

UNCLASSIFIED

AD 296 002

*Reproduced
by the*

**ARMED SERVICES TECHNICAL INFORMATION AGENCY
ARLINGTON HALL STATION
ARLINGTON 12, VIRGINIA**



UNCLASSIFIED

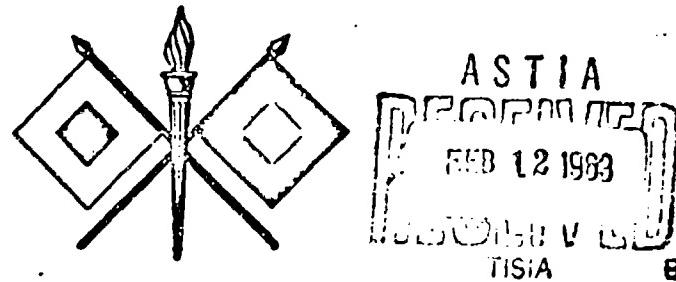
NOTICE: When government or other drawings, specifications or other data are used for any purpose other than in connection with a definitely related government procurement operation, the U. S. Government thereby incurs no responsibility, nor any obligation whatsoever; and the fact that the Government may have formulated, furnished, or in any way supplied the said drawings, specifications, or other data is not to be regarded by implication or otherwise as in any manner licensing the holder or any other person or corporation, or conveying any rights or permission to manufacture, use or sell any patented invention that may in any way be related thereto.

63-2-4

CATALOGED BY ASTIA
ACYAD NO 296002

PROCEEDINGS
OF THE
SEVENTH SYMPOSIUM
ON

HYDROGEN THYRATRONS & MODULATORS
HELD AT
THE HEXAGON — FORT MONMOUTH, N.J.
MAY 22, 23, 24, 1962



CO-SPONSORED BY
THE ADVISORY GROUP ON ELECTRON DEVICES
AND
U.S. ARMY SIGNAL RESEARCH & DEVELOPMENT LABORATORY

PROCEEDINGS

of the

SEVENTH SYMPOSIUM ON HYDROGEN THYRATRONS
AND MODULATORS

Held at

The Hexagon, Fort Monmouth, New Jersey

on

22, 23, and 24, May 1962

The services and materials required for the
arrangement, handling, and reporting of this
Symposium have been furnished under Signal Corps
Contract DA36-039 sc-89076

by

ELECTRON DEVICES GROUP
ENGINEERING RESEARCH DIVISION
NEW YORK UNIVERSITY

ASTIA AVAILABILITY NOTICE

Qualified requestors may obtain copies
of this report from ASTIA

The papers compiled herein are prepared in their entirety as submitted. Each paper reflects the viewpoint of its author, and USASRDL and AGED do not necessarily subscribe to the ideas and opinions expressed therein.

SEVENTH SYMPOSIUM ON HYDROGEN THYRATRONS AND MODULATORS

COMMITTEE

S. Schneider, USASRDL (Co-Chairman and Editor)
G. W. Taylor, USASRDL (Co-Chairman)
H. L. Beard, Rome Air Development Center
R. A. Hill, Bureau of Ships
A. J. Paturzo, AGED (Secretary)
M. S. Green, USASRDL (Assistant to Editor)

Session B (continued)

Page No.

A HIGH PEAK POWER MODULATOR FOR RESEARCH IN PULSE COMPRESSION 94
R. Banks
Marconi's Wireless Telegraph Company, limited

A SIMPLIFIED MODULATOR FOR LONG PULSES AND HIGH MEAN POWER 105
N. S. Nicholls and R. E. Jarvis
Royal Radar Establishment

PERFORMANCE TESTS AND LIFE DATA OF THE 36-MEGAWATT MODULATORS 124
DEVELOPED FOR THE ASTRON 1000-MEGAWATT ELECTRON ACCELERATOR
Vernon L. Smith
Lawrence Radiation Laboratory, University of California

ANALYSIS OF MODULATOR DESIGN PROBLEMS BY SIMULATION 165
Robert A. Hill
Westinghouse Electric Corporation

HIGH-POWER VLF PULSE GENERATION USING HYDROGEN THYRATRONS 179
E. R. Besenfelder and C. J. Eichenauer
General Electric Company

THE GRID SPIKE PROBLEM ASSOCIATED WITH HYDROGEN THYRATRONS 195
AND A PRACTICAL MEANS FOR ITS SOLUTION
R. W. Sedgwick
The Bendix Corporation

Session C. - Solid State and Magnetic Modulators

Chairman: H. Beard
Rome Air Development Center

A TWT FLOATING DECK GRID PULSER EMPLOYING PNPN (SHOCKLEY) 200
TRANSISTOR DIODES
Albert R. Luna and Stephen P. Delligatti
Burvac Electronics Company, Inc.

SOLID-STATE GATE MODULATOR 207
Roy T. Courtney
ITT Federal Laboratories

Session C (continued)

Page Nr.

SOLID STATE MODULATOR

223

T. Hamburger, C. H. Wood, and R. A. Gardenghi
Westinghouse Electric Corporation

TWO EXPERIMENTAL SEMICONDUCTOR-MAGNETIC PULSE MODULATORS

240

R. Jordan, C. Price, and L. Swain
Electronic Systems Laboratory
Massachusetts Institute of Technology

DEVELOPMENT OF A 50-MEGAWATT MAGNETIC MODULATOR TO
SIMULTANEOUSLY TRIGGER 500 THYRATRONS

260

Bernard M. ... h
Lawrence Radiation Laboratory, University of California

A LONG PULSE MAGNETIC MODULATOR

290

R. J. Froelich and J. V. Stover
Hughes Aircraft Company

THE DESIGN OF A MODULATOR-POWER SUPPLY SYSTEM FOR THE
STANFORD TWO-MILE LINEAR ACCELERATOR

312

W. I. Smith
Radio Corporation of America

Session D.- Ignitrons and Hard Tubes

Chairman: E. Spitzer
Radio Corporation of America

PERFORMANCE OF IGNITRONS IN PULSE SERVICE

328

T. F. Turner and H. S. Butler
Stanford University

RESEARCH STUDY OF HARD TUBE MODULATOR LIMITATIONS

348

C. V. Weden
The Machlett Laboratories, Inc.

DESIGN AND APPLICATION OF THE "INJECTRON" (Abstract)

360

Lowell J. Fox
Litton Electron Tube Corporation

Session D (continued)

Page No.

SOME ADVANCES IN THE TECHNOLOGY OF MODULATING ANODE PULSERS
FOR HIGH-POWER KLYSTRONS

361

C. Pappas
Radio Corporation of America

FIELD EMISSION SWITCH TUBE STUDY
E. E. Martin and F. H. Charbonnier
Linfield Research Institute

388

HARD TUBE MODULATOR TECHNIQUES THAT PERMIT UTILIZATION OF
MINIMUM SIZE CAPACITOR BANKS

415

Vadim N. Martirovitch
Lockheed Electronics Company

Session E.- Special Topics and Crowbar Technology

Chairman: F. J. Rutter
Westinghouse Electric Corporation

MODULATOR CONSIDERATIONS FOR MODULATING ANODE BEAM TUBES
IN BURST MODE RADARS

421

E. F. Weinburg and W. A. Vail
Rulytheon Company

A REVIEW OF THE U.K. GOVERNMENT PROGRAMME ON DEVICES FOR
PULSE MODULATORS

No Paper

N. S. Nicholls
Royal Radar Establishment

THE HIGH SPEED PROTECTION OF MICROWAVE TUBES AND SYSTEMS
Albert J. Morris and Joseph P. Swanson
RADIATION at Stanford

436

PROTECTIVE CIRCUITRY CAPABLE OF AUTOMATIC OPERATION OVER
A WIDE DYNAMIC RANGE
H. F. Onusseit
Sylvania Electronic Systems

454

FAULT SENSING AND PROTECTION FOR HIGH POWER KLYSTRON
TRANSMITTERS
C. Pappas
Radio Corporation of America

460

<u>Session E (continued)</u>	<u>Page Nr.</u>
A VERSATILE ELECTRONIC CROWBAR SYSTEM S. Schneider, M. H. Zinn, and A. J. Buffa USASRDL	482
A 300-KV MULTIGAP CROWBAR G. Grotz Sperry Gyroscope Company	507
 <u>Session F. - Crowbar Technology</u>	
Chairman: J. E. Creedon U. S. Army Signal Research & Development Laboratory	
THE USE OF TRIGGERED SPARK GAPS AS CROWBARS Lawrence B. Woolaver Edgerton, Germeshausen and Grier, Inc.	521
A HIGH POWER GAS DISCHARGE SWITCH B. O. Baker and K. G. Cook The General Electric Company, Limited	532
INFINITE VOLTAGE RANGE TRIGGERED ARC CAPS FOR CROWBAR APPLICATION Joseph P. Swanson RADIATION at Stanford	549
PRESSURIZED, TRIGGERED, HIGH VOLTAGE SPARK GAP - A POSSIBLE PROTECTIVE DEVICE W. F. Westendorp General Electric Research Laboratory	553
RECORD OF ATTENDEES	565
AUTHOR INDEX	573

OPENING REMARKS

by

M. H. Zinn

U. S. Army Signal Research and Development Laboratory
Fort Monmouth, New Jersey

I would first like to add my welcome, to that of Colonel Kimbrough's, to all of you on this occasion of the Seventh Symposium on Hydrogen Thyratrons and Modulators. I would also like to thank Colonel Kimbrough and the Laboratory for making these facilities available to us, so that we can continue to carry on this effort of bringing together on a biennial basis the foremost experts in the field of modulator devices and modulators.

Our objective for this Symposium remains the same as it has been from the first, to provide a meeting ground for the device designer and the device user to discuss their achievements and their problems so that each may stimulate the other in turn. To this end the Symposium Committee has assembled a program that covers a wide range of topics in both the device area and in modulator design and techniques. The devices to be covered include hydrogen and deuterium thyratrons, ignitrons, spark-gaps, magnetic modulators, high-vacuum modulator tubes, and solid state devices. Modulator discussions will include both line-type and hard-tube type as well as the need for and methods of providing protection in high-energy storage systems.

The Symposium Committee has, in my opinion, done a magnificent job in providing this well-balanced program. Obviously, however, this could not be accomplished without the existence of two factors: first, the great cooperation of industry, the universities, and the military services in providing the speakers the opportunity to report on their efforts; and, second, the large scale of activities in the modulator field in the three countries represented here today. This large scale of activities is directly reflected in the size of the program for the next three days. This year the Committee has scheduled thirty-seven papers, compared to approximately thirty-one at the last meeting, and it was forced to reject a number of worthy papers over and above those that were scheduled. In addition, they were also forced to forego the general discussion session that has traditionally been a part of the format of these meetings. Since, as I have stated, one of the prime objectives of the Symposia has always been to discuss our mutual problems, omission of a general discussion session leaves the obligation of attaining the discussion goals to you, the audience. The Committee has left ample time for discussion after each paper so that, if the speakers adhere to their allotted times, the opportunity for discussion will be there. Please use this time to bring out into the open any problems you may have that bear a general resemblance to the topic under discussion at the moment.

A close examination of the program indicates that the major portion of the device effort directly sponsored by the military services here and abroad is covered by papers. Before you leave the Symposium you should be well aware of where we stand today as far as the power-handling capabilities of hydrogen thyratrons and ignitrons are concerned. The discussions on

high-vacuum modulator tubes will show that entirely new concepts of tube design are being explored and hold promise of providing new capabilities in the future. The solid state field is well represented, covering modulator design and solid state application in both the low-power region, where they are the natural type of device to be considered, and in the high-power field where they may provide advantages for general or particular applications.

Reviewing the modulator equipment portions of the program indicates that we will receive a clear picture of how most of these devices have fared in different applications, with data presented on both performance and life. The program promises to continue the discussion started by Mr. Eichenauer in his paper presented at the last Symposium, entitled "Superpower Klystron Pulsing Considerations," on the line-type modulator versus the hard-tube modulator. The emphasis of the last day's program on crowbar technology is indicative of the amount of effort presently being expended on one of the side results of having resolved this question of line-type versus hard-tube modulator in favor of the hard-tube modulator.

All of this will be covered, and, I am sure, will be covered in a more than adequate manner, by the speakers who will follow me, and I would not want to steal any of their thunder by expounding in any detail on any of these subjects.

I see the possibility, however, for some confusion in the minds of some of you when we are through. You may well ask, where are we going? What is the major trend in the modulator field? Truthfully, I cannot provide you with an adequate answer. I feel that I can give you instead my own opinions of where we should be going. To my mind there is no need to settle, if indeed it is possible to settle, any arguments on line-type modulators versus hard-tube modulators on a general basis. Each particular system requirement, if intelligently examined from the standpoints of equipment performance characteristics against such items as weight, size, and initial and maintenance cost, will provide the answer for that particular system. What we must guard against is that when this answer is reached the modulator device required to do the optimum job is not available; that the optimum answer is never reached at all because available devices have biased the considerations; or that having arrived at the answer and finding no device available, a crash development is initiated to obtain it. I firmly believe that the equipment designer must have available to him a complete family of both line-type and hard-tube modulator devices to enable him to do his job properly. Furthermore, the available devices should be capable of switching the full input power into an rf generator as well as to gate the rf device on and off. It is a common fallacy to view the employment of an rf device, such as the anode-modulated linear beam tube, as having eliminated the need for a full-power modulator. I call this a fallacy because the full-power modulator is still there although some people can't see it. In this case the rf tube is the modulator tube. The circuit is automatically restricted to a hard-tube modulator circuit and must be laid out and treated and protected as one. While this may or may not result in equipment simplification, I feel that we in the modulator device research and development area should be more considerate of our fellow engineers in the RF Generator Tube Design Area. If they knowingly wish to take on our problems, good luck to them, but we should not be forcing them to such designs, which may, and have, complicated the already severe problem of achieving the desired rf performance because modulator devices capable of switching the full input power are not available.

This, then, is the direction in which we should be going, towards full-power capability in both line-type and hard-tube modulator devices. You may next ask, are we moving in that direction? I can only state that we have started a small amount of effort in this direction and a large amount of plans to move further. The systems management concept of leaving device development to the systems manager, however, does not do much to encourage the initiation of such an expensive broad-based program and I cannot predict whether it will ever truly be launched.

I hope that my remarks have served the purpose intended by the Symposium Committee when they invited me to make them, that of whetting your appetite for the papers to follow. I also hope that they have served my purpose in giving them, that of setting a framework against which you could view the Symposium and take back to your separate establishments a more meaningful understanding of its purpose and objectives. I hope that you will all enjoy your stay with us on the Jersey shore and that you will be looking forward to the next Symposium with as great an anticipation as you did this one.

CATHODE PHENOMENA & LIFE IN HYDROGEN THYRATRONS

by

Seymour Goldberg

Edgerton, Germeshausen & Grier, Inc.

Careful consideration of the cathode in hydrogen thyratrons is particularly important since it is uniquely this area of the tube that is subject to a basic continuous wearing-out or depletion process during life and thus, it is the cathode and these depletion processes which eventually determine the life capability of the hydrogen thyratron. (Hydrogen cleanup is not normally too serious a life-determining process due to the use of reservoirs.) In this paper we will discuss these processes for conventional oxide-coated cathodes as commonly used in American thyratrons.

The effects of the cathode wearing-out process is to eventually deplete the cathode of its oxide coating resulting in loss in triggering performance. Tubes will thus fail due to exceeding t_{ad} , Δt_{ad} or jitter specifications or they may reach a point where they will not trigger at all with the specified trigger pulse.

CATHODE DEPLETION

Cathode depletion occurs in two manners: first, as a gradual and continuous loss of emissive coating from the cathode, and, second, a more violent ejection of discreet pieces of the cathode occurring rather rapidly. The latter process occurs when cathode arcing occurs due either to excessive peak currents or poor cathode activity. The gradual continuous process is the more fundamental one and occurs to a greater or lesser extent in all hydrogen thyratrons. Figure 1 illustrates the cathode depletion in 4C35 thyratrons at progressive stages of life and the steady loss of cathode coating may be seen. The time scale for this process depends on the operating conditions. At rated conditions complete loss of coating occurs at about 2500 hours.

By carefully measuring the temperature dependence of the rate of steady depletion of cathode coating in tubes under operating and quiescent conditions, we have established that the rate of cathode coating loss is purely temperature dependent. At a given cathode temperature the rate of coating loss is the same in a pulsed tube as in a tube operating at the same cathode temperature but without a discharge.

These observations indicate that the depletion mechanism is a thermal evaporation process. Figure 2 shows our measurement of coating loss rate on thyratron cathodes compared to the evaporation data of Herrmann and Wagener⁽¹⁾; and Leverton & Shepherd⁽²⁾. This data shows that at the normal

operating temperature of the thyatron cathodes, life is decreased about a factor of 2 for every 25°C rise in cathode temperature. Thus, understanding the factors responsible for determining the operating temperature of the cathode is basic to obtaining long-life thyatrons.

CATHODE DISSIPATION

It is well known that the temperature of the cathode increases from its quiescent value when pulsed current is passed through the tube. This occurs because the cathode coating has a small but finite resistance through which the pulsed current must pass. The dissipation is thus given by the square of the R:S current multiplied by the net effective resistance of the cathode coating. This resistance is equal to the specific resistance of the cathode coating, i.e., the resistance of 1 cm² of cathode surface, divided by the area of the cathode supplying current. Assuming the total cathode area is reasonably uniformly utilized by the discharge, the set of equations shown in Figure 3 may be derived for calculating the magnitude of the temperature rise. The other major assumptions for these derivations are:

1. that cathode temperature is related to the cathode input power by a simple power function. Since most of the cathode thermal losses are due to radiation, the exponent is typically between 3 and 4, and of course, cannot exceed 4.
2. that the cathode filament power increases linearly with cathode area.
3. that $\frac{\Delta T}{T_0}$ is small compared to 1 that is, does not exceed 0.2
4. that the cathode is iso-thermal, that is, that it has sufficient thermal conductivity over its entire area so that power input from the filament or by dissipation results in the same uniform temperature rise.

This derivation shows that ΔT is strongly influenced by the R:S current and cathode area and also by the specific coating resistance.

FILAMENT DERATING

Operationally, it is possible to eliminate the cathode temperature rise by reducing the cathode filament power under operating conditions by an amount equal to the cathode dissipation. Life test data on 4C35 thyatrons indicated that the operational life of the cathode was increased by over a factor of two by reducing filament voltage from 6.3 to 5.4 volts. An EG&G 1802/7322 thyatron was tested under standard operation 1 conditions using a filament derating technique where E_f was reduced to 4 volts. After 2800 hours the cathode was only 1/4 depleted indicating a life capability of over 10,000 hours by reducing cathode power. (The tube failed at 2800 hours due to a reservoir filament short.) These results confirm that the essential cathode life problem in thyatrons is due to a cathode temperature rise which may be solved by appropriate reduction in filament power.

CATHODE UTILIZATION

The problem in building thyratron cathodes of large area for high powered tubes is to assure that the entire area is utilized by the discharge. The degree of spreading of a discharge along the axial dimensions of the cathode, i.e., parallel to the axis of the discharge, is given by:

$$L_{ut} = \sqrt{\frac{2I_b R_o}{W E_p - \frac{dV_s}{dx}}}$$

E_p = plasma field

$\frac{dV_s}{dx}$ = gradient of cathode sheath voltage

W = ratio of total cathode area to length = cathode periphery

$$E_p - \frac{dV_s}{dx} \approx 21 \text{ volts/cm}$$

Actually, the cathode current is far from uniform over this length and for obtaining a length which is reasonably evenly utilized one would used a length of half this.

This relation thus indicates a well-utilized axial length of about 1 cm per 5 amp/cm² of average current density.

The effects of non-uniform utilization may be seen in Figure 1 where the current density was greatest at the top of the cathode and thus this region was hottest causing more rapid evaporation. Since one is thus limited in the length of the cathode one may utilize further increases in area can only come about by increasing the cross section of the cathode. This then brings up the question as to the extent of the radial spreading of a discharge along the cross section of a cathode. This was studied at EG&G by means of the tube shown in Figure 4. The cathode length is 1 inch and its width is .265".

It was found that when the large planar anode was used (plane parallel anode-cathode) the discharge was fairly evenly spread over the 1" cathode length. However, in a more typical case, the cathode would normally have a baffle in the place of the large anode and the discharge would have to enter the cathode region through the space of the small anode and then spread radially along the cathode. The utilized length was measured using the small anode by photographing the discharge light and also scanning the discharge light with a photomultiplier over the cathode length.

Figure 5 plots the utilized length vs. peak current and it may be seen that the results agree very closely with the lengths predicted from the axial utilization theory.

Actual cathode design for many thyratrons involves a combination of axial and transverse cathode utilisation. While a quantitative theory for this case has not been derived it is probably true that the discharge will spread evenly over a cathode having a limited access aperture about 1 cm in any axis for every 5 amp/cm² of average cathode current density.

COATING RESISTANCE

Figure 6 shows some measurements of coating resistance for a cathode of 2.74 cm² area. This figure compares double and triple carbonate cathodes on 499 Ni and also A-31, a tungsten-nickel alloy. The A-31 yields significantly lower values of R_o. The results one obtains on a measurement of this type can fluctuate widely due to processing and cleanliness factors. These curves are representative of what can be obtained with a very well-processed cathode.

CATHODE ARCING

The current density limitation at which cathode arcing occurs is also a major cathode design parameter as it determines the maximum peak current that can be supplied by a given area of cathode. Figure 7 shows the current densities at which arcing occurred for a .75 millisecond pulse length. It was found in this experiment that with pulses this long appreciable cathode temperature rise occurs during the pulse. Since arcing occurs at the end of the pulse, the arcing limit of the cathode is enhanced by the temperature rise and the true arc limit is determined by the end of the pulse temperature. These results show that rather large peak currents can be passed without arcing even at .75 msec at reasonable cathode temperatures. The peak current limit increases as the pulse width is made shorter.

MATRIX CATHODES

In an effort to obtain cathodes of large peak current capability with less resistance than the conventional oxide coating, matrix and impregnated cathodes have been studied. Being largely metallic in nature one would expect these types of cathodes to have very low resistance and thus operate with a small temperature rise.

Work on the Phillips type of impregnated cathode has been discouraging in that these cathodes show very low or almost no activity in hydrogen tubes. A few minutes of operation will generally completely deactivate them.

The matrix or B-N type of cathode as described by Beck (3) has shown more promise. These consist of a mixture of nickel and triple carbonate powders with a 1% zirconium activation which are compacted under pressure and sintered in our case in vacuum. The cathodes contain sufficient nickel (70% by weight) to have very low, essentially metallic bulk resistivity.

The emission drop data, however, shows a relatively high apparent resistance as shown in Figure 8 for 1.2 cm² area cathode. However, colori-

metric measurements of cathode temperature rise (which were rather low) indicated that the high emission drop was not due to resistance of the cathode but were rather due to the cathode operating in a temperature-limited mode and the emission drop is largely due to a high cathode sheath.

A diode has been successfully life-tested, however, at 37 amp/cm² for 1000 hours in this mode. The emission drop started at 80 volts and was 200 volts at end of life.

During the first 20 to 100 hours of life some of the cathodes have yielded very low emission drops indicating a space charge limited mode. Our test results on this cathode type are as yet incomplete, however.

-
1. Herrmann & Wagener, "The Oxide Coated Cathode", Vol. I, Chapman & Hall, Ltd., 1951
 2. Leverton & Shepherd, "The Use of Radioactive Isotopes to Study Evaporation of Thermionic Cathodes" JOURNAL OF APPLIED PHYSICS, Vol. 23, No. 7, July 1952
 3. Beck et al, "A New Diffusion Cathode", LeVide No. 54, November 1954
-

This work was supported by USASRDL under Signal Corps contract DA36-039 SC-85338.

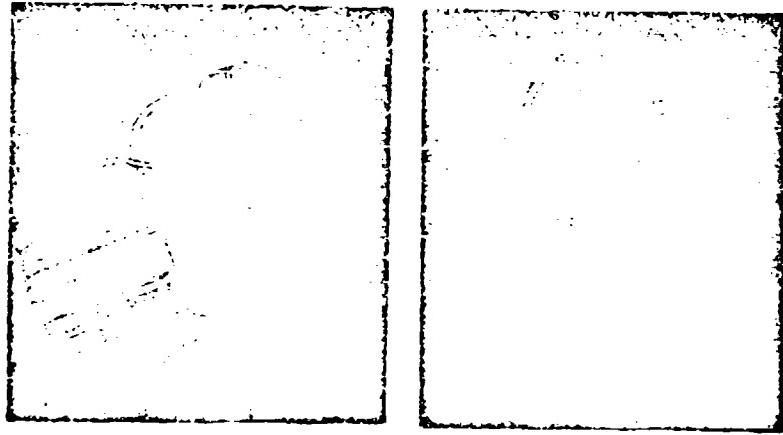


Figure #1. 4C35 Thyratron Cathodes Showing Cathode Depletion During Life

CATHODE DISSIPATION P_d

$$① P_d = I_{RMS}^2 \frac{R_c}{A_c} \quad I_{RMS} = \sqrt{I_s I_m}$$

$$② P_{Ra} = R_c A_c T_c \quad n = 3 to 6$$

TOTAL CATHODE POWER = $P_{Ra} + P_d$

$$③ P_{Ra} + P_d = R_c A_c (T_c + \Delta T)^n$$

$\Delta T = \text{TEMP. RISE}$

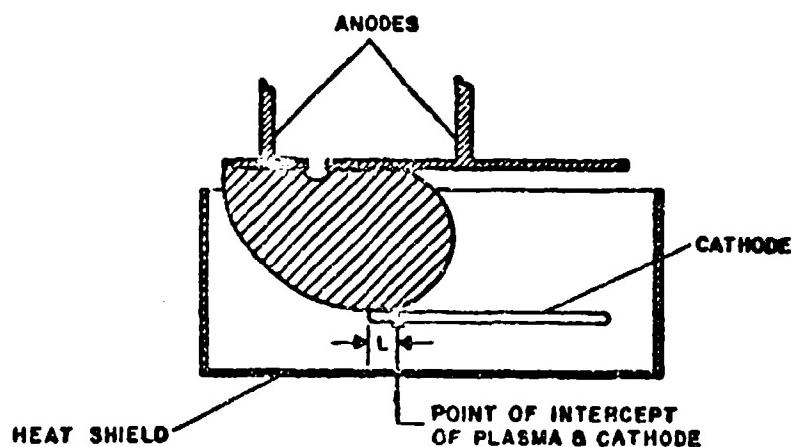
$$④ \frac{P_d}{P_{Ra}} = \left(1 + \frac{\Delta T}{T_c}\right)^n - 1$$

FOR $\frac{\Delta T}{T_c} \ll 1$

$$\frac{\Delta T}{T_c} = \frac{1}{n} \frac{P_d}{P_{Ra}}$$

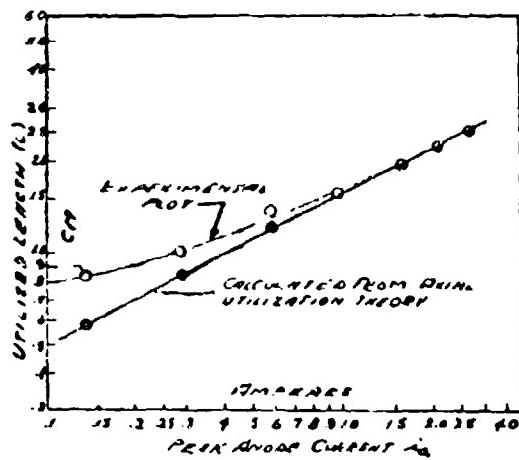
$$⑤ \Delta T = \frac{I_{RMS}^2 R_c}{n A_c R_c T_c} \quad \text{OR} \quad A_c = I_{RMS} \sqrt{\frac{R_c}{0.4 k n \Delta T}}$$

Figure #3. Derivation of Cathode Temperature Rise



Typical discharge plasma in transverse utilization tube with extended flat cathode.

Figure #4. Transverse Utilization Geometry



THE TRANSVERSE UTILIZATION
OF A FLAT RADIALLY EXTENDED
CATHODE AS A FUNCTION PEAK
ANODE CURRENT

Figure 75. The Transverse Utilization of A Flat Radially Extended Cathode As A Function of Current.

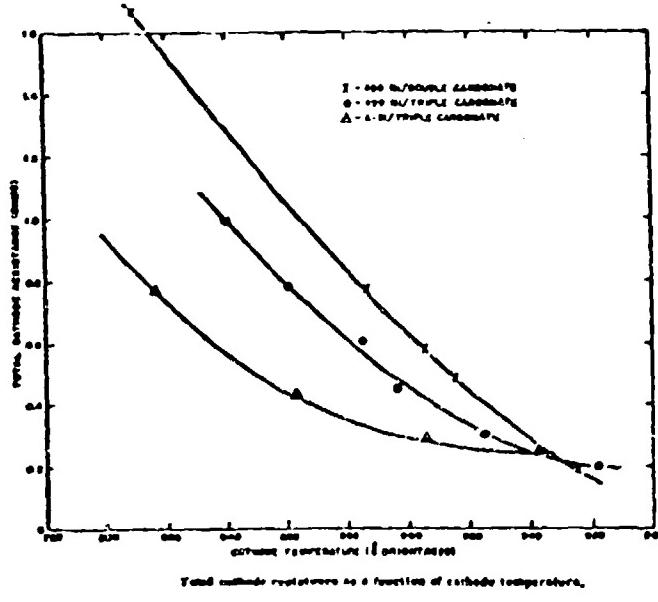


Figure 76. Total Catnode Resistance As A Function of Temperature For A 2.74 cm^2 Cathode.

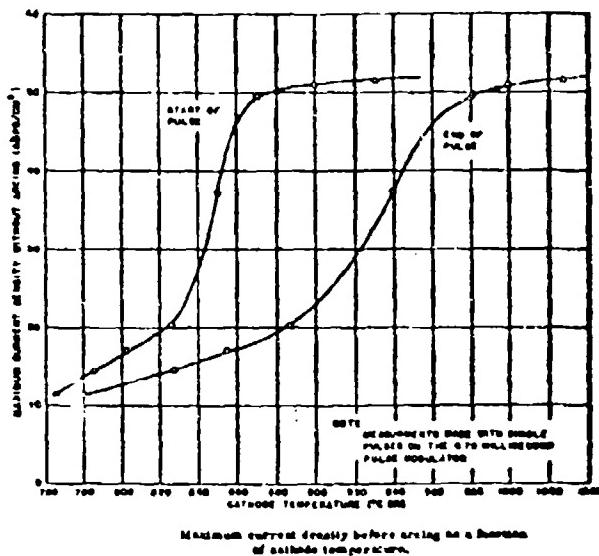


Figure #7. Minimum Current Density Before Arcing As A Function of Cathode Temperature

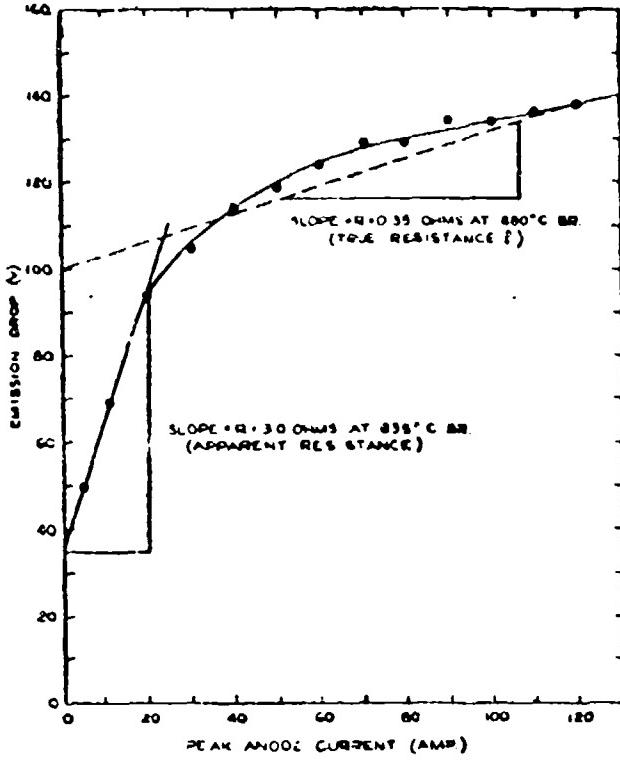


Figure 78. Emission Drop Versus Current For A 1.2 cm² Flat Matrix Cathode

CATHODE-GAS PRECIPITATION IN HYDROGEN THYRATRONS

by

J. E. Creedon, S. Schneider, and F. Cannata

U. S. Army Signal Research and Development Laboratory
Fort Monmouth, New Jersey

To obtain a better understanding of cathode limitations in hydrogen thyrators, a number of tubes of various types were studied for emission characteristics at pulse lengths of 5, 30, and 1000 microseconds. The results indicate that a rating curve can be derived from which the peak current capability of a cathode at any pulse length can be determined.

A diagram of the test circuit is shown in Figure 1. The value of the tube drop (V_T) of the diode under test was measured with an oscilloscope, and the peak current (i_b) was measured with a current transformer. The emission properties of the cathode were studied using single-shot techniques. Also shown in Figure 1 are two plots of the tube drop as a function of peak current. Over a large range of current the form of the curve is given by

$$V_T = V_g + R i_b \quad (1)$$

where the constant V_g is the intercept at zero current and R is the slope of the line. To a good approximation, V_g is the gas drop in volts and it is relatively independent of current. R is the resistance of the cathode in ohms, and it is an inverse function of the cathode temperature.¹

At a given cathode heater power the peak current was increased until arcing was observed towards the end of the pulse. Although the presence of an arc could be visually detected, an abrupt drop in the voltage presentation gave the time of the arc and was used to determine the presence of an arc in all the tests. The quiescent temperature of the cathode was then varied by changing the heater power, and the cathode resistance and the current level for arcing were redetermined. To account for a pulse heating effect, the tube drop was measured at a time corresponding to 60 percent of the pulse width. Using this procedure, a large number of experimental points were obtained of the arcing current limit as a function of R . The data were normalized by dividing the current level at which arcing occurred by the nominal cathode area (A_c) and by multiplying the measured cathode resistance by A_c . This gives a J_{arc} in amperes per square centimeter for a corresponding R_o in ohms (centimeters squared), and, in this way, a variety of tube sizes could be compared.

For emission data at a pulse width of 1000 microseconds, a millisecond modulator was used, where the impedance of the pulse-forming network is 4 ohms. At this pulse length, a total of ten tubes were studied. The types and numbers of the tubes used were: 5C22 (2); 5949 (3); 5948 (1); 1257 (3); and 7390, Phase I, (1).

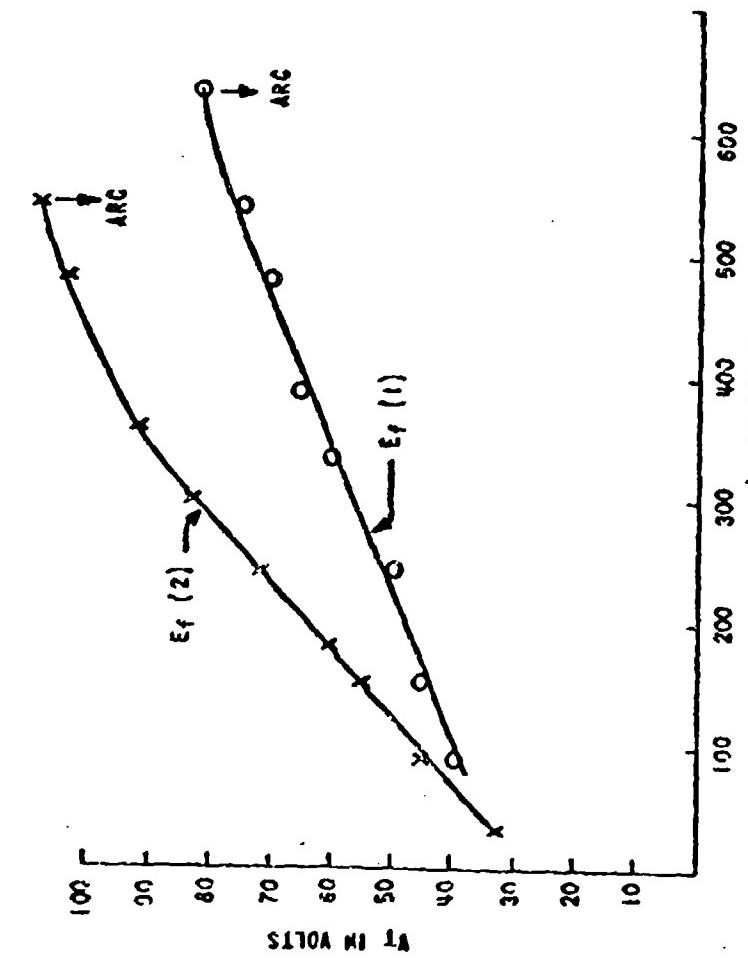
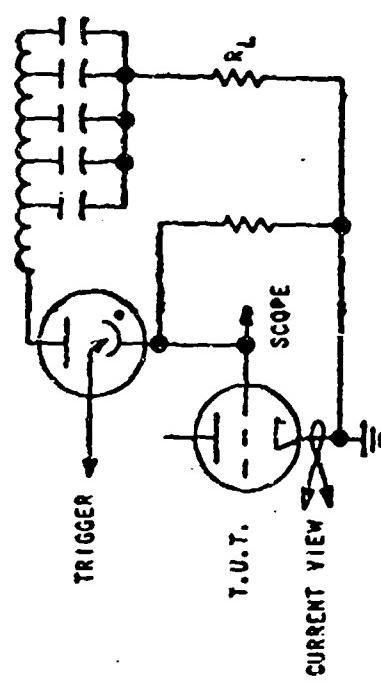


FIG. 1 EMISSION CIRCUIT AND CURVE

The experimental results are shown in Figure 2, where the logarithm of J_{arc} is plotted as a function of R_o^{-1} . The slope of the solid line is one-half, which indicates that the limiting mechanism is due to a power dissipation density in the cathode, since the experimental dependence of J_{arc} on R_o^{-1} is given by

$$\log J_{arc} = \frac{1}{2} \log R_o^{-1} + \log C \quad (2)$$

and

$$\frac{J_{arc}}{C} = \left(\frac{1}{R_o}\right)^{\frac{1}{2}} \quad (3)$$

$$J_{arc}^2 \times R_o = C^2 = P_d \text{ arc} \quad (4)$$

where $P_d \text{ arc}$ is in $\frac{\text{watts}}{\text{cm}^2}$ per pulse.

Experimentally, the value of $P_d \text{ arc}$ for the millisecond pulse length is 250 watts per cm^2 . Expressed in terms of energy, an arc occurs when 0.25 watt-sec per cm^2 is dissipated in the cathode.

Figure 3 shows data obtained for a 5948 thyratron operating as a switch tube in the millisecond modulator. In this test, the root-mean-square current (I_{rms}) was kept constant by adjusting the pulse repetition rate as the peak current was varied. The grid-cathode drop was measured on an oscilloscope at 600 microseconds, and emission curves were obtained for I_{rms} currents of 10, 15, 20, and 25 amperes at several cathode heater powers. Cathode resistances were calculated from the slopes of these curves. The J_{arc} values versus R_o^{-1} obtained with this procedure are the plotted points. The solid line is the single-shot data from Figure 2, and the agreement of the slopes is reasonably good. Although the points consistently lie above the line, the limiting current density values shown are for arcs occurring on 10 to 40 percent of the pulses, whereas the line represents an averaging of the occurrence of an arc on the single-shot data.

An interesting observation on this test was that the grid-cathode voltage as a function of peak current at constant rms current was essentially linear up to the arcing limit. Figure 4 shows the observed values of grid-cathode voltage drop measured at 0.60 millisecond after the start of current flow. In curve (1), the 5948 thyratron was pulsed once every two minutes, and the plateauing off of the voltage drop is quite commonly observed in emission drop measurements at high values of peak current. For curves (2) through (6), the pulse repetition rate was varied to maintain constant I_{rms} currents of 10, 15, 20, 25, and 30 amperes respectively. In general, the curves are linear and of the form of equation (1) to within 100 to 150 amperes of the current level where arcing occurs on 10 to 40 percent of the pulses. The decrease in the slope of the curves as the I_{rms} value is increased illustrates the dependence of R and R_o on cathode temperature mentioned previously. Extrapolating the curves to zero current gives a V_g value of 38 volts.

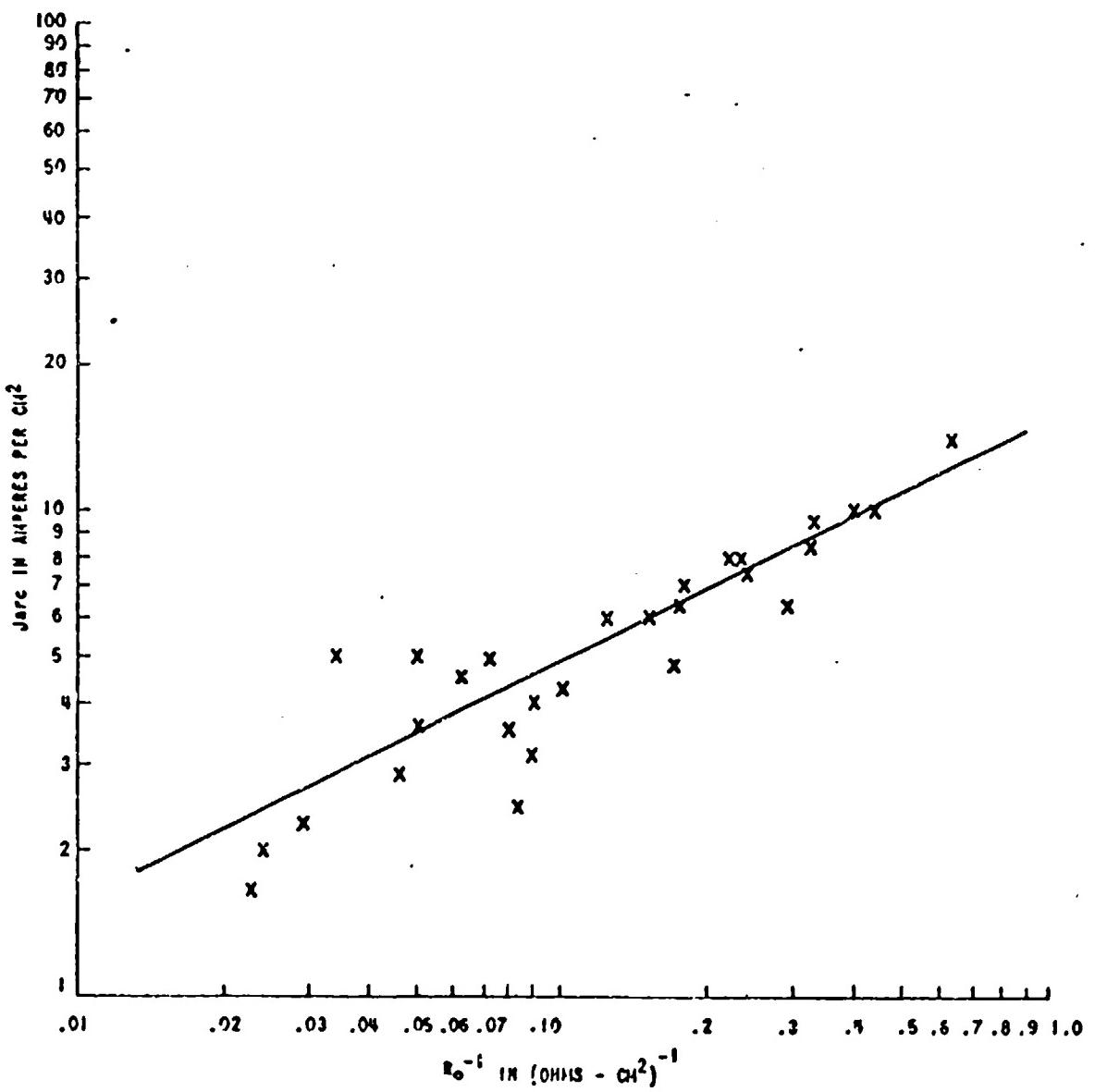


FIG. 2 CURRENT DENSITY FOR ARCING VS R_0^{-1} - MILLISECOND PULSE

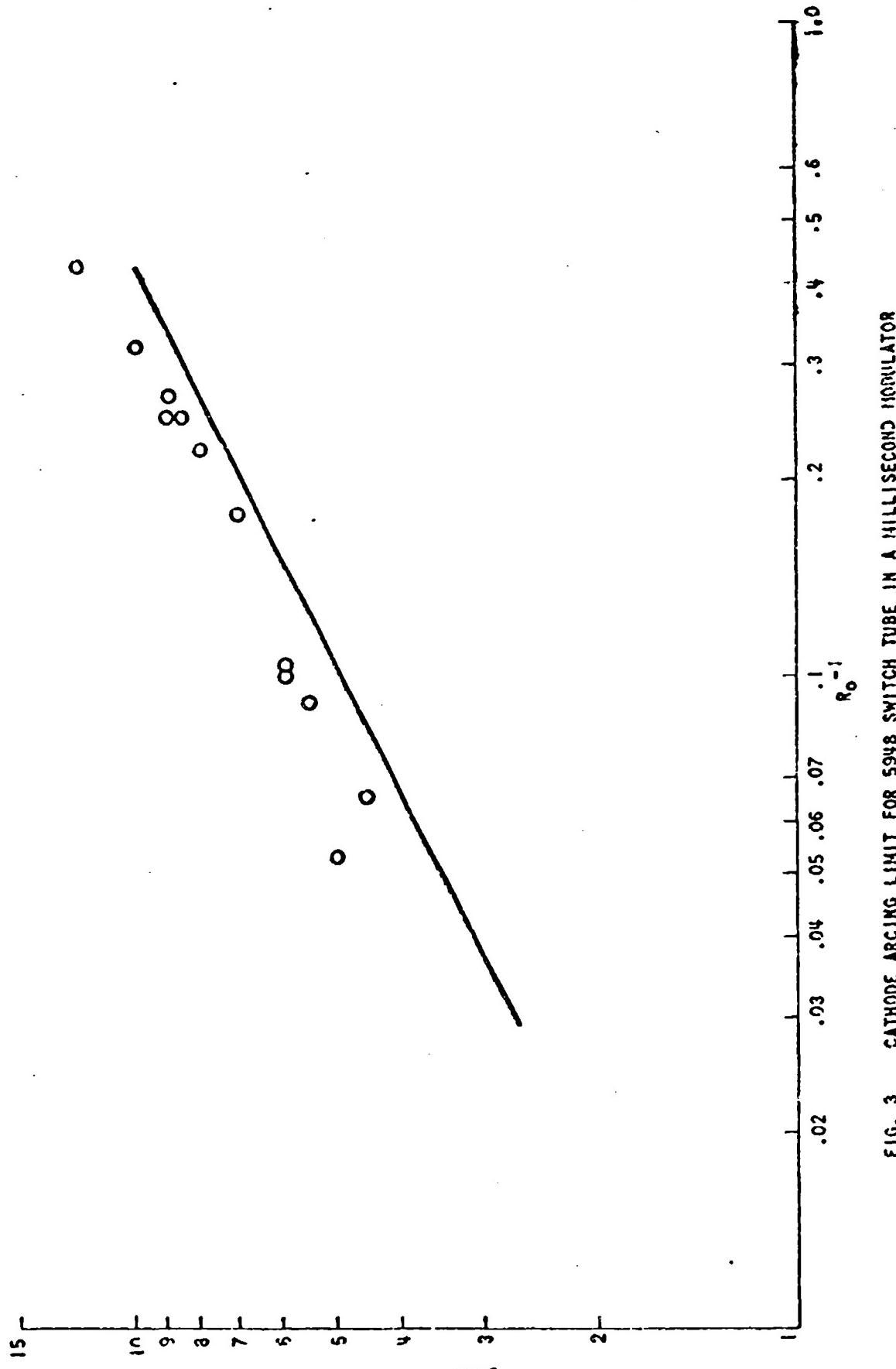


FIG. 3 CATHODE ARCING LIMIT FOR 5948 SWITCH TUBE IN A MILLISECOND IONIZER

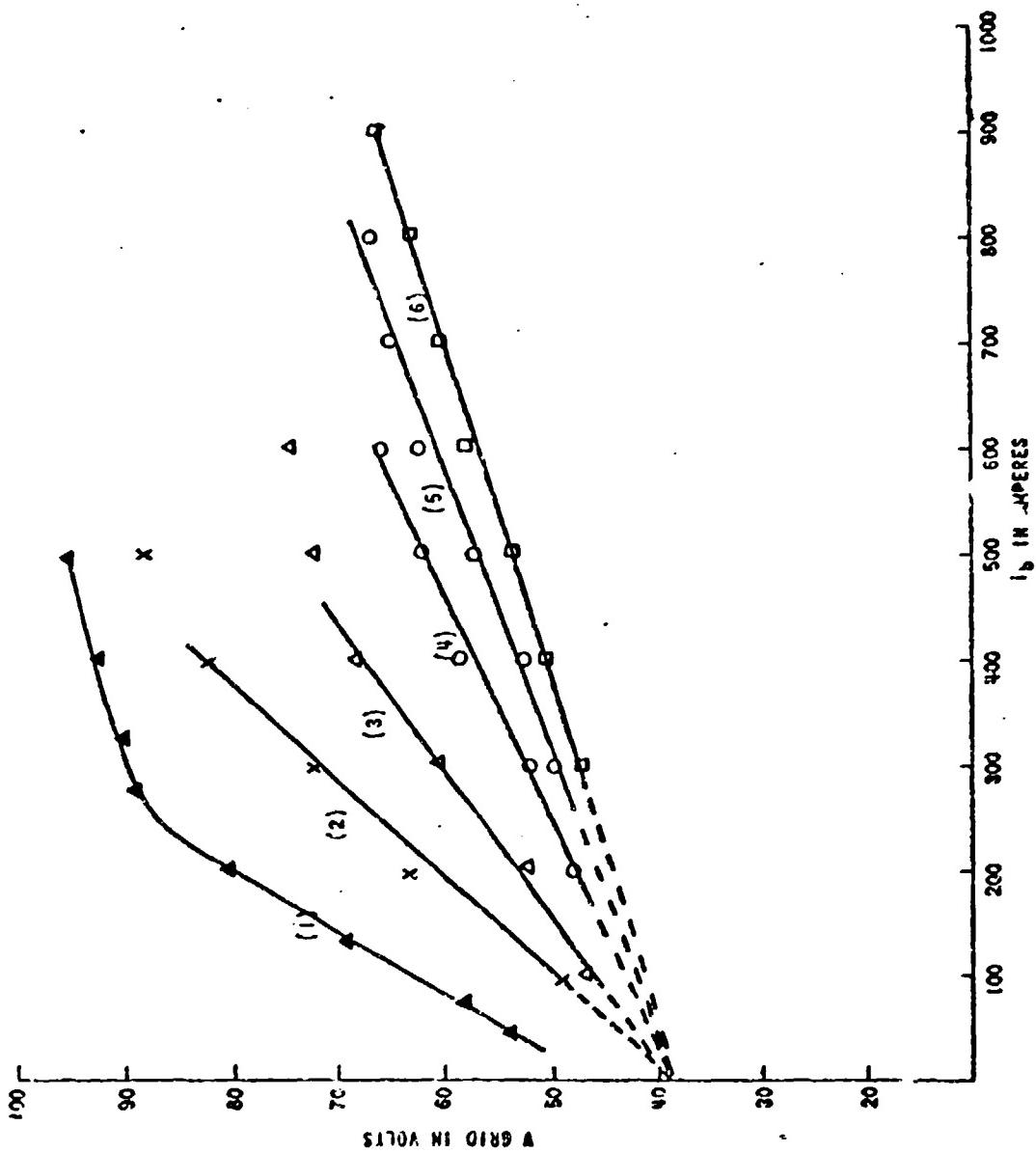


FIG. 4 GRID-CATHODE VOLTAGE VS PEAK CURRENT

Figure 5 shows the results obtained for a 30-microsecond pulse. At this pulse length the value of current density for arcing has increased considerably in comparison with the millisecond pulse. At an R_0 value of 4 ohms - cm^2 , corresponding to R_0^{-1} value of 0.25, the observed J_{arc} value of 25 amperes per cm^2 is larger than the millisecond value by a factor of three. The dependence of J_{arc} on R_0 is also given by the 1/2 power law, and the value of $P_{d \text{ arc}}$ from these data is equal to 2500 watts per cm^2 per pulse.

For a 5-microsecond pulse width, the conventional emission checker used did not have the peak current capability required to arc the larger-size tubes, and the results shown in Figure 6 were obtained on 5C22 tubes. Empirically, the same dependence of J_{arc} on R_0 was observed as at the longer pulse widths, and $P_{d \text{ arc}}$ was calculated to be a nominal 8100 watts per cm^2 for this pulse length.

The values of $P_{d \text{ arc}}$ obtained from this type of experimental data are plotted as a function of time in Figure 7, and the result can be expressed as

$$P_{d \text{ arc}} = C t_p^{-k} \quad (5)$$

where

$$C = 2.5$$

$$k = 2/3$$

t_p = pulse width in seconds

For a cathode that is uniformly utilized, equations (5) and (3) may be used to predict the current density capability at any pulse length, since

$$P_{d \text{ arc}} = C t_p^{-k} = J_{\text{arc}}^2 R_0 \quad (6)$$

and

$$J_{\text{arc}} = \frac{1.58 t_p^{-1/3}}{(R_0)^{1/2}} \quad (7)$$

If the R_0 value for the cathode is known, then the value of J_{arc} can be obtained immediately.

Figure 8 shows the emission current density limit for a 5948 thyratron, which was obtained in our millisecond modulator about a year prior to the data discussed so far. In this case, as the peak current was increased the time during the pulse at which the arc occurred was determined. At 0.9 millisecond, arcing was observed at 6 amperes per cm^2 , and for the arc to take place at 0.1 millisecond, the current density had to be increased to 12 amperes

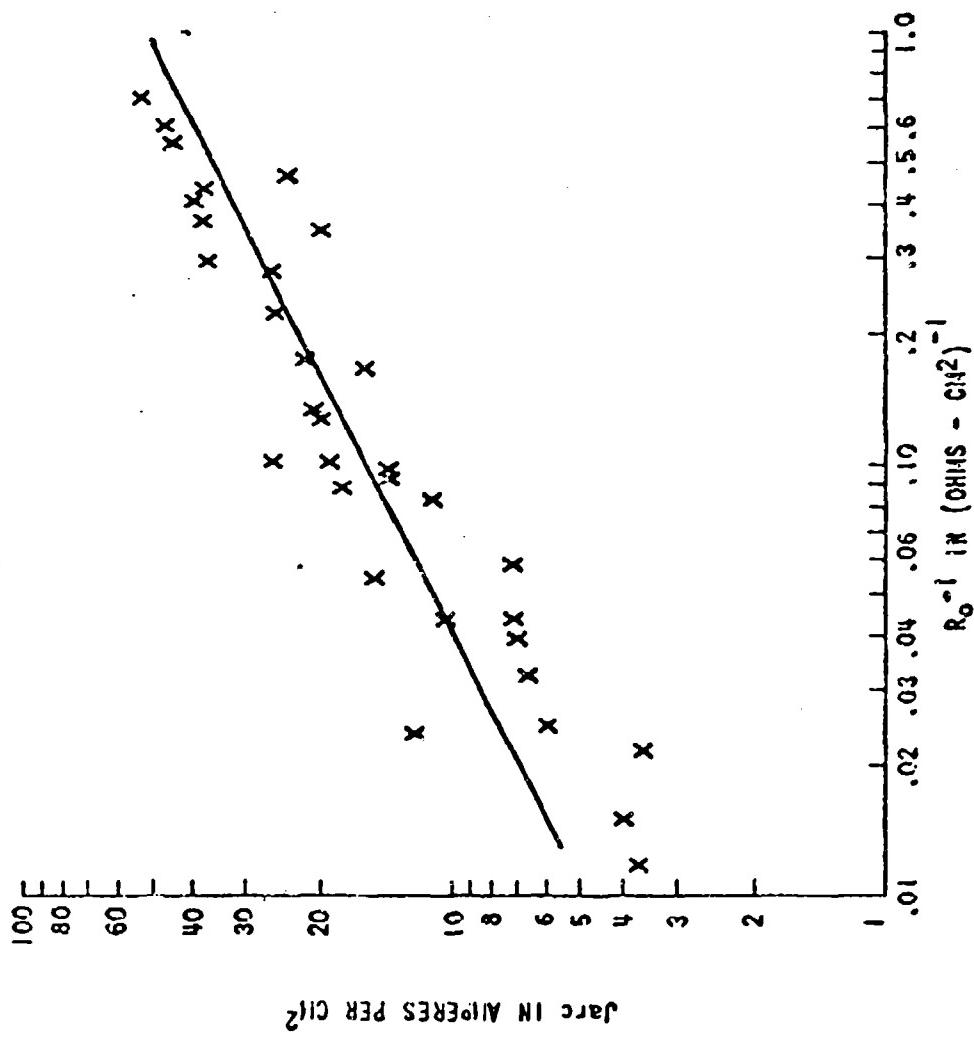


FIG. 5 CURRENT DENSITY FOR ARCING vs R_0^{-1} = 30 MICROSECOND PULSE

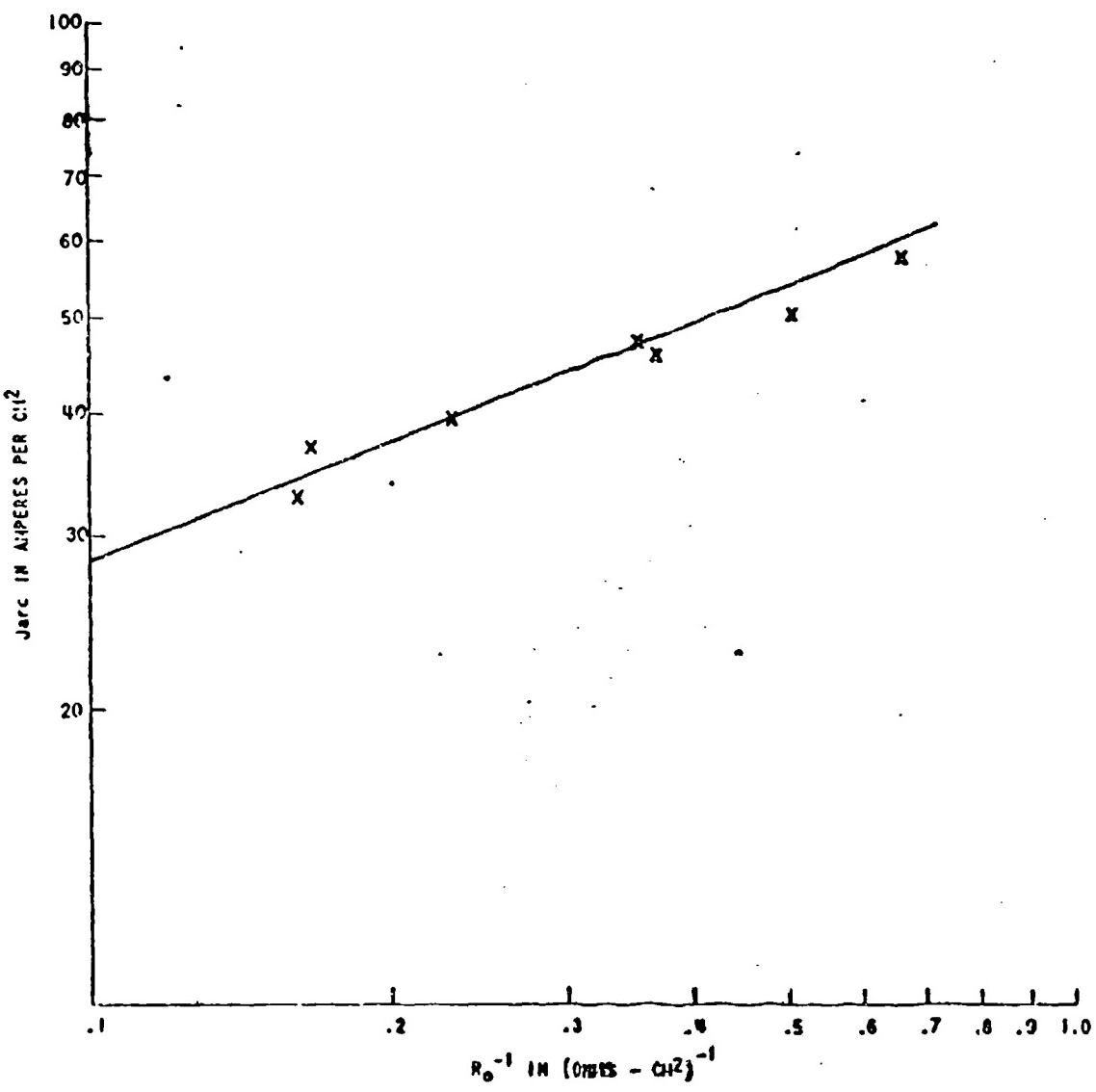


FIG. 6 CURRENT DENSITY FOR ARCING vs R_0^{-1} - 5 MICROSECOND PULSE

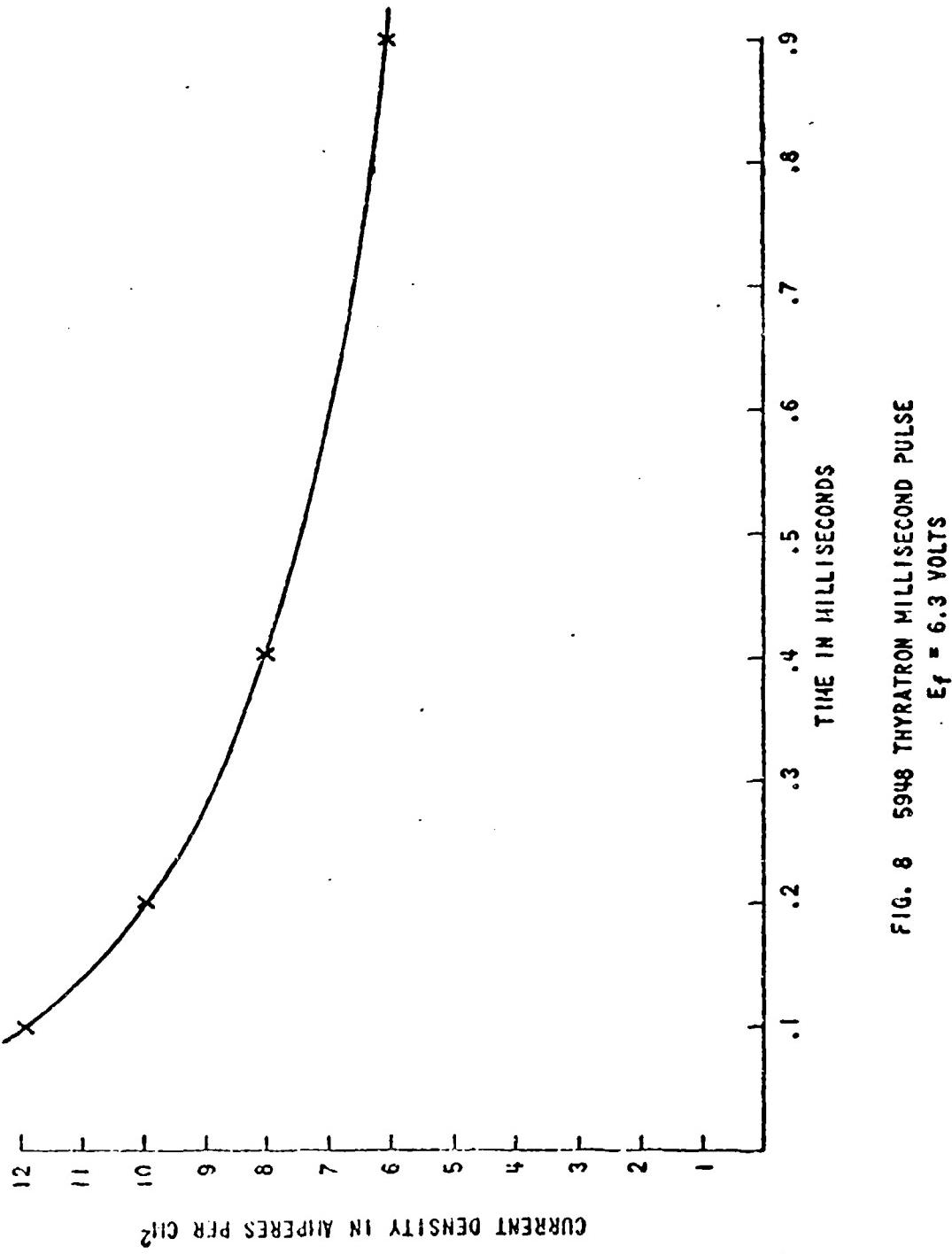


FIG. 8 5948 THYRATRON MILLISECOND PULSE
 $E_f = 6.3$ VOLTS

per cm^2 . This particular tube had a constant voltage drop during the pulse after the first 100 microseconds and for times greater than 100 microseconds the R_0 value was equal to 7.7 ohms - cm^2 . Using this value of R_0 in equation (4), P_d arc values were calculated for times of 0.1, 0.2, 0.4, and 0.9 millisecond. These values are plotted in Figure 9. The solid line is the P_d arc dependence given by equation (5).

In summary, the arcing limit of oxide-coated cathodes has been studied for several pulse lengths. The current density for arcing has been empirically related to R_0 , and it is found that a maximum power density dissipation factor is the limiting factor. The power density is related to pulse width, and it is shown that this dependence may be used to determine the maximum current capability of a cathode.

REFERENCE

1. "Research Studies for Cathode and Grid Elements for Superpower Switches," Fourth Quarterly Progress Report, Signal Corps Contract DA36-039 sc-85338, Edgerton, Germeshausen and Grier, Inc.

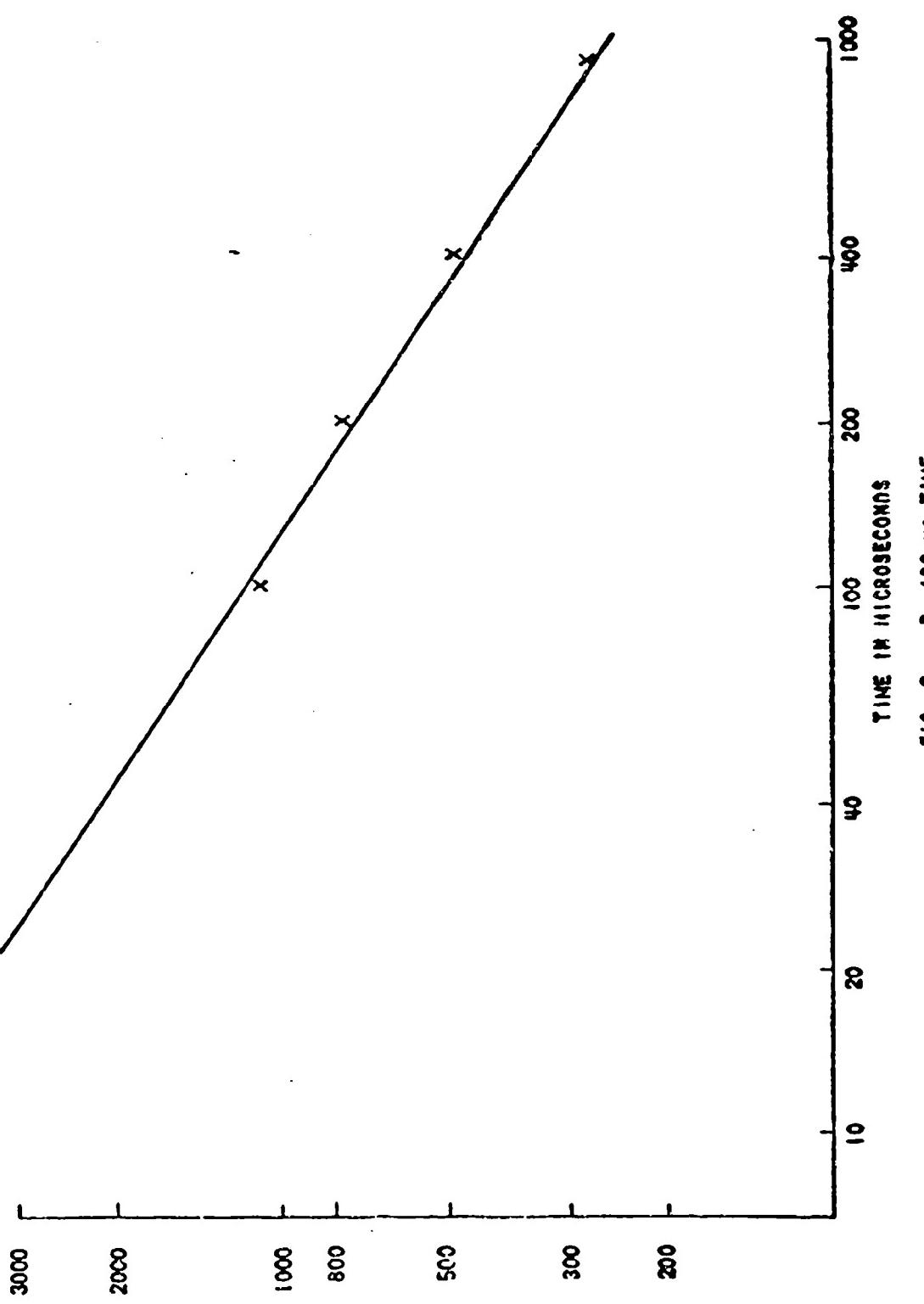


FIG. 9 P_d ARC vs TIME

HYDROGEN RESERVOIR MATERIALS

by

A. Huartson and H. Menown

English Electric Valve Company Limited

The property of sorption of hydrogen by the interstitial hydrides at different temperatures and pressures is used in gas-filled tubes when a reservoir of gas is required. As a result of work by Yeaman¹ we decided to find out what happened if the starting material were a finely divided hydride powder. In our experiments, measured quantities of hydrogen were removed in stages from a hydride powder of known mass. The pressure of hydrogen, produced by this depleted hydride for temperatures between 300°C and 700°C, was noted. At the same time a mathematical relationship which might help in the design of a reservoir was sought. Most of the work has been done on titanium hydride, some on zirconium hydride, and some on lanthanum and neodymium hydride powders of dubious purity. The average particle size of the lanthanum and neodymium hydrides was too large for them to be classed strictly as powders.

The reaction of hydrogen with titanium is mainly a surface effect, and so the amount of hydrogen available from a reservoir of "solid" metal is limited. In the case of powdered hydride, which is "saturated" with hydrogen, a greater reservoir of gas is available at a given temperature. It was therefore decided to use the powdered hydride as a starting material, and minimise sintering effects by making the time of its operation at higher temperatures as short as possible.

When using titanium and zirconium hydrides, a thin-walled palladium capsule fitted with a thermocouple was filled with a known amount of hydride powder, mounted on a stem, and sealed into a bulb whose volume was approximately the size of a CX1140 (1 litre). The bulb was then mounted on a vacuum system fitted with McLeod gauges for pressure measurement and vacuum taps for controlling and monitoring the flow of hydrogen gas. The data obtained was used to follow the metal-hydrogen reaction as the hydride was depleted of hydrogen.

It is known experimentally that when small amounts of hydrogen are taken up by a metal to form an interstitial compound at constant temperature, the concentration is proportional to the square root of the pressure. This may be written as

$$P = K'c^2 \quad (1)$$

where P is the pressure of hydrogen

molecules in the gas phase, C is the concentration of hydrogen atoms in the metal and K' is the equilibrium or solubility constant and is independent of C and P but dependent on temperature. Application of the van't Hoff equation² in this connection gives

$$-\frac{d(\ln K')}{dT} = \frac{Q}{RT^2} \quad (2)$$

Integrating gives

$$-\ln K' = -Q/RT + \text{a constant}$$

Thus

$$1/K' = \phi \cdot \exp(-Q/RT)$$

$$P/C^2 = \phi \cdot \exp(-Q/RT)$$

Therefore

$$P = \phi \cdot \exp(-Q/RT) \quad (3)$$

where ϕ is a molar entropy factor.

Fig. 1 shows the family of curves produced when the log of pressure is plotted against temperature in the form $1000/T$. These curves, and others for different weights of hydride (not shown), show that the change in slope of the lines is associated with a phase change from a single (alpha) phase to a mixed (alpha + beta) phase region. In the case of low loadings the slope of the $\ln P$ against $1/T$ curve is $-Q/R$. An evaluation of Q from the graphs in Fig. 1 gives a value in the alpha phase of $20,000\text{cal/mole}$, which is in agreement with values quoted by Mc Quillan³ and Barrer⁴. Substitution of our experimental data gives a value for ϕ of 6.0×10^3 which is of the same order as that given by McQuillan (9.616×10^3). The decrease in slope of the lines from high to low loading regions is due to a progressive reduction in the concentration of hydrogen in the titanium, which, by consideration of equation (3) above, will result in a decreasing value of Q. The values of the slopes agree substantially with those given by Yeamans, except that higher loadings were required to give the same slope. This may be due in some way to the physical state of the titanium. In other words, the difference may result from the use of finely divided powder as against a sintered matrix or macroscopic titanium particles.

Again applying the considerations of solubility in dilute solutions to the hydrogen-metal reaction

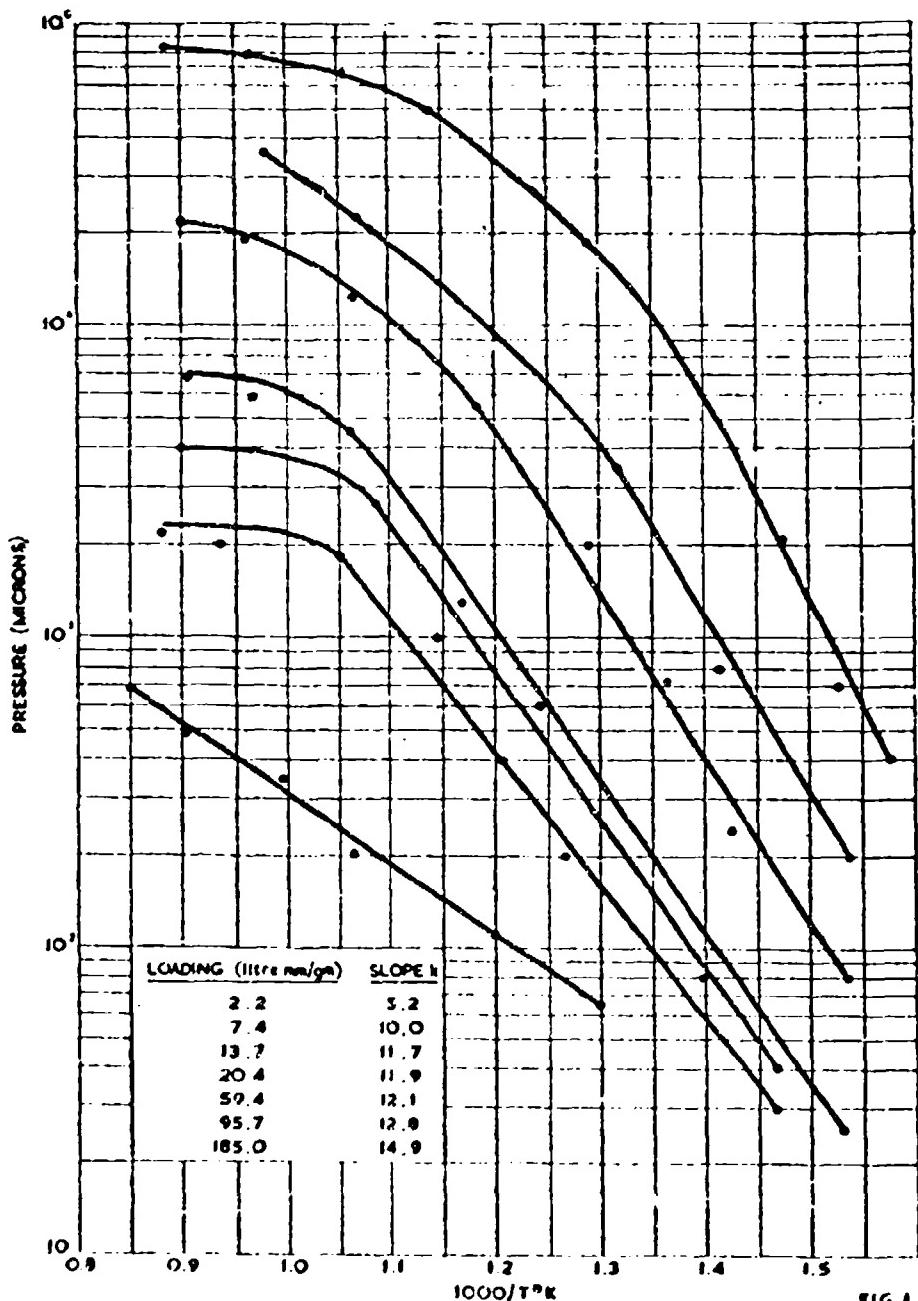
$$P^{1/2}/C = K$$

where K is a form of the equilibrium constant and is proportional to $(K')^{\frac{1}{2}}$, P the pressure and C the concentration by weight. If X is the weight of hydrogen in the gas phase, the number of moles = $X/2$, and it follows that

$$P = XKT/2V$$

since $PV = nRT$ where n is the number of moles of hydrogen.

TITANIUM HYDRIDE



If m grams is the total mass of hydrogen in M grams of metal, and loss of hydrogen to the gas phase is X grams, then

$$K = \frac{(XRT/2V)^{1/2}}{(m-X)/M}$$

Thus X is a function of M and m . This means that the amount of hydrogen in the gas phase and so the pressure can be computed for constant temperature, given K , a mass of titanium, the volume of a tube, the total amount of hydrogen available, and a temperature. We have therefore a mathematical relationship between the different parameters, temperature, pressure, volume and amount of hydrogen and titanium. Values of K have been calculated for temperatures between 450°C and 600°C. Fig. 2 shows the plot of $\ln K$ against $1000/T$ as a straight line. Substitution of values of K in the van't Hoff equation for different values of K and T give a value for Q of 18,400cal/mole, compared with the published value of 20,000cal/mole.

Fig. 3 shows values of dP/dT plotted against capsule loading. The values of dP/dT were computed from

$$dP/dT = 1000kP/T^2$$

and are presented for pressures from 100 microns to 600 microns. It will be seen that dP/dT is smallest in the low loading alpha region, and that although dP/dT is almost independent of loading in the mixed phase region where loading is very much higher, the value of dP/dT is such that operation in this region requires close control of reservoir heater voltage in high power high voltage tubes. One may deduce little of theoretical significance from this but it is obviously preferable to operate as low down the dP/dT curve as possible, taking into consideration reservoir capacity. Because dP/dT is proportional to pressure, and equation (3) shows that pressure is an inverse exponential function of the heat of solution, it is also obvious that the best reservoir material is that with the lowest heat of solution of hydrogen.

Other hydrides have been examined to find if they have any advantages over titanium hydride for reservoirs. Fig. 4 shows a family of curves obtained for zirconium hydride. These are similar in nature to those of Fig. 1. Here again similar considerations may be applied where the curves show the linearity associated with a single phase region. From the values of slopes in the alpha region the heat of solution Q has been computed as 36,000cal/mole which compares favourably with that of Sieverts at 35,000cal/mole. These values of slopes (Yeaman's k) are substantially in agreement with those of Yeaman's. The difference may be attributed to a known small percentage of hafnium in the zirconium. Furthermore, its limiting composition did not approach a "saturated" value of $ZrH_{1.9}$ but was around $ZrH_{0.6}$.

The work on lanthanum and neodymium hydrides could not be done in a palladium capsule because they react with palladium at temperatures above 500°C. The experiments were made using a sintered high alumina ceramic tube as a container.

Fig. 5 shows the plot of log pressure against $1000/T$ for lanthanum hydride. The slope (k) of the pressure temperature curve in the region of dilute solution is about 1.2 compared with 10 for titanium. Thus the use

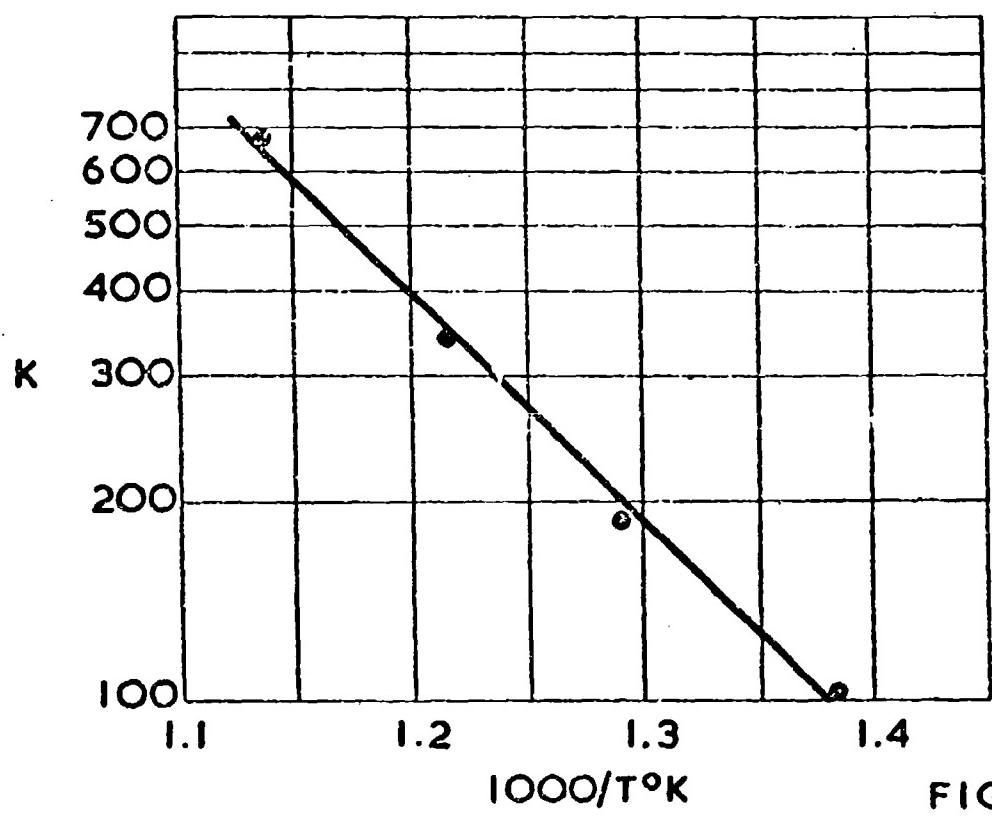
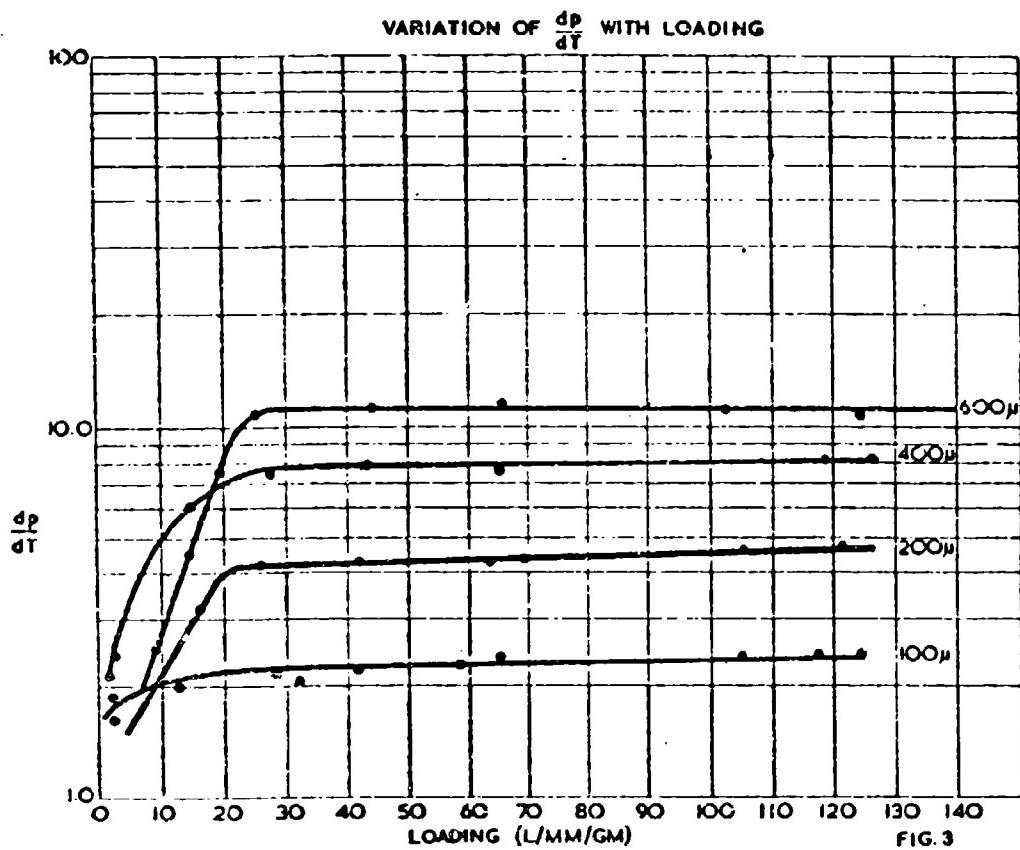


FIG. 2



ZIRCONIUM HYDRIDE

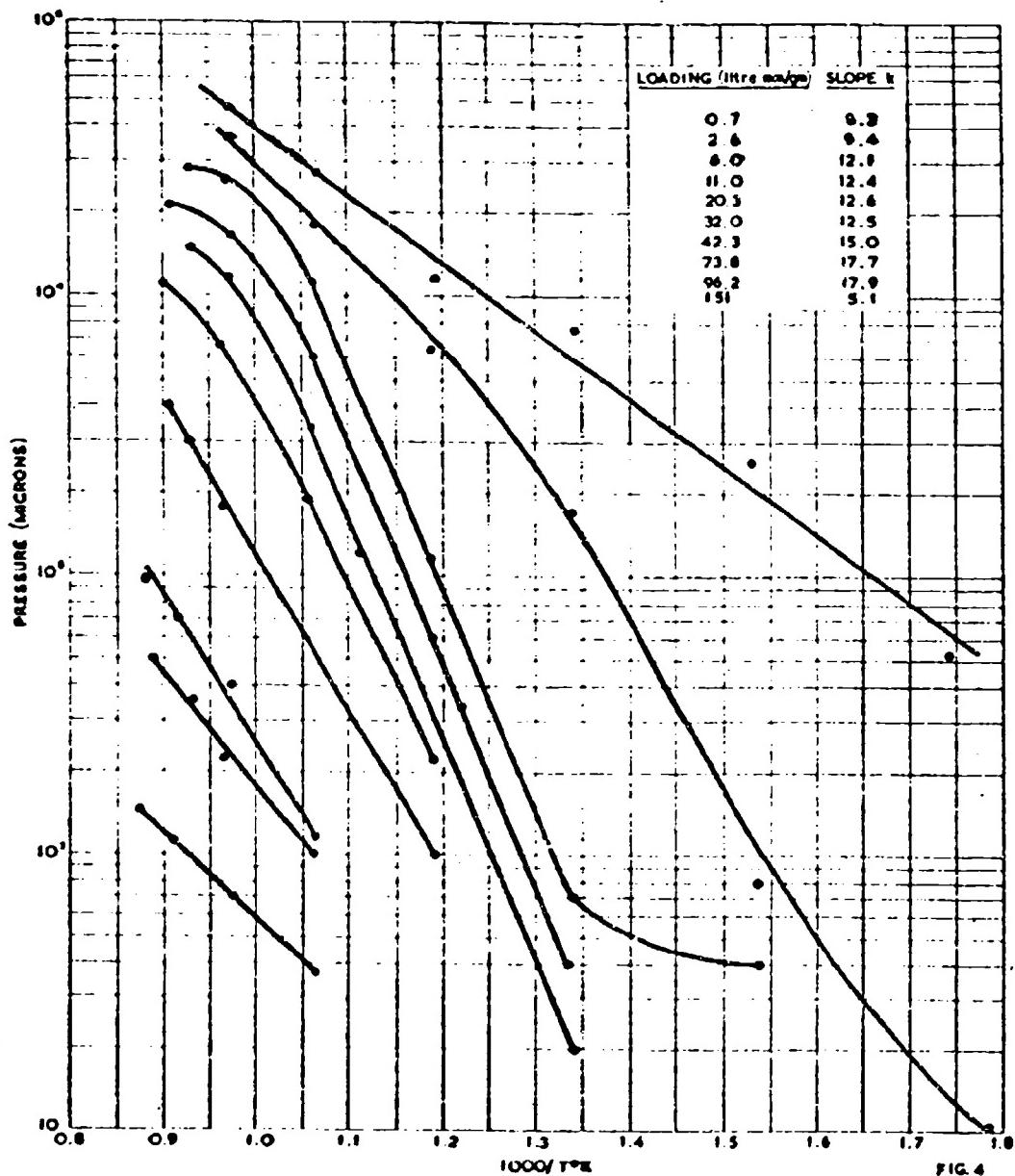
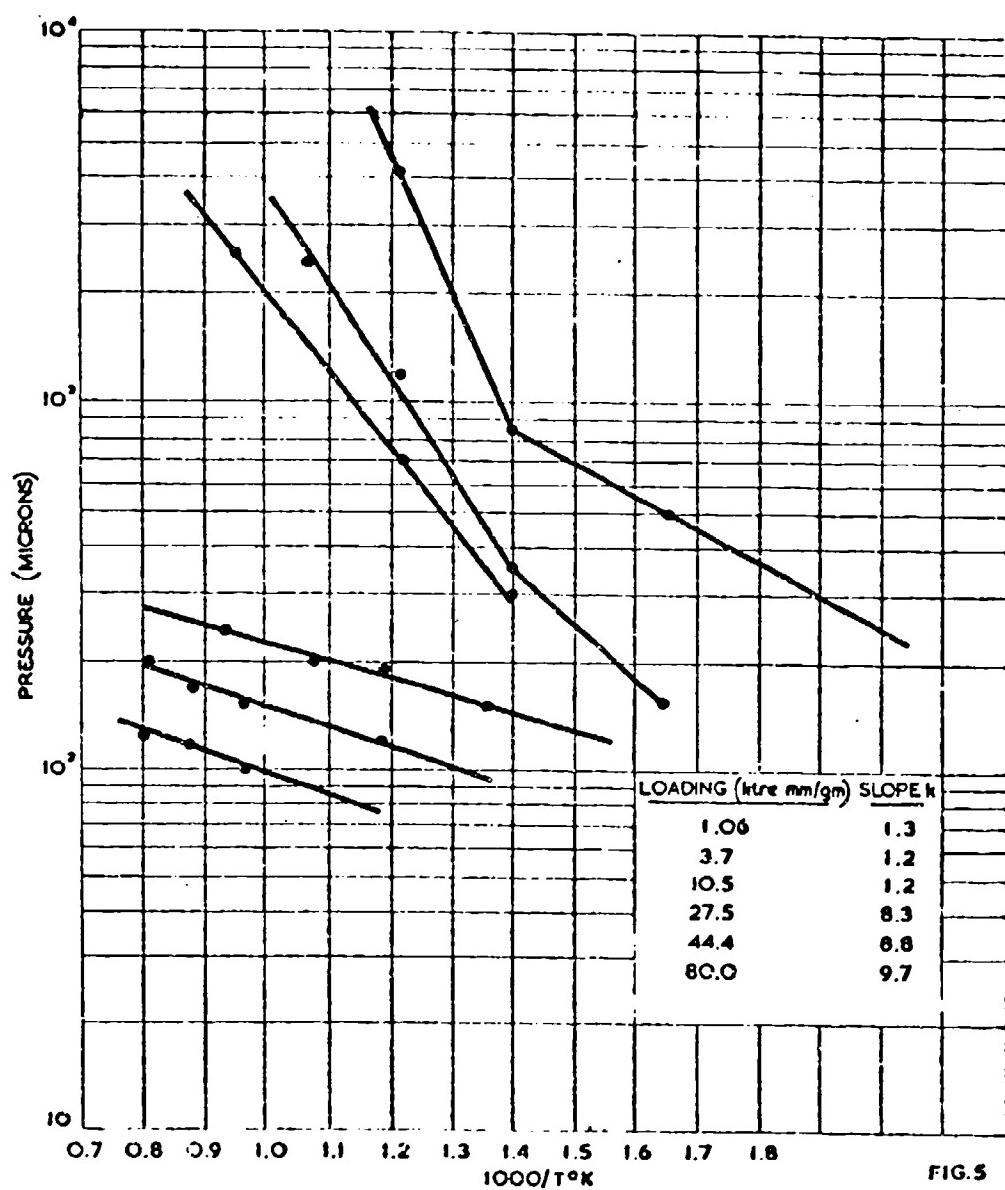


FIG. 4

LANTHANUM HYDRIDE



of Lanthanum hydride as a reservoir material has the advantage of a lower slope of the pressure-temperature curve in the region of dilute solution. This, coupled with a low value of dP/dT would be of some use at pressures around 100 microns. In the region of higher concentration it gives values of dP/dT close to those of titanium.

Fig. 6 shows a plot of log pressure against $1000/T$ for neodymium hydride. The slope (k) of the pressure temperature curve is about 8.0 in the low concentration region, as compared with values of 1.0 to 3.0 for lanthanum hydride.

A palladium capsule containing titanium hydride had its hydrogen removed with the capsule temperature kept below 700°C . Fig. 7 shows the effect of reloading this titanium with hydrogen, and the characteristic flattening of the pressure/loading curve at constant watts input. It will be noted that there is a temperature variation of approximately 100°C along the curve. There is also a marked increase in pressure above 100 litre-mm per gram. Fig. 8 shows that similar conditions apply in the case of zirconium. The loading curve for 20 watts input shows a marked deviation from that of Yeomans. In this connection, the possibility of contamination by oxygen was considered, but exhaustive tests did not produce hysteresis effects. In the case of the rare earth hydrides it was found that they would not reabsorb hydrogen above loadings of 10 litre-mm per gram. This was probably due to their reactivity under the experimental conditions.

We have produced three types of hydrogen thyratrons with reservoirs which consist of palladium tubes containing titanium hydride depleted of hydrogen (Fig. 9). These reservoirs are connected in series with the heaters and tube warm up time is 5 mins for a heater supply of 6.3V and a range of $\pm 5\%$. First is the CX1140, which is a plug-in replacement for 7384, is tested to 175 μ levels and has similar ratings. It is the highest power plug-in thyratron available anywhere. Next comes FX297, (a hydrogen inverse or clipper thyratron) with the same dimensions and connections as 5949. For the lower operating pressure requirements of the inverse thyratron, the reservoirs have been further depleted. A deuterium version of this thyratron has been made by substitution of deuterium for hydrogen in the exhausted capsule. Care is taken to avoid sintering of the titanium during exhaust. The CX1154 is a ceramic development from CX1140. This tube has a heater and reservoir current of 25A at 6.3V, a five minute warm up, and maximum hold off voltage of 30kV. One hydrogen filled tube has completed 1500 hours at 30kV epy, 600pps, 1200A, 6,750A/micro sec mean. The tube was working all this time with inverse voltage of 7.5kV produced by discharging a 30 ohm p.f.n. into a 20 ohm non-inductive load. There is some evidence that deuterium filling improves the performance of the tube for arc back, and later valves have been made using deuterium. One is now undergoing life test under the above conditions.

Acknowledgement

A large part of this work was done under Admiralty contract. Acknowledgement is made to Admiralty and the Managing Director, English Electric Valve Company Limited, for permission to publish this paper.

NEODYMIUM HYDRIDE

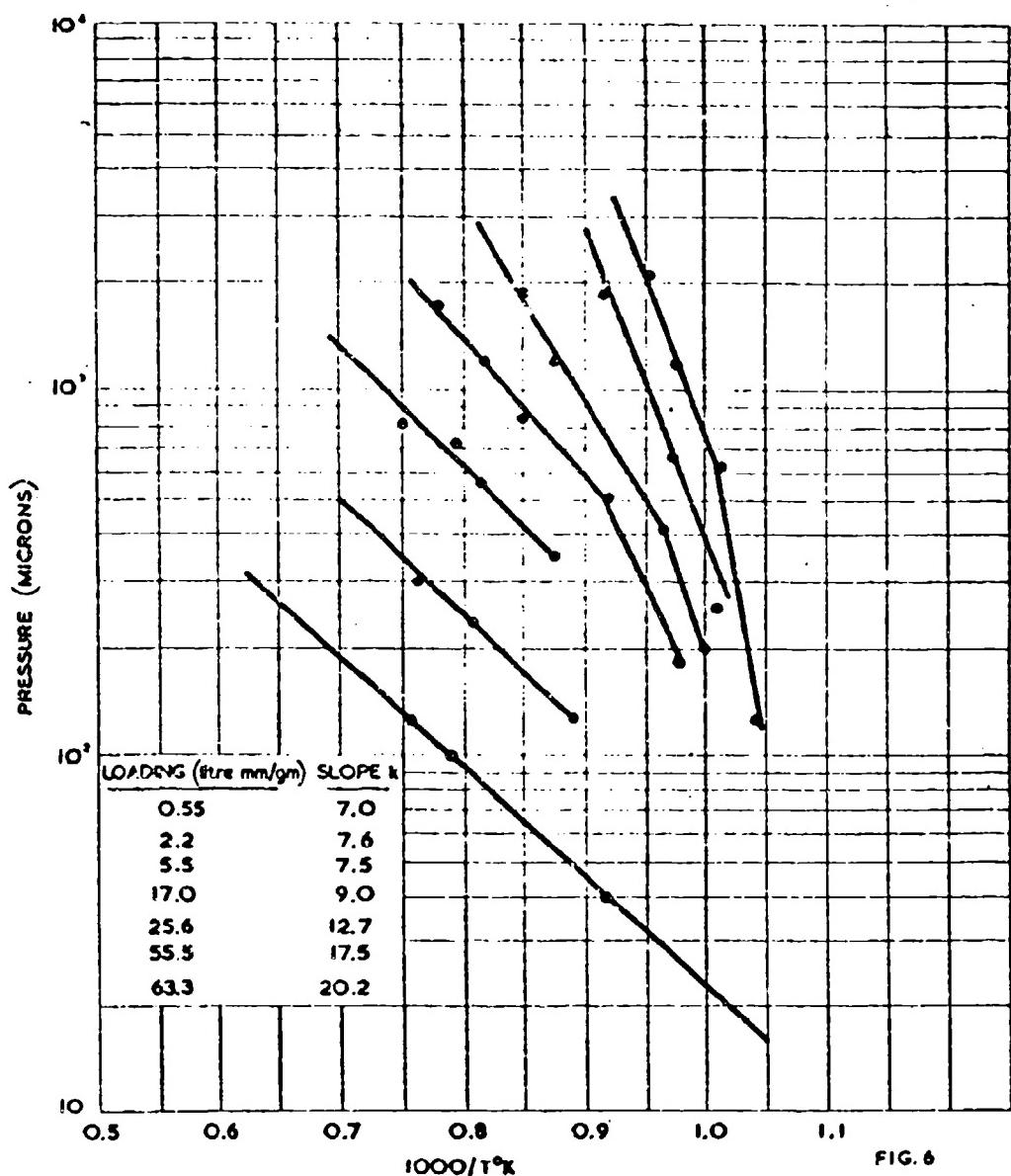


FIG. 6

EFFECT OF CAPSULE LOADING
ZIRCONIUM

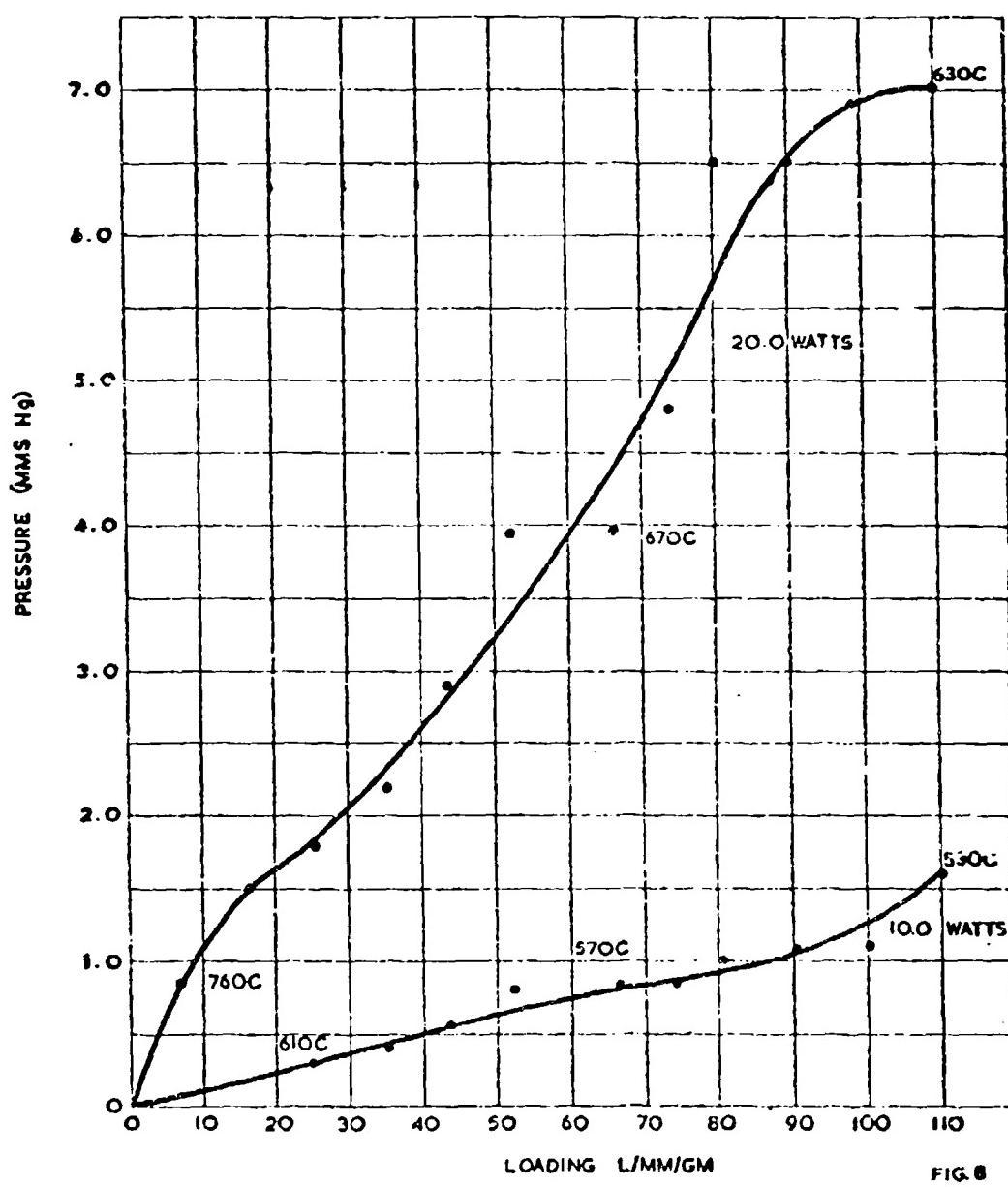
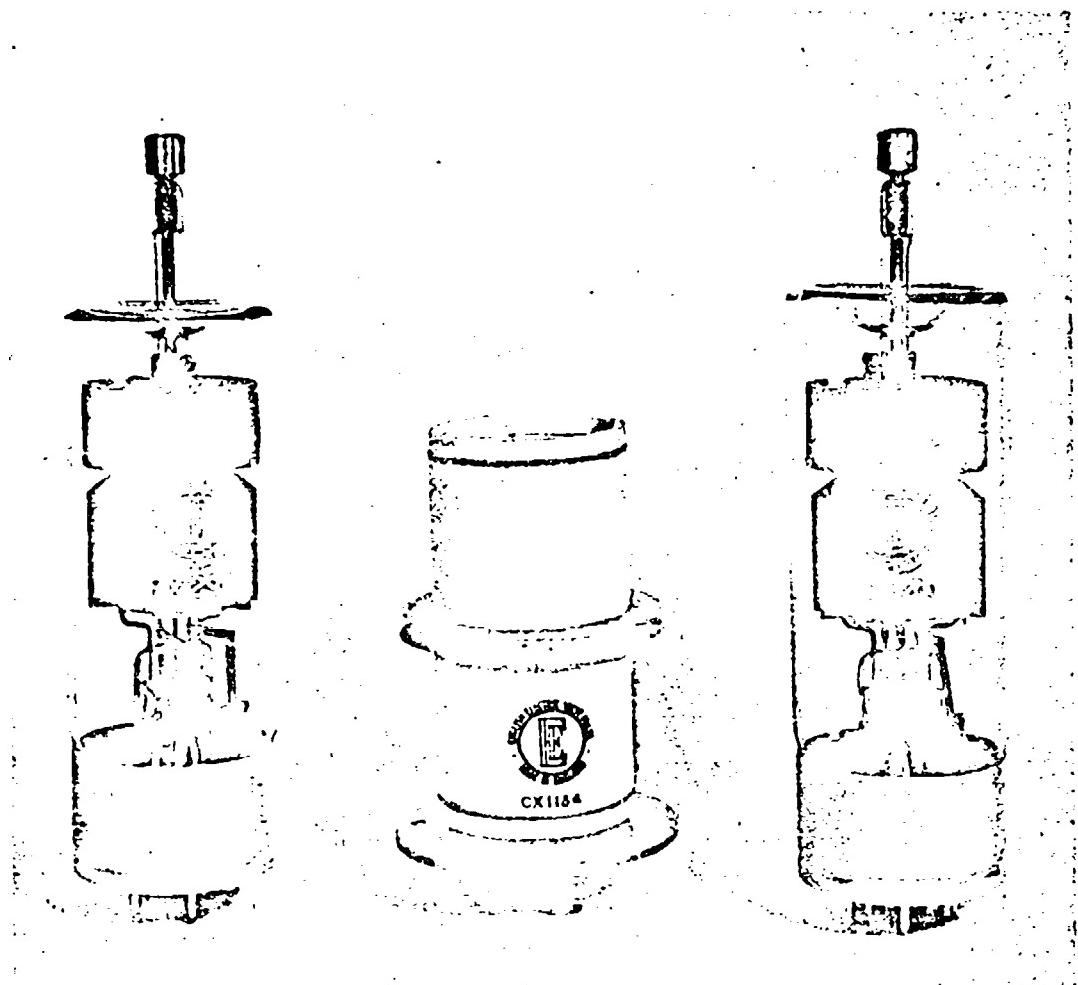


FIG. 6



References

1. Properties of Hydrogen Reservoir Materials. Teamans, Schneider and Creedon. Sixth Symposium on Hydrogen Thyratrons and Modulators May 1960.
2. Textbook of Physical Chemistry. Glasstone.
3. An experimental and Thermodynamic investigation of the hydrogen-titanium system. McQuillan A.D. Proc. Roy. Soc. A.204 (1950) 309.
4. Diffusion in and through solids. Barrer. Camb. Univ. Press.

A COMPACT METAL-CERAMIC DEUTERIUM THYRATRON

by

K. G. Cook, B.Sc.(Eng.) and R. J. Wheldon, B.Sc.

The General Electric Company Limited,
Central Research Laboratories, Hirst Research Centre,
Wembley, England.

1. INTRODUCTION

At the Sixth Symposium a paper¹ was presented comparing the metal envelope and ceramic envelope types of thyatron shown in Figure 1. The advantages of the metal valve are as follows:-

- (a) The grid, in which 50% of the valve dissipation may occur, can be more readily cooled, thus preventing grid emission and reduction of gas density in the grid slots.
- (b) The grid-anode insulator is situated behind the anode and cannot become coated with sputtered material.

These considerations lead to the development of a large water cooled valve type VX3336, shown in Figure 2, which is rated at 200Mw peak power and 150kw mean power. The present paper describes the development of a compact metal envelope valve, type VI3351, which is similar in rating to the 1257.

2. VX3351 RATING

Figure 3 shows a photograph and Figure 4 a sectional drawing of the VX3351. The target ratings of this valve are as follows:-

Peak Anode Voltage 40kv, Peak Anode Current 2000A, Cathode Heater Voltage 6.3v, Cathode Heater Current 15A, Reservoir Heater Voltage $6.3 \pm 10\%$, Reservoir Heater Current 2A, Warm up time 5 minutes, Mean Anode Current (a) as a rectifier $3\frac{1}{2}$ A (b) as modulator or clipper diode $2\frac{1}{2}$ A, Peak Rate of Rise of Anode Current $7500A/\mu sec$. The valve is air cooled, overall length 10", body diameter $2\frac{1}{2}$ ".

3. VX3351 DESIGN

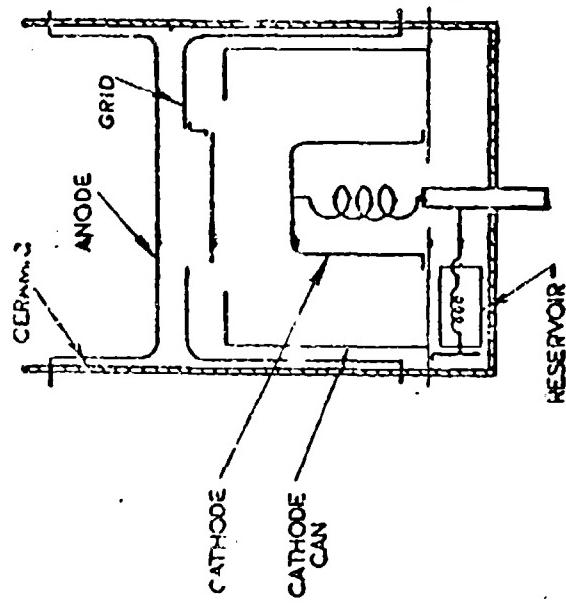
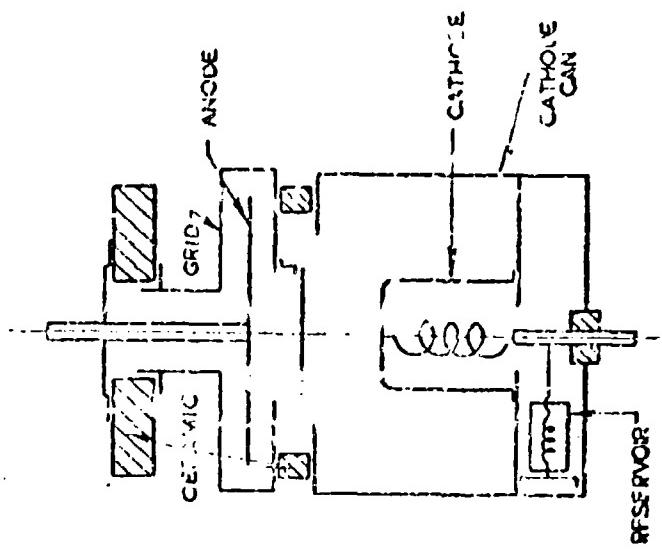
3.1. Anode

It is desirable to use ceramic seals in a metal envelope valve for

FIG. 1.
METAL AND CERAMIC THYRATRONS

(a) METAL ENVELOPE
THYRATRON

(b) CERAMIC ENVELOPE
THYRATRON



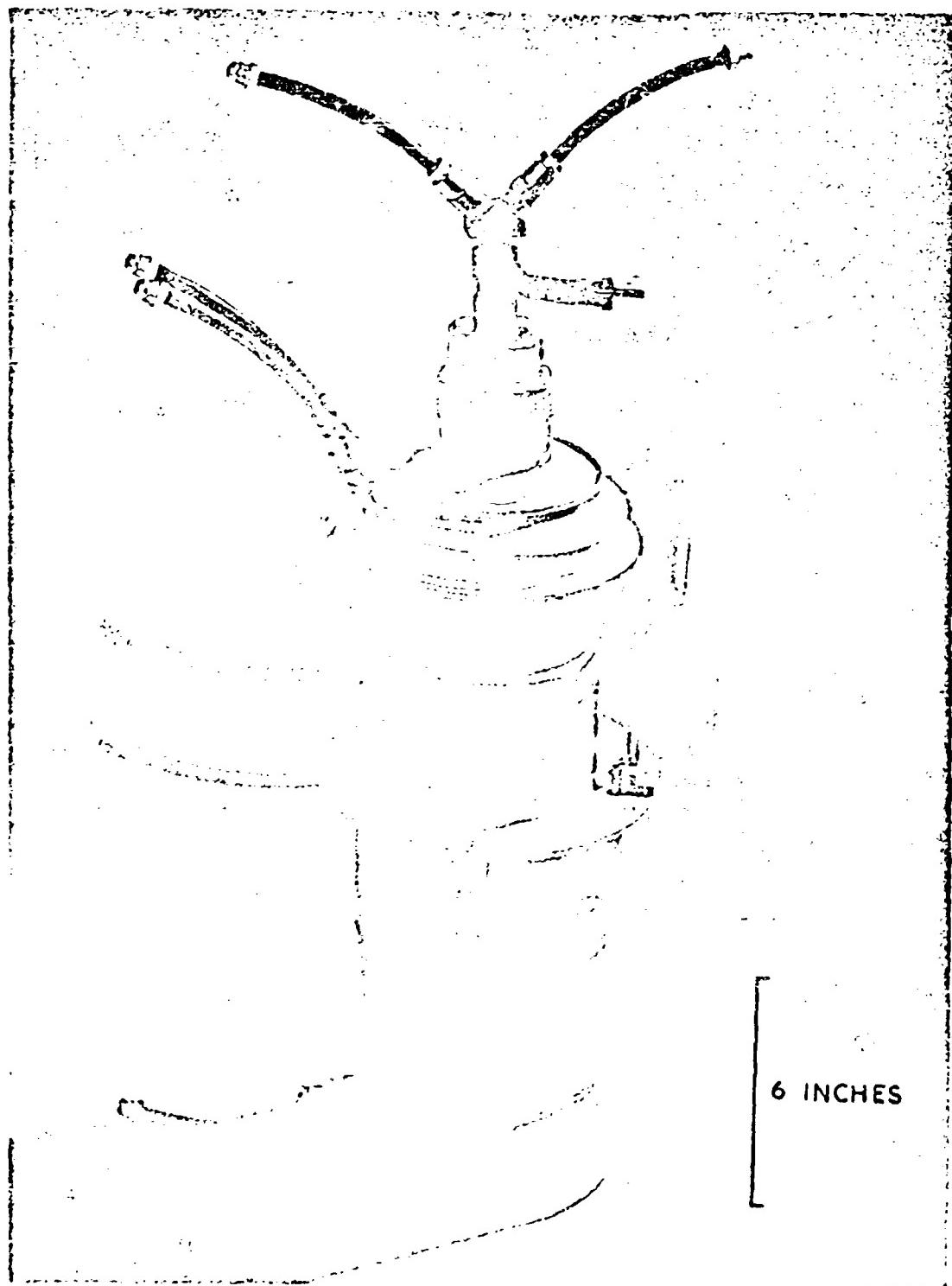


Fig. 2. V63336 Thyratron

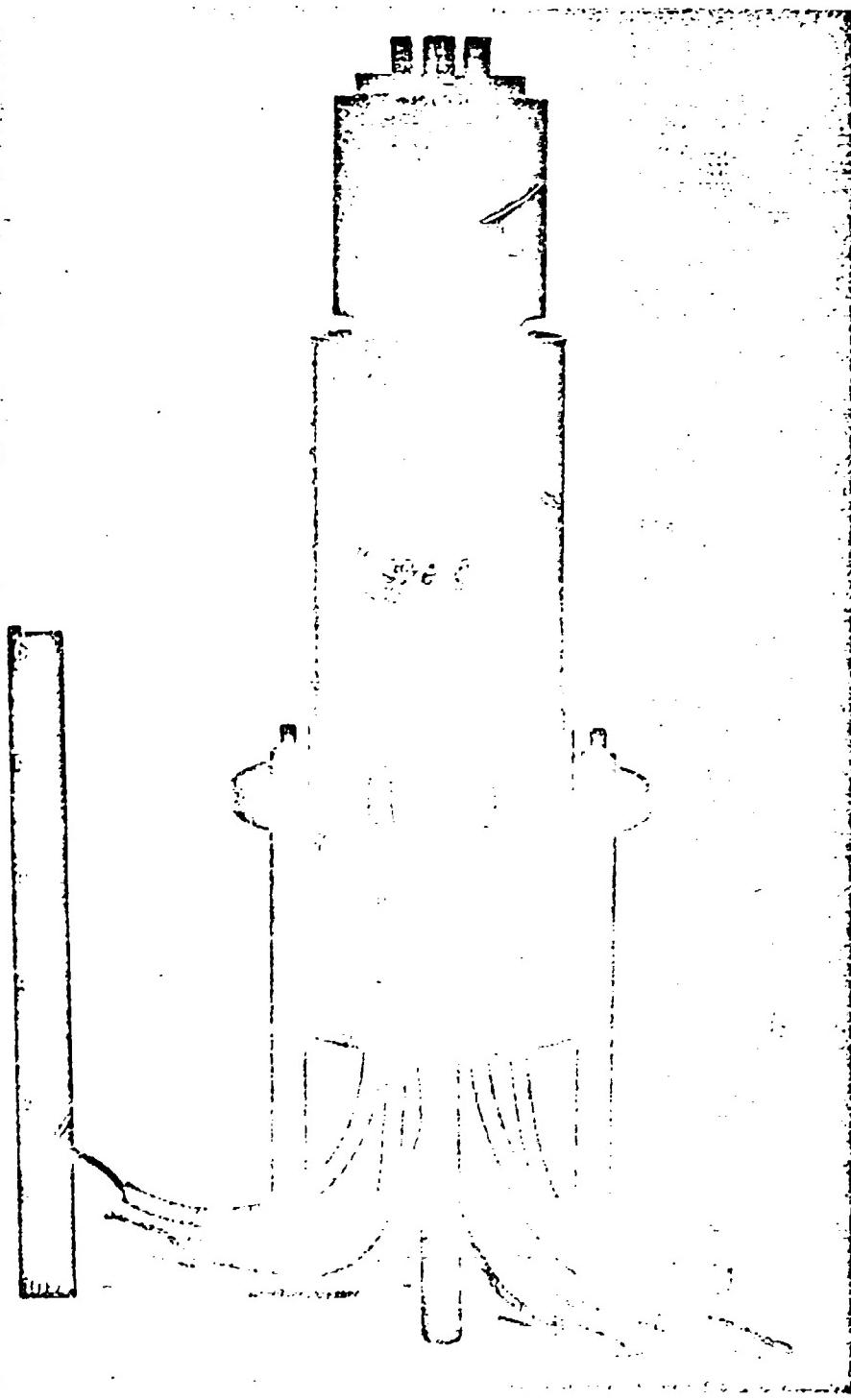
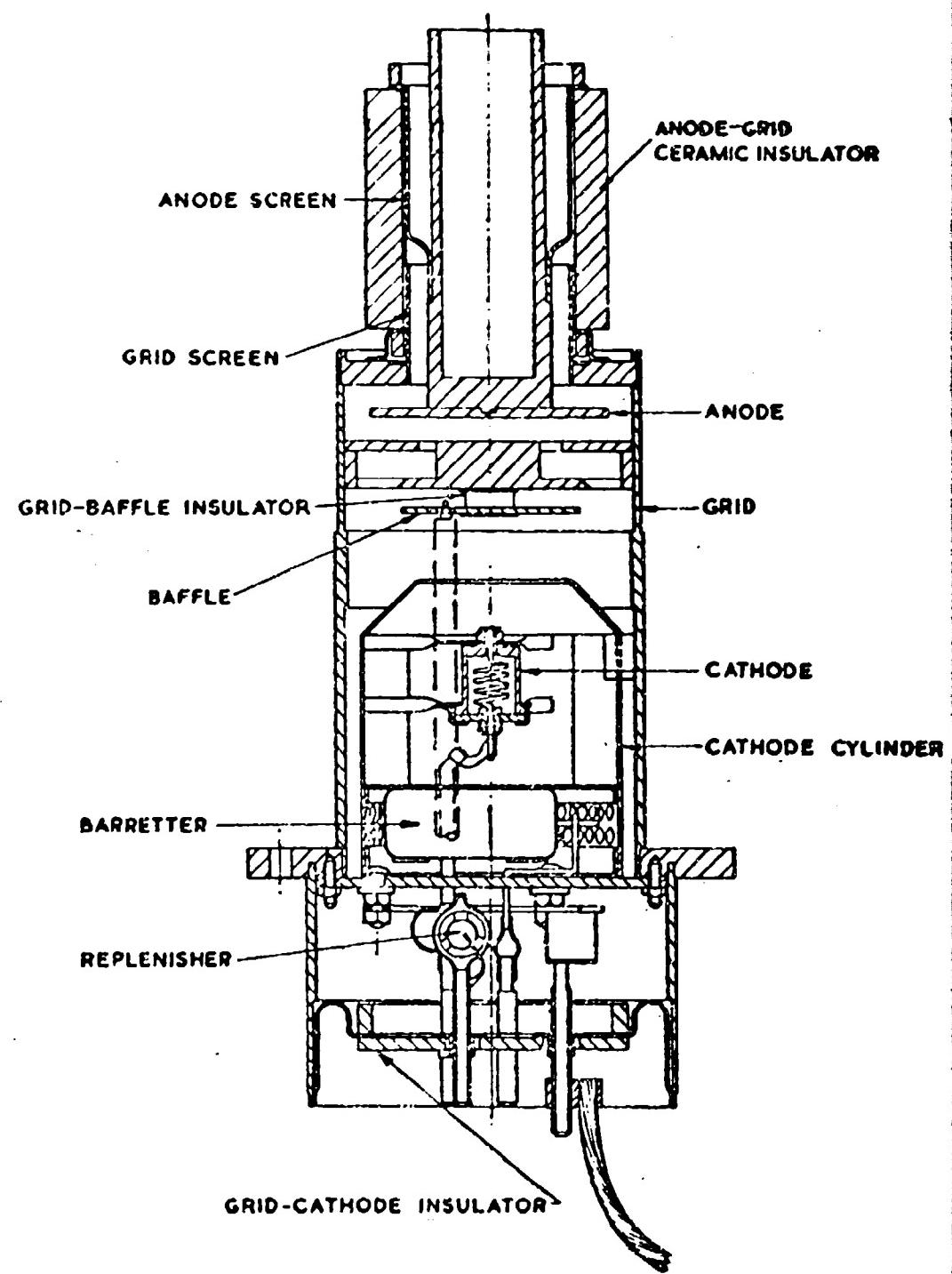


Fig. 3. VX3351 Thyratron

FIG. 4
SECTIONAL DRAWING OF VX3351



two reasons: firstly, the metal components cannot be outgassed by normal eddy current heating techniques, and therefore it is necessary to bake up to 700°C during manufacture; secondly, ceramic seals are more rugged than those in glass.

The design of a high voltage anode seal involves three main requirements: (a) the lengths of the lines of force between anode and grid through the gas should be short, to prevent Paschen breakdown, (b) the anode-grid spacing should not be so small that field emission can occur, (c) there should be adequate external spacing between anode and grid, to prevent breakdown in air.

The ceramic anode seal shown in Figure 4 incorporates these features. The anode is enclosed by the grid, the mean anode grid spacing being 5 mm, enabling a maximum Paschen breakdown voltage of greater than 40kv to be achieved at about 0.3 torr deuterium pressure. The lines of force between anode and grid lengthen in the region of the anode and grid screens, but Paschen breakdown is prevented in this region by virtue of the close clearance ($\frac{1}{2}$ mm) between the ceramic and the screens.

The basic principle of the seal is not unlike that used in the ceramic envelope design of valve. The metal valve has an advantage, however, since the ceramic insulator is situated behind the anode where it is unlikely to become coated by material sputtered from the electrodes by the discharge.

Deuterium has been used in place of hydrogen because its higher Paschen breakdown potential enables 40kv anode voltage to be achieved at a gas pressure sufficiently great to support a high current discharge.

3.2. Grid

Dissipation studies have shown that a large fraction of the steady state and trailing edge dissipation in a modulator valve can occur at the grid. At normal gas pressure the grid dissipation usually exceeds that at the anode. Failure to cool the grid adequately can result in gas density reduction in the region of the grid slots, leading to reduced rate of rise of current, and in grid emission.

The metal valve offers the most efficient means for cooling the grid, since the active part of the electrode is joined directly to the envelope, which may be air or conduction cooled.

The precise form of the grid and the grid slots depends upon the application. For the modulator and clipper diode it is desirable to use a molybdenum electrode, to prevent sputtering. In the rectifier valve a copper electrode is satisfactory.

In the modulator valve a closely baffled structure is required to achieve a short recovery time. In the clipper diode and controlled rectifier, where recovery time is unimportant, it is desirable to reduce the arc losses in the grid and to reduce the trigger current. A more open grid structure is therefore used.

The baffle, which is separately triggered, shields the grid from emissive material evaporated from the cathode, and hence helps to prevent grid emission. The baffle also serves to direct the electrons in the grid-cathode triggering discharge into the region of the grid slots where anode field penetration is greatest. As a result the grid current required to initiate anode conduction is reduced.

3.3. Cathode

The cathode is an indirectly heated impregnated tungsten emitter, surrounded by a finned metal cylinder. In operation the cylinder becomes coated by emissive material evaporated from the impregnated tungsten, and can contribute a large fraction of the total emission.

A cathode of this type was described at the previous symposium¹. The mechanism of the emission from the cylinder is still imperfectly understood, but certain practical results have now been established. The emission is a function of pulse length. For pulse durations of the order of 5 μ sec the cylinder temperature need not exceed 350°C; the emission is only present if a discharge is being drawn from the impregnated tungsten cathode. With pulse lengths of the order of 1 millisecond, satisfactory emission is only achieved if the cylinder temperature exceeds 550°C.

The VX3351 cathode consumes 100 watts and reaches emitting temperature in less than 5 minutes. At 2000A peak current and 5 μ sec pulse length the cylinder contributes over 95% of the pulse current. In rectifier applications the major part of the emission is drawn from the impregnated tungsten, since the cylinder temperature does not exceed 350°C.

3.4. Reservoir

The indirectly heated titanium hydride replenisher is controlled by a barretter and permits a supply voltage variation of $\pm 10\%$. The barretter is situated inside the envelope of the valve; thus any back heating from the discharge produces a drop in barretter current which compensates for the effect of back heating on the replenisher.

4. FUTURE DEVELOPMENTS

The successful development of the VX3336 and VX3351 thyratrons has shown that the metal envelope has many desirable features. It is now

proposed to extend the range by developing a valve about 4" in diameter which would be suitable for about 100kw mean power, and a smaller 6kw mean power valve.

ACKNOWLEDGEMENT

The authors are indebted to the Admiralty for permission to publish this paper.

REFERENCE

1. K. G. Cook. A High Power Metal Envelope Deuterium Thyratron. Sixth Symposium on Hydrogen Thyratrons and Modulators, 1960.

PROGRESS REPORT ON PHASE II SUPERPOWER THYRATRON

by

A. W. Coolidge, Jr.

General Electric Company

At the last symposium a brief report was submitted on the status of the Phase II hydrogen thyratron (Z-5212) being developed under Signal Corps contract No. DA 36-039 sc-7485C. Objective ratings are given in Table I.

Table I - Objective Ratings - Phase II Hydrogen Thyratron

Peak Forward Voltage (A) (kilovolts)	50
Peak Anode Current (B) (amperes)	2000
Pulse Repetition Rate (C) (pulses per second)	4000
Average Current (amperes direct current)	8.0
Anode Dissipation Factor ($A \times B \times C \times 10^{-9}$)	400

At the time of that report consistent operation had been achieved to 25 KV at a repetition rate of 4,000 PPS in a tube design depicted in Figure 1. Because this same tube would perform to the full 50KV anode voltage when the resonant charging and actual repetition rates were reduced to 500 PPS the importance of reducing the recovery time was indicated.

In the intervening two years the major effort has been expended on the problem areas involving recovery time, and electrode dissipations at the anode and gradient grid.

RECOVERY TIME

The approach to the recovery time problem was made by modifying the tube design so that large interelectrode spacings would be eliminated. As a form of insurance a charging triode circuit was developed which could be integrated with the test equipment to provide an increased period for tube recovery after each pulse.

Electrode Spacings

Perhaps the most effective way to minimize the recovery time would be to keep all interelectrode spacings to a low value of one-eighth inch. In the grid-anode region this would present no novelty as all hydrogen thyratrons have evolved with such spacings because of Paschen Law considerations. In the grid-cathode region, however, such a small spacing would represent a vast departure from tradition.

A flat disc cathode having an area equivalent to that of the vane cathode already designed would be more than a foot in diameter. Holding the grid-cathode spacing constant at one-eighth inch over such a large span would be difficult mechanically. In addition, barium deposition on the grid would be excessive and the prospect of even utilization of the cathode and grid would be poor.

Accordingly, a compromise was effected resulting in the design depicted in Figure 2 wherein the vane cathode is retained but the cathode is mounted higher and the grid lower so that their minimum separation is about one-quarter inch.

Equipment Modification

The equipment change was accomplished in such a way that it is a simple matter to change from one type of charging (diode) to the other (triode). The triode charging circuit was constructed in a portable cabinet and contained the following of the units shown in Figure 3:

- a) charging reactor
- b) charging triodes
- c) trigger amplifier and driver
- d) trigger generator
- e) variable delay.

After some operating experience was obtained with the triode charging circuit clipping and damping components were added to reduce spurious voltage swings across the charging triodes. More recently a Z-5212 has been substituted for the two GL-7390's in the charging triode position.

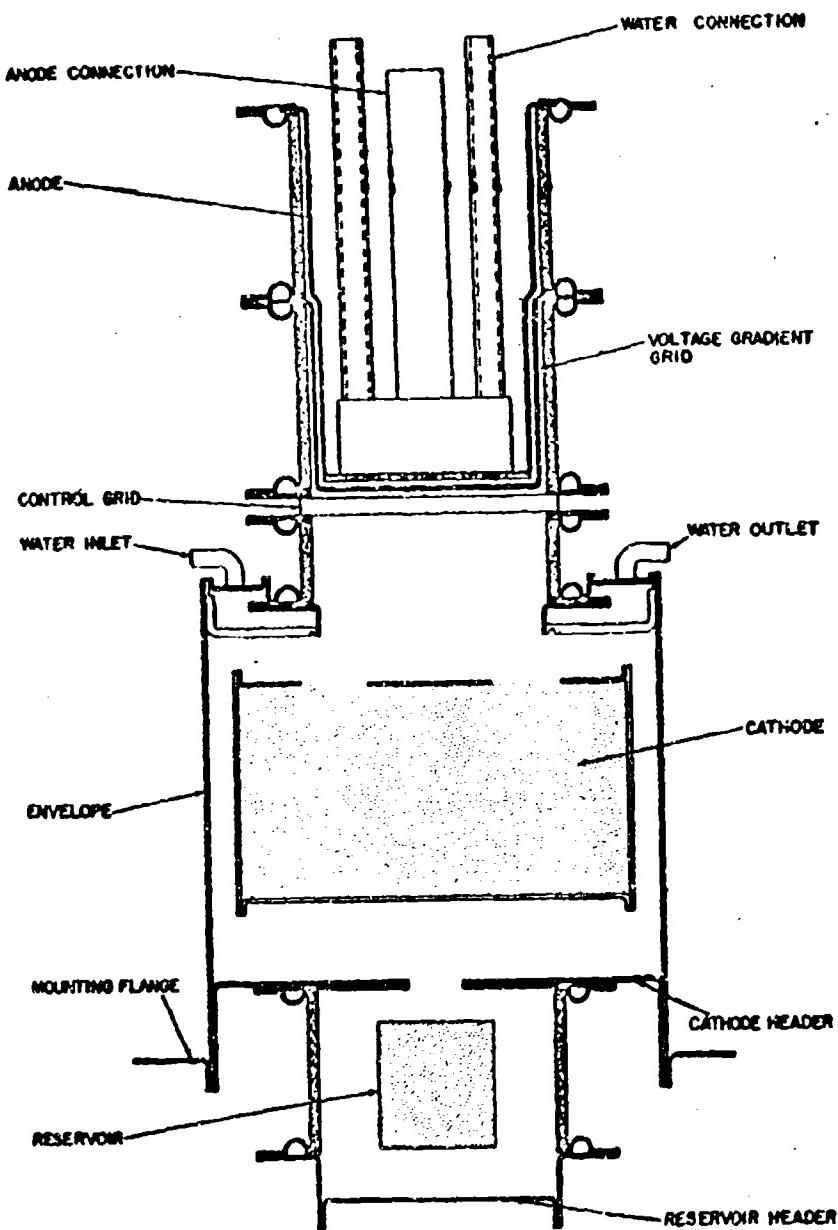


Figure 1 - Superpower Thyratron, G-E Developmental Type Z-5212,
Proposed Design Q

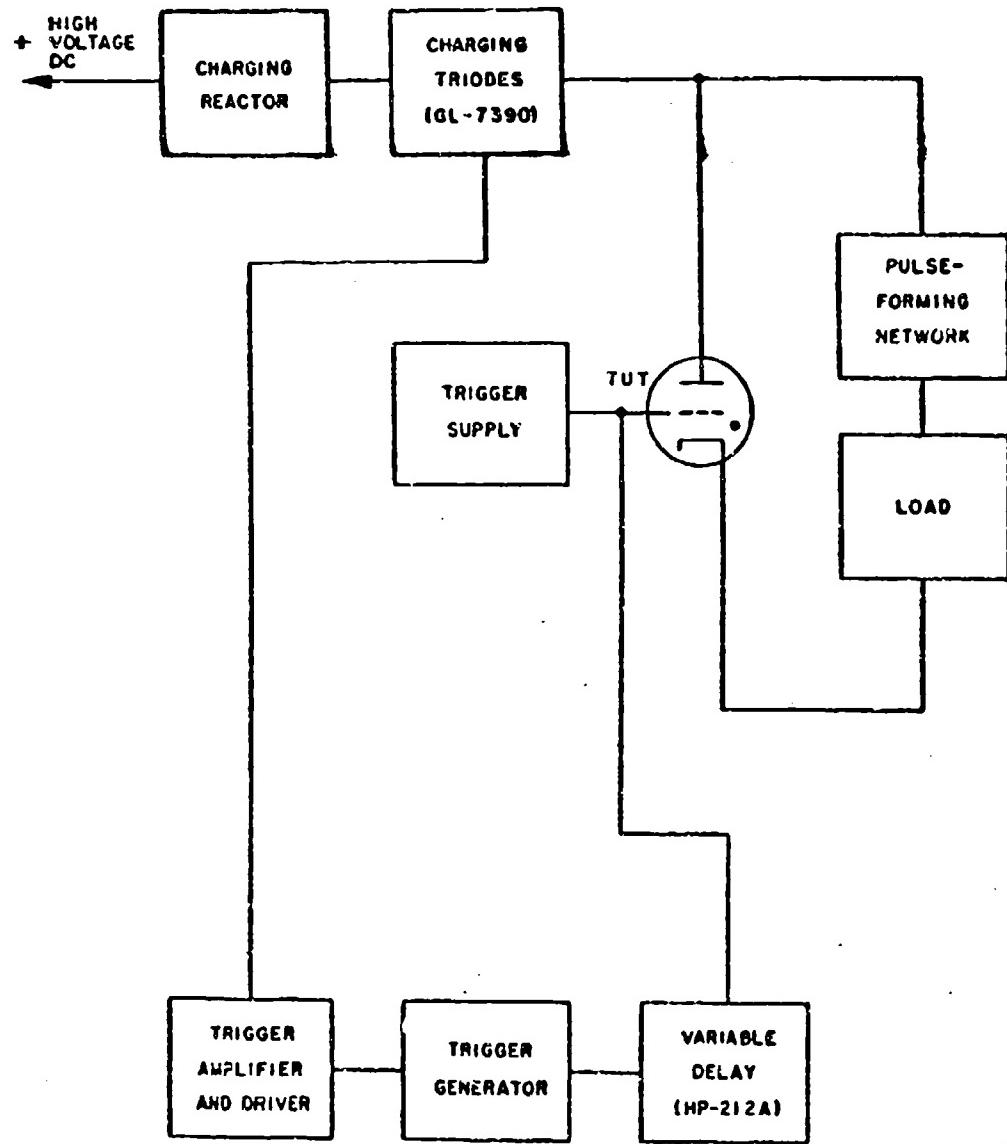


Figure 3 - Block Diagram of Triode Charging System for Phase II Test Set

As matters have turned out it may not be necessary to resort to triode charging for successful high repetition rate operation. It is handy, however, in case subsequent results prove the above to be optimistic. Because of its built-in variable delay feature, it has been used on a number of occasions for determining actual recovery time data.

Test Results on Modified Tube Design

The benefit of reducing grid to cathode spacing was affirmed when test results on the first tube with such a modification, No. 9, indicated that operation at 4,000 repetition rate was stable to a maximum anode voltage of 35 KV. This represented an increase of 10 KV over earlier tubes with large grid cathode spacings. Four new bits of information indicated that at least one limitation other than recovery time prevented No. 9 from reaching full power operation.

- 1) Intermittent inverse voltage clipping accompanied by intermittent inverse current (Figure 4) was observed near the ceiling power of the tube.
- 2) Highest voltage performance was reached with a matched load of 12 ohms (Figure 5) where the time available for recovery would be the least.
- 3) Excessive gradient grid emission was sometimes observed.
- 4) When tube No. 9 was finally opened, severe distortion of the gradient-grid bars was evident, Figure 6.

Attention was focused on heat dissipations at the anode and gradient grid.

ELECTRODE DISSIPATIONS

Anode

Calorimetry measurements indicated that only a few kilowatts of average power dissipation were removed by the cooling water, but it is well understood that transiently at the front part of the current pulse the instantaneous power dissipated at the anode may reach a relatively high value. Figure 7 displays a typical transient dissipation curve where the maximum power is reached about 0.1 microsecond after the start of the discharge. This data was obtained on a GL-7890 operating under Phase I, Operation II conditions where the anode voltage was 30 KV and the peak current was 1,000 amperes. It can be conservatively estimated for Phase II conditions (50 KV and 2,000 amperes) that the peak power dissipation would be more than twice that shown in Figure 7 or nearly 20 megawatts while the width of

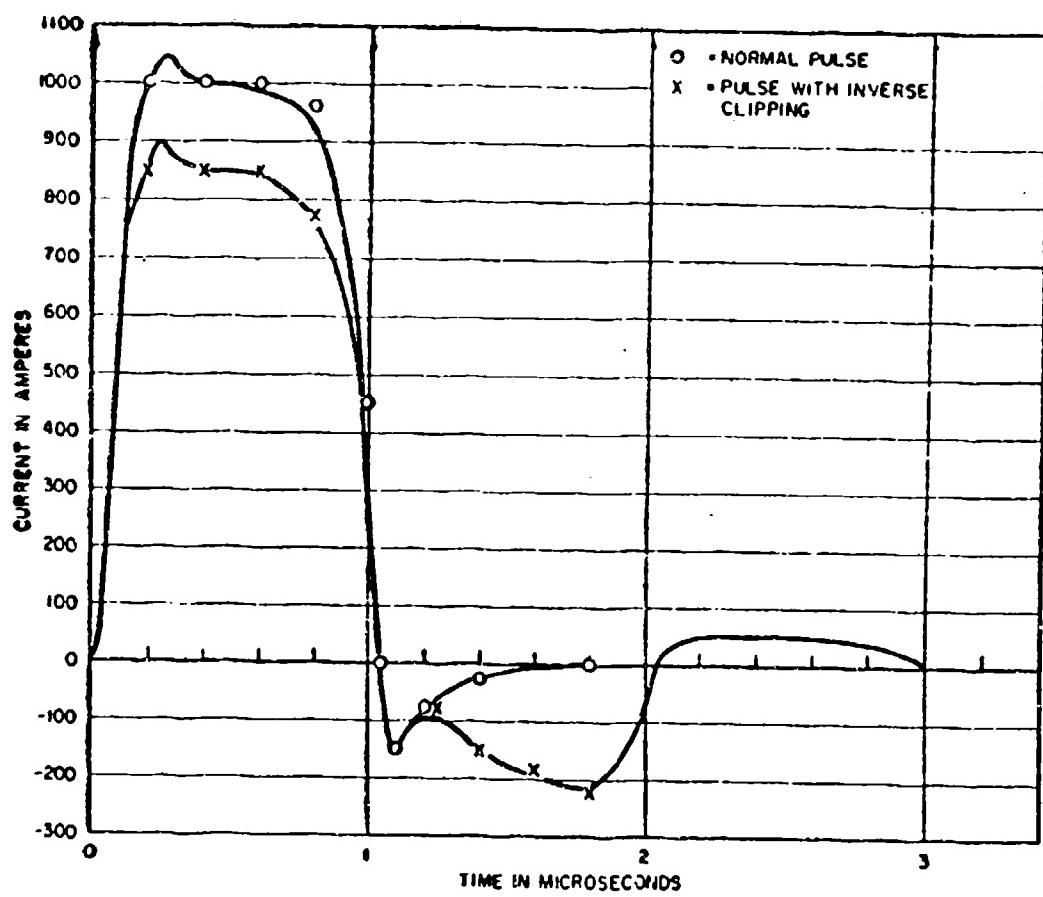


Figure 4 - Approximate Current Wave Shapes With and Without Inverse Clipping

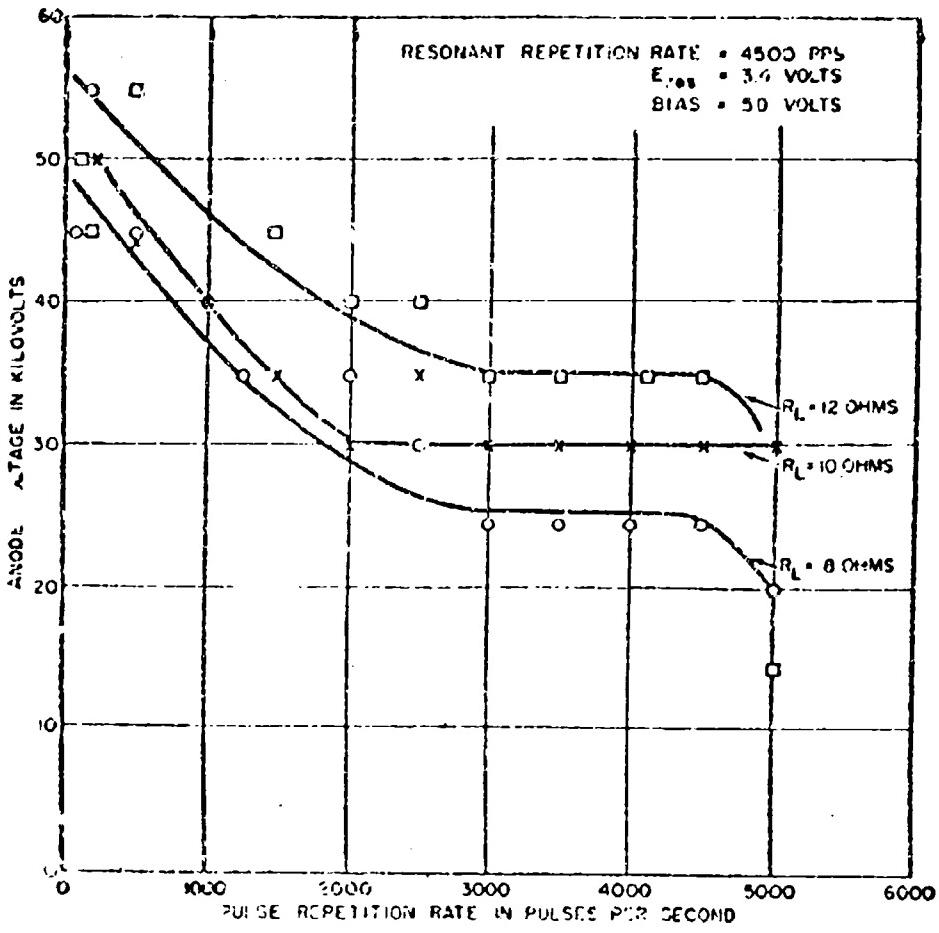


Figure 5 - Comparison of Seiling anode Voltages vs. Repetition Rates at Three Different Load Settings for Z-5212, No. 9

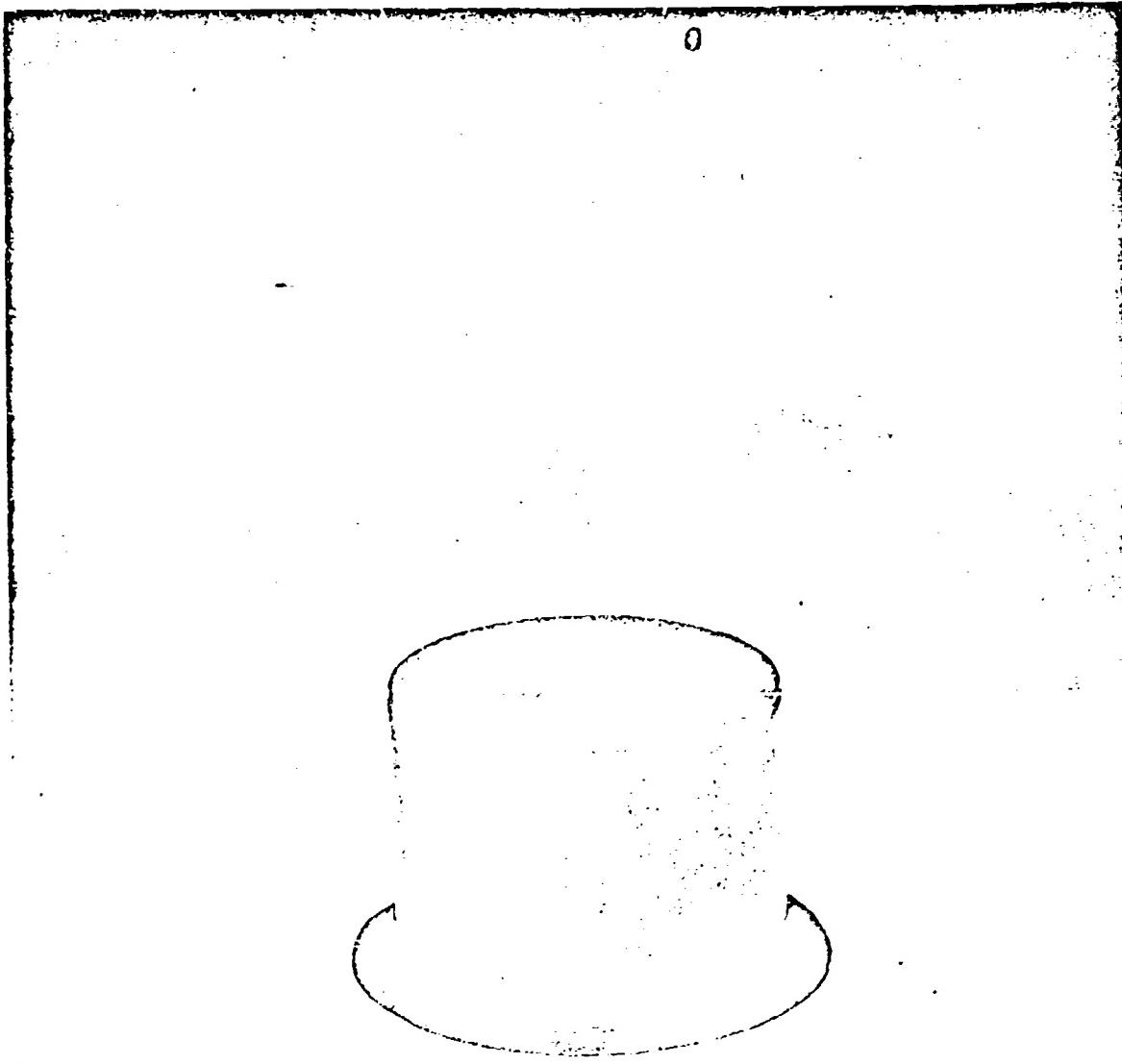


Figure 6 - Gradient Grid Taken from Z-5212, No. 9

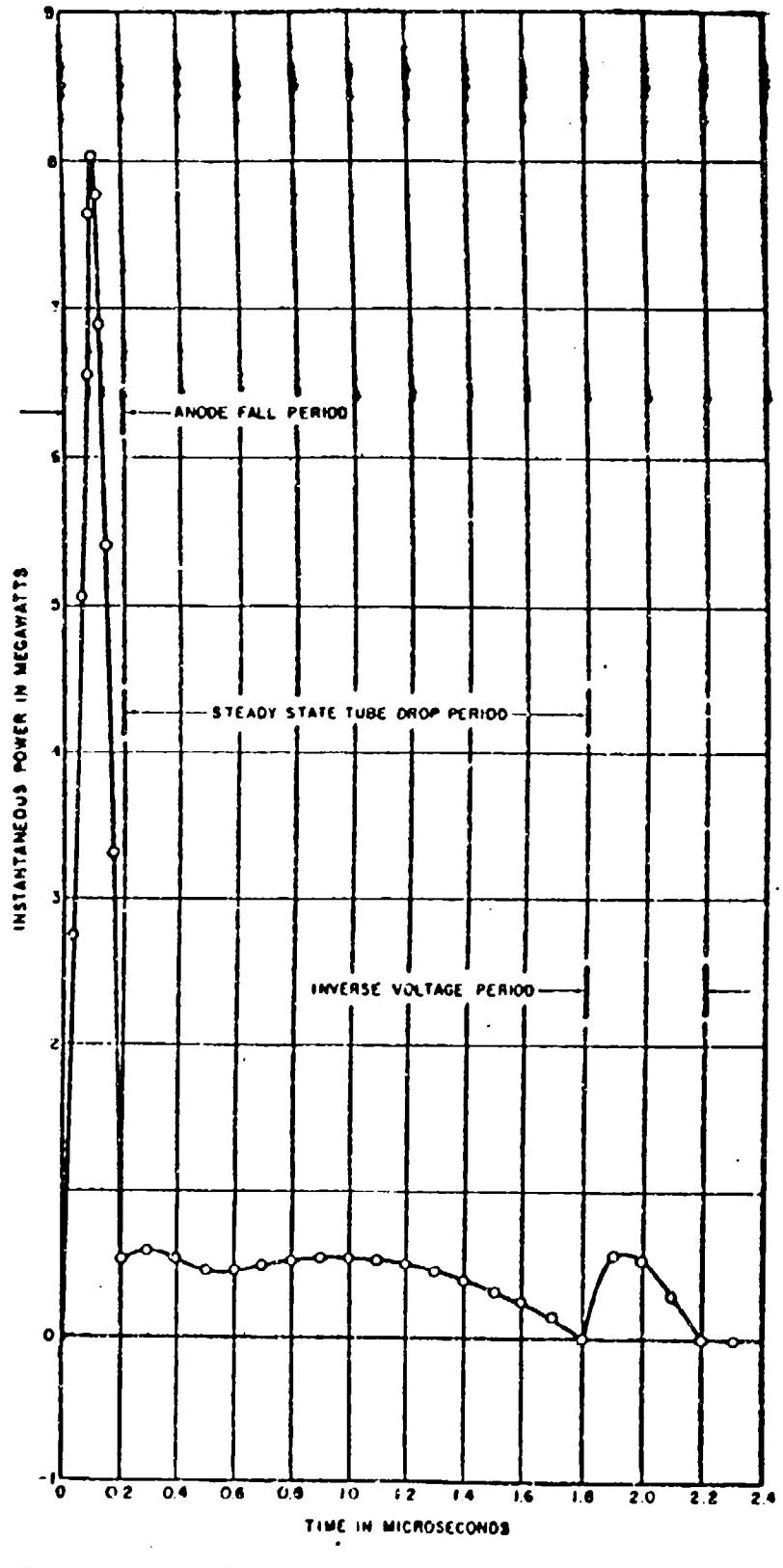


Figure 7 - Instantaneous Power Loss in Thyratron During and After Anode Current Pulse

the base of the high dissipation triangle would be only 0.1 microsecond (since in the Phase II equipment the rise of the current pulse is nearly complete in 0.1 microsecond).

An approximate expression was derived for the temperature rise at the anode surface which depends only on the events of the anode fall period:

$$\Delta t_s = \frac{0.34 p \sqrt{t^1}}{a \sqrt{C_s d K}}$$

where: Δt_s = temperature rise, C at anode surface

p = power (amplitude) in watts of rectangular pulse of anode dissipation. It is assumed for the above expression that the power dissipation at the anode during the anode fall period is constant. While a plot of power dissipation versus time is actually more of a triangle than a rectangle, the rectangle may be defined as one having a width equal to the anode fall time and height such that the area represents the energy given up during the anode fall time.

t^1 = time that above pulse is applied

a = area of anode section in CM^2 through which energy is absorbed

C_s = specific heat of material in calories/gram/C

d = density of anode material in grams/ CM^3

K = thermal conductivity coefficient in calories/(second) (CM^2)(C/CM)

The anode surface temperatures may be estimated for Phase II operation,

where: p = 10×10^6 watts

t^1 = 0.1×10^{-6} seconds

a = area of one grid slot 1-1/8 inch x 1/8 inch, a condition encountered if all the anode current were to concentrate and flow through one slot. Thus a = 0.91 CM^2 and for molybdenum

$$C_s = 0.008$$

$$d = 10$$

$$k = 0.26$$

The rise in surface temperature then equals 2600°C .

The surface temperature might exceed the melting point of molybdenum which might result in the generation of a local cloud of molybdenum vapor and ions.

If the inverse clipping is attributed to the high-temperature considerations presented, the most logical way of reducing the problem would be to minimize the losses during the anode fall period.

Anode fall losses can be minimized to a degree by inserting a saturable reactor in series with the anode lead of the tube.

Saturable reactors have been used previously in conjunction with hydrogen thyratrons. They reduce appreciably the anode dissipation by holding the current to a low level while the anode voltage is falling as shown in Figure 8. When the current reaches point "x" the reactor saturates and its inductance is reduced to virtually nothing. The current, thereafter, rises rapidly as if the saturable reactor were not in the circuit.

The Signal Corps made available a high current saturable reactor of unique design wherein the magnetic core is, in a sense, wrapped around the current conductor. This type of reactor has been described at an earlier symposium¹. To handle Phase II power requirements and to obtain 0.1 to 0.2 microseconds delay in the fast build-up of current, 29 coils of special alloy strip are mounted on one-half inch diameter copper tubing which doubles as the electrical anode lead and water conduit to the anode cooling area. Each coil has an inner diameter of 0.52 inch, an outer-diameter of 1.15 inch, a height of 0.50 inch and is wound from 0.001-inch thick tape of 50/50 iron-nickel, grain-oriented, square-hysteresis-loop material (known to the trade as "Deltamax"). The coils are separated about one-half inch by teflon spacers.

The above design is not only relatively compact but provides for some water cooling to each individual core. Enough measurements have been made with this saturable reactor to clearly establish the potential benefits. The

1. Creedon, J. E. and Schneider, S., A Magnetic Assist for High Power Hydrogen Thyratrons, Proceedings of the Fifth Symposium on Hydrogen Thyratrons & Modulators held at the Hexagon, Ft. Monmouth, N.J. on May 20-22, 1958.

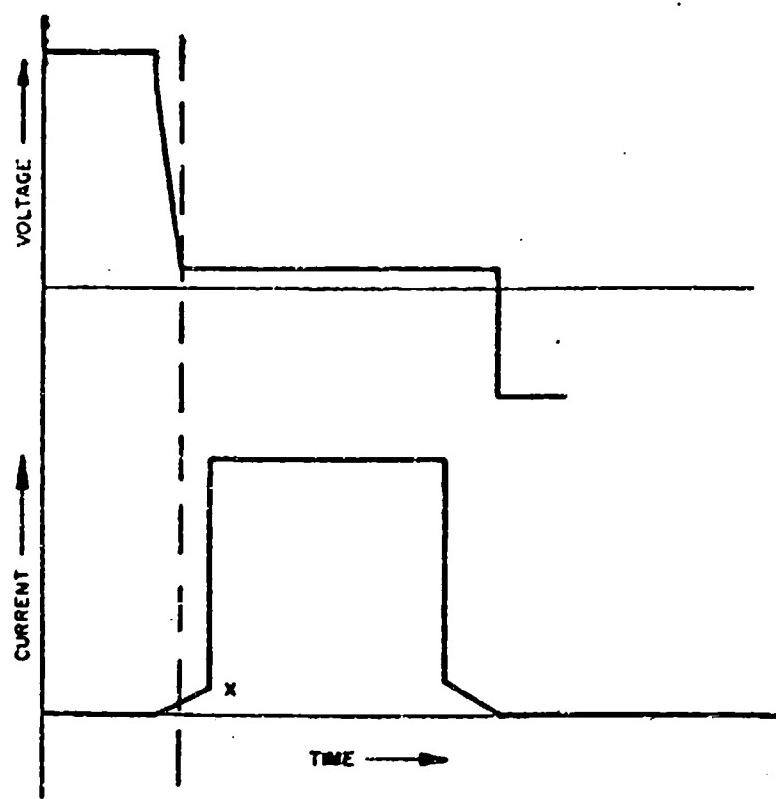


Figure 8 - Hypothetical Current and Voltage Wave Shapes with Saturable Reactor

inverse clipping is much reduced and anode dissipation has been observed to be as much as an order of magnitude lower. The reactor has the greatest effect when the tube pressure is low and when anode dissipation (without a reactor) would tend to be excessive. A comparison of anode dissipations with and without a saturable reactor is given in Figure 9 where average current was varied by varying the anode voltage.

Figure 10 indicates the extension in tube performance at the full 4000 repetition rate that could be credited to the saturable reactor. Gradient grid emission was considered to be the culprit that now prevented full power operation.

Gradient Grid

Accordingly a tube (No. 11A) was assembled with a gradient grid fashioned from 3/16-inch thick copper to be substituted for the 0.070-inch thick molybdenum used previously.

Although gradient-grid emission was eliminated, No. 11A fell short of attaining full power either with or without a saturable reactor. Suspicion was directed at the quality of the bottom gap, between control and gradient grids, when it was found that the optimum operating potential for the gradient grid was a small percentage of the anode potential, Figure 11. Indeed, it was found that the tube would operate to 35 KV when the gradient grid was connected directly to the control grid.

Subsequent examination revealed severe distortion of the 3/16-inch thick copper gradient grid. Not only had the grid bars been bent, but the grid disc as a whole was out-of-round. Whereas the original diameter was 4.030 inches, Figure 12 shows that the lifting of the bars had reduced the diameter in one plane by 0.030 inch and increased it in another by 0.019 inch. There was a sufficient upset of the normal spacings between the two grids to account for the poor performance of the bottom gap.

A fuller analysis of the mechanical stresses at the gradient grid was called for.

By calorimetry it was determined that more than 500 watts dissipation was occurring at the control grid. It was assumed that a similar dissipation would occur at the gradient grid and would moreover, be distributed between only two grid bars if the anode current flowed through only one of the grid slots. Knowing the temperature of the gradient-grid seal it could be calculated that the temperature at the bottom of the gradient-grid cup would be about 450°C . The hottest parts of the grid would be the bars receiving the powers of 250 watts respectively. The maximum temperature could be determined by calculating the temperature gradient along the bars and assuming that the ends were attached to a heat sink at 450°C . The distortion problem is accentuated by the fact that the bars, whose ends are fixed, try

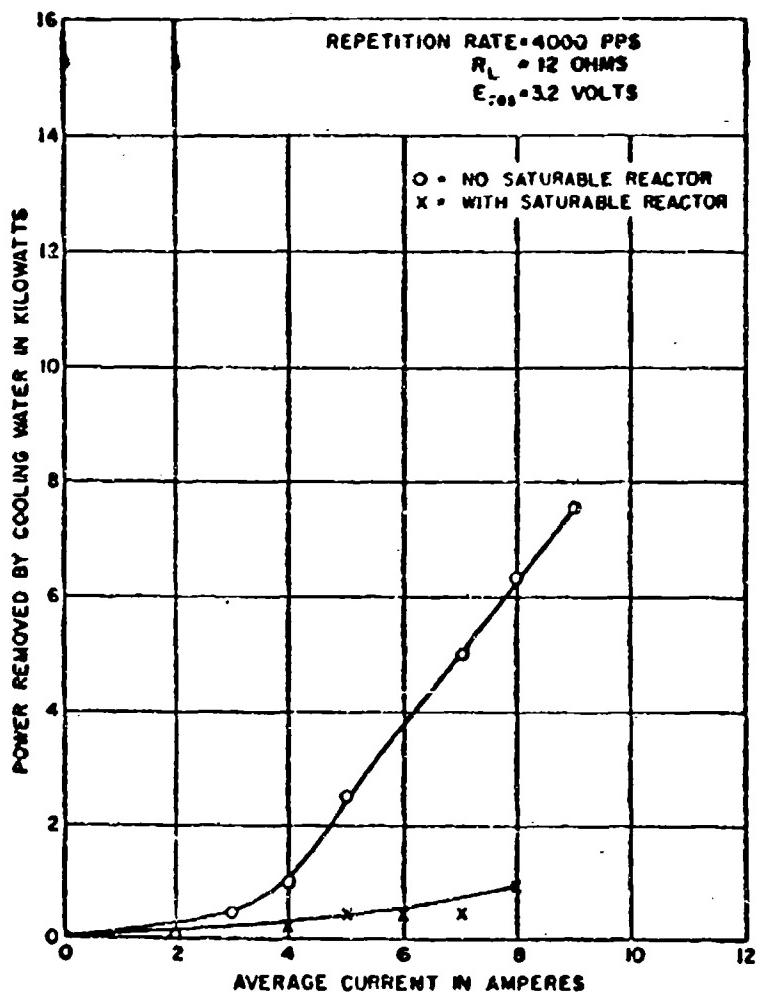


Figure 9 - Power Removed by Cooling Water vs Average Current for Z-5212, No. 11A

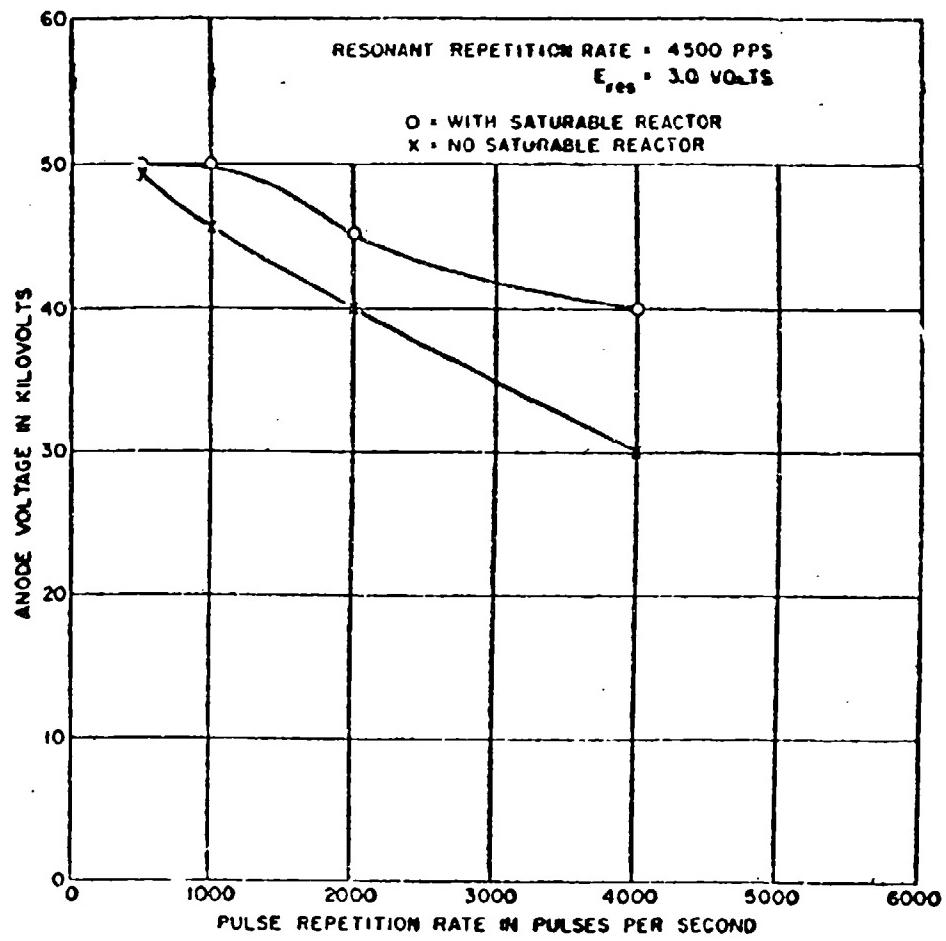


Figure 10 - Ceiling Anode Voltage vs Repetition Rate for Z-5212, No. 9A

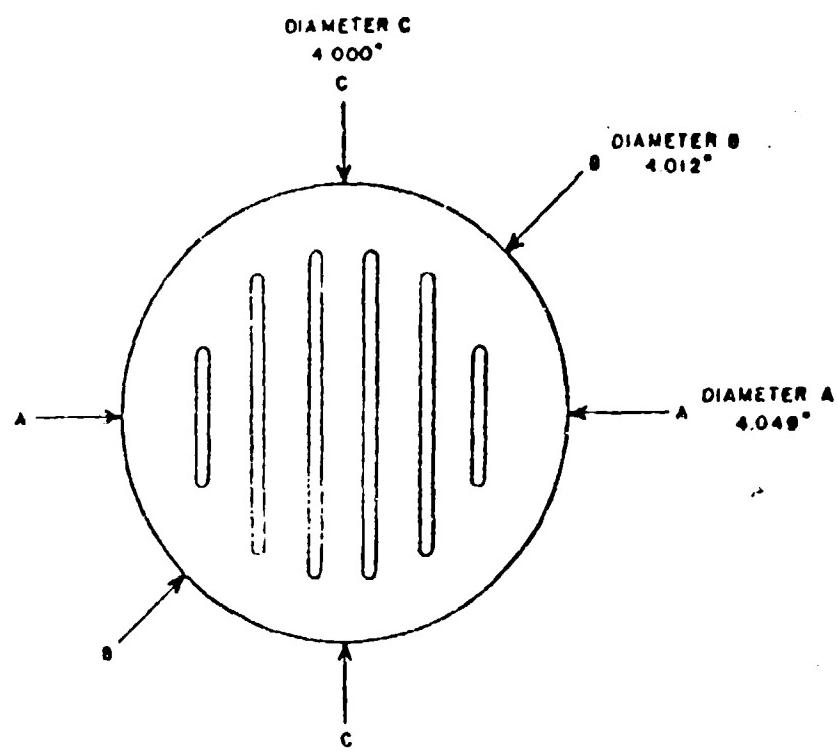


Figure 12 - Gradient-Grid Baffle Taken from Z-5212, No. 11A

to expand. Thus, it is possible to calculate the mechanical stress in the bars. If the calculated stresses exceed known safe limits, there would be a good chance of buckling or distortion of the bars. Table II summarizes the stresses for the two gradient grids that had been used. It also shows stresses that might be encountered if the gradient grid were fashioned from thicker molybdenum.

Table II - Gradient-Grid Temperature and Stress Considerations

{Based on 250 watts power to center of 4-CM x 3/8-inch bar whose ends are attached to 450°C heat sink}

<u>Material</u>	<u>Grid</u> <u>Thickness</u> (inch)	<u>Bar Temperature</u>		<u>Unit Stress</u>
		<u>Hot Spot</u>	<u>Average</u>	<u>(LB/SQ IN.)</u>
Molybdenum	0.070	1700	1075	180,000
Copper	3/16	570	500	15,000
Molybdenum	3/16	950	700	80,000
Molybdenum	1/4	830	640	65,000
Molybdenum	5/16	750	600	60,000

<u>Material</u>	<u>Grid</u> <u>Thickness</u> (inch)	<u>Safe Limits</u>	
		<u>Elastic Limit</u>	<u>Yield Point</u>
Molybdenum	0.070	-	15,000 (at 1075°C)
Copper	3/16	1,000 (at 500°C)	-
Molybdenum	3/16	-	45,000 (at 700°C)
Molybdenum	1/4	-	48,000 (at 640°C)
Molybdenum	5/16	-	50,000 (at 600°C)

A comparison of the theoretical unit stresses and the safe limits indicated that even a 5/16-inch thick molybdenum grid might be subject to buckling. On the other hand, in choosing a new gradient-grid thickness it seemed appropriate to keep the thickness to the minimum consistent with freedom from distortion.

As a result of the above considerations a calculated risk was taken with a 1/4-inch thick molybdenum gradient grid which was incorporated in tube No. 11B.

Full power operation at 50 KV and high repetition rate was achieved for the first time with No. 11B. Improvement at the gradient grid was also indicated by the fact that the optimum operating potential for the gradient grid was nearly 50 percent of the anode potential, Figure 13. (This data was taken before the tube was fully conditioned, which may explain the anode ceiling voltage reaching only 45 KV.) Although the saturable reactor was not initially needed for full power operation, the widest reservoir range was achieved with the reactor, Figures 14 and 15.

LIFE TESTS

Tube No. 11B was placed on life test deliberately without a saturable reactor and after three hours an instability developed whereby the anode voltage ceiling was depressed to about 25 KV. Efforts to re-age the tube were fruitless until the saturable reactor was inserted in the anode lead. After this step was taken, however, the tube recovered in a short time and was again capable of full power operation. With the saturable reactor, life testing was continued at full power until at 75 hours the tube failed because of a puncture in a small ceramic seal at the bottom of the tube. Post-mortem examination revealed that this seal had been attacked by corona.

Z-5212, No. 13A, similar in design to No. 11B, followed on life test with the following additional precautionary changes:

- 1) all seals that might be subject to corona were encapsulated in rubber
- 2) the bottom end of the tube was cooled by an air draft
- 3) the saturable reactor was used at all times in the anode lead

To date the tube has operated in excess of 700 hours and some of the characteristics as a function of life are given in Figures 16 and 17. At 270 hours it was necessary to reduce the anode voltage to 40 KV but life testing was continued in order to determine whether further degradation was imminent. At 350 hours a bad component was located in the test set and when this was replaced the anode voltage could be raised to 45 KV. Figure 18 depicts

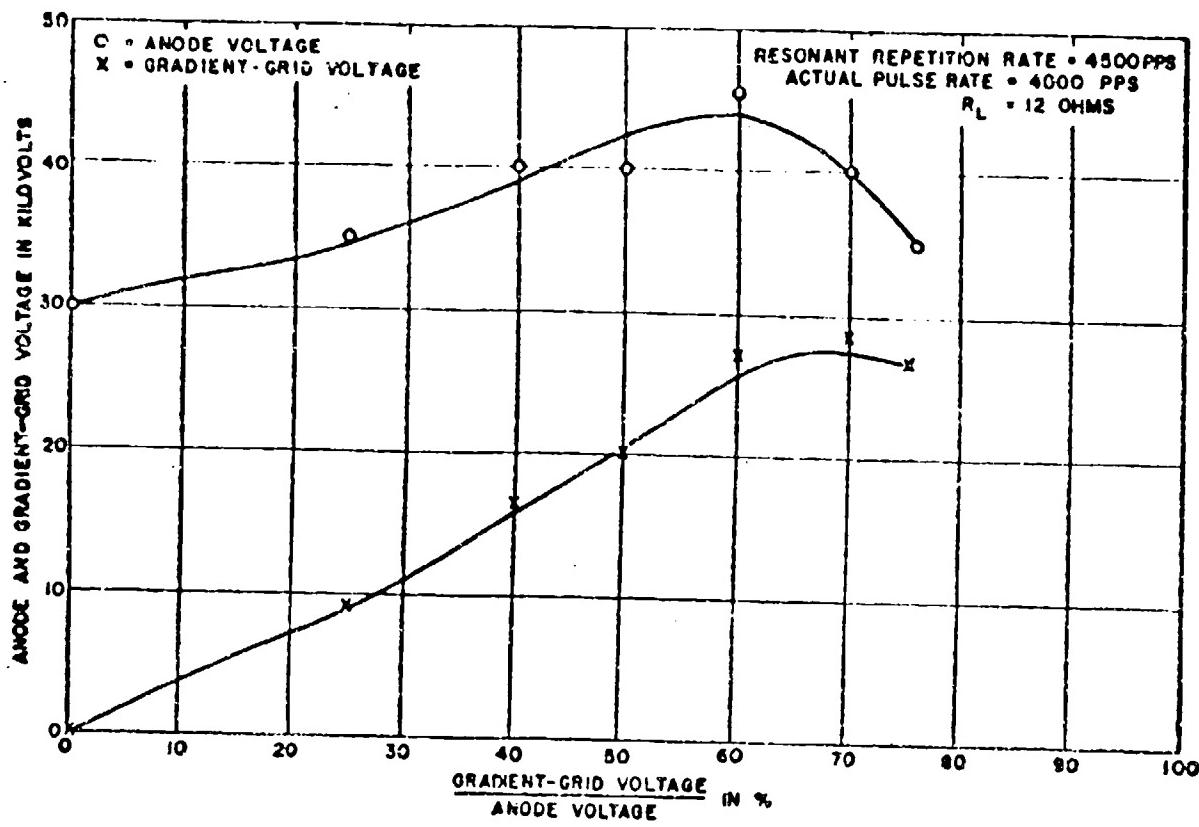


Figure 13 - Ceiling Anode Voltage vs Ratio of Gradient-Grid to Anode Voltage for Z-5212, No. 11B

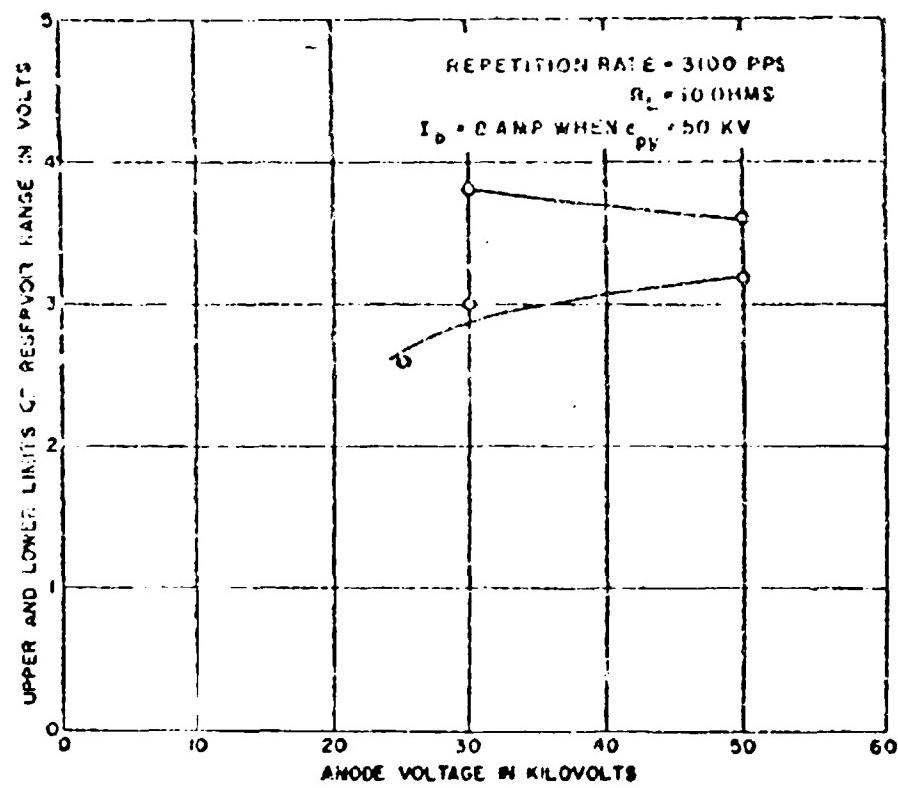


Figure 11 - Reservoir Range for Z-521Z, No. 11B with Saturable Reactor

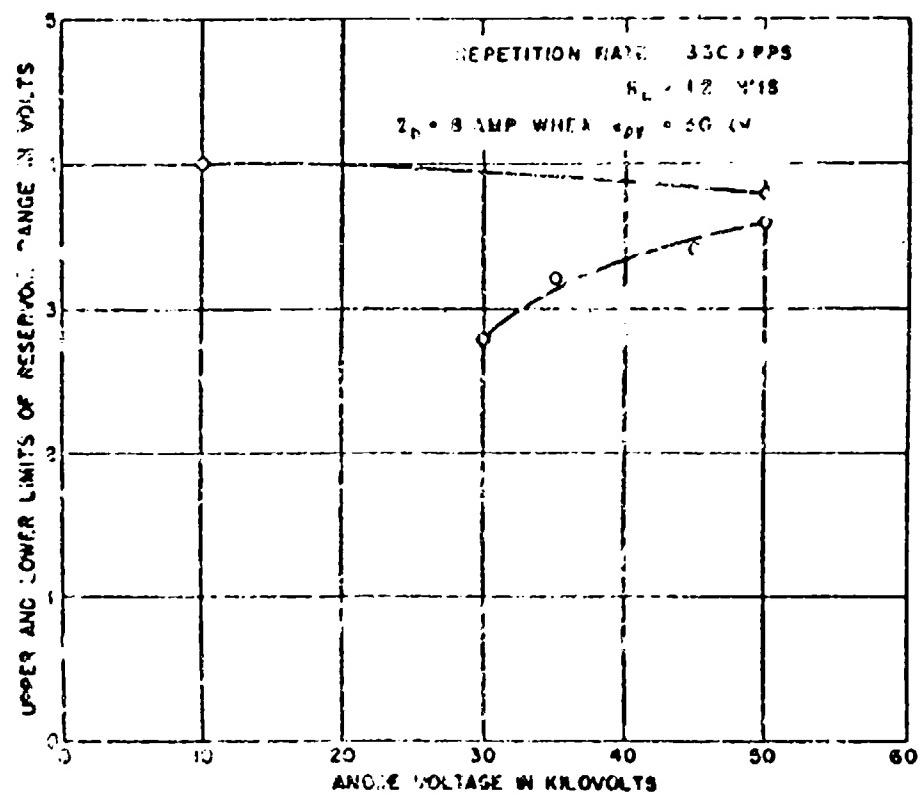


Figure - Reservoir Range for Z-5212, No. 11B with No Saturable Reactor

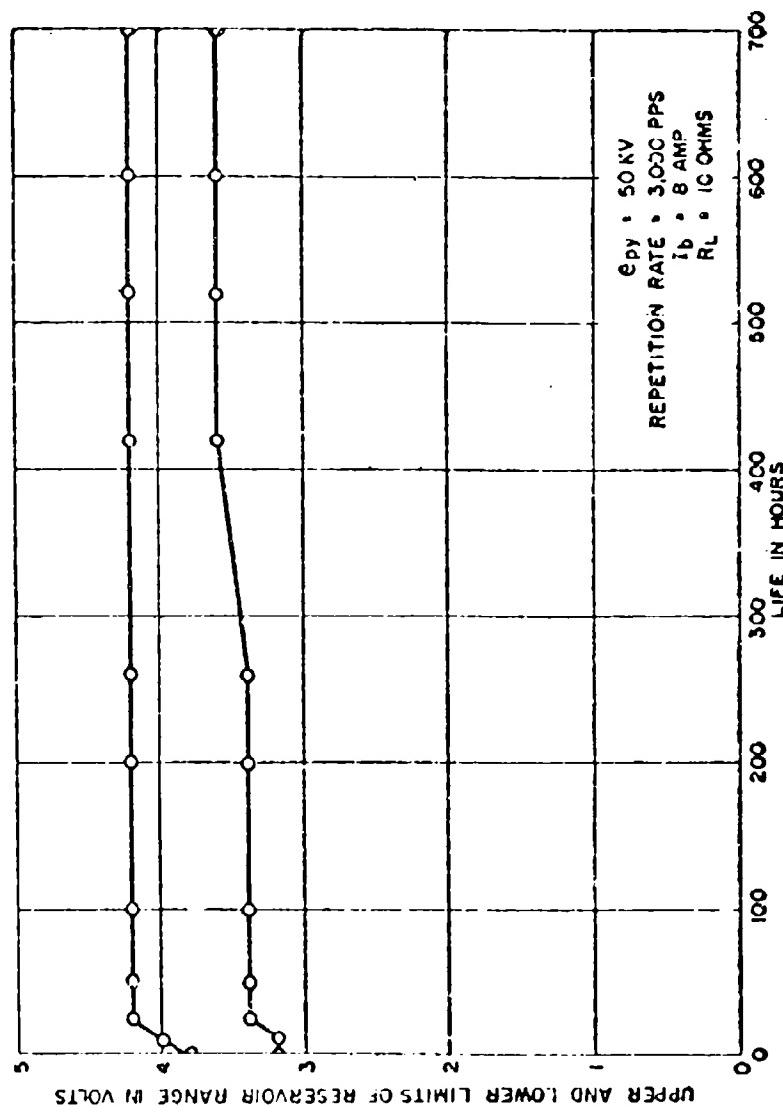


Figure 16 - Z-5212, No. 13A Range vs Life

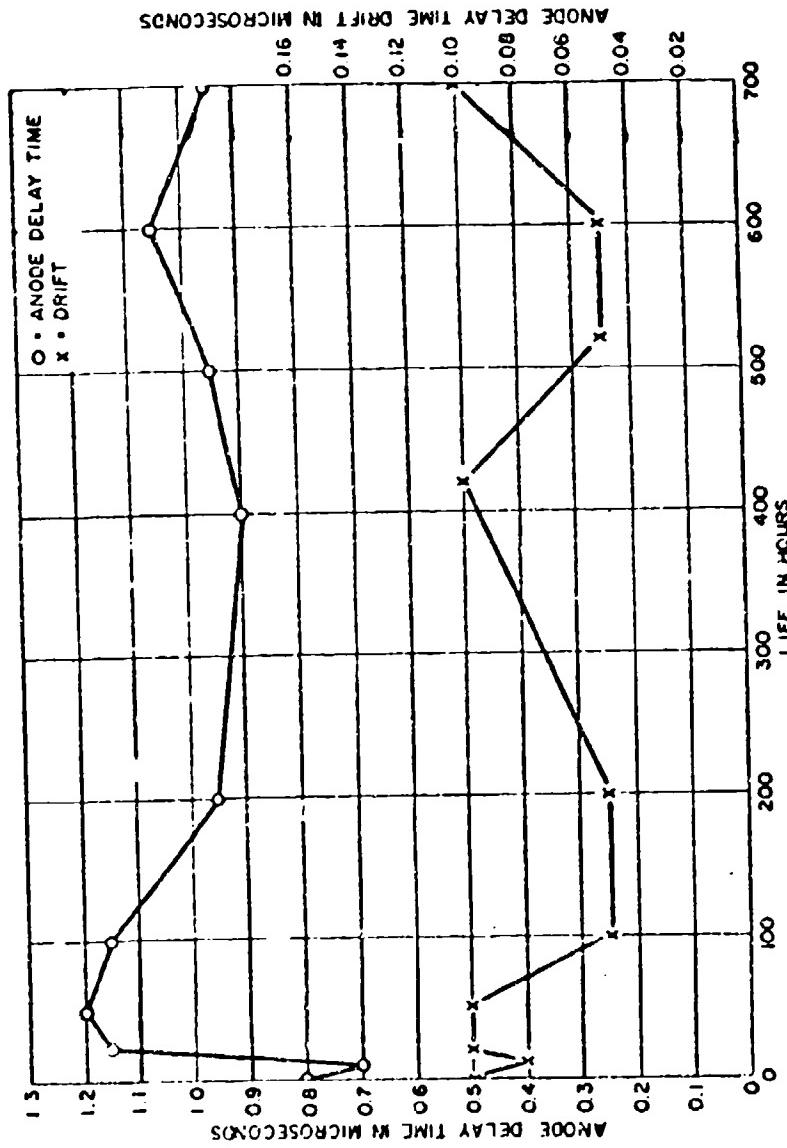


Figure 17 - Anode Delay and Delay Time Drift During Life for Z-5212,
No. 13A

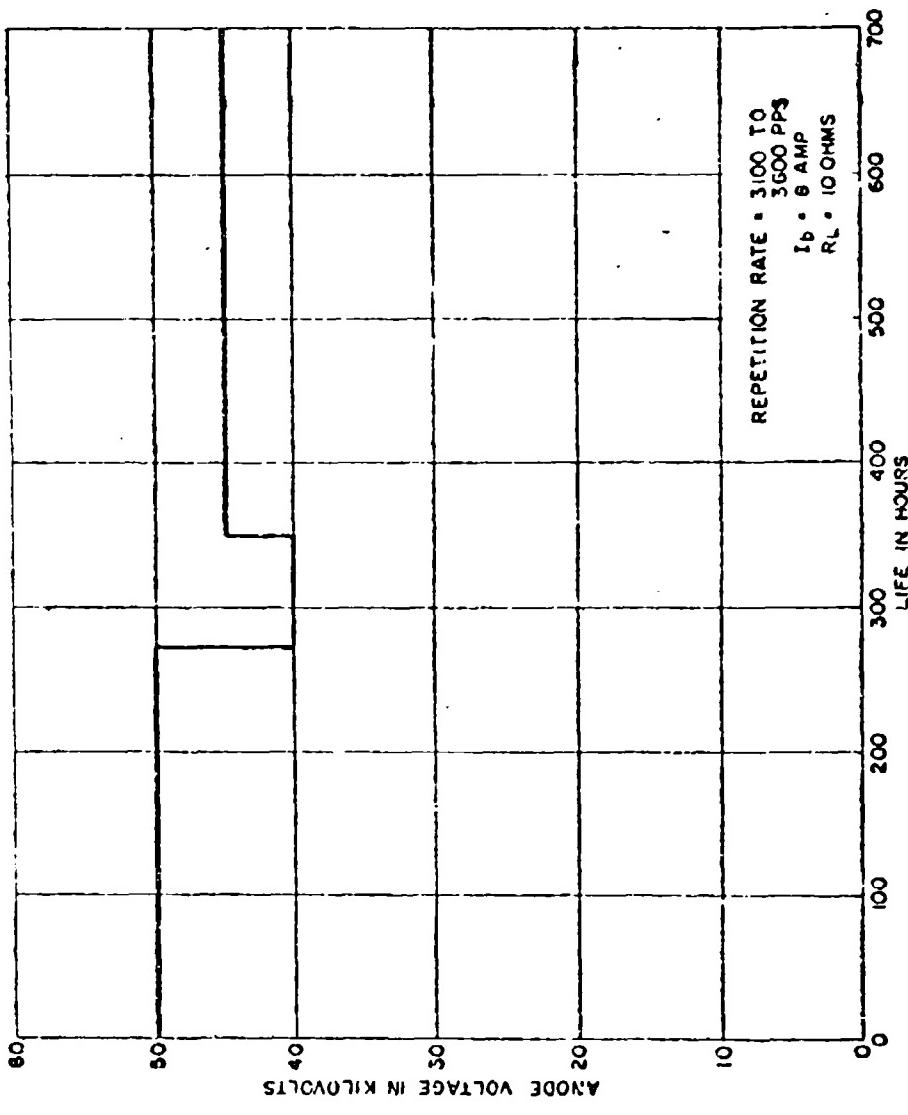


Figure 18 - Z-5212, No. 13A Anode Voltage Setting vs Life

the operating conditions that have prevailed during this life test.

CONCLUSIONS

At the present stage of development of the Z-5212 and with the limited operating experience to date the following conclusions can be stated.

- 1) High repetition rate operation is enhanced by keeping all interelectrode spacings to a small value so that the length of path from cathode to anode is small.**
- 2) A saturable reactor can materially reduce anode dissipation and as a result reduce or eliminate inverse clipping at the anode.**
- 3) Substantial grid dissipations can be tolerated by**
 - a. water cooling the control grid**
 - b. using 1/4-inch thick molybdenum at the gradient grid.**
- 4) The results of early life testing indicate the desirability for:**
 - a. increasing the anode voltage ability of the tube by some 10 KV**
 - b. increasing the width of the reservoir range.**
- 5) Water cooling at 50 KV presents no unique problems.**

In the remaining time on the contract small refinements in electrode spacings will be studied, additional life testing will be performed, technical data will be published, sample tubes will be made available for Signal Corps evaluation and a final report will be written.

MODULATOR DESIGN FOR A NEW FAMILY OF HIGH-POWER THYRATRONS

by

N. S. Nicholls, B.A.

R.R.E., Malvern, England

Introduction

The development of a new family of high-voltage thyatrons is projected, based upon the design of the VX 3351, which has been described by Cook and Wholdon(1).

It is planned to develop, in this family, valves suitable for all the known fields of application of high-voltage thyatrons.

Initially, work is being concentrated on valves having a $2\frac{1}{2}$ " diameter envelope, but smaller and larger sizes will probably be introduced later.

In this paper choice of target characteristics for the VX 3351 and its variants is discussed in relation to likely methods of use.

Controlled Rectifier and Charging Service

The advantages of using controlled rectification for power supply to radar modulators have been outlined in an earlier paper(2).

The use of controlled charging is often necessary in thyatron modulators when the effective duty ratio exceeds about .005 in order to ensure recovery of the other valves in the circuit.

The VX 3351 valve is being developed for these types of service, and has the characteristics given in Table I. Note that as a controlled rectifier, an output of 25 KV 10 A. D.C. is readily obtainable from six valves in a 3 phase bridge circuit.

The metal envelope design is particularly advantageous for these purposes because the excellent cooling of the grid permits the use of the most open design compatible with voltage hold-off requirements without danger from grid emission or contamination of the anode. This confers a low aro-drop and easy triggering. However, in comparison with the VX 3287 which was described in the earlier paper(2) and in which a screened construction was employed, this valve has a much greater anode-grid capacitance. This would often prevent full advantage being taken of the high permiss. , grid-circuit impedance of about 4 Kohms. However, it has proved possible to avoid the difficulty by using the "Grounded-Grid" circuit shown in Fig. 1. In this circuit the valve is fired by the application of a negative pulse to the cathode, while passage of the anode current through the

trigger pulse generator is prevented by the semi-conductor diode connected between cathode and grid. This semi-conductor diode has to pass the full thyratron anode current (including fault-condition surges) but has only to withstand an inverse voltage equal to the trigger pulse amplitude. Present experience indicates that it is adequately protected by the thyratron grid from the effects of inverse flashover in the valve. In cases where grid-bias is required, this can be inserted in series with the thyratron grid lead, but the supply must be able to withstand surges due to flashover in the thyratron without excessive voltage rise or the semi-conductor diode may be damaged.

The recovery time of the valve after passing its rated fault current of 500 A. should be sufficiently short without the use of grid bias to ensure reliable circuit-breaking when used as a controlled rectifier at supply frequencies up to a kilocycle. On the other hand, the recovery at small currents is sufficiently rapid to involve some risk of complete extinction by commutation oscillations when impulse firing is employed with a 50 c.p.s. supply. This trouble is particularly liable to occur with equipment required to operate from a variety of power sources, including small generator sets. It has been successfully cured in one case by the use of small saturable reactors in series with the H.T. transformer primary together with CR elements in shunt.

Pulse Modulation

The variant of the VX 3351 intended for switching duty in network-type modulators is the VX 3359. Its target ratings and characteristics are given in Table II. Note that a peak power of up to 40 MW at 10 μ sec. pulse length and an average power of up to 50 KW, is allowed, although the size and heater power are little more than those of a 5C22.

The design is particularly well adapted to this class of service. Knight and Lord⁽³⁾ and Isaacs⁽⁴⁾ have shown that a substantial additional dissipation in the grid normally occurs in pulse service, due to reverse current. With VX 3359 good cooling of the grid maintains a high gas density in its vicinity and thus permits reliable operation at high rates-of-rise of current under these conditions.

A somewhat less open grid design than for the VX 3351 is employed primarily to maintain the voltage hold-off performance with the higher gas pressure required.

The grid is still, however, somewhat more open than has been general practice hitherto in modulator valves, and this, together with the use of Deuterium, gives a rather long recovery time. By the use of -100 V. grid bias in conjunction with a grid circuit impedance of 500 ohms, a recovery time of 30 μ sec. at a peak anode current of 2 KA should be obtained. This is adequate for operation at p.r.f.'s up to several kilocycles in conventional modulators having low duty ratio (see Fig. 2). It is important that the grid-circuit impedance should not exceed the specified value during the danger period following the first appearance of forward anode voltage after the pulse. To cover the usual case where the thyratron grid

circuit contains reactances and non-linear circuits, the term Recovery Impedance has come into use in the U.K.

This is defined for each instant subsequent to the current pulse as follows:-

$$\text{Recovery Impedance} = \frac{(\text{Instantaneous grid potential}) - (\text{Specified grid bias})}{(\text{Instantaneous grid current})}$$

The use of this quantity relies on the hypothesis, originally advanced by Malter and Johnson⁽⁵⁾, that the progress of deionization is unaffected by the potentials of the electrodes, provided, of course, that additional ionization is not generated. The departures reported by Knoop⁽⁶⁾ are confined to long recovery times, and are therefore probably not important in the present context.

Unfortunately the value of the Recovery Impedance obtaining in a particular equipment is in general affected by the grid-current of the valve operated in it and therefore depends on the particular valve used and on the value of the anode current. Consequently its usefulness is mainly limited to circuits which are predominantly dissipative in character, so that uncertainties in the temporal dependence of thyratron grid-current only affect small corrections.

One method of achieving a low Recovery Impedance without heavily loading the trigger pulse generator is to employ a saturable choke (or transformer) in shunt with the trigger-pulse generator. Some means of re-setting the magnetic core between pulses is required.

The mode of operation will now be explained with reference to Fig. 3. In the figure, a typical modulator anode voltage waveform is shown. From this, and the value of the peak anode current, the unique critical-grid potential curve may be obtained from the measured valve characteristics. The critical-grid potential passes through a minimum shortly after the anode first becomes positive, and subsequently returns to the static value as deionization proceeds. The grid-current must next be obtained. The variation of grid-current with grid-voltage shows current saturation like a negatively biased probe provided that the grid voltage is low. The value of the saturation current was found by Malter and Johnson (loc. cit.) to decay exponentially with time from an initial value which is a function of the peak anode current. Departure from the exponential law at short times had been reported by Gavrilov⁽⁷⁾, but does not affect the qualitative argument. Prior to saturation of the reactor, the grid current will be limited to a low value by the unsaturated inductance of the reactor. After saturation of the reactor, the grid current will be limited initially to about $\frac{V}{R}$ until the saturation grid current falls below this. Thereafter the current will be controlled by the valve only. The grid voltage waveform may not be drawn, and it may then be deduced whether satisfactory recovery will be obtained. Any reduction in the initial value or increase in the rate of decay of the saturation grid current will result in an earlier return of the grid potential to the bias level and therefore increase the safety margin. Thus, only straightforward unilateral tolerancing is involved.

additionally useful to have a valve whose recovery time is to a large extent under the control of the circuit designer.

Inverse Diode Operation

The desirable attribute of the VX 3358 design for inverse diode service is that the grid-current-to-fire may be kept down by using a fairly open structure, while still maintaining an effective evaporation baffle between cathode and anode.

The target ratings are given in Table III.

To minimize the risk of failure to trigger, the lowest possible grid-current-to-fire and the longest possible recovery time compatible with reliable inverse voltage hold-off will be sought during the development.

Because of the danger, which is always present with gas-filled inverse diodes, of a valve reaching end-of-life by failing to strike, with consequent serious risk of damage elsewhere, it is wise to back it up by connecting directly across the P.F.N. a sealed spark-gap in series with a matching resistor.

Cooling

The heat requiring to be dissipated varies from around 300 watts for operation at full rectifier rating to as much as twice this for the pulse modulator under severe conditions. It should be possible to attain such dissipations by free convection because the envelope will withstand high temperature, and, though small, may be finned over its entire length.

Nevertheless, assisted cooling will often be indicated for the benefit of surrounding less refractory components. This is particularly true in compact installations.

Moreover, another cooling problem arises from the inevitable sensitivity to ambient temperature of the hydrogen reservoir system. The main source of heat is usually the cathode region which is adjacent to the reservoir, and thermal coupling is increased by the high conductivity of the envelope. Although some compensation is inherent in the design, the difference between the temperature of the reservoir surroundings for a cold start at -25°C compared with that in operation at full power at 85°C, would present a severe problem if not restricted by assisted cooling.

Since the reservoir is the most temperature sensitive part of the valve, a heat sink is applied to a flange on the envelope in its vicinity. This also serves as the mechanical support. Some forms are suggested in Fig. 6. The heat sink may be convection or forced air or liquid cooled. The form of the heat sink and the disposition of the fins when air cooling is employed is left to the choice of the user, who is thereby given the maximum possible freedom in the thermal design of his equipment.

Pins will probably be fitted to the top of the envelope to assist in dissipating the grid heat, as indicated in the figure.

The anode is intended to be cooled by natural convection from a small radiator fitted permanently to its lead, since a fairly high anode temperature is permissible, particularly in the high-dissipation pulse modulator roles.

Conclusions

By the use of this family of valves, a major advance in compactness and reliability should be possible in many pulse modulators.

As rectifiers, their power loss, including heater power, is no more than a third of that of any semi-conductor arrangement, with the further advantage of being able to dispose of their waste heat at a much higher temperature. They should also compare favourably in compactness, first cost, and, on account of their simplicity and resistance to surges, in reliability, with alternative semi-conductor arrangements.

As modulators they have substantially lower power losses than existing glass valves, as well as being much more compact and rugged. Their long life (the target is 5000 hours), and the ease of storage and handling of spares, is expected to make them more economical in use at average powers at least down to 50 KW.

As inverse diodes they will have advantages in compactness, robustness, reliability and simpler cooling requirements than possible semi-conductor alternatives, though the heat dissipation will generally be a little higher.

It thus appears that for most modulator applications, at least down to the 50 KW average power level, the valves of this family will represent the best available devices for all applications for some time to come.

Acknowledgments

Thanks are due to workers at the Hirst Research Centre of the General Electric Co., England, who supplied useful information, and to the Controller of Her Majesty's Stationery Office for permission to publish. Crown Copyright is Reserved on the illustrations.

References

1. Cook, K. G. and Wheldon, R. J., "A Compact Metal-Ceramic Deuterium Thyratron" - 7th Symposium on Thyratrons and Modulators.
2. Jarvis, R. M., Price, E., Bradshaw, J. D. and Nicholls, N. S., "Grid Controlled Rectifiers for Radar Transmitter R.T. Supply." - Proceedings of the 6th Symposium on Thyratrons and Modulators, p. 278.

3. Knight, H. de B. and Lord, J., "Measurement of Energy Losses in a Hydrogen-filled Thyratron in Modulator Duty". - Proc. I.E.E., Vol. 108, Part B., 40, (1951), p.455.
4. Isaacs, G. C., Unpublished progress reports on C.V.D. Research Project RP.3-1.
5. Malter, L. and Johnson, E. O., "Studies of Thyratron Behaviour". - R.C.A. Review, Vol. XI 165, 178 (1958).
6. Knoop, Ernst. Sch. f. Angew. Physic. Vol. IV No. 10 (1952) and Vol. IX No. 3 (1957).
7. Gavrilov. Reps. Acad. Sci. U.S.S.R. Vol. 71, No. 2 (1950).
8. Goldberg, S., "Research Study on Hydrogen Thyratrons" Vol. II, Edgerton, Germeshausen & Grier, Inc., Boston.

TABLE I

VX 3351 - CONTROLLED RECTIFIERTarget Ratings

<u>Parameter</u>	<u>Unit</u>	<u>Limits</u>
Heater voltage	V. R.M.S.	6.3 $\pm 7\%$
Reservoir voltage	V. R.M.S.	6.3 $\pm 7\%$
Cathode heating time	secs.	300 min.
Peak forward anode voltage	KV	40 max.
Peak inverse anode voltage	KV	40 max.
Mean anode current	A	3.5 max.
Peak anode current, normal operation	A	25 max.
Peak anode current, surge (Note A)	A	500 max.
Ambient temperature	$^{\circ}$ C	-25 to +85

Note A For a maximum of two successive half-cycles of current at a supply frequency of 50 c.p.s.

Tentative Data

Heater current	A. R.M.S.	15
Reservoir current	A. R.M.S.	2
Unloaded trigger pulse voltage	V.	200
Trigger current	mA.	50
Recovery time (Note 1)	usec.	175

Note 1 Measured with a 1 KV. test pulse following 12 A. peak anode current, with zero-bias and 4 Kohms grid circuit impedance.

Dimensions

Overall length	-	10"
Envelope diameter	-	2 $\frac{1}{2}$ "

TABLE II
VX 3359 - PULSE MODULATOR

Target Ratings

<u>Parameter</u>	<u>Units</u>	<u>Limits</u>
Heater voltage	V. R.M.S.	6.3 $\pm 7\%$
Reservoir voltage	V. R.M.S.	6.3 $\pm 7\%$
Cathode heating time	secs.	300 min.
Peak forward anode voltage	KV.	40 max.
Mean anode current	A.	2.5 max.
Peak anode current (Note A)	A.	2000 max.
Peak rate of rise of current	A/ μ sec.	7500 max.
Operation factor (Note B)	V x A x p.p.s.	20×10^9 max.
Ambient temperature range	$^{\circ}$ C	-25 to +85

Notes: A. For 5 μ sec. (max.) pulses. Derating for longer pulse lengths is to be determined.

B. This applies for a rate of fall of current not exceeding 2500 A/ μ sec. and a peak inverse voltage not exceeding $0.25 \times \sqrt{A_{pk}}$.

Tentative Data

Heater current	A. R.M.S.	15
Reservoir current	A. R.M.S.	2
Unloaded trigger pulse voltage	V.	500
Trigger source impedance	ohm,	500
Recovery time (Note 1)	μ sec.	30

Note 1. Measured with a 1 KV. test pulse following 2000 A. peak current, with -100 V. bias and a grid circuit impedance of 500 ohms.

Dimensions

Overall length = 10"
Envelope diameter = 2 $\frac{1}{2}$ "

TABLE III
VX 3358 - INVERSE DIODE (TRIGGERED)

Target Ratings

<u>Parameter</u>	<u>Units</u>	<u>Limits</u>
Heater voltage	V. R.M.S.	6.3 \pm 1%
Reservoir voltage	V. R.M.S.	6.3 \pm 7%
Cathode heating time	secs.	300 min.
Peak inverse voltage	KV.	40 max.
Mean anode current	A.	2.5 max.
Peak current, normal (Note A)	A.	500 max.
Peak current, fault condition (Note B)	A.	2000 max.
Ambient temperature range	°C	-25 to +85

- Notes: A. For 10 μ sec. (max.) pulses. Derating for longer pulses to be determined.
- B. For 10 μ sec. (max.) pulses at 400 p.p.s. (max.). Maximum duration of fault 1 sec.

Tentative Data

Heater current	A. R.M.S.	15
Reservoir current	A. R.M.S.	2
Unloaded trigger pulse voltage	V.	200
Trigger current	mA.	50

Dimensions

Overall length	-	10"
Envelope diameter	-	2 $\frac{1}{2}$ "

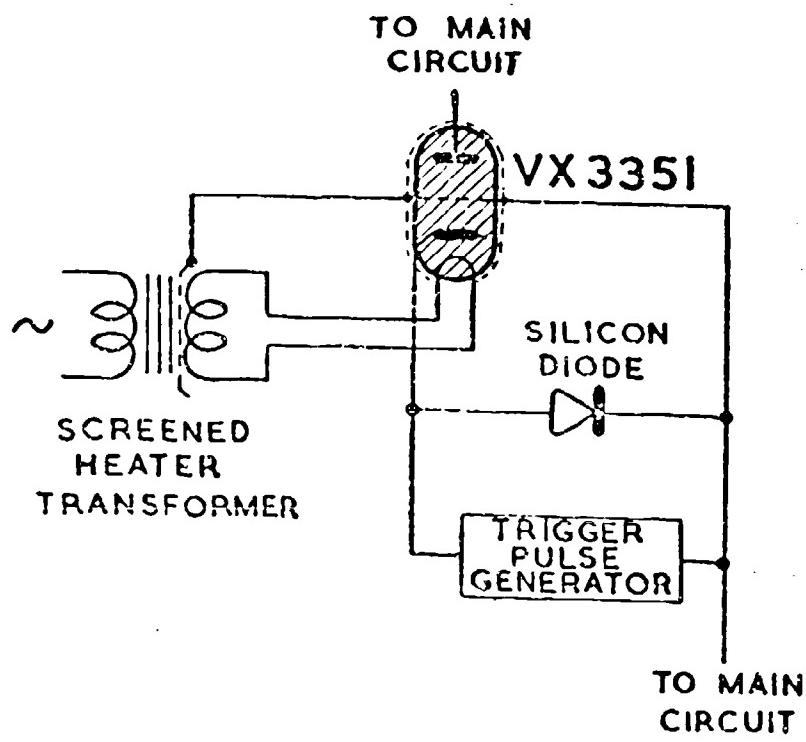


FIG. 1

THE "GROUNDED GRID" RECTIFIER CIRCUIT

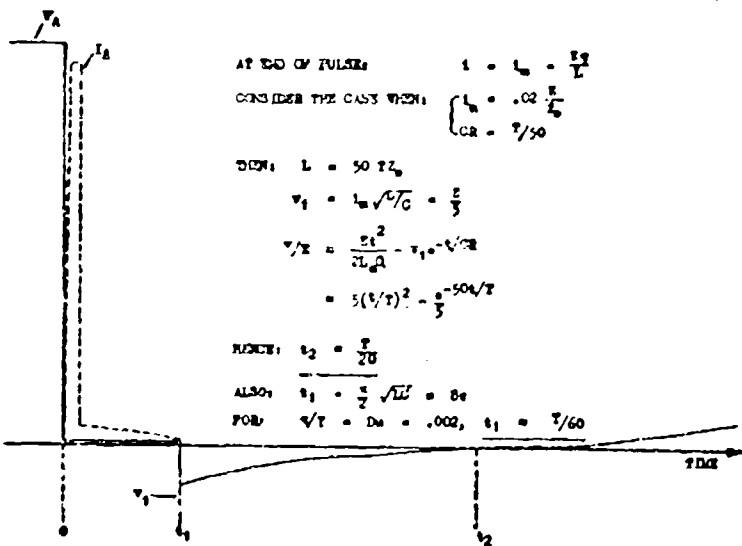
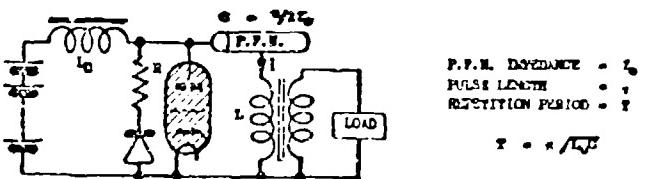


FIG. 2.

TYPICAL MODULATOR ANODE VOLTAGE AND CURRENT WAVEFORMS

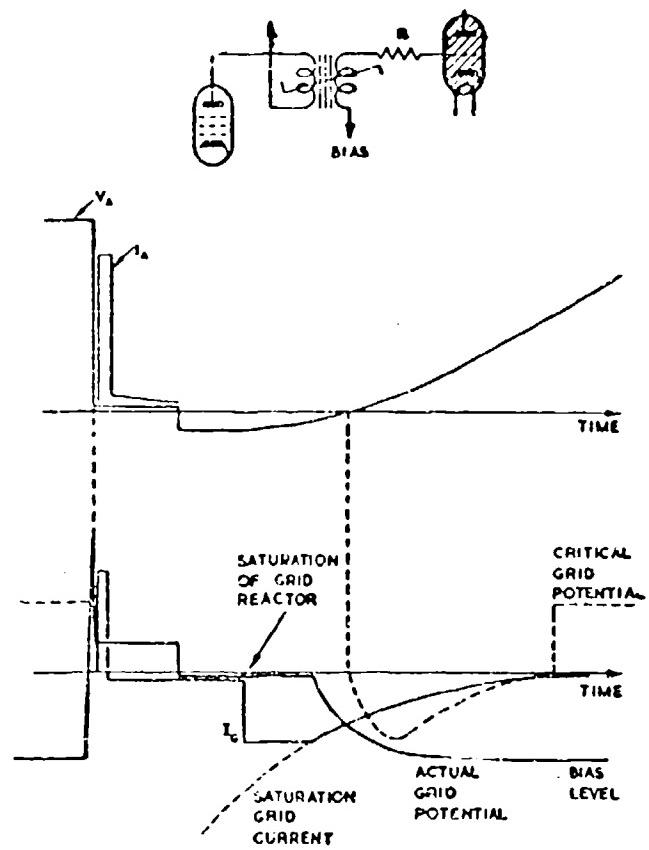


FIG. 3.
SATURABLE REACTOR GRID CIRCUIT AND WAVEFORMS

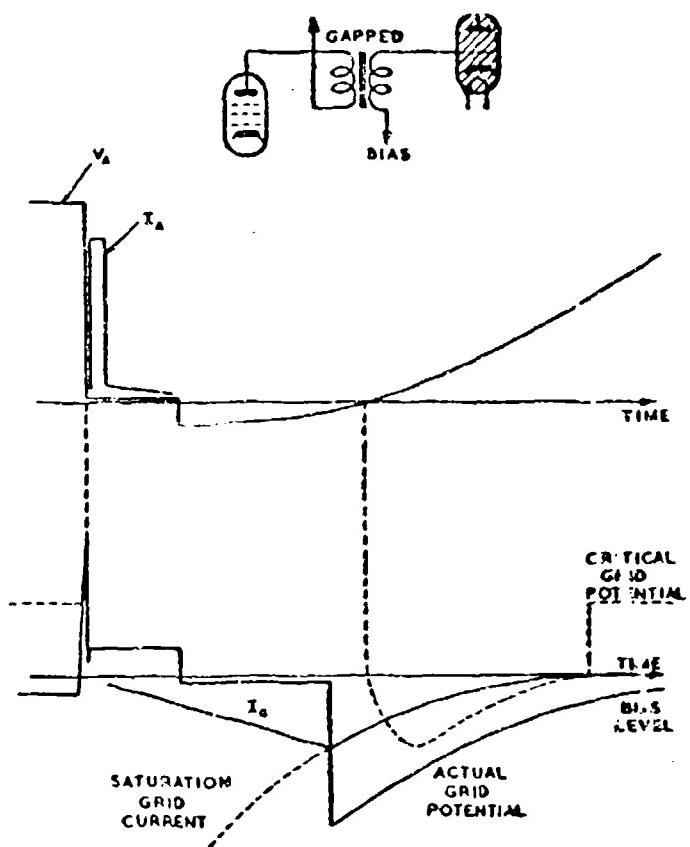


FIG. 4
INDUCTIVE GRID CIRCUIT AND WAVEFORMS

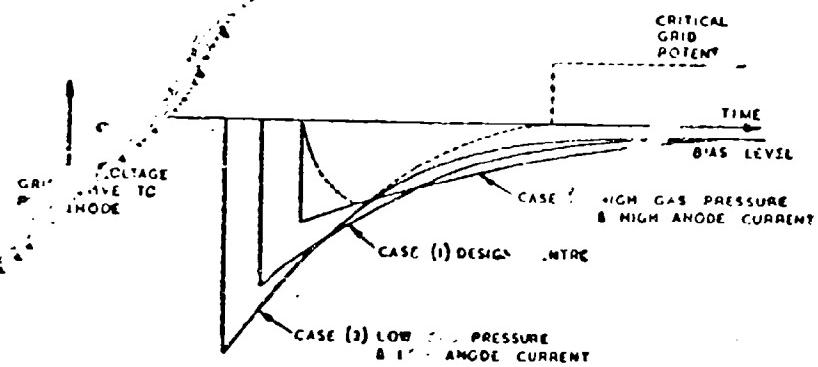


FIG. 5

LIMITING GRID VOLTAGE WAVEFORMS WITH THE INDUCTIVE GRID CIRCUIT

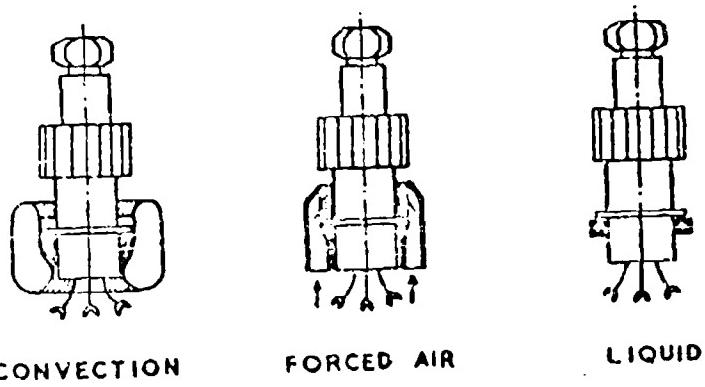


FIG. 6.
ALTERNATIVE COOLING ARRANGEMENTS

HIGH PEAK POWER MODULATOR
FOR RESEARCH IN PULSE COMPRESSION

by

R. Banks,

Marconi's Wireless Telegraph Company Limited.

SPECIFICATION OF EQUIPMENT.

The prime requirement of the equipment described below was that within two years of commencement of its design it should be available for the initial testing of the high power T.W.T. which forms its load. This precluded the application of advanced techniques beyond those essential to the fulfilment of the tight target specification on output waveform - e.g. thyratrons rated at 35 KV are being operated at only 25 KV, primarily because at the initiation of the development it was uncertain at what date the 35 KV thyratrons would be available and development had to proceed with over-run 25 KV thyratrons.

(Fig.1) shows the specified output voltage waveform having a guaranteed departure from an ideal flat pulse top of not more than 2% over the 4.1 μ s in which R.F. drive is applied to the T.W.T., and having a design target of individual fourier components of this departure from ideal of the order of 0.1% to 0.6%.

This output voltage is specified to be stable to 0.1% short term (1 second) or 0.75% medium term (5 minutes) and is developed at a peak power of 250 KW into a T.W.T. of nominal porveance 1.41×10^{-6} (1.25×10^{-6} minimum, 1.56×10^{-6} maximum), corresponding to 500 KV peak 500 Amps peak into 1000 Ohms mean resistance. Dynamic resistance of the load would be 670 Ohms but for relativistic corrections which increase it to 750 Ohms at the design working point.

Rated P.R.F. is 250 pulses per second corresponding to 250 KW useful mean output, but actual mean output including power in leading and trailing edges is 440 KW. This illustrates the point that 4 μ s pulse length is near to the economic minimum value practicable in a load of 1.4μ s at this peak power.

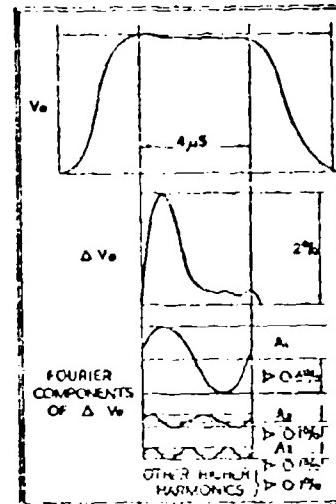


Figure 1.

GENERAL DESCRIPTION.

T.W.T. and Lead Shield.

The T.W.T. forming the lead is of 18ft to 20ft overall length, weighs about 5 Tons, and gives rise to an X-Ray flux of the order of 100 Rad/minute at 5ft distance, of which the significant components are at energies of from 500 KeV to almost 1 MeV. The resulting problem in biological shield design greatly influences the layout of the High Voltage circuitry shown in section in (Fig.2) together with

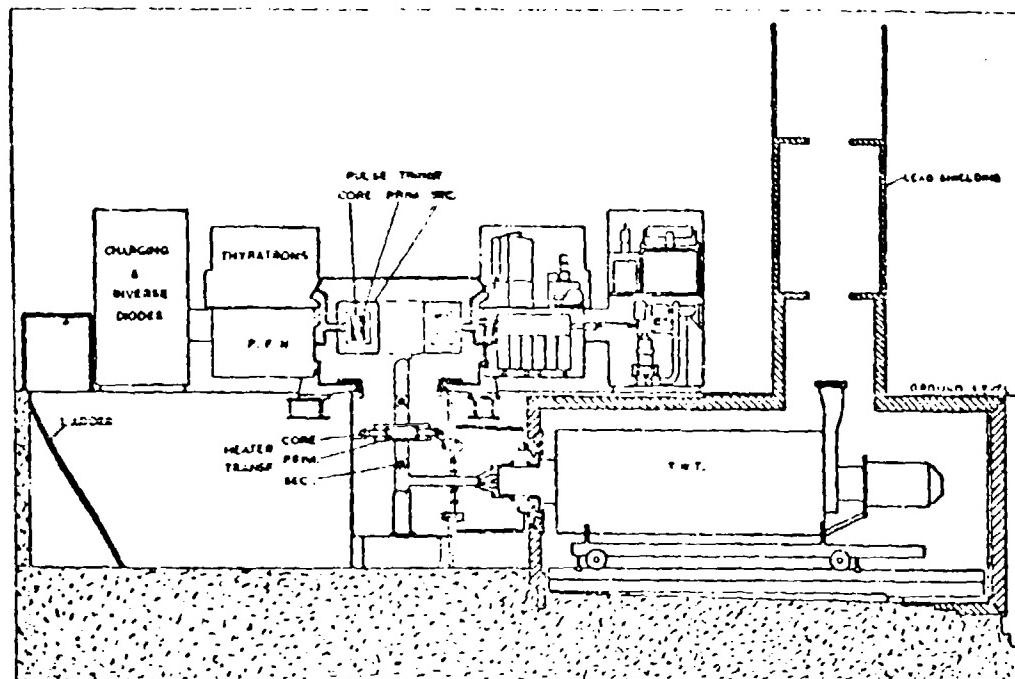


Figure 2.

the T.W.T., lead shield and low voltage circuitry. The T.W.T. with axis horizontal is carried on rails in a concrete pit with lead roof at the general ground level, lead doors close behind the T.W.T. to complete shielding of 8" lead or lead equivalent.

High Voltage Structure.

The cathode insulator of the T.W.T. protrudes through the smallest practicable aperture in the lead shield into a lightly screened (1 $\frac{1}{2}$ " lead) connection chamber which is oil filled but isolated from the main transformer tanks by a Perspex disc insulator in the plane of the current and voltage monitors. In this region, which is subject to high X-Ray flux, voltage gradients are held to 150 KV/inch maximum except on the T.W.T. itself. This connection tank, together with the oil filled tank of the main low capacitance heater transformer

of 8 KW 80 V 100 Amps 250 c/s rating, forms the biological shield for the X-Ray beam emergent via the cathode structure of the T.W.T. To minimise stray capacitance the main pulse transformer is placed immediately above the heater transformer and the heater and pulse transformer tanks form a single vacuum vessel for elimination of air bubbles from the high voltage structure during initial filling with Shell Diala B oil. This High Voltage structure, including the pulse transformer secondary, has a total shunt capacitance to ground of 430 pF, distributed as 150 pF Transformer, 80 pF T.W.T., and 200 pF heater transformer, monitors and connection chamber. These last three elements also form the X-Ray shield.

Low Voltage Structure.

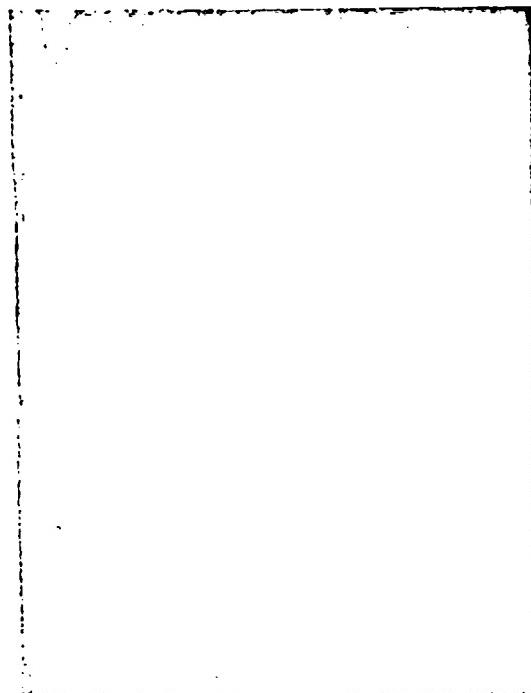


Figure 3.

The need for control of series stray inductance in the primary circuits of the pulse transformer has dictated the layout of the modulator shown by (Fig.3) which is a view from a 10 Ton overhead crane. Twelve identical P.P.H.'s operating in parallel are mounted in the six lower steel tanks around the central hexagonal pulse transformer tank. Thyatrons are mounted in the wire mesh enclosures, over the P.F.H.'s and the inverse diodes with their loads and the charging circuits are mounted in the six cabinets outside the P.P.H.'s.

theoretical 10 KW at 2.5^o magnetising current. This heat is removed from the vicinity of the core by forced oil distribution via the headers visible in (Fig.4) which are fed with 50 C.P.H. by a pump and oil to air heat exchanger system.

Primary Pulse Circuit.

The twelve parallel basic primary circuits are each as shown in (Fig.5). In the interim form of the modulator the main thyratron (V1) was a VX.3250 Hydrogen Thyratron over-run on anode current. In the final form of the modulator pairs of identical circuits in parallel operate from each of six VX.3336 Deuterium Thyratrons. To minimise effects of stray shunt reactances to earth one side of each P.F.N. is earthed at the cathode terminal of the Thyratron and considerable care has been taken in the arrangement of the main pulse circuit leads to obtain low loop inductance.

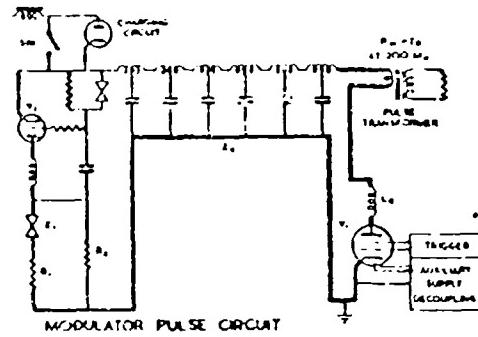


Figure 5.

Each of the twelve VX.3533 Deuterium Inveras Diodes is connected at the back of its associated P.F.N. of impedance Z_0 in series with an air cooled load R_1 , Z_1 ; R_2 of $R_1 \approx 0.7 Z_0$ and non-linear element $Z_2 \propto V^{-3}$. To protect against thyratron reverse conduction and consequent oscillatory discharge of the P.F.N. when the load short circuits ($R_1 + Z_1$) is made to equal Z_0 near to the full load short circuit condition. ($Z_1 = 0.2 Z_0$ at full load short circuit). To control the demagnetisation cycle of the pulse transformer $R_2 \approx 7 Z_0$ provides damping of the overshoot ($Z_1 \approx 7 Z_0$ at peak of magnetising overshoot).

The charging circuits, resonant at 250 P.R.F., have provision for insertion of a total of six English Electric Valve Co. AR.1121 thoriated filament air cooled external anode charging diodes for variable P.R.F. working during T.W.T. processing.

Power Supply and Control.

The main reservoir capacitor of 140 μF 13 KV rating is fed via a 2H choke with shunt surge protection by a non-linear resistor from an English Electric 6 phase full wave bridge mercury Excitron rectifier employing grid blocking for fault protection. The modulator is fed by a motor alternator set comprising induction motor, main and pilot alternator with magnetic amplifier automatic voltage controllers. Machine inertia and the voltage regulators provide stabilisation of supplies against mains supply transients and D.C. feedback to the

main A.V.R. stabilises the main H.T. against a reference source adjustable from the control desk ((Fig.6)), ... which full control and monitor facilities are centralised.

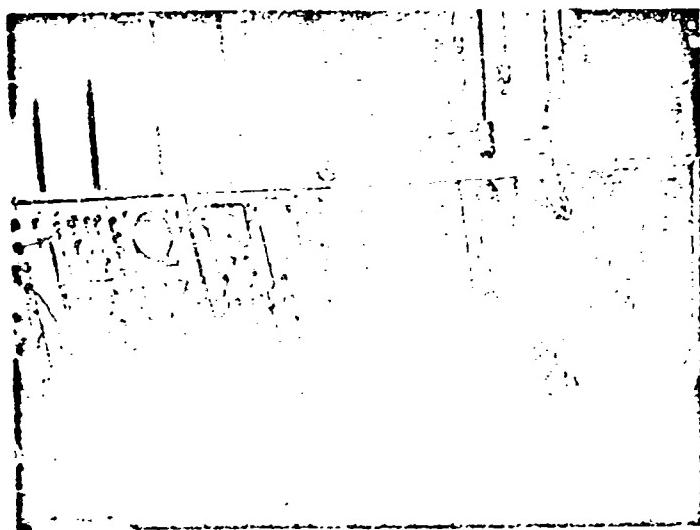


Figure 6.

Independently of A.C. and D.C. overload relays, high speed protection is provided by blocking of grid drive to modulator thyratrons and rectifiers. 48 individual transistor fault detectors of 2 μ s response time are fed from monitor points throughout the modulator and operate this protection. To assist in fault diagnosis, fault detectors indicate individually at the control desk the presence at the associated monitor point of a signal either above or below a preset reference level which may be constant or proportional to H.T. To test these monitors and fault detectors a routine periodically alters individual reference voltages to values which should produce fault detector operation with a normally functioning modulator. Simple transistor and diode logical circuitry separates modulator fault and detector test indications and, when necessary, programmes the transmitter for instantaneous shut down after a preset number of fault pulses, and also for H.T. lock off or recycle according to the nature of the fault.

METHOD OF DESIGN TO MEET THE PULSE SHAPE REQUIREMENT.

It was decided initially that it would be necessary to employ linear network theory throughout and to apply empirical corrections to the completed modulator to correct for the effects of the non-linear load. The mean value of load impedance has been employed in most of our work to permit experimental verification of the theoretical results but checks have been made of the effect of changing to the dynamic impedance.

Layout of the High Voltage circuitry was governed by the need to minimise shunt capacitance and thus power loss in the leading and trailing edges of the pulse. Complicating this were demands, firstly for good separation of the pulse transformer secondary windings from the voltage monitor capacity potentiometer so as to permit an accurate knowledge of the monitor capacity ratio from low frequency measurements, and secondly for large size to provide X-Ray shielding and to provide space for transient damping resistors should these prove necessary to reduce fault energy input to the T.W.T. in the event of flashing.

Once a provisional value of secondary capacitance had been derived, transient responses were computed for the load R and C fed via various values of series inductance with a Heaviside step as from an ideal P.F.N. plus thyratrons. The optimum value of series inductance was selected from the resulting graphs and was that which produced 1% overshoot.

Primary voltage was determined by the decisions to provide for initial operation with VX.3250 Hydrogen Thyratrons of 25 KV rating and to accept that in the final equipment subsequent 25 KV hold off working of the 35 KV rated VX.3336 would be justified as conducive to the high reliability of operation needed in a modulator operating several valves in parallel. This voltage determined the transformer ratio of 47/1 which, with the previous transient analysis, determined the required primary circuit inductance of about 0.6 μ H. At 25 KV each Thyratron requires a rate of rise inductance of 2.5 μ H, and four parallel VX.3336 Thyratrons which would meet the mean power requirement would thus contribute 0.625 μ H rate of rise inductance to the primary circuit. This would neither allow practical transformer leakage and circuit strays nor provide a design margin to allow for corrections of the linear load theory. Thus we adopted the present 6 valve layout in which rate of rise inductance contributes 0.4 μ H, leads 0.10 μ H and pulse transformer 0.15 μ H to a total of 0.65 μ H minimum achievable primary inductance. The end sections of the P.F.N.'s absorb 0.19 μ H of this, each of their twelve coils in parallel being made 2.3 μ H below theoretical value.

The need to minimise lead inductance and the convenient availability of 12 Pulse Transformer primary windings suggested that 12 P.P.N.'s would be desirable. Consultations with capacitor manufacturers confirmed this and showed that even with 12 P.F.N.'s it would be necessary to use only a small number of sections if the effects of capacitor lead inductance were to be corrected by adjustment of inductor mutual coupling. A small number of sections was also felt desirable to provide a large end section inductance to absorb circuit strays.

It was decided at this stage that equal capacitor networks were desirable both to assist in manufacture of close tolerance capacitors of equal temperature coefficients and temperature rise, and to avoid aggravating the capacitor lead inductance problem. It was decided on the basis of some provisional calculations of inter-section mutual inductance from section n of a P.F.N. to sect' ns n + 1, n + 2, etc., that in order to obtain adequate agreement of a manageable theory with the practical circuit it would be necessary to screen individual sections.

$$C = 0.094 \mu F. \quad L_s = 0.07 \mu H.$$

L_1	1.30 μH	M_1	0.41 μH
L_2	1.32 μH	M_2	0.52 μH
L_3	1.23 μH	M_3	0.52 μH
L_4	1.28 μH	M_4	0.48 μH
L_5	1.36 μH	M_5	0.38 μH
L_6	1.76 μH		

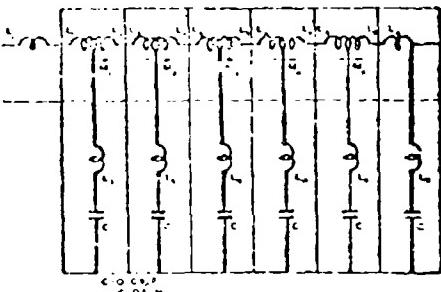


Figure 7.

Each section of the network was therefore designed, as shown in (Fig.7), as a T section and built with separate screens for the inductor and for the capacitor connected to its centre point. Series stray inductance of each capacitor was thus minimised and could be measured accurately. The theoretically required values of mutual inductance between the two halves of the inductor were adjusted to allow for the observed mean value of the capacitor inductance.

Component tolerances were expected to be better than $\pm 3\%$ relative, $\pm 5\%$ absolute, for capacitors or $\pm 2\%$ relative, $\pm 3\%$ absolute, for inductors. This has been achieved with an observed $\pm 1\%$ selection tolerance in the capacitors as received and temperature coefficients of 0.03 to 0.05% per $^{\circ}C$. With a statistical improvement of about $\sqrt{12}$ to be expected from the parallel connection of 12 networks, departures from calculated waveforms of the order of $\frac{1}{2}\%$ may be expected, with a small further error in pulse duration.

To achieve a theoretical waveform of a similar order of goodness has involved considerable computation. The basic approach has been to design a network by Guillemin's method, computing the component values for the equal capacitor form, and then to compute the pulse waveform in load $R = Z_0$ for the circuit so derived. It is a weakness of the iterative method of calculating the components of the equal c network that it has been necessary to work initially to 60 or more binary digits to obtain three significant figures in the final component values, but a programme to perform this realisation on a DEJCE computer has been prepared. Guillemin networks of the parabolic, cubic, and quartic forms of leading and trailing edges were explored. Designs to the cubic and quartic laws and of the higher number of sections tended to lead in general to networks not realisable in the equal capacitor form, or only marginally superior in performance to the parabolic type of the same number of sections. The parabolic rise case proved most promising and accordingly the graph shown in (Fig.8) was computed showing % ripple of the nominally flat top of pulses generated by 4, 5, 6 and 7 section networks of varying value of "a", the ratio of parabolic rise time to base-line pulse length.

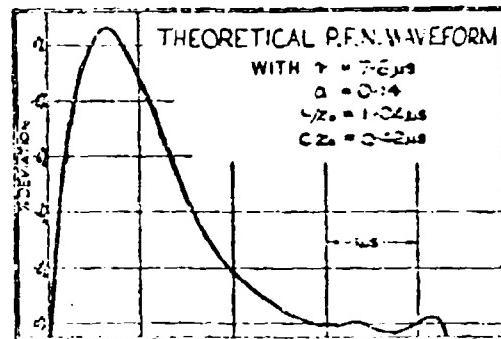
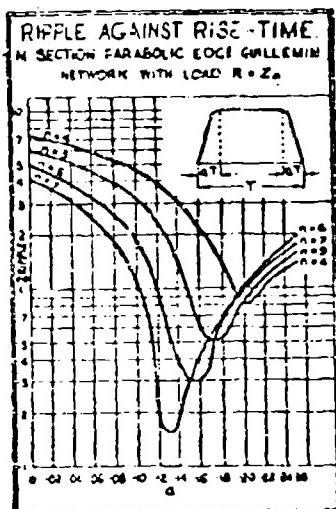


Figure 9.

Figure 8.

From this data the parabolic Guillemin network of six sections and $a = 0.15$ was chosen as giving acceptable ripple for minimum total energy storage and further computations made of the waveform developed in a load of $R = Z_0$ paralleled by C to give $Ck = 0.42 \mu s$ as in the expected high voltage circuit, and fed via an inductor of arbitrary value. The best results, as shown in (Fig.9), were obtained with $a = 0.14$ and $L/Z_0 = 1.04$ which led to the primary circuit inductance of $0.53 \mu H$ adopted in the final equipment. This allows $0.07 \mu H$ padding inductance for final empirical adjustment of the output waveform.

During this phase of trial and error selection of networks and of adjustment of the load inductance, we had initially believed that the major errors in our logical design process lay in the rounding off of infinite series at an arbitrary nth term. In the Guillemin method, however, a further discrepancy arises from the use with a matched load of a network designed by summing the periodic currents produced by n parallel sections each of L and C in series operating into short circuit and equating these to corresponding terms of a Fourier analysis of a repetitive waveform of the desired type. With the network we have adopted the computed output waveform in short circuit in an order of magnitude better than that in matched load. This emphasises the fact our design is essentially empirical and does not therefore necessarily produce optimum performance for the number of variables at our disposal. Though there is thus a theoretical need for further effort to be devoted to analysis of the network design problems - preferably of the P.F.N. coupled with the load L, C and R, we have already achieved a result adequate for the accuracy of construction practicable in our high power equipment, and have not therefore continued this work.

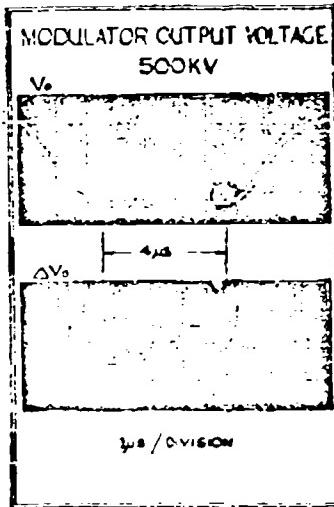


Figure 10.

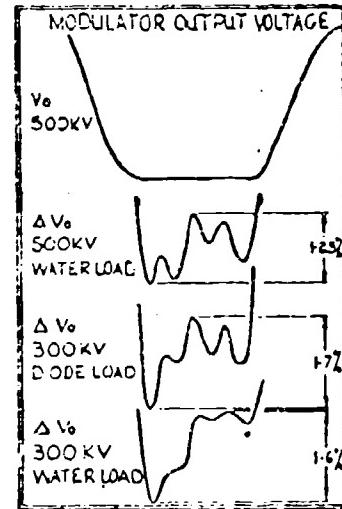


Figure 11.

OPERATING EXPERIENCE TO DATE.

A photograph of the typical output voltage waveform obtained at 500 KV into linear load is shown in (Fig.10). To measure the waveform errors two independent methods have been adopted, one by photographic enlargement of a well focussed oscilloscope trace and, for normal use, the more convenient one shown in (Fig.10) of electrical "windowing" or selection of only the pulse top for amplification prior to display. These methods agree well and (Fig.11) shows typical waveforms as obtained at 500 KV into matched resistive load, 300 KV in $I = KV^3/2$ diode load, and 300 KV in a resistive load equal to diode mean impedance at that level. Waveform is naturally dependent on the load but a top flat to within the guaranteed 2% has been achieved and fourier components with the exception of the fourth are generally within specification. The cause of this ripple in the pulse top has not yet been investigated as our main effort has been centred on the testing of a "Short Diode" - comprising the cathode, anode and collector of the final T.W.T. with slow wave structure omitted.

With the "Short Diode" in circuit operation at up to only 350 KV to 380 KV has proved practicable as severe flashing of the diode occurs at this level. This has caused no problems in modulator operation but even with next pulse shut down of the modulator following a flash the normally beneficial spot knocking process ceases to improve the Short Diode at this level.

This raises an interesting problem in valve protection on which we are at present collecting data illustrated by (Fig.12) which is compiled from photographic records not suitable for reproduction. The three modulator output waveforms are on identical time and amplitude scales.

The first shows normal output at 320 KV. The second is typical of the output current when the "Short Diode" flashes and was recorded at 320 KV following very similar flashes at 325 KV, 325 KV, 340 KV and 345 KV spread over 6 minutes operation. The third waveform is an abnormal one occasionally observed. This record was obtained 1 minute after the record above and this flash was followed by others at 200 KV from which recovery to even 280 KV took 20 minutes. Though the severe 9 Mc/s ring of the modulator high voltage system on short circuit has been observed only occasionally the correlation between this and apparent damage to the "Short Diode" appears to justify inclusion in the modulator of a series damping circuit in the high voltage lead as close as possible to the "Short Diode".

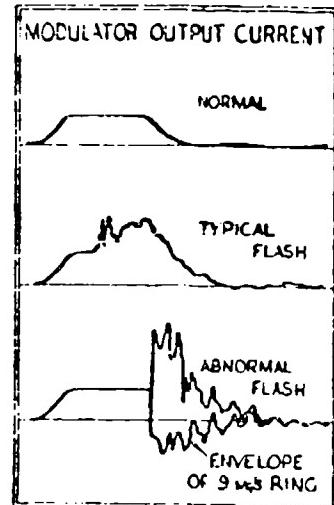


Figure 12.

To hold off stray capacitance from the T.W.T. or "Short Diode" and to damp the 9 Mc/s ring discussed above, a damping circuit of $R = 100 \text{ Ohms}$ and $L = 5 \mu\text{H}$ in parallel is to be included in the modulator high voltage lead. Operation of a complete T.W.T. which should be available shortly will then take precedence over other work, which will include investigation and improvement of the output waveform after full power operation has been achieved by either modulator or T.W.T. modification. Life experience at full power has so far been limited by flashing of the "Short Diode" and by the VX.3250 Thyratrons which have been run to the 50% overload necessary for full output for only limited periods. With the VX.3336 Thyratrons now in circuit, further life experience is urgently required and will be obtained with T.W.T. load if possible or, failing this, with resistor load.

ACKNOWLEDGMENTS.

I thank the Director of Research of Marconi's Wireless Telegraph Company for permission to publish this interim description of our work to date. I wish also to thank Mr. J.W.E. Jones of Marconi's Wireless Telegraph Company who has supplied most of the detailed information summarised here.

A SIMPLIFIED MODULATOR FOR LONG PULSES AND HIGH MEAN POWER

by

N. S. Nicholls, B.A. and R. E. Jarvis, B.Sc.(Eng.)

R.R.E., Malvern, England

1. Introduction

The modulator to be described, which is now nearing completion, is rated at 400 kW mean power and 40 MW peak power, with a nominal pulse length of either 200 μ sec. or 67 μ sec. It was designed as a test source for the VX 523 klystron. The cost was to be kept to a minimum, and the installation was to fit into existing accommodation with limited internal floor space.

The majority of high power modulators, whether of network, hard-valve or floating-deck type, contain a D.C. energy-storing or smoothing capacitor in which the energy stored is often ten times greater than the energy contained in a single pulse. This component is large and costly, and gives rise to the problem of diverting the stored energy on the occurrence of a fault.

The capacitor has been eliminated by employing an A.C.-charged network-type modulator, resulting in an appreciable saving in size and cost. The total energy stored is never more than the pulse energy, which has a maximum value of 8000 joules. Thus the problem of energy diversion, while not eliminated, is alleviated.

In order that the A.C.-charged modulator presents a balanced load to the three-phase supply, with a reasonably high power factor and low harmonic content, three pulse-forming networks are employed. These are charged sequentially via a network of valves, which also eliminates D.C. in the supply transformer.

2. Basic Circuit

The basic circuit of the modulator is shown in Fig. 1.

An 11 kV 50-cycle 3-phase A.C. supply is fed via a tapped auto-transformer with off-load tap changing, which is used as a coarse control of modulator output voltage, and a double-wound step-up transformer. To the secondary winding of this transformer are connected 6 valves arranged as in a 3-phase bridge rectifier circuit. The circuit differs from a 3-phase bridge however, in that the cathodes of the valves V_1 , V_2 and V_3 are not strapped together but are each connected to a charging reactor and pulse-forming network. These three valves are grid-controlled charging thyratrons whose firing determines the times of commencement of the three separate charging periods of the three networks, relative to the supply voltage waveform. Delayed firing is essential in order to secure time for the recovery of

valves associated with the discharge circuit, as will be shown later. Variation of grid firing phase is used to control the output of the modulator.

The charging current of each network is an approximate half-sine-wave whose duration is determined principally by the product LC where L is the inductance of each charging reactor and C is the total capacity of one pulse-forming network. The charging current returns to the supply via the three return diodes V_4 , V_5 and V_6 , between which there is free commutation.

Each pulse-forming network has its own discharge thyratron, the cathodes of these three valves V_7 , V_8 and V_9 being strapped together and connected to the primary winding of the pulse transformer.

There are two principal modes of operation as shown in Fig. 2. (A) The three networks may be charged in succession and discharged simultaneously, with a pulse repetition frequency equal to the frequency of the supply. (B) The three networks may be charged and discharged in succession, independently, giving a pulse repetition frequency equal to 3 times the supply frequency.

In mode (A) the impedance of each network must be equal to 3 times the effective load impedance, since the 3 networks are discharged in parallel. In mode (B) the impedance of each network must be nominally equal to the effective load impedance. The change from mode (A) to mode (B) is conveniently made by removing the network coils and replacing them with coils of one-ninth the inductance. This changes the network impedance from 18 ohms to 6 ohms, and the nominal pulse length from 200 microseconds to 67 microseconds. At the same time the triggering of the discharge valves is rearranged. The mean power and peak power remain the same.

It will be apparent that sufficient time must be allowed between successive charging periods for the pulse-forming networks to be discharged and for recovery of valves associated with the discharge. However, the charging periods should not be made shorter than is necessary, otherwise the charging current becomes more peaky, its R.M.S. value increases and the utilisation factor of the supply decreases.

3. Charging Circuit

Let us now consider the charging of the pulse-forming networks in more detail.

The upper set of sine waves in Fig. 3 represents the phase voltages of the supply, that is the voltage of the three bushings with respect to the star point. Consider valve V_1 fired at the angle ϕ_1 , as the voltage of red phase is approaching its maximum positive excursion. An approximate half sine wave current flows into network 1 via L_1 , returning initially to the phase which is most negative with respect to the red phase, i.e. to yellow phase, through diode V_5 . At the instant ϕ_2 , blue phase becomes more negative than yellow phase so the current transfers from V_5 to V_6 . The current decreases to zero at the angle ϕ_3 , and V_1 and V_6 extinguish leaving

network 1 fully charged. Networks 2 and 3 charge in similar fashion, through valves V_2 and V_3 as yellow and blue phase become positive in turn.

During the charging of network 1, the voltage applied to the charging circuit, v_c , during the interval from ϕ_1 to ϕ_2 is the difference between red phase and yellow phase, which is the line voltage of red with respect to yellow, and from ϕ_2 to ϕ_3 it is the line voltage of red with respect to blue. The voltages applied to the three charging circuits are therefore as shown in the lower waveforms of Fig. 3. At the assumed angle of firing, ϕ_1 , the value of v_c is almost equal to the peak line voltage, and it remains near to the peak line voltage over the whole charging period. Because of the well-known transient behaviour of an LC circuit the network voltage swings up to approximately twice the mean value of v_c over the period of current flow, i.e. for the interval of conduction shown it approaches twice the peak line voltage of the supply.

Let us define a quantity β which is the ratio of the natural resonant frequency of the charging circuit to the supply frequency, i.e. $\beta = \frac{1}{\omega \sqrt{LC}}$.

The behaviour of the circuit has been computed for several values of the parameter β and for a range of values of the firing angle ϕ_1 , assuming a lossless charging circuit, and free commutation between the return diodes at the fixed angle ϕ_2 , at which one line voltage is zero. For any given value of ϕ_1 , the greater the value of β the greater the peak charging current and the shorter the duration of current flow. The value chosen for β must be large enough to ensure that the interval remaining between successive charging periods is never less than the required minimum for any value of ϕ_1 likely to be used, but no longer than necessary.

In the modulator under construction β is 1.70 giving (at the smallest value of ϕ_1 which is used) a maximum charging period of 106° and a minimum interval between charging periods of 14° , corresponding to 780 μ sec. The desired value of β is obtained by appropriate choice of the total charging circuit inductance L , since the network capacity is fixed by the desired network impedance and pulse length. In the present case, the total value of L is 0.53 henry of which 0.50 henry is in the charging reactor itself and the remainder is in the transformer and supply reactance.

As the value of ϕ_1 is increased, for a fixed value of β , the charging period decreases slightly, while the peak charging current falls off rapidly, resulting in a decrease in the voltage obtained on the pulse-forming network. Variation of ϕ_1 can therefore be used to control the power output from the modulator. The form of variation obtained is shown in Fig. 4. The angles on the horizontal axis are referred to the instant when red phase voltage passes through zero, going positive. Over the range of ϕ_1 from 45° to 155° , which is what we propose to use, the ideal network voltage, expressed as a multiple of the peak line voltage of the supply transformer, varies from 1.91 to 0.67, giving a variation in output from full power to $\frac{1}{8}$ power.

The valve used in the charging position (and also in the charge position) is a deuterium filled thyratron, the VX 3356. The current

through the valve is 10 amps and the maximum inverse voltage is equal to the pulse-forming network voltage, which is 51 kV. The maximum inverse voltage on the return diodes is ideally equal to the peak line voltage of the supply transformer which is in the region of $16\frac{1}{2}$ kV, so that one can use a valve with a considerably lower inverse voltage rating than the charging valve. For this reason, and for economy, the 3V/561E hot-cathode mercury valve has been chosen.

The return diodes are in fact triodes, in order that they may be cut off for fault suppression. The grids are driven by a rectified 10 kc/s sine wave which is square-wave modulated at 50 c/s in phase with the anode voltage, so that each valve is free to conduct when the anode is positive. Care is taken not to excite the grid when the anode is negative because this results in increased sputtering of the anode by ion bombardment and consequent deterioration of the insulation to both grid and anode.

Fig. 5 shows the transformer secondary current waveform for two values of ϕ_1 . When ϕ_1 is greater than ϕ_2 , which is 90° , there is no commutation between return diodes, i.e. the charging current returns through one diode only. The utilisation factor of the transformer for $\phi_1 = 45^\circ$ is 0.81.

4. Pulse Circuit

Each of the three pulse-forming networks (Fig. 6) consists of 10 equal capacitors, each of $0.57 \mu F$, and a long single-layer tapped coil. One side of the network is earthed, the load being placed in the common cathode circuit of the three discharge valves. This simplifies insulation problems, particularly within the capacitors themselves, resulting in a smaller capacitor bank; it eliminates problems due to the capacity to earth of the network; it also means that the currents in the various auxiliary valves associated with each network (other than the discharge thyratrons) do not pass through the load, and thus avoids problems arising from interaction between the three sections of the modulator. The disadvantage of having the cathodes of the discharge valves at high potential (this also applies to the charging valves) is overcome by the design of a special valve mounting box for the VY 3336, (Fig. 7) containing all necessary auxiliary supplies, together with control, pressure monitoring and protective circuits, and isolating coils for the cooling water supply.

Fig. 8 is a diagram of one of the three pulse-forming networks and its associated valves.

As with the majority of high duty ratio modulators, one of the more difficult aspects of the circuit design is to ensure recovery of the discharging thyratron. The problem is aggravated by the non-linear nature of the load which causes the network to be left positively charged when working at low voltage.

We aim to achieve recovery by the use of a tail-biter thyratron, which is triggered immediately after the end of the main pulse. If the load impedance is high the tail-biter will conduct, short-circuiting the network, and sending a negative voltage wave to the back end. Since the cathode of

the tail-biter is biased to -400 volts the anode of the discharging thyratron is forced down to about -350 volts. The voltage on the cathode of the discharging thyratron is determined by the decay of the pulse transformer magnetising current through the overswing diode and non-linear resistor, and by appropriate choice of the latter can be arrested at not more than 200 volts negative. We are thus left with a reverse voltage of 150 volts across the discharge thyratron, to enable it to recover. If the load impedance is low there will of course automatically be a reverse voltage, limited by the inverse diodes to about 500 volts at full power.

Following once more the case of high load impedance, the falling wave front caused by the firing of the tail-biter travels to the back end of the network, producing a negative voltage there half a pulse length later and causing the inverse diodes to conduct. The inverse diode load is designed to have an impedance about $1\frac{1}{3}$ times the network impedance, so that some negative voltage remains temporarily on the network, and a negative wave returns to the front end. Now the anodes of the inverse diodes are also returned to -400 volts, so that when this negative wave reaches the front end of the network, the anode of the tail-biter is taken negative with respect to its cathode. Thus the tail-biter is given its chance to recover.

The pulse transformer ratio is such that the networks are matched to the load at $7\frac{1}{3}$ of full network voltage. The maximum positive residual network voltage occurs at $2\frac{2}{3}$ of full voltage and is about equal to the maximum negative residual voltage, which of course occurs at full voltage. This condition minimises the required power rating of the inverse diode series resistors.

An upper limit to the value of these resistors is set by the need to remove substantially all reverse voltage from the networks before recharging commences. In addition the peak reverse voltage occurring at the back end of the networks must be limited to protect the charging valves from excess forward voltage.

The mean currents flowing from the -400 volts bias supply through the inverse diodes and through the tail-biter are in opposition so that the total current drain on this power supply is quite small.

The primary function of the crowbar tube is to divert energy from the load in the event of an arc in the load. It also serves to protect the comparatively small tail-biter and inverse diodes from the consequences of flashever. The crowbar is triggered from high speed overcurrent detection circuits, short-circuiting the pulse-forming network, and at the same time the grids of the charging valves and return diodes are suppressed for a few seconds.

The load fault current flows through the leakage inductance of the pulse transformer, which is quite large, - about $60 \mu H$. referred to the primary - and if one merely short circuits the source of energy the fault current will decay only slowly, with a time constant of several hundred microseconds. In order to force the current down within a few microseconds

it is necessary to return the cathode of the crowbar to a capacitor charged to a large negative potential. The crowbar has to hold off a forward voltage of about 41 kV at full power. The valve used is an ignitron type BK 178, and it is fired by discharging a capacitor charged to 1 kV into the ignitor circuit by means of a cold-cathode thyratron.

5. Triggering

It will be apparent that the triggering of the various valves in this modulator must be carefully controlled in order to ensure that the required interval between charging periods is maintained, that the pulse occurs at the optimum instant within the interval and that all valves are given ample time for recovery. A schematic diagram of the arrangements is given in Fig. 9.

The firing signals for the 3 charging thyratrons are derived from a voltage transformer on the incoming high voltage supply. The 3-phase output from the transformer drives regenerative peaking transformers which produce pulses variable in phase over a minimum range of $\pm 10^\circ$. These are fed to the grids of the charging thyratrons via step-up pulse transformers having high voltage insulation between primary and secondary. The square-wave gate for the 10 kc/s grid drive on the return diodes is derived from the same voltage transformer but is fixed in phase.

The firing signal for the discharging thyratrons must be related to the cessation of charging current and this event is detected by saturating current transformers. The signals from these transformers are fed into variable delay units, which give the delay necessary to allow the charging thyratrons to recover, and are then used to lock separate trigger pulse generators, which fire the discharging thyratron via insulated pulse transformers.

Signals from these three trigger pulse generators are also fed to three more variable delay units which in turn feed the tail-biter trigger pulse generators.

The inverse diodes are in fact triggered diodes containing a grid and are fired automatically whenever forward voltage appears on them, by means of a high vacuum diode connected between anode and grid. This system responds to both high and low rates of change of voltage, ensuring that the inverse diodes will function under all conditions and reducing the chances of over-charging of the pulse-forming networks.

6. Pulse Transformer

The pulse transformer, of which the main parameters are given in Fig. 10, steps up the modulator output pulse from ± 14.7 kV, 2,600 amps to ± 240 kV 170 amps. In the design of the unit major importance has been attached to the mechanical design, to the thermal characteristics, and to the high voltage insulation, the leakage inductance and distributed capacity being regarded as less important.

8. Conclusions

It might be objected that the modulator, although simple in principle, is rather complex in its realization. However, in making comparison with possible alternative forms of network-type modulator for the same purpose the following points should be borne in mind.

- (a) The high average power output of 400 kW in relation to the available thyatrons dictated the use of three discharging valves operating in parallel. Separate pulse-forming networks are advisable.
- (b) The high duty ratio of .01 in combination with the non-linear load, dictated the use of controlled charging, tail-biters, and a pulse-transformer overswing diode.
- (c) Safety as well as valve ratings dictated the use of at least two independent reverse diodes per pulse-forming network.
- (d) Crowbar provision is necessitated by the long pulse length and maximum stored energy of 8000 joules.

When these factors are taken into account, it will be appreciated that a conventional D.C.-charged modulator would require even more than the 25 high-voltage gas-filled valves employed here.

Further, in this modulator, the number of passive high power components has been reduced to an absolute minimum. The absence of a D.C. smoothing circuit means that the modulator will be free from the transient overvoltages which occur in many D.C.-charged modulators, particularly on the occurrence of an arc-through in the discharging thyatron.

It is hoped to have the modulator in operation within the next 3 months.

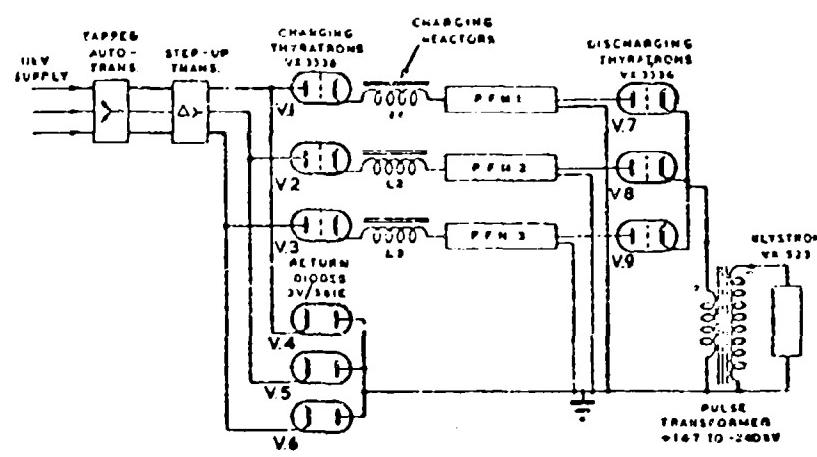


FIG. I
BASIC CIRCUIT

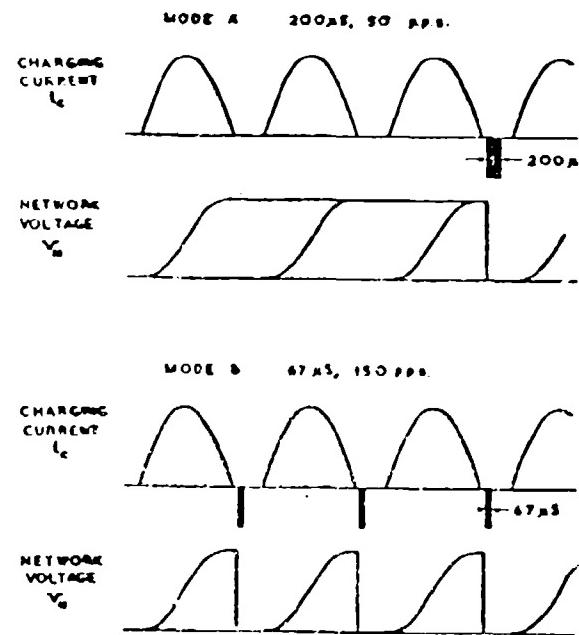


FIG.2.
MODES OF OPERATION.

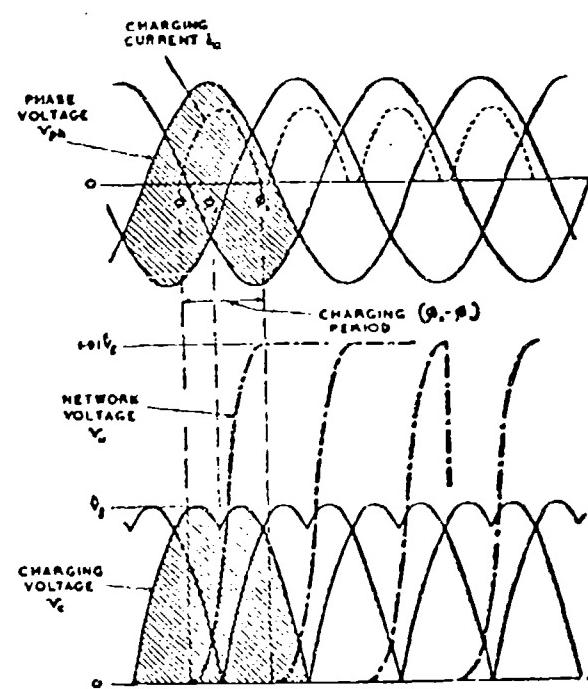


FIG: 3.
CHARGING WAVEFORMS.

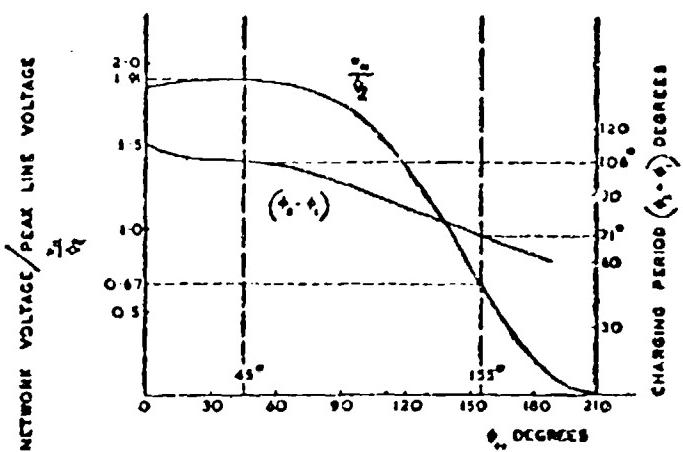


FIG. 4

NETWORK VOLTAGE AND CHARGING PERIOD,
AS A FUNCTION OF FIRING ANGLE ϕ_0 ,
FOR $\beta = 1.70$

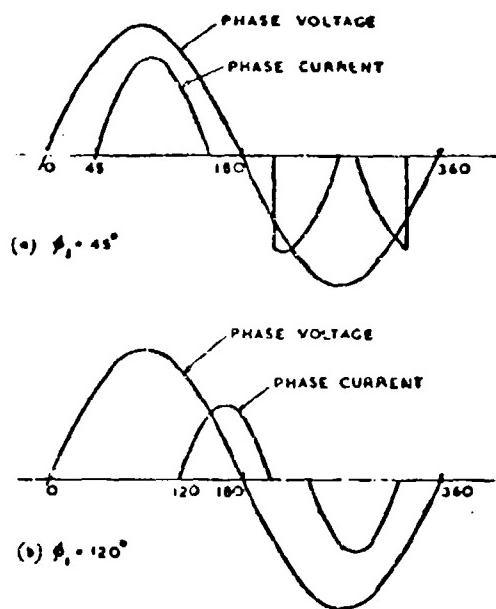


FIG. 5.
TRANSFORMER SECONDARY CURRENT.

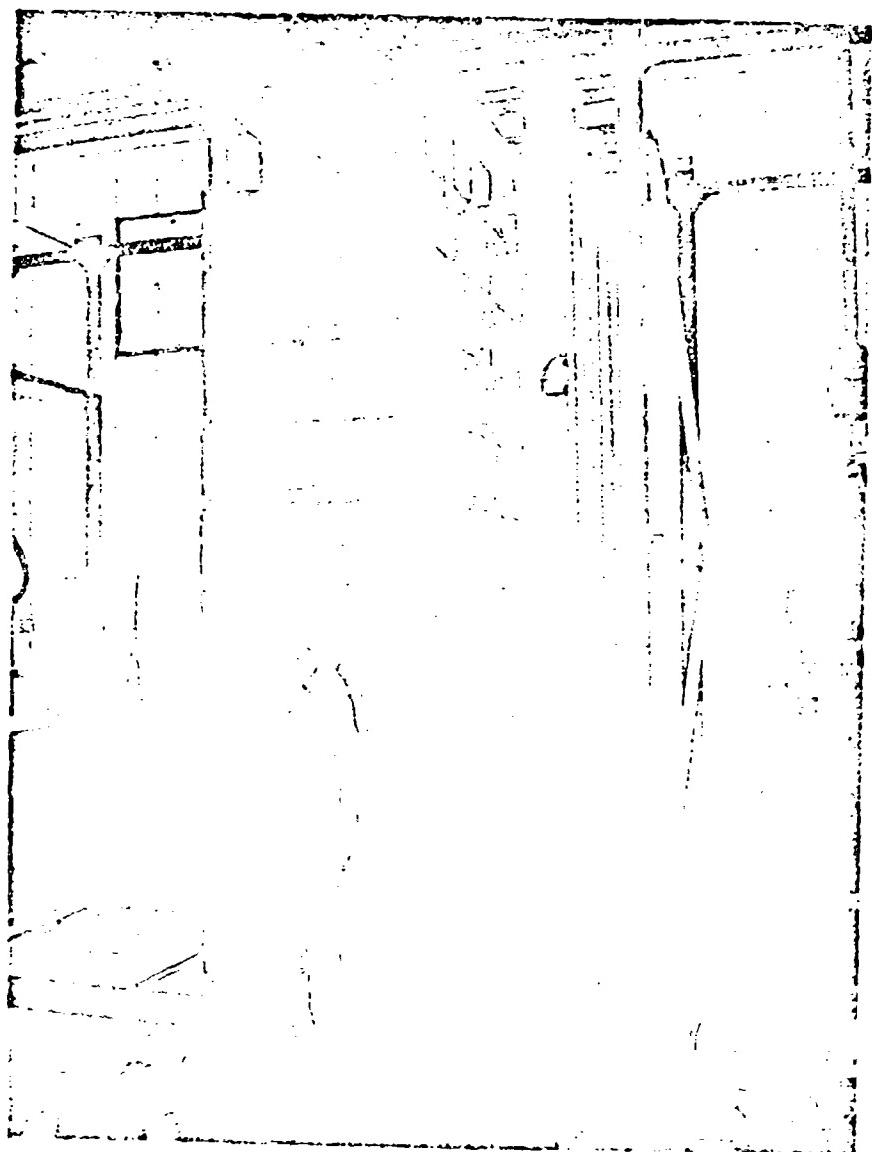


FIG. 6.

PULSE-FORMING NETWORKS

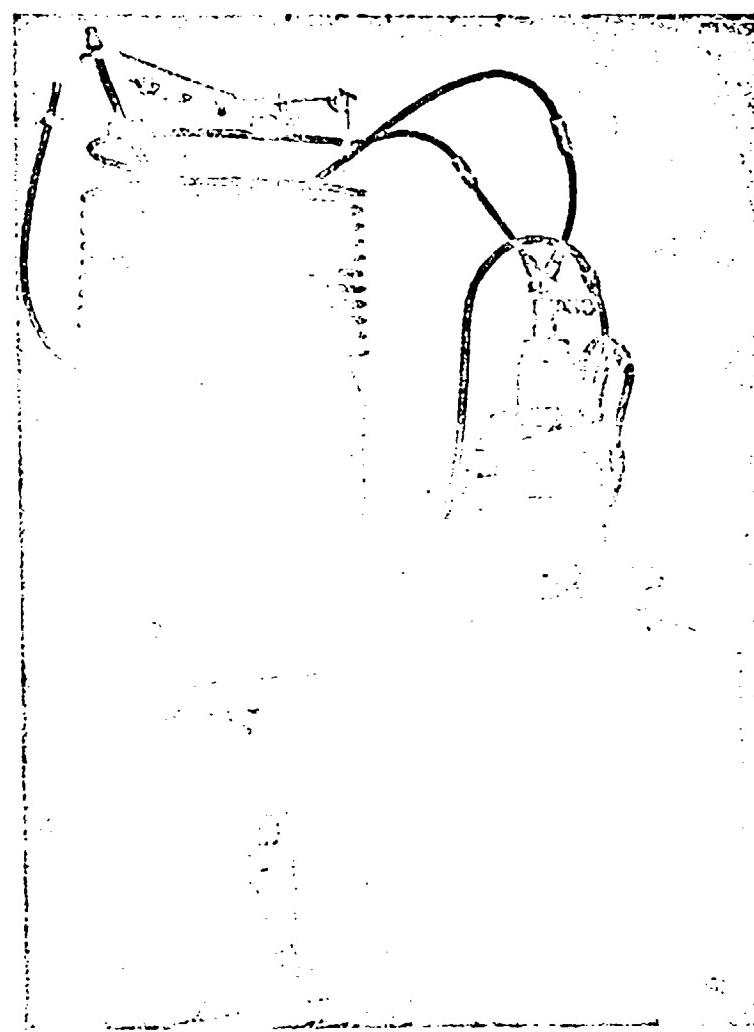


FIG. 7.

VX 3336 IN MOUNTING BOX

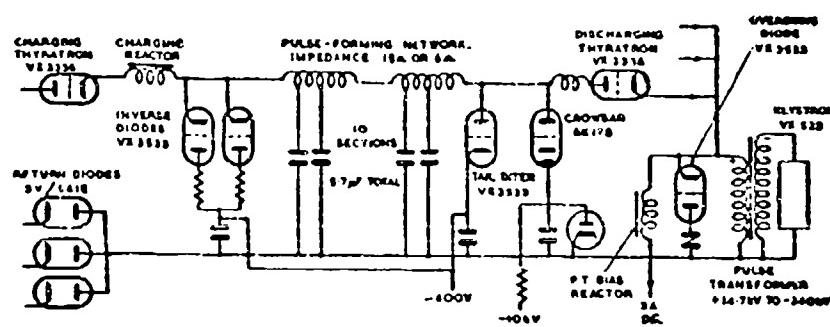


FIG. 8.
PULSE CIRCUIT.
(ONE THIRD OF MODULATION)

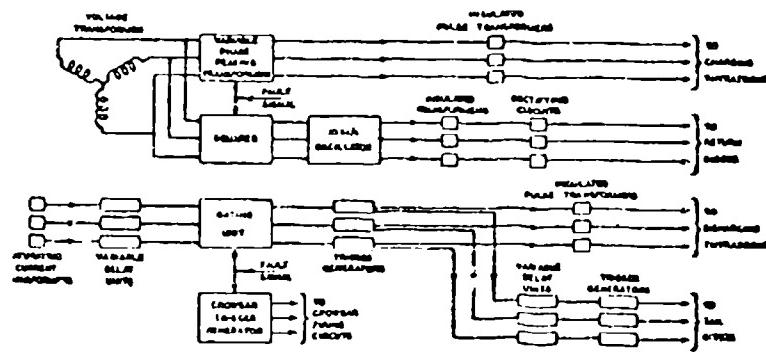


FIG. 8
TRIGGERING DIAGRAM

Input voltage	14.7 kV	Output voltage	24.0 kV
Input current	2,800 A.	Output current	170 A.
Primary turns	38	Secondary turns	628
Mean power	400 kW	Duty ratio	0.01

Core:- Material 0.004" grain-oriented silicon steel strip.
 Core circle diameter 9 ins.
 Window 25 ins. x 8 ins.
 Nett core area 52.5 sq. ins.
 Mean path 94 ins.
 Weight 1,300 lbs.

Flux swing -0.8 to +0.8 webers per sq. metre.

Magnetising current	1%	Primary copper loss	1½ kW
Core loss	3½ kW	Secondary copper loss	2½ kW

Winding spacing, low voltage limb 7/8 ins.
 Winding spacing, high voltage limb 1¾ ins.

Leakage inductance referred to primary	60 µH.
Leakage inductance referred to secondary	16 mH.
Distributed capacitance referred to secondary	250 pF.
Estimated load capacitance	250 pF.

FIG. 10 PULSE TRANSFORMER PARAMETERS
(For 200 Microsecond Pulses at 50 P.P.S.)

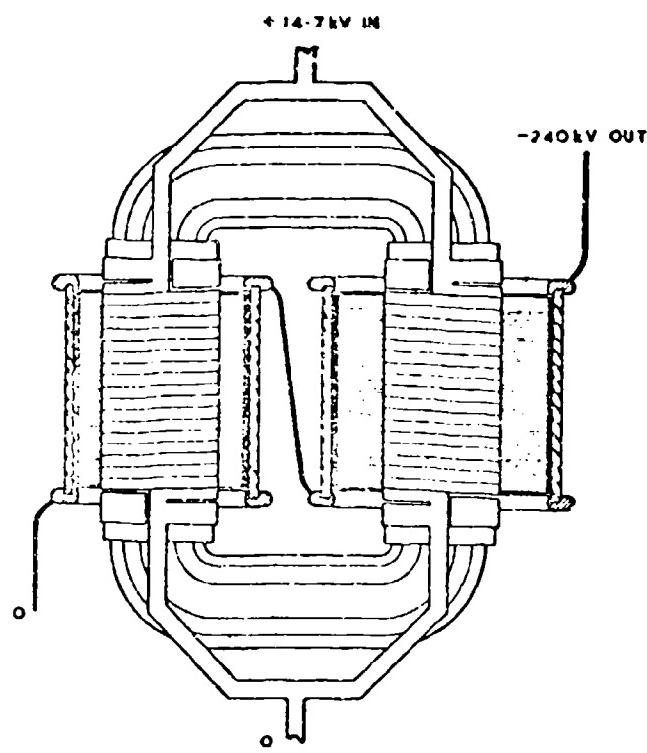


FIG.II.
PULSE TRANSFORMER SCHEMATIC DIAGRAM.

PERFORMANCE TESTS AND LIFE DATA OF THE 36-MEGAWATT
MODULATORS DEVELOPED FOR THE ASTRON 1000-MEGAWATT
ELECTRON ACCELERATOR

by

Vernon L. Smith

Lawrence Radiation Laboratory, University of California
Livermore, California

Summary

A 36-megawatt modulator, utilizing a Type 5949A hydrogen thyratron has been developed to pulse magnetic cores used in the 1000-megawatt peak-power Astron linear electron accelerator. The accelerator will be used for the injection of electrons into a thermonuclear fusion experimental device, called the Astron, which is now under construction at the Lawrence Radiation Laboratory in Livermore, California.

The type 5949A hydrogen thyratron is run at 32 kV, 2500 amperes peak current (5X rating), 0.4- μ sec pulse length, and at 60 pps. The system requires 500 thyratrons operated in parallel which results in a peak-power output of over 15,000 megawatts.

Data will be presented on the following subjects:

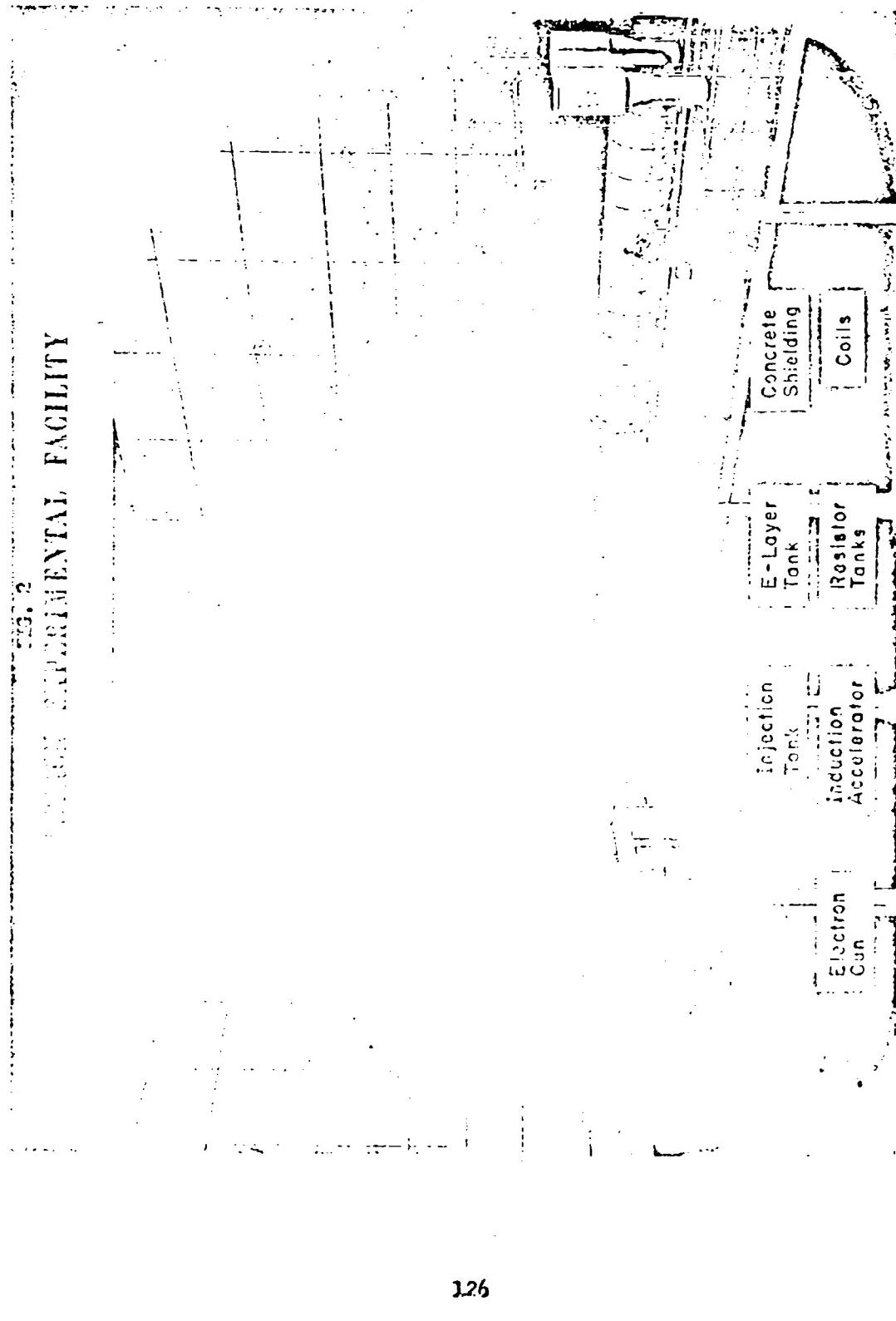
- A. General description of the accelerator and modulator.
- B. Performance tests of the 36-MW modulator.
 - 1. Peak current
 - 2. Hold-off voltage and tube aging procedure.
 - 3. Peak power.
 - 4. Average power.
 - 5. Trigger characteristics.
 - 6. Prefire characteristics.
 - 7. Output pulse shape.
- C. Life data of the 36-MW modulator operated at 28 to 32 kV, 60 pps.
 - 1. Switch tube, Type 5949A, used at 2500 amperes peak.
 - 2. Pulse-forming network (RG-218/u at 32 kV).
 - 3. Load cables, RG-213/U.
 - 4. Connectors.

Introduction

A possible method to attain the long-sought goal of a controlled thermonuclear reaction is to utilize high-energy electrons to produce magnetic confinement and, simultaneously, heat the plasma by transfer of some of the electron energy to the plasma particles.

The Astron¹ thermonuclear fusion experimental device, (see Figs. 1 & 2) which is now under construction at the Lawrence Radiation Laboratory in Livermore, California, will be used to determine if these principles can be utilized to make a power-producing fusion reactor. A 1000-megawatt, linear

Fig. 2
SUBSIDIARY FACILITY



electron accelerator²⁻⁴ capable of producing a relativistic beam of electrons of high intensity and quality is required to perform these experiments. Table I lists the specifications for the accelerator.

TABLE I
Accelerator Specifications

Electron energy	5 MeV
Peak beam current	200 amperes
Peak beam power	1000 megawatts
Pulse length of $\pm 0.5\%$ flat portion	0.25 μ sec
Repetition rate, variable	0 to 60 pps
Energy spread (during the pulse and/or from pulse to pulse, and at a variable repetition rate)	$\pm 0.5\%$
Beam diameter	~1 cm
Beam quality	$< 10^{-2}$ radian - cm

Development of Core Pulsing Requirements

After considerable study by the Physics Staff of the Lawrence Radiation Laboratory, it was decided to build an accelerator utilizing a basic induction principle,⁵⁻⁷ known for many years, but never before employed in a practical linear accelerator. This basic principle is to use an accelerating induction electric field generated by changing the magnetic flux in a ferromagnetic material. This method is inefficient with low beam currents because of the extremely high exciting currents of known magnetic materials. An efficiency approaching 10% may be realized in the Astron accelerator when operating at beam currents of 200 amperes. An increase in the number of primary turns affects the input impedance, as in a pulse transformer, but results in a corresponding stepdown of accelerating potential. The Astron accelerator is designed⁸ to utilize tape-wound, toroidal, doughnut-shaped, magnetic cores with the electrons accelerated through the center of the core. Figure 3 is a diagram of the principle using axial symmetry in the core material. A one-turn primary is used in order to keep the system voltage as low as possible. This results in a one-to-one pulse transformer and a large number of cores (429) are needed in series to obtain the required output energy.

The choice of magnetic material vastly affects the core modulator requirements because the pulse permeability⁹ (at 0.4 μ sec) can easily vary orders of magnitude depending on material composition, thickness of lamination, and annealing methods.

Many different materials were tested^{10,11} and optimization studies were made comparing the combined costs of magnetic materials and pulse modulator systems. One-mil, 50% nickel-iron, tape-wound cores were found to represent a reasonable compromise. The final design uses two sizes of cores: The electron gun section uses forty-five 18-inch i.d. \times 33-inch o.d. \times 1/2-inch-thick cores; the eight accelerator sections (48 cores each) use 384 eight-inch i.d. \times 24-inch o.d. \times 1/2-inch-thick cores. See Fig. 4 for a side view of the complete accelerator.

The large cores will be pulsed to 16,000 volts and the small ones to 12,000 volts. Under optimum conditions this would yield an output of 5.32 MeV, however, beam loading effects and variations of the magnetic properties between cores (as much as $\pm 30\%$) will reduce the output.

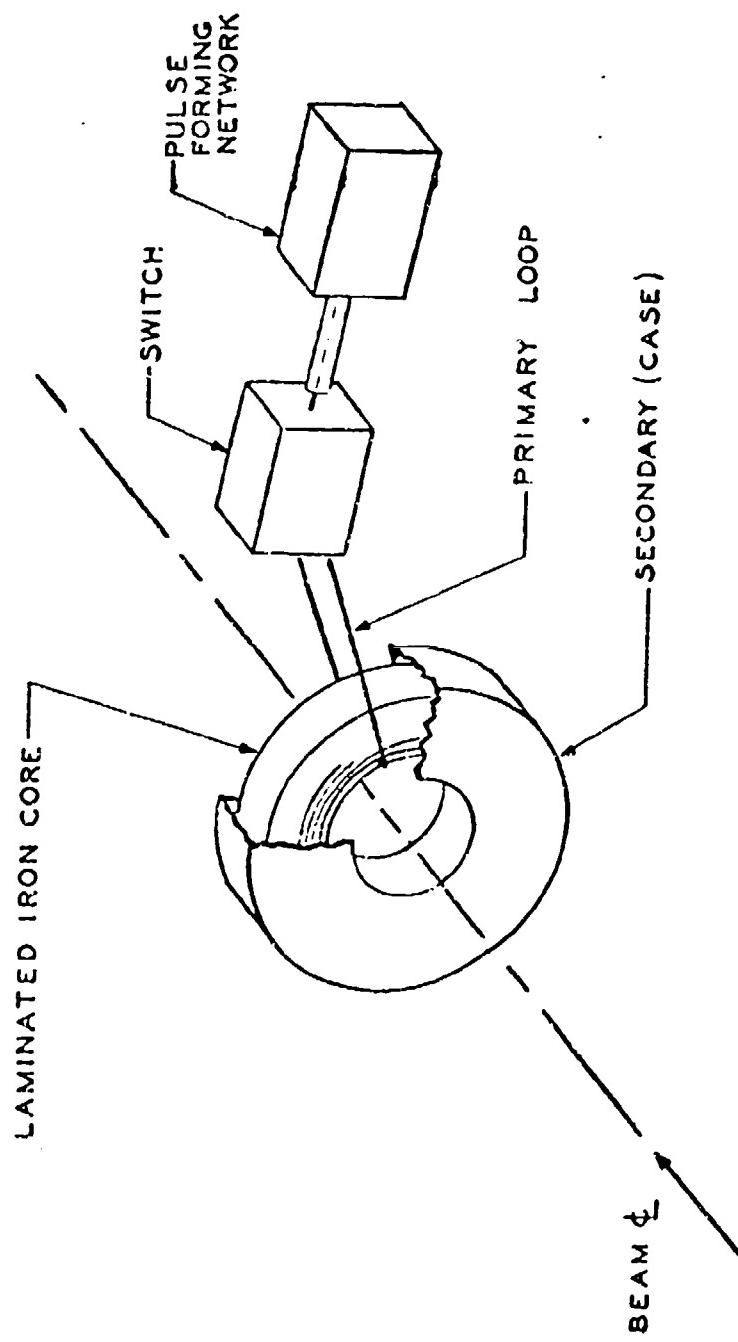


FIG. 3 INDUCTION ACCELERATOR PRINCIPLE

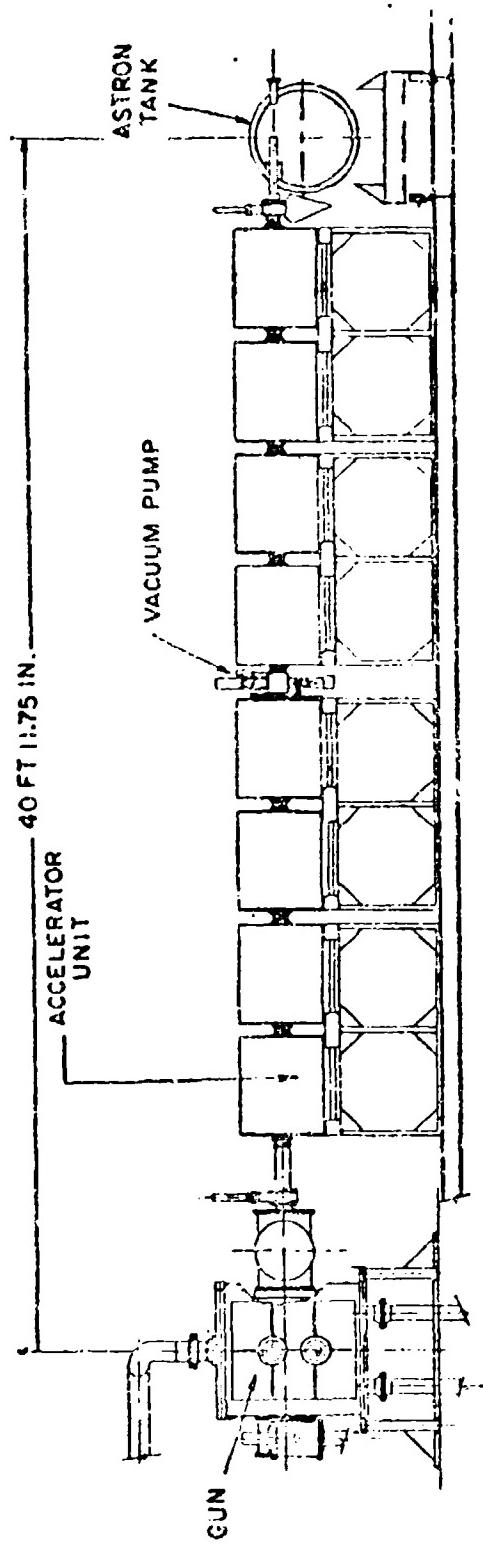


FIG. 4 SIDE VIEW OF COMPLETED ACCELERATOR

The electron injection requirements of the Astron dictate that a square-wave pulse voltage be developed across the secondary plates¹² of the accelerator. The waveforms of Fig. 5 show test results for gun and accelerator cores. The apparent core input impedance (primary voltage/input current) is shown in Fig. 6. These data reveal the need for a modulator that can deliver a constant voltage across a load impedance that varies approximately 4 to 1 during a 0.4- μ sec pulse.

The core pulsing requirements for each type of core are summarized in Table II.

TABLE II
Typical Core Pulsing Requirements For a Single Core

Item	Gun Core	Accelerator Core
1. Peak primary voltage *	16,000 volts	12,000 volts
2. Peak input current *	4,500 amp	1,800 amp
3. Peak power input *	72 MW	21.6 MW
4. Maximum input impedance	12.5 ohm	17.5 ohm
5. Minimum input impedance	2.9 ohm	6.0 ohm
6. Primary voltage rise time	40 nsec	40 nsec
7. Secondary voltage rise time	40 nsec	40 nsec
8. Primary voltage fall time	60 nsec	60 nsec
9. Secondary voltage fall time	60 nsec	60 nsec
10. Pulse duration over $\pm 0.50\%$ portion	0.25 μ sec	0.25 μ sec

* Measured at the end of the 0.25- μ sec flat region of pulse

Description of Overall System

Discussion of System Requirements

A detailed review of core pulsing requirements reveals the need for a pulsing system capable of a peak power input of approximately 13,530 megawatts to the cores. The system chosen employs 519 line-type thyratron circuits, each one capable of 36 megawatts peak power with a combined peak power output of about 18,600 megawatts. There are unavoidable mismatches that result in losses which account for a peak power capability in excess of the core requirements. The system current rate of rise is approximately 1,000,000 amperes in 40 nsec or 25×10^6 amp/ μ sec at a maximum repetition rate of 60 pps.

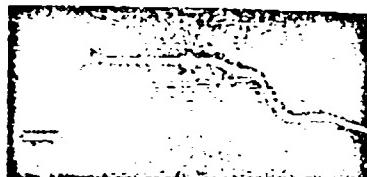
The timing of the 519 thyratrons has to be held very precise because variations of anode delay will reduce available pulse width.

The Project schedule and budgetary considerations did not allow an extended research and development investigation. Therefore, the system was designed with existing commercial products.

A basic modulator channel, utilizing a Type 5949A hydrogen thyratron at five times rated peak current, was developed. The major problem has centered around the construction and operation of a system of over 500 thyratrons in parallel with stringent reliability and timing considerations.

A summary of test results and comments about various thyratron tubes is given in Table III. This work concluded with the choice of the Type 5949A tube.

(a) ACCELERATOR CORE



COMPENSATED CORE
WAVE FORMS

PRIMARY VOLTAGE

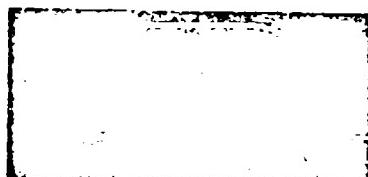
7900 V/cm

PRIMARY CURRENT

900 A/cm

PRIMARY VOLTAGE
SCOPE BIASED
790 V/cm

(b) GUN CORE



PRIMARY VOLTAGE
7240 V/cm

PRIMARY CURRENT
2700 A/cm

PRIMARY VOLTAGE
SCOPE BIASED
724 V/cm

FIG. 5 COMPENSATED WAVEFORMS: SWEEP SPEED 100 NSEC/CM

FIG. 6

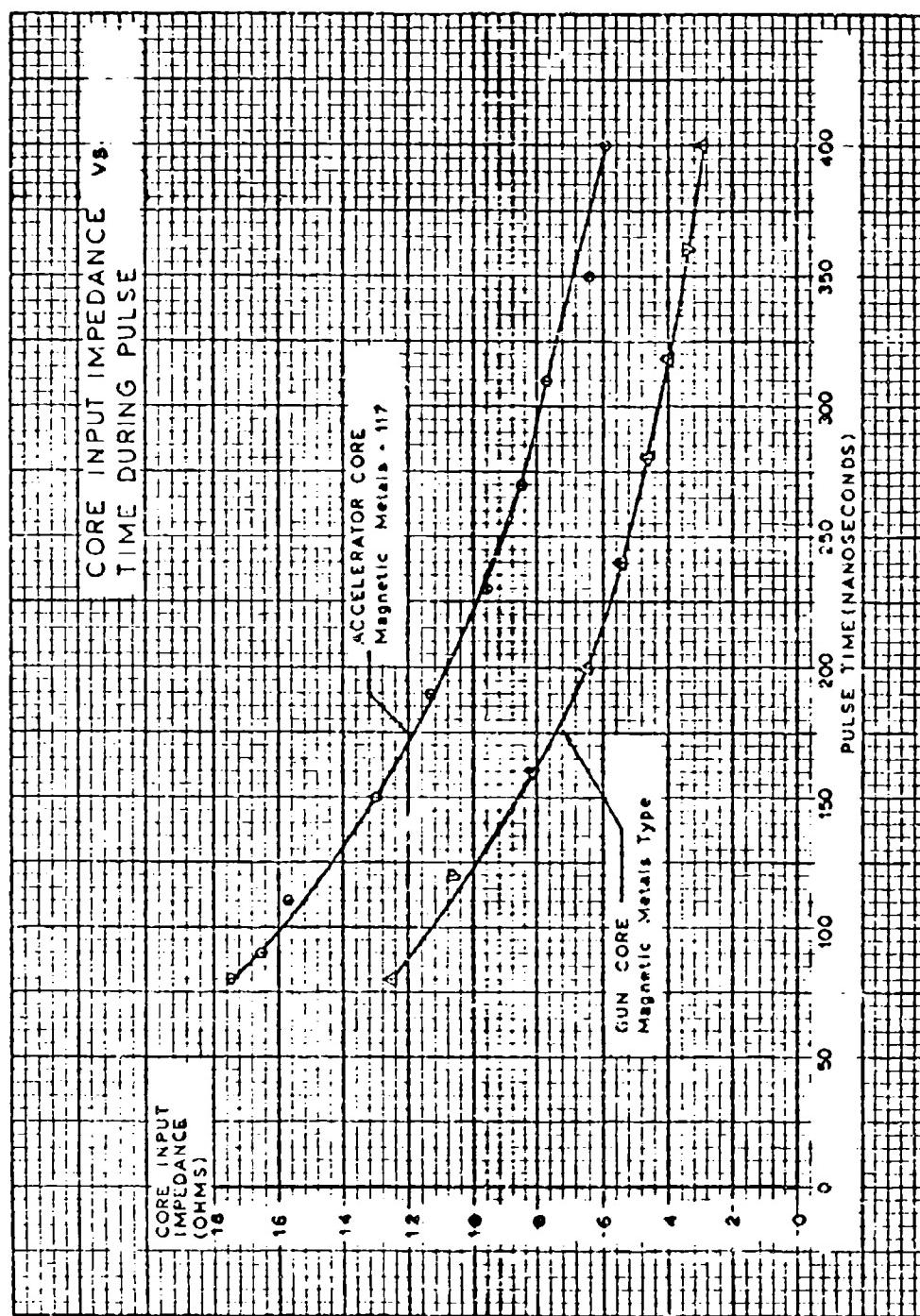


TABLE III
Test Results of Thyratron Tube Testing (0.4- μ sec Pulse)

Rating	Tested At:					Circuit Impedance	Rise Time	Cost in Large	Approx.
	Peak	Peak	P _B	Peak	P _B				
Type	Volts	Current	Power	Factor	Volts	Current	Power	Factor	Source
MFG.	kV	MW	amp	$\times 10^{-9}$	kV	amp	MW	$\times 10^{-9}$	ohms
Kuthe	5C22	16	325	2.6	3.2	16	1600	12.8	1.5
									10
									60
									21
									Did not attempt higher voltage
Kuthe	6587	16	325	2.6	3.2	32	2240	36	4.3
									14.3
									40
									Used a low inductance version & preaged at 35kV
Kuthe	1257	33	2000	33	20	32	3850	61	7.4
									8.3
									100
									600
									Rise time long
GE	GL739C	33	2000	33	30	32	3850	61	7.4
									8.3
									25
									1200
									High cost/amp
Kuthe	KU-74	33	2000	33	40	32	3850	61	7.4
									8.3
									25
									1200
									High cost/amp
Kuthe	5949A	25	500	6.25	6.25	32	2240	36	4.3
& Tung-	Sol								14.3
									45
									60
									Prefire good, Low cost/amp

The voltage drop at the core (load impedance) due to the mismatch between the coaxial transmission line characteristic impedance and the core is eliminated by a pulse shaper located in the output circuit of the modulator. However, the flatness was obtained with a sacrifice in efficiency. The pulse shaper can be adjusted to produce an approximate ramp voltage to be transmitted to the core (see block diagram, Fig. 7). Secondary voltages from the cores have been observed with a ripple less than $\pm 1/4\%$ when the pulse shaper is properly adjusted.

The output pulse is positive and is taken from the cathode of the thyratron. A positive pulse improves the life of the RG-213/U transmission lines to the cores by at least an order of magnitude greater than when a negative pulse is used. The peak pulse voltage on the output cables can be 18 kV under maximum output conditions and pulse shaper adjustment. The cable can withstand many times (100 kV or more) this voltage under dc or long rise time pulse conditions. However, under fast pulse conditions, corona bursts occur during the rise and fall of voltage and holes are bored through from the braid to the inner conductor.¹³

The minimum electrical length of the transmission lines to the cores is set at one-half the pulse width (130 feet) in order to prevent reflections from arriving back during the pulse. The maximum length is limited by cable attenuation and will not exceed 200 feet. The final design utilizes 170-ft lengths. The pulse-forming network consists of three 260-ft reels of RG-218/U and one 130-ft length of RG-218/U to an isolating resistor which is connected to the high-voltage charging power supply.

The gun core, at an output of 16 kV, requires three times the peak power of the accelerator core. Three modulators in parallel will be used to power the gun core instead of using a different design modulator.

Detailed Description of System Under Construction

A simplified block diagram of the modulator system is shown in Fig. 7.

The PFN's consist of three 260-foot and one 130-foot reels of RG-218/U (see Figs. 8 and 9) per modulator channel. There will be over 2000 reels in the final system and Fig. 10 shows nearly half of the final installation.

The PFN's are charged by a pulse charging system of four 125-kW power supplies. They are charged up in approximately 2 milliseconds and discharged about 1 millisecond later (see Fig. 11). A de-Q'ing circuit,¹⁴ plus hard-tube regulation, is used to obtain the $\pm 1/4\%$ regulation needed. The power supplies are still under construction, and, therefore, are not reported on in detail.

Each switch, the Type 5949A thyratron, is mounted in a low-inductance cast aluminum housing (see Fig. 12). The housing is incorporated in a chassis (see Fig. 13) which includes an adjustable trigger delay (short sections of RG-58A/U switched in or out), grid and cathode isolation, and a cathode monitor. A complete schematic of the switch chassis is shown in Fig. 14. The switch chassis is plugged in or out of a back panel (see Figs. 15 and 16).

The switch chassis is mounted on sliders in racks and plugs into a back panel (see Fig. 17). The PFN cables (RG-218/U) and load cables (RG-213/U) are permanently mounted in the connectors on the back panel. The switch chassis and pulse shapers are mounted in racks. Figures 18 and 19 show 40% completion of this layout.

Several varieties of co-axial connectors were designed to use with RG-213/U at high pulse voltages. The allowable spacings created a corona problem which was solved by using corona-resistant isomica (silicone

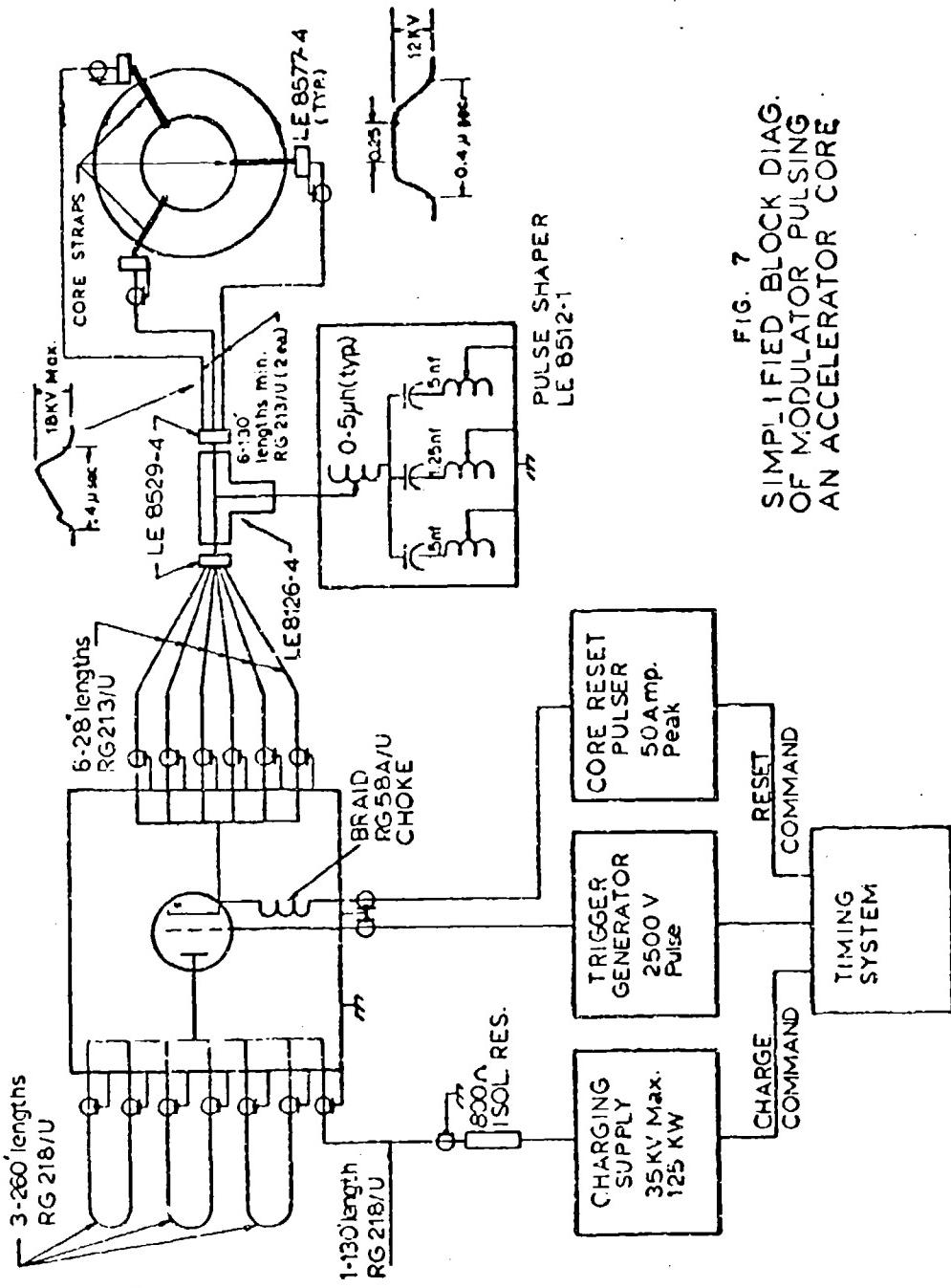


FIG. 7
SIMPLIFIED BLOCK DIAG.
OF MODULATOR PULSING
AN ACCELERATOR CORE

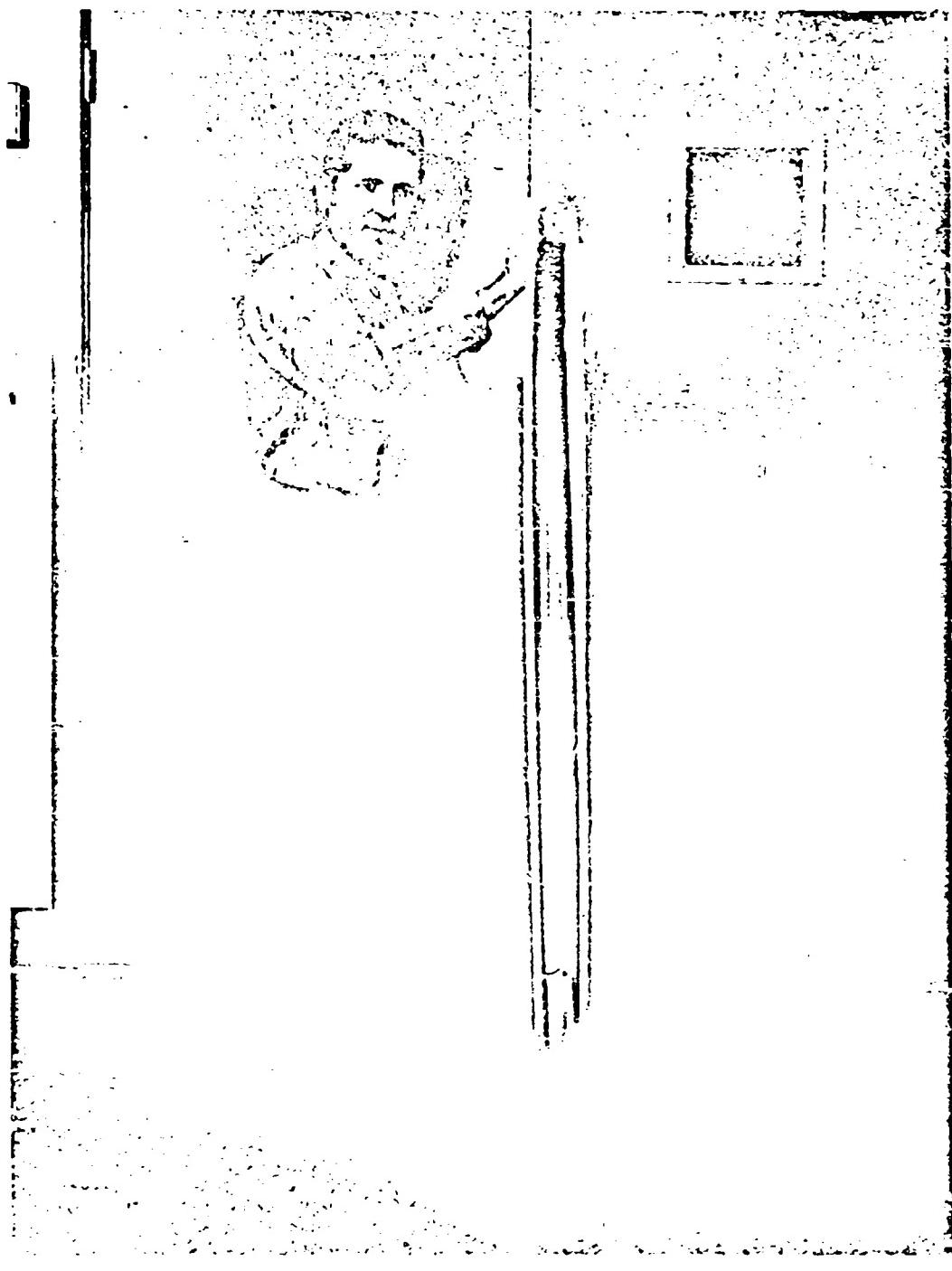
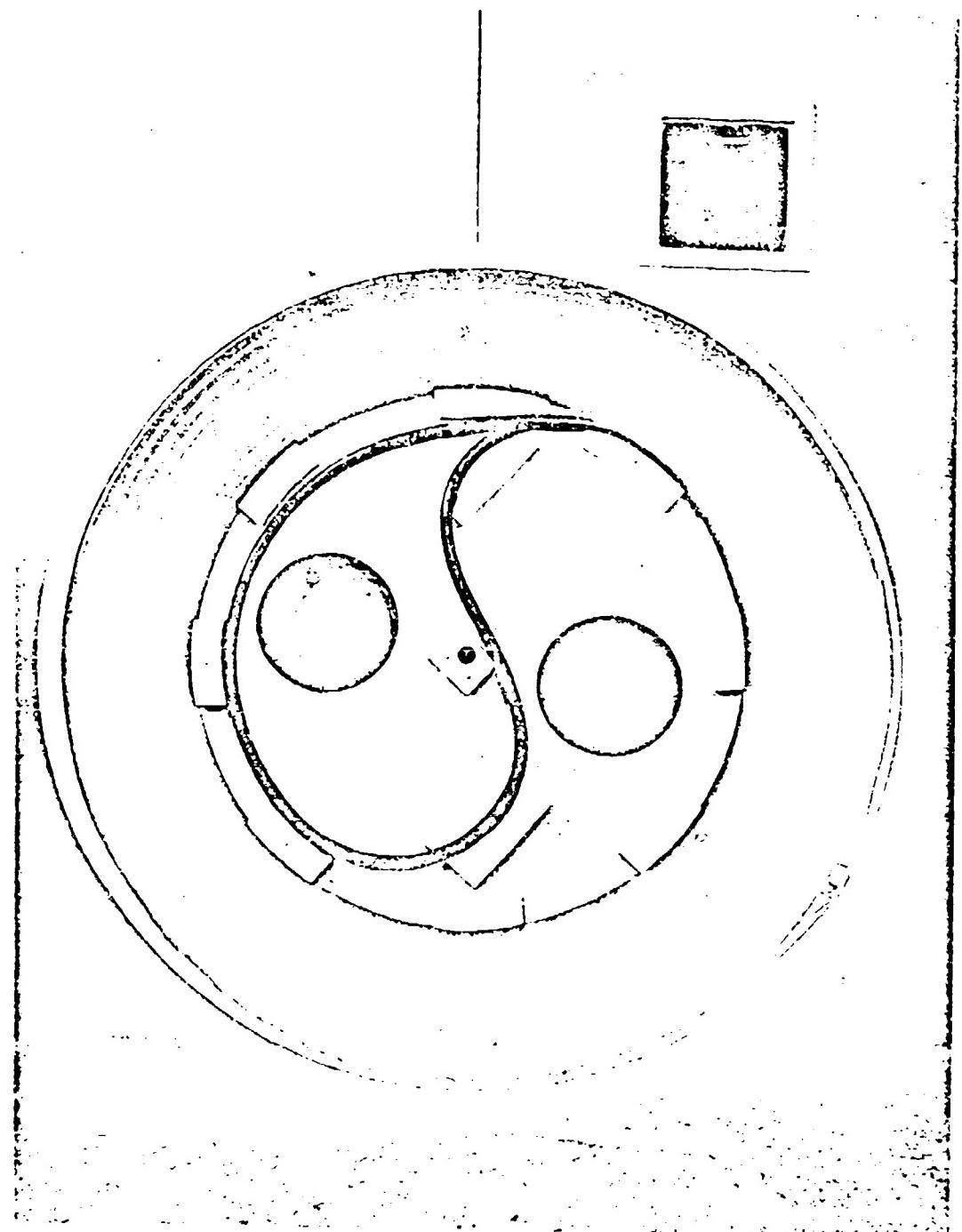


Fig. 6 One 260-foot PEN of RG-216/U.



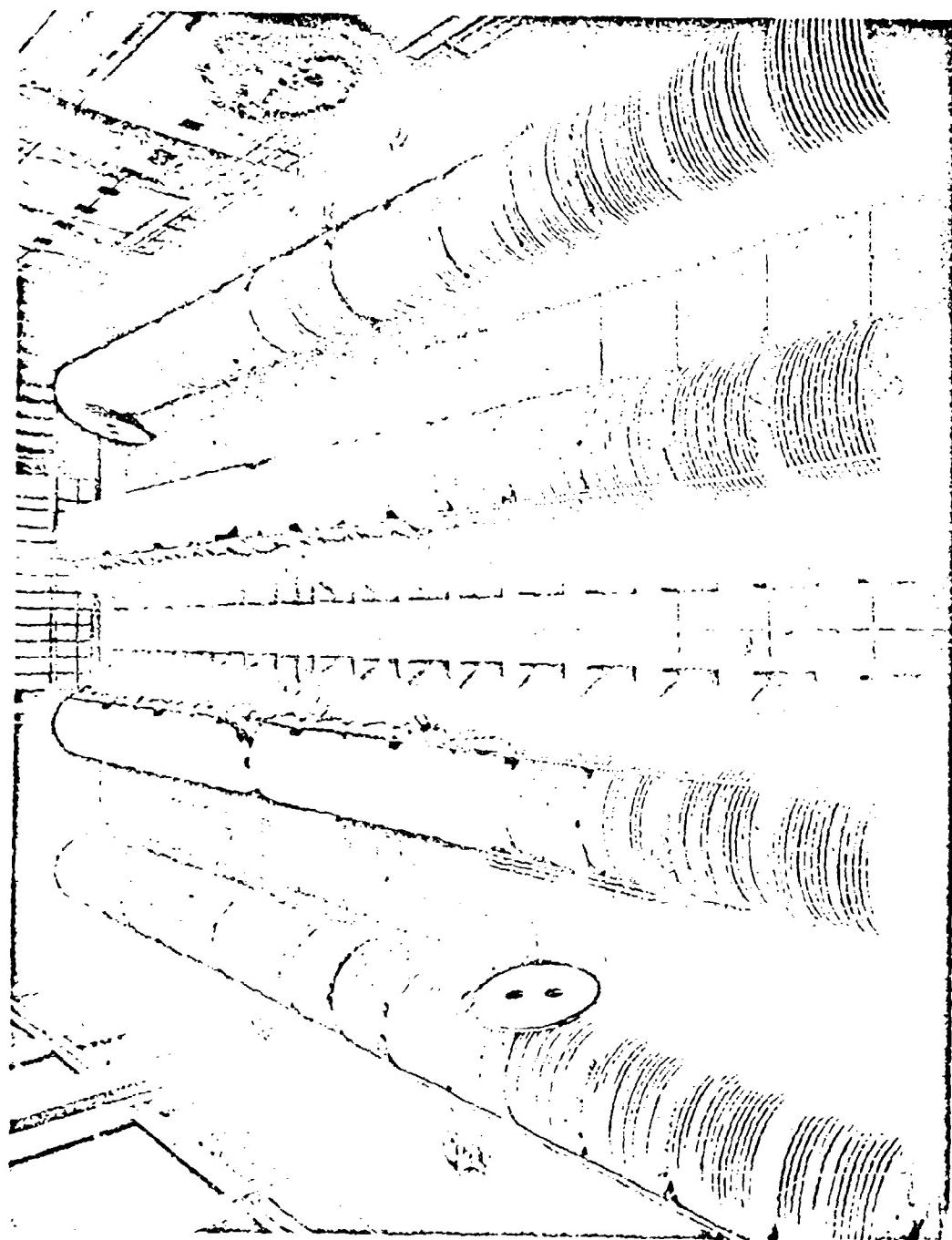


Fig. 10 Top view of 50% PFN installations.

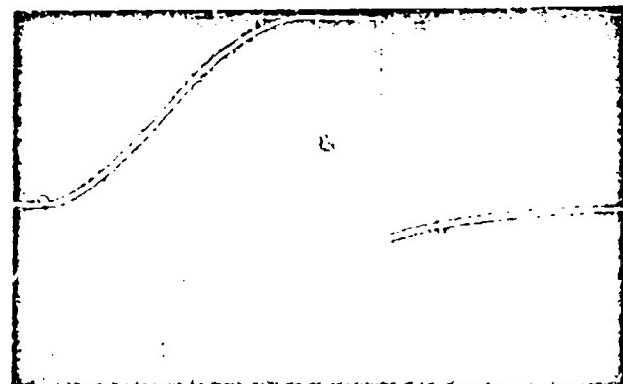


FIG. 11 WAVEFORM OF PULSE CHARGING OF ZEN OF MODULATOR

Sweep speed - 500 microsec/cm

Vertical sensitivity 10,000 volts/cm

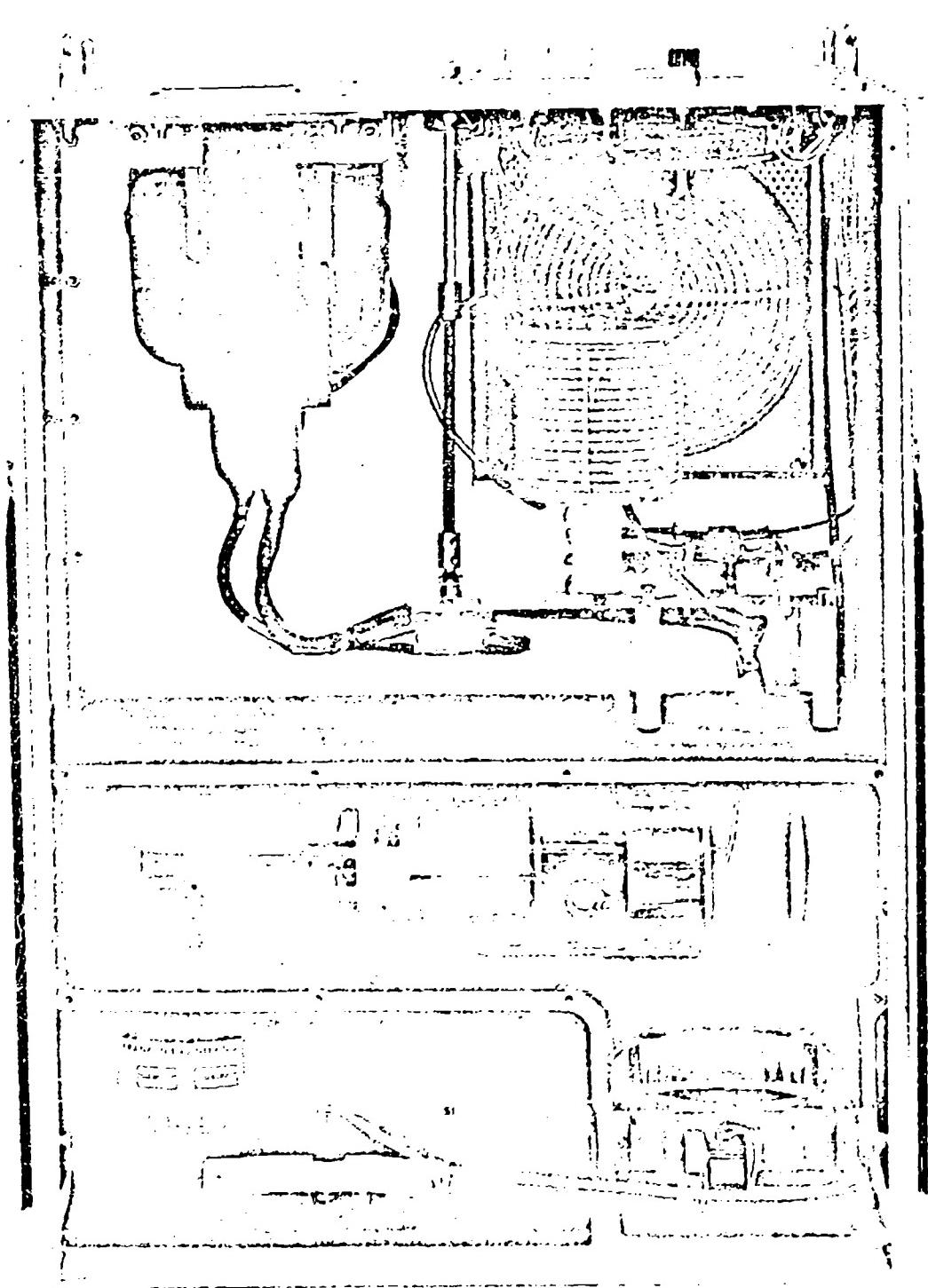


FIG. 12 SWITCH CHASSIS, TOP VIEW

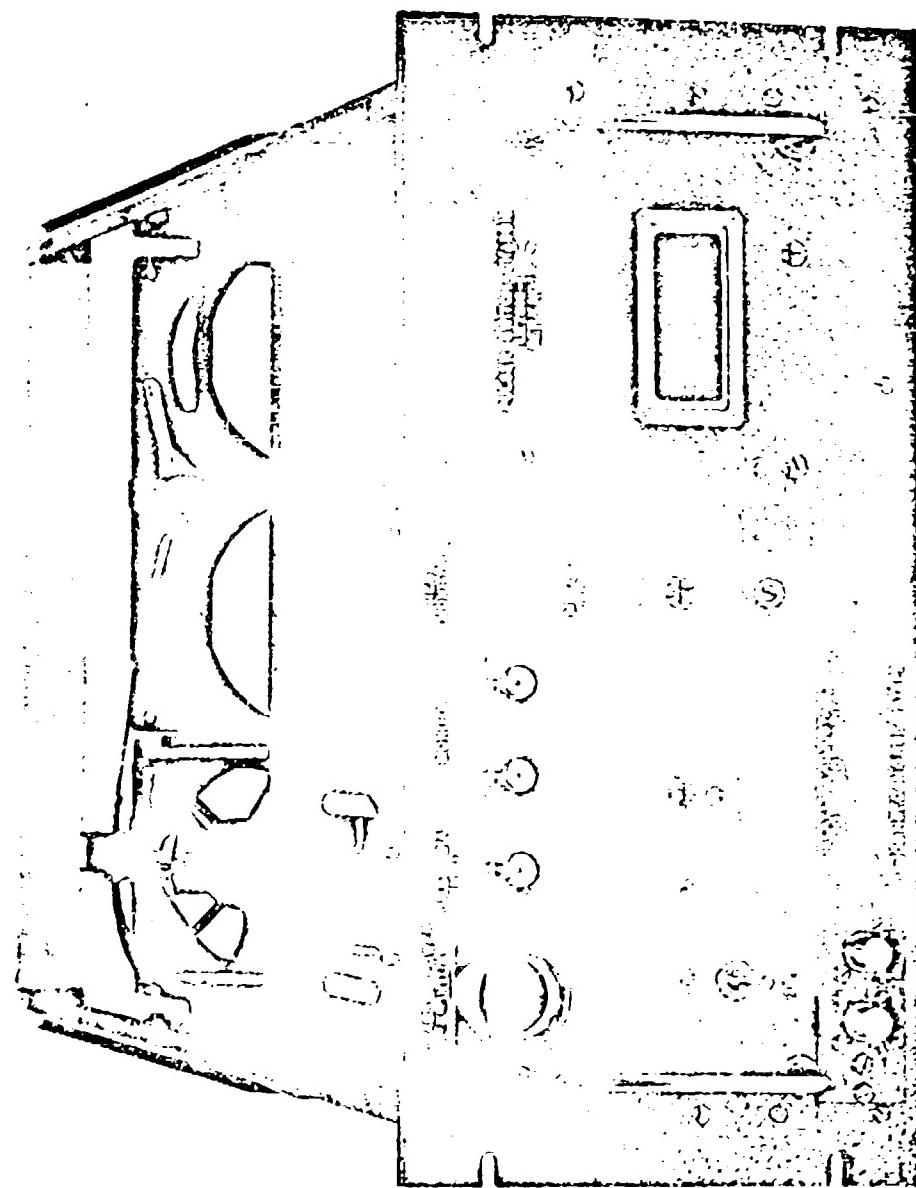
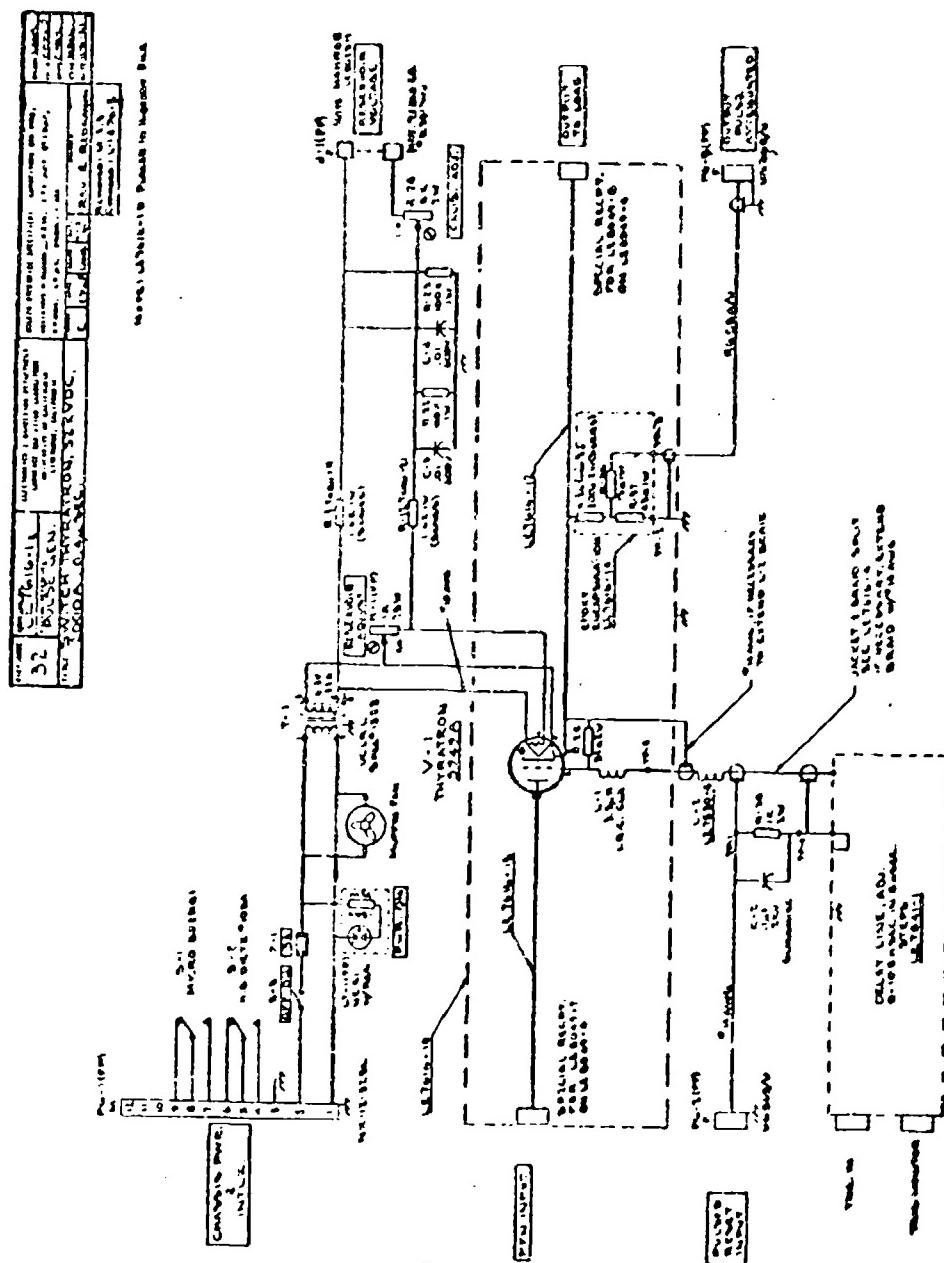


Fig. 13 Switch chassis, front view.

FIG. 24. SCHEMATIC OF SWITCH CHASSIS



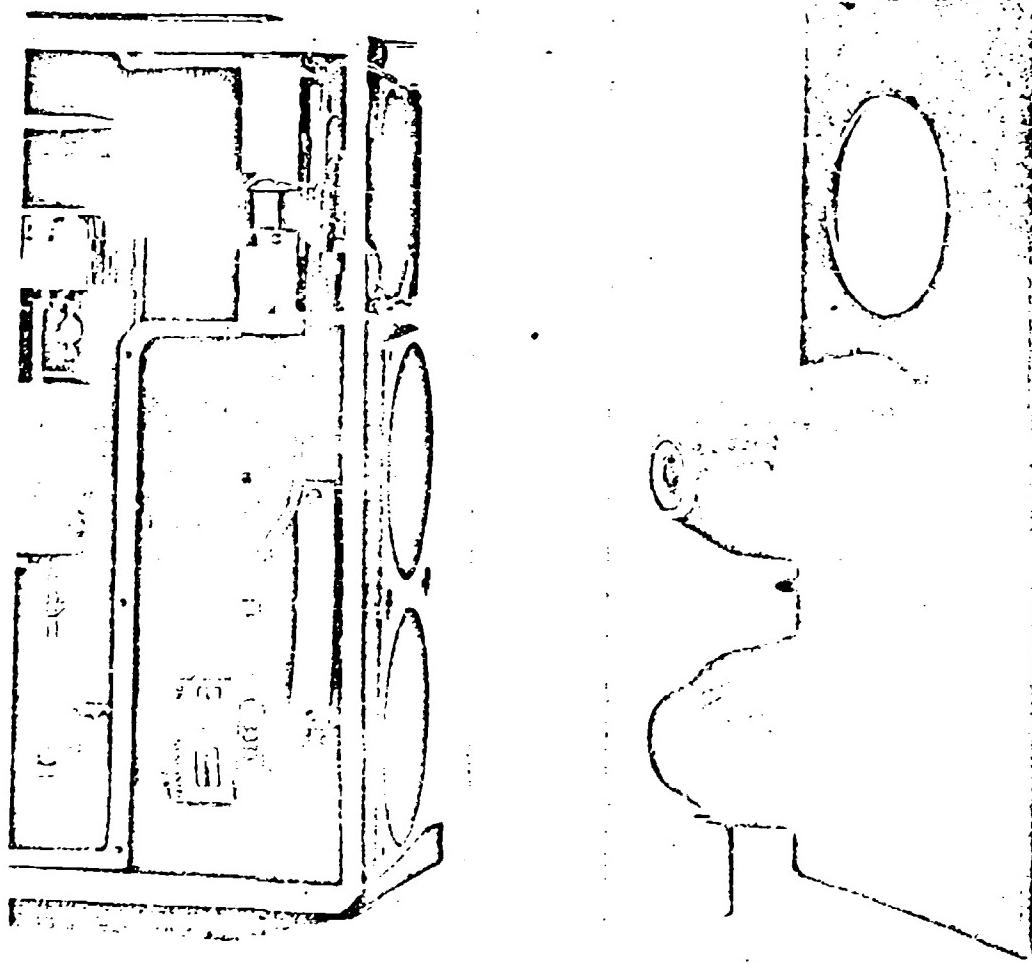


Fig. 15 Back Panel Plug-in connectors.

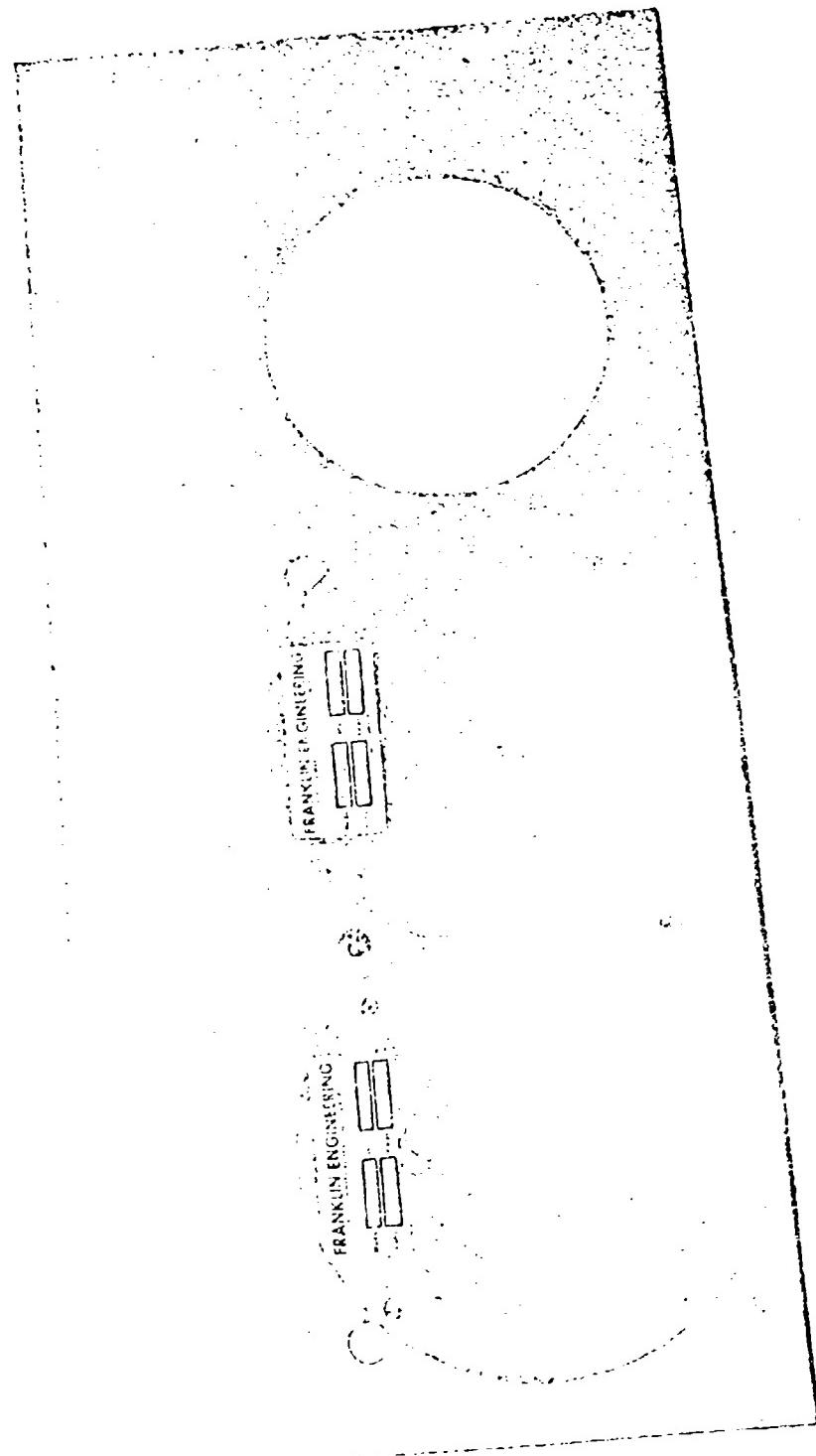


FIG. 16 BACK PANEL, CABLE END

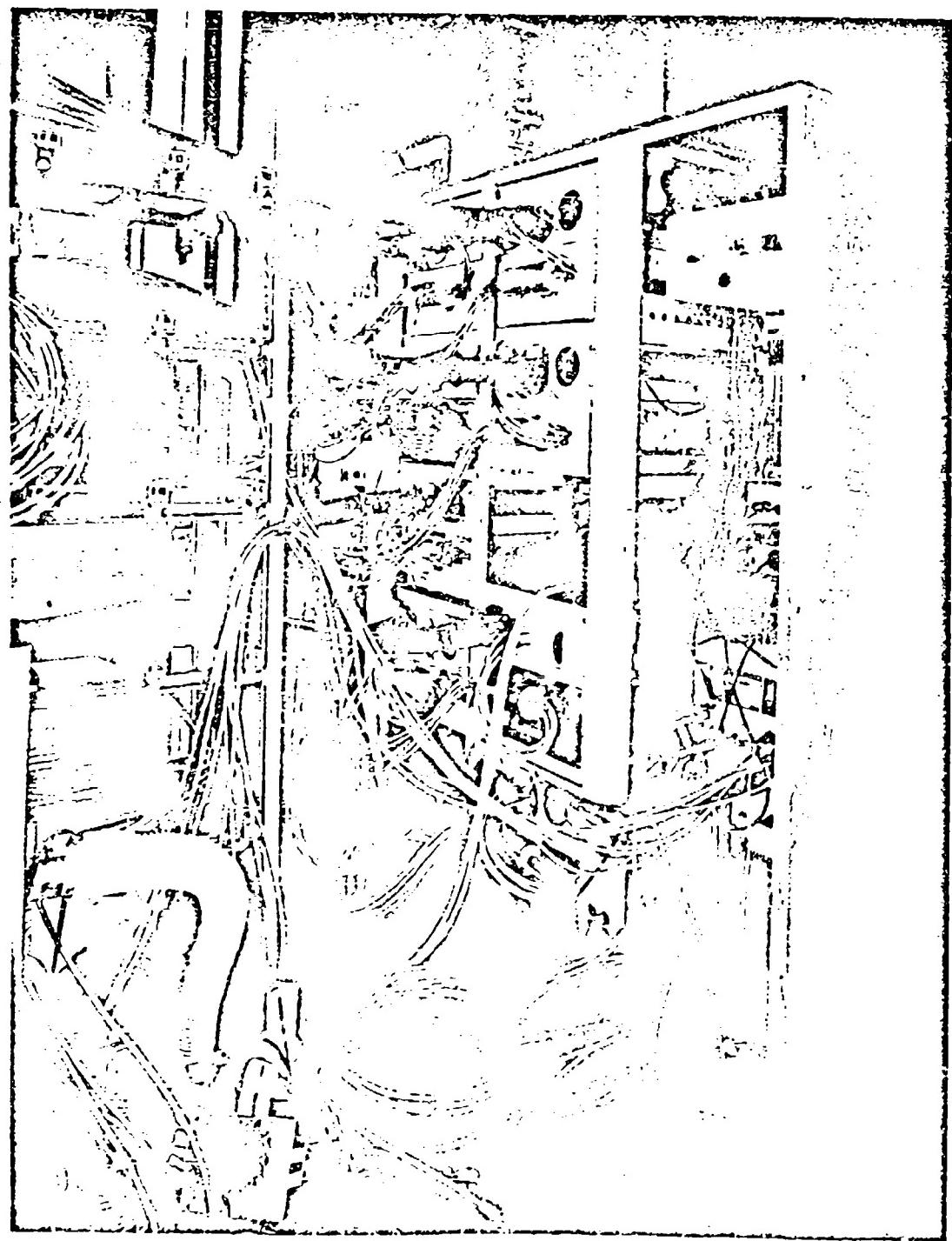


Fig. 17. Back view of eight pulsers showing cable connections to back panels and pulse shapers.

Fig. 18 Installation of PFN reels and racks for switch chassis (showing about 40% of the final system).

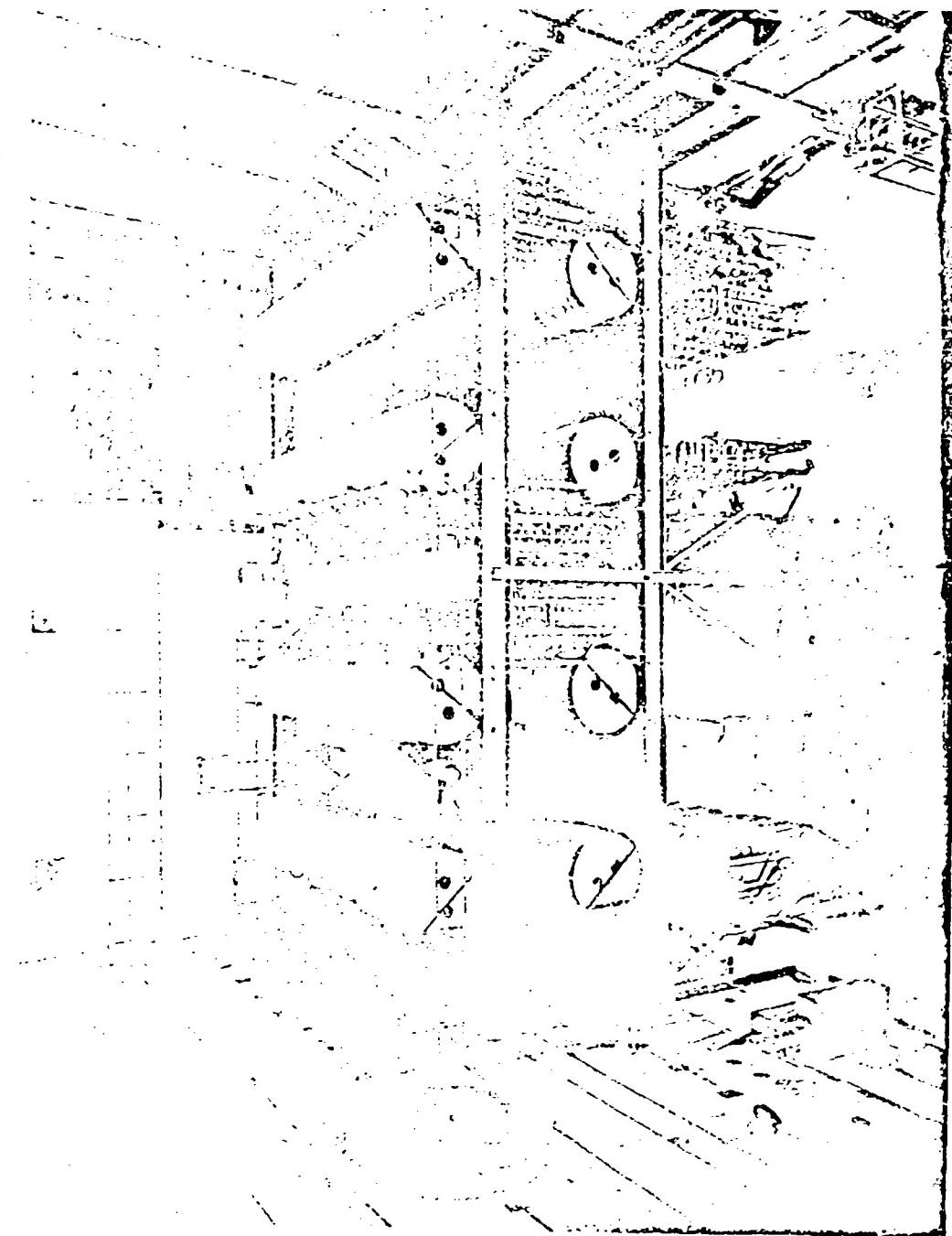
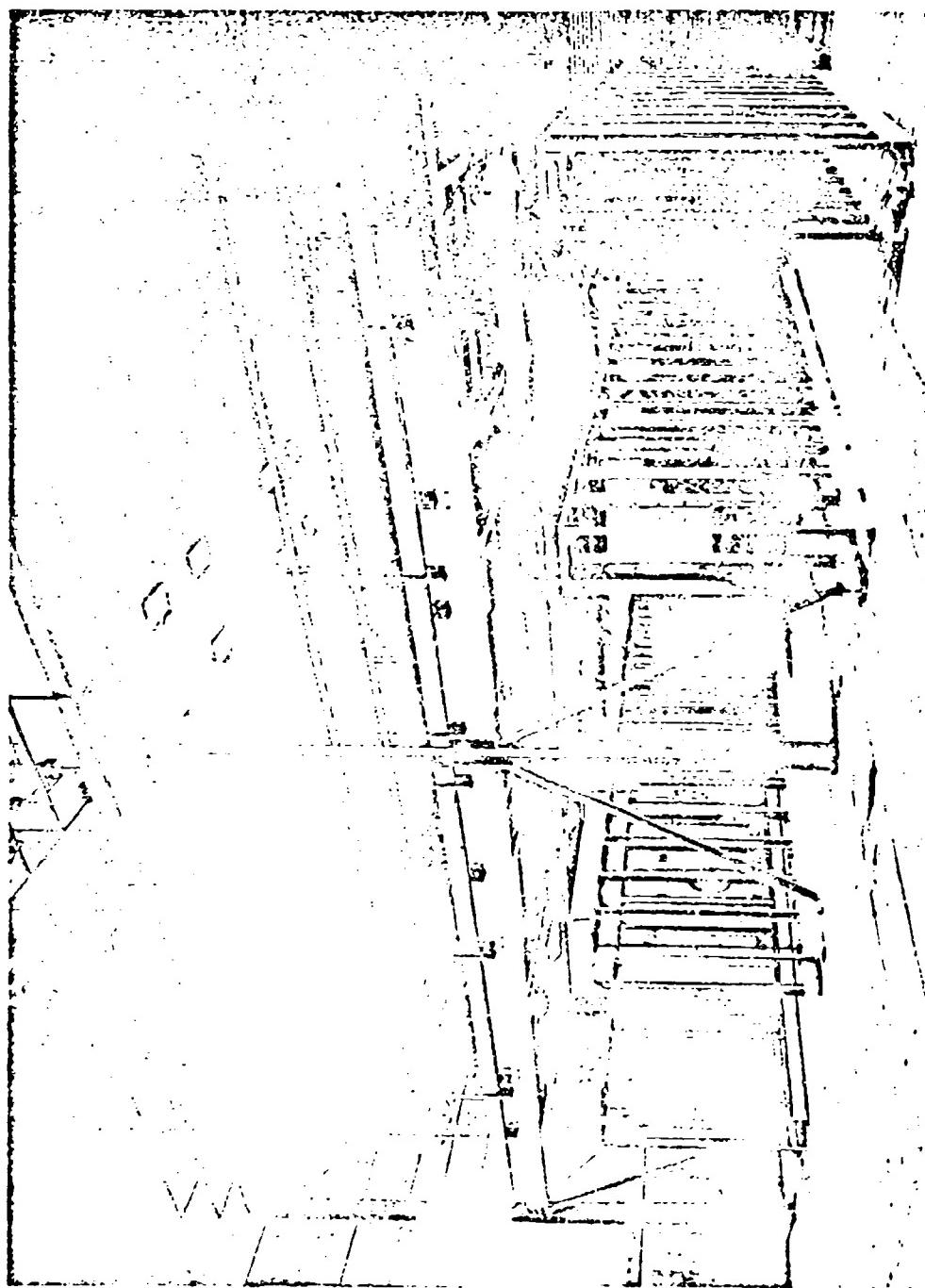


Fig. 19 Rack installation, 40% complete.



bonded mica) shields. RG-213/U cable fails very rapidly when subjected to corona bombardment. This technique eliminates the use of oil and allowed use of a small, inexpensive connector (see Figs. 20, 21, 22, and 23).

Performance Tests of The 36-MW Modulator

The modulator specifications operating into a matched load are shown in Table IV. Waveforms under these conditions are shown in Fig. 24.

Peak Current

The peak current under matched conditions ($Z_L = 50/7$ ohm) is 2240 amperes. In the system the pulse shaper is added in parallel with a Z_L of 50/6 ohm. The current waveform, with the pulse shaper adjusted for a typical core, is shown in Fig. 25. The peak current through the thyratron is approximately 2830 amperes. This maximum is reached after 0.1 μ sec and decreases to about 2200 amperes at the end of the pulse. The modulator performs satisfactorily in either case. No attempt was made to determine the maximum possible current pulse, however, it is possible to affect the current rate of rise by setting the reservoir too low. Waveforms of such conditions are shown in Fig. 26.

TABLE IV

Peak power	36 MW
Output voltage	8 to 16 kV
Output current	1120 to 2240 amp
Average power	680 watts
Load impedance	50/7 ohms $\pm 2\%$
Average anode current	0.054 amp
RMS anode current	11 amp
Pulse length (flat region)	0.3 μ sec
Rise time (10 - 90%)	50 nsec
Fall time (10 - 90%)	50 nsec
Pulse repetition rate	0 - 60 pps
Time jitter	± 5 nsec
Pulse-to-pulse amplitude jitter	$\pm 0.25\%$
Pulse ripple	$\pm 0.25\%$

Hold-Off Voltage and Tube Aging Procedure

The anode voltage rises in about 2 msec and the thyratrons are fired about 1 msec after the peak voltage is reached. The modulator has worked well up to 32 kV under such conditions. In order to obtain such performance on 25-kV rated tubes, we have preaged the tubes. The aging process is a run-in time of 12 hours at 32 kV in a circuit with matched load conditions and at 60 pps. The anode voltage rises in 2 msec, however, it stays up about 10 msec before the tube is fired.

The optimum reservoir setting is determined during this aging process. In addition, cathode arcs to ground and prefires are monitored during the run. The prefires are of most concern in this system, because no attempt has been made to isolate PFN's other than by a 750-ohm resistor at the power supply to each PFN. This means about 125 PFN's are tied together and one early prefire could reduce the voltage on all the others. Ultimately it may be necessary to isolate each PFN, however, this will be costly.

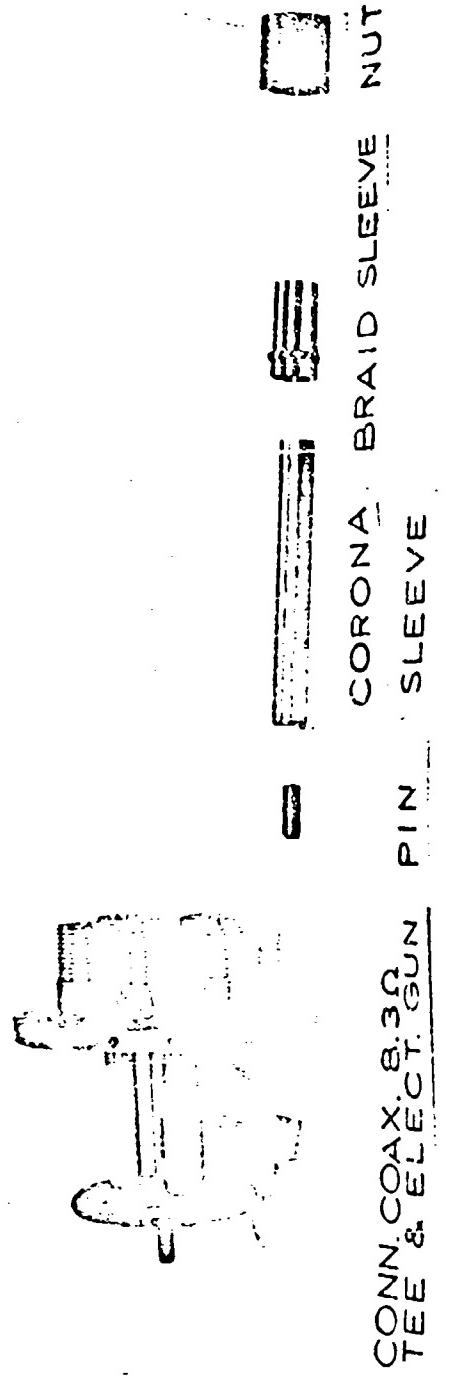
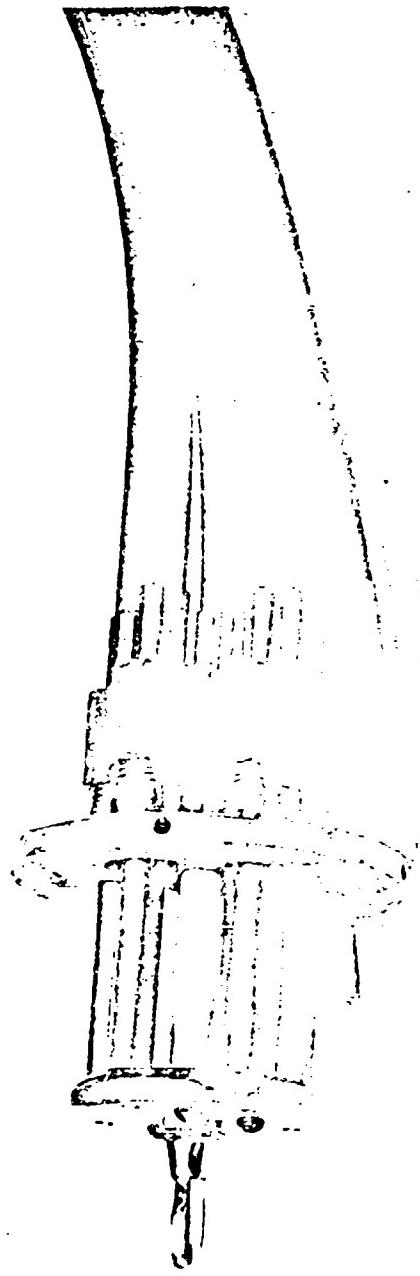


FIG. 20 SIX-CABLE CONNECTOR, PARTS

RG 2131U



CONN. COAX. 8.3Ω
TEE & ELECT. GUN

FIG. 21 SIX-CABLE CONNECTOR, ASSERATED

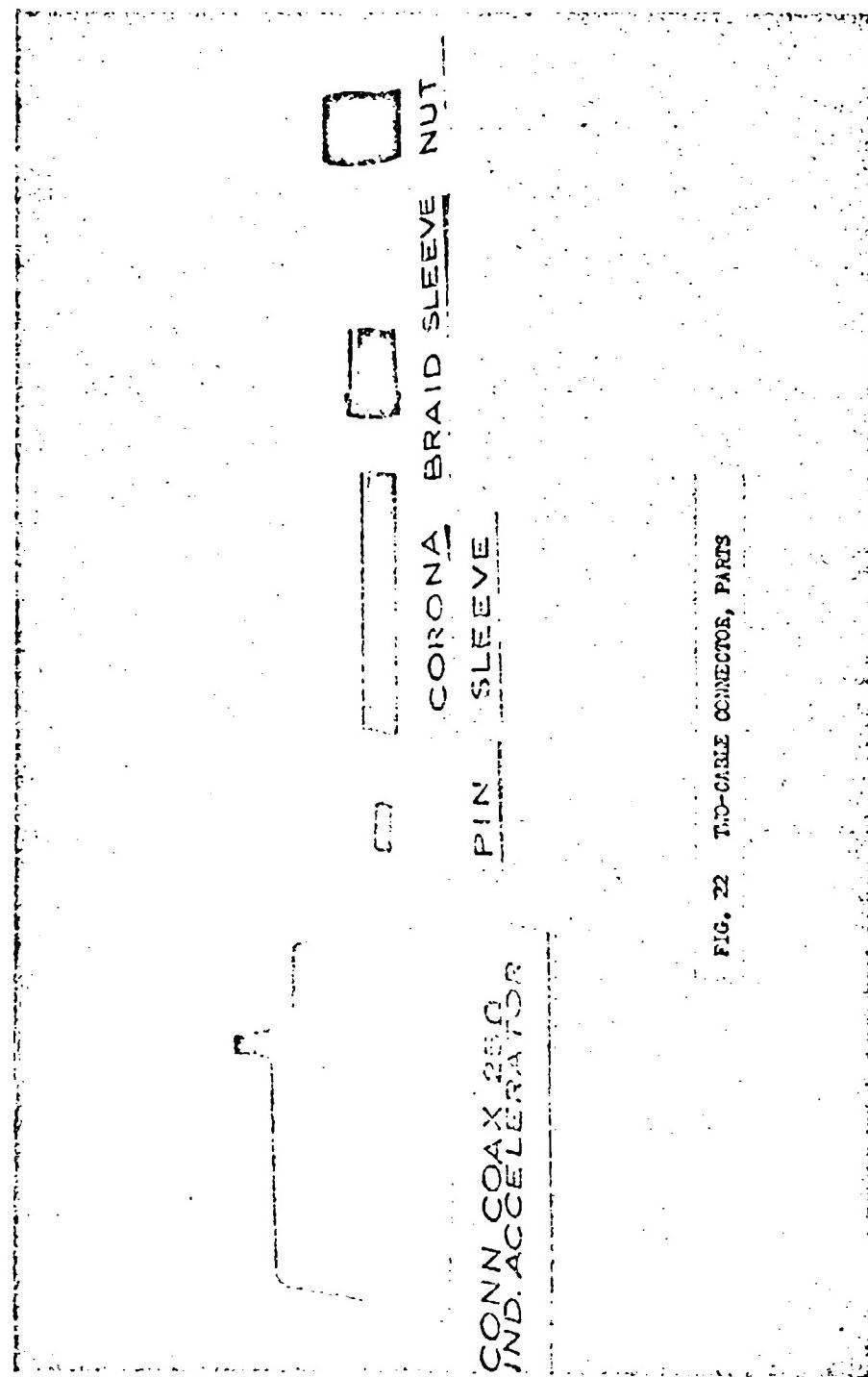
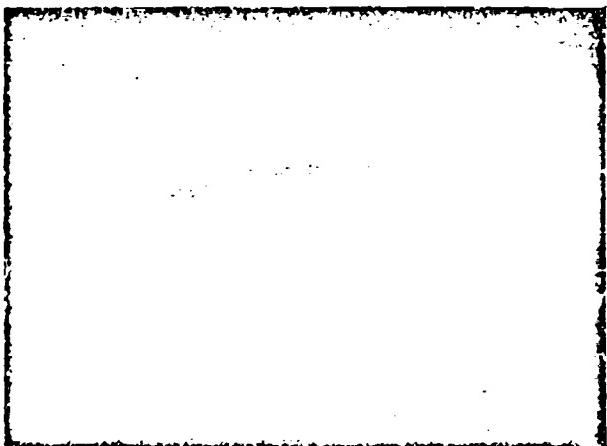


FIG. 22 T.O.-CABLE CONNECTOR, PARTS

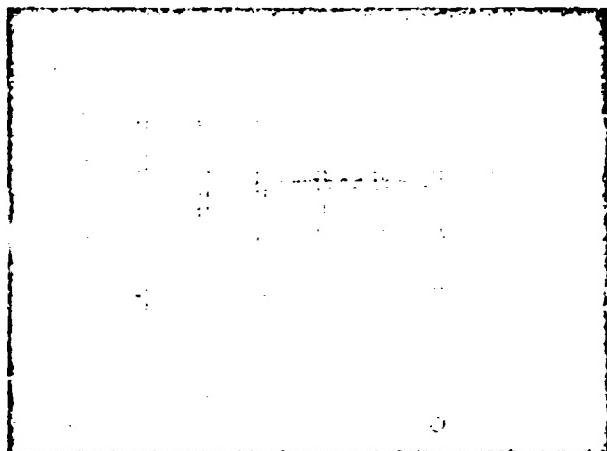
CONN COAX 25Ω
IND. ACCELERATOR

FIG. 23 TWO-CABLE CONNECTOR, ASSEMBLED

RG 213/U



SWEET SPEED: 50ns/cm
TIMING FREQ: 100mc
applied to Horizontal
Deflection Plates
(Dot Rossi Technique)



SWEET SPEED: 100ns/cm

FIG. 24. WAVEFORMS OF OUTPUT OF SWITCH CHASSIS
TERMINATED IN A 7.14-OMH LOAD

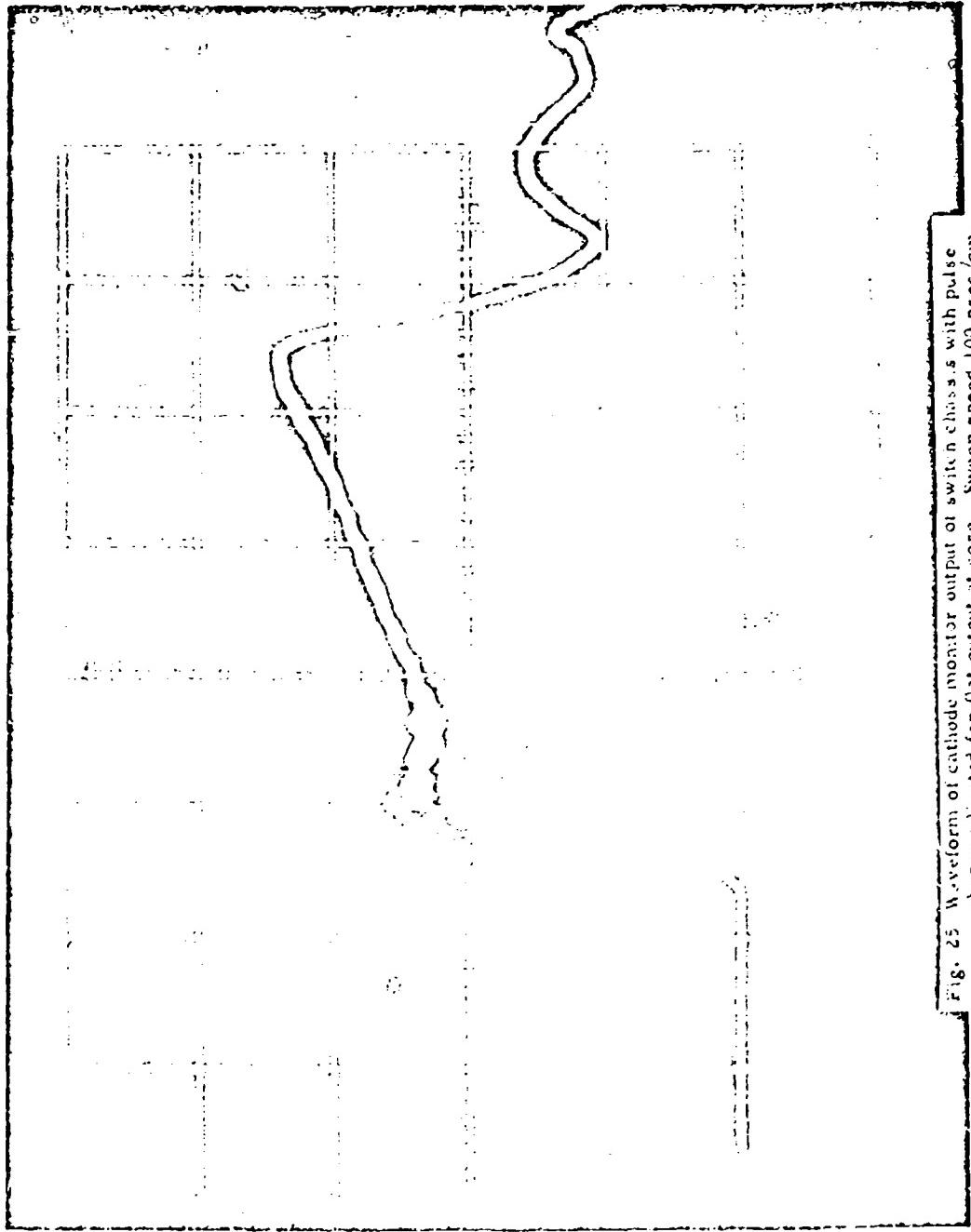
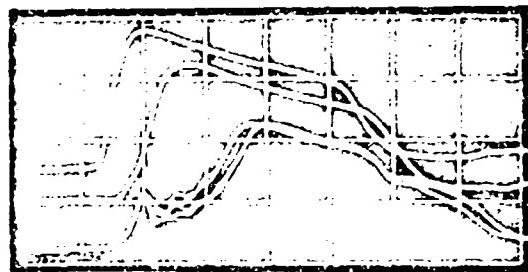


Fig. 25. Waveform of cathode monitor output at switch chassis with pulse shaper adjusted for flat output at core. Sweep speed 100 nsec/cm.
Vertical sensitivity of 4920 volts/cm.



TOP TRACE: NORMAL RESERVOIR SETTING 5.1 V
CENTER TRACE: 30 sec. AFTER CHANGING RES. TO 4.4 V
BOTTOM TRACE: 2 min. AFTER CHANGING RES. TO 4.4 V

FIG. 26 WAVEFORMS OF CORE OUTPUT SHOWING EFFECTS OF LOW RESERVOIR SETTINGS

Sweep speed - 100 nsec/cm

Vertical sensitivity - 7,000 volts/cm

Peak Power

The maximum peak power is approximately 36 MW and operation at 60 pps under such conditions was satisfactory. We have not attempted to make higher peak-power runs.

Average Power

Twelve test modulators have been run at an average power of 680 watts each, with a combined running time of over 20,000 unit hours.

Trigger Characteristics

We have experienced low jitter of the order of ± 2 nsec when using a sufficiently high voltage trigger. However, the tube shows variations of anode delay of up to ± 50 nsec over an operating time of 700 hours at 60 pps (see Fig. 27) and about ± 20 nsec over short runs of 2 to 5 hours when anode voltage and repetition rate are varied. The anode delay drift has been negligible (± 5 nsec) on short runs (2 to 5 hours) when anode voltage and repetition rate were constant. Variations occur slowly and can be taken care of manually by adjusting the delay in each switch chassis. The causes of these changes have not been determined.

The variation of anode delay vs trigger voltage of four tubes is shown in Fig. 28. A 50-ohm source trigger is used. It should be noted that the differential in delay is nearly a constant above 500 volts, the spread in anode delay is about ± 70 nsec, and the variation in delay above 1500 volts is less than 3 nsec per 100 volts. A trigger voltage of 1500 to 1700 volts is used to minimize any effects from changes in trigger voltage.

Variations in anode delay are compensated by changes in trigger delay within each switch chassis. This method eliminates costly electronic delays and each chassis can be monitored and adjusted properly. However, the greater the variation of anode delay, the more delay required inside each switch chassis. Therefore, the anode delay (after the aging cycle of each tube) was measured in order to select tubes. The results of 222 tubes are shown in Fig. 29. All the tubes are from the same production run of one manufacturer. An initial variation of ± 30 nsec can be achieved by using $2/3$ of the run.

Prefire Characteristics

The anode voltage operation allows approximately 2 msec for a prefire to occur. A prefire is defined as a premature firing of a tube prior to the arrival of the trigger pulse. This phenomenon is not important in many applications because the rate is so low. However, in a system with many thyratrons in parallel and not completely isolated, a high prefire rate would make the system inoperable. In this system, because of protection devices, a single prefire will reduce the beam output considerably and require readjustment. Under such conditions a reasonable prefire rate should be under five per hour. Tests have been made that show an average prefire rate of about one per 2 hours at the end of a 12-hour period (see Fig. 30). Subsequent testing shows a further reduction of the prefire rate until the tube nears the end of life. We attempted to correlate these data with reservoir range (see Fig. 31), however, no direct conclusions were made.

Therefore, the system prefire rate could run as high as 250/hour, which is intolerable. This problem is obviously being given considerable study. It may be necessary to isolate each PFN and thyratron from the high-

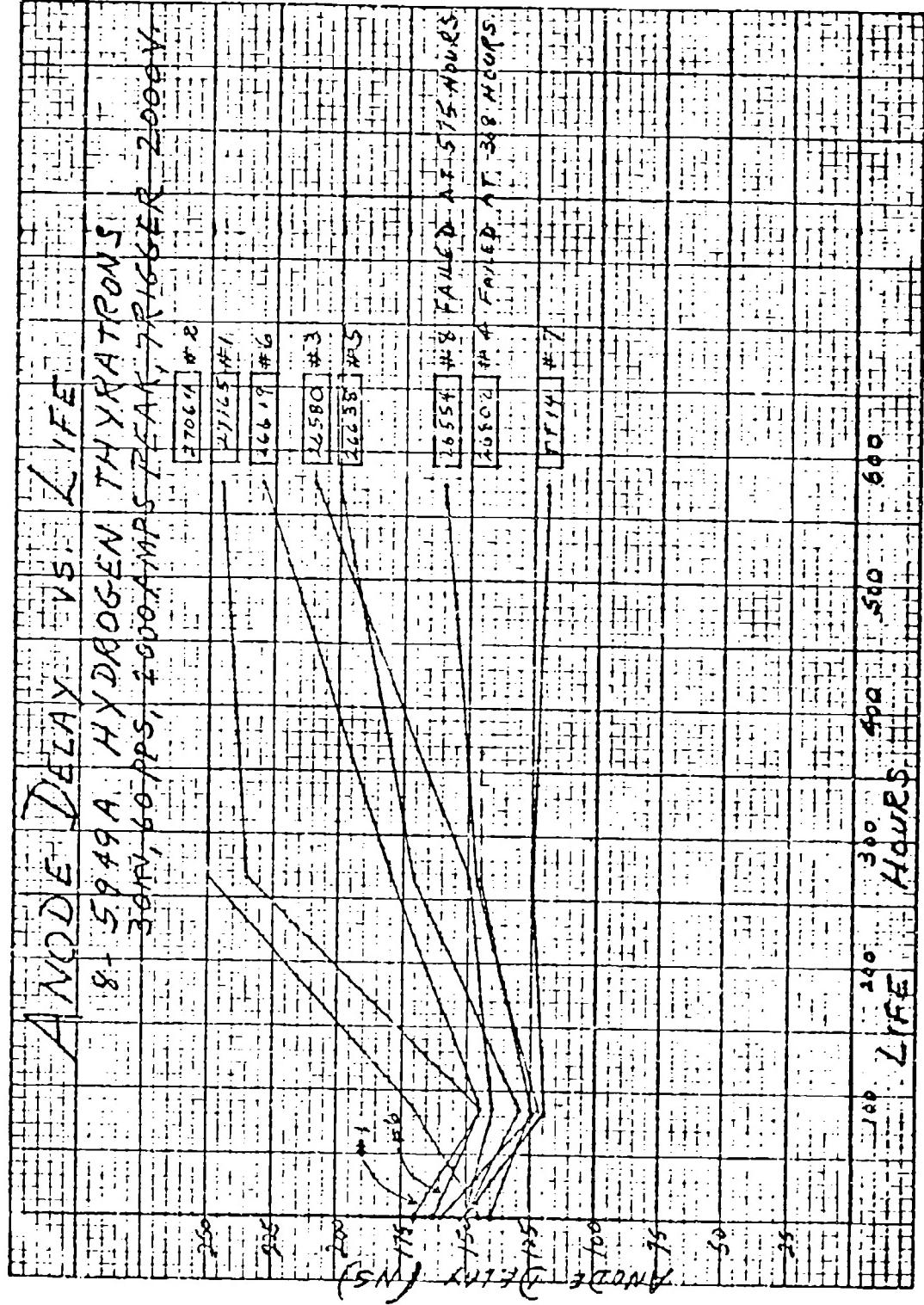


FIG. 27

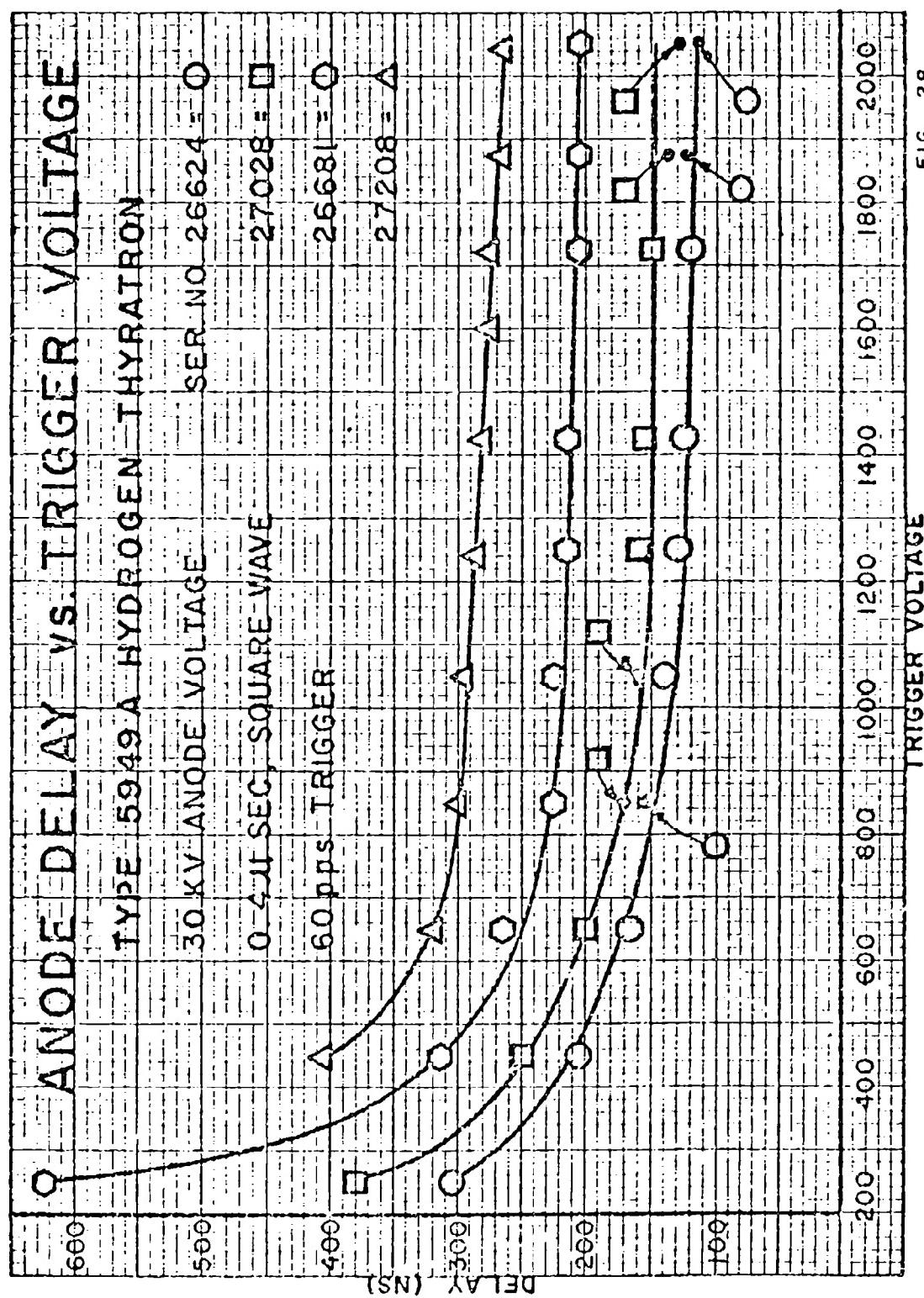
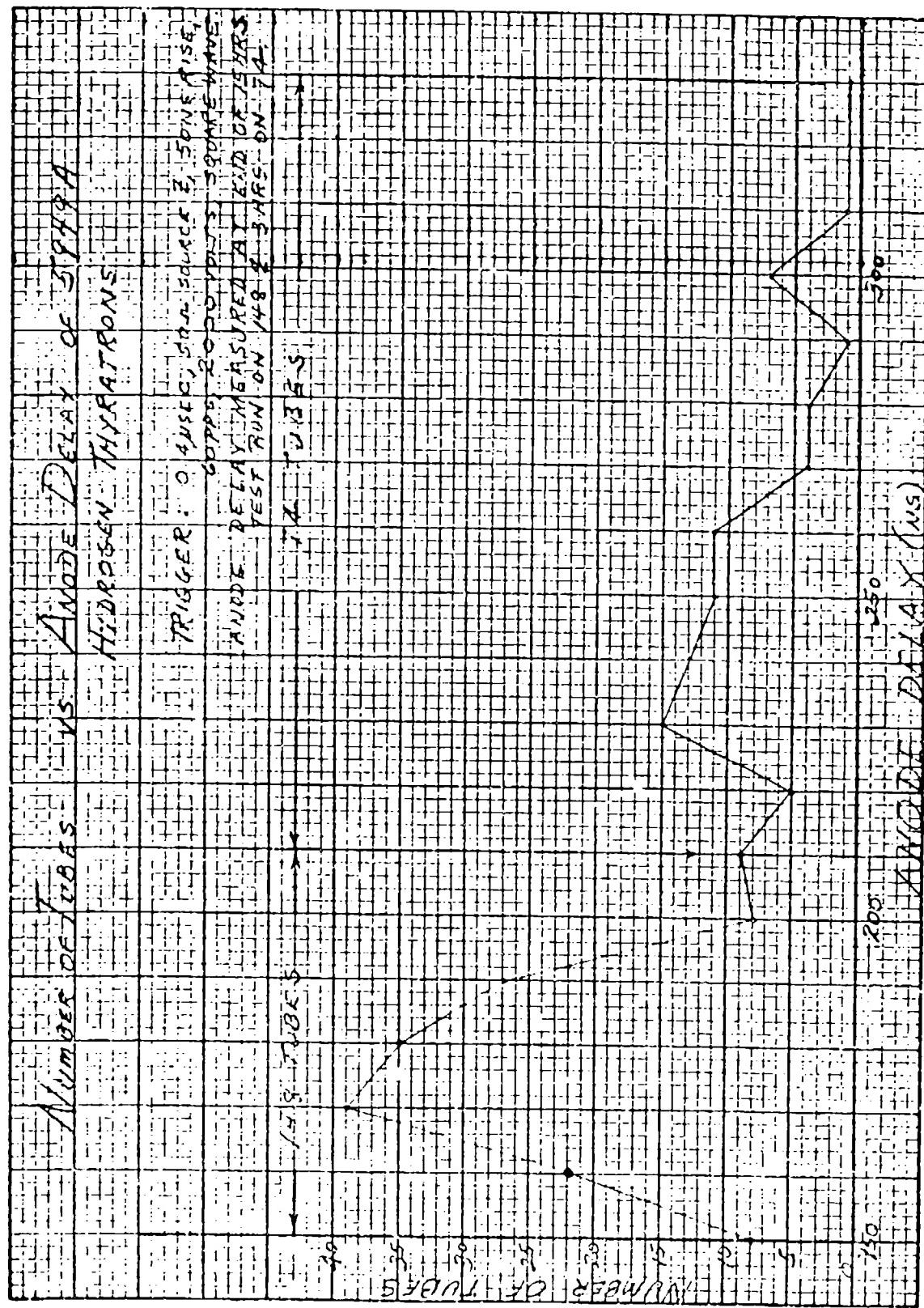


FIG. 28



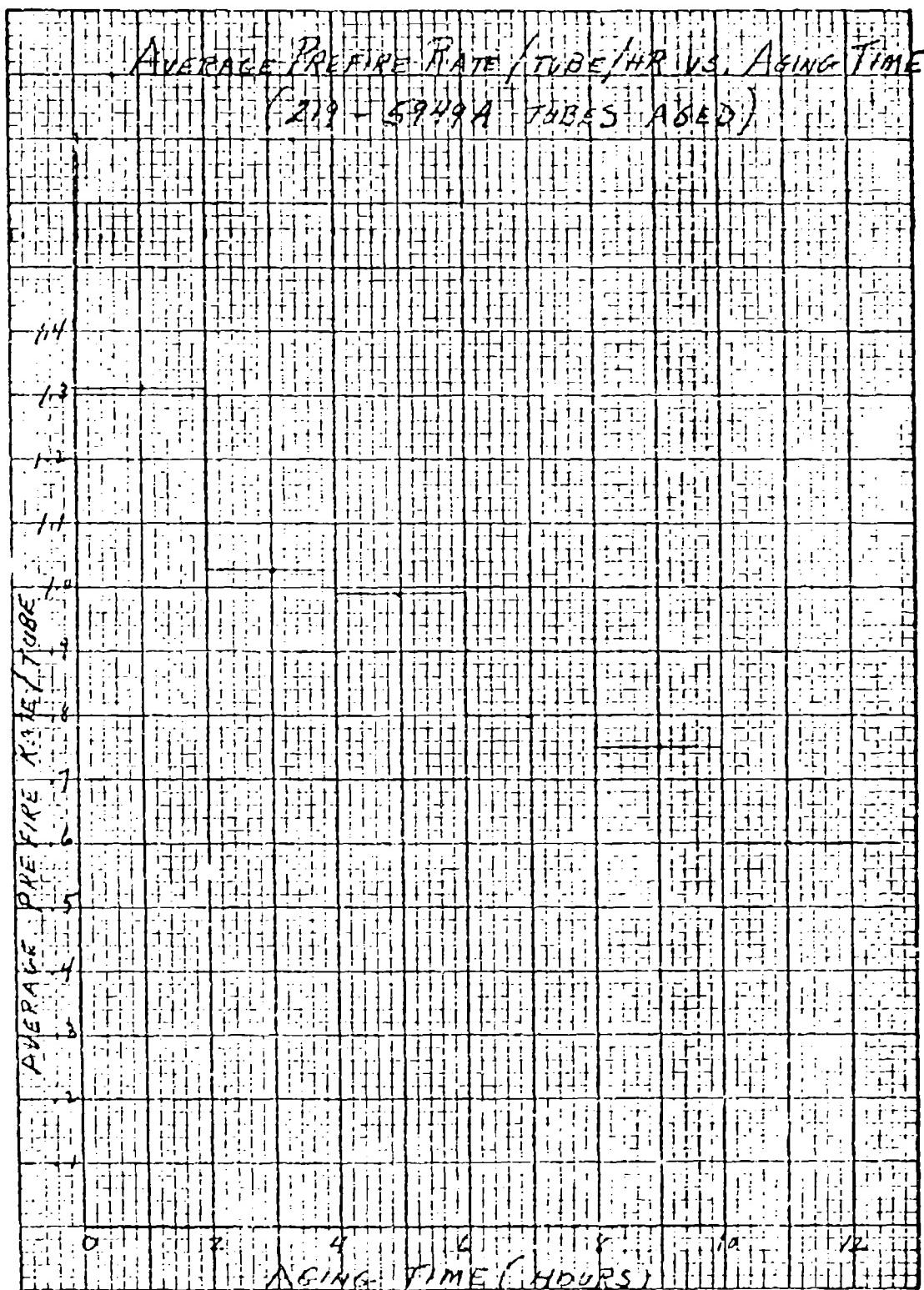


FIG. 30

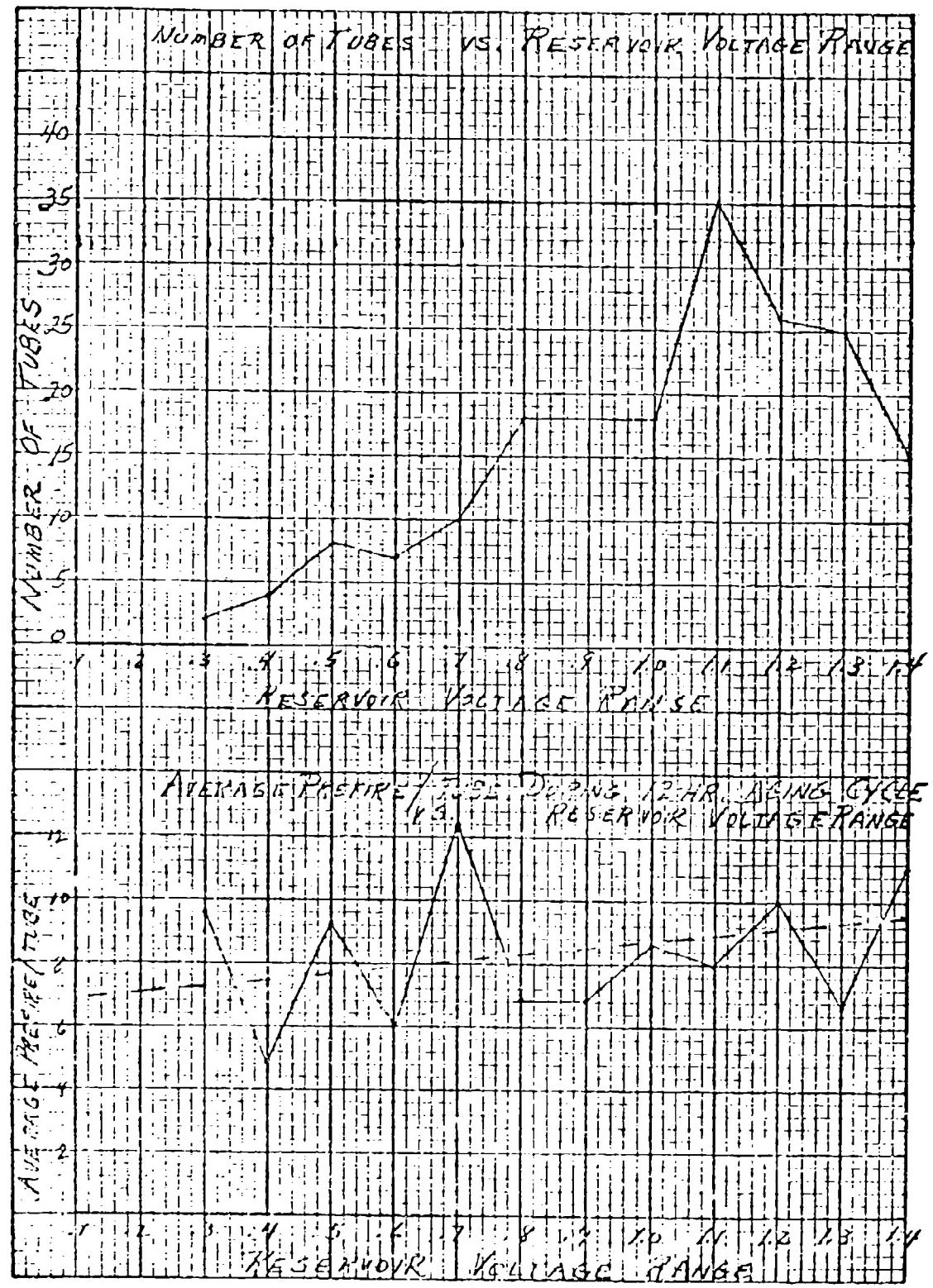


FIG. 31

voltage power supply charging system and also isolate trigger inputs so that random prefires can be tolerated. Under conditions of proper isolation, a random prefire would reduce the beam output by only 0.2% and only occur about once per 1,000 pulses at 60 pps.

Output Pulse Characteristics

Rise times of 50 nsec (10 to 90%) have been realized into a load impedance consisting of seven RG-213/U cables (7.14 ohms). The waveforms (see Fig. 24) of primary voltage and current into the cores show the low ripple attainable with the system when the pulse shapers are properly adjusted. The secondary core voltages are almost identical because of the excellent coupling.

Life Data of the 36-MW Modulator Operated at 28 to 32 kV, 60 pps

Switch Tube, Type 5949A, Used at 2500-Ampere Peak

A single tube was run constantly at 28 kV for over 6000 hours. The tube apparently failed to hold voltage and was removed from the test setup. It was later retested and seemed satisfactory. This tube has been returned to the manufacturer for examination. These data seemed quite encouraging and the design continued around the Type 5949A.

The following test data are not quite as encouraging, but still show reasonable life considering the low cost of the tube. It is anticipated that a special tube may be designed specifically for this application.

No. Tubes	Hours of Life	Total Tube Hours
2	1180	2360
3	810	2430
2	710	1420
1	570	570
1	370	370
9		7150

The average life is about 800 hours. It is obvious from the above that it will be necessary to replace tubes on a maintenance schedule of 600 hours in order to obtain reasonable reliability for the operating system.

Pulse Forming Network (RG-218/U at 32 kV)

Twelve pieces of RG-218/U (nine 260 feet long and three 130 feet long) were run a total of 3200 hours at 32 kV, 60 pps. Three of the surviving pieces ran an additional 3300 hours before all had failed. This added to a total of 34,070 unit operating hours with three failures, or a MTBF of 11,290 hours. The wearout appears to be about 6500 hours. This life seems reasonable for an experimental system of this nature.

Load Cables, RG-213/U

Thirteen 2-foot sections of 213/U were tested at 30-kV pulses (two times actual expected voltage in service) and nine failures were experienced in 32,000 unit operating hours for an average MTBF of about 3600 hours. Individual 170-foot-long sections have been tested to 5650 hours at 16 kV, 60 pps.

Connectors

Nine sets of RG-213/U load cable connectors (Figs. 21 and 23) have been run a total of 20,800 unit operating hours with six failures, giving an MTBF in excess of 3400 hours. Measures were taken to eliminate early connector failures caused by:

- (a) Poor connections of inner conductor pins.
- (b) Nicking of polyethylene.
- (c) Poor mica sleeves.

Conclusions

A compact, low cost, 36-megawatt modulator can be built utilizing a Type 5949A hydrogen thyratron for short pulses at five times rated peak current and attain the following:

- (a) 800-hour tube life.
- (b) Low anode delay drift of ± 5 nsec at constant operating parameters.
- (c) Low anode delay drift of ± 20 nsec over a wide range of anode voltage and repetition rates.
- (d) Long term (up to 800 hours) anode delay drift of ± 50 nsec.
- (e) Rise time of 50 nsec with low ripple in a 7-ohm circuit giving a current rate of rise of 50,000 amp/ μ sec.
- (f) Positive output pulse without significant deterioration of the rise time.
- (g) Prefire rates as low as one per 400,000 pulses.

Acknowledgments

The major portion of the life tests were performed by L. L. Steinmetz, H. M. Graham, and K. A. Saunders. This work was performed under the auspices of the U. S. Atomic Energy Commission.

References

1. N. C. Christofilos, "Astron Thermonuclear Reactor," Proceedings Second U.N. International Conference on the Peaceful Uses of Atomic Energy, Geneva, vol. 32, p. 279; 1958.
2. N. C. Christofilos, "High Current Electron Accelerator," Lawrence Radiation Laboratory, Univ. of Calif., Livermore, UCRL-5463-T, January, 1959.
3. N. C. Christofilos, "Induction Electron Accelerator," Lawrence Radiation Laboratory, Univ. of Calif., Livermore, UCRL-5783-T, November, 1959.
4. N. C. Christofilos, "High Current Pulsed Electron Accelerator," Lawrence Radiation Laboratory, Univ. of Calif., Livermore, UCRL-5951-T, April, 1960.
5. E. T. S. Walton, "The Production of High Speed Electrons by Indirect Means," Proc. Cambridge Phil. Soc., vol. 25, p. 469, July, 1929.
6. D. W. Kerst, "Acceleration of Electrons by Magnetic Induction," Phys. Rev., vol. 58, p. 841, September 1, 1940.
7. D. W. Kerst, "The Acceleration of Electrons by Magnetic Induction," Phys. Rev., vol. 60, p. 47, July 1, 1941.
8. W. A. S. Lamb, "Design Features of a High-Current Pulsed Electron Accelerator," Lawrence Radiation Laboratory, Univ. of Calif., Livermore, UCRL-6699, November, 1961.
9. W. S. Melville, "Use of Saturable Reactors as Discharge Devices for Pulse Generators," Proc. Inst. Elec. Engrs. (London), vol. 98, pt. 3 (Radio and Communication Engineering) No. 53, p. 185, May, 1951.
10. K. Aaland, "Magnetic Core Evaluation For a 0.3 Microsecond Pulse," Lawrence Radiation Laboratory, Univ. of Calif., Livermore, UCID-4167, December, 1959.
11. K. Aaland and B. M. Loth, "Acceptance Tests of Astron Induction Accelerator Cores," Lawrence Radiation Laboratory, Univ. of Calif., Livermore, UCID-4203, August, 1960.
12. V. L. Smith, "Development of 36 Megawatt Modulators for The Astron 1,000-Megawatt Electron Accelerator," IRE Trans. on Nuclear Science, April, 1962.
13. C. D. Nail, "The Failing of Dielectrics," Electronic Industries, p. 74, September, 1958.
14. R. G. Schonberg, "High Power Pulse System Regulation," 6th Symposium on Hydrogen Thyratrons and Modulators, Fort Monmouth, N. J., 1960.

ANALYSIS OF MODULATOR DESIGN PROBLEMS BY SIMULATION

by

Robert A. Hill

Westinghouse Electric Corporation
Electronics Division

Through use of equivalent circuits for the components, the model of a modulator circuit can be described by a set of differential equations. Equation coefficients are determined by circuit elements. Solution of these equations on an analog computer yields familiar graphical information. The analog model obtained in this manner inherently yields freedom of experimentation and observations without restrictions imposed by physical circuits.

Illustrative examples of this approach can be taken from design problems typically encountered with the line type modulator. The area of interest in this report will be limited to the four basic components in the pulse loops shown in Figure 1. These components are treated as an integral group to determine the transient response of the entire system in producing the output pulse. Before proceeding with computation of the complete system, it is necessary to determine component equivalents and the influence of each on over-all response characteristics.

(a) Pulse Forming Network

The simulated network is equivalent to a four section Type E with equal capacitance per section as shown in Figure 2. A four section network was selected as a compromise between minimum mathematical computations and obtaining front end element values nearly equal to a network having a greater number of sections. This amounts to removing all but the first four sections of any network to study pulse front edge response. The pulse length obtained is sufficient to observe leading edge transient behavior of the transformer and provide decay time for anticipated overshoot and transient ringing.

Starting point for the network design was that given in Chapter 6 of Vol. 5 (Rad. Lab. Series). Using values given for the 5 section network, the pulse shape was in agreement with Figure 6-27. The third section was then removed to obtain the desired

four sections. As inductance was adjusted for minimum ripple, the network became load sensitive. This design was abandoned in favor of the design given in Evans Signal Lab Report T-43. Initially this network had approximately 5% r p/c; however, it could be adjusted for minimum ripple without increasing load sensitivity. Ripple was reduced to $\pm 1\%$ with very good stability. Waveform of the network is shown in Figure 3.

Load sensitivity was found to be the major problem in network design. This is the ability of a pulse forming network to maintain its pulse shape when the load impedance is changed. In actual practice, a network is usually adjusted for desired ripple tolerance with a matched resistive load during manufacture, but is operated in service with a slightly mismatched transformer load. This sequence was carried out in the simulation program to examine various network designs and manufacturing techniques. The general criterion for both low ripple and stability of pulse shape appeared to be symmetry of internal loop currents. It can be seen in Figure 3 that all loop currents are symmetrical about an axis through the time center of the pulse. A constant impedance of the network is maintained in the analog model to determine true system droop. Actual networks would require compensation for transformer droop.

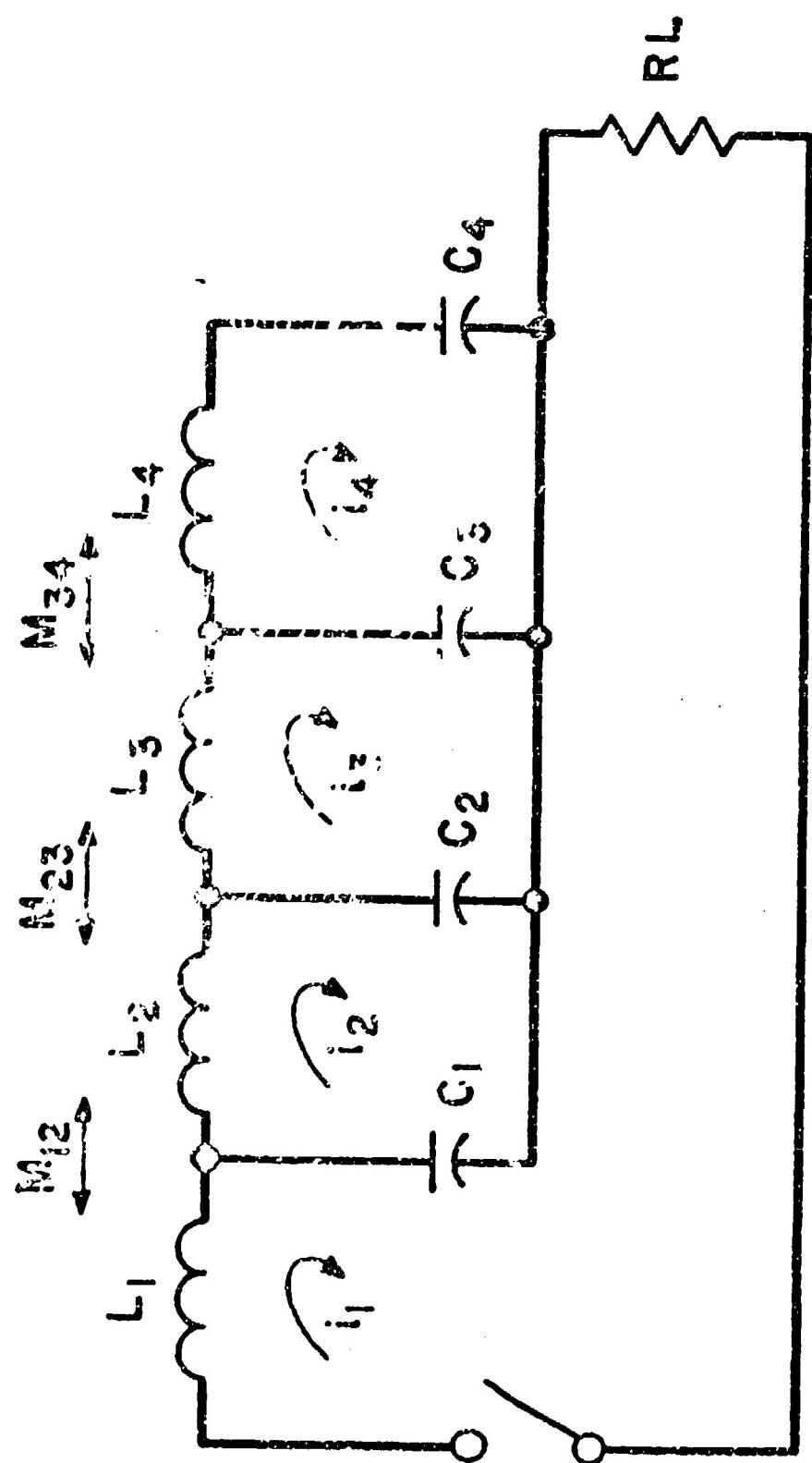
(b) Load

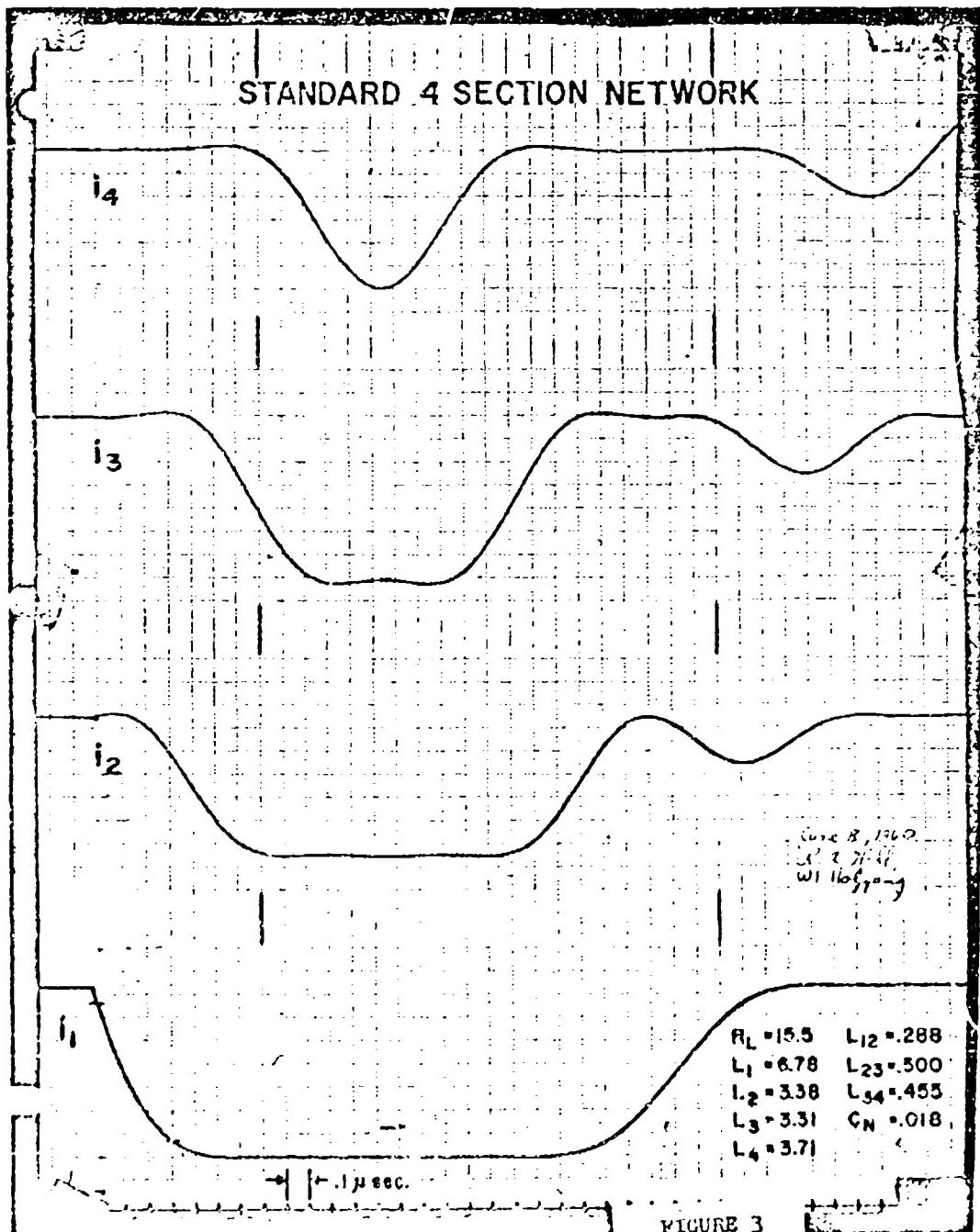
Upon examining the discharge loops of the modulator circuit, it can be seen that the only major dissipative element is the load. Since other components are mainly composed of reactive elements, all energy dissipation and circuit damping will essentially be accomplished by the load. Most useful loads are non-linear and will depart radically from the ideal characteristics of pure resistance. To accurately compute pulse rise time, overshoot, ripple, backswing, etc., the dynamic impedance, represented by the equivalent load circuit is used. In the analog model, this can be achieved by non-linear function generators or series-parallel combinations of resistors and biased ideal diodes.

(c) Thyratron

Non-linearities of a thyratron preclude exact simulation of all its characteristics. Fortunately, the thyratron acts as a low impedance, unidirectional

PULSE FORMING NETWORK





switch, and therefore lends itself to considerable simplification. Generally, for large modulators the internal inductance and plate voltage drop are taken into account. The resistance may be assumed constant during the pulse; however it must be considered variable during the backswing period in the absence of active transformer clippers.

(d) Pulse Transformer

Over-all performance of the line type modulator depends largely upon pulse transformer characteristics. Output pulse shape, component operating levels, and energy transfer are all inter-related with transformer parameters. This complex function results mainly from imperfections in the electrical characteristics introduced by its physical properties and dimensions. The imperfections are for the most part stray reactances and losses. These are usually distributed throughout various voltage levels of a transformer and the position of any increment will determine its effectiveness. To develop a complete equivalent circuit for this is all but impossible.

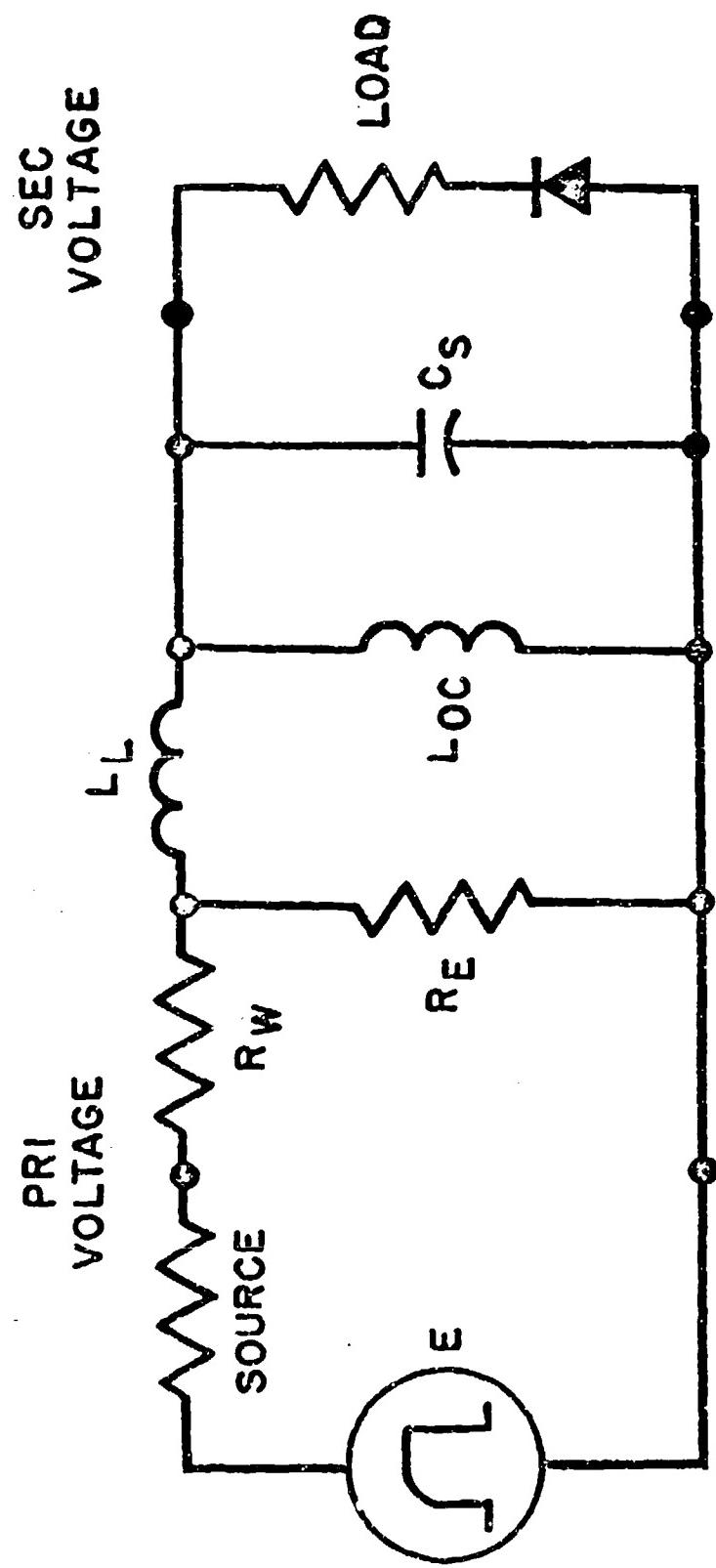
Most of the pulse transformer effects, but certainly not all, can be described by elements in the elementary equivalent circuit shown in Figure 4. The elements include effective values of stray capacitance (C_s), leakage inductance (L_L), open circuit inductance (L_{oc}), core loss (R_e) and copper loss (R_w). Figure 5 shows the response of such a circuit. For a given primary voltage, output voltage and output current may be computed. Rise time, overshoot, droop, fall time, and backswing may be seen. It is of interest to also note magnetizing current may be plotted. In some cases, a more elaborate equivalent circuit is required.

TYPICAL PROBLEMS

Having developed a model of the circuit with appropriate element values (Figure 6), special problem areas may be simulated for investigation.

A commonly encountered problem of line type modulators with a magnetron load is that of double tracing. The pulse is seen to alternate between two conditions. A comparison of an observed waveform from an actual modulator and computed waveform is shown in Figure 7. It was found from operating the modulator that this condition existed within a given range of the operating voltage. Computed

ELEMENTARY TRANSFORMER
EQUIVALENT WITH 1:1 RATIO



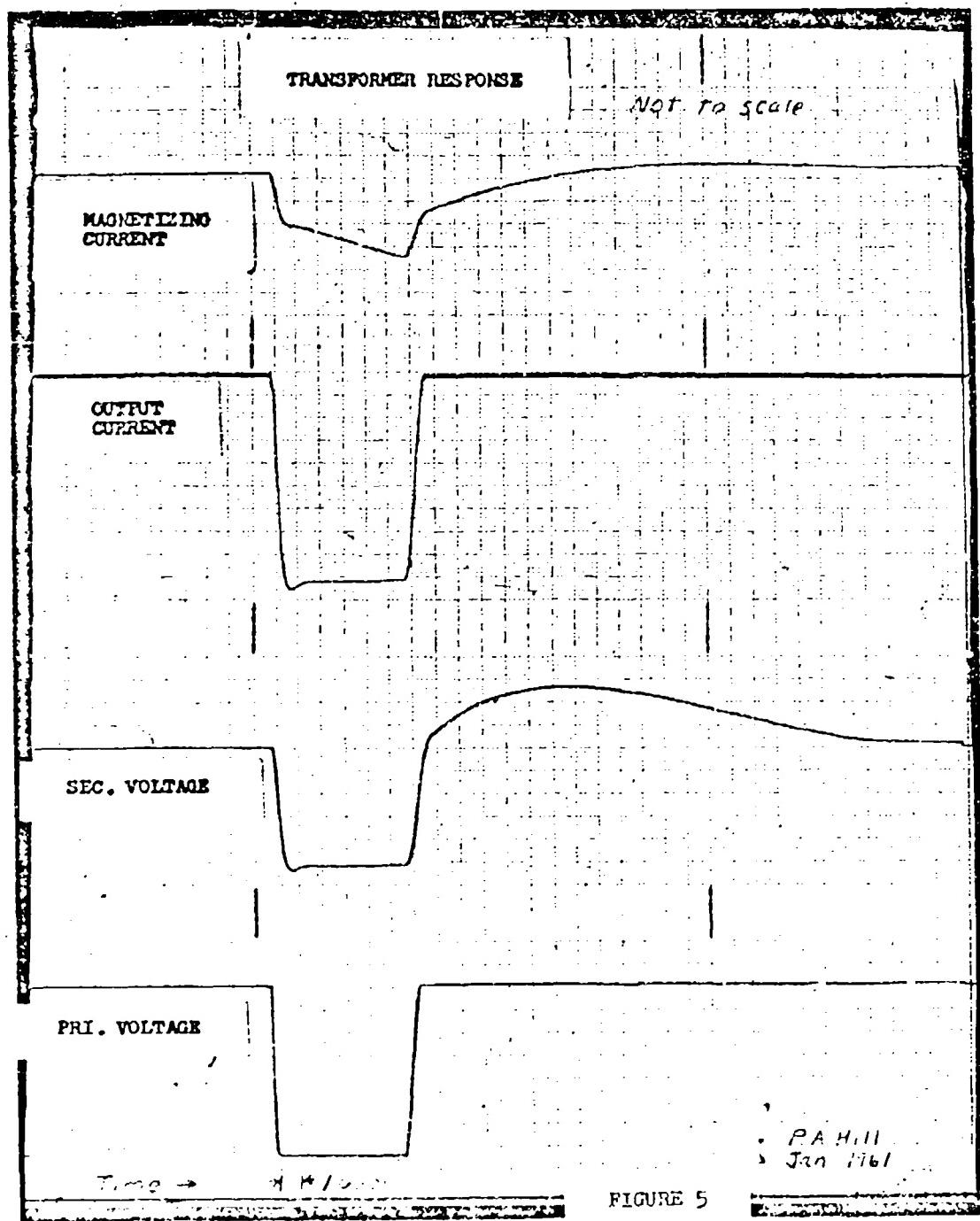


FIGURE 5

MODULATOR EQUIVALENT

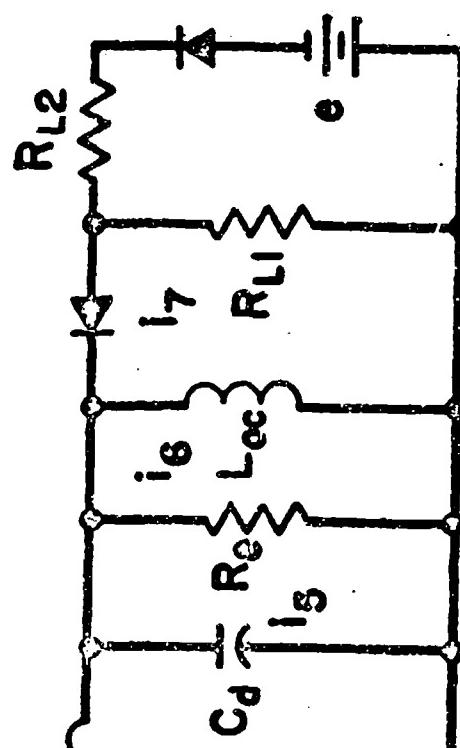
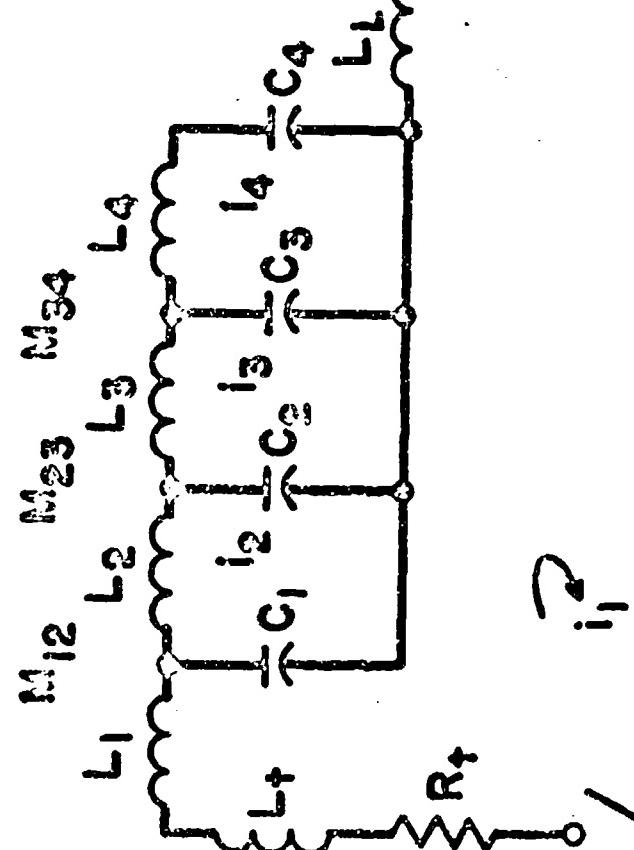


FIGURE 6

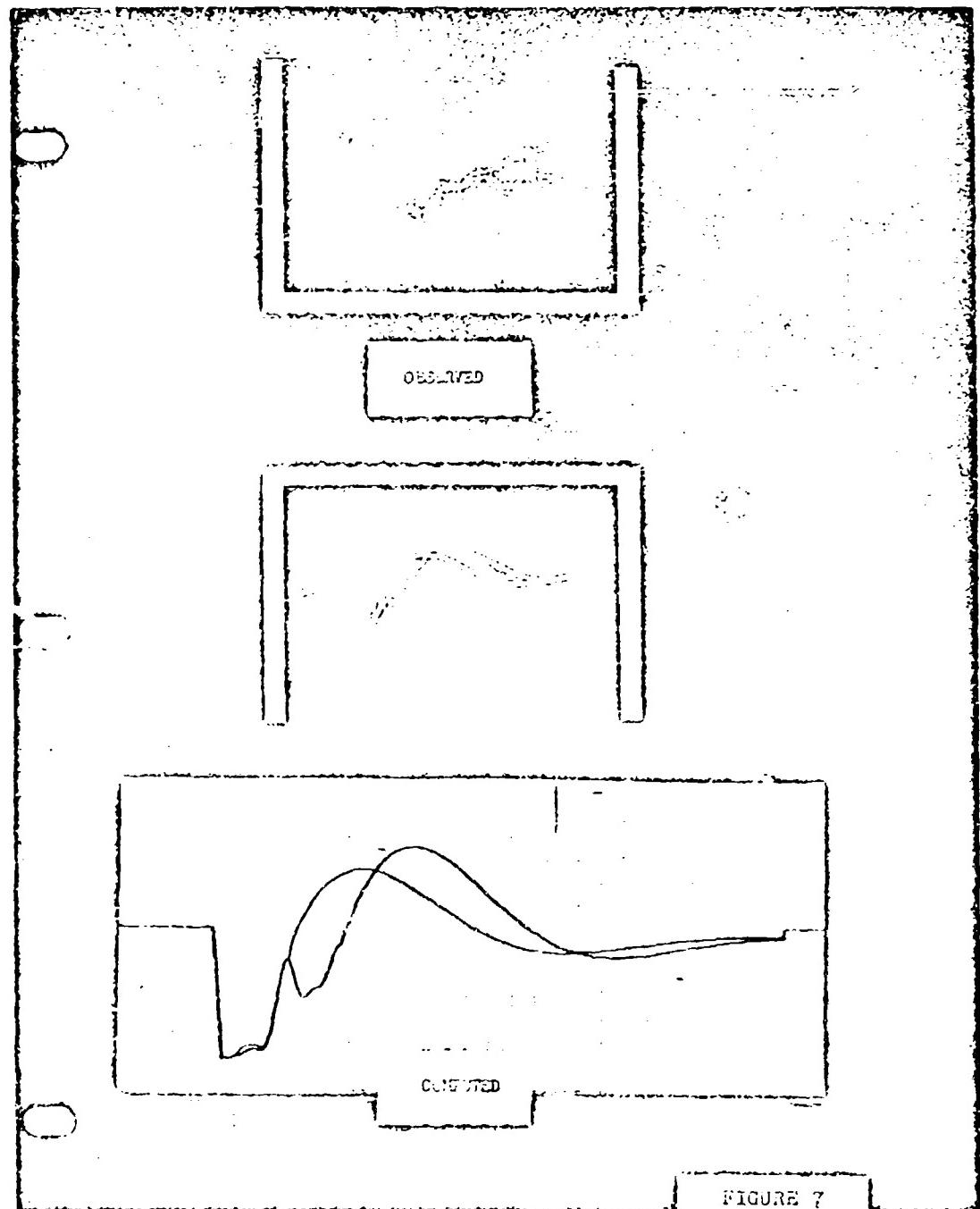


FIGURE 7

waveforms for this operating region indicated that primary current had large superimposed ripple during the decay time. Ripple peaks caused the thyratron to conduct during the post pulse period. This in turn changed the succeeding charging cycle in such a way as to cause the pulse shape to vary.

In another example, the analog model was used to investigate transformer ringing. Ripple was observed on the secondary winding during the pulse plateau. The elementary equivalent circuit of a transformer will not produce high frequency ripple, rather it acts as a low pass filter. The transformer equivalent shown in Figure 8 was used to investigate ringing. With this scheme the transformer is reduced to a 2:1 step up ratio rather than a 1:1. It can be seen that coupling is accomplished entirely by mutual inductance instead of series leakage. DC isolation between primary and secondary is retained. This circuit lends itself to the general practice of transformer construction where half of the secondary winding is wound on each core leg. It includes leakage inductance of each half winding to the primary, individual capacitance of the windings to ground, and intrawinding leakage inductance of the secondary. A comparison of observed waveform and computed waveform for an actual transformer is given in Figure 9. (NOTE: Transformer droop shown the oscilloscope was due in part to the pulse generator used during the test.) Study work done with this equivalent circuit has been confirmed by laboratory experiments with excellent agreement. Ringing has been shown to be a function of incremental leakage inductance and stray winding capacitance. The magnitude of ringing produced by the stray loops depend in part upon excitation caused by the input pulse rise time. Thus, network rise time must be slower than resonant frequencies of the stray loops if ringing is to be avoided.

Most modern systems using wavetube amplifiers require an extremely flat pulse plateau with minimum rise time. Limitations imposed by physical considerations within the transformer, network, and load force a compromise. The layout of components within a package must also be considered. Packaging does not necessarily add new components to the equivalent circuit of a modulator but does alter element values. Compatibility of the network, transformer, and non-linear load depends on the proper choice of element values of the components. As previously mentioned, the PFN must have minimum load sensitivity. There are several potential sources of waveshape distortion in a pulse transformer. Characteristic impedance, $Z = \sqrt{L_L/C_d}$, of the transformer was investigated as to its significance with a three-halves power diode load. Except in the case of a

TRANSFORMER EQUIVALENT

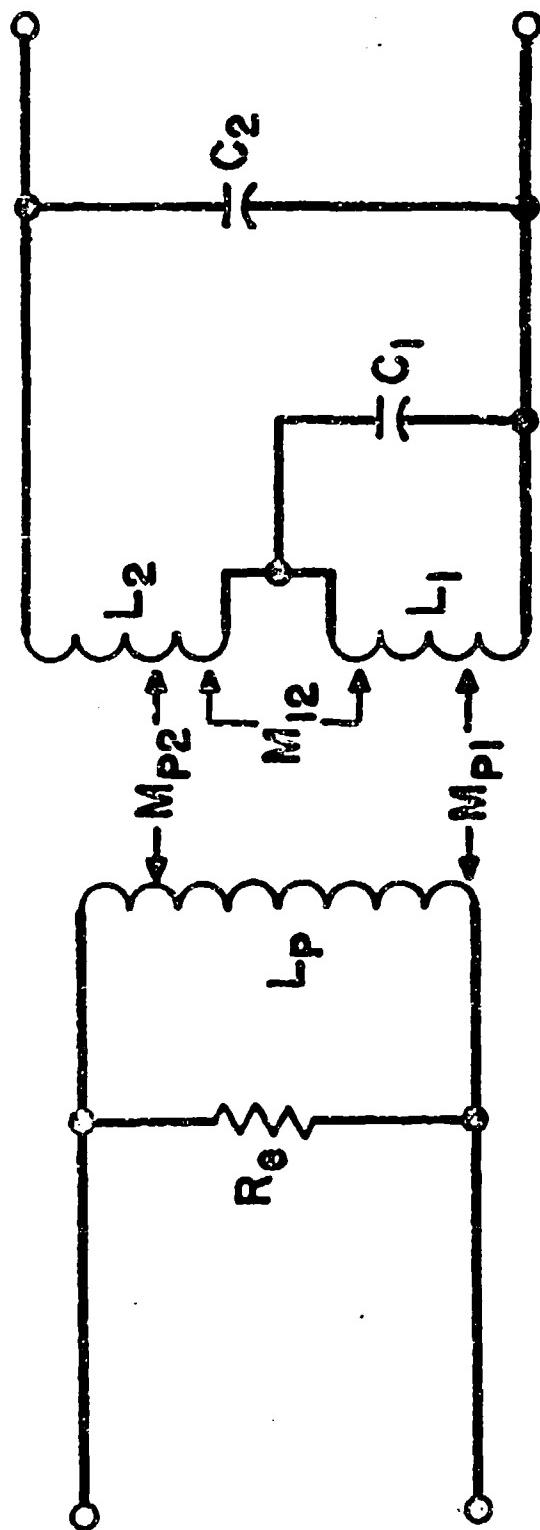


FIGURE 8

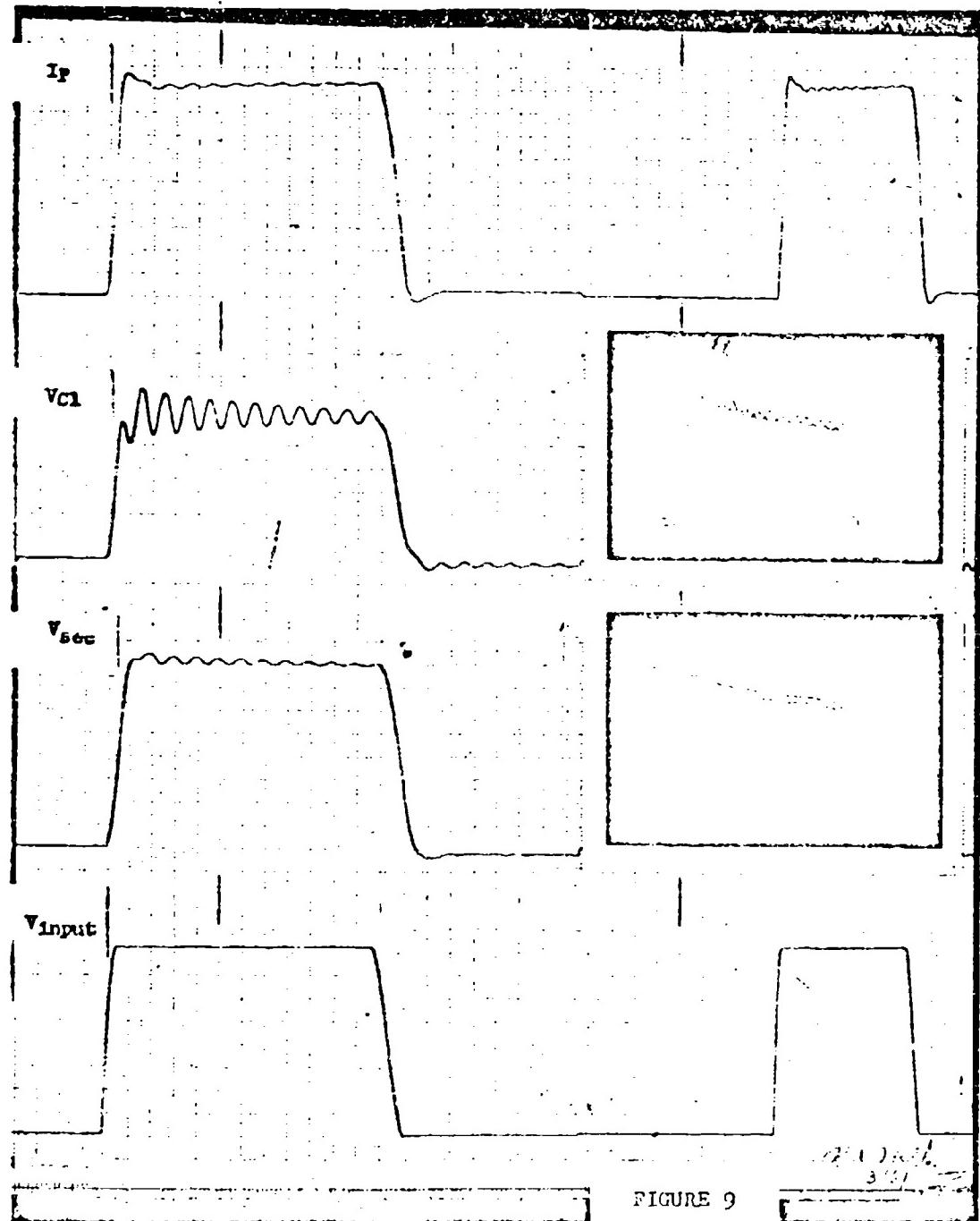


FIGURE 9

highly load sensitive network, characteristic impedance matching was found to be of little importance. In a total of 50 computations using various values of $Z = \frac{I_L}{C_d}$ each one indicated a high impedance of the transformer is desirable. In effect, this is reducing the total capacitance and thereby reducing surge current during rise time. It appeared that the best over-all compromise occurred when the transformer leakage inductance equaled the nominal section inductance and total stray capacitance of the transformer and load was less than section capacitance. With this criterion, network section values become a function of transformer parameters with the total number of sections determined by pulse length. Since equivalent values are used in the model the same holds true for parallel operation of networks.

HIGH POWER VLF PULSE GENERATION USING HYDROGEN THYRATRONS

by

E. R. Besenfelder and C. J. Eichenauer

Heavy Military Electronics Department
General Electric Company, Syracuse, New York

The versatility of the hydrogen thyratron as a high level energy discharge device has been firmly established over the course of many years. Similarly, the use of the type E pulse forming network, as an efficient energy storage and shaping means has been clearly established.

A somewhat unusual application of these two elements was brought about by a recent equipment requirement. A pulsed VLF transmitter was required which would be capable of producing an output power of one megawatt, an output frequency in the one to five kilocycle region, and an output pulse duration in the 10 to 100 millisecond region. Specifically, the approach taken in this development was to use a hydrogen thyratron inverter as the VLF generator, and a type E pulse forming network as the pulse energy source for the inverter. While this approach appears a direct one, justification of several of the techniques proposed was necessary, since they represented a great departure from those normally associated with inverter technology, and since the final equipment had to occupy the minimum possible cubic content.

One of the first areas which required review was the use of a pulse forming network for the pulse power supply element. Figure 1 shows the alternate means considered. The first of these, the DC rectifier power supply was eliminated on the basis of its size and weight. For example, if the longest pulse duration is considered, the supply would require a storage capacitor of approximately half a million joules in order to limit the 100,000 joule output pulse to a ten percent droop. The second course of action, was the AC to AC flywheel motor generator set in conjunction with a high voltage rectifier. In addition to its size, weight and audible noise level there was some question about the ability of this technique to provide a sufficiently flat pulse due to the inherent regulation of the AC generator. The third possibility, the AC to DC flywheel motor generator set was eliminated on the basis of size, weight, audible noise, commutation generated RF noise, and possibly poor regulation. In addition, all three of these approaches have the potential disadvantage of delivering a high fault current into the inverter in the event of a malfunction in its operation. Based upon the above considerations, a pulse forming network system was selected as most appropriate for this application.

Figure 1 shows in simplified form the main elements of the power supply and pulse forming network arrangement. Briefly described, the equipment functions as follows:

1. Line power, at 1100 volts three phase, is supplied to the primary of a conventional high voltage three phase rectifier circuit by means of a constant 1100 current network.
2. The DC supply charges the main pulse forming network at constant DC current due to the action of the constant AC current network.
3. When the potential across the pulse forming network reaches its specified level, the voltage level comparator circuit turns on the charging level triode which short circuits the DC power supply and discontinuing the charging of the network.
4. Network discharging back through the charging level triode is prevented by the holdoff action of the charging diode.
5. At the prescribed time, the pulse forming network is discharged by the inverter, following which the above sequence of events repeat themselves.
6. In the event of a fault in the inverter, the pulse forming network energy is absorbed by an end of the 1100 clipper circuit.

Two items deserving of a more detailed treatment are the constant current charging circuit and the pulse forming network. Constant current charging was employed for two reasons, first, because it allowed the use of a high voltage DC power supply having a relatively low current rating, and second, because this type of charging allowed the pulse forming network capacitors to operate at a lower effective value of voltage during the long charging period than would resistive or recurrent charging. As a result of the second point it was possible to use a capacitor rated for more energy storage in a given case size than would have been possible otherwise.

The constant current charging circuit employed is shown in figure 3. This circuit, invented by Blumlein in the early days of alternating currents has seen relatively little use in recent years. It is known as the homopolar network and has the characteristic of delivering constant current to the load resistor R₁ regardless of its ohmic value. Both single phase and three phase variations are shown along with their simplified design procedures. Figure 4 shows a more detailed view of the charging circuit where the three primary legs of rectifier transformer have replaced the load resistors of the previous figure. The secondary legs of the transformer are then connected to a conventional

FIGURE 2

SIMPLIFIED DIAGRAM OF ONE TENTH MEGAJOULE PULSER

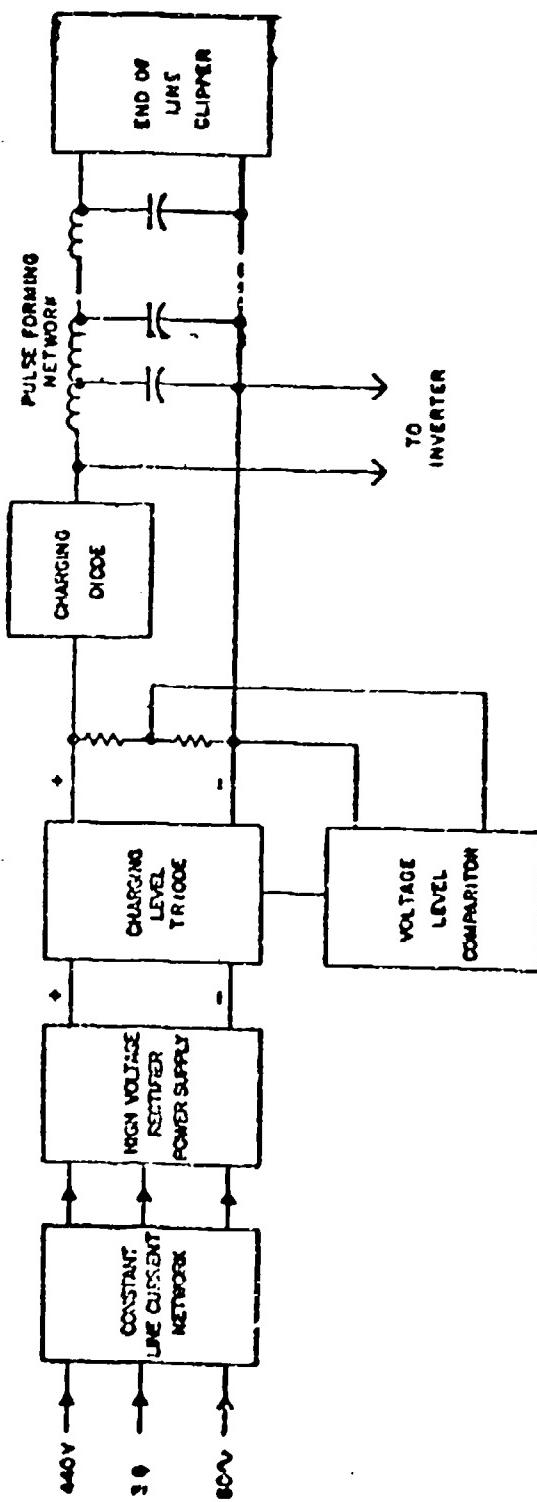
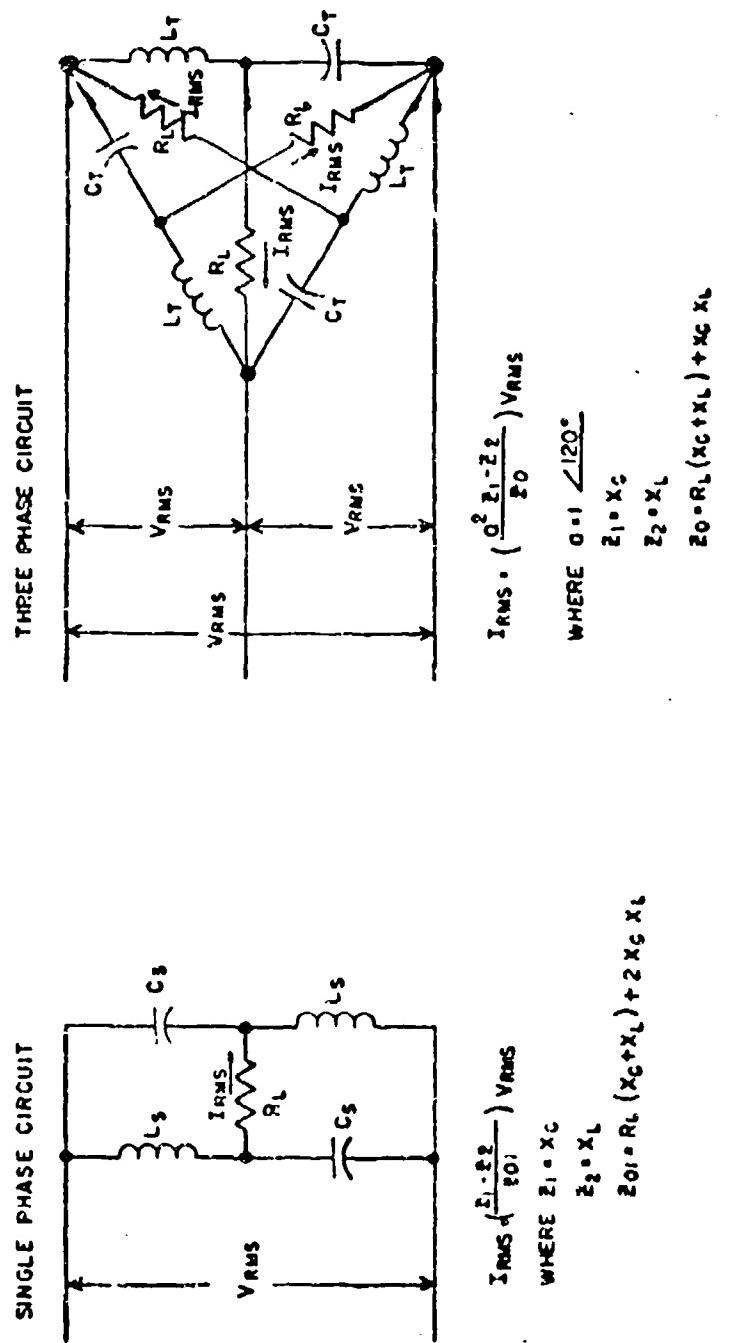
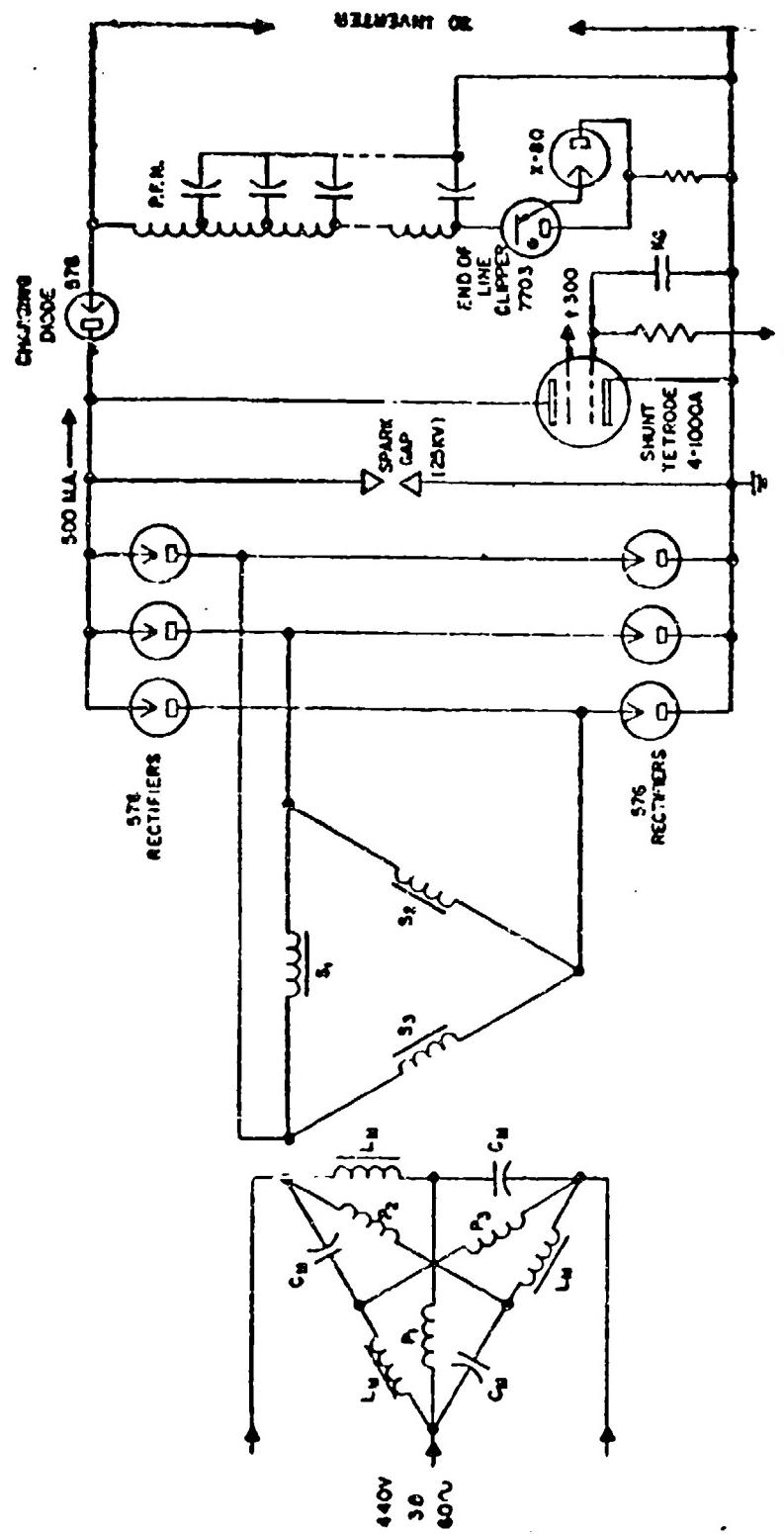


FIGURE 3





SIMPLIFIED SCHEMATIC DIAGRAM OF PULSER

FIGURE 4

three phase rectifier which in turn charges the pulse forming network at a constant value of DC current. The ratio of the constant DC current to the constant RMS line current is an almost direct function of the turns ratio of the rectifier transformer and the type of rectifier circuit employed. As noted previously, when the charging voltage on the pulse forming network has reached the predetermined value, relay contacts K_C close causing the 4-1000A shunt tetrode to conduct, thus diverting the charging current through that path. A most important part of this type of charging circuit is a spark gap across the output of the DC supply. In its absence, should the electronic shunt circuit fail to operate, the DC voltage will continue to rise until some component flashover occurs or until some magnetic component saturates.

The design of a pulse forming network capable of providing pulses in the one tenth megajoule region at long pulse durations involves special consideration of several mechanical and electrical characteristics of the device. For example, a 100 ohm, 100 millisecond network would require 500 microfarads of capacitance and 5 henrys network inductance. These values can be reasonably obtained by using conventional capacitor cans, and air core coils. Assuming the network was designed using approximately twenty sections, a structure similar to figure 5 could result. The following factors are relevant to such a design:

1. The DC resistance associated with twenty large coils of one quarter henry each may be large compared to the load resistance. For this reason the network should be designed with tapered characteristic impedance to compensate for the pulse droop which would otherwise result.
2. For greatest ease of final adjustment the coils should be adjustable relative to one another thus providing for proper mutual coupling adjustment in such a tapered design.
3. Once adjusted the coils should be adequately braced since magnetic forces of several thousand pounds between coils can easily result due to the large numbers of turns involved.
4. Network capacitors should be specified which reflect the peak current, voltage stress and duty cycle on a per capacitor basis. It is possible that a properly rated network capacitor may be little larger per unit volume than a conventional filter capacitor design.
5. Particular attention should be given to the rating of end of the line clipper tubes and resistors since similar elements found satisfactory in short pulse service may not have adequate emission and/or thermal capacity for long pulse service.

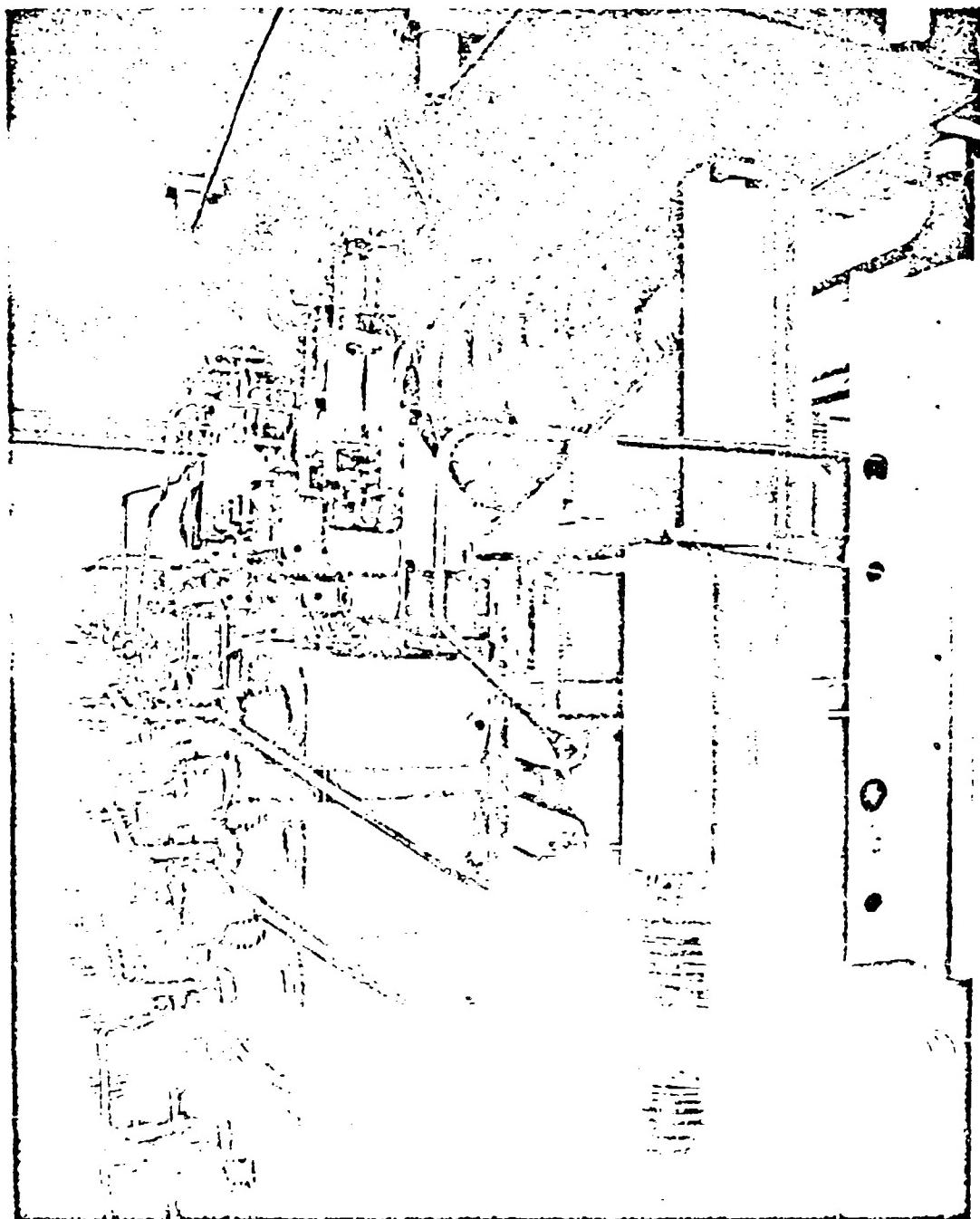


Figure 5 Pulse Forming Network Assembly

A typical wave shape obtained from the equipment shown in the previous figure is shown in figure 6. This wave shape does not represent the best pulse top characteristic possible since portions of the network were optimized for operation at a different pulse duration and hence some compromise was necessary. It does serve to illustrate how the tapered network design effectively overcame what would have been a 30% droop in the pulse had the coil resistance not been properly compensated.

As has been mentioned the hydrogen thyratron is a high level energy discharge device and for this reason it was chosen to operate in a parallel inverter circuit to generate high power VLF pulses. However, the hydrogen thyratron inverter involved several unique design problems.

First, during switching the device used in the inverter must withstand inverse voltage of the same magnitude as forward voltage. Also turn-on and turn-off times of the device used must be short. Specifically, in the design circuit, the ionization time is small and was ignored and the allowed time for de-ionization equals one tenth of the time for one cycle.

Second, the output power of the inverter must vary with the DC level of the power supply, hence, the switch device must be capable of firing at low values of supply voltage.

The General Electric Power Tube Department evaluated the GL-7390 hydrogen thyratron for this application. The test results indicated that the GL-7390 thyratron would withstand the expected inverse switch potential of 24,000 volts. Also the grid would regain control in approximately 5 microseconds by controlling grid bias and reservoir voltage. Also the device would fire at potentials lower than 1000 volts, allowing the inverter output level to be varied the required 20 dB. With the de-ionization time in the order of 5 microseconds the inverter could be operated at frequencies up to 20 KC or approximately four times the frequency of interest. Our breadboard models using smaller devices have recently been operating at frequencies in the order of 100 KC. It would be well to note here that from the tests conducted, thyratrons seem to have a different set of characteristics for inverter use than for modulator or clipper use. Hence, the writers would like to promote the publishing of such data to better evaluate thyratrons for inverter applications.

Figure 7 shows the basic inverter circuit. This circuit was developed using a paper written by C. F. Wagner as a guide. The grids are alternately triggered by 2 microseconds pulses developed by 3C45 thyrtatrons in combination with 2 microsecond pfn's. Gated pulses to the 3C45's control the start and stop of the inverter. The 2 microsecond pfn in a resonant charge circuit is designed to charge for the highest desired output frequency. As the current drawn by the inverter has a ripple frequency of 2 fo a series trap tuned to 2 fo reduces the

FIGURE 6 OUTPUT WAVEFORM OF
PULSE FORMING NETWORK

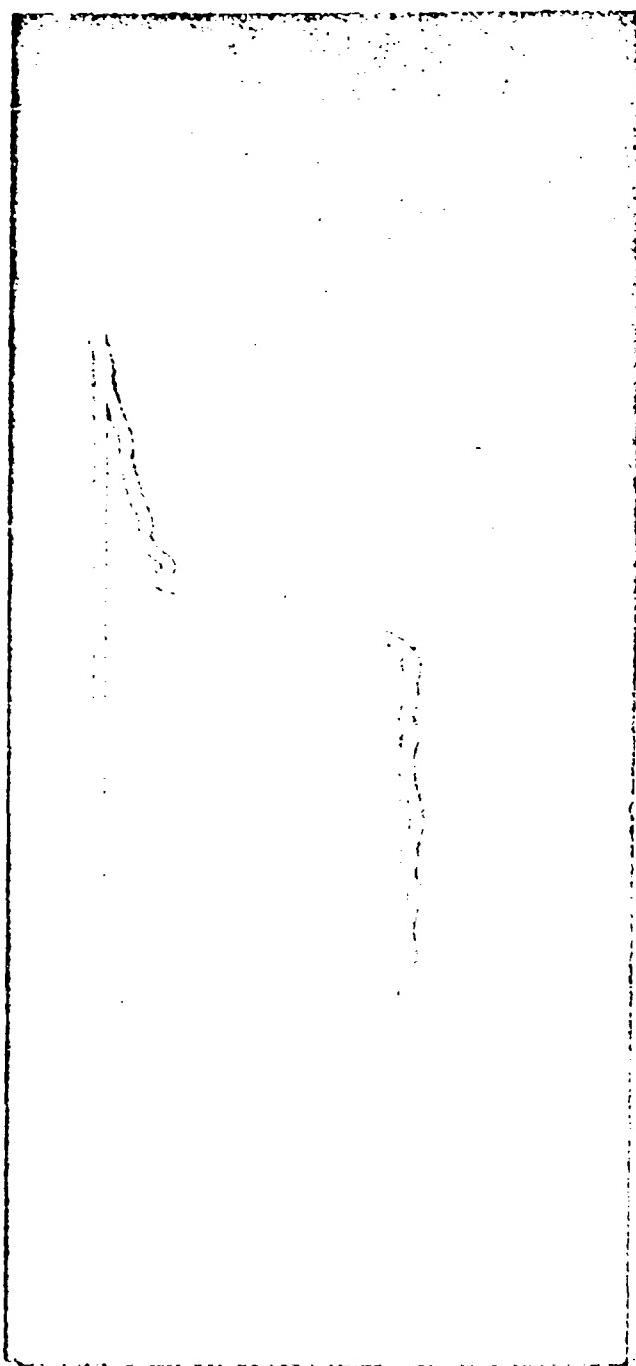


FIGURE 7

SIMPLIFIED SCHEMATIC OF HYDROGEN THYRATRON INVERTER

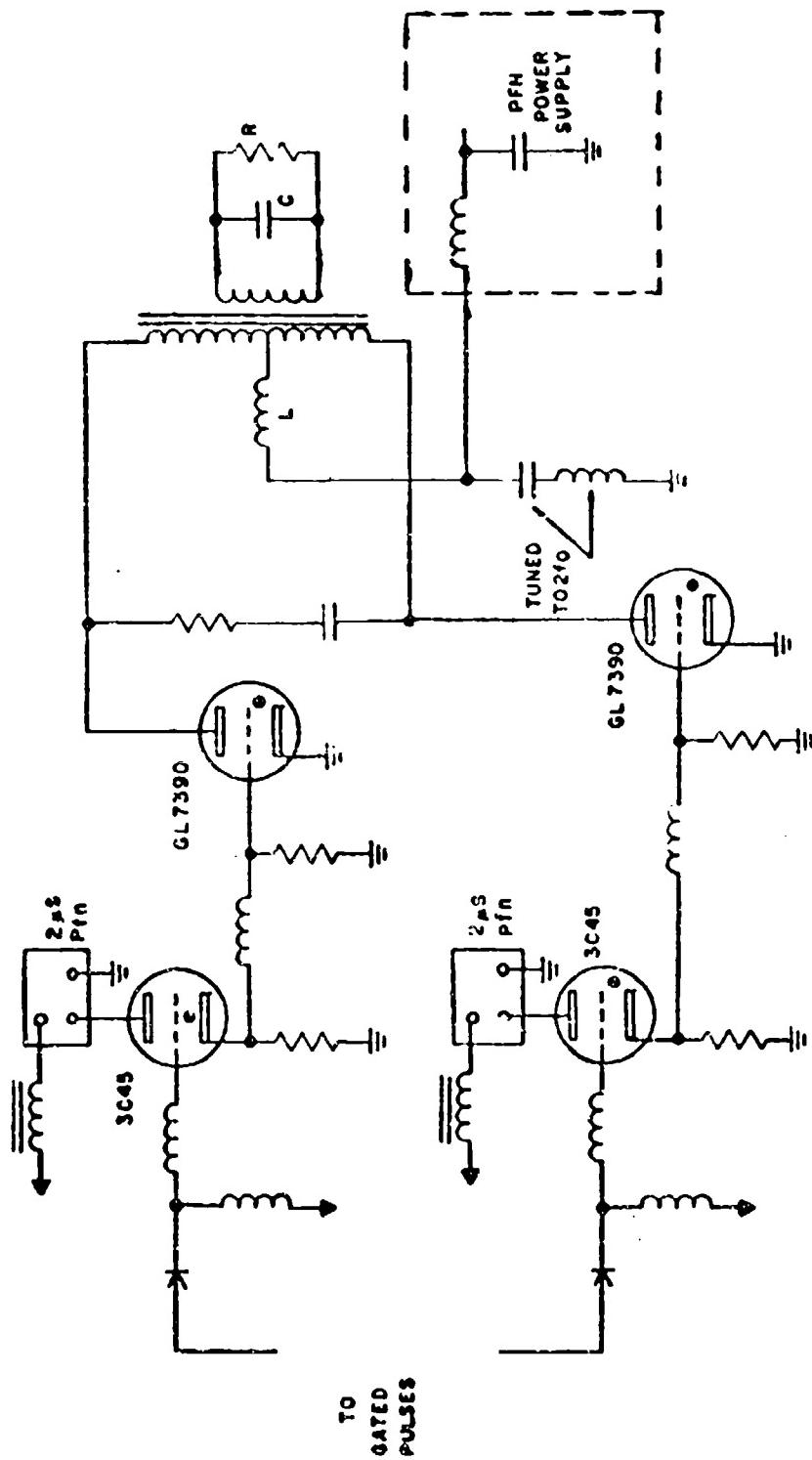


FIGURE 8 INVERTER OUTPUT WAVEFORM OF
ONE TENTH SECOND PULSE

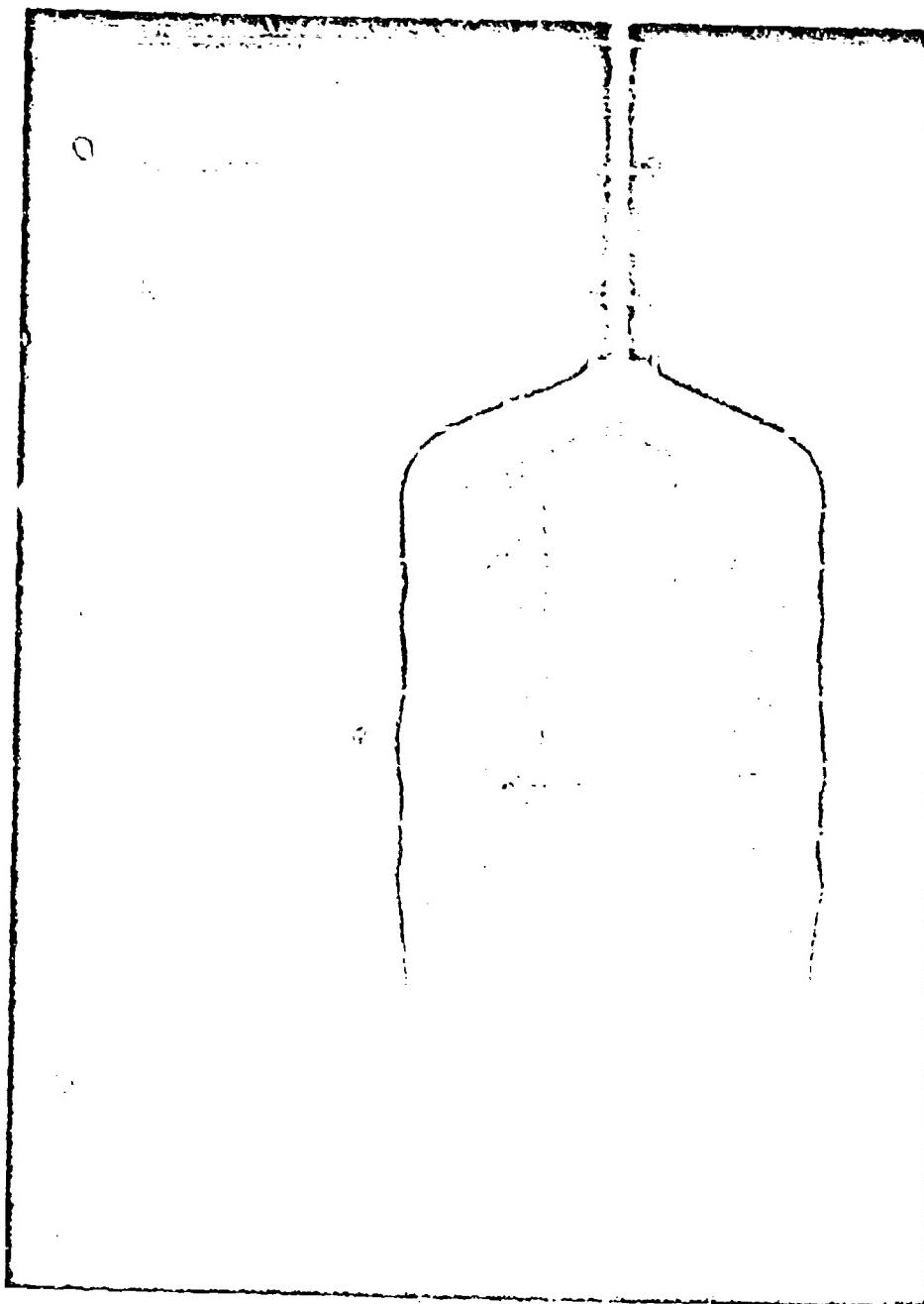


FIGURE 9 INVERTER OUTPUT WAVEFORM OF
THIRTY FIVE MILLISECOND PULSE
(PFN ADJUSTMENT NOT OPTIMUM)

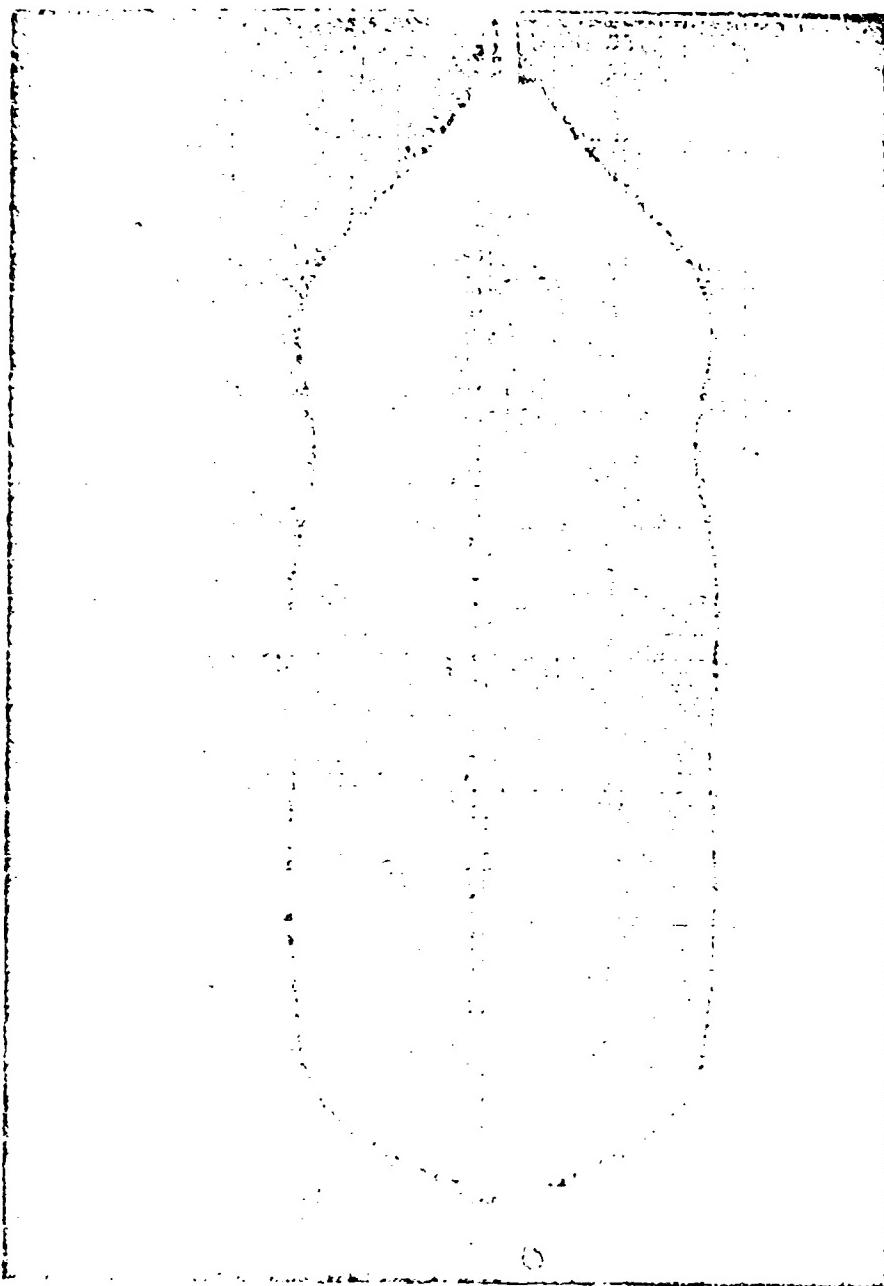
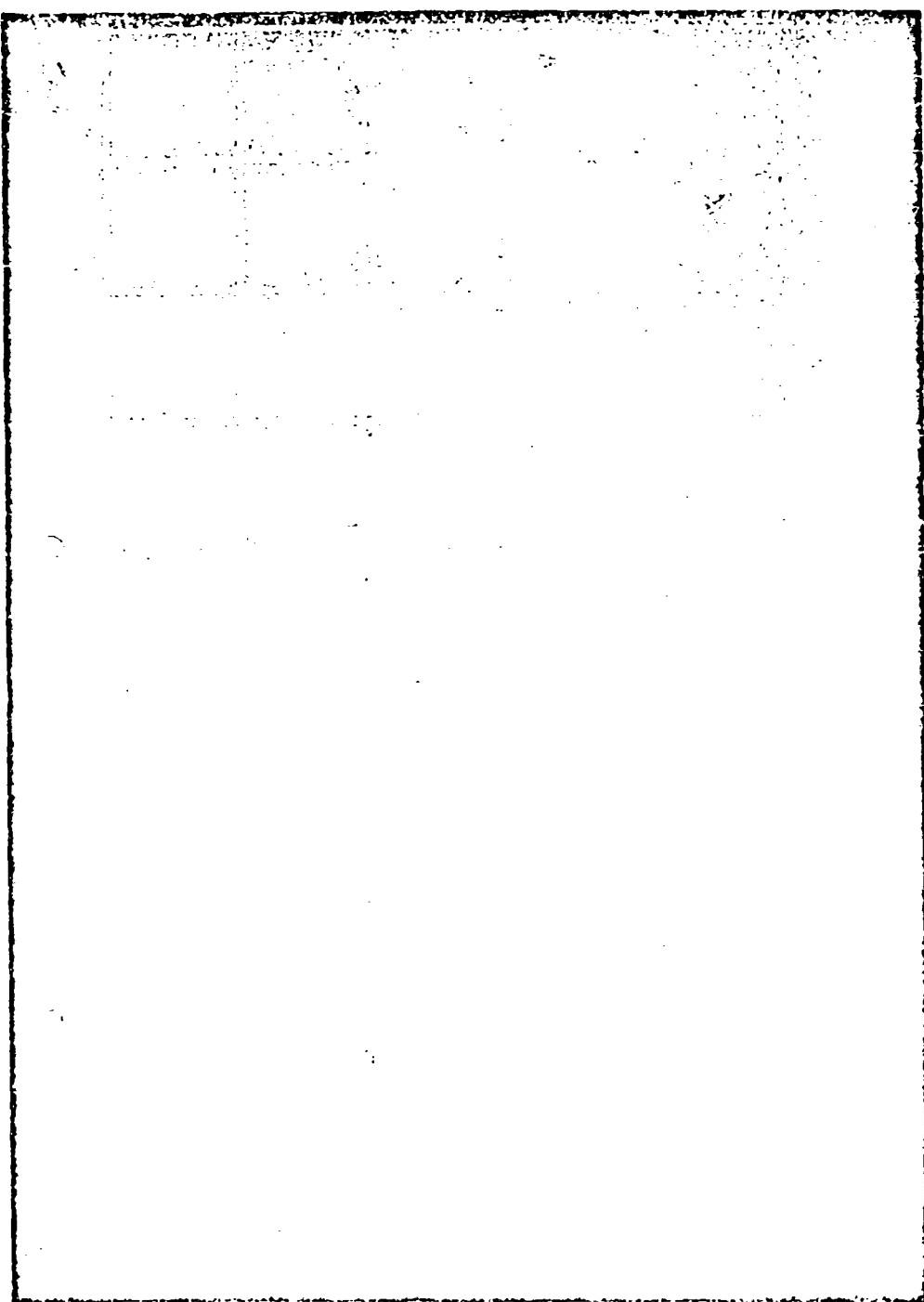


FIGURE 10 INVERTER OUTPUT WAVESHAPE



In summary, this development program has conclusively demonstrated the effectiveness of hydrogen thyrectrons as VLF power generating devices, when used in properly designed inverter circuits. In addition, a properly designed type E pulse forming network has been shown to be an effective and versatile means of supplying pulse energy to such an inverter. An operating system employing these concepts has been in continuous operation in the field for the past six months.

- REFERENCES:
- (1) Wagner, C. F. "Parallel Inverter with Resistive Load"; Transactions of the American I.E.E. 1935 p1227.
 - (2) Grabowski, S. J. "Monocyclic Constant Current Networks"; GE Technical Information Series 101124H - General Electric Company, Schenectady, New York.

THE GRID SPIKE PROBLEM ASSOCIATED
WITH HYDROGEN THYRATRONS AND A PRACTICAL
MEANS FOR ITS SOLUTION

by

R. W. Bedgwick

The Bendix Corporation
York Division

It is well known to the designers of line-type radar modulators that, when the grid of the hydrogen thyratron switch tube is triggered, high voltage spikes occur at the grid terminal. These spikes, although of exceedingly short duration, can approach the peak voltage applied to the anode from the fully charged pulse forming network. When the trigger is applied to the grid, the potential rises during the discharge current rise¹ until it closely approaches the peak anode voltage, thereby generating the spike. As soon as full tube current is established, the grid potential returns to the trigger generator output voltage level. The literature² recommends that a low-pass filter be placed between the output of the trigger generator and the thyratron grid. It also recommends that the grid circuit components be designed to withstand instantaneous voltages of several kilovolts between grid and ground.

The author has been closely concerned with the development of a number of lightweight line-type radar modulators during which the breakdown of grid circuit components assumed serious proportions, and it became necessary to investigate the problem further. In the particular case under consideration, a 2:1 step up transformer was used to raise the output of the trigger generator to the proper level, thus raising the grid circuit impedance considerably. Many failures of these transformers occurred due to high grid spike voltages. The first step in solving the problem was to view the spike and determine its characteristics. It was found that the grid spike had a width of approximately 40 nanoseconds at the 50% point, and its amplitude varied from tube to tube. Amplitudes ranging up to over 7 KV have been observed where the peak anode voltage was 8 KV.

Three circuits are shown in Figure 1 for coupling the trigger generator to the thyratron grid. Figures 1 (a) and 1 (b) show, respectively, conventional RC filter and biased diode arrangements. Neither arrangement would withstand the grid spike voltages unless made impractically large, and with adequate high voltage ratings for the insulation and diodes. Since the spikes have a width of approximately 40 nanoseconds at the 50% point, it seemed practical to attempt to design a suitable

1 Hydrogen Thyratrons - Theory and Application General Electric Company (Bulletin)

2 M.I.T. Radiation Laboratory Series, Vol. 6 - McGraw Hill

filter resonant at the equivalent frequency of 12.5 mc. The filter would offer a high impedance to the spike, and thus, attenuate the high voltage sufficiently to afford protection to the trigger generator output circuit. At the same time, this circuit would also pass the trigger to the grid with minimum attenuation because of its low impedance at the trigger generator frequency. The circuit shown in Figure 1 (c) was developed and successfully attenuates the grid spikes in the ratio of approximately 8:1. It was found that a 220 μ h choke layer wound on a specially insulated powdered iron core with the comparatively low Q of about 30 and self-resonant out of the circuit at 3.5 mc was the optimum value for this service. When the choke is connected into the circuit, however, the circuit self-resonant frequency is about 12.5 mc as read on a grid-dip meter, which incidentally, affords a simple method of checking the grid circuit parameters. It should be mentioned that this paper only covers one particular case, but there appears to be no reason why the same principles should not be successfully applied to protect any thyratron grid circuit from grid spikes.

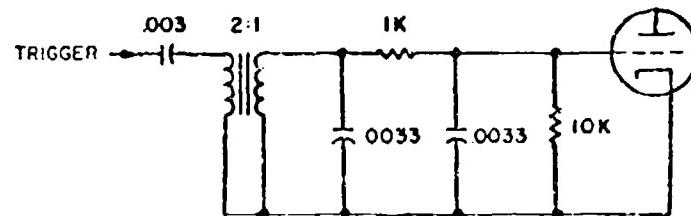
Slides

- Slide #1 - Figures 1(a), 1(b), 1(c).
- Slide #2 - Figure 2 Trigger Pulse, tube out.
- Slide #3 - Figure 3 Trigger Pulse, tube in, filament voltage applied.
- Slide #4 - Figure 4 Grid Spike, tube pulsed.
- Slide #5 - Figure 5 Spike at choke input, tube pulsed.

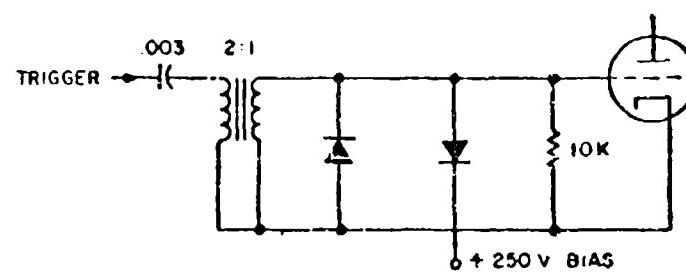
Acknowledgement is made of the considerable assistance rendered to the author in the preparation of much of the data for this paper by D. P. Clark, E. Kepner, and J. Wible of the York Division of The Bendix Corporation.

References

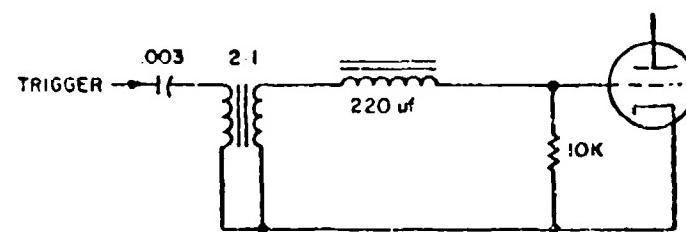
1. Hydrogen Thyratrons - Theory and Application General Electric Company (Bulletin)
2. M.I.T. Radiation Laboratory Series, Vol. 5 - McGraw Hill



(a)



(b)



(c)

FIGURE I

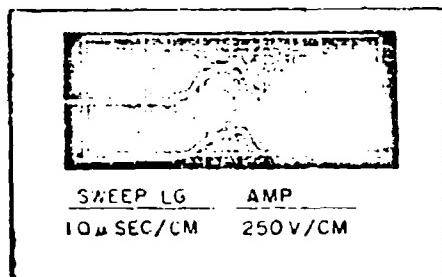


FIGURE 2 TRIGGER PULSE, TUBE OUT

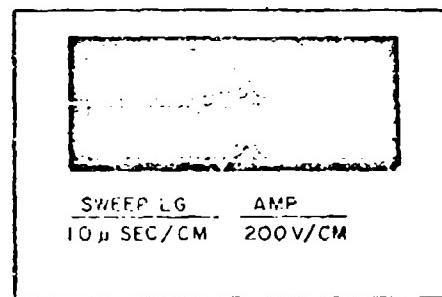


FIGURE 3 TRIGGER PULSE, TUBE I,
FILAMENT VOLTAGE APPLIED

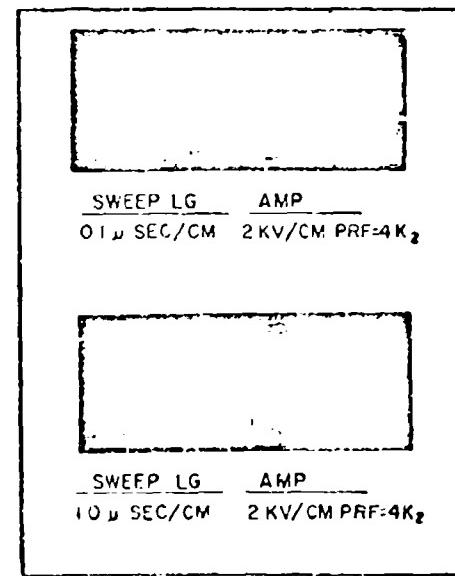


FIGURE 4 GRID SPIKE, TUBE PULSED

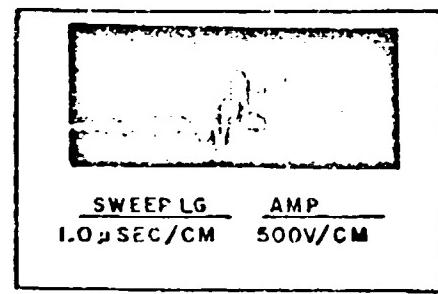


FIGURE 5 SPIKE AT CHOKE INPUT,
TUBE PULSED

A TWT FLOATING DECK GRID PULSER
EMPLOYING PNPN (SHOCKLEY) TRANSISTOR DIODES

by

Albert R. Luna - Stephen F. Delligatti

Burmac Electronics Company, Inc.

Introduction

This paper describes in one pulser three uses of the PNPN (Shockley) transistor diode. This device was used, (1) to enhance the trigger pulse, (2) to operate as the switch device of a line-type modulator and, (3) to act as a tail biter. The pulser displays characteristics comparable to those achievable with a hard tube modulator. This is accomplished in a fraction of the space and weight that would otherwise be required. By virtue of the completely solid-state design, maximum efficiency and extreme ruggedness are obtained.

Requirements

The customer had need for a grid bias supply and a pulser (Figure 1). The only unusual feature of the bias supply was that, because it would be in series with the pulser, its dynamic impedance must be so low as to not adversely affect the pulse characteristics.

The pulser requirements referenced to the bias voltage were:

Peak Voltage; 700 volts positive
Peak Current; 800 milliamperes maximum
Duty Cycle; 0.01 maximum
Pulse Width; 13.1 microseconds
Rise and Fall Times; 0.2 microseconds maximum
Droop plus Ripple; 0.1 percent maximum peak to peak

Since the cathode was to be fixed at -30,000 volts dc, these units were to operate as a floating deck. The ultimate use was to be in an airborne application, so that minimum size and weight, and the greatest possible ruggedness were an important consideration.

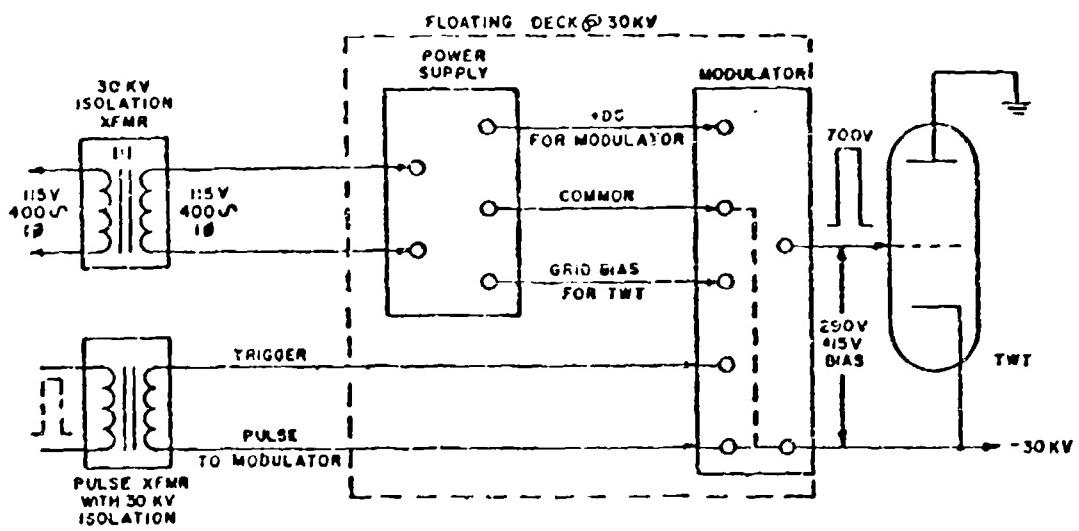


FIG. 1

The customer's reason for requiring an extremely flat-top pulse was in order to achieve the constant phase shift necessary for a pulse compression radar system. The fast rise and fall times were required in order to pass through the critical oscillation region of his TWTs as quickly as possible, and to achieve maximum effective duty cycle within the operating specifications of the tube.

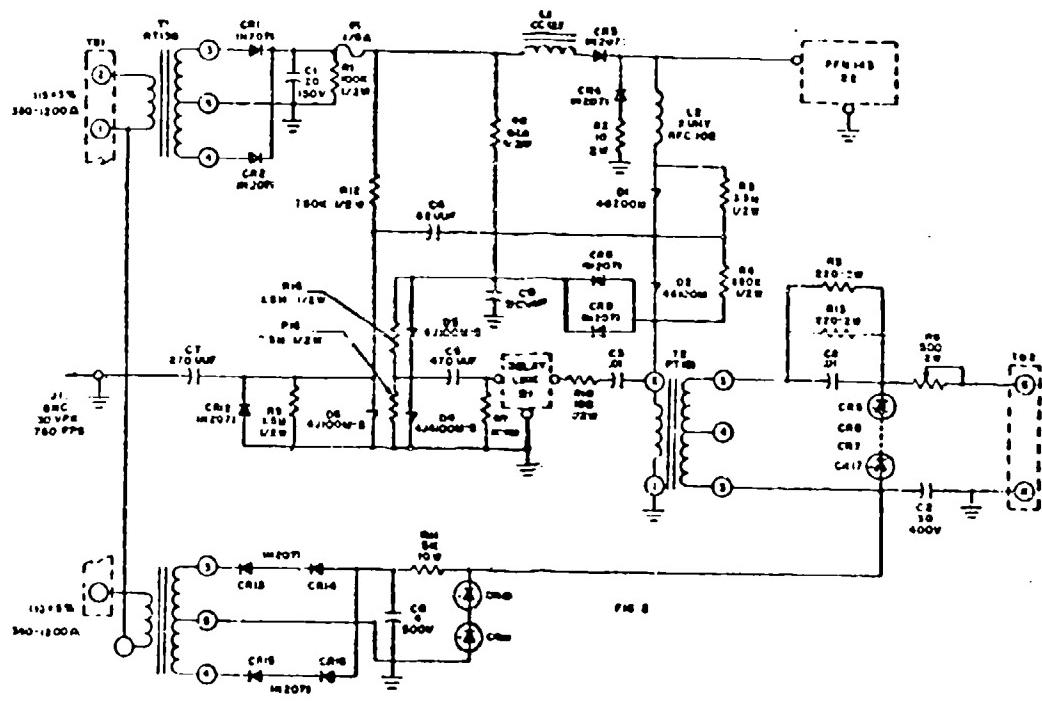
Approach to Solution

The customer had an operating hard tube pulser which met the specifications and a line type pulser which did not. Still, to achieve minimum size and weight, they felt that a line type pulser was necessary. Our past experience with the PIPN diode in line-type pulsers indicated to us that this was the device around which to design our pulser. It is certainly smaller, more rugged and more efficient than comparable hydrogen thyratrons. With this device, the required fast rise time is no problem. Because fall time at 13.1 microseconds would be difficult to achieve directly, we decided to speed the fall time by means of a tail-biting circuit. We were of the opinion that the pulse flatness could be achieved by using zener diodes across the output of the modulator, essentially in shunt with the grid of the tube. We had the advantage that the customer was able to prove out the zener philosophy in their line-type pulser even before the order was placed.

The final schematic is as shown in Figure 2. Since the customer wished to provide us with a positive trigger pulse of 30 volts peak amplitude, we decided to amplify that trigger by means of PIN diode D5. In that way the trigger pulse is increased to roughly 100 volts amplitude. This pulse, which incidentally is negative, applied at the junction of D1 and D2, causes D1 to switch to a conducting state, followed by D2. A positive pulse appears on the primary of T2, is stepped up and fed through limiting resistors R5 and R13 to the zener diodes C5, 6, 7 and 17. Capacitor C8 is used to reduce a round off on the top of the pulse. Potentiometer R6 is used to vary the amplitude of the pulse, since grid current flows. The same positive pulse on the primary of pulse transformer T2 is fed through delay line Z1 to the junction of PIN diodes D3 and D4 which when they switch act to "bite" the tail of the pulse. Delay line Z1 therefore determines the pulse width. Pulse forming network Z2 is made to be slightly wider than delay line Z1.

Difficulties Encountered

In the development of this modulator we found some difficulty in three areas. First, the tail-biter circuit was originally more conventional. There was no dc voltage on the PIN diodes, and the pulse into the delay line came from the output of trigger diode D5. In order to prevent the switching of the tail-biter diodes during the leading edge of the pulse it was necessary to decouple them from the pulse voltage on the



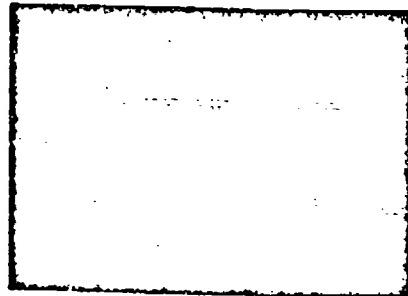


FIG 3A PULSE SIGNAL

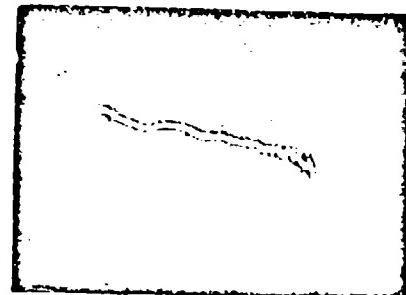


FIG 3D R6 = 0 OHM
SENSITIVITY 0.25 V PER CM

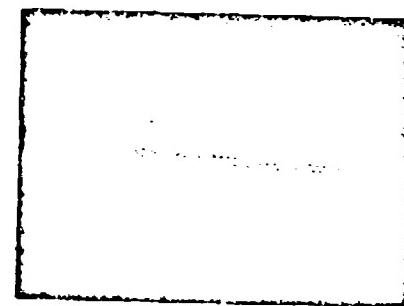
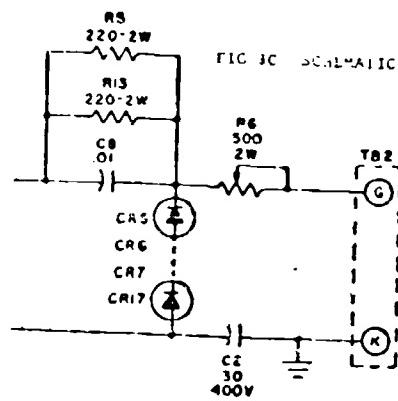


FIG 3D R6 = 500 OHMS
SENSITIVITY 0.25V PER CM

pulse with R6 set at 500 ohms, a condition of minimum pulse amplitude. Deviation from flatness is 0.5 volt total.

We have learned that of the four modulators delivered, the one in longest operation is one which has been in actual operation some 35 hours. However, this is 35 hours of operation on a floating deck at 30 kv. Every time the TWT was put on the air, the operation of the crowbar was checked. Also, there were several instances during the 35 hours when the crowbar was caused to fire during the operation of the tube. There have been no failures in the modulators, and there has been no cause for alarm. We regret that for security reasons we are not permitted to state the TWT tube types nor the frequencies employed.

Subsequent Work

In one subsequent contract for a different customer, Burmac has produced a 15 microsecond pulser at 0-200 pulses per second for pulsing the RCA 312H TWT. In that pulser, both bias and pulse amplitude are variable over a large range. The pulse characteristics achieved were comparable to those which were described. Life so far is in excess of 75 hours.

For another customer, we have proven the feasibility of producing similar pulsers in the order of 2 milliseconds pulse duration. Naturally, it was necessary to come up with an entirely new concept of pulser design, which might be the subject of some future paper.

Acknowledgments

The authors are indebted to Mr. Thomas Massey and his associates at the Surveillance and Reconnaissance Division of Naval Air Development Center in Johnsville, Pennsylvania, for the pulse photos, and for their assistance and advice in the preparation of this paper.

SOLID-STATE GATE MODULATOR

by

Roy T. Courtney
Development Engineer

ITT Federal Laboratories
Nutley, New Jersey

Introduction

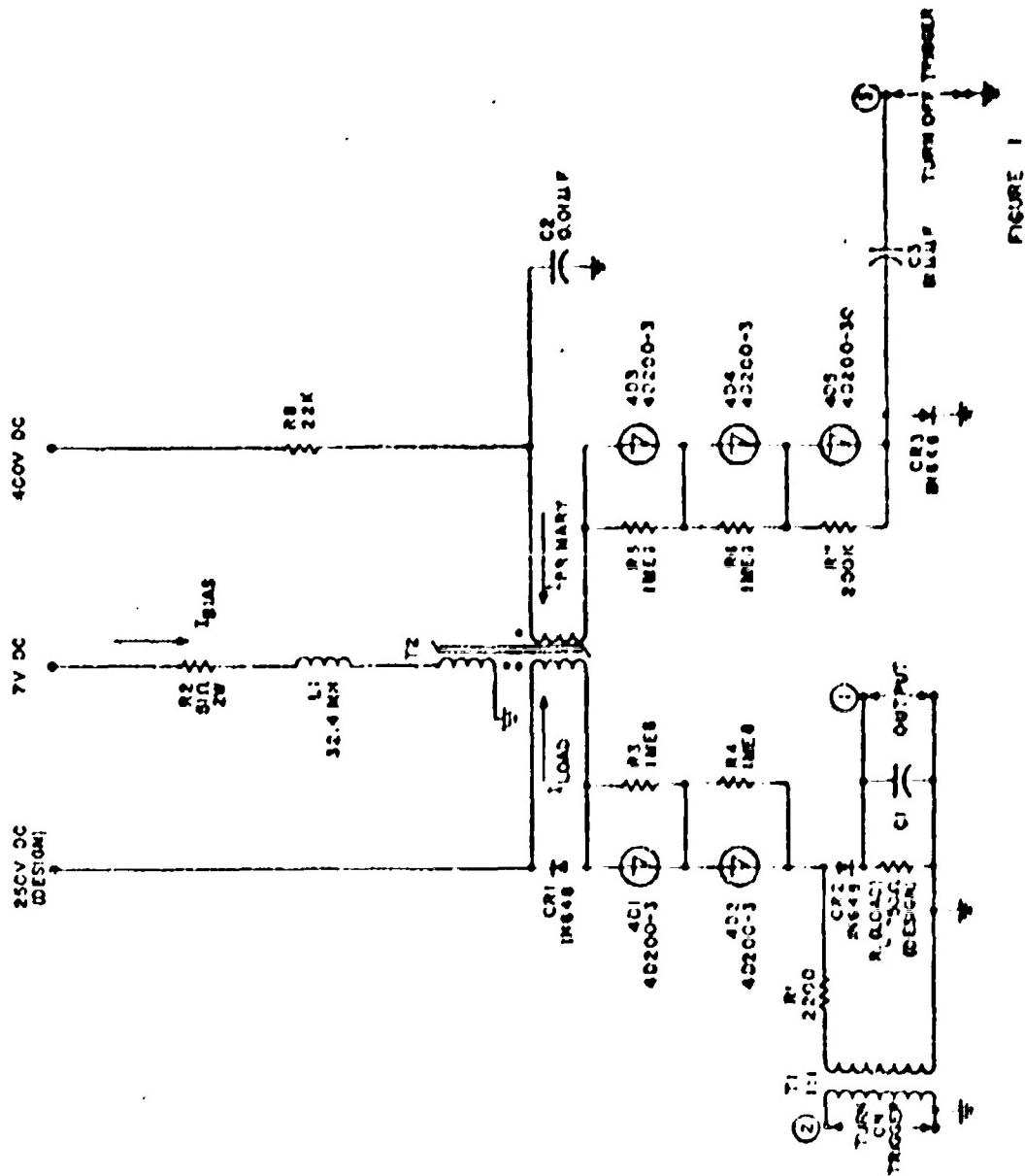
The solid-state gate modulator is an unique modulator in that it is essentially a constant voltage device; that is to say, its output voltage is independent of load impedance over wide limits. The modulator uses four-layer PNPN silicon diodes and a saturable transformer as an almost ideal switch. This type of modulator is ideal for pulsing a gridded traveling wave tube whose input impedance varies greatly from tube to tube. It is also adaptable to pulsing klystrons and magnetrons. Because of the variable pulse width and repetition rate characteristics, this type of modulator is readily adapted to pulse coded systems.

Solid-State Switch

The four-layer PNPN silicon diode is a self-actuated diode with operating characteristics based on the principles of transistor action. It is a two terminal device which has two stable states: (1) an "open" or high resistance state with a forward resistance of more than one megohm, and (2) a "closed" or low resistance state with a forward resistance of one ohm or less. The characteristics are similar to those of a gas thyratron except that its recovery time is much less. The device is switched by controlling the voltage across it or the current flowing through it. When the voltage across the unit is equal to or greater than its "switching" voltage, the device switches to its closed state. It will remain in this state until the current passing through the diode is reduced below "holding" current or the voltage across the diode is reduced below holding voltage at which time the unit returns to its open state. The diodes can be placed in series to increase the switching voltage of a circuit.

250 Volt Solid-State Gate Modulator

Figure 1 is the schematic for a 250 volt modulator with a maximum repetition rate of 1500 pps and pulse width of 66 microseconds. Two negative pulses with their leading edges separated by a time equal to the width of the desired output pulse are required to activate the modulator. The first pulse will be the "turn-on" trigger and the second pulse will be the "turn-off" trigger.



20 NOVEMBER 1942
RECORDED BY SGT. GENE COOPER

The four-layer diodes 4D1, 4D2, 4D3, and 4D4 have a nominal switching voltage of 200 volts each. The four-layer diode 4D5 has a nominal switching voltage of 50 volts. Transformer T2 is set to the quiescent operating point by a d-c current flowing from the 7-volt supply through the bias winding. Capacitor C2 is charged to 400 volts, when 4D3, 4D4 and 4D5 are in the open state.

The negative turn-on trigger pulse is applied to the cathode of four-layer diode 4D2 across diode CR2 and load resistor R_L through transformer T1 and resistor R1. CR2 is back biased by the negative trigger pulse and presents a high impedance to it. The amplitude of the trigger at the cathode of 4D2 when added to the 250-volt supply voltage brings the voltage across 4D1 and 4D2 to the switching voltage; the diodes switch to the closed state, and load current flows. The core of transformer T2 is saturated by the bias current even when full load current flows in its secondary winding. Consequently, the impedance between the load terminal and the 250-volt modulator supply voltage consists primarily of the forward conducting impedance of diodes 4D1, 4D2, and CR2. Since this impedance is less than 5 ohms, better than 98 per cent of the modulator supply voltage appears across the output terminals of the modulator. This means that the output voltage of the modulator is relatively independent of the load impedance; in effect the modulator is almost an ideal voltage source.

The negative turn-off trigger pulse is applied to the cathode of the four-layer diode 4D5 across the back biased diode CR3 through coupling capacitor C3. The sum of the 400-volt charge on capacitor C2 and the turn-off trigger is greater than the switching voltage of the string of four-layer diodes. Consequently, the turn-off string of diodes switch to the closed state and capacitor C2 discharges through the primary of transformer T2 and diodes 4D3, 4D4, 4D5, and CR3 to ground. This discharge current drives transformer T2 out of saturation, thereby developing a negative pulse voltage across the transformer primary winding. A negative pulse of approximately 380-volts peak appears across the secondary of the transformer. This pulse will cause a current to flow in the opposite direction through the load to the load current. A negative voltage is developed thereby reducing the positive load voltage. When the voltage across 4D1 and 4D2 is reduced below holding voltage by this negative pulse, these diodes switch to the open state. This removes the voltage from the load. The width of the negative switching pulse at the 250 volt point must be greater than the recovery time of 4D1 and 4D2 or these diodes will not remain in the open state. Diode CR1 removes any positive overshoot of the negative pulse. This positive overshoot, if not removed, would switch the four-layer diodes back into the closed state.

Resistor R8 limits the current flowing from the 400-volt supply to a value less than the holding current for the string of turn-off four-layer diodes. When the charge on capacitor C2 can no longer supply holding current for the turn-off diodes, these diodes switch to the open state. Capacitor C2 then recharges through resistor R8 to 400 volts and the modulator is ready for the next set of trigger pulses.

Resistor R1 increases the source impedance of the trigger generator to the point where the modulator may override the turn-on trigger pulse when 4D1 and 4D2 switch to the closed state. In addition, R1 prevents the secondary of transformer T1 from shorting the load during long output pulse widths. Resistors R3, R4, R5, R6 and R7 equalize the voltage drops across the four-layer diodes when they are in the open state. Resistor R2 limits the current flowing in the bias winding of transformer T2. The inductor L1 prevents turn-off pulse current from flowing in the bias winding of T2.

Saturable Transformer

The core of transformer T2 is composed of magnetic material having a rectangular hysteresis loop. The operation of the transformer will be explained using the ideal B-H curve or hysteresis loop in Figure 2. A transformer is saturated when a change in magnetizing force (H) does not produce a change in flux density (B).

H1 (Point 1) is the magnetizing force due to the d-c current flowing in the bias winding. This is the quiescent operating point of the transformer. The secondary winding of the transformer is wound so that load current flowing in the secondary produces a magnetizing force that opposes the bias magnetizing force. The net magnetizing force is then H2 (Point 2). Since this point is still in the saturated region and the flux density (B) has not changed, the secondary winding presents no impedance to the load current during the pulse interval.

The primary winding produces a magnetizing force that aids the magnetizing force produced by the load current as long as the transformer is in the saturated region. As the primary current drives the transformer out of saturation toward Point 3 the load current is reduced toward zero. The magnetizing force produced by the primary current maintains the net magnetizing force at H3 until the flux density (B) goes from B1 to B2. When primary current ceases, the magnetizing force due to the bias current resets the transformer core to the quiescent operating point and the cycle is complete.

The core used for the transformer in the 250 volt modulator was a 1 mil ovthonik tape wound core. Ovthonik material, composed of grain oriented 50 per cent nickel and 50 per cent iron alloy has an hysteresis loop which approaches the ideal rectangular hysteresis loop of Figure 2.

Waveshapes for the 250 Volt Solid-State Gate Modulator

A circuit was built with a layout similar to the layout of the schematic in Figure 1. A photograph of this circuit is shown in Figure 3. Figures 4 through 12 are photographs of waveforms between the points indicated on the schematic and ground.

The turn-on and turn-off negative trigger pulses in time reference to the output pulse are shown in Figure 4 and 5, respectively. The waveshape of Figure 6 is the minimum pulse width that could be obtained with the available turn-on and turn-off trigger source. Figure 7, 8 and 9 are photographs of the output pulse with widths of 3, 7 and 11 microseconds, respectively.

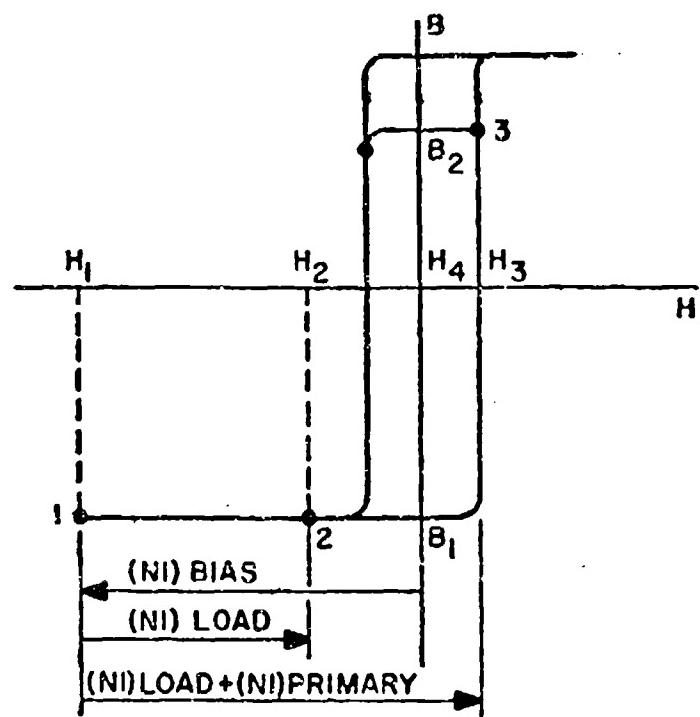


FIGURE 2
B-H CURVE

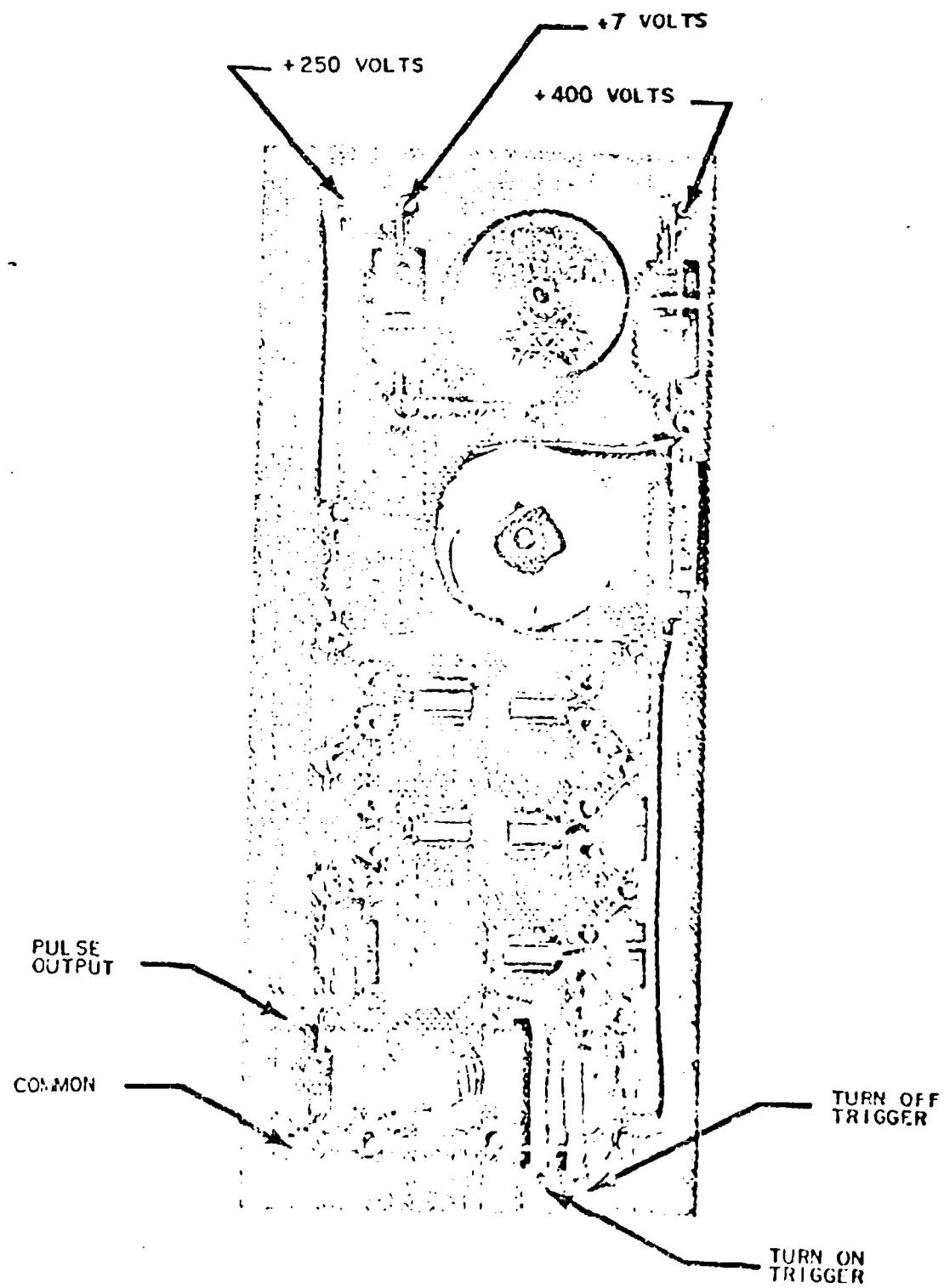


FIGURE 3. SIMPLE SOLID STATE GATE MODULATOR

4a - TURN-ON
TRIGGER (Point 2)
PULSE

4b - OUTPUT PULSE
(Point 1)

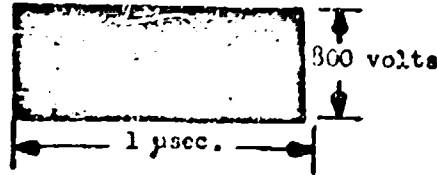


Figure 4 - Reference of the TURN-ON TRIGGER PULSE with respect to the OUTPUT PULSE.

5a - TURN-OFF
TRIGGER (Point 3)
PULSE

5b - OUTPUT PULSE
(Point 1)

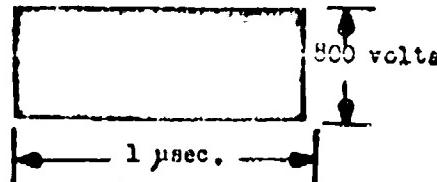


Figure 5 - Reference of the TURN-OFF TRIGGER PULSE with respect to the OUTPUT PULSE.

Note: Point numbers referred to in above figures correspond to ... points in Figure 1.

All voltages were measured with respect to ground.
All waveshapes are read from right to left.

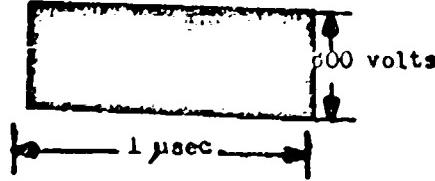


Figure 6 - Minimum pulse width obtainable with the available TURN-ON and TURN-OFF Trigger Pulses.

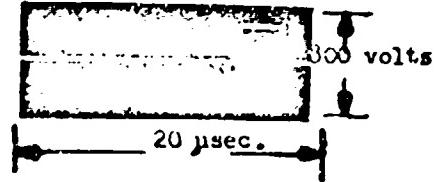


Figure 7 - 3 μsec OUTPUT PULSE

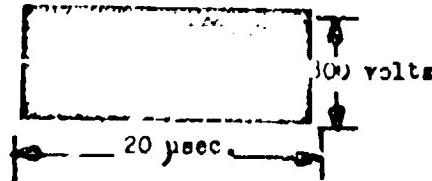


Figure 8 - 7 μsec OUTPUT PULSE

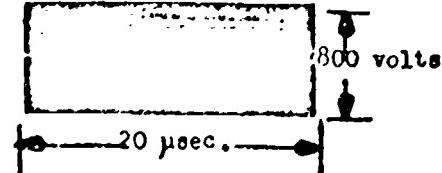


Figure 9 - 11 μsec OUTPUT PULSE

Note: All voltages were measured with respect to ground.

All waveshapes are read from right to left.

Figure 10 is a set of waveshapes of the output pulse as the load resistor was varied from 1200 to 220 ohms. Figures 10a through 10f show that the output pulse was not affected as the load resistor was varied from 1200 to 470 ohms. Figures 10g and 10i show that the output pulse amplitude was reduced for load resistors of 300 and 220 ohms. For the output pulses of Figures 10a through 10g and Figure 10i, the bias current was 140 ma (nominal). The value of the load resistor for Figures 10g and 10i allowed a load current that drove transformer T2 out of saturation; therefore part of the modulator supply voltage was dropped across the transformer winding. In Figures 10h and 10j the bias current was increased to 400 ma. This bias current did not maintain the core completely saturated with load current flowing but did reduce the impedance of the secondary winding presented to the load current. Thus for a load variation of 3 to 1 the output voltage remained constant without any adjustments made to the circuit. By adjusting the bias current, the circuit could be made to supply approximately a constant output for a load variation of 6 to 1.

Figure 11 is a set of waveshapes of the output pulse as the modulator supply voltage (250 volts nominal) was varied from 100 to 280 volts. The output pulse shape was not affected. The amplitude varied directly as the modulator supply voltage varied.

As can be seen from Figures 10 and 11, the modulator is a constant voltage source. Changing load impedance has little or no effect on the output voltage. The output voltage is primarily a function of the modulator supply voltage.

Figure 12 is a set of waveshapes of the output pulse as capacitance is added across the load resistor. Figure 12 has no capacitance except wiring and stray capacitance. As can be seen in Figures 12b, 12c, and 12d, the additional capacitance has to be charged and discharged at the beginning and the ending of the output pulse.

Projected Capabilities of the Simple Circuit

The maximum width of the output pulse is limited only by the capability of the four-layer diodes. If the peak load current is equal to or less than the d-c rated current of the switching diodes, the pulse width can have any value.

The minimum output pulses width is limited by the turn-on and turn-off trigger pulse spacing. This modulator should be capable of producing an output pulse with a width of approximately one tenth of a microsecond. The minimum pulse width of Figure 6 was limited by the available trigger pulses.

The rise time of the output pulse was less than 50 nano-seconds with no capacitance across the load except the wiring capacity. Adding capacitance across the load decreases the rise time as can be seen in Figure 12. The decay time of the output pulse is less than 0.1 microsecond but is affected by capacitance across the load as can be seen in Figure 12.

Pulse output voltages of approximately 15 volts peak to approximately 1000 volts peak can be obtained from this type circuit. The four-layer diodes can be placed in a series string to hold off the necessary voltage.

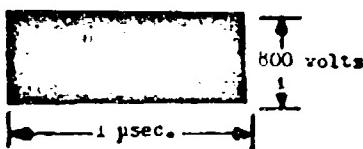


Figure 10a - $R_L = 1200 \text{ ohms}$
Bias current = 140 MA.

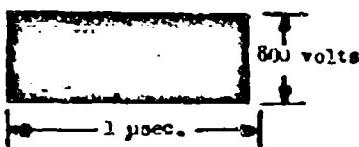


Figure 10b - $R_L = 1000 \text{ ohms}$
Bias current = 140 MA.

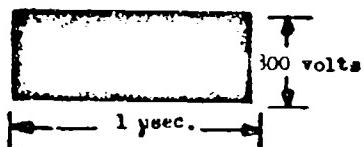


Figure 10c - $R_L = 820 \text{ ohms}$
Bias current = 140 MA.

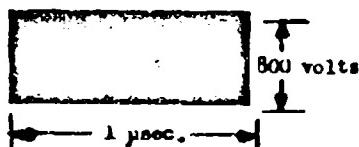


Figure 10d - $R_L = 750 \text{ ohms}$
Bias current = 140 MA.

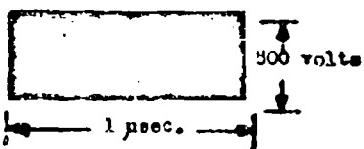


Figure 10e - $R_L = 620 \text{ ohms}$
Bias Current = 140 MA.

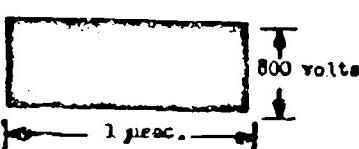


Figure 10f - $R_L = 470 \text{ ohms}$
Bias current = 140 MA.

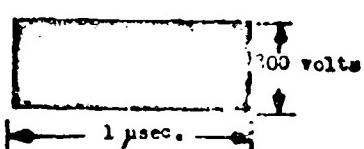


Figure 10g - $R_L = 300 \text{ ohms}$
Bias current = 140 MA.

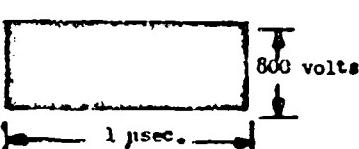


Figure 10h - $R_L = 330 \text{ ohms}$
Bias current = 140 MA.



Figure 10i - $R_L = 220 \text{ ohms}$
Bias current = 140 MA.



Figure 10j - $R_L = 220 \text{ ohms}$
Bias current = 400 MA.

Figure 10 - Effect of varying the load resistor R_L on the output pulse. modulator supply = 250 volts and $C_1=0$

NOTE: All voltages were measured with respect to ground. All waveshapes are read from right to left.

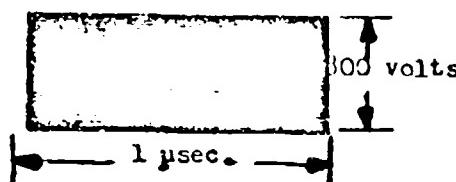


Figure 11a - $V=100$ volts

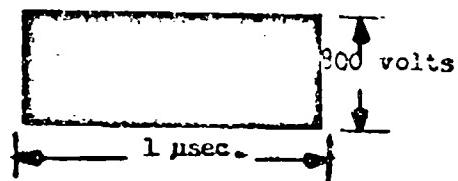


Figure 11b - $V=150$ volts

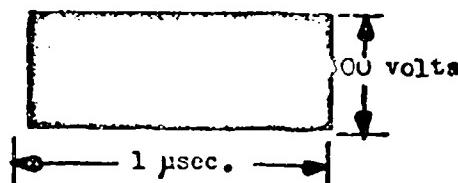


Figure 11c - $V=200$ volts

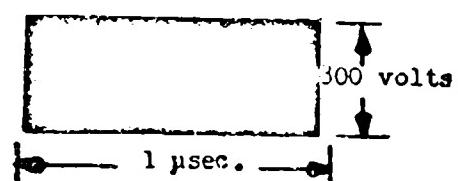


Figure 11d - $V=250$ volts

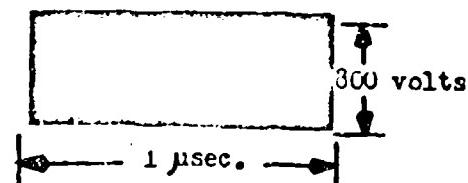


Figure 11e - $V=280$ volts

Figure 11 - effect of varying the modulator supply voltage
on the output pulse. $R_L = 750$ ohms and $C_L = 0$.

Note: All voltages were measured with respect to ground.
All waveshapes are read from right to left.

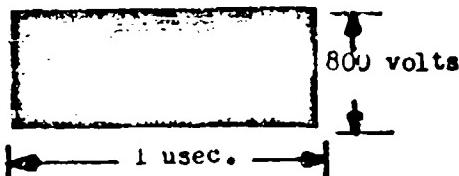


Figure 12a - $C_1=0 \mu\text{uf}$.

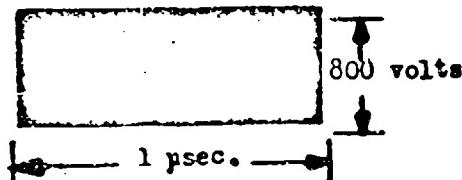


Figure 12b - $C_1=51 \mu\text{uf}$

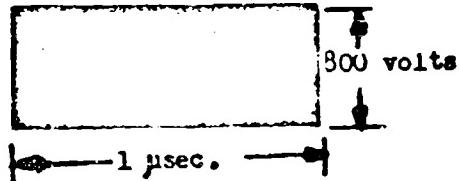


Figure 12c - $C_1=100 \mu\text{uf}$

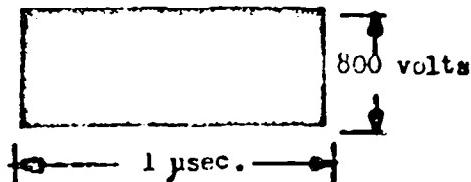


Figure 12d - $C_1=220 \mu\text{uf}$.

Figure 12 - Effect of varying the capacitor C_1 on the output pulse. Modulator supply = 250 volts and $R_L = 750 \text{ ohms}$.

NOTE: All voltages were measured with respect to ground. All waveshapes are read from right to left.

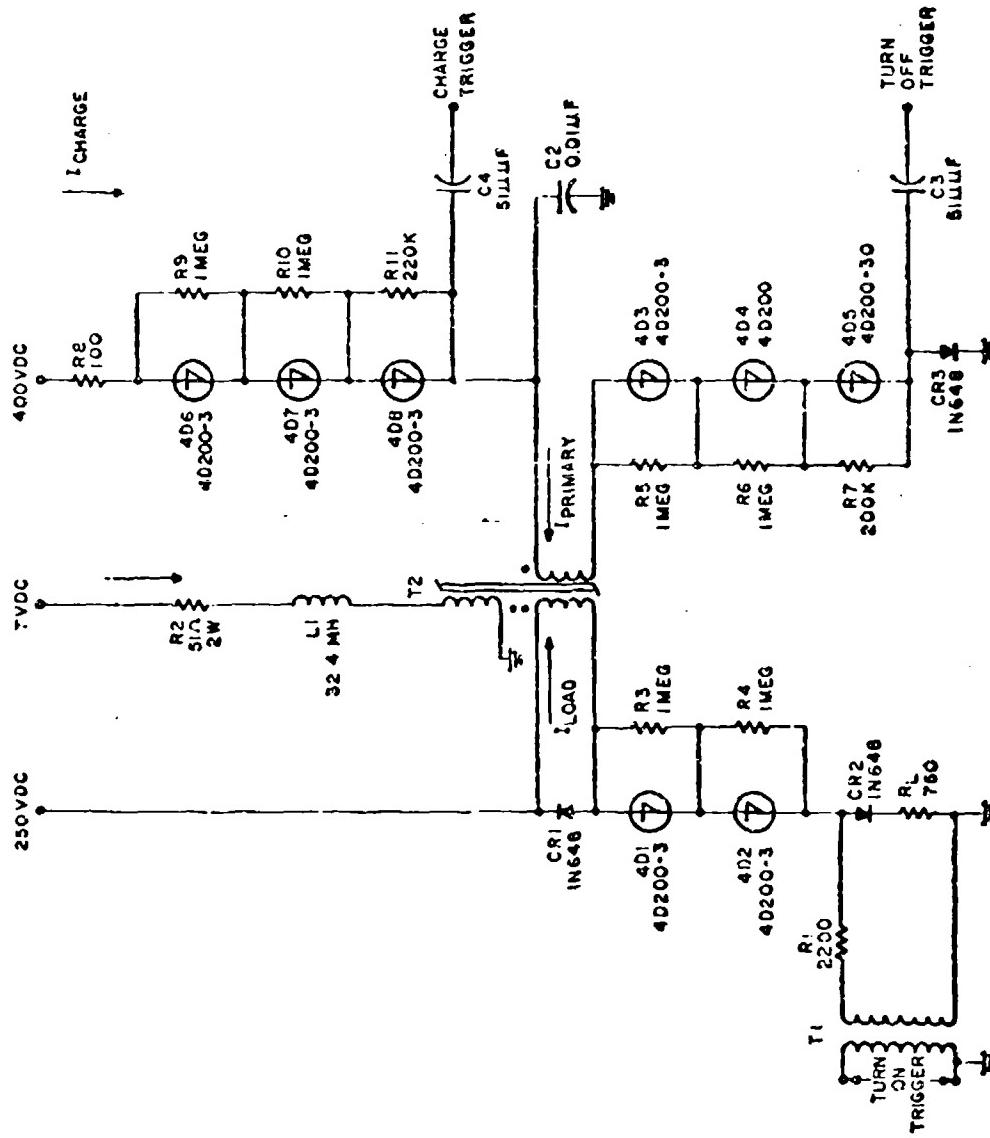


FIGURE 13
100 KC SOLID-STATE GATE MODULATOR

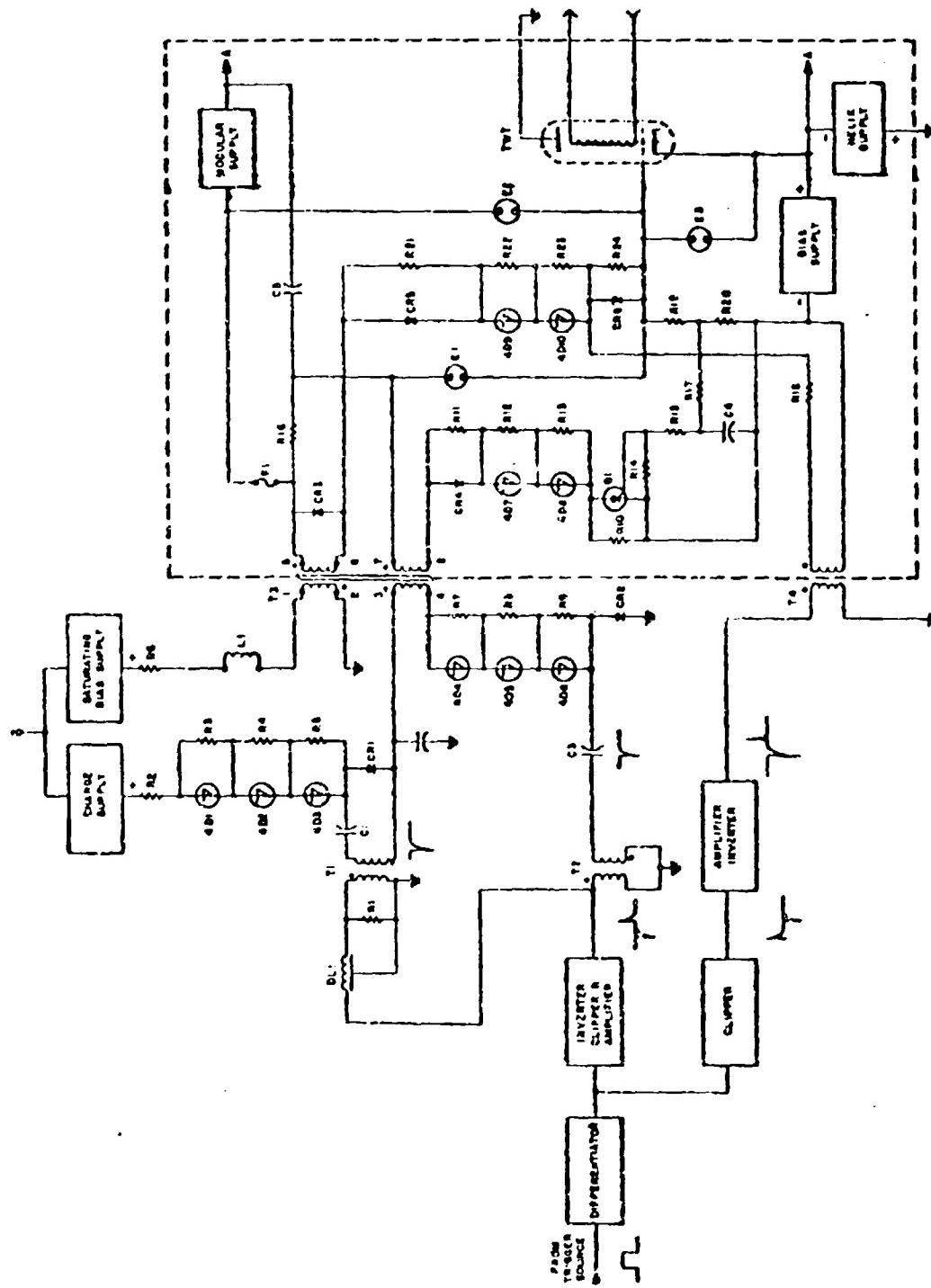


FIGURE 14
CIRCUIT ADAPTER

When an arc occurs within the tube from grid to shell, the helix supply capacitor will discharge through the Bias Supply and resistors R19 and R20 in an unprotected circuit. The elements will not withstand the high surge current. To protect these elements, spark gap E3, with a breakdown potential larger than the normal operating potential, is shunted across them. When the tube arcs, the breakdown potential of the gap is reached and the gap conducts, discharging the helix supply capacitors.

When an arc occurs, the stray capacitance to ground of the modulator and modulator supply must be discharged or a high inverse voltage will be applied across the modulator four-layer diode strings. Spark gaps E1 and E2, with breakdown potentials larger than the breakdown voltage of spark gaps E1 and E2, diodes CR4 and CR5 are placed in series with the modulator elements. (CR4 and CR5 may each consist of several diodes in series.)

Since the four-layer diodes can withstand the peak pulse current for a limited time only, the turn-on section of the modulator has to be protected against malfunction in the turn-off section. This can be accomplished by sampling the output pulse, integrating the sample over a safe limit of pulse interval, and using this integrated voltage as a trigger for an auxiliary turn-off circuit. In Figure 14, resistor R20 is a sampling resistor having a small value compared to the load of the modulator. The sampled pulse is fed to the integrating network consisting of resistor R15 and capacitor C4. If the pulse width is wide enough, capacitor C4 will charge to a value large enough to trigger the avalanche transformer T2 developing a negative pulse between terminals 5 and 6 which will switch four-layer diodes 4D9 and 4D10 to the open state. The auxiliary turn-off section will be reset by resistor R16 limiting current flow through diodes 4D7 and 4D8 below holding current.

The fuse, F1 of Figure 14, would be used only to prevent possible damage to the power supply in the event of a component failure in the modulator where the auxiliary turn-off circuit is employed. A simple way of protecting the turn-on section of the modulator would be to utilize a fast-blow fuse in the position of F1 and eliminate the auxiliary turn-off circuit entirely. The disadvantage of using a fast-blow fuse is that it would have to be replaced after a transient fault. The auxiliary turn-off circuit would reset automatically.

Summary

While the solid-state gate modulator discussed in this paper was developed with the requirements of systems employing gridded traveling wave tubes and klystrons in mind, these applications are by no means the limit of its applicability. A very interesting application would be to drive low-power magnetrons, particularly in airborne or satellite beacons where variable pulse widths are required. This type of modulator would have the distinct advantage of being small, lightweight, efficient and stable.

"SOLID STATE MODULATOR"

by

T. Bamburger
C. H. Wood
R. A. Gardenghi

Westinghouse Electric Corporation
Electronics Division
Baltimore 3, Maryland

I. INTRODUCTION

This paper represents a study in the use of solid state devices in radar modulator applications. Of particular interest are radar modulators capable of switching peak pulse powers in the megawatt range. As the basic switching element, both the Transistor and the Trinistor (RNPN switch) are considered. The former would be applicable to the "Hard Tube" type of modulator while the latter would be used in a "Line Pulsing" type of modulator.

II. APPLICATION OF TRANSISTORS TO RADAR MODULATOR CIRCUITRY

At this time, the maximum power which can be switched by a single transistor is approximately 6 kilowatts. Hence, both series and parallel operation of transistors was considered in an effort to attain peak pulse powers in the megawatt region.

Two or more Transistors can be connected in series as shown in Figure 1. Equal voltage division across the Transistors in the "off" state is ensured by connecting Resistors in parallel with each unit. The necessary base drive for each unit is provided by the multiple secondary trigger transformer shown in the figure.

One of the major difficulties encountered with series operation of transistors is that unless all units switch "on" coincidentally, the full hold off voltage will appear across the slowest switching transistor. This will undoubtedly result in destruction of the transistor.

To increase the current switching capability, two or more transistors can be connected in parallel, as shown in Figure 2. The maximum current that can now be switched is equal to the current rating of a single transistor multiplied by the number of transistors in parallel. However, to obtain maximum power output, the impedance

level becomes far too low for a practical modulator design. In addition the division of the load current among the paralleled transistors is inversely proportional to the transistor saturation resistance. Hence, compensating resistances must be provided which will reduce the overall circuit efficiency.

Finally, the power gain of transistors is low. Therefore, the required driving power is a significant proportion of the output power.

It may thus be concluded that the use of transistors is highly inefficient in high power radar modulator circuitry.

There are, however, many applications for low power pulsers where transistors could adequately handle the power. Many high power transistors have a relatively slow switching time and special circuitry has been designed for these transistors. Figure 3 shows a circuit which eliminates the storage time effects and reduces the effects of shunt capacity on the trailing edge of the output pulse. Figure 4 shows a circuit for generating very narrow pulses with fast rise and fall times. Each of these circuits uses relatively slow speed transistors for the generation of pulses with a very fast rise and fall times. One circuit was built which generated a 225 watt, 10 microsecond pulse with rise and fall times of 0.6 microseconds.

III. APPLICATION OF TRINISTORS TO A RADAR MODULATOR CIRCUITRY

The Trinistor, which is also known as the PNPN switch, silicon controlled rectifier, silicon controlled switch, is a three junction semi-conductor device with thyratron-like characteristics. It will block relatively high voltage in both the forward and reverse direction until turned on by a low level pulse into its gate. When the Trinistor is in the conducting state, its forward impedance is extremely low. Consequently, it is ideally suited to radar modulator circuitry. Figure 5 illustrates the use of the Trinistor in a conventional line-type pulser circuit. The pulse forming network (PFN) is resonantly charged to approximately twice the supply voltage. The Trinistor is triggered "on" by applying a low amplitude pulse to its gate. The PFN then discharges through the Trinistor and load resistor R_L . When the discharge current falls below the Trinistor maintaining current, the Trinistor will revert to its high-impedance state and the entire cycle will be repeated.

The following sections describe various techniques whereby the Trinistors may be used to switch peak-pulse powers in the megawatt range.

A. Reliable Resonant Charging

The usual method of resonant charging consists simply of a choke in series with a diode. The choke performs two functions. Firstly, it resonates with the PFN capacitance to produce the charging cycle. Secondly, it provides an isolating impedance between the power supply and the load switching element of the modulator. During the pulse output time interval, however, the current through the choke rises exponentially. This is ordinarily of little consequence as long as the value of current at the end of the pulse has not reached the maintaining current level of the switch device. The switch will then turn off at the end of the pulse, and the resonant charging cycle will recur.

The maintaining or "holding" current of Trinistors, however, is very low. A typical holding current for a 70 ampere Trinistor is 20 milliamperes. Therefore, the charging choke must have sufficient inductance to prevent more than 20 milliamperes to build up during the output pulse interval. This value of inductance, however, may not be comparable with the other circuit constants selected for a particular modulator. To overcome this difficulty, reliable resonant charging with any value of charging inductance, can be obtained by replacing the charging diode with a Trinistor as shown in Figure 6.

When a Trinistor is used for charging, it must be triggered "on" to allow the PFN to charge. Once the PFN reaches its peak charge, the charging Trinistor turns off since the current through it drops to zero. When the load switching Trinistor is turned on to deliver the output pulse, current cannot start to build-up in the charging choke because the charging Trinistor is "off" and is a virtual open circuit. The next charging cycle will not be initiated until the charging Trinistor is triggered "on" again. Therefore, with suitable delays between the triggering of the load switching Trinistor and the charging Trinistor, reliable operation can be achieved even with very wide pulses and very low inductance charging chokes.

The charging Trinistor for resonant charging not only gives reliable operation but also allows a much more flexible system. For example, a wide range of pulse repetition rates can be obtained with a single value of charging inductance. Also, for low repetition rates, leakage of the PFN (droop) can be virtually eliminated since the charging cycle can be initiated at some long interval after the end of the previous pulse. This will also allow the use of lower inductance (and physically smaller) charging chokes for applications where size and weight must be at a minimum.

B. Saturable Reactor

The Trinistor, when switching from the "off" state to the "on" state, exhibits a high resistance. If high currents are being switched,

considerable amounts of power are dissipated in the Trinistor even though the transition from "off" to "on" is very fast. In addition, the turn-on mechanism of the Trinistor is such that the entire area of the junction does not turn on simultaneously. Consequently, the rate of rise of current through the junction must be limited if localized excessive heating of the junction is to be avoided. The total dissipation can be markedly decreased if the volt-ampere produce is kept to a minimum during the switching time of the Trinistor. In addition, the Trinistor when "on", can handle peak currents which are 10 to 20 times its average current rating.

The aforementioned desirable characteristics can be achieved by inserting a saturable reactor in series with the PPN as shown in Figure 7.

The operation is as follows: When the Load switching Trinistor is triggered on, during the switching time, the amount of current that can flow is limited by the unsaturated inductance of the reactor. After the Trinistor has switched completely on and is in its low resistance state, the current in the reactor builds up sufficiently to cause the core to saturate. Once the core saturates, the inductance of the reactor becomes negligible and the full load current can flow. Therefore, the saturable reactor delays the current sufficiently so that the volt-ampere produce, while the Trinistor is switching, is greatly reduced. Since the current is delayed, the output pulse is also delayed. The amount of delay is determined by the saturable reactor design. This delay can be clearly seen by comparing Figure 8A with 8B. These waveforms show the Trinistor anode voltage and the inverted output pulse with and without a saturable reactor.

The delay time, t , of the saturable reactor is given by:

$$t = \frac{NABt}{V_p}$$

where N = number of turns

A = cross sectional area of core

B_t = total flux change

V_p = peak voltage applied to PPN

The current required to switch the core must be a small percentage of the peak current. The switching current is given by:

$$i_s = \frac{Hl}{N}$$

where i_s = current to saturate core

A = magnetizing force for saturation

l = mean length of core

N = number of turns.

Resetting of the core after each pulse is accomplished automatically in this application by the resonant charging current (which flows in an opposite direction to the load current.)

It is important that the saturated inductance of the saturable reactor be considered in the design of the Pulse Forming Network.

While the Trinistors dissipate much less power with the use of a saturable reactor, there is some power dissipation in the saturable reactor. For high power applications at high repetition rates, some means of cooling the saturable reactor must be provided. It has been calculated that for a specific 5 megawatt modulator operating at 300 pps, the power dissipated by the saturable reactor is approximately 40 watts.

C. Series Operation of Trinistors

When power in excess of a single Trinistor's capability is required, multiple units must be used. Trinistors may be connected in parallel to increase the overall power handling capabilities but there are several disadvantages to this approach. Current equalization means must be used to prevent damaging an individual Trinistor. In addition, the impedance of the circuit elements, such as the PFN, will be so low as to be impractical. Furthermore, the required step-up turns ratio of the pulse transformer will be prohibitively large.

Connecting Trinistors in series, however, is a very practical way of increasing the power handling capabilities of the modulator. This method of connection reduces the required step-up turns ratio of the pulse transformer and allows the use of PFN impedance levels in a practical range.

One of the problems in seriesing Trinistors is to ensure equal voltage sharing. The simplest method is to use resistors as shown in Figure 9.

There are, however, several disadvantages to using resistors for voltage equalizing. The equalizing resistors dissipate a relatively large amount of power, tend to discharge the PFN, and do not equalize the voltage for fast transients.

Figure 10 shows a method of voltage sharing using zener diodes. This method overcomes the disadvantages noted for resistor equalization. The leakage current through the zener diode need only be slightly larger than that of the worst Trinistor. The operating voltage chosen should be equal to or slightly less than the minimum hold-off voltage capability of the Trinistor at its maximum temperature of operation.

D. Gate-Cathode Biasing

When using charging Trinistors, false triggering can result because of transient voltages or dv/dt effects. For example, a 400 volt Trinistor subjected to a voltage rate of change of 1000 volts per microsecond, will trigger at approximately 180 volts. It can be seen that point A of Figure 6 is subjected to a large "rate of change" of voltage (dv/dt). The charging Trinistors are then prone to trigger.

It was found that the ability of a Trinistor to resist dv/dt breakdown can be greatly enhanced if reverse bias is applied to the gate-cathode junction (see Figure 11).

Bias is easily applied to a single Trinistor. However, when Trinistors are operated in series it is very difficult to apply reverse bias to the gate-cathode junction since the gates must be isolated from each other. Therefore, circuitry was developed to effectively produce reverse bias in the gate circuit.

The first method is a dynamic type of bias and is shown in Figure 12. This circuit was used successfully to prevent the charging Trinistors from breakdown due to the large dv/dt caused by the firing of the load-switching Trinistors.

The circuit operates as follows: A gate pulse is coupled to the charging Trinistor through the transformer causing it to fire. This allows the PFM to charge up as usual. Some time later the load-switching Trinistors are fired to deliver an output pulse. This causes a large negative going pulse to appear at the cathode of the charging Trinistor, tending to turn it on. Simultaneously, some of the pulse is coupled to the gate of the Trinistor through resistor, R_f , C_f , and the transformer. The pulse is inverted by the transformer so that it effectively produces a reverse bias on the gate of the Trinistor.

It is interesting to note that the normal gate pulse occurs at some definite interval of time before the load-switching Trinistors fire and the feedback occurs. This ensures that there be no conflict between the trigger pulse and the feedback. Therefore, no additional drive is required when this feedback circuit is used as described.

The second method actually develops a D.C. bias on the gate-cathode junction. The D.C. is developed from the trigger pulse itself. The circuit is shown in Figure 13(a); the gate waveform is shown in Figure 13(b); the diode, D, is a zener diode. Its action is to drop a portion of the gate trigger pulse across it and charge up the capacitor, C. This capacitor maintains its charge in between pulses and effectively appears as a battery, reverse biasing the gate.

Obviously, this circuit is applicable only to instances where a repetitive trigger is used. Fortunately, such is the case in radar modulators. Also, the drive pulse must have a greater amplitude than formerly required since a portion of it is used to develop the bias. This scheme has worked well and has been applied in a modulator to be described later in this report.

E. Triggering

A single medium power transistor is capable of supplying the necessary drive required by a series string of Trinistors. For example, a Trinistor having an average current rating of seventy amperes and, switching a peak current of 1000 amperes, can be triggered by a 2 volt, 100 milliamperc (200 milliwatts) pulse. The duration of the pulse must be sufficiently long to permit the Trinistor anode current to reach its maintaining value. There are, however, several other aspects to triggering when Trinistors are operated in series. The most important consideration is the D.C. isolation which must be produced between gates when Trinistors are connected in series. This may be accomplished by the use of transformers, as shown in Figure 9. A single transformer with multiple secondary windings can also be used.

IV. CONCLUSIONS

The basic principals of using Trinistors in line-pulsing modulators were verified in several laboratory breadboards.

A 160 KW modulator was built to prove the feasibility of switching high peak currents with Trinistors. The circuit used is shown in Figure 14. Figure 15 is a photograph of the actual modulator chassis.

The switching Trinistors used in this chassis were two Westinghouse 809H, 50 ampere, 400 volt units connected in series. A saturable reactor designed to give a 3 microsecond delay was used with the Trinistors. A single C35D (16 ampere, 400 volt Trinistor) was used for the charging Trinistor. A one ohm, non-inductive load resistor was used. The output was a 400 volt, 400 amp, 5 microsecond pulse. This pulse is shown in Figure 14.

Another modulator was built using 20 Trinistors in series as the switch element. The purpose of this circuit was to prove the feasibility of using a large number of Trinistors in series. Figure 16 shows the circuit used. Figure 17 shows the actual breadboard model with output pulse transformer and load resistor.

The 20 switching Trinistors used in this circuit were 16 ampere, 250 volt units. Ten 3 ampere, 250 volt Trinistors connected in series were used for charging.

A peak power output of 200 KW was obtained by switching 100 amperes at 4000 volts with the Trinistors. Three different PFN's and pulse transformers provided operation with pulse widths of 1, 5, and 100 microseconds. The turns ratio of the pulse transformers was 1:8, providing a peak amplitude of 16,000 volts for the output pulse.

If the features of these various experimental circuits were combined, very high powers could be obtained. For example, if 20 or the 70 ampere, 700 volt Trinistors were used in series, a peak power output of 7 megawatts could be obtained. Even higher powers could be obtained with Trinistors having higher voltage and peak current ratings.

The results of this work have shown, therefore, the feasibility of high power, solid-state line-type modulators. The use of a saturable reactor enables the Trinistor to switch peak currents which are 10 to 20 times its average current rating. High voltage ratings are obtained by series strings of Trinistors. Reliable resonant charging and turn-off of the switching Trinistors can be achieved by using Trinistors instead of a charging diode. Gate bias has been used to reduce transient effects on Trinistors. The combinations of these ideas can vary to suit the particular application.

V. ACKNOWLEDGEMENT

This paper is based on work performed under contract AF 30(602)-2207 with the Rome Air Development Center, Griffis Air Force Base, New York.

The authors gratefully acknowledge the cooperation of this agency as well as members of the Advanced Development Subdivision of the Westinghouse Electronics Division.

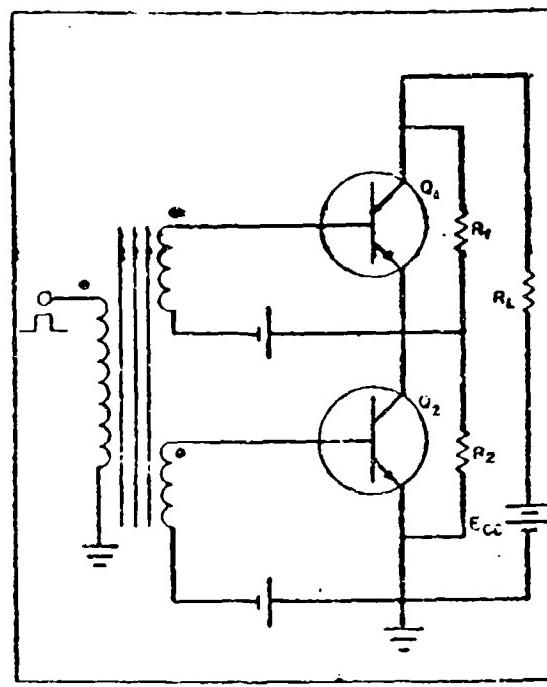


Figure 1. Transistors in Series

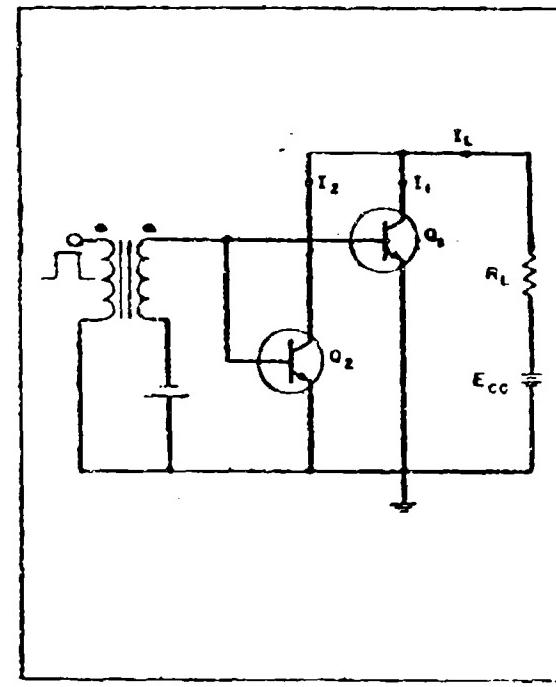


Figure 2. Transistors in Parallel

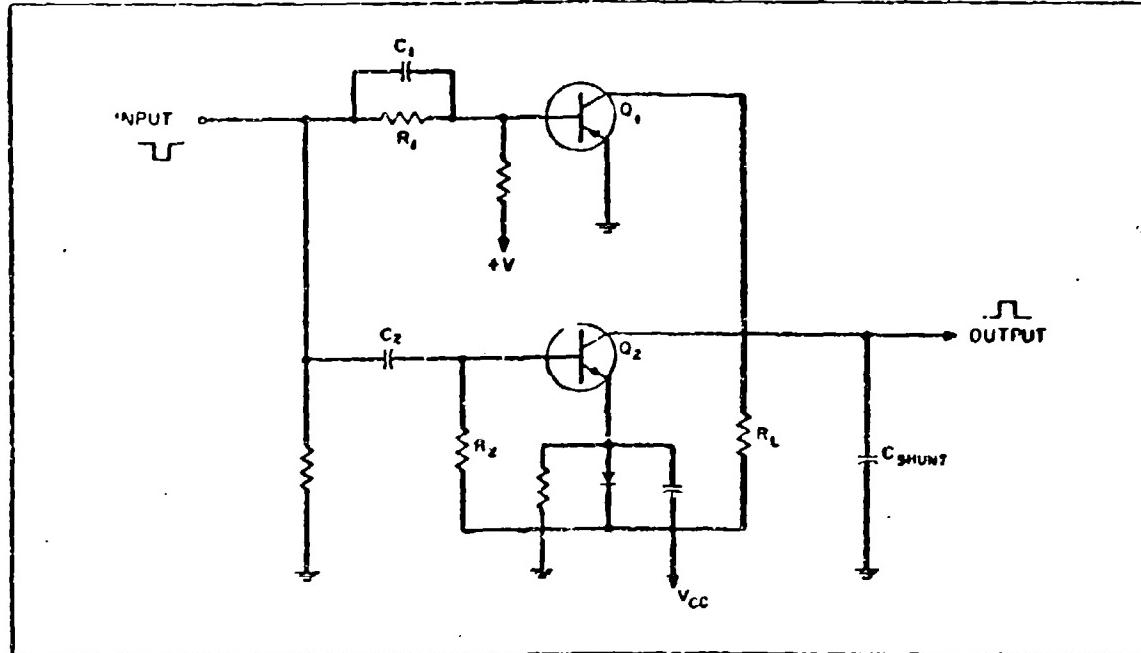


Figure 3. High Speed Circuit

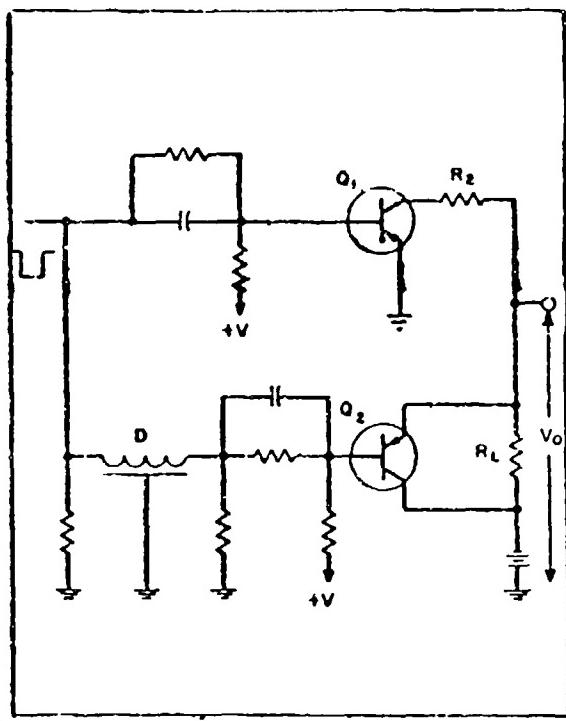


Figure 4. Narrow Pulse Circuit

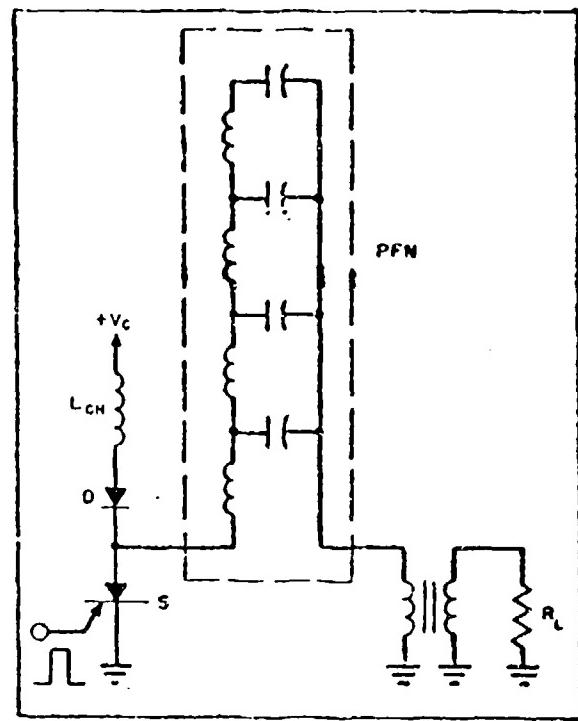


Figure 5. Solid State Line-Type Pulser

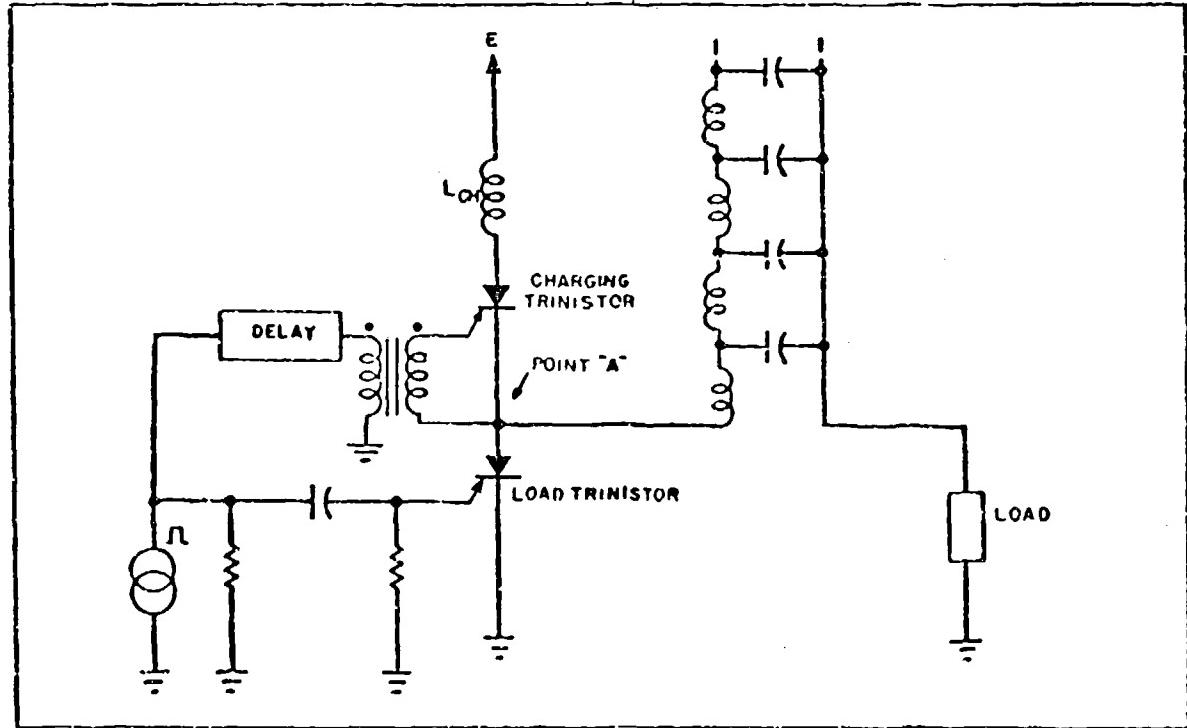


Figure 6. Basic Solid State Pulse Circuit with Charging Triistor

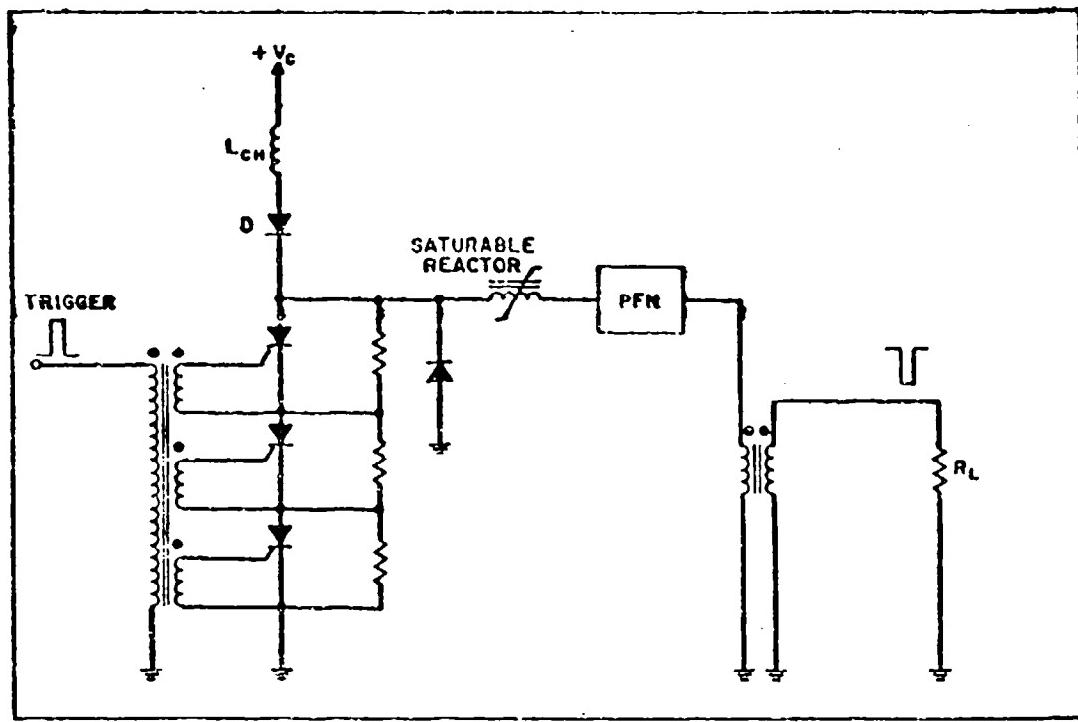


Figure 9. Series-Connected Tristors with Saturable Reactor

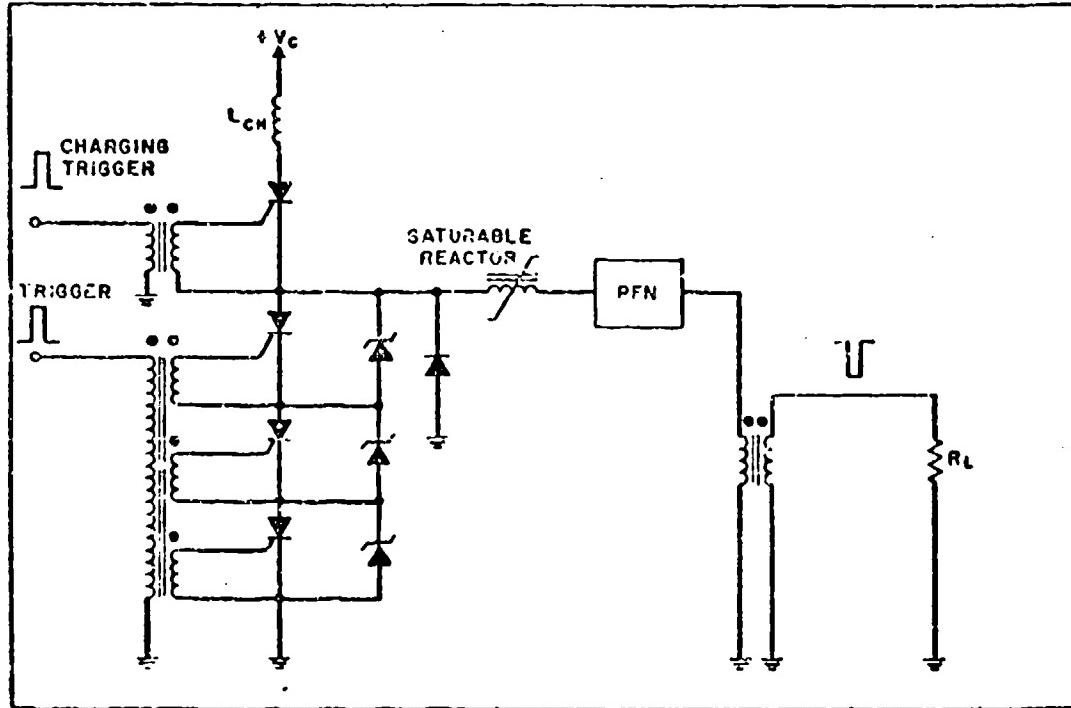


Figure 10. Series-Connected Tristors with Zener Diode Voltage Divider

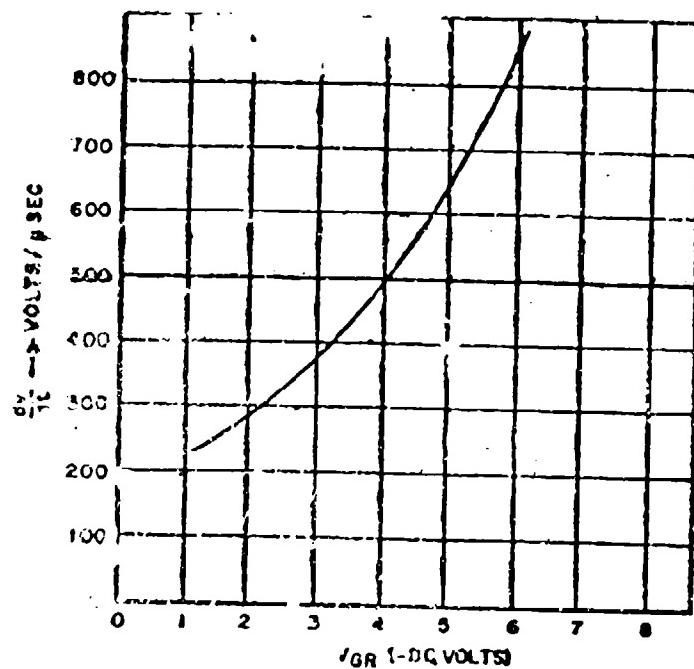


Figure 11. Breakover dv/dt versus Reverse Bias

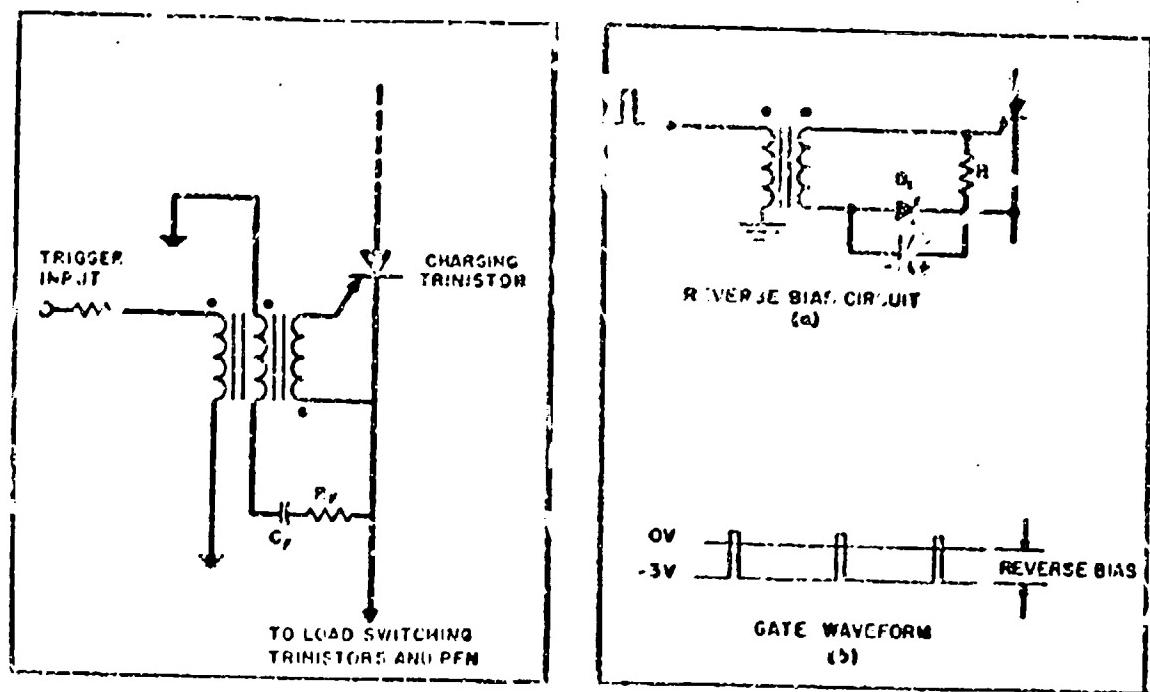


Figure 12. Feedback Circuit to Reduce Effect of dv/dt

Figure 13. Reverse Bias

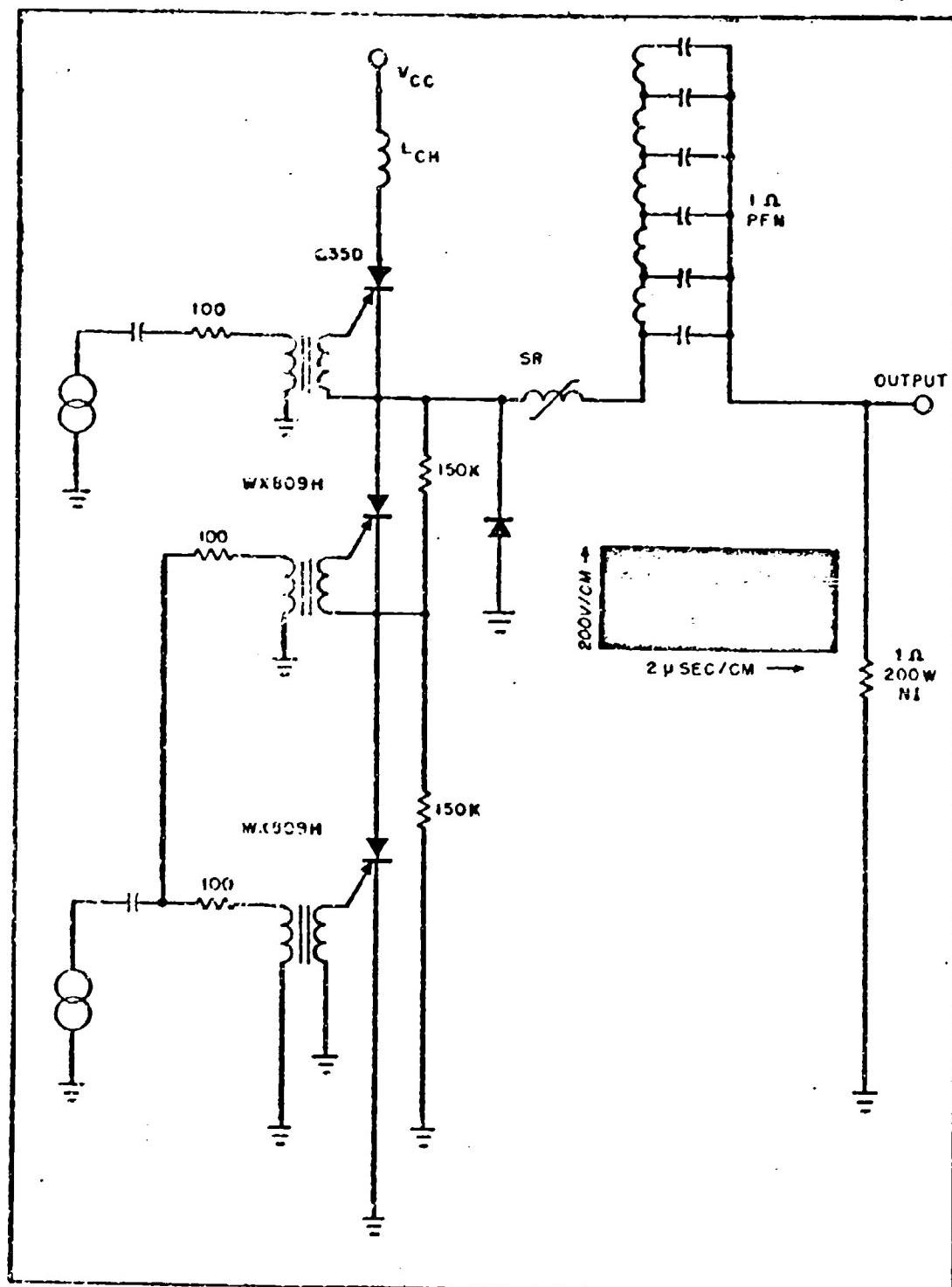
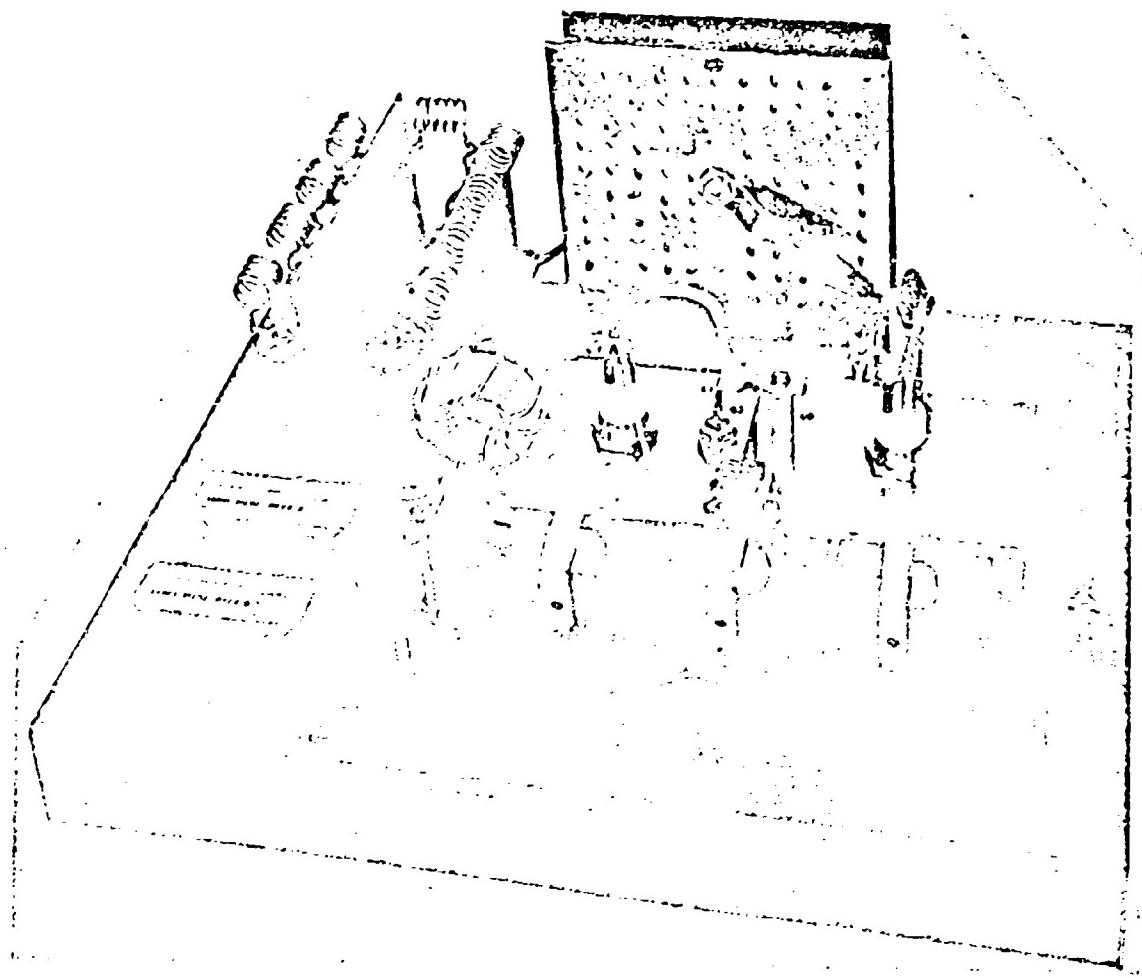


Figure 14. 160 KW Modulator



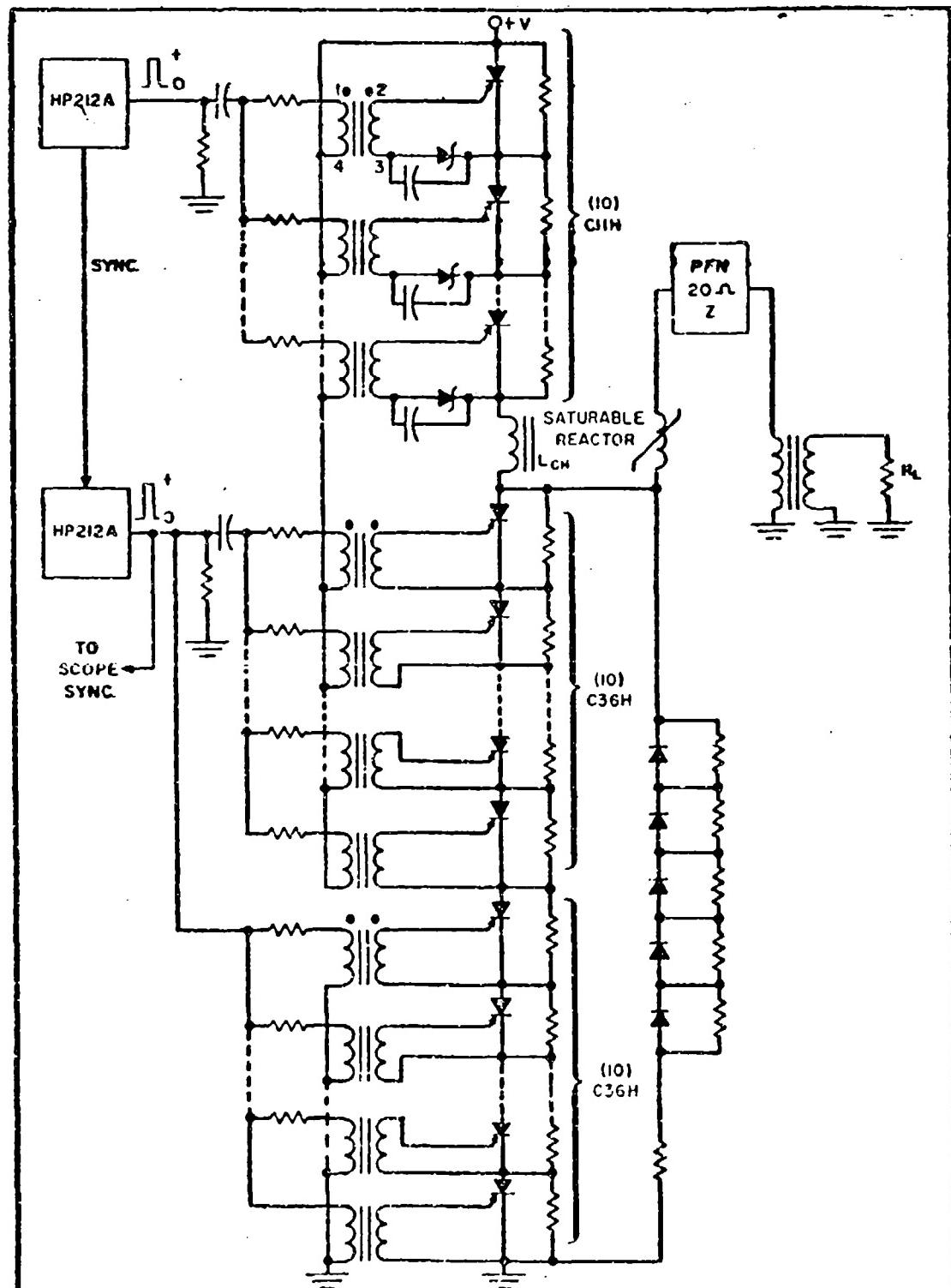


Figure 16. 20 Trinitron Switch Schematic Diagram

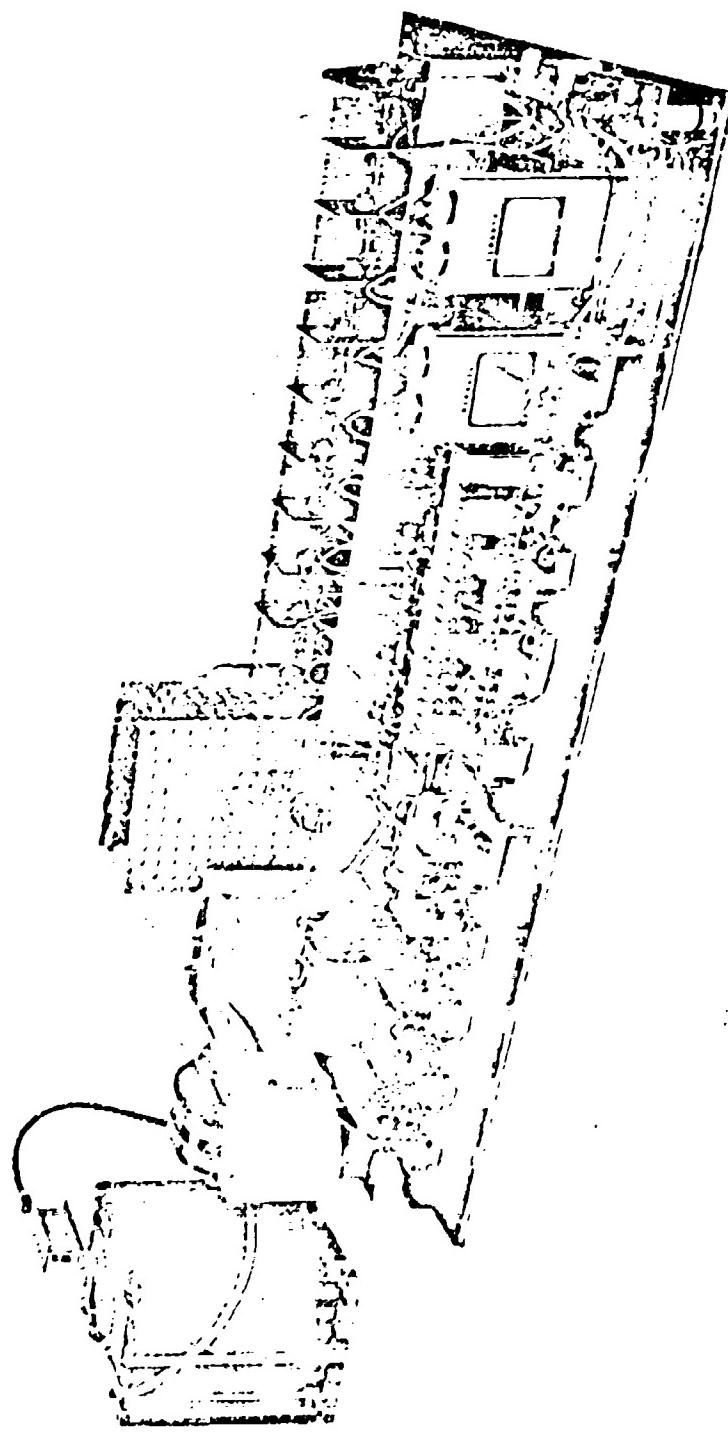


FIG. 17 20-TRANSISTOR SWITCH WITH RESISTOR LOAD

TWO EXPERIMENTAL SEMICONDUCTOR-MAGNETIC PULSE MODULATORS

by

R. Jordan, C. Price, and L. Swain

... Electronic Systems Laboratory
Massachusetts Institute of Technology
Cambridge 39, Massachusetts

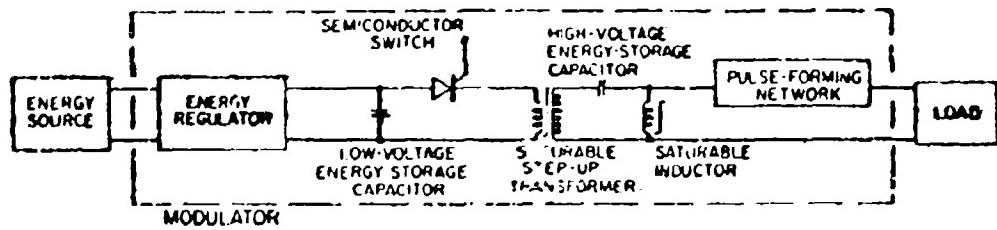
I. INTRODUCTION

For several years an investigation at the M.I.T. Electronic Systems Laboratory has been directed toward developing airborne pulse modulators which are small and lightweight, and operate reliably and with high efficiency. Thanks to new semiconductor devices and square-loop magnetic materials the study has led to the design of modulators which possess these characteristics to a greater degree than previously known types. The basic modulator circuit that has evolved can be tailored to a wide range of output powers, pulse widths, and power-supply requirements.

The operating principles and some design considerations pertinent to semiconductor-magnetic modulators are presented here in a discussion of two recently designed circuits. The first has been designed to generate 2-kw (kilowatts) average output power, and is intended for operation from a 400-cps a-c power line. The second circuit, intended to operate from a battery or dc-to-dc-converter power supply, is capable of 160 watts average power output. Experimental data obtained from tests on the tests on both modulators are also included.

II. BASIC OPERATING PRINCIPLES

A simplified circuit diagram applicable to both modulators appears in Fig. 1a. Energy derived from an unregulated d-c power supply is delivered to a transmitting-tube load as brief pulses. The modulator circuit generates the desired output pulse in three distinct steps (refer to Figs. 1b, 1c, and 1d):



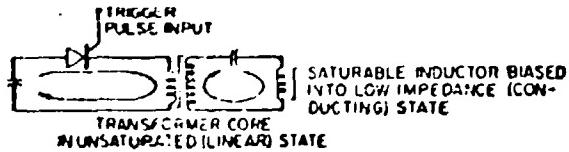
(a)

SIMPLIFIED CIRCUIT DIAGRAM - MODULATOR WITH SOURCE AND LOAD



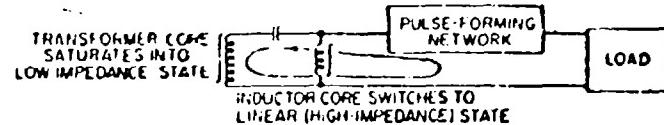
(b)

STEP I ENERGY REGULATOR CHARGES LOW-VOLTAGE CAPACITOR WITH PRECISELY THE ENERGY REQUIRED FOR A SINGLE OUTPUT PULSE PLUS LOSSES



(c)

STEP II TRIGGER PULSE CLOSES SEMICONDUCTOR SWITCH. LOW-VOLTAGE CAPACITOR DISCHARGES INTO TRANSFORMER PRIMARY, CHARGING HIGH-VOLTAGE CAPACITOR THROUGH TRANSFORMER SECONDARY AND SATURATED INDUCTOR



(d)

STEP III HIGH-VOLTAGE CAPACITOR DISCHARGES THROUGH LINEAR PULSE FORMING NETWORK INTO LOAD

Fig. 1 Simplified Circuit Diagram - Modulator with Source and Load

Step I. Energy is drawn from an unregulated source (battery, transformer-rectifier-filter, etc.) to charge a low-voltage energy-storage capacitor. The charging time is somewhat less than the interpulse period. An energy-regulator circuit assures that despite supply-voltage fluctuations the capacitor receives the exact amount of energy required to produce a single output pulse and to supply circuit losses.

Step II. A semiconductor switch is triggered closed, and the energy is transferred from the low-voltage capacitor through a saturable voltage-step-up transformer to a high-voltage capacitor. The discharge time is only a few times greater than the duration of the output pulse.

Step III. The transformer saturates and the shunt inductor switches out of saturation (i. e., the inductor becomes a high impedance), discharging the high-voltage capacitor through a linear pulse-forming network and into the load. A rectangular output pulse appears across the load.

A more detailed discussion of circuit operation is given in the sections that follow.

The principal advantages of this circuit stem from the pulse-energy regulator, which assures pulse-to-pulse uniformity in time and amplitude, and from combining semiconductor and magnetic switching elements to achieve pulse-time compression, which results in a modulator that is unusually lightweight, efficient, and reliable.

The next two sections describe in detail the operation of two modulators, each with a different application but both with the basic circuit of Fig. 1a.

III. 2-KW MODULATOR

The basic circuit of the modulator described in this section can be used in a wide variety of pulser applications where primary power is supplied by an a-c line. The principal difference between this circuit and the one described in Sec. IV is that each uses a different kind of energy regulator. The d-c power for the modulator described in this section is provided by an ac-to-dc power supply with a simple inductance-capacitor filter output. Under these circumstances an energy-regulator circuit can be designed that returns excess energy to the d-c power supply, rather than dissipating it--a technique that leads to high regulator efficiency.

The component values given in Sec. B, below, were determined for a modulator intended to produce 2-kw average output power in 2-microsecond, 1-megawatt pulses.

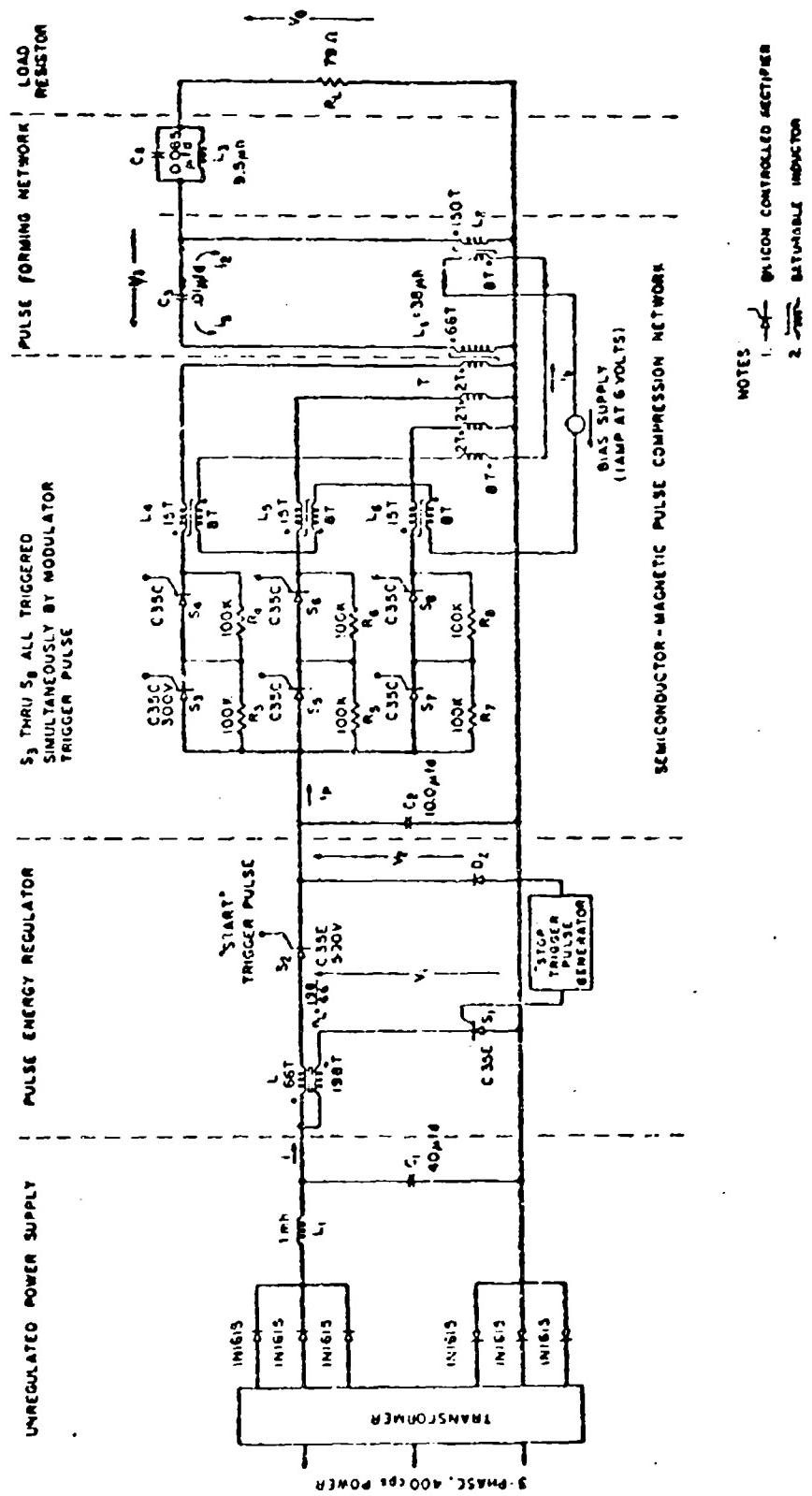
A. Circuit Operation

A simplified schematic diagram of the 2-kw modulator appears in Fig. 2. Voltage waveforms for a typical pulse cycle are given in Fig. 3, and operation of the circuit is described below.

The pulse-generation cycle is initiated when the energy regulator is triggered. When silicon controlled rectifier (SCR) S_2 is triggered, energy is transferred from the d-c power supply to C_2 through the primary winding of inductor L . At time t_1 (see Fig. 3a), when v_2 reaches the desired voltage E_o , reference Zener diode D_z conducts, triggering the "stop"-trigger pulse generator. The stop-trigger pulse fires S_1 , connecting the secondary winding of L across the power supply. The turns ratio of L is chosen so that when S_1 switches on, v_1 decreases to a value less than E_o . The reverse voltage thus applied across S_2 forces it to turn off. Any current in the primary winding of L is transferred to the secondary, so that energy stored in L at t_1 is returned to the power supply (see Fig. 3d). After all the energy stored in L is returned to the source, the supply voltage turns S_1 off. At this point the energy-regulator cycle is over until the next pulse cycle begins.

Shortly after C_2 becomes fully charged, the parallel-series-connected bank of SCR's S_3, \dots, S_8 is triggered (at time t_2 in Fig. 3d). In order to avoid excessive power dissipation in the controlled rectifiers while they are switching from the nonconducting to the conducting state, the saturable inductors L_4 , L_5 , and L_6 present a high impedance so that conduction is delayed for the few microseconds (t_3-t_2 in Fig. 3a) required for the controlled rectifiers to turn on completely. The cores of the inductors have square B-H loops (as shown in Fig. 4)* and are biased at some point A, in negative saturation with respect to i_p . At t_3 the inductors have absorbed sufficient volt-time integral to become positively saturated (and hence, low impedances), so E_o is applied to the primary of transformer T. The core of T is negatively saturated (point B in Fig. 4), so T behaves initially as a linear transformer; and C_3 is resonantly charged by C_2 through the saturated inductances of L_4 , L_5 , L_6 in the primary circuit and the saturated inductance of L_2 in the secondary circuit. At t_4 , when v_3 has reached its maximum value E'_o in Fig. 4b, the transformer core switches into positive saturation and the secondary winding assumes a low impedance. Inductor L_2

* The B-H loops for all the cores of L_2 , L_4 , L_5 , L_6 , and T in Fig. 2 are identical.



is negatively saturated with respect to i_s , and is effectively an open circuit. Thus C_3 is connected in series with the saturated T secondary, the pulse-forming network tank circuit, and the load, so energy stored in C_3 is delivered to the load as a rectangular pulse of width $(t_5 - t_4)$ (see Fig. 3c).

Before a new pulse cycle can begin, a reverse volt-time integral must be applied to each saturable core to reset it to its original state of saturation. This is accomplished by a bias circuit consisting of a bias-current supply and a separate winding on each saturable core. The bias circuit prevents the currents i_p , i_s , and i_L from becoming zero until sufficient volt-time integral has been provided for each core by linearly changing voltages on C_2 and C_3 . The variation of capacitor voltage resulting from the bias current during the resetting period is shown in Figs. 3a and 3b for a magnetron load, which is an open circuit during the resetting interval.

R. Design

The component values in any modulator depend upon the output pulse requirements and the nature of the load. The design of the circuit of Fig. 2 proceeds from output to input in the sequence of steps outlined in this section.

1. Pulse-Forming Network. The modulator is designed to operate with a magnetron load. Modulator output requirements are:

Magnetron impedance R_L	79 ohms
Pulse energy J_o	2 joules
Pulse duration $(t_5 - t_4)$	2 microseconds
Pulse repetition rate (F)	1000 pulses per second

The pulse-forming network (PFN) in Fig. 2 is a two-stage Guillemin type¹ and comprises C_3 , C_4 , L_3 , and the saturated inductance L_8 of the transformer secondary winding. The network is designed to produce an approximately rectangular output pulse. The PFN element values are determined from Reference 1, and are completely specified by the load impedance, pulse duration, pulse rise time, and pulse shape desired.

2. Pulse-Compression Network. The volume of each of the cores for L_2 , L_4 , L_5 , L_6 and T of Fig. 2 is constrained by the total volt-time integral each of the cores is required to absorb before saturating and by the saturated inductance desired of each winding. From these considerations it can be shown that

¹ G. M. Glascoe and J. V. Lebacqz, Pulse Generators, M. I. T. Radiation Laboratory Series, Vol. 5, Chapter 6, McGraw-Hill Book Co., N. Y., 1948.

$$V_{4-6} = \frac{\mu_s}{4L_{4-6}} \left[\frac{E_o(t_3 - t_2)}{B_s X_k} \right]^2 \quad (1)$$

$$V_2 = \frac{\mu_s}{16L_2} \left[\frac{E'_o(t_5 - t_4)}{B_s X_2} \right]^2 \quad (2)$$

and

$$V_T = \frac{\mu_s}{16L_T} \left[\frac{E'_o(t_4 - t_3)}{B_s X_T} \right]^2 \quad (3)$$

where V_{4-6} , V_2 , V_T , and L_{4-6} , L_2 , L_T are respectively the core volumes and saturated inductance of inductors L_{4-6} , L_2 and the saturable transformer secondary, and μ_s , B_s , and X represent respectively the core-material properties--saturated permeability, saturation flux density (see Fig. 4), and stacking factor. In Eq. 3 it can be shown that $(t_4 - t_3)$ is a function of the independent variables L_{4-6} , L_2 , and E_o , and all other quantities are determined from the output pulse shape and the type of core material used.

Values of the variables are selected according to one of a number of optimization criteria (e.g., minimum cost, minimum weight, or maximum efficiency) that have been developed. The maximum efficiency criterion was used in the design of the 2-kw modulator.

The combined losses of the transformer T and the controlled rectifier switches S_3, \dots, S_8 in Fig. 2 may be written as a function of $(t_4 - t_3)$; when $(t_4 - t_3)$ is 6 microseconds, these losses are a minimum. A value of 660 volts was selected for E_o , and L_2 and L_{4-6} were chosen as respectively 0.57×10^{-4} and 0.4×10^{-6} henries, so that the total core volume of L_2 , L_4 , L_5 , and L_6 is minimized.

Another consideration in selecting the saturable reactor cores is that the window area must be large enough to accommodate the wire in the windings; in the case of L_2 and T , additional space had to be provided for high-voltage insulation.

The value of C_2 (10.0 microfarads) depends upon the required output pulse energy J_o and the regulated voltage E_o . The number and configuration of controlled rectifiers (S_3, \dots, S_8 in Fig. 2) in the pulse-compression network is determined by their breakdown voltage and root-mean-square current (rms) ratings and by the average power output of the modulator. Resistors R_3, \dots, R_8 are voltage dividers which ensure that each SCR blocks its share of the voltage E_o on C_2 .

It should be recognized that the design procedure outlined above does not result in a modulator having absolute maximum efficiency since only the combined losses of S_2, \dots, S_8 , and T were minimized. The analysis required to determine parameters that assure minimum total loss is extremely lengthy, and experience has shown that the use of the alternative procedure described here gives nearly the same results.

3. Energy Regulator. The dashed waveforms in Fig. 3d show the variation in power-supply current when the d-c supply voltage E_s has both the highest (E_h) and the lowest (E_l) values for which regulation of the energy delivered to C_2 is desired. If the regulation range $a = E_h/E_l$ is known, the design of the regulator components can be accomplished; the basic relationships which must be satisfied are summarized here.

(a) In order that C_2 cease charging when v_2 reaches E_o for all values of supply voltage between E_h and E_l , the anode-to-cathode voltage across S_1 in Fig. 2 must be positive just before the stop-trigger pulse occurs and v_2 must be greater than v_1 just after S_1 is triggered. If E_l is taken to be $E_o/2$, then it can be shown that these conditions are satisfied when

$$n_L = \frac{a}{2-a} \quad (4)$$

where n_L is the turns ratio of the two-winding inductor L .

(b) The pulse period $1/F$ must exceed the maximum total time required to charge C_2 and to return the energy stored in L to the power supply. The maximum occurs when $E_s = E_h$; hence from Fig. 3d it follows that

$$\frac{1}{F} \geq \tau - t_o \quad (5)$$

(c) The maximum amount of energy J_m is stored in the airgap of L at t_1'' in Fig. 3d, when $E_s = E_h$. Therefore the airgap volume V_g must satisfy the relation

$$\frac{J_m}{V_g} = \frac{B_s^2}{2\mu_0} \quad (6)$$

where μ_0 is the permeability of air.

(d) In order to prevent saturation of the magnetic material the volt-time integral across the primary of L must be

$$L \int_0^{t_1/2} \frac{di_{1h}}{dt} dt = N_L B_s A_L \quad (7)$$

where i_{1h} is the current when $E_s = E_h$ (see Fig. 3d), N_L is the number of turns on the primary winding of L , A_L is the core cross-section area, and L is the primary inductance.

(c) The area of the wire A_w in each winding of L is limited by the rms current I_{rms} in the winding and is given by

$$A_w = \frac{I_{rms}}{K_c} \quad (8)$$

where K_c is the current-carrying capacity of the wire in amperes per unit area.

IV. 160-WATT MODULATOR

A. Operation

The basic circuit of a 160-watt semiconductor-magnetic modulator, designed to operate with battery prime power, is shown schematically in Fig. 5. Circuit operation is very similar to that of the circuit of Fig. 2 and the waveforms in Figs. 3a and 3b apply; differences between the two circuits are discussed below.

The energy regulator circuit in Fig. 5 functions differently from the one used in the 2-kw modulator. The energy stored in L when v_2 in Fig. 5 reaches E_0 (at t_1 in Fig. 3a) is not returned to the power supply, but instead is dissipated in Zener diodes D_{Z2} and D_{Z3} . When S_1 is triggered on by the "stop"-trigger pulse, S_2 and S_3 turn off and the current i in Fig. 5 becomes zero; however, a current i_L still exists (see Fig. 6) in the inductor L by virtue of the path provided through L , S_1 , D_{Z3} , and D_{Z2} . When i_L becomes zero, S_1 turns off. This type of energy regulator is used because the modulator power supply is a battery which will not recharge as quickly as energy would be returned to the source in the circuit of Fig. 2. Closer regulation of v_2 can be achieved with the circuit of Fig. 5 because the detrimental effects of leakage inductance in the windings of L in the regulator (Fig. 2) are not present; regulator efficiency, however, is lower.

The rest of the modulator circuit is basically the same configuration as the 2-kw circuit, with the most noticeable differences being series-connected discharge SCR's S_4 , S_5 , and S_6 , and an additional tank circuit in the P.F.C.

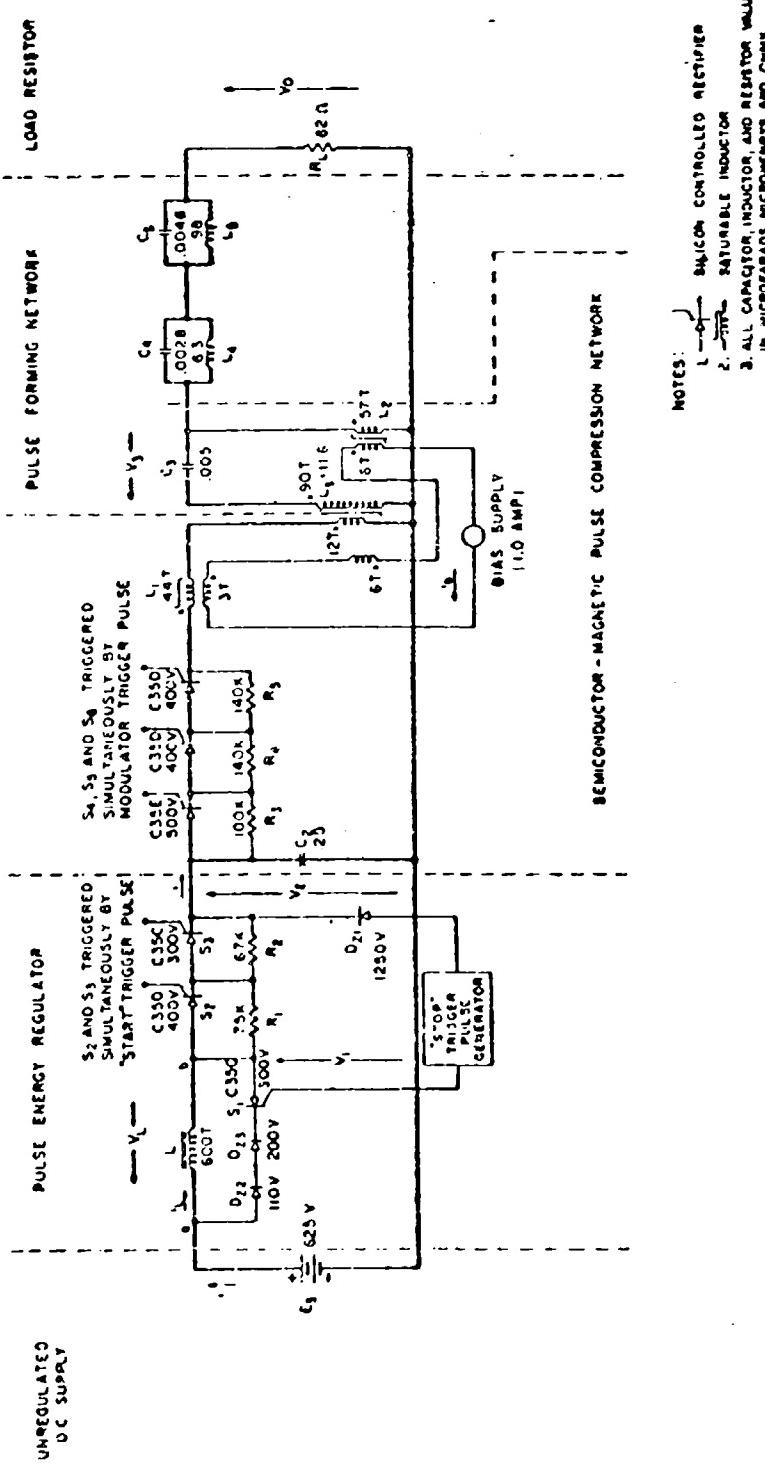


Fig. 5 160-Watt Semiconductor-Magnetic Modulator--Simplified Schematic Diagram

B. Design

1. Pulse-Forming Network. The 160-watt modulator is designed to operate with a magnetron load. The modulator output requirements are:

Magnetron impedance R_L 82 ohms
Pulse energy J_0 0.16 joules
Pulse duration ($t_5 - t_4$) 1.0 microsecond
Pulse repetition rate F 1000 pulses per second

The pulse-forming network in Fig. 5 is a three-stage Guillemin type¹ and comprises C_3 , C_4 , C_5 , L_4 , L_5 , and the saturated inductance L_s of the transformer secondary winding. The network is designed to produce an approximately rectangular output pulse. As in the case of the 2-kw modulator, the element values given in Fig. 5 have been determined from Reference 1.

2. Pulse-Compression Stage. Equations 1, 2, and 3 respectively apply as constraints on the volumes of L_1 , L_2 , and T in Fig. 5. The minimum-weight criterion was the basis for selection of the variables E_0 , L_2 , and L_1 . Values for L_2 and L_1 were chosen to be respectively 27.0 and 4.3 microhenrys so that the total core volume of L_1 , L_2 , and T is minimized, and E_0 was selected to be 1250 volts to permit the use of a physically small capacitor C_2 (0.25 microfarads).

3. Energy Regulator. The dashed waveforms in Fig. 6 show the variation in inductor current i_L in Fig. 5 when the d-c supply voltage has the extreme values of E_h and E_f ; the times t_0 , t_1 , t'_1 , t''_1 , and τ have the same significance as in Fig. 3d. The definition of the regulation range a is the same as for the circuit of Fig. 2, and Eqs. 5, 6, 7, and 8 must be satisfied. In addition, by the same reasoning employed in deriving Eq. 4, it can be shown that

$$V_z = \frac{E_0}{2} (2 - a) \quad (9)$$

where V_z is the combined reference voltage of D_{Z2} and D_{Z3} .

The supply voltage E_s is much higher than in the 2-kw modulator. Hence a series bank of controlled rectifiers S_2 and S_3 is required to realize the proper breakdown-voltage rating for the semiconductor switch in the pulse-energy regulator stage of Fig. 5. Resistors R_1 and R_2 are voltage dividers

¹ Ibid., Glascock and Lebacqz.

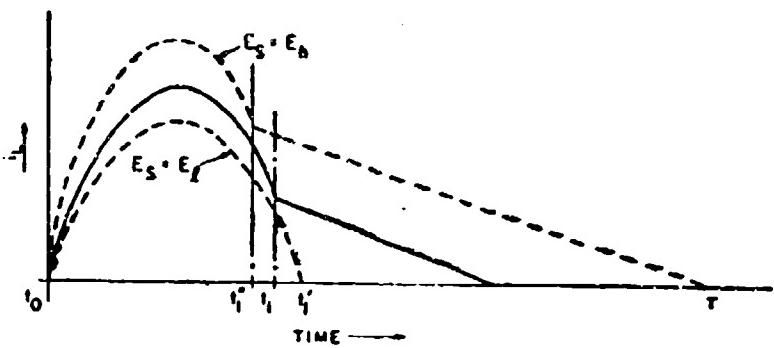


Fig. 6 Inductor Current i_L in Fig. 5 Versus Time for Different Values of E_s

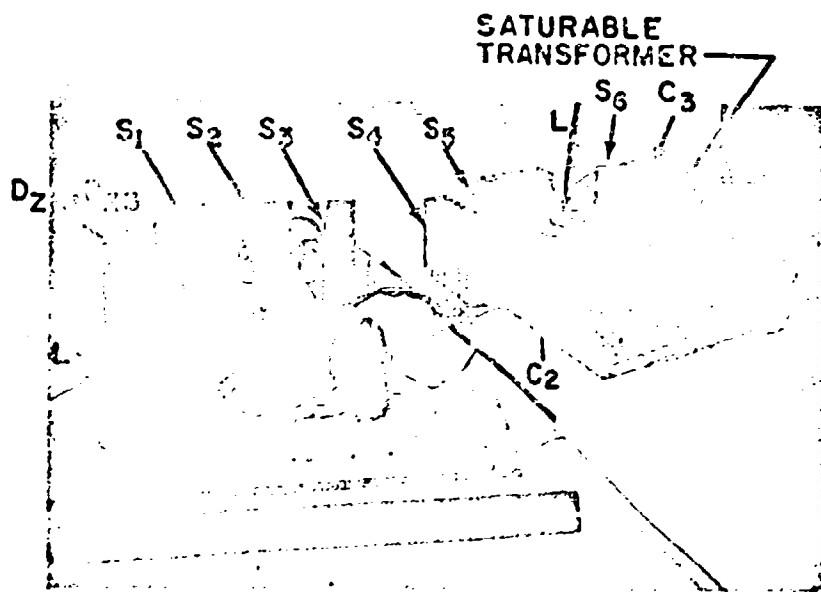


Fig. 7 Experimental Model of 160-Watt Modulator

which ensure that each SCR blocks its share of the total voltage.

V. PERFORMANCE CHARACTERISTICS

A. 160-Watt Modulator

The 160-watt modulator circuit shown in Fig. 5 has been constructed. Preliminary test data are reported here; as of this writing a complete evaluation of the circuit, and some needed minor parameter adjustments, have not been made. An a-c driven d-c power supply capable of providing an output voltage in the range 600-900 volts was used, and the load was simulated with an 82-ohm resistor. A photograph of the apparatus, excluding the power supply, appears in Fig. 7. Oscillographs of several voltage waveforms in the circuit are given in Figs. 8 through 13.

Figures 8, 9, and 10 show the variation of v_L in Fig. 5 for several different values of the source voltage E_s . In Fig. 8 v_L is a nearly perfect half cosine beginning at t_0 and ending at t_1 (see Fig. 3a); E_s has the value E_f , which is just sufficient to charge C_2 to the regulated voltage E_o . In Figs. 9 and 10 the regulating action provided by the energy regulator shows up as the sharp discontinuity in the negative portion of each waveform at t_1 , at which point C_2 ceases charging and the voltage across L is the combined Zener reference voltage of D_{22} and D_{23} . At t' all the energy stored in L has been dissipated and v_L becomes zero.

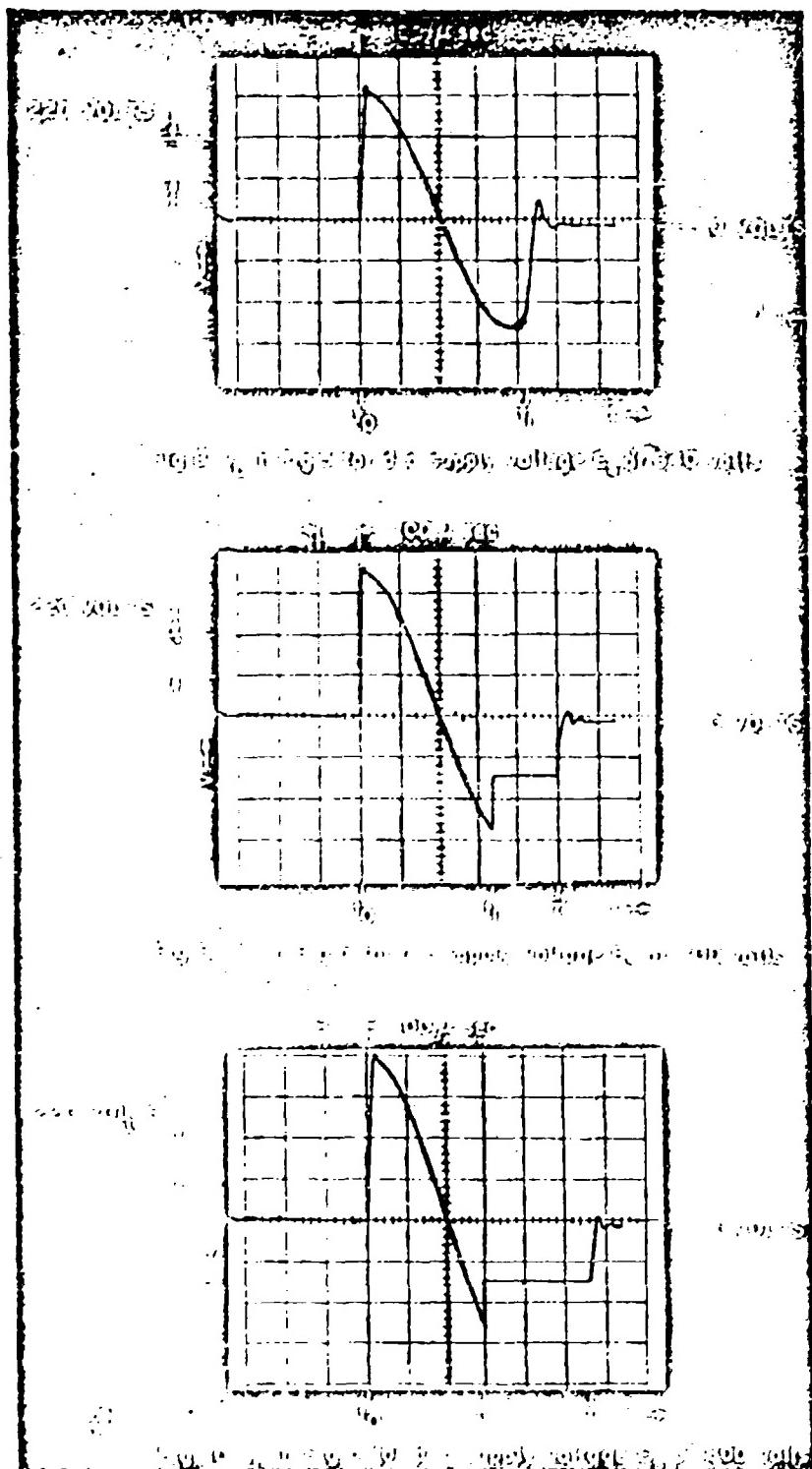
Figure 11 shows the variation of v_2 as C_2 is charged. The abrupt break-over at E_o , the maximum voltage, results when the energy regulator interrupts the charging circuit. As C_2 is discharged, v_2 varies as in Fig. 12.

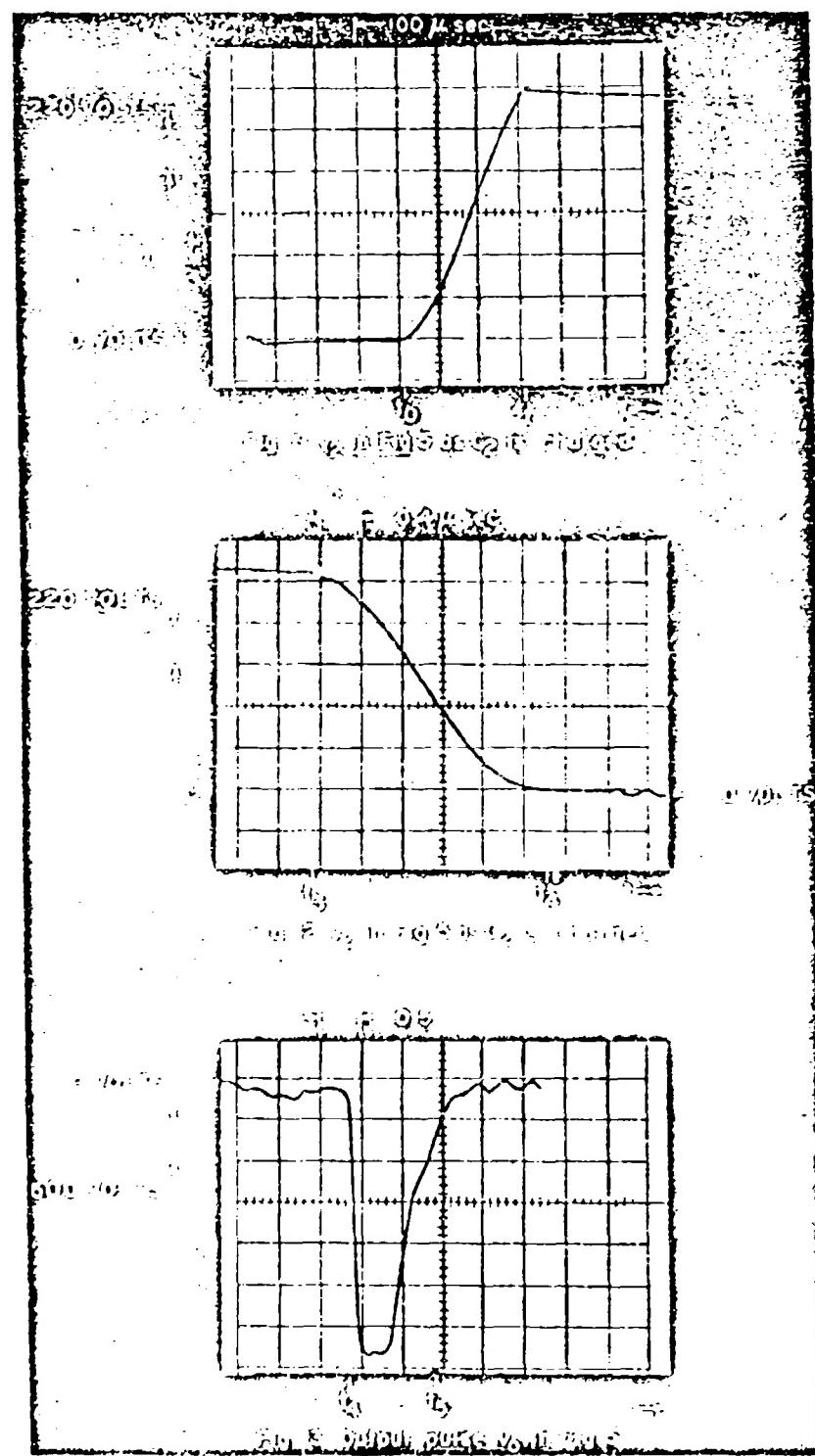
Figure 13 shows the output voltage pulse shape when the energy is delivered to a resistive load.

The energy-regulator circuit restricts the change in E_o to be from 1200 to 1260v when the d-c power-supply voltage E_s varies from E_f (900v); most of the increase in E_o occurs when E_s is in the 800- to 900-volt range. The regulation range a was chosen to be 1.5.

The overall efficiency of the circuit in Fig. 5 varies from approximately 45 percent when $E_s = E_h$ to approximately 70 percent when $E_s = E_f$.

The total weight of circuit components shown in Fig. 7, including heat sinks, is 5 pounds.





B. 2-kw Modulator

A breadboard version of the 2-kw modulator shown schematically in Fig. 2 has been constructed. A photograph of the breadboard exclusive of the power supply is shown in Fig. 14. A three-phase a-c driven 275-volt d-c power supply was used for testing the circuit, and the load was simulated with a 79-ohm resistor. Oscillographs of several important voltage waveforms appear in Figs. 15 through 20.

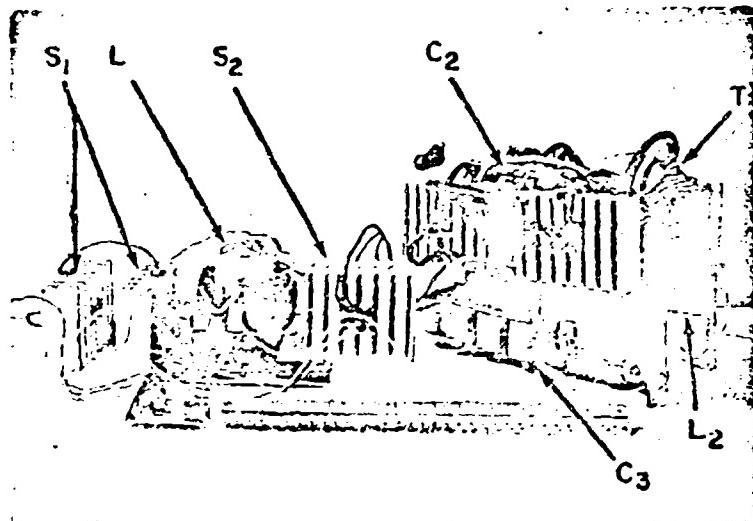


Fig.14 Experimental Model of 2-kw Modulator

Figure 16 shows the time variation of v_1 (see Fig. 2). The voltage v_1 has the value E_s until S_2 is triggered at t_o (see Fig. 3) after which v_1 becomes identical to v_2 , the voltage across the low-voltage storage capacitor C_2 . The waveform shows the voltage build-up during the charging of C_2 . At t_1 C_2 reaches E_o and S_1 is triggered, thus lowering v_1 to a value less than E_o ; this action causes S_2 to turn off and v_2 remains at the regulated value E_o . After all the energy stored in L is returned to the power supply at τ' (see Fig. 16), v_1 again assumes the value of E_s . In the oscilloscope the second value of E_s is less than the first because C_1 in the power supply has not fully charged. Figures 15 and 17 show the variation of v_1 when E_s has respectively smaller and larger values than in Fig. 16. In the limiting

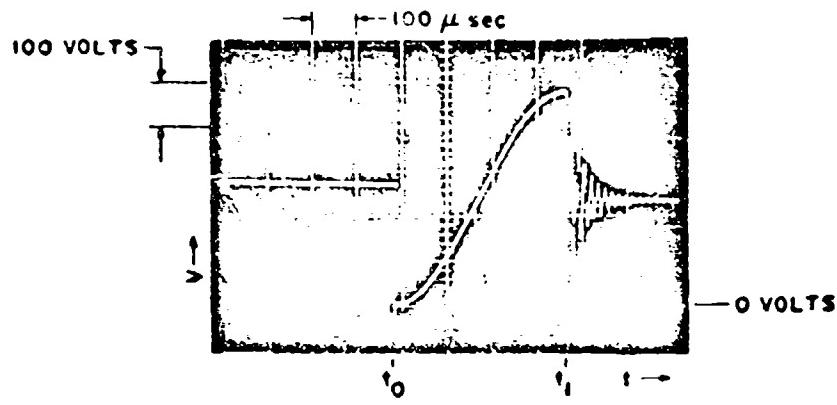


Fig. 15 v_i in Fig. 2 for d-c supply voltage E_s of 260 volts

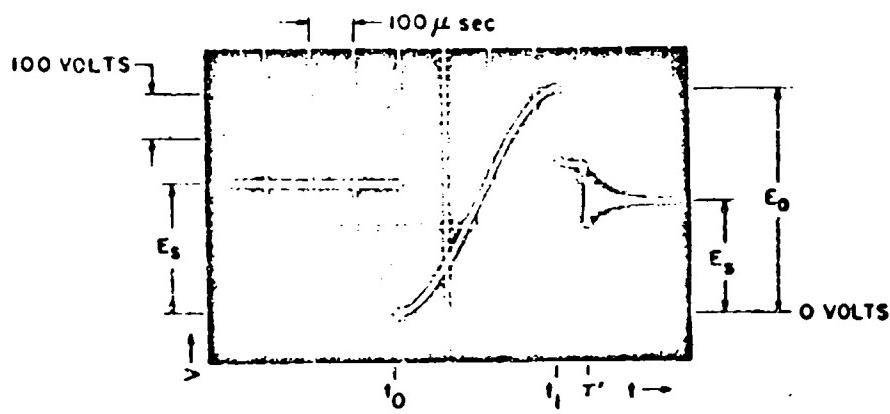


Fig. 16 v_i in Fig. 2 for d-c supply voltage E_s of 280 volts

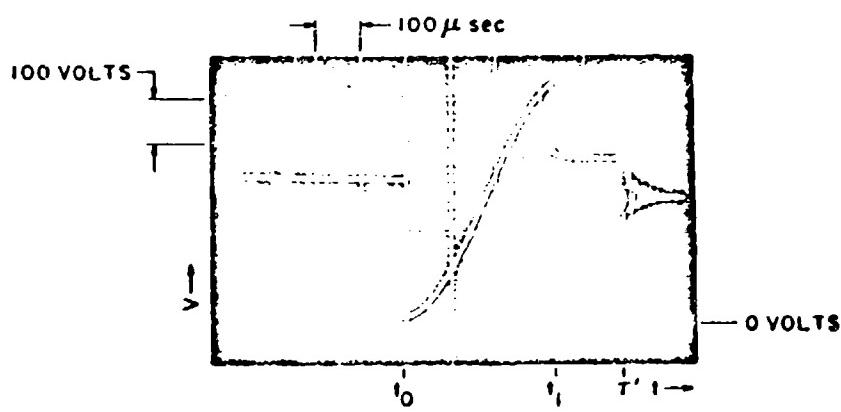


Fig. 17 v_i in Fig. 2 for d-c supply voltage E_s of 300 volts

case shown in Fig. 15 E_g is just sufficient (E_f) to charge C_2 to the voltage E_o ; therefore, no energy regulator action is required and S_1 does not trigger.

Figures 18, 19, and 20 show voltage waveforms similar to those in Figs. 11, 12, and 13 respectively. There is more ripple in the output pulse of Fig. 20 than in that of Fig. 13 because the 2-kw modulator has one less PFN stage than does the 160-watt modulator, and the 2-kw load was mismatched by 20%.

The overall efficiency of the circuit in Fig. 2 is estimated at approximately 80 percent for all values of E_g between E_h and E_f . The estimate is based on a calculated efficiency of 95 percent for the energy regulator and a measured efficiency of 85 percent for the discharge network. The smaller efficiency of the 160-watt modulator is caused by power dissipation in D_{Z2} and D_{Z3} of that circuit and relatively high switching losses in the magnetic cores and capacitors of the pulse-compression network.

The total weight of the breadboard circuit shown in Fig. 14 is 15 pounds. With the power supply included the total modulator weight is 25 pounds.

VI. CONCLUSION

The circuit techniques described here permit the design of rugged light-weight, reliable, compact pulse modulators. While only two working examples are presented here, other circuits have been constructed that are only one-third the weight of conventional circuits with the same output characteristics.

A detailed report covering all phases of semiconductor-magnetic modulator operation and design is in preparation by Mr. Rolando Jordan, and should be completed later this year.

ACKNOWLEDGEMENT

The research reported here was made possible through support extended the Massachusetts Institute of Technology, Electronic Systems Laboratory, by the United States Air Force, Navigation and Guidance Laboratory, Aeronautical Systems Division, under Contracts AF-33(616)-5489 and AF-33(657)-7644.

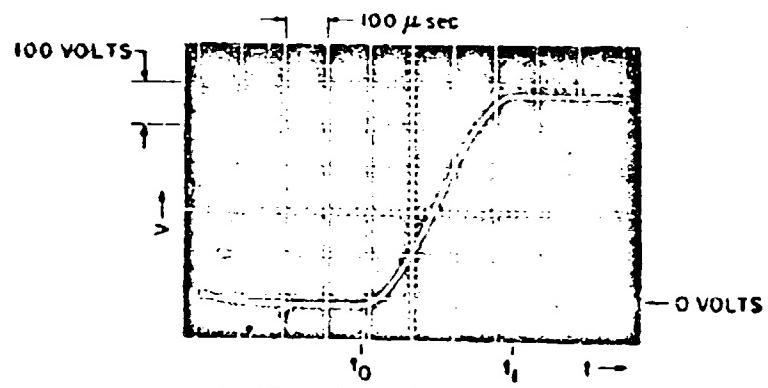


Fig. 18 v_2 in Fig. 2 as C_2 is charged

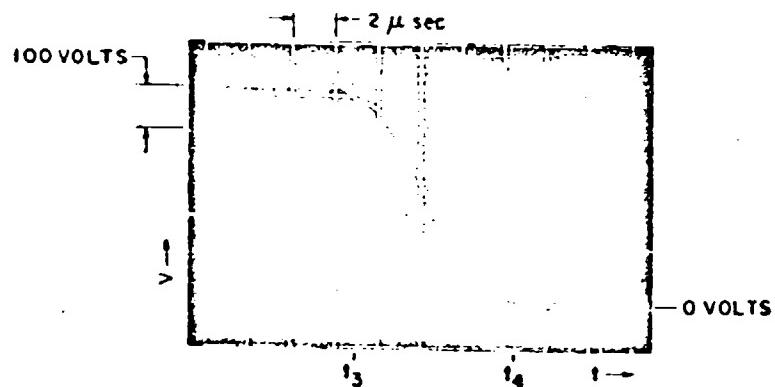


Fig. 19 v_2 in Fig. 2 as C_2 is discharged

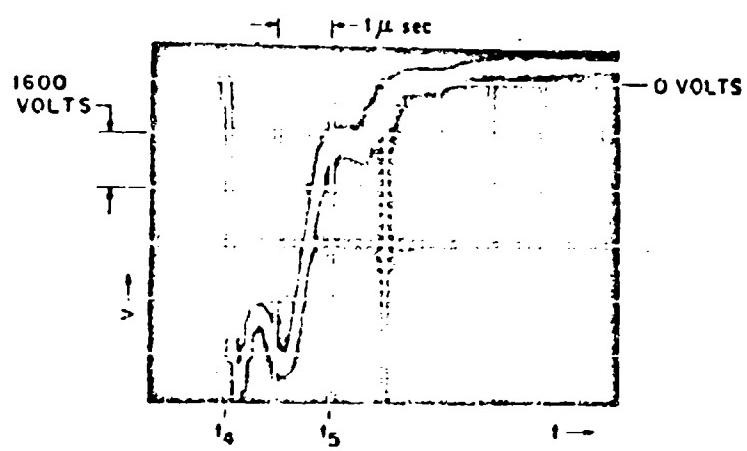


Fig. 20 Output pulse, v_0 , in Fig. 2

so that the electrons rotate in a helical path. Magnetic mirrors confine the ends of the helix so that the rotating electrons form a cylindrical layer.

The magnetic field associated with this rotating electron current will confine a plasma. The plasma will be heated by collisions with the rotating electrons. In this manner, conditions making possible thermonuclear reactions will hopefully be obtained.

The requirements for the pulsed electron beam are a beam of 200 amperes at 5 Mev $\pm 0.5\%$ with the regulated portion of the beam at least 0.25 μ sec wide and the beam turn-on time less than 100 nanoseconds.

A linear magnetic induction accelerator will be used to accelerate the electrons to the proper energy. The electrons will be accelerated by induction as they pass through a series of pulsed magnetic cores. The action of the pulsed core on the electron beam is analogous to that of a pulse transformer. The accelerator is divided into several sections, each section consisting of 48 cores. Each core must be excited to a voltage of 12-kv with a flat top pulse, that is 250 nsec wide.

In order to maintain the accelerator gradient, the cores had to be limited to 1/2-inch thickness. To support the volt-seconds required, the core build-up is 8 inches. Since the accelerator column must pass through the cores, an 8-inch inside diameter was required.

To pulse magnetic cores at these short pulse widths, very high exciting currents are required. The maximum current is 2,000 amperes.

Each core is excited by a line-type modulator⁶ using a type 5949A thyratron. The impedance match to the core is achieved by using a one-turn primary winding. Since the magnetizing current is not constant, compensating networks are utilized to produce the required current waveshapes.

Investigation of various core materials at this pulse width⁷ found that a 1-mil, 50% nickel-iron tape wound core would be a satisfactory choice.

REQUIREMENTS OF TRIGGER SYSTEM

Since each core must be excited simultaneously, a system that would simultaneously trigger 500 thyrtatrons was needed. Since each thyratron has its own individual firing delay, compensations must be made on an individual basis. An analysis of anode delay vs trigger voltage and wave shape indicated that a firing voltage of over 2 kilovolts, with a pulse duration of at least 400 nanoseconds, was required (figure 1). The rise time of the trigger pulse at the grid of each thyratron should be a maximum of 100 nanoseconds. Since each thyratron grid is terminated in 50 ohms, the equivalent load resistor for 500 thyrtatrons would be 0.1 ohm. For a 2,000-volt pulse this represents 40 Mw of peak power.

Magnetic modulators offer a reliable method of producing high-power, short-duration pulses at repetition rates of 60 pps. The accelerator cores being constructed of a square loop material of sufficiently thin gauge, offered a source of modulator cores.

Two basic avenues of approach to trigger generation are possible. The first is to produce the output pulse at a high voltage and high impedance and then use transformers to reduce the voltage to the proper operating point. The second is to produce the triggers at their final value and trigger all thyrtatrons directly. Both approaches have been investigated.

PRINCIPLES OF OPERATION OF MAGNETIC MODULATORS

The theory of operation of magnetic modulators and the conditions for optimum operation have been described in many reports.⁸⁻¹⁴ The basic principles governing magnetic modulator operation can be simply described by reference to figure 2.

Capacitor C_1 is initially charged to voltage E . At time t_0 the electronic switch S_1 is closed. Capacitor C_1 will then discharge into the series resonant circuit consisting of L_2 , C_1 , and C_2 . If C_1 and C_2 are equal, the energy stored in C_1 will be transferred to C_2 during the first half period of the resonant cycle.

Saturable reactor L_2 is initially biased to negative saturation, thus having a high impedance to current flow from C_2 to C_3 . Reactor L_2 is designed to saturate when capacitor C_2 is fully charged. This will occur at time t_1 .

Saturation of L_2 discharges C_2 into the resonant circuit formed by the saturated inductance of L_2 , C_2 , and C_3 . If the capacitances of C_1 , C_2 , C_3 , and the output pulse forming network are equal, the operation of each stage is similar.

As a practical consideration, the charging time of the pulse forming network should be a minimum of five times the network delay. The operation of the output stage is similar to that of any modulator utilizing pulse forming networks. The saturated inductance of L_4 can be included as part of the pulse forming network (PFN). Output pulse width and rise time are then determined by the PFN and load characteristics.

The impedance of each subsequent stage in a magnetic modulator is lower than that of the preceding stage. This results in each energy storage device discharging faster than it was charged. A magnetic modulator will thus transform a long pulse of low peak energy into a narrow pulse of high peak energy. Magnetic modulators, by compressing the input pulse, have inherent time delay. The longer this delay, the higher the peak power gain of the modulator.

Equations Governing Modulator Operation

For the charging cycle:

$$V = \frac{E}{2} (1 - \cos \omega t)$$

$$\omega = \frac{1}{\sqrt{LC}}$$

For toroidal reactors:

$$L_{sat} = \frac{4 \pi N^2 A}{l_m} \times \mu_{sat} \times 10^{-9} \text{ henrys}$$

The time for each reactor to saturate is governed by the relation

$$\int_0^t V dt = N B_{sat} A \times S.F. \times 10^{-8}$$

The magnetizing current in the reactor winding at saturation.

$$I = \frac{H_{sat} l_m}{0.4 \pi}$$

Where:

- μ_{sat} = Saturated permeability of core
S.I. = Core stacking factor
 I = Current, amperes
 B_{sat} = Magnetizing force at B_{sat} , oersteds
 ω = Resonant frequency
 L_{sat} = Saturated inductance of reactor
 N = Number of turns on core
 A = Core area, square centimeters
 l_m = Mean magnetic path, cm
 V = Voltage, volts
 t = time, seconds

THE EFFECTS OF TRIGGER SYSTEM REQUIREMENTS ON MAGNETIC MODULATOR DESIGN

The Astron trigger system must provide jitter-free triggers to 500 504 1 thyatron under conditions of variable repetition rate operation. This means that the relative time of arrival of each trigger at the thyatron grid must remain constant. Since the anode delay of each tube is a function of trigger voltage, the output voltage of the trigger generator must remain constant at all repetition rates.

There are several parameters that must be closely controlled in order to maintain output stability at varying repetition rates. The energy storage capacitors must have low dissipation factors at their apparent operating frequency. Thermal changes in capacitors will affect both the output voltage and the delay time of the trigger system.

The input voltage to the magnetic modulator must be closely regulated. Variations in charge voltage will cause proportional changes in modulator delay time and output voltage.¹⁵

The magnetic properties of the modulator cores must be maintained constant under conditions of varying core losses. Saturation flux density and core loss are both functions of core temperature.¹⁶ To find the conditions for stable operation, saturation flux density and core losses must be measured under actual operating conditions. From these data the cooling required to maintain the required temperature limits can be calculated.

The combination of high peak power and low output impedance required for the modulator, make the generation of the output pulse from a single core winding a difficult design problem. This has been solved by dividing the last two stages of the modulator into multiple channels. The capacitors and pulse forming networks of these channels are electrically isolated. The saturable reactor windings for each stage are all wound on a common core. All channels are then magnetically coupled until discharge of that stage.

When the reactor saturates, the multiple windings are decoupled due to the reduction of core permeability. This results in no cross-talk between channels after core saturation. Timing between channels remains constant since stage discharge is governed by core saturation.

The isolation of channels after stage discharge has been investigated for several modulators using multiple winding reactors. In all cases it has been found to be adequate for use in a multiple trigger system. Since each channel is isolated after reactor saturation, different output pulses can be generated by the same modulator, with the time synchronization provided by the saturation of the output reactor. Faults occurring in one channel do not affect the operation of adjacent channels during the time of the output pulse.

AN EXPERIMENTAL 72-MEGAWATT MAGNETIC MODULATOR

In order to investigate the feasibility of constructing a magnetic trigger generator at a high voltage, an experimental 72-megawatt, single-stage, magnetic modulator was built. A simplified diagram of this modulator is shown in figure 13.

The input switch for this modulator is a type 5649A thyratron. In this unit the thyratron is operated above its rating. A final design would include several intermediate stages for reliable operation.

The output stage is divided into twelve individual channels, each having its own pulse forming network and output winding. Each channel is designed to produce a 10-kilovolt, 0.4 microsecond pulse into three parallel 50-ohm loads. The combined output impedance of all channels is 1.7 ohms. For a 10-kv, 0.4- μ sec pulse, the peak output power is 71.4 megawatts. Operating at the maximum system repetition rate of 60 pps, the average output power is 1714 watts. Impedance matching to the thyratron grid circuit would be made by step-down pulse transformers.

A comparison of design and actual operating conditions is shown in Table I.

Table I. Operation of 72-Megawatt Magnetic Modulator

Item	Design Value	Operating Value
Discharge time for input capacitor	2.27 μ sec	2.25 μ sec
Charge time for PFN	2.27 μ sec	2.25 μ sec
Peak charge current for all PFN's	2170 amp-turns	*
PFN required	70 amp-turns	30 amp-turns
Magnetizing force at core saturation	2019 amp-turns	2178 amp-turns
Output pulse width	0.4 μ sec	0.46 μ sec
Output pulse rise time	122 nsec	125 nsec
Pulse amplitude	10 kv	10 kv

* Not practically measurable

This modulator worked very close to its design specifications. The most serious difficulty in operation was insulation breakdown in the output windings. This was the main reason that development of this modulator was not extended to the design of intermediate stages.

Details of the modulator construction can be seen in figure 5.

The output reactor details are summarized in Table II.

Table II. 72-Megawatt Output Reactor

Number of legs	3
Material	1-mil, 50% nickel-iron tape wound
Outside diameter	15.5 inches
Inside diameter	8.5 inches
Thickness	0.5 inch
Core area	11.25 square centimeters
Magnetic path length	81.6 centimeters
Stacking factor	0.8
Output winding	12 each, 3 turns, No. 16 A.W.G.
Bias winding	1 each, 1 turn, No. 10 A.W.G.

Core Loss and Saturation Flux Density Measurements

To find the cooling required to maintain constant magnetic properties it was necessary to measure the core losses under operating conditions. Core loss can be measured in two ways. First, the core can be operated at a constant temperature and the heat generated by the core can be measured. The second method is to measure the area of the dynamic B-H loop.

To make the calorimeter measurement, cooling ducts were placed in the modulator and forced-air cooling was used to stabilize the core temperature. Measurements of inlet and exhaust temperatures at a fixed-volume cooling air yielded the following result.¹⁶

Mean core temperature - 89°F
Pulse repetition rate - 60 pps
Heat generated - 390 watts

From these data:

$$\text{Core heating ergs/cc/cycle} = \frac{\text{watts} \times 10^7}{\text{pps} \times A \times S.F. \times I_m} = \frac{390 \times 10^7}{60 \times 33.75 \times 0.8 \times 81.6} \\ = 29.5 \text{ ergs/cc/cycle}$$

Measurements of dynamic hysteresis loops at various temperatures are shown in figures 6 - 11. The poor resolution in the oscilloscope trace is caused by the different writing rates at various portions of the trace. The oscillations are parasitics induced in the monitoring system.

A plot of core loss vs temperature is shown in figure 3. At 89°F the loss is 27.7 ergs/cc/cycle. The values of the core losses agree within the experimental error of both measurements.

The saturation flux density measured at a magnetizing force of 340 oersteds is plotted vs temperature in figure 4. Saturation flux density increases approximately 0.1% per degree Fahrenheit for temperatures below 100°F.

Temperature Profile

Several thermocouples were placed on the output reactor core in order to measure the uniformity of heat generation in the core. The core material, being a stainless steel, has a poor thermal conductivity. Since the material is laminated there is very little heat flow radially.

The modulator was permitted to operate without cooling for a period of fifteen minutes. At that time the temperature profile shown in figure 12 was recorded. The temperatures measured at the same radius were the same for each core.

The temperature of the core increases with increasing radial distance. Measurements on similar cores used as pulse transformers show a thermal profile that decreases with increasing radial distance.

In pulse transformer operation the inner laminations receive the greatest excitation since they have the shortest magnetic path. Higher excitation in this case would cause more core loss and consequently, higher temperatures.

One can visualize the cause of this to be as follows: In a saturable reactor the inner laminations receive the greatest excitation. Since, in this mode of operation, the core drive is sufficient to cause complete saturation, the inner lamination saturates first. As more of the core saturates, a saturation wave front propagates radially from the inner

lamination. As this wave moves outward the time rate of flux change increases. This results in the outer laminations operating at a higher apparent frequency than the inner laminations. The net result is increasing core losses with increasing radius.

Operating Stability

The Astron trigger system must be capable of stable operation at all machine repetition rates. Sufficient cooling must be provided to all the modulator cores to maintain narrow temperature limits in their operation.

Saturation flux density varies $0.1\%/\text{°F}$. This means that the delay through the trigger system would vary 0.1% of the total delay per degree Fahrenheit of core temperature change.

The change in output voltage can be expressed for small temperature changes by the relation

$$\frac{\Delta E}{E} \% = \left[1 + \cos \pi \left(1 - \frac{\Delta B}{B_{\text{sat}}} \right) \right] \times 100\%;$$

for a 10°F temperature change the output voltage would change 0.05% .

Thus, the modulator delay time is twenty times as sensitive to temperature change as is the output voltage.

AN EXPERIMENTAL TWO-STAGE MAGNETIC MODULATOR FOR 50-MEGAWATTS OUTPUT, 25 CHANNELS

To investigate the feasibility of building a multistage magnetic modulator that would develop a 1.5-kilovolt, $0.4\text{-}\mu\text{sec}$ pulse into a $0.1\text{-}\Omega$ resistive load, an experimental two-stage magnetic modulator was constructed. A re-evaluation of the trigger requirements for type 5949A thyatron indicated that a pulse of at least 2 kilovolts was required at the thyatron grid.⁶ The input voltage to the magnetic modulator was increased until an output pulse of 2 kilovolts was obtained.

The modulator has been operated to a peak output voltage of 2.3 kv. At this voltage many of the components used in construction are operating above their voltage ratings. The modulator has been operated at a 60 pps rate with an output pulse of 2 kv. Since the prototype model does not have provisions for cooling, operating time at 60 pps was very limited. Most test data were obtained at an output voltage of 2 kv and a repetition rate of 30 pps.

The modulator is of the series reactance type and utilizes a Size A ignition as a primary switch. Both stages of this modulator utilize a multiple winding technique which provides electrical isolation of outputs after reactor saturation. Figure 14 shows details of the modulator construction. Figure 16 is a simplified equivalent circuit of the modulator.

The output waveshape is determined by the characteristics of the output pulse-forming network and its individual winding on the output reactor. During the charging time of the output networks, they are coupled together by the magnetic properties of the output core. The output reactor saturates at the peak of the PFN charging voltage. This effectively switches all PFN's into their respective loads. When the core is saturated, its magnetic permeability is reduced to a value close to unity. This destroys the magnetic coupling between the output sections. As a consequence of this loss of coupling, the output loads are electrically isolated from each other. Since the generation of the output waveform is dependent on the saturation of a single core, all outputs must start from a common time.

Both stages of this modulator are constructed to operate in this manner. The only electrical connection between outputs is in the input to the first magnetic stage. This point is isolated from the output by the delay of the entire modulator. A reflection at an output stage must be transmitted through twice the delay time of the modulator before appearing at any other output. In the application of this modulator to a trigger system, this delay is long enough to eliminate any cross-talk effect between outputs.

The simultaneity of isolated outputs is dependent on two factors. The first is uniformity of output winding and PFN characteristics. A non-uniformity in these parameters will cause differing output waveforms. The second factor in determining output simultaneity is that the core may not saturate in all sections at the same time.

Figure 15 shows the result of an investigation of the combined effect of both factors. All outputs were timed at the 50% point of the output rise time. The times are normalized to the 50% point of output No. 1. A maximum time difference of 37 nanoseconds was measured between outputs at the 50% point.

The time jitter between all outputs was investigated and found to be lower than the resolution of the recording equipment. This was less than 40.5 nanosecond. The relative output times of all outputs were found to be stable over periods of several hours operation and at no time was any jitter measurable on the leading edge of the pulse.

Investigations of the electrical isolation of output sections were made by short-circuiting each channel in turn and observing the effect on all other channels. The effect of this test on output waveforms was not measurable, making the effect less than 2%.

Table III compares the design parameters and the actual operating conditions. The effect of increasing the input voltage can be seen in the early saturation times of P_1 and P_2 .

Table III. Operating Parameters of Experimental 50-Megawatt Magnetic Modulator

	Calculated	Measured
Input dc voltage	4.0 kv	5.25 kv
Discharge time for C_1	10.5 μ sec	7 μ sec
Charge time for C_2	10.5 μ sec	7 μ sec
Peak charge current for C_2	1570 amp	...
Discharge time for C_2	3.4 μ sec	2.7 μ sec
Peak discharge current for C_2	5390 amp	...
Bias required for P_1	1.5 amp	2.5 amp
Magnetizing current to saturate P_1		
Per channel	29.7 amperes	...
Total	743 amperes	...
Charge time PFN	3.4 μ sec	2.7 μ sec
Peak charge current PFN (per channel)	213 amp	230 amp
Bias required for P_2	40 amp	40 amp
Magnetizing current to saturate P_2		
(per channel)	95 amp	54 amp
Total	2375 amp	1350 amp
Output pulse rise time	140 nsec	100 nsec
Output pulse width	0.12 μ sec	0.6 μ sec
Output pulse amplitude	1500 volt	2000 volt

*Not easily measurable.

Table IV. Design Data for Saturable Reactors of the 50-Mega-watt 25-Channel Magnetic Modulator

Reactor P₁:
Core:
1-mil 50% nickel-iron tape wound
Outside diameter - 17 inches
Inside diameter - 16 inches
Thickness - 1/2 inch
Mean magnetic path - 137.5 cm
Core area - 1.75 cm ²
Stacking factor - 0.7
Winding:
25 windings, each 48 turns No. 14 wire
Bias winding, 25 turns No. 16 wire
Reactor P₂:
Core:
1-mil 50% nickel-iron tape wound
Outside diameter - 24 inches
Inside diameter - 17 inches
Thickness - 1/2 inch
Mean magnetic path - 163.5 cm
Core area - 13.65 cm ²
Stacking factor - 0.7
Winding:
25 windings each 2 turns - 1/2-inch x 19 mil copper
Bias winding 1 turn 1/2-inch x 19 mil copper

DESIGN OF A THREE-STAGE MAGNETIC MODULATOR TO PRODUCE 50 MW OF PEAK POWER TO TRIGGER 500 THYRATRONS

The curve of anode delay vs trigger voltage for a type 5949A hydrogen thyratron (figure 1) shows the anode delay of an individual 5949A tested at a unique condition of anode voltage and pulse repetition rate. The firing characteristics of 5949A thyratrons are also functions of anode voltage and firing rate. There are, in addition, variations of anode delay between individual thyratrons.

To insure all thyratrons firing simultaneously, the variations of firing characteristics must be individually compensated for under each operating condition. For the operation of this trigger system, adjustments of pulse delay from the trigger generator to the grid of individual thyratrons will be made.

The trigger requirements for simultaneously firing 500 thyratrons are to produce a specified trigger wave shape at the grid of each thyratron so that individual anode delays result in simultaneous output pulses. Since the delay time from the trigger system to each tube is adjustable, the triggers do not have to be synchronous at the generator. They must be jitter-free with respect to each other.

An analysis of the entire system indicates that the trigger generator must have the following output requirements:

- Number of outputs - 500
- Pulse width of output - 0.4 μ sec minimum
- Impedance of each output - 50 ohm
- Pulse rise time - 100 nsec maximum

Pulse amplitude - 2250 volts ± 5%
 Jitter between outputs - ± 1 nsec maximum
 Output time variation - 50 nsec maximum
 Pulse repetition rate - variable 0 to 60 pps

Design of Modulator

In order to design a magnetic modulator to produce a specific output pulse, the design must be started at the output and proceed toward the input.

Since the magnetic properties of cores required for operation as magnetic modulators vary from core to core, final design must be done empirically on the finished model.

In order to facilitate construction, the outputs are arranged in groups of twenty. The requirements for each channel then become:

$$Z_{ch} = \frac{Z_{out}}{20} = \frac{50}{20} = 2.5 \text{ ohm}$$

Pulse width - 0.4 μsec
 Amplitude - 2,250 volts

Design of PFN

$$C = \frac{\tau}{2} \div Z = \frac{0.2 \times 10^{-6}}{2.5} \\ = 0.08 \mu\text{f}$$

$$L = Z^2 C = (2.5)^2 \times 0.08 \times 10^{-6} = 0.5 \mu\text{h}$$

A prototype PFN is shown in figure 19.

Discharge of Output Stage

Referring to figure 17 the output pulse is generated by the saturation of L_2 . Output reactor L_2 consists of twenty-five windings. Each winding consisting of two turns of insulated copper strap 0.5 inch × 19 mils. Reactors T_1 , L_1 , and L_2 are all wound on the same size and material core.

Table V. Reactor Core Data

Core material - 50% nickel-iron, 1 mil, tape wound
Outside diameter - 24 inches
Inside diameter - 15.5 inches
Thickness - 0.5 inches
Mean magnetic path - 163.5 cm
Core area - 13.65 cm ²
Core volume - 2250 cc
Core weight - 13 kilograms
Stacking factor - 0.70

The rise time of the output pulse can be approximated by calculating the saturated inductance of each winding. For all windings on the output core

$$L_{sat} = \frac{4\pi N^2 A}{l_{in}} \mu_{sat} \times 10^{-9} \text{ henrys}$$

Experience with the two-stage prototype indicates that an assumption of $\mu_{sat} = 1$ will yield the proper L_{sat} in the above formula.

$$L_{sat} = \frac{4\pi(2)^2(13.65)}{163.5} \times 10^{-9} = 4.2 \times 10^{-9} \text{ henrys}$$

The effective saturated inductance referred to an individual channel is

$$L_{sat}/\text{channel} = 25 L_{sat} = 105 \times 10^{-9} \text{ henrys}$$

The output rise time is then:

$$RT = 2.2 L/R = 2.2 \frac{105}{2.5} \times 10^{-9} = 92.3 \text{ nsec}$$

At the maximum repetition rate of the modulator the peak power delivered to the output is:

$$\text{Peak Power} = 25 \frac{V^2}{R} = 25 \frac{(2.250)^2 \times 10^6}{2.5} = 50.6 \text{ Mw}$$

The total output power is

$$P_{ave} = P_{peak} \times \tau_p \times \text{pps} = 50.6 \times 10^6 \times 0.4 \times 10^{-6} \times 60 = 1215 \text{ watts}$$

The dominant losses in this design will be core losses. From figure 3, at 95°F operating temperature the core losses are 26.3×10^3 ergs/cc/cycle.

The volume of active core material is:

$$V = 1 \times 2250 = 1575 \text{ cc}$$

$$\text{Total core losses} = 26.3 \times 10^3 \times 1575 \times 60 \times 10^{-7} = 248.5 \text{ watts}$$

In order to maintain stable operating conditions this core must be maintained to within $\pm 5^\circ\text{F}$ of its operating temperature.

Charging of Output Stage

Since the design of the output reactor is determined by the output rise time requirement, the charging waveshape must be shaped to cause saturation at the charging peak. Experience with the two-stage prototype indicates a peak charge voltage of 5380 volts will be required.

$$\frac{\text{Volt-sec}}{\text{Turn}} = B_{sat} A \times \text{S.F.} \times 10^{-8}$$

The volt-sec for a cosine wave can be approximated by $E \Delta t/2$

$$\Delta t = \frac{2 B_s A \text{N.S.F.}}{E} \times 10^{-8}$$

E = Peak voltage

Δt = time for half period

B_s = saturation flux density

A = Core area

S.F. = Core stacking factor

$$\Delta t = \frac{2(32) \times 10^3 \times 13.65 \times 0.7}{5380} = 2.28 \mu\text{sec}$$

This represents an apparent frequency of 219 kc. The output reactor is of the shunt type, this results in the output PFN charging current flowing through the load. Since each load is remote from the modulator, charging

current is permitted to flow through the load. There are several methods to shunt the charging current across the output terminals. The most straightforward method would be a diode across the output terminals. This method is currently under investigation.

The charging voltage is of a cosine form and the peak current required to charge $0.08 \mu\text{f}$ in $2.28 \mu\text{sec}$ would be 320 amperes. This diode must recover in less than 100 nsec in a 2.5-ohm circuit.

Another approach to shunting the charging current across the output is to use a saturable reactor shown in figure 17 as L_3 . This reactor would be saturated in the direction of charging current flow. The impedance offered the charging current would be the saturated inductance of this reactor. This would then be included in the reactance of the resonant charging source. The reactor would represent a high impedance in parallel with the output cables under modulator discharge conditions. This type of saturable reactor-diode operation seems to offer the best approach to load charging isolation and is being actively studied.

The output winding is of the multiple channel isolating type described for the two-stage prototype.

Discharge of C_3

The discharge of capacitor C_3 is made by a series saturable reactor L_1 . Capacitor C_3 is divided into five sections, each section discharging into five PFN's. The total capacitance at C_3 is $2 \mu\text{f}$.

The design of reactor L_1 is determined by the value of saturated inductance required to charge all PFN'S in $2.28 \mu\text{sec}$.

For an apparent frequency of 219 kc, the inductance required per channel is then $13.25 \mu\text{h}$. Allowing $2.75 \mu\text{h}$ for lead inductances and local isolation per channel, a sixteen-turn reactor winding will have a saturated inductance of $10.5 \mu\text{h}$ per channel. This will produce the required discharge frequency of 219 kc. Measurements on prototype modulators indicate an efficiency of 84% for this stage.

Charging of C_3

C_3 is charged by the resonant discharge of C_2 through the saturated inductance of the secondary winding of T_1 . The charging requirements of C_2 are a peak voltage of $\frac{5380}{0.93} = 5800$ volts.

The saturation time of L_2 is:

$$\Delta t = \frac{2NBA(SF)}{E} = \frac{2(16)(32)(0.7)(13.65)}{5.8} \times 10^{-8} = 17.2 \mu\text{sec}$$

The peak charging current for each $0.4-\mu\text{f}$ section of C_3 would be 684 amperes at an apparent frequency of 29 kc.

Discharge of C_2

Capacitor C_2 discharges through the saturated inductance of transformer T_1 secondary. T_1 has six secondary windings, all directly paralleled. An analysis of the number of secondary turns indicates 117 secondary turns. A saturated permeability of 1.5 is assumed due to the high leakage reactance expected in this stage.

$$L_{\text{sat}} \text{ needed} = 30 \mu\text{h total}, f = 29 \text{ kc for 117 turns}$$

$$L_{sat} = \frac{4\pi N^2 ASF}{l_m} \mu_{sat} \times 10^{-9}$$

$$L_{sat} = \frac{4\pi (117)^2 \times 13.65 \times 0.7}{163.5} \times 10^{-9} \times 1.5 = 22.5 \times 10^{-6} \text{ h}$$

The additional inductance will be added to the windings to produce the required value.

Charge of C₂

Capacitor C₂ is charged through transformer T₁ from the discharge of C₁. The required charge on C₂ would be 6150 volts. The time required to saturate T₁ on the secondary windings.

$$\Delta t = \frac{2NBA(SF)}{E} \times 10^{-8} = 110 \mu\text{sec}$$

This is an apparent frequency of 4.55 kc.

The total capacitance at C₂ is 2 μf and the peak charging current is 178 amp. This current is conducted through diode D₁ in five channels. The current per channel = 178/5 = 37.6 amp.

The turns ratio of T₁ is approximately 20 to 1. This reduces the voltage in the primary to 308 volts. This is the proper magnitude for silicon-controlled rectified switching. The peak current through a single SCR would be 3560 amperes.

The primary inductance for this circuit must be 3.6 μh. This is the total for all components in the primary and the leakage inductance of the transformer. In order to handle the large amounts of primary current and reduce the leakage reactance, six windings are used in parallel.

Tests of Silicon-Controlled Rectifiers

A test assembly was built to measure the peak current carrying capacity of SCR's for narrow current pulses (figure 18). In order to prevent excessive losses in the SCR during turn-on, a magnetic assist was used to prevent high current flow until the entire junction was in a conducting state.

The duration of peak conduction was then 30 μsec. Extrapolating from figure 20, for a peak conduction current of 3500 amp, gives a total loss in the SCR at 60 pps operation of 57.2 watts.

$$P_{rms} = \frac{I E}{2} P \times \text{conduction time} \times 60 \text{ pps}$$

$$= \frac{3500 \times 5}{2} \times 110 \times 10^{-6} \times 60 = 57.2 \text{ watts}$$

Since these results are based on low repetition rates, provision is being made to utilize six SCR's as a primary switch.

Delay Time in Magnetic Modulator

The delay time in the three stages of this modulator is the sum of the charging times of C₂, C₃, and the PFN.

$$\text{Total delay} = 110 + 17.2 + 2.28 = 129.48 \mu\text{sec}$$

The delay of each stage is a function of the saturation flux density of the core material.

From figure 4, B_s varies 1% for a thermal change of 10°F . Therefore, the output delay will change at the rate of $0.13 \mu\text{sec}/1^{\circ}\text{F}$.

The output voltage will change as

$$\% \frac{\Delta E}{E} = \left[1 + \cos \pi \left(1 - \frac{\Delta B_s}{B_s} \right) \right] \times 100\%$$

$$\% \frac{\Delta E}{E} = (1 + \cos 0.99 \pi) \times 100\% \approx 0.05\% \quad \% \frac{\Delta E}{E} / ^{\circ}\text{F} = 0.005\%$$

Changes in input charging voltage will, however, cause the same percentage change in both the output voltage and output delay time.

Table VI. Tabulated Design of 50-Megawatt Three-Stage Magnetic Modulator

	Calculated
Peak discharge current C_1	3560 amp
Charge time C_2	$110 \mu\text{sec}$
Discharge time L_2	$17.2 \mu\text{sec}$
Peak charging current C_2 (Total all units)	178 amp
Charge time C_3	$17.2 \mu\text{sec}$
Discharge time C_3	$2.2 \mu\text{sec}$
Peak charging current L_3 (Total)	3420 amp
Charge time PFN	$2.2 \mu\text{sec}$
Output pulse rise time	92.3 nsec
Output pulse width	$0.4 \mu\text{sec}$

CONCLUSIONS

1. Magnetic modulators can be used to generate peak pulse powers in excess of 100 megawatts, with pulse rise times of less than 100 nanoseconds.
2. Magnetic modulators can be constructed with electrical isolated synchronous channels.
3. The limiting factor in the further development of efficient high-power magnetic modulators is the lack of suitable core materials.

ACKNOWLEDGMENTS

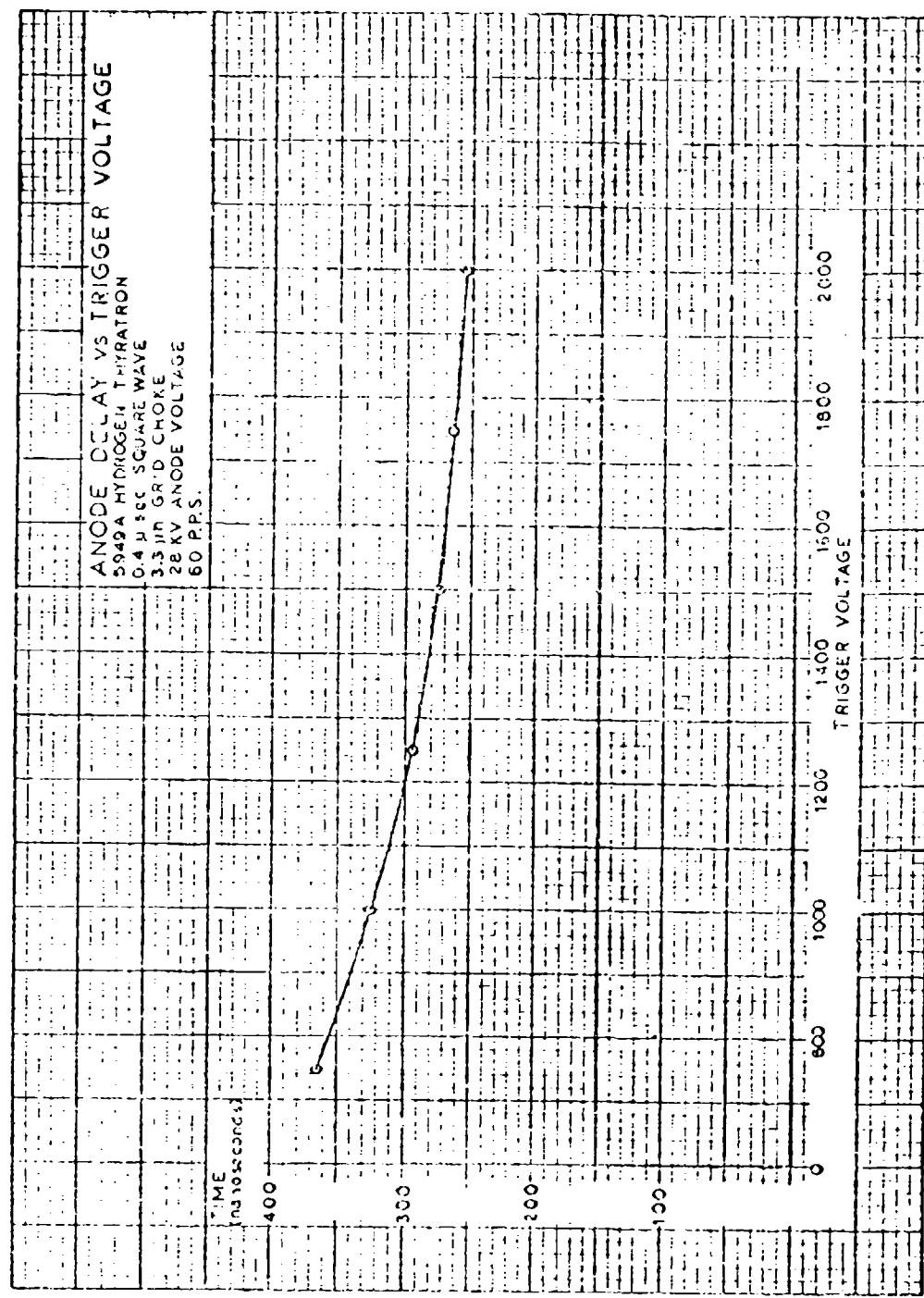
I am indebted to Kristian Aaland for the many suggestions and ideas that he has contributed to this work. I wish to thank Vernon L. Smith for the support he has given this project. I am grateful for the contributions of R. Morgret, A. Foote, D. Leigh, and D. Mummaugh in constructing and operating the experimental modulators.

This work was performed under the auspices of the U. S. Atomic Energy Commission.

REFERENCES

1. N. C. Christofilos, "Astron Thermonuclear Reactor," Proceedings Second U.N. International Conference in the Peaceful Uses of Atomic Energy, Geneva, Vol. 32, p. 279, 1958.
2. N. C. Christofilos, "Induction Electron Accelerator," Lawrence Radiation Laboratory, University of California, Livermore, UCRL-5783-T, November, 1959.

Fig. 1 Anode delay vs trigger voltage.



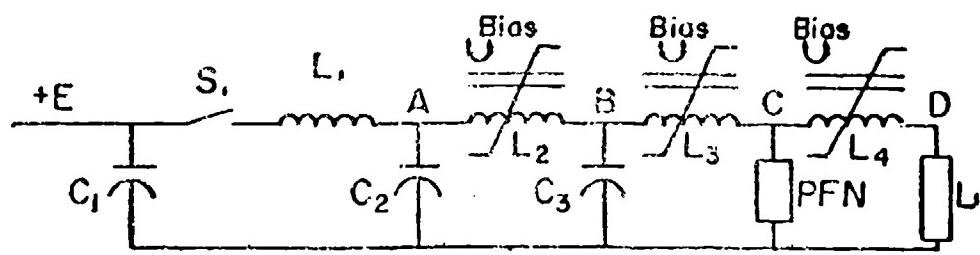


Figure 2 Basic Magnetic Modulator

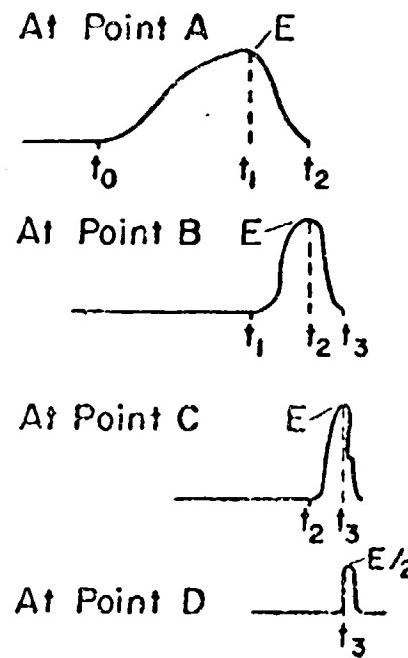


FIG. 2. BASIC MAGNETIC MODULATOR.

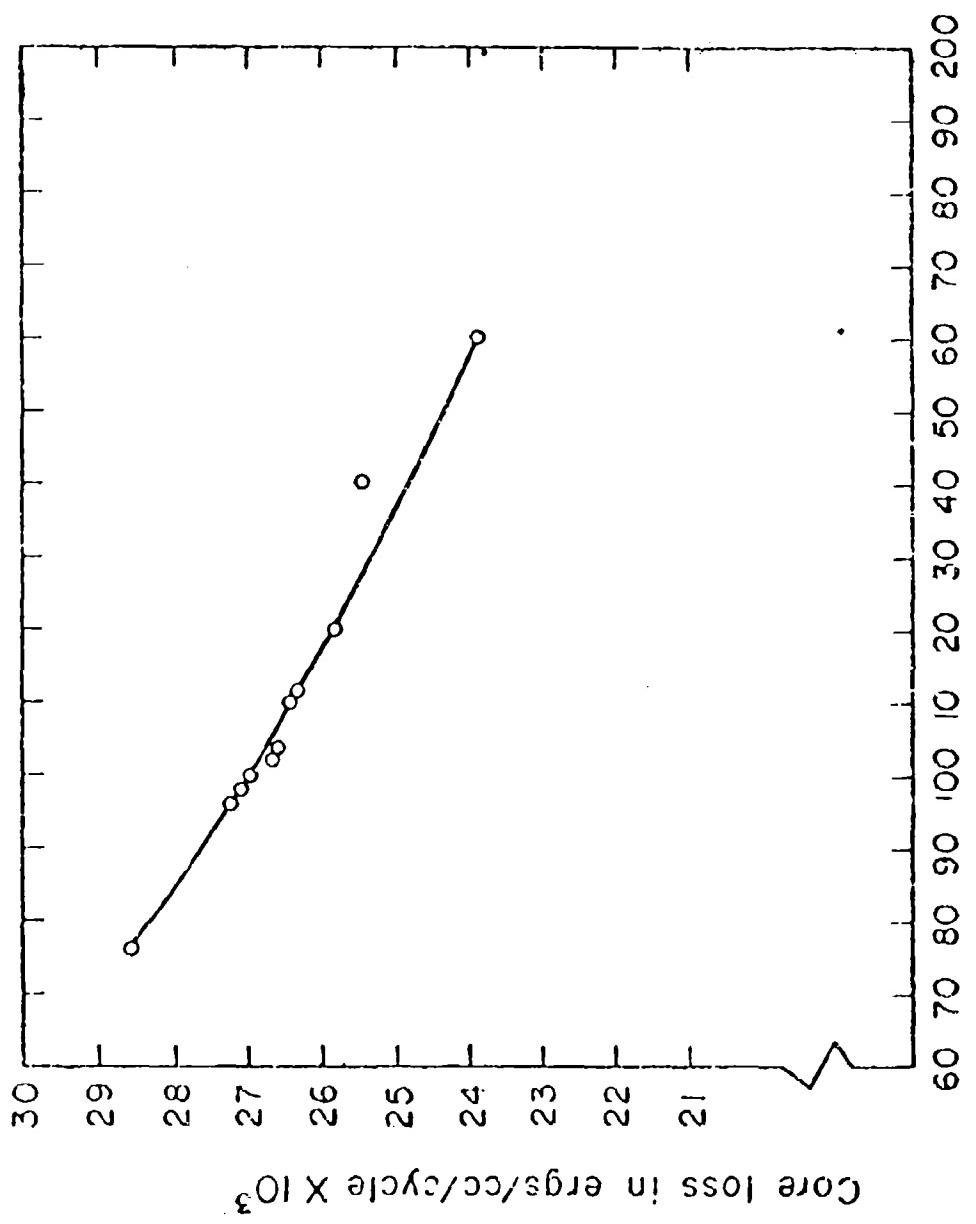


FIG. 3. CORE LOSS VS TEMPERATURE FOR 1-mil 50% NICKEL-IRON AT 270 Hz.

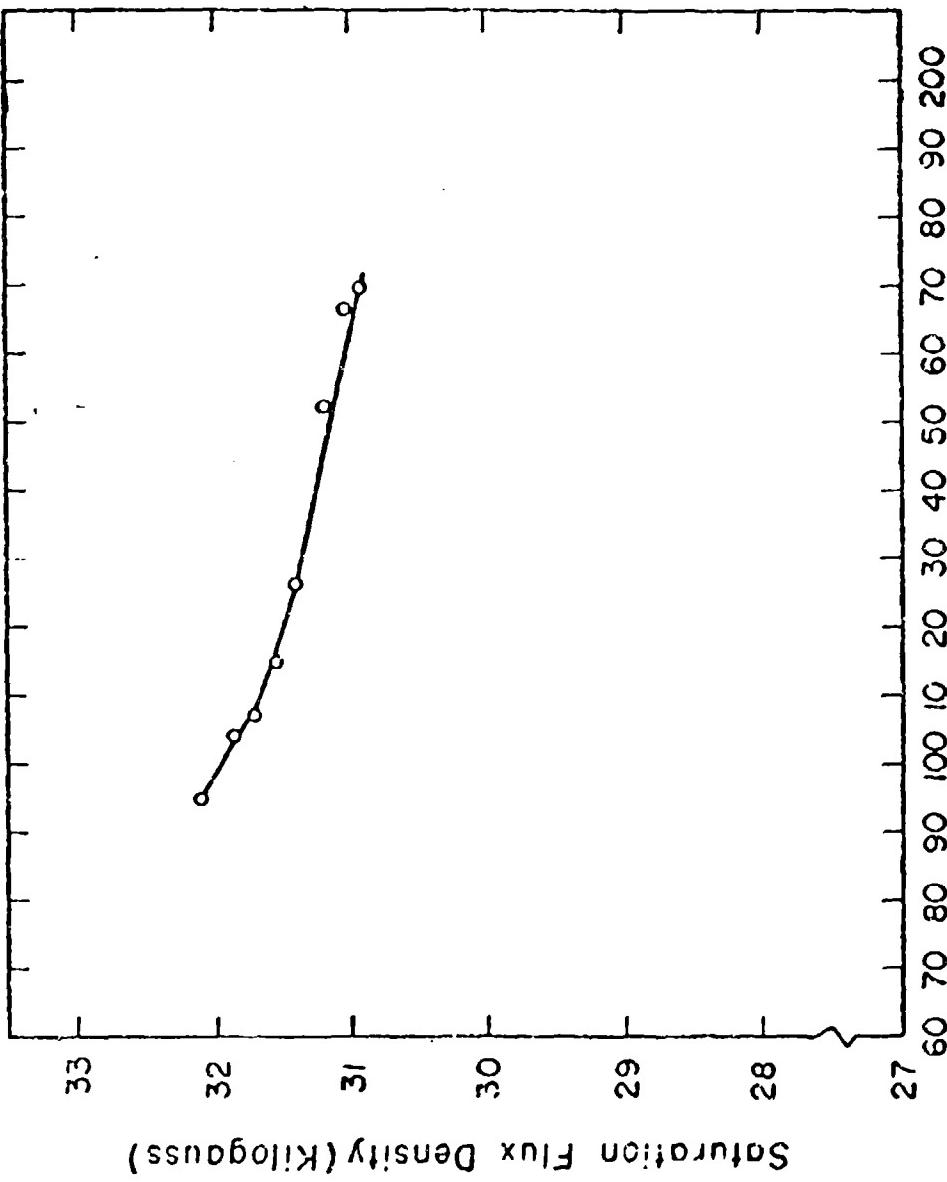
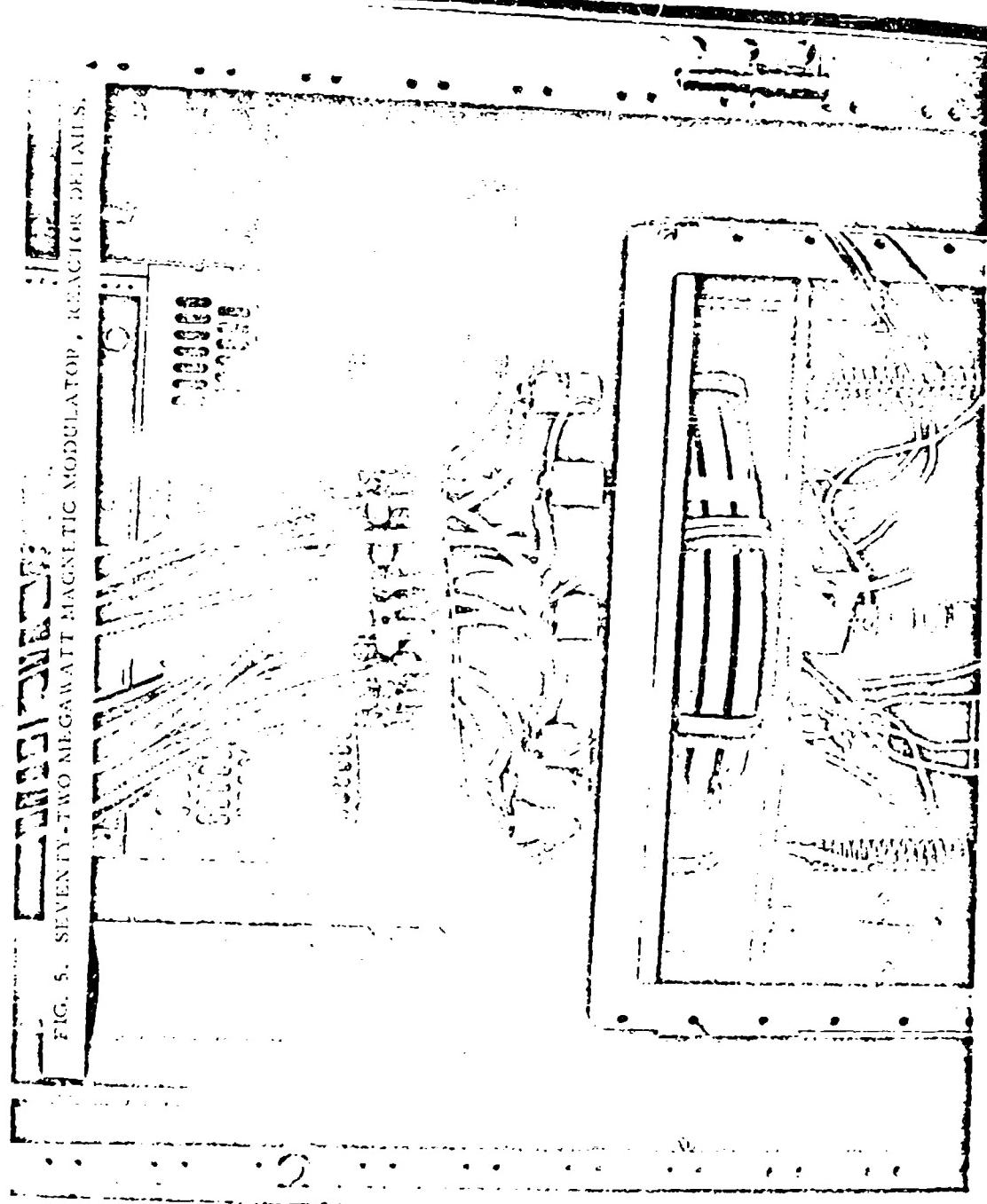


FIG. 4. SATURATION FLUX DENSITY VS TEMPERATURE FOR
1-mm 50% NICKEL-IRON AT 230 kC (B_s MEASURED AT 340 OERSTEDS).

FIG. 5. SEVENTY-TWO MEGAWATT MAGNETIC MODULATOR, REACTOR DETAILS.



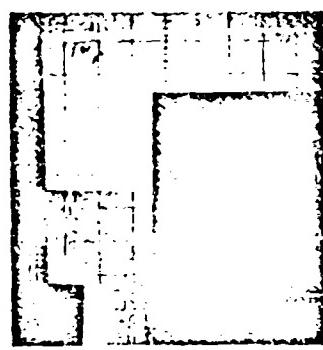


FIG. 6. MEAN CORE TEMP., 96°F.

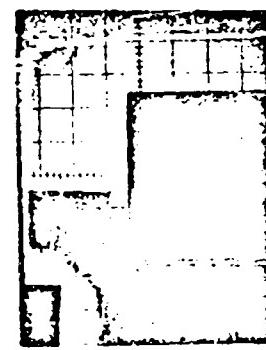
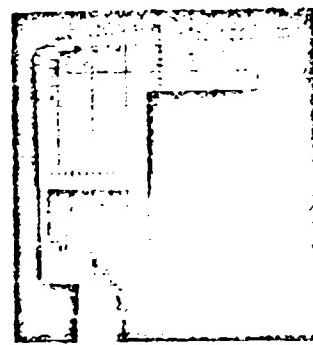


FIG. 7. MEAN CORE TEMP., 116°F.



2.62 X 10 gauss / division

FIG. 8. MEAN CORE TEMP., 127°F.

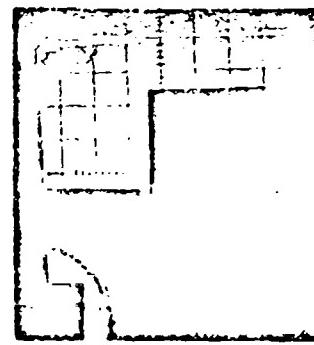


FIG. 9. MEAN CORE TEMP., 138°F.



FIG. 10. MEAN CORE TEMP., 147°F.

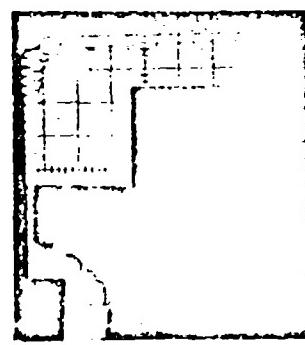


FIG. 11. MEAN CORE TEMP., 156°F.

500 Oersteds / division

FIGS. 6-11. DYNAMIC HYSERESIS LOOPS FOR 1-mil 50% NICKEL-IRON AT 250 kc.

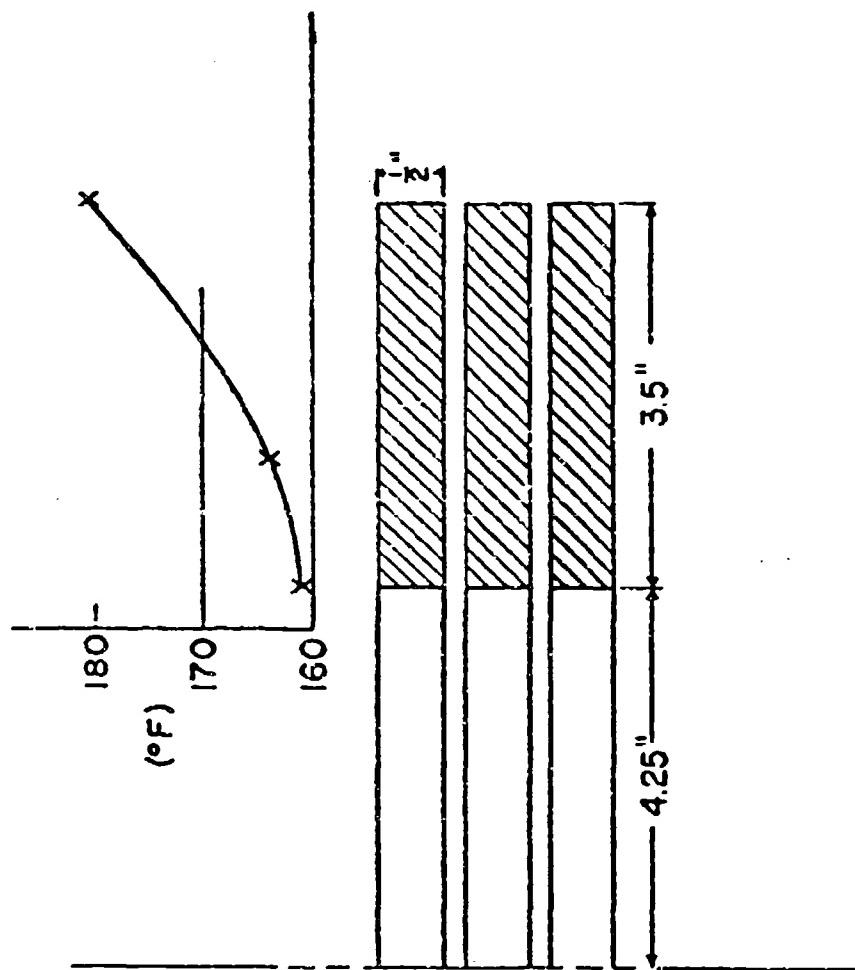
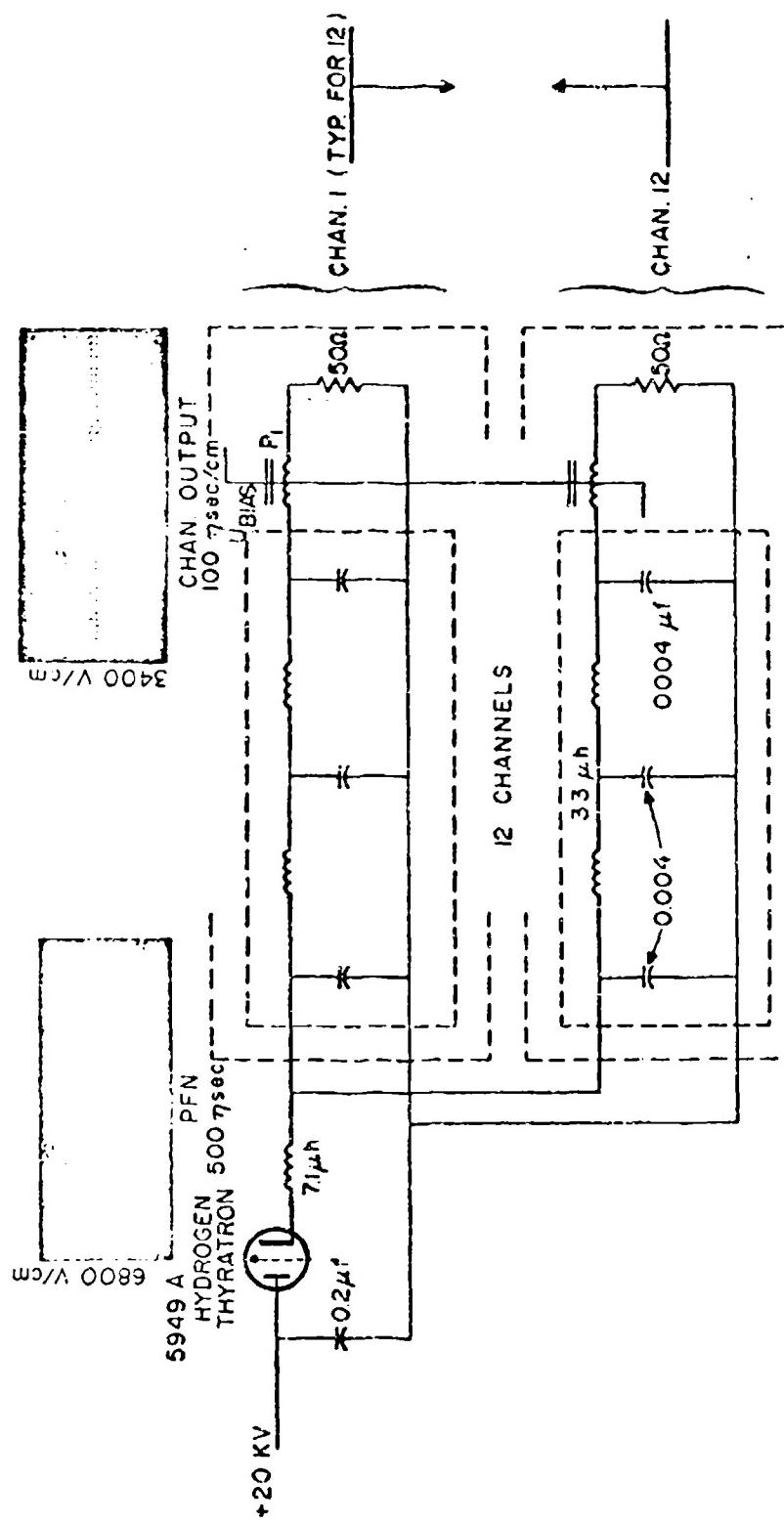


FIG. 12. THERMAL PROFILE OF 1-mil NICKEL-IRON CORE FOR 72-Mw MAGNETIC MODULATOR OPERATING AT 60 p.p.



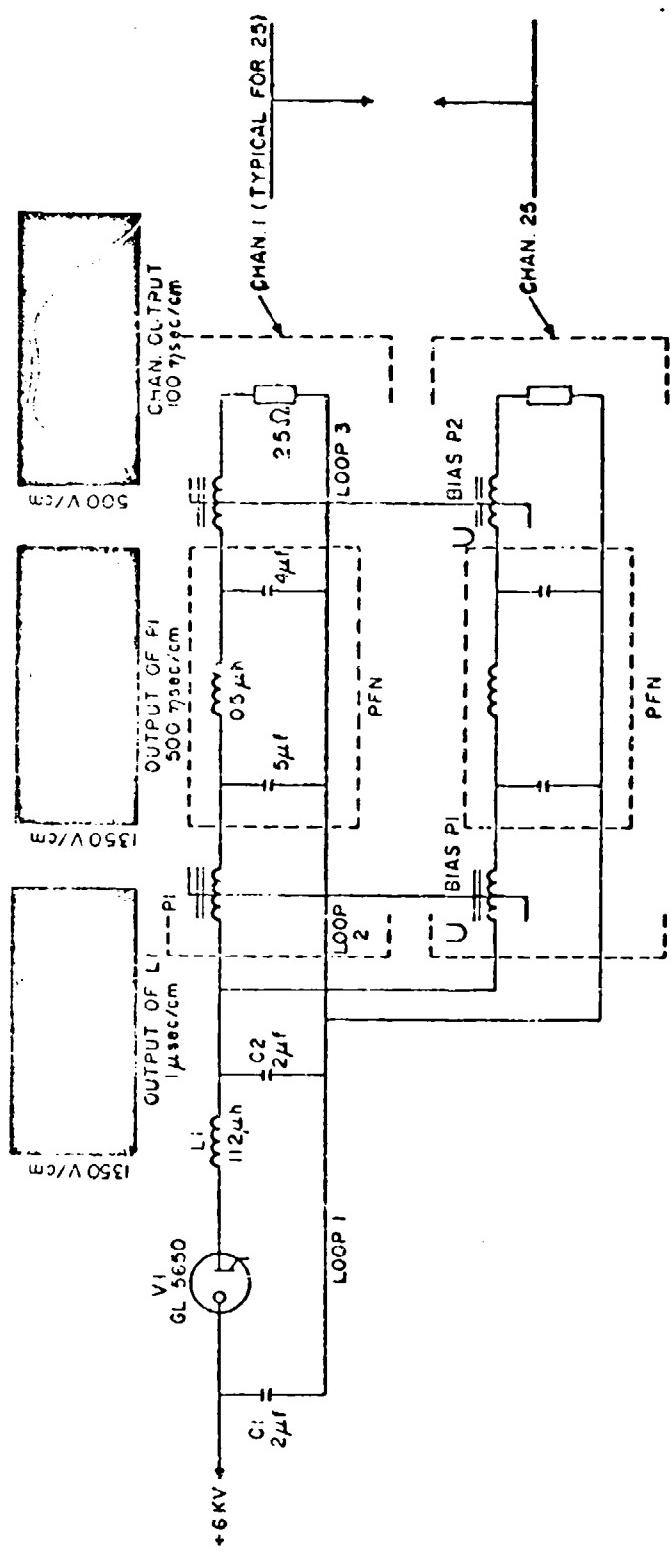
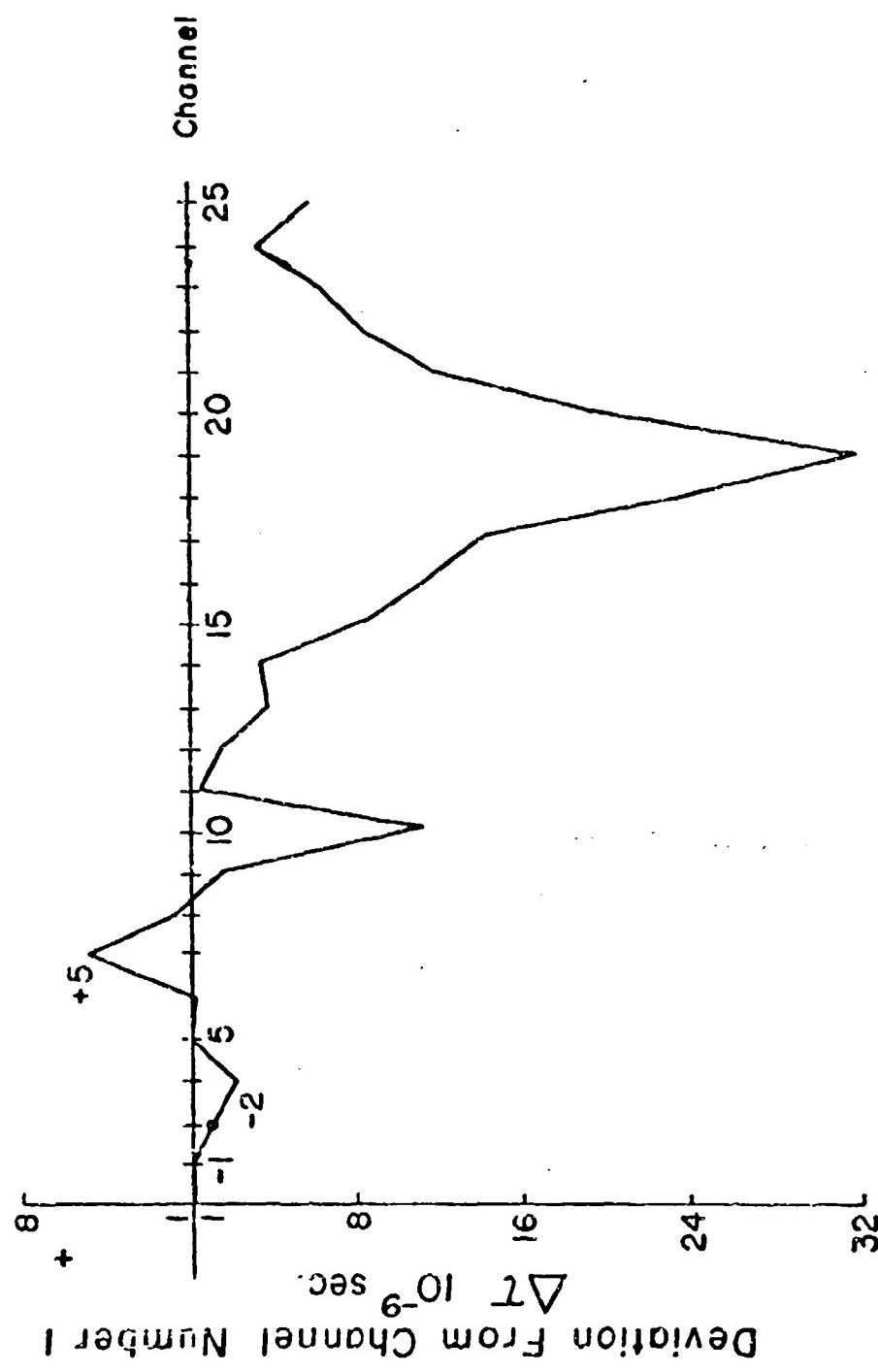


FIG. 10. EXPERIMENTAL SLOW MAGNETIC MODULATOR, AS CHANNEL 1 NO CHANNELS.



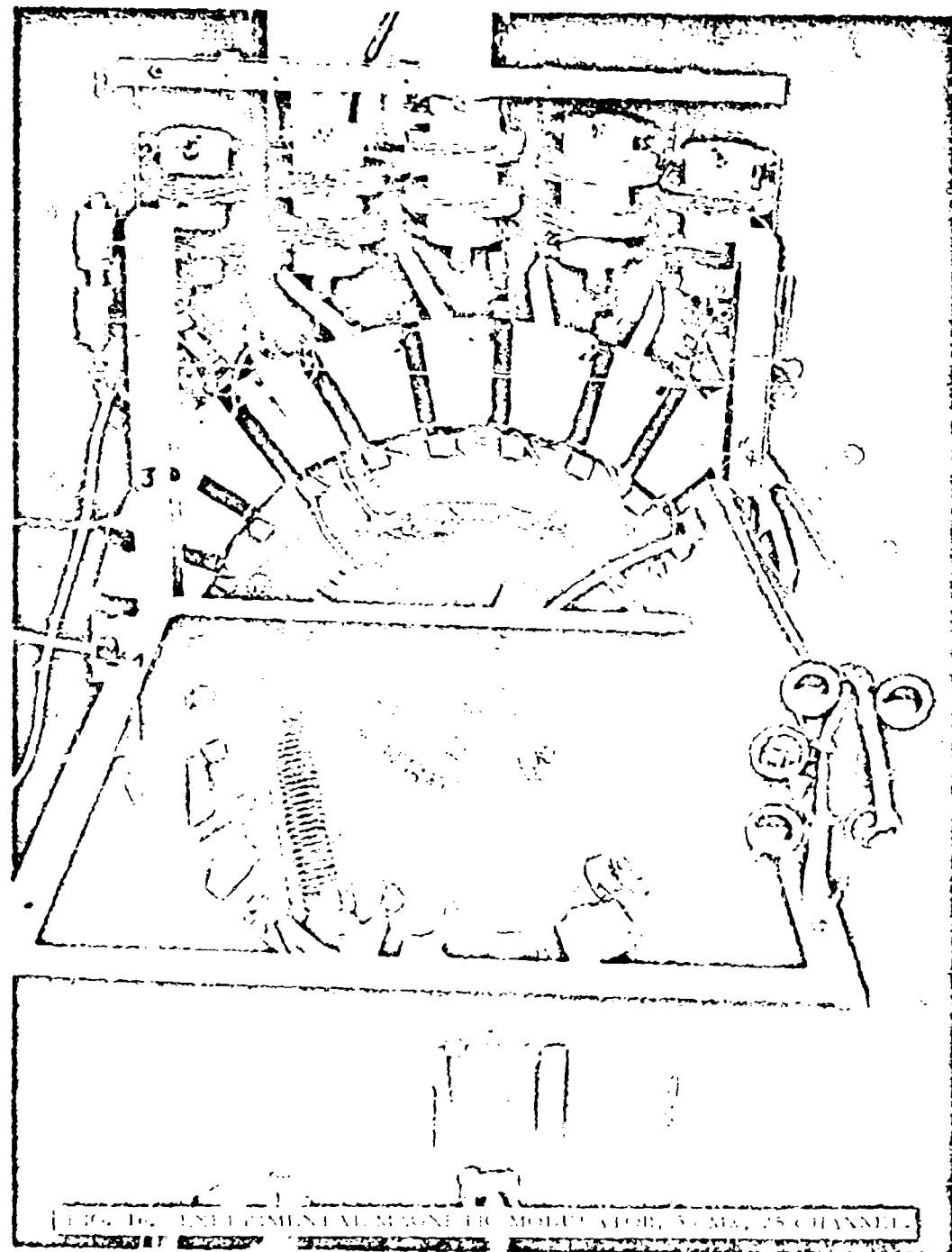
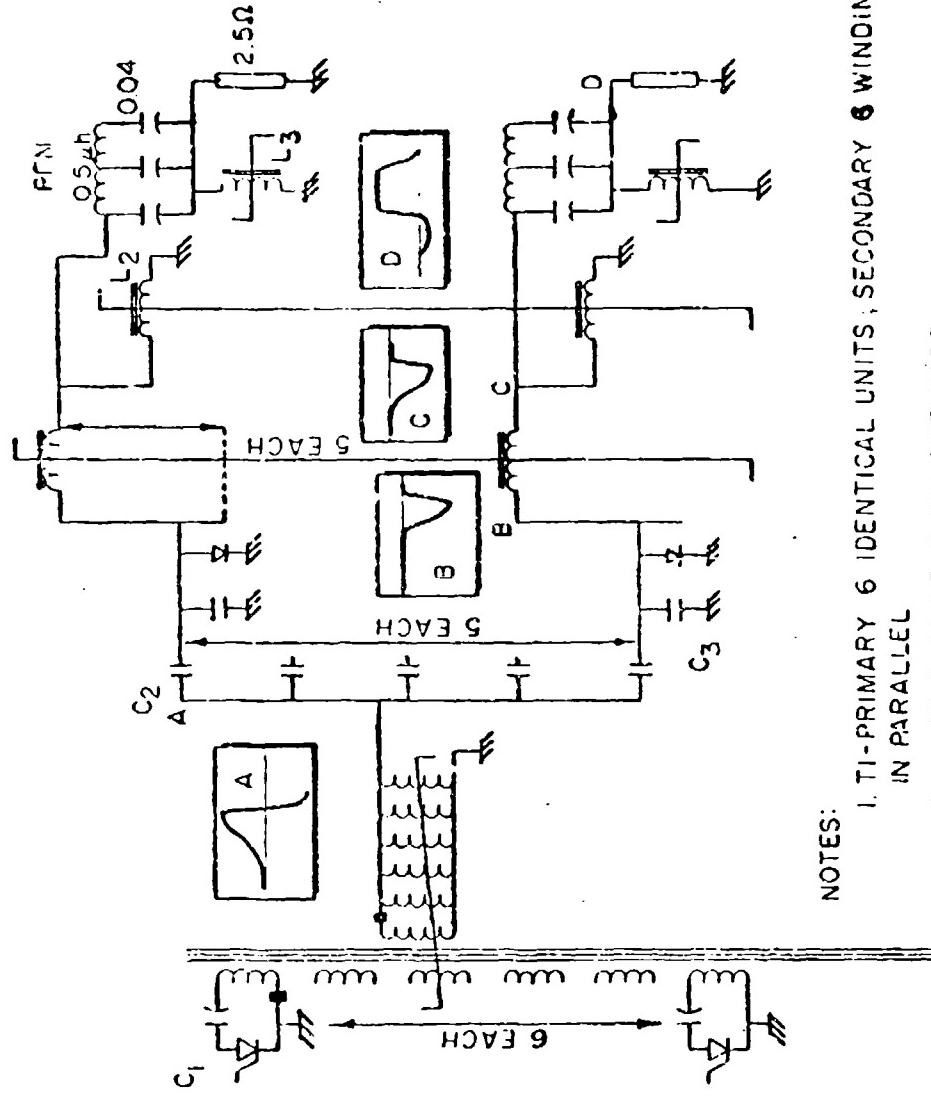


FIG. 16. EXPERIMENTAL MAGNETIC MODULATOR, 3.5 Mhz, 25 CHANNEL.

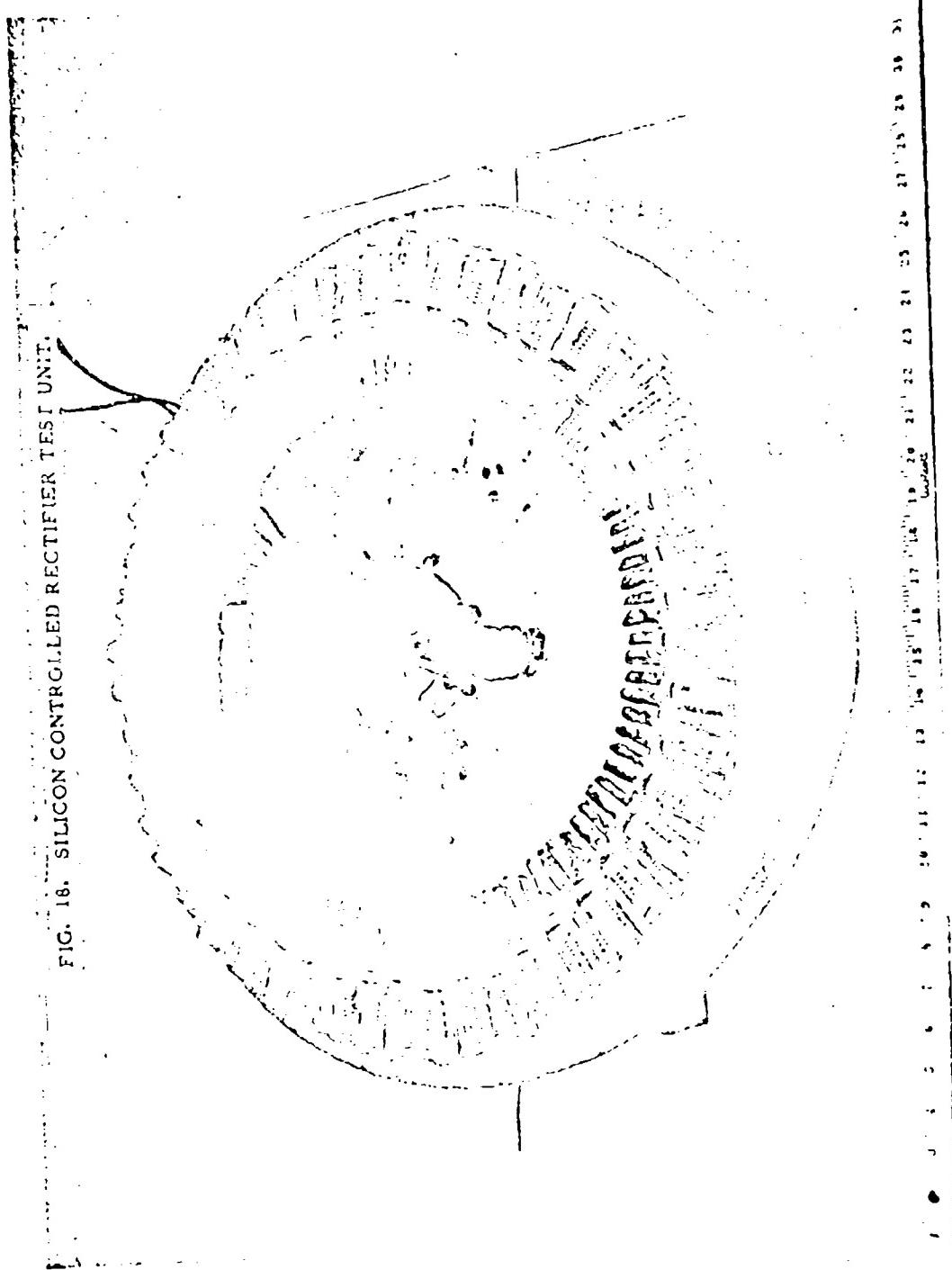


NOTES:

1. T1- PRIMARY 6 IDENTICAL UNITS, SECONDARY 6 WINDINGS IN PARALLEL
2. L1- 25 CHANNELS ON ONE CORE
3. L2- 25 CHANNELS ON ONE CORE
4. L3- 25 CORES ONE CHANNEL PER CORE

FIG. 17. THREE-STAGE MAGNETIC MODULATOR. 50 MHZ. 25 CHANNEL

FIG. 18. SILICON CONTROLLED RECTIFIER TEST UNIT.



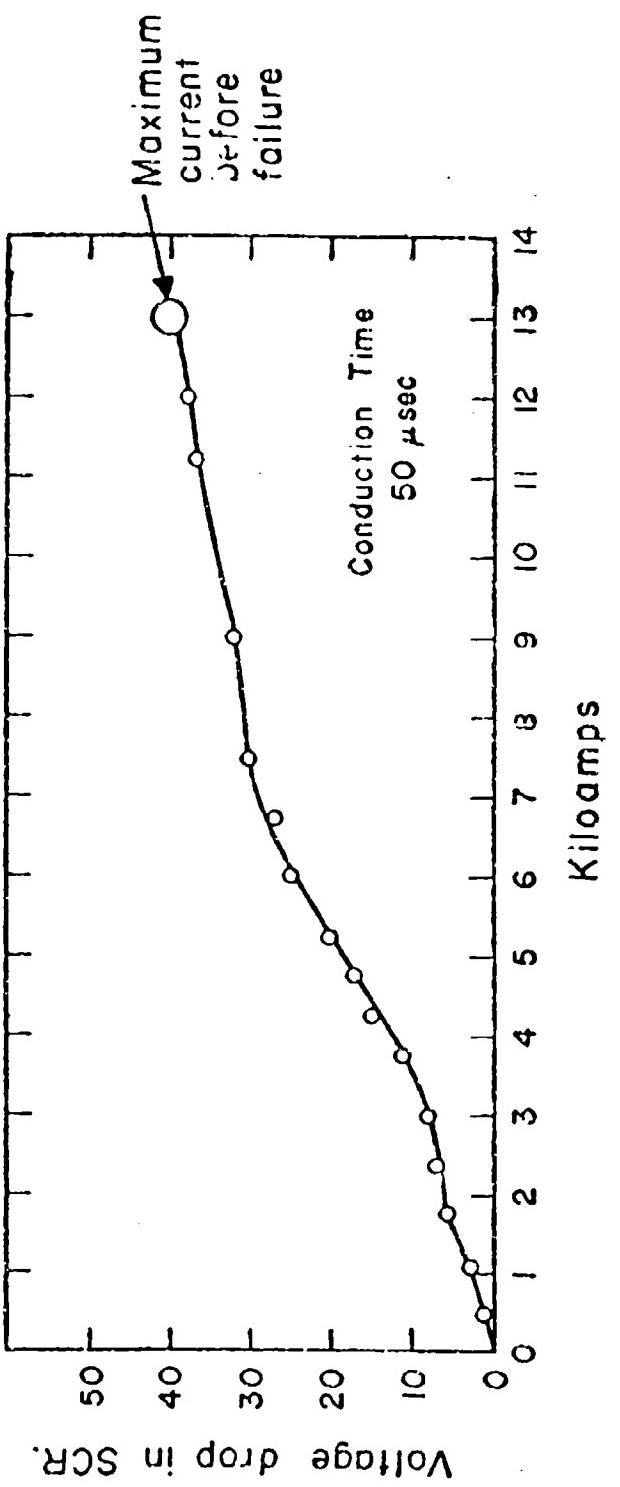


FIG. 20. VOLT-AMPERE CHARACTERISTICS OF WX-809F SILICON-CONTROLLED RECTIFIER.

A LONG PULSE MAGNETIC MODULATOR

by

R. J. Froelich
J. V. Stover

Hughes Aircraft Company - Fullerton, California

A. Introduction

This paper discusses some aspects of designing a magnetic modulator for generating the long pulse requirements of a high power radar modulator. The magnetic modulator has attractive features for this application since it offers high reliability and efficiency at the long pulse widths used in many high power radar systems. The magnetic modulator design objectives were (1) to obtain maximum efficiencies approaching 90% at pulse widths in the vicinity of 600 microseconds, and (2) to evaluate fabrication techniques applicable to magnetic modulators having average power capabilities up to 10,000 kilowatts.

In this study particular emphasis has been placed on investigating various types of core material and core material stacking for the switching reactors.

B. Modulator Circuit Requirements

The magnetic modulator circuit configuration under consideration is fundamentally a series reactor, shunt capacitor type with the saturated inductance progressively decreasing in value. This circuit is shown in Figure 1a. The charging voltage, $V_{cn}(t)$, and charging current, $i_{cn}(t)$, for the nth capacitor are shown together with the flux density, $\theta_n(t)$, in Figure 1b.

From the mathematical expressions for charging voltage, $V_{cn}(t)$, and the saturated inductance, L_{sn} , of the nth switching reactor, the following equation is established which is derived in the Appendix.

$$\frac{L_{sn-1}}{L_{sn}} = \frac{\Delta \theta u_n^2 U_n}{2.47 \mu_{sn} W_{cn} K_m^2} \quad (1)$$

where

- $L_{s_{n-1}}$ = saturated inductance of the (n-1)th reactor.
 $\Delta \theta_{u_n}$ = peak-to-peak flux density change of the nth reactor.
 U_n = core volume of the nth reactor.
 W_{c_n} = energy stored in the nth capacitor.
 μ_{s_n} = saturated permeability of the nth reactor.
 K_m = dimensional constant.

Figure 2 illustrates the typical time compression of the discharge current, $i_n(t)$, as it is switched between stages. Defining

$$\rho_{n-1,n} = \frac{T_{n-1}}{T_n}$$

the following expression is established which is derived in the Appendix.

$$(\rho_{n-1,n})^2 = \frac{\Delta \theta_{u_n}^2 U_n}{2.47 \mu_{s_n} W_{c_n}} \quad (2)$$

C. Core Material Requirements For The Switching Reactor

The total core volume, U_n , of a switching reactor is a function of the pulse compression ratio, $\rho_{n-1,n}$, and the energy stored in the nth capacitor, W_{c_n} . By rearranging equation 2, into the form

$$U_n = \frac{2.47 W_{c_n} (\rho_{n-1,n})^2}{\Delta \theta_{u_n}^2 / \mu_{s_n}}$$

it is readily apparent that minimum core volume per stage is obtained when the ratio, $\frac{\mu_{u_n}}{\mu_{s_n}}$, is a maximum. This ratio will be referred to as the figure of merit of the core material.

This figure of merit has been investigated for Hy-Mn 80, 48 Alloy, and Orthonol magnetic materials using stacked DJ laminations. Orthonol, a 50% NiFe material, has the highest figure of merit with a saturated permeability variation which is a linear function of magnetizing force. It has been given primary consideration in the evaluation of "I" laminations.

In the unsaturated state the nth reactor must have sufficient inductance, L_{u_n} , to prevent negligible loading during the charging of the nth capacitor. The following inequality is derived in the Appendix and expresses this condition:

$$\frac{\mu_{u_n}}{\mu_{s_n}} >> 0.5 \frac{L_{s_{n-1}}}{L_{s_n}} \quad (3a)$$

or

$$\frac{\mu_{u_n}}{\mu_{s_n}} >> 0.5 (\rho_{n-1,n})^2 \quad (3b)$$

Thus a good switching reactor core material should possess a high ratio of unsaturated to saturated permeability.

In addition a low coercive force, H_{ac} , is required to achieve negligible loading. The approximate requirement for coercive force, H_{ac} , is expressed in the following inequality:

$$\bar{H}_{ac} \leq \frac{K_u W_{c_n} (1 - \eta_n)}{4B_s U_n} \quad (4)$$

where K_u = Dimensional constant

η_n = Stage energy transfer efficiency

\bar{H}_{ac} = Mean coercive force

This expression is derived in the Appendix.

Summarizing, the following criteria must be adhered to in selecting the core material for a particular application:

(1) High Figure of Merit, F_m

$$F_m = \frac{\Delta \sigma_{u_n}^2}{\mu_{s_n}}$$

$$(2) \frac{\mu_{u_n}}{\mu_{s_n}} >> 0.5 (\rho_{n-1,n})^2$$

$$(3) \bar{H}_{ac} \leq \frac{\kappa_0 W_{c_n} (1 - \eta_n)}{4 B_s U_n}$$

D. Core Material Stacking For The Switching Reactor

The possible usage of DU type laminations in a low level modulator with a 600 microsecond output pulse was investigated. The basic properties of interest, as previously mentioned, were the peak-to-peak saturation flux density, $\Delta \sigma_{u_n}$; the saturated permeability, μ_{s_n} ; and the coercive force, H_{ac} . These parameters were evaluated using three different methods.

The first method was basically a hysteresis loop measurement. Schematically this test method is illustrated in Figure 3 with switch, S, in the closed position. This test method consists of applying a sinusoidal voltage of the desired frequency to the core material specimen and driving the core material to its positive and negative saturation flux densities. The magnetizing current and integrated flux voltage are simultaneously displayed on a Tektronix Model No. 536 oscilloscope resulting in the well known dynamic E-H loop. Since the core material presents a high impedance to the driving source, the core is sinusoidally voltage driven in the unsaturated state. Thus this test method is considered to give measurements of saturation flux density, $\Delta \sigma_{u_n}$, and coercive force, H_{ac} which closely represent actual switching reactor service in the unsaturated operating region.

The second test method is illustrated schematically in Figure 3 when switch, S, is in the open position. In this test the cores are sinusoidally current driven in the saturated state due to the diode which blocks voltage reset. The output voltage waveform is again integrated and displayed with the exciting current waveform using a Tektronix Model 536 oscilloscope. From this display saturated permeability data is obtained.

The third test method is a saturated impedance measurement consisting of measuring the impedance offered to a 20 kilocycle test current when the core material is heavily d-c biased. If capacitive reactance, d-c resistance, and a-c resistances are minimized, values of saturated permeability can be accurately obtained. The measurements obtained using this test method were compared with measurements made using a Tektronix Model 130 LC meter. This test method is shown schematically in Figure 4.

In all of the tests performed, the auxiliary windings were closely coupled to the core material to minimize errors in measurement.

Figure 5 illustrates the saturated permeability dynamic B-H curves obtained using HyMu80, 43 Alloy, Orthonik, and Orthonol stacked DU laminations when tested by the second test method. Test results indicate a well defined transition from the unsaturated to the saturated state for HyMu80 and indicates it has the lowest saturated permeability of the four. However, Orthonol has the highest figure of merit with a saturation flux density, B_m , of 13.9 Kilogauss and was given primary consideration in the further investigation of laminations.

In Figure 6 the saturated permeability of these same core material specimens is shown as a function of dc magnetic field intensity, H_{dc} , when tested using test method 3. Comparison of this data to the saturated permeability dynamic B-H curves reveals that HyMu80 has the lowest saturated permeability and the sharpest transition between states.

The results of both measurements are tabulated in Table I. A consistent discrepancy in the value of the saturated permeability as measured using the two different measurement methods is attributed to the different methods of core material excitation used in the two test methods.

The use of I laminations for switching reactor use was considered for the following reasons:

- (1) Fabrication of the I laminations is economically feasible.
- (2) I laminations can be stacked in a wide variety of geometries.

(3) Pre-wound windings can be used.

(4) Windings can be more easily supported to withstand high mechanical forces present in operation using pre-wound coils.

Orthonol (50% NiFe) has a face centered cubic crystalline lattice structure and the directions of easy magnetization are along the cube edge. The directions of easy magnetization are (1) in the direction of rolling, (2) normal to the direction of rolling and in the direction of the strip thickness, and (3) normal to the direction of rolling and in the direction of the strip width. Thus oriented 50% NiFe appears attractive for use in laminations where the flux must traverse from laminate to laminate.

Oriented 50% NiFe I laminations were considered because:

- (1) Oriented 50% NiFe core material has a high figure of merit.
- (2) Directions of easy magnetization of oriented 50% NiFe core material were compatible with laminated core structures being considered.

Figure 7 indicates the results of hysteresis loop measurements using 6 mil thick Orthonol I laminations assembled in the four stacking methods shown.

Observation of the hysteresis loops using stacking configurations B and C reveals undesirable switching properties due to reduction of the core material saturation flux density and the non-linear variation of saturated permeability with peak driving force. Stacking configurations A and D appear more promising because the saturating flux density, B_m , of the core material is not degraded and the saturated permeability, μ_{sp} , is reasonably linear with peak driving force and had the lowest value of all the I lamination stacking configurations investigated.

Since configuration A and D employ a 50% stacking factor, the air reluctance path, R_a , in parallel with the saturated iron reluctance path can cause deviation between intrinsic saturated permeability, μ_{si} , and measured or apparent saturated permeability, μ_{sn} . The following relationship expresses the difference:

$$\mu_{sn} = \mu_{si} + \frac{A_T}{A_{F_E}} - 1$$

A_T = Total cross sectional area

A_{PE} = Cross sectional area of core material

With 50% stacking factor, $\frac{A_T}{A_{PE}} = 2$, hence

$$\mu_{s\eta} = \mu_{s1} + 2 - 1$$

$$\mu_{s\eta} = \mu_{s1} + 1$$

The measured permeabilities of stacking configurations A and D were approximately 12, hence little deviation exists between the measured permeability and the intrinsic permeability especially where the intrinsic permeability is 10 or greater.

The variations of the core material properties using "I" laminations stacked in the D configuration were investigated at excitations of 400 and 800 cycles per second.

The dynamic hysteresis loops and saturated permeability B-H curves are shown in Figure 8. As expected, the coercive force increased with frequency, but no noticeable change in saturated permeability occurred. This implies that the saturated permeability of the core material is independent of frequency in the range of frequencies tested.

E. Summary

The results of the core material and stacking configuration evaluations are summarized in Table II.

The results of the data to date indicate that all methods of stacking "I" laminations presently evaluated result in inferior magnetic properties compared to core material fabricated using toroidal and DU lamination configurations. The Epstein frame and its modifications retained the superior switching properties of Orthonol better than other "I" lamination configurations tested.

Computations using formulae derived herein indicate that usage of Orthonol "I" laminations in an Epstein configuration is practical and feasible for long pulse magnetic modulators. At present a 10 kilowatt average power, 600 microsecond output pulse width magnetic modulator is being fabricated using Orthonol "I" laminations in an Epstein configuration.

A low level prototype magnetic modulator has been constructed using 6 mil DU laminations. An efficiency of 70% has been attained.

APPENDIX

A. Modulator Circuit Requirements

(a) The Figure of Merit of the Core Material

Consider the typical nth stage waveforms shown in Figure 1. The equation for the charging voltage, $v_{c_n}(t)$, of the nth capacitor is:

$$v_{c_n}(t) = \frac{E_{p_{n-1}}}{2} [1 - \cos \omega_{n-1} t] \quad \text{assuming } Q > 10$$

where

$E_{p_{n-1}}$ = Peak voltage before energy transfer to the nth capacitor.

ω_{n-1} = Discharge current angular velocity in the n-1 stage.

Q = Quality factor of the n-1 stage during energy transfer.

The total flux density excursion in reactor L_{u_n} before saturation is expressed by the following integral,

$$\Delta \theta_{u_n} = \frac{K_m}{A_n N_n} \int_0^{T_{n-1}} v_{c_n}(t) dt$$

where

N_n = Total number of turns on the nth reactor.

A_n = Net core cross sectional area of the nth reactor.

T_{n-1} = Discharge half period of the n-1 stage.

K_m = Dimensional constant.

which results in

$$\Delta \theta_{u_n} = \frac{\pi K_m E_{p_n}}{2 N_n A_n \omega_{n-1}}$$

Upon proper substitution, solving for $N_n A_n$ yields,

$$(N_n A_n)^2 = \frac{2.47 W_{c_n} L_{s_{n-1}}}{\omega_{n-1}^2} K_m^2$$

where

W_{c_n} = Energy stored in the nth capacitor.

$L_{s_{n-1}}$ = Saturated inductance of the n-1 stage.

The basic inductance equation for the saturated inductance, L_{s_n} , is:

$$L_{s_n} = \frac{K_m N_n^2 A_n \mu_{s_n}}{l_{c_n}}$$

where

l_{c_n} = Core mean magnetic path length.

μ_{s_n} = Saturated permeability of the nth reactor.

Rearranging and substituting for $(N_n A_n)^2$ yields

$$\frac{L_{s_{n-1}}}{L_{s_n}} = \frac{\Delta \beta u_n^2 U_n}{2.47 \mu_{s_n} W_{c_n} K_m^2} \quad (1)$$

where

U_n = Core material volume in the nth reactor.

The discharge current pulse time compressibility, $\rho_{n-1,n}$ of the discharge current from stage to stage is defined as:

$$\rho_{n-1,n} = \frac{T_{n-1}}{T_n}$$

where T_n , T_{n-1} are defined in Figure 3.

$$\rho_{n-1,n} = \sqrt{\frac{L_{s_{n-1}}}{L_{s_n}} - }$$

hence

$$(\rho_{n-1,n})^2 = \frac{\Delta\beta u_n^2 u_n}{2.47 \mu_{s_n} w c_n} \quad (2)$$

or upon rearranging

$$u_n = \frac{2.47 w c_n (\rho_{n-1,n})^2}{F_m}$$

where

$$F_m = \frac{\Delta\beta u_n^2}{\mu_{s_n}}, \text{ the figure of merit.}$$

(b) The Core Material Permeability Requirements

The n th reactor inductance, L_{u_n} , must be sufficient to prevent loading of the n th capacitor during uncharging. The following inequality expresses this condition:

$$\omega_{n-1} L_{u_n} \gg \frac{1}{\omega_{n-1} C_n}$$

However,

$$L_{s_n} = (\rho_{n-1,n})^2 L_{s_{n-1}}$$

and

$$0.5 \omega_{n-1} L_{s_{n-1}} = \frac{1}{\omega_{n-1} C_n} \text{ assuming } C_n = C_{n-1}$$

therefore

$$L_{u_n} \gg 0.5 L_{s_{n-1}}$$

Since

$$\frac{L_{u_n}}{L_{s_n}} = \frac{\mu_{u_n}}{\mu_{s_n}}$$

then

$$\frac{\mu_{u_n}}{\mu_{s_n}} \gg 0.5 \frac{L_{s_{n-1}}}{L_{s_n}} \quad (3A)$$

or

$$\frac{\mu_{u_n}}{\mu_{s_n}} \gg 0.5 (\rho_{n-1,n})^2$$

(c) The Core Material Coercive Force Requirements

Assume the switching reactor core material can be represented by a dynamic hysteresis loop which is a parallelogram as shown in Figure 9.

The energy required to set the flux level is given by

$$W_s = U_n \int_{-B_s}^{+B_s} H(t) dB$$

where U_n = Total core volume of the nth reactor.

$H(t)$ = Instantaneous magnetic field intensity.

and $H(t) = \frac{B(t)}{\mu_e} + H_{ac}$

where $B(t)$ = Instantaneous flux density.

μ_e = Effective permeability.

H_{ac} = Set coercive force.

upon substitution and integration

$$W_s = 2H_{ac}B_sU_n$$

and the total energy is

$$W_T = 4B_sU_n \left[\frac{H_{ac} + H_{ac}'}{2} \right]$$

$$= 4B_sU_n\bar{H}_{ac}$$

where $\bar{H}_{ac} = \frac{H_{ac} + H_{ac}'}{2}$

H_{ac}' = reset coercive force

If $W_{c_n} \gg W_T$

or

$$W_{cn} \gg 4B_s \bar{H}_{ac} U_n$$

and if the efficiency of energy transfer is

$$\eta_n = \frac{W_{cn} - W_T}{W_{cn}}$$

then

$$\frac{W_{cn}}{W_T} = \frac{1}{1 - \eta_n}$$

Hence

$$W_{cn} \geq \frac{1}{1 - \eta_n} 4B_s \bar{H}_{ac} U_n$$

Converting to the CGS system

$$W_{cn} = \frac{1}{1 - \eta_n} \left[\frac{4B_s \bar{H}_{ac} U_n}{K_u} \right]$$

where

$$K_u = 4\pi \times 10^{17}, \text{ a dimensional constant.}$$

or

$$\bar{H}_{ac} \leq \frac{K_u W_c (1 - \eta_n)}{4B_s U_n} \quad (4)$$

TABLE II
Summary of Core Material Characteristics

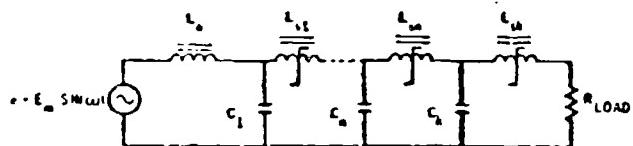


Figure 1a. The general a-c charged series type magnetic modulator.

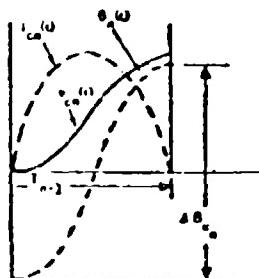


Figure 1b. Typical operating waveforms during the discharge of the n-1 stage.

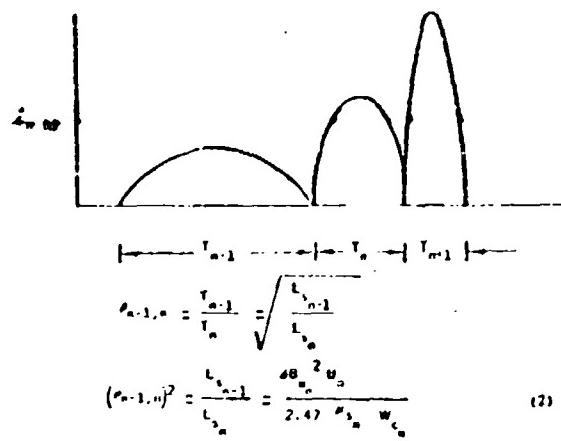


Figure 2. Typical discharge current waveforms for the various modulator stages.

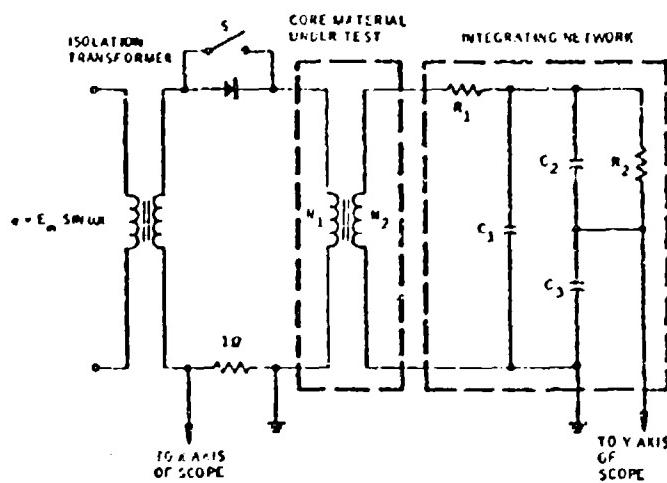


Figure 3. Schematic diagram of test circuit used to obtain values of saturation flux density, ΔB_{u0} ; coercive force, H_{ac} ; and saturated permeability, μ_{B0} .

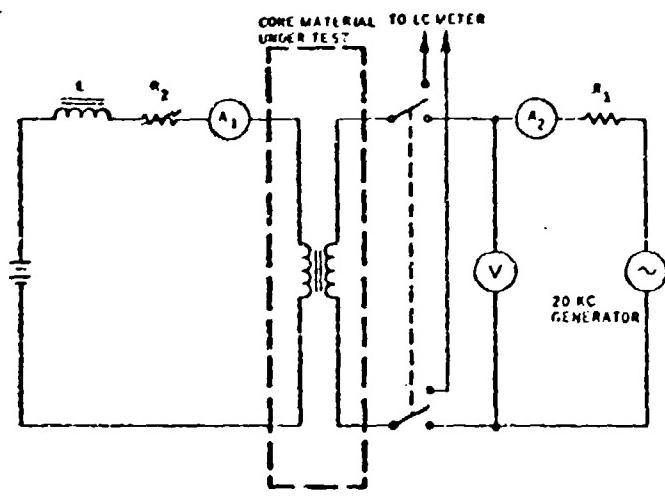


Figure 4. Schematic diagram of test circuit used for the saturated impedance measurements.

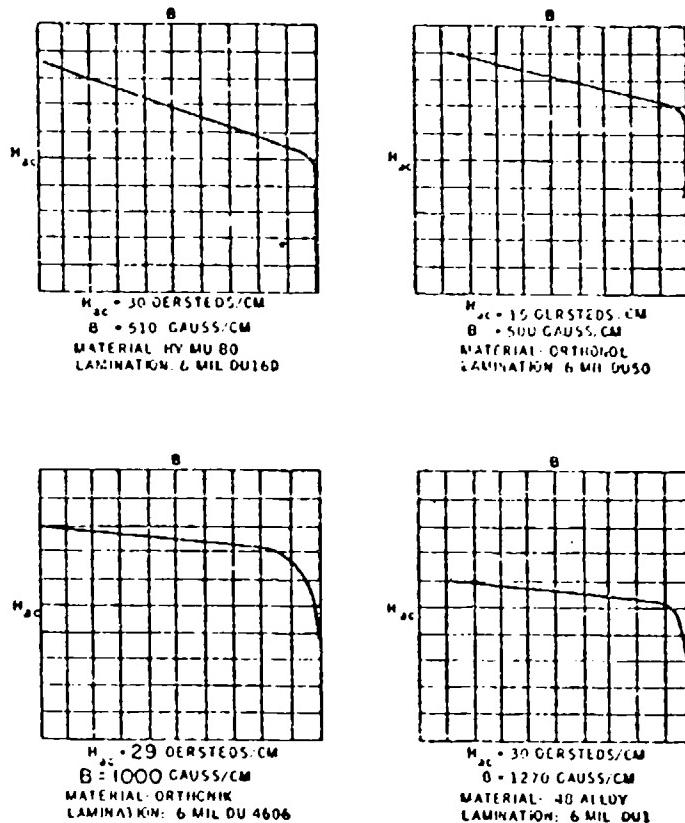


Figure 5. Dynamic B-H curves for various magnetic materials using test method 2.

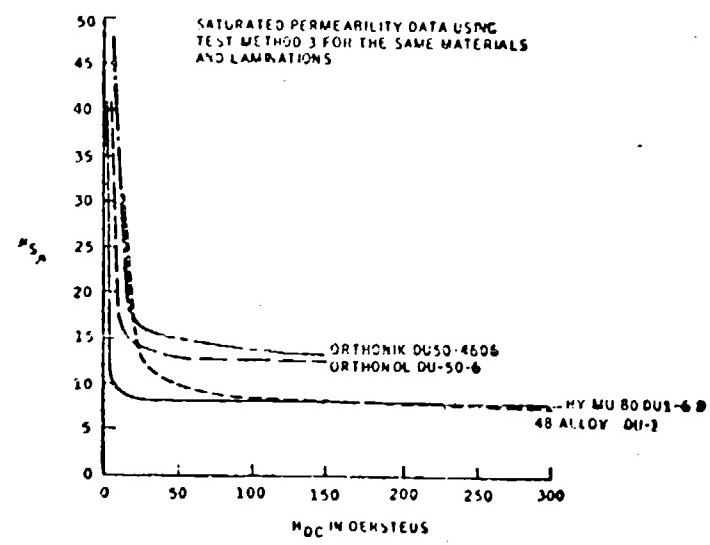


Figure 6. Saturated permeability data using test method 3 for the same materials and laminations illustrated in Figure 6.

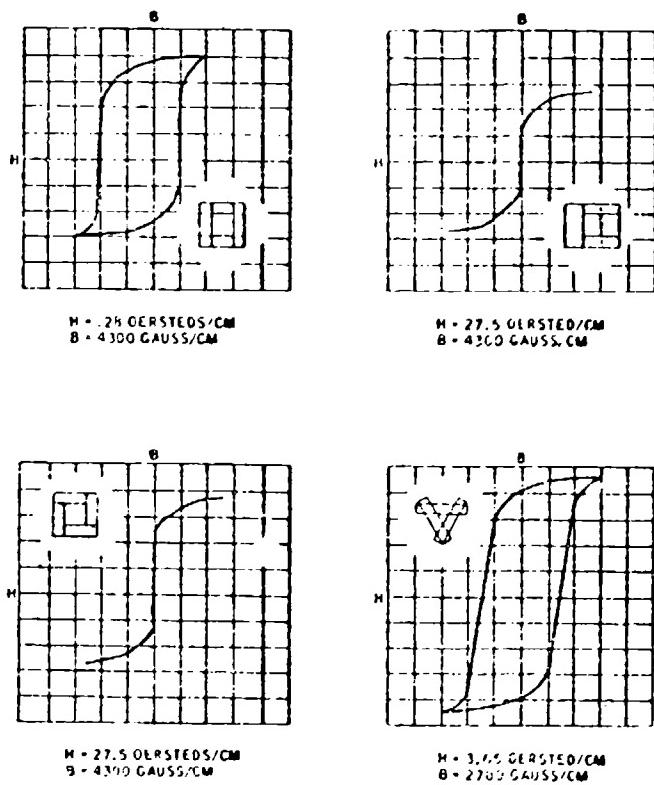
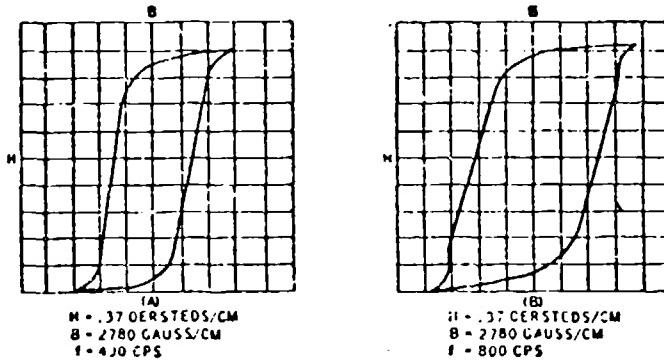
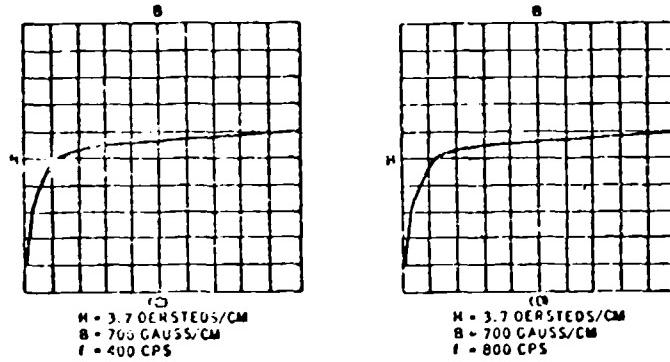


Figure 7. Influence of stacking configuration
of I bar magnetic characteristics.



Curves a and b: Using test method 1



Curves c and d: Using test method 2

Figure 8. Influence of frequency upon
 Orthonol I laminations using
 stacking configuration D.

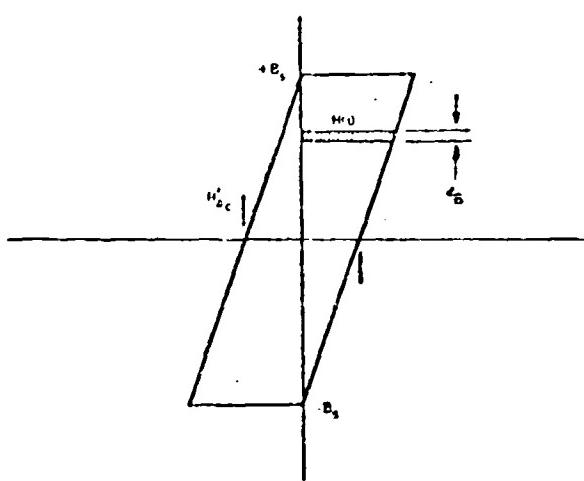


Figure 9. Hysteresis loop of nth reactor.

THE DESIGN OF A MODULATOR-POWER SUPPLY SYSTEM
FOR THE STANFORD TWO-MILE LINEAR ACCELERATOR

by

W. I. Smith

Radio Corporation of America

Under subcontract S-125 between Stanford University and RCA, a research and development program was undertaken commencing December 12, 1960, to establish the design of a modulator-power supply system suitable for utilization in the Stanford 45 bev linear electron accelerator.

This program and some results are discussed hereafter. The work was conducted with close cooperation between representatives of RCA and the University. Allowance must be made for continued improvements in the system prior to the period of final quantity equipment procurement; and the purpose of this paper is to report on modulator considerations of general interest to the art, rather than to identify the final form of Project H equipment.

Recognition should be extended to Thomas F. Turner, formerly of Stanford University, for his early studies in adapting the ignitron to relatively short pulse modulator applications.

A team of approximately ten (10) RCA engineers, for whom the author serves as spokesman, contributed to the effort.

General Requirements

Before discussing design approaches, a brief review of basic system requirements for the machine is in order.

The system design includes the simultaneous use of 960 klystron beam pulse modulators spaced at ten-foot intervals along the two-mile accelerator tube. Each unit must provide 64 megawatts of pulse power for 2.5 microseconds up to 360 times per second. The klystron cathode pulse must be flat to \pm 3.5 percent during the 2.5 microsecond period, and the pulse-to-pulse amplitude level must be maintained to within \pm .25%. These characteristics are required to provide the precise accelerator beam energy control necessary to the nuclear experiments to be conducted. (Radiation from beam filters may mask experimental results when the beam energy level is distributed rather than discrete.)

The impact on beam energy stability of even occasional modulator trip-out when the tripout rate is multiplied 560 times is obvious. The impact on maintenance requirements and impact on complexity of machine operating procedures are equally obvious.

Hence, a high order operational stability is required. High overall power efficiency is mandatory on an economic basis. The modulator system DC power consumption is in the order of 70 megawatts; and AC power for the complete modulator system, nearly 100 MVA.

The power cost initially estimated was such that one percent power waste was priced at about \$500,000 for the ten-year operational period. Purely on an efficiency basis, the pulse rise time was limited by specification to 0.7 microseconds maximum which was considered as the fastest attainable for the application, consistent with other requirements. Even this relatively fast rise time involves about an eight percent power waste at a corresponding cost of roughly four million dollars to the program.

Fortunately, detailed studies early in the cycle showed in general a clear compatibility between high performance, high reliability and high efficiency.

Choice of the System Elements

The Power Supply System: A substantial number of design approaches are entirely feasible, and some are used in existing HVPS applications. Those seriously considered here were:

1. Grid controlled ignitron rectifiers
2. Several 360 cps MG sets providing "AC Diode Charging"
3. Phase-staggered silicon rectifiers with external control and regulation circuits.

Ignitrons were eliminated based on reliability estimates and power line noise considerations.

AC diode charging appeared quite attractive for reasons such as:

1. Ease of voltage control
2. Ease of voltage stabilization
3. Complete electrical isolation from the power line
4. Quiescence of the modulator switch during half of each 360 cps charging period assuring negligible switch deionization problems
5. Ease of disconnect of a faulty modulator from the system during the quiescent half period
6. Overall simplicity
7. Reliability comparable to the utilities.

Three major drawbacks were:

1. Relatively low efficiency
2. Large size of the MG set due to the low utilization factor
3. The problem of obtaining a sufficiently low sub-transient reactance to provide optimum charging gain.

The system selected as superior comprised 30 three-phase, full-wave, phase staggered silicon rectifiers, providing the equivalent of 48-phase rectification. The phase staggering, accomplished through the design of the rectifier transformers, provides sufficiently low composite harmonic line currents that AC line filters will very probably prove unnecessary.

An induction regulator was selected to control the voltage and provide several-second line voltage correction to $\pm 1\%$. The rectifiers, transformers and regulator will be packaged in outdoor weather-proof structures to eliminate building costs. The circuit breakers are also in weather-proof housings centrally located at the hi-line feed center to protect the AC distribution lines as well as the rectifier units.

It is expected that the rectifiers will have reliability equivalent to that of AC substation equipment. The design and reliability of all parts are such that maintenance will be virtually unnecessary and operation fault free. Spare power supplies with automatic switching equipment are not considered necessary. Rectification is efficient, and operation and maintenance costs both low.

Figure I shows the relative economy of various transformer size options and helps explain why thirty units were selected to meet overall requirements. The cost advantage of larger sized units is exploited to near maximum; and machine capability is still close to maximum, notwithstanding the possible down time of one in thirty units.

Pulse Voltage Regulation $\pm 0.25\%$

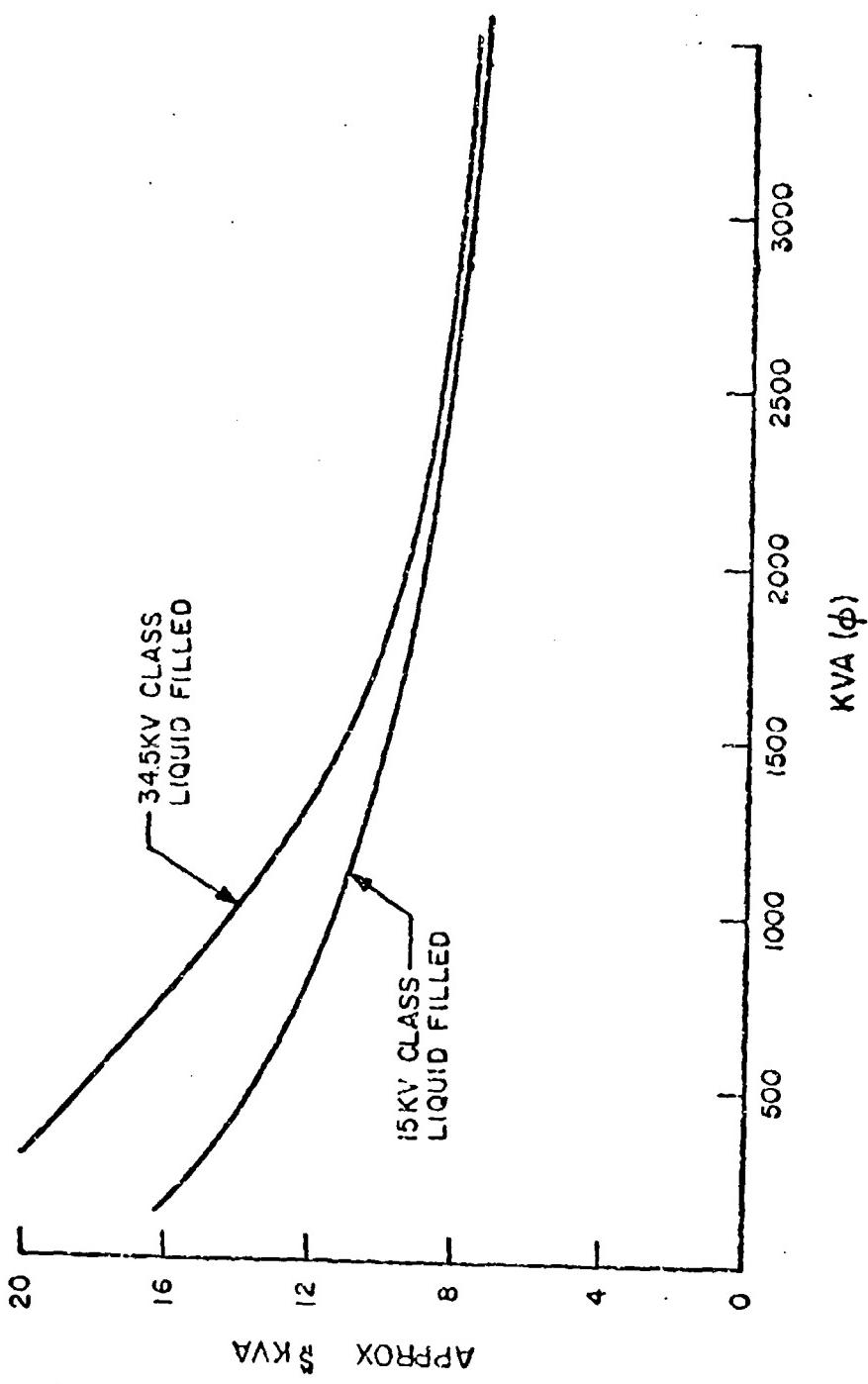
Some variation in residual PWM voltage was anticipated due to random variation in modulator switch deionization time. This would cause variation in subsequent peak charging level and pulse voltage. Also, the induction regulator corrective action is not fast enough to offset anticipated line voltage variations. Therefore, a system was incorporated in the prototype design for automatically regulating the PWM peak charging level. This system provides for returning excess energy stored in the charging inductor to the power supply filter rather than dissipating it. Figure II is a block diagram of the circuit.

Transformer T_1 serves as a charging inductor but has an extra winding used for returning the energy stored in the iron core to the power supply filter capacitor when network charging action is interrupted. With the turns ratio equal to 1.5, the secondary voltage exceeds V_b , wherever the primary voltage exceeds $0.67 V_b$, or the network voltage exceeds $1.67 V_b$. The comparator reference can, therefore, be set so that V_1 fires at any given network voltage between $1.67 V_b$ and $2 V_b$ for idealized charging. When V_1 fires, charging immediately ceases since the secondary voltage is clamped to V_b , and the primary voltage to $.67 V_b$ and diode CR-1 isolates the PWM from further action. The transformer amper-turns cannot change instantly, so the primary residual charging current is instantly replaced by a corresponding secondary current which flows into the filter capacitor against the relatively fixed power supply voltage. This current reduces linearly to zero in a fraction of one millisecond according to the rate

$$\frac{di}{dt} = - \frac{V_b}{L_{\text{secondary}}}$$

CR-2 assists V_1 in sustaining the reverse voltage present at terminal B during the first half of the charging cycle.

FIGURE I
APPROXIMATE COST VERSUS POWER
SUPPLY CAPACITY FOR 15KV AND 34KV
TRANSFORMERS



The observed performance is greatly complicated by the presence of the distributed capacitance and leakage inductance of T-1.

- Figure III shows additional parameters which must be considered.
 L_1 is the total primary circuit lead inductance.
 C_1 is the primary component of the transformer distributed capacitance.
 L_2 is the transformer leakage inductance.
 C_2 is the secondary winding distributed capacitance.

These parameters respond to three distinct changes in circuit conditions, including:

1. The firing of V_1 , the DeQ'ing switch
2. The discharge of C_1 , C_2 when the charging current has fallen to zero and the voltage at point 1 must fall from 1.67 V_b to V_b .
3. The firing of the main switch tube. This behavior is quite complicated and provides sufficient material of itself for a lengthy technical paper. However, the net effects which must be considered in the design can be readily appreciated.
 - A. Secondary transient voltage swings at the time the main switch fires, are considerably greater than simplified, idealized theory would indicate, causing insulation problems.
 - B. A relatively "fast" ringing current is superimposed on the declining ramp current which should flow in the secondary. If its amplitude is permitted to exceed the ramp current maximum, the net current will swing through zero causing deionization of V_1 and resumption of PFN charging, disrupting regulation.

Damping circuits were added to control the overall performance with considerable success but with some reduction in circuit efficiency. Study of improved damping arrangements continues. Figure IV shows a family of curves demonstrating the independence of pulse voltage and DC voltage over nearly full theoretical dynamic range.

The Switch

Three major alternatives considered for the switching device included the spark gap, thyratron and ignitron. Stanford had proven the feasibility of the spark gap in this service; but its shortcomings including significant maintenance requirements, audio and RF noise generation, and deionization problems are well known. The latter can be handled satisfactorily by careful design, but no method of eliminating the necessary maintenance was known.

A thyratron having full capability was not available early in the effort, but rapid progress has been made in the art; and we feel a suitable tube will be available prior to the major procurement. However, the ten year tube complement cost is presently considered excessive; and operating life expectations are not as lengthy as desirable.

Available ignitrons had been operated at Stanford at the full power requirement of the system. Ignitron life in other forms of service had been sufficiently lengthy to strongly encourage the judgement that the ignitron would prove the minimum ten-year cost device. Optimum igniter circuitry from a life standpoint is still under study, and performance data

FIGURE III
SIMPLIFIED PULSE REGULATION

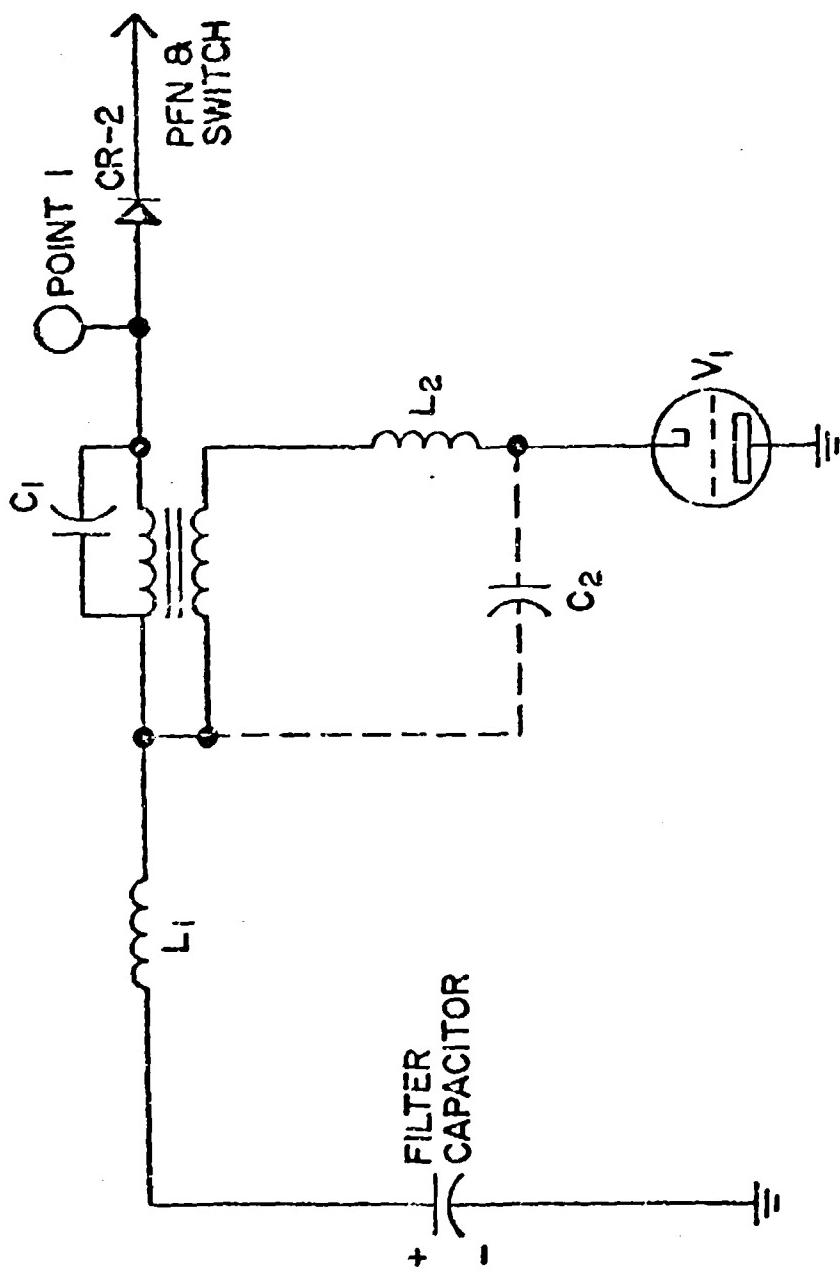
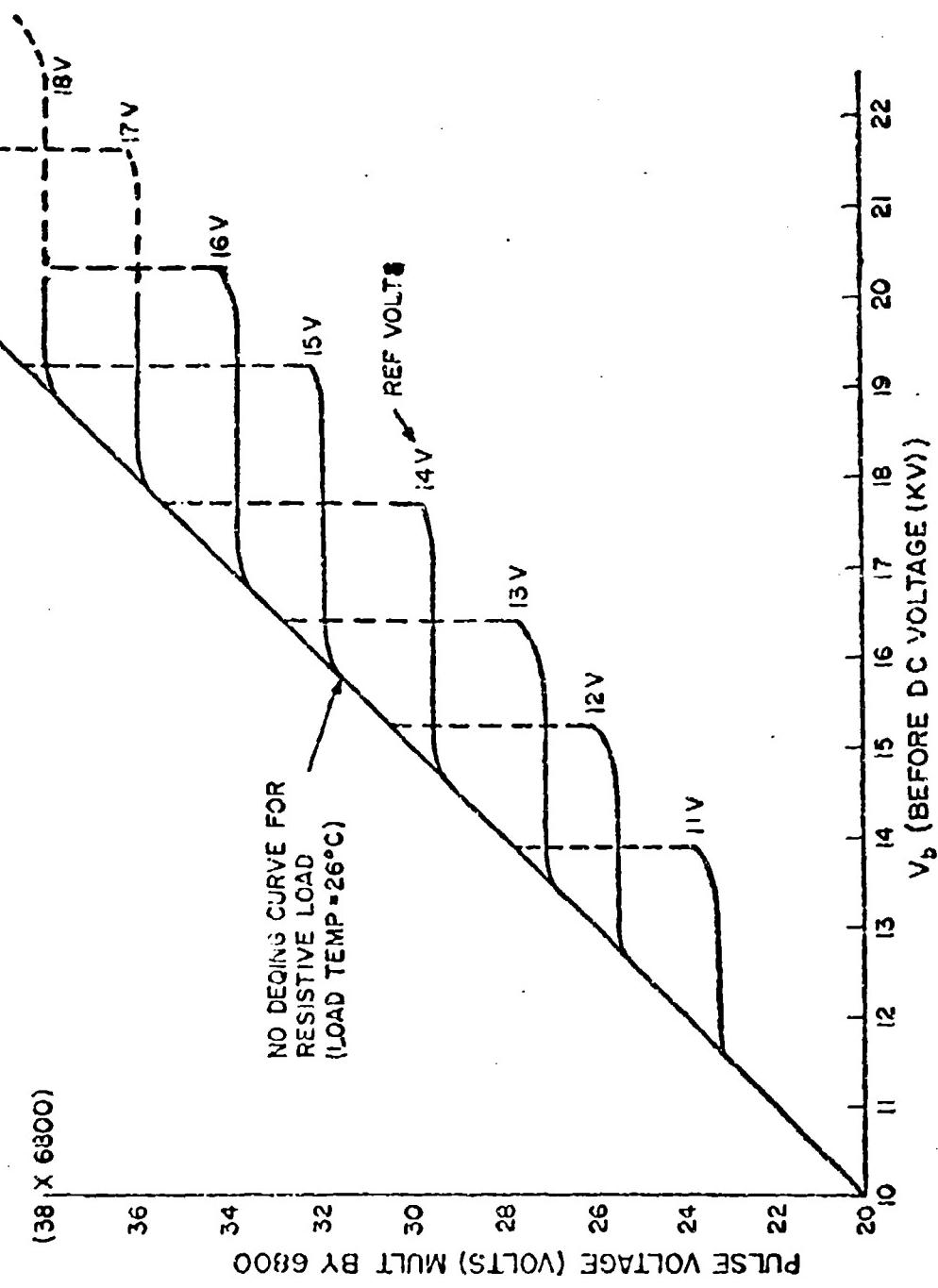


FIGURE IV
 V_b vs V_{pulse} WITH DEQING



are being accumulated. The arc-thru rate is also under study. Should this device prove disappointing it is considered that one of the alternative devices could be substituted without significant change in operating philosophy or performance characteristics. While a reliable solid-state switch seems very desirable in this application, no development known to us had offered encouragement that such a device will be available in the necessary time cycle.

The power supply voltage level was selected with consideration of the expected capability of the ignitron, the suitability of the required pulse transformer turns ratio, and nominal corona suppression requirements. Adjustment downward seems most likely if any departure from the existing design proves meritorious.

The Pulse Forming Network

A number of pulse forming network configurations were devised and tested in a scale model pulser. Blumlein circuit operation was included among the tests. A unit using coils without mutual coupling was considered promising for a number of reasons. It was known that a rectangular pulse into a resistive load could be approximated to any desired degree simply by increasing the number of identical sections. Moreover, without mutual coupling each section has first order level control on only a restricted portion of the pulse duration. There is a linear correspondence between points in time on the pulse and physical points down the length of the network. This arrangement promised rapid and easy adjustment to compensate for the droop and overshoot distortions caused by the pulse transformer equivalent circuit parameters.

The scale model tests clearly confirmed the anticipated performance. Coil adjustability was obviously the most flexible arrangement. These were constructed as in Figure V. Coarse control is available with strap ties and vernier control by adjustment of the copper slugs.

Polyethylene insulation was chosen for the capacitors in order to minimize losses. Added expense is compensated for by reducing power cost and the absence of required cooling apparatus. We estimate that the losses are about one third of the equivalent paper insulated network. This is supported by Q measurements. The temperature rise of the three capacitors nearest the front end is significantly higher than the others as expected, but well within design tolerances.

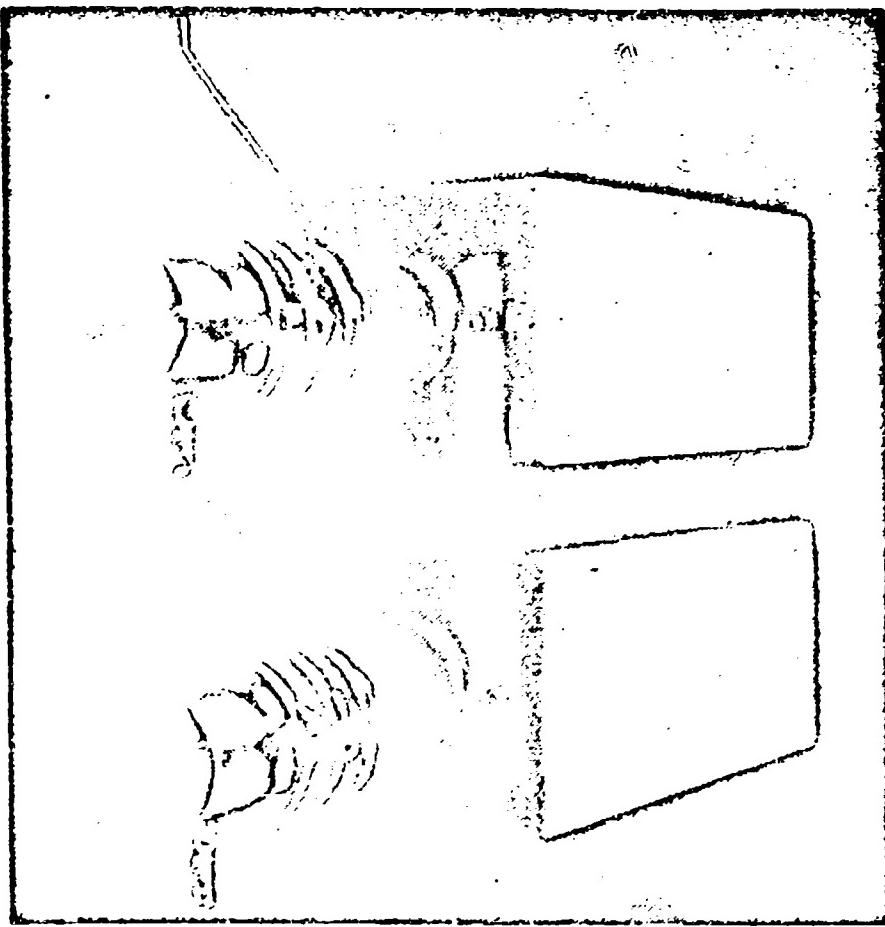
The unit can tolerate a surprising amount of series lead inductance although this disturbs the theoretical configuration.

Full scale results are very close to the scale model test results. A mathematical analysis of this type of pulse forming network was performed by Mr. T. Douma, of RCA. It was determined that versatility of the unit is theoretically supported. The mathematics involved was sufficiently interesting that the analysis will be the topic of another paper.

The Pulse Transformer

Mr. Douma also performed a very interesting mathematical analysis of the pulse transformer equivalent circuit response. This extends the analy-

FIGURE V
PULSE FORMING NETWORK COIL ASSEMBLY



sis presented in Volume V of the M.I.T. Radiation Series. Many interesting graphs were drawn showing the relative impact of design choices. Figure VI depicts one particularly interesting curve showing two possible L/C ratios (leakage inductance to load circuit capacitance) for any given pulse overshoot, using an ideal transmission line driving source. The low L/C ratio is rarely used in practice because a sufficiently low leakage inductance is difficult to attain physically, but analysis shows that if the art progresses to provide this need, much more efficient transformers will result. The M design approaches this goal, but PFIJ adjustment is relied on where the pulse transformer parameter attainment falls short.

Two broad aims guided the transformer approach. The first was to minimize the volume of insulation between the windings to minimize leakage inductance. The second was to minimize the volume of iron, to minimize core losses.

To minimize the volume of insulation, an oil insulated transformer was selected with the oil stressed to a maximum safe limit and stressed uniformly. The latter requires graded winding spacing so that stress is uniform.

The low core loss requirement is achieved by biasing the core to permit use of the full 3-H loop; also, of course, by careful core selection.

These ideas are not new but were firm considerations for selection of a transformer design. An important additional advantage considered was that the oil could be flushed after a flashover and operation continued without significant maintenance. In the case of several arcs actually experienced, some damage to the coil form resulted. However, the units are designed to run with the oil processed and the core sealed under a slight vacuum, and this was not done.

Air bubbles on the coil form surface are suspected as the prime cause of arc-over. Following repair of two which had arced, three units were operated at full voltage without incident. (These were vacuum pumped to remove air bubbles.)

While accurate loss measurements have not been made, the transformer operation is exceptionally efficient, with core losses less than one kilowatt in 75 handled - and uncompensated droop less than 1%. The leakage inductance referred to the secondary is approximately 240 microhenrys. The primary pulse voltage is 20 KV; and the secondary, 250 KV.

Figure VII is a photograph of the core and coil assembly.

Paralleled primaries and secondaries are wound on each leg providing bifilar characteristics. Tests on a Jord winding arrangement revealed a second-order oscillatory mode which disturbs pulse flatness, so this was avoided. Design of the isolation inductor for core resetting did not present any significant problems, and the level of resetting current did not prove critical or touchy.

Modulator High Voltage Diodes

A study of modulator diodes showed that silicon diode assemblies would present minimum ten-year cost if they are designed to last the life of the

FIGURE VI

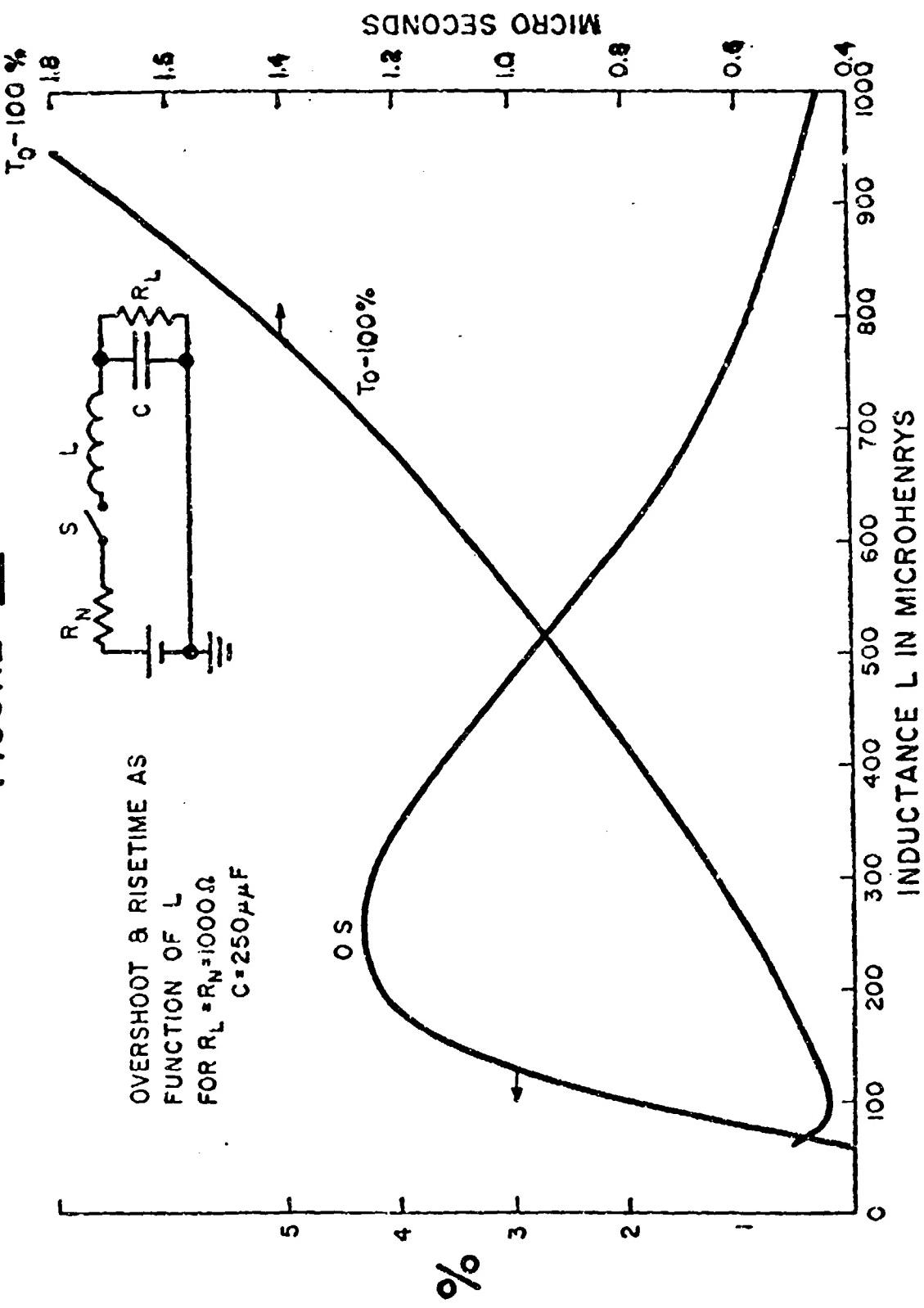
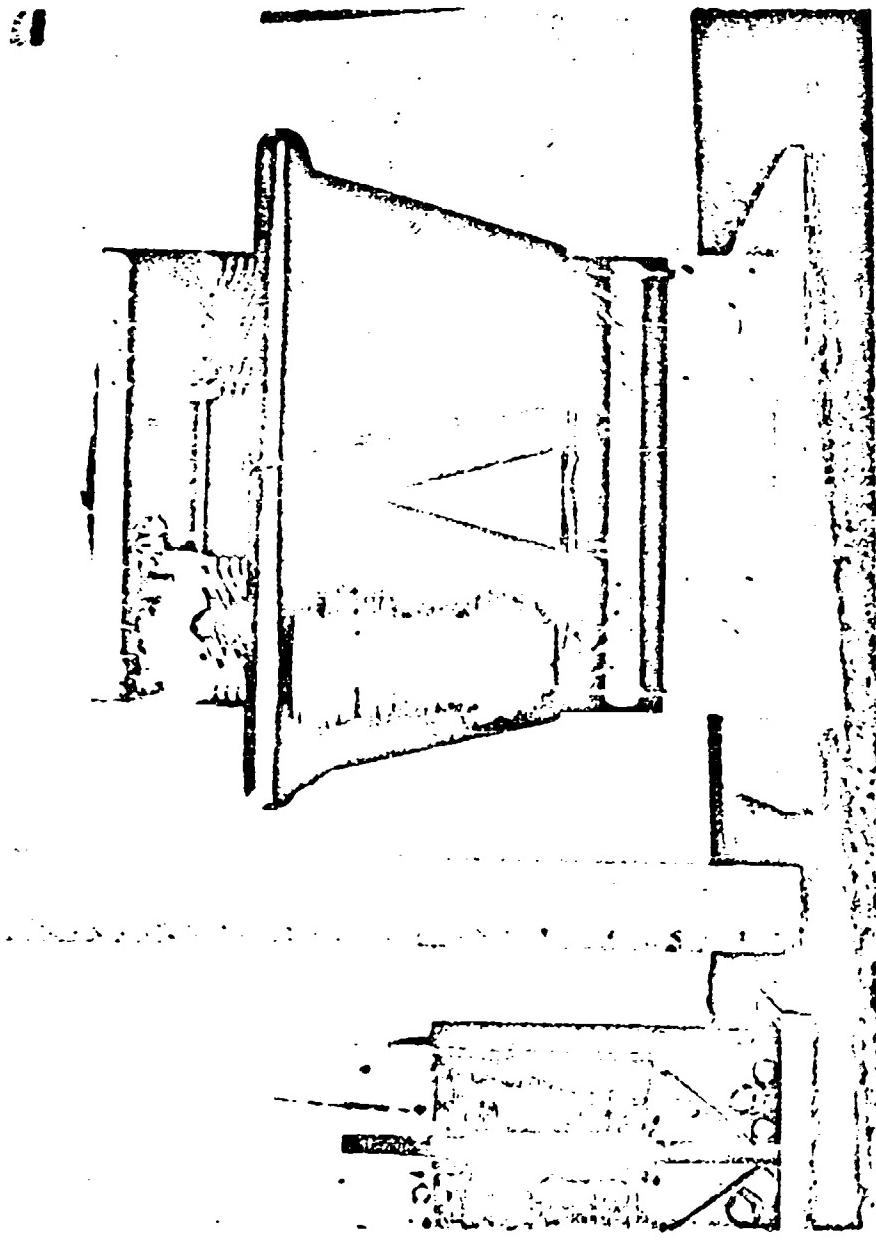


**FIGURE VII
PULSE TRANSFORMER PACKAGING ARRANGEMENT**



equipment.

The development problem presented was to determine minimum safe diode ratings by identifying the worst exposure to transient stresses in the equipment. For economic reasons it is essential that the diode does not fail under even occasional fault conditions. As is well known, gas tubes and vacuum tubes will frequently tolerate transient overstresses, but silicon assemblies disappear functionally from the circuit when overloaded. More than twenty-five resonant circuit modes are shock excited by normal operation or equipment faults. Most of these which can be ignored when solid-state devices are not employed had to be considered here. The most vexing and uncertain problem contended with was diode failure due to inverse voltage appearing too quickly following forward conduction. However, the ratings are difficult to determine under any circumstance. The worst case of heating due to the combination of forward conduction losses, steady-state inverse voltage losses and post-conduction inverse voltage heating must be identified and accounted for.

High voltage silicon diode assemblies are employed for the "holdoff", "DeQ'ing" and "end-of-line-clipper" functions.

Diffused junction diodes were employed for the "charging" and "end-of-line-clipper" diodes because their lower leakage current minimizes PFM discharged during the pulse interval at low repetition rates. More economical alloy junction units were used in the DeQ'ing diode assembly.

Fault Sensing and Protection

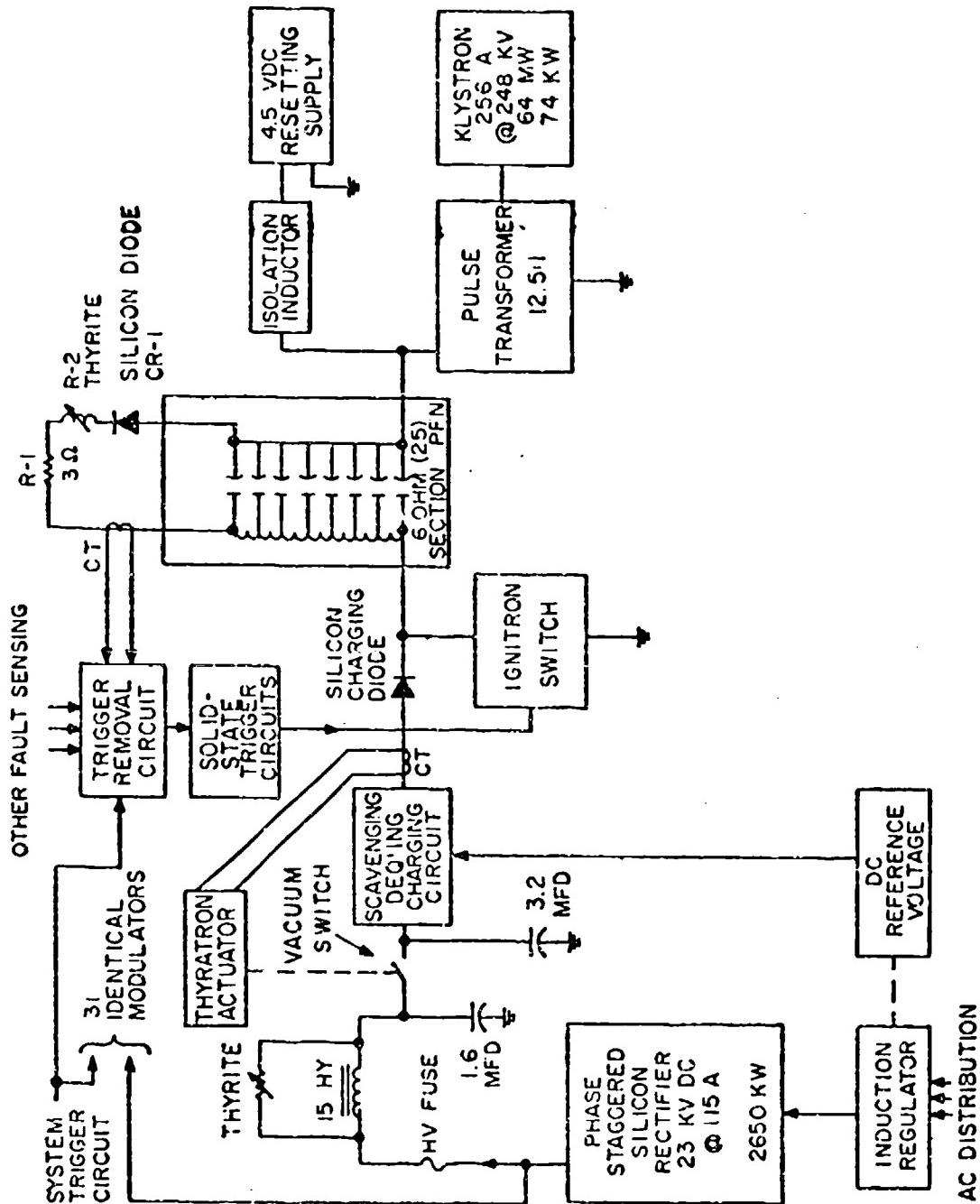
Thirty-two modulators are fed from each DC rectifier supply. It is undesirable to lose operation of a thirty-two unit sector for more than several milliseconds in the event of modulator failure. Original concepts of dumping the sector bus to permit disconnect of a faulty unit were discarded early in favor of a system providing successful DC interruption to remove the faulty unit without interruption of the other units. To facilitate this the ripple filter was divided to provide per/unit filters in each modulator of 15 by and 5 mfd's each. A series fast-breaking vacuum switch with each terminal by-passed by segments of the filter capacitor interrupts the fault in about two-and-one-half milliseconds. (See Figure VIII) Rigorous transient analysis was undertaken with this arrangement and the saturation levels and residual inductances of the charging inductance and filter choke are controlled to cause a current zero through the vacuum switch in the vicinity of the time of opening.

The vacuum switch is operated from a thyratron-switched storage capacitor for accelerated operating speed.

The thyratron is triggered by a signal derived from a specially designed current transformer which detects charging current levels in excess of the normal maximum. A thyrite element across the filter choke is necessary to damp transient swings following the overload current interruption. A high voltage, slower acting fuse provides backup protection.

Klystron arcing is sensed and the arcing current integrated. If the integral exceeds a selected value in a given ten pulse train, modulator

FIGURE VIII
STANFORD ACCELERATOR MODULATOR



triggering is interrupted to protect the klystron. Several consecutive arcs can be tolerated without shutdown, to aid in klystron seasoning.

A matched silicon diode inverse clipper or "end-of-line-clipper" is connected across the remote end of the pulse forming network. When the klystron arcs and short circuits the PFN, the energy is drained from the PFN without significant inverse voltage appearing at the switch tube end. The next charging cycle is thus normal in all respects. Significant current flows in the inverse clipper only when a klystron arc occurs. Hence, a current transformer in this loop provides a sampling for the arc-current integration discussed.

Other more conventional protection circuits such as klystron filament undervoltage and undercurrent devices and cooling system switches cause modulator trigger removal under abnormal conditions.

Ignitron Deionization Control

In most line-type modulator designs, the PFN is slightly undermatched to cause switch deionization promptly after the pulse.

With the parameters in the modulation described here, it was determined that if the switch were kept in conduction immediately after the pulse, it could serve as a pulse transformer backswing clipper. In this mode of operation the transformer exciting current flows through the series PFN capacitance and switch tube after the pulse, until the transformer core energy is transferred to the PFN capacitance. At the moment the exciting current passes through zero, the resultant inverse PFN voltage shuts off the switch. The "end-of-line-clipper" previously described disturbed this arrangement since it shunted the PFN preventing necessary reverse voltage buildup. Deionization problems resulted. Hence, a thyrite resistor was added in series with the clipper circuit matching resistor. Its resistance is negligible at current levels resulting from klystron arcing but is several hundred ohms at the pulse transformer exciting current level. This is sufficiently high that deionization control was restored.

DC Distribution

To pipe the DC voltage to the modulator stations, a system of prefabricated harnesses using #2, 7-strand power cable with a beefedup shield to handle return current is presently considered optimum. Specially designed connectors will permit prefabricated sections to be joined into continuous lengths or end fed from a feeder cable of the same size from a sector power supply. Each harness will consist of a length of cable with as many permanent takeoffs at 10-foot intervals as shipping and handling requirements will permit. In Phase I when only 240 equipments are operated, the unused ends which will eventually tie into the modulator units are capped with rubber boots. When switchover to Phase II for operation of 960 modulators is required, the harness lengths can be reconnected one sector at a time, without machine shutdown. A service-disconnect switch is housed in the modulator with the hot terminal shielded. The disconnect switch must be opened to permit entry to the modulator. Noise radiation problems are minimized by maintaining coaxial integrity from the power supply unit to each modulator.

Figure VIII shows in broken diagram form the highlights of the design which have been discussed here.

PERFORMANCE OF IGNITRONS IN PULSE SERVICE

by

T. F. Turner^f and H. S. Butler

Stanford Linear Accelerator Center

The results of various performance tests on three multi-grid ignitrons (GL-6228, Z5233 and Z5234) are presented. These tests were conducted to evaluate the feasibility of using these tubes as the high-power switch in the modulators for the two-mile linear electron accelerator being built at Stanford University. Measurements relating to peak current, peak power, average power, hold-off voltage and jitter are described. In addition, a number of general observations relating to the operation of ignitrons as switch tubes are reported.

A number of experimental observations relating to the deionization and recovery of ignitrons following a pulse are described. They compare the effects of peak pulse current, cooling water temperature and pulse repetition frequency on the deionization time of the GL-6228 and the Z5233. Results of tests on an experimentally designed ignitron are also reported.

The accumulated observations from our test program provided clues to the deionization mechanisms operating during the recovery period. These mechanisms are discussed and formulated mathematically. Comparisons between theory and experiment are presented. On the basis of this theory suggestions are made for design changes to improve ignitrons for pulse service. Additional suggestions for future theoretical studies are also given.

INTRODUCTION

In the spring of 1959 a research program was initiated to find a device to serve as the high-power switch for use in the modulators for the Stanford two-mile linear electron accelerator.¹ The switch had to make possible the development of modulators having the following principal specifications.

Peak power output (max)	64 MW
Average power output (max)	74 kW
Output pulse voltage range	158-248 kV
Output pulse current range	120-258 amps
Load impedance range	1320-962 ohms
Pulse length (flat-top)	2.50 μ sec
Rise and fall times (max 0-100%)	0.7 μ sec
Pulse repetition rate	60, 120...360/sec
Pulse height deviation from flatness (max)	$\pm 0.5\%$

^fNow with General Capacitor Co., Palo Alto, Calif.

Pulse time jitter (max)	± 10 μ sec
Pulse-to-pulse amplitude jitter (max)	$\pm 0.25\%$

In addition, the modulator had to be the design that would be most economical when maintenance and operating costs over a ten-year period were taken into account.

As a result of our investigation we have established that commercially available multi-grid ignitrons can be used successfully as high-power switches. Specifically, they make possible the development of modulators which not only satisfy the requirements outlined above but which surpass the specifications in many ways. We believe that ignitrons afford a major advance in high-power switch capabilities plus very long switch-tube lifetimes.

To date, three different gridded ignitrons have been tested at Stanford. They are the GL-6228, the Z5233 and the Z5234. The performance data for the GL-6228 have been reported elsewhere² and will not be repeated here. However, we do have one additional observation to report in connection with the GL-6228. It relates to pulse repetition frequency. While visiting another laboratory, we were privileged to watch a modulator having a GL-6228 for the high-power switch operate at a PFR of 1 kc/s. The average power level was 150 kw; the pulse length was 3 μ sec. The success of this test aids confidence to our belief that ignitrons can be operated at much higher rep rates than normally attributed to mercury vapor tubes.

The second multi-grid ignitron to be tested extensively in our laboratory was the Z5233, which was designed specifically for pulse service. We found that this ignitron fulfilled all the requirements set forth earlier and surpassed several of them. For instance, we operated successfully at an average power level of 120 kw, twice that required. We noted that the operation of the Z5233 was somewhat less sensitive to cooling water temperature. It would continue to perform with a water temperature near 20°C whereas the GL-6228 would not operate below 25°C. The control grid bias required for optimum results was around 2.5 kv.

We also tested a Z5233 without a splash baffle and found it to be as satisfactory, if not more so, as the Z5233 with baffle. In one test we started the modulator 25 times without failure at a peak power of 21 Mw with the cooling water at 20°C, directly from the water tap. Also some of the spurious signals which we observed on the oscilloscope trace of the pulse current following the conduction period were noticeably less frequent when the Z5233 without baffle was in the modulator. These observations are reported without comment.

Considerable success has also been achieved in using the Z5234 in pulse service. This ignitron, which is a scaled-up version of the Z5233, has been incorporated in the modulator for the Mark IV linear accelerator at Stanford University. This modulator drives a pair of klystrons with the Z5234 switching up to 8000 amperes evenly divided between the two loads. Typical

performance parameters are

Peak Power	260 MW
Average Power	56 kw
Hold-off Voltage	35 kv
Pulse Length	3 μ sec
Rep Rate	60 pps

The Mark IV modulator has now logged some 600 hours of service and the ignitron is performing satisfactorily in all respects. We did observe that a cooling water temperature of 40°C for the 25234 led to most satisfactory operation. This is some 4 degrees higher than we use for the GL-6228. The performance characteristics of the 25234 at higher rep rates was not investigated.

One final series of tests was run on an ignitron of our own design. On the whole the tube was disappointing as compared to the other tubes we tested. We could achieve only about 5 MW peak power with any reliability. There are two reasons for this. Because of the grid design, we could not raise the bias voltage above 1.5 kv without obtaining a long path discharge to the cathode. Thus we could not maintain proper control. Also, the anode-gradient grid region was too small and deionized too quickly. This prevented the inverse anode voltage from reaching the magnitude necessary to prevent a re-ignition of the discharge before recovery was complete. Both these design faults can be corrected, but the shifting emphasis of the work at the accelerator center will probably curtail any further development work. Both the GL-6228 and the 25233 will function satisfactorily and are readily available for use in the project modulators.

GENERAL OBSERVATIONS

In addition to the results of specific performance tests, there are a number of general observations to be made regarding the performance of ignitrons as switch-tubes. The first deals with tube life. Our experience to date has shown that only two things can limit the life of an ignitron tube. One is ignitor failure, and the other is some mechanical damage that lets the tube down to air. With regard to ignitor life, we make use of an observation by Cummings³ who found experimentally that the velocity of cathode spot migration was a function of tube current. Therefore, we pre-fire the ignitor several microseconds before application of the grid pulse. During the interval between the firing of the ignitor and the application of the grid pulse, current should be drawn to the holding anode. The advantage of this type of operation is to improve ignitor life by allowing time for the cathode spot to migrate away from the ignitor itself before the main pulse current flows. While it is impossible to assign precise numbers at this time, experience indicates that a 10 microsecond delay with a holding anode current of the order of 500 amperes is satisfactory. We have now operated two tubes in accordance with these parameters in excess of 4,000 hours with no sign of ignitor failure. The reader is referred to the earlier work of Cummings for a more detailed discussion of the mechanism of cathode spot migration.

Other groups have had significant success in using ignitrons in pulse service. In particular, we have knowledge of one radar installation which has had 48 ignitrons, Type 5630, in continuous operation for about four years without a single tube replacement. The total down time on this radar has been 0.05%. While these tubes are operating at a low repetition rate and with very long pulses, we believe this experience, added to that gained in our own laboratory, gives ample ground for presuming an indefinite tube life for ignitrons.

We have recovered in working with tubes other than the GL-6228 that the grid bias voltage required for most stable operation does vary from tube to tube by a few per cent, and varies a great deal between different tube types. The control bias voltage ranges from -1500 volts for the GL-6228 to as high as 3 kv for the 25234. This range seems to reflect the difference in grid hole diameter--the lower bias going with the smaller hole diameter (assuming the two grids have the same thickness). In practice, it seems best to adjust the bias for correct operation on each individual tube.

In using ignitrons as modulator switch-tubes it is desirable to mismatch the load in the opposite direction from the conventional mismatch employed for hydrogen thyratrons, that is, the load impedance must be somewhat higher than the line impedance. This requirement stems from the fact that during the pulse, magnetizing current is drawn by the pulse transformer. We find empirically that the amount of mismatch is determined by equating the energy in the mismatched portion of the pulse to the energy stored in the pulse transformer during the main pulse. This degree and direction of mismatch will cause an inverse voltage of the proper magnitude to appear on the anode of the ignitron. Experience has shown that to operate stably at power levels of the order of 100 or 200 kw average and with pulse currents of 5,000 to 5,000 amperes, the post-pulse voltage at the anode should be about 300-500 volts for a time comparable with the recovery time. Voltages appreciable greater or less than this range will cause malfunctions leading to a fault. While it is possible to achieve these results with various clipper circuits, mismatching in the manner described is far more economical in that it does not require expensive clipper components. Moreover, it has been shown that the total power wasted is the same whether mismatching is utilized or a backswing clipper is employed.

In considering the problem of pulse forming network design, not only must the mismatch be provided as outlined above, but generally the impedance of the network must be tapered to make up the magnetizing current and still yield a flat-top portion of the pulse at the output. With reference to Fig. 1, the required mismatch is given by equating the energy in the reflected portion of the pulse to that stored in the pulse transformer.

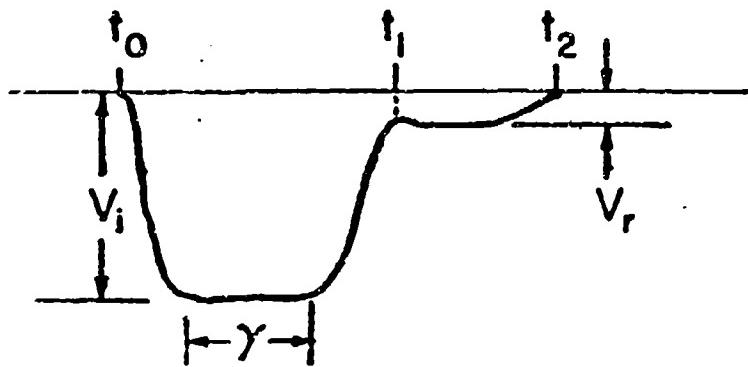


Fig. 1--Mismatch required between line and load.

The energy stored in the pulse transformer is

$$U_T = \frac{1}{2} L i^2 \approx (V_L^2 \tau^2) / 2L \quad (1)$$

where

$$i = (1/L) \int_{t_0}^{t_1} V_1 dt \approx V_1 \tau / L .$$

The energy in the mismatched portion of the pulse is

$$(1/R_L) \int_{t_1}^{t_2} V_r^2 dt \approx V_r^2 \tau / R_L \quad (2)$$

We equate this to the energy stored in the pulse transformer and solve for the reflection coefficient, $\rho = V_r/V_1$. We obtain

$$\rho = \frac{R_L - Z_0}{R_L + Z_0} = (R_L \tau / L)^{\frac{1}{2}} \quad (3)$$

While we realize that both the load and the line impedance are complex, experience has shown that the magnitude of mismatch as indicated above is adequate.

The value for the initial Z_0 is given by

$$(Z_0)_{\text{initial}} = R_L (1 - \rho)/(1 + \rho) \quad (4)$$

It is required that Z_0 reduce as a function of time (or length) to make up the magnetizing current and present no droop in the load pulse. The necessary taper is calculated to a first order by assuming the simple circuit shown in Fig. 2.

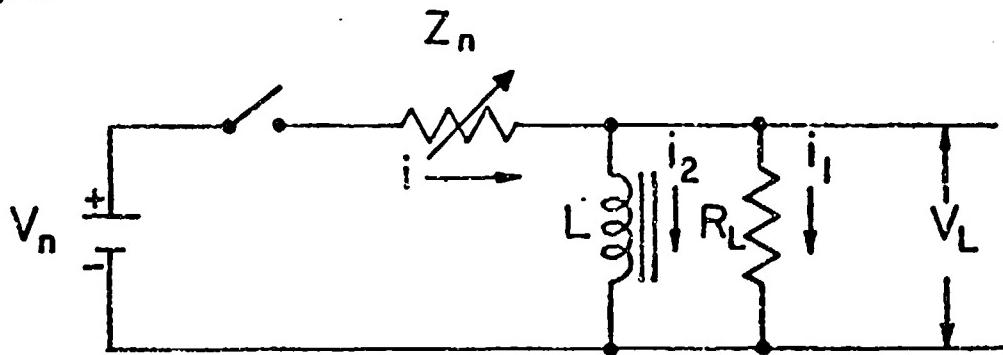


Fig. 2--Approximation to discharge circuit

For this circuit $V_L = V_n - i_2 Z_n(t)$. Solving for $Z_n(t)$ and approximating i_2 as before, namely

$$i_2 = (1/L) \int_0^t V_L dt = V_L t / L$$

we obtain an expression for the final network impedance. It is

$$(Z_n) = \frac{V_n/V_L - 1}{1/R_L + t/L} \quad (5)$$

In practice, a linear taper or the network impedance between the value given by Eq. (5) and that given by Eq. (4) is satisfactory for design purposes.

EXPERIMENTAL OBSERVATIONS

The basic modulator circuit which was used in these tests is shown in Fig. 3. The pulse forming network with impedance Z_n is charged up by the supply voltage E_{bb} through the charging choke. The gradient grid of the ignitron is directly grounded while the shield grid is grounded through a 500 ohm resistor. The ignitor is held at ground potential until triggered to

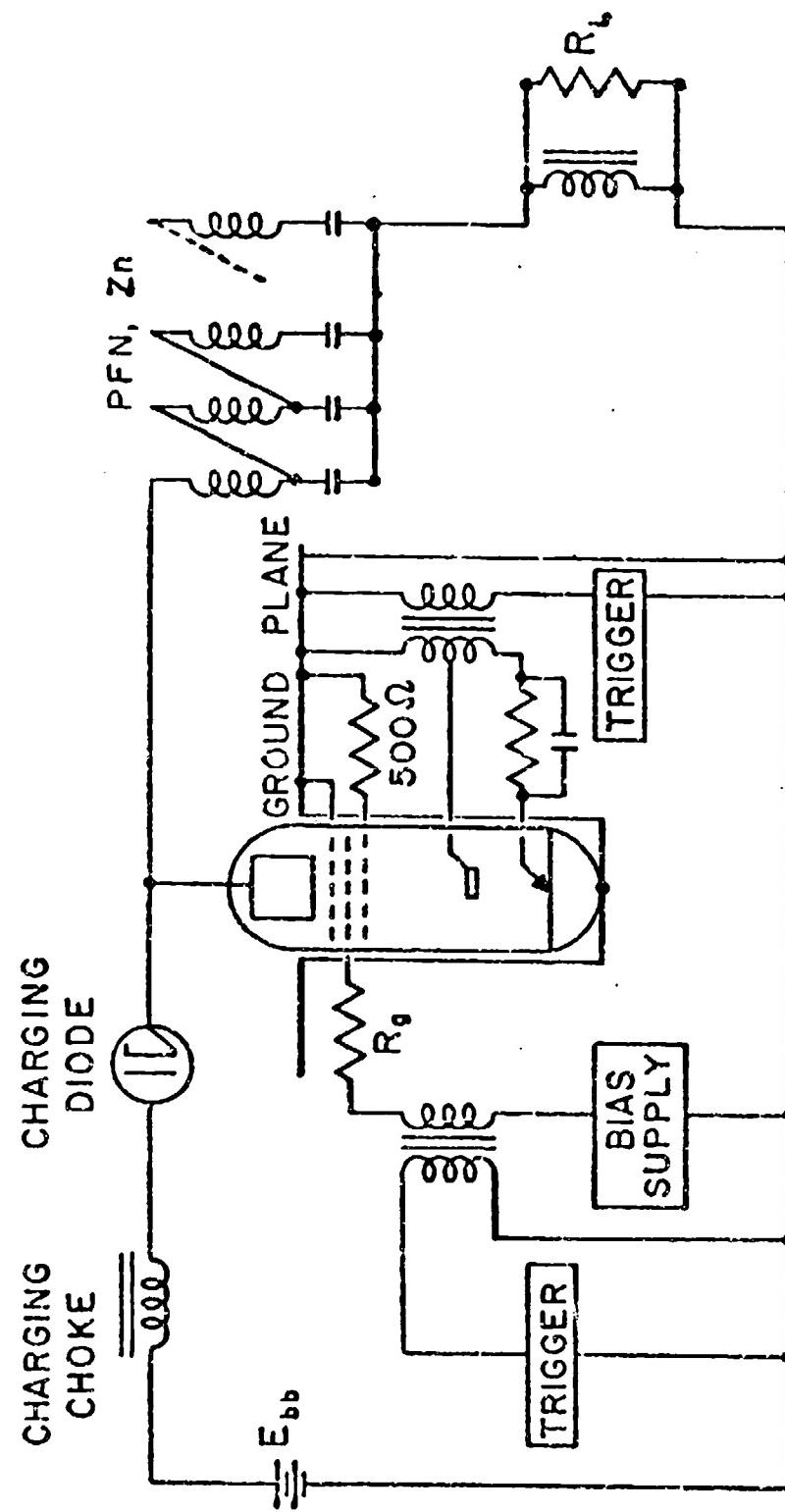


FIG. 3--SCHEMATIC CIRCUIT DIAGRAM OF THE MODULATOR
USED IN OUR IGNITRON TEST PROGRAM.

form the cathode spot. The control grid is maintained at the bias voltage until triggered to start the pulse.

The operation of the ignitron over one pulse cycle is depicted in Fig. 4. The cycle begins with the firing of the ignitor to form the cathode spot. Current is drawn to the holding anode and the cathode spot migrates away from the vicinity of the ignitor stub. After 10-20 microseconds the control grid is triggered on. The electrons in the cathode spot are attracted to the grid region where they come under the influence of the high anode potential. The pulse current through the tube begins to develop as the electron and ion densities and temperatures begin to increase. In a fraction of a microsecond a low pressure arc discharge in mercury develops. The anode voltage falls to a few tens of volts positive and the control grid stabilizes at a voltage some 10-15 volts less than the anode. The pulse forming network delivers its energy through the load, the ignitron now acting effectively as a short circuit.

After an interval of time equal to the pulse length of the line, the pulse network has delivered most of its energy and the pulse current drops to a smaller value determined by the degree of mismatch. After a second equal interval of time, the line is totally discharged and the pulse current falls to zero. This marks the beginning of the deionization and recovery period. As an after effect of the mismatch, an inverse voltage appears on the anode. The presence of this inverse voltage prevents reignition of the discharge until the control grid regains control. During this time the control grid is acting as a probe, extracting ions from the residual plasma and forcing the electrons out through the grounded gradient and shield grids. When the ion density drops to such a value that the Debye sheath fills the whole grid region, deionization proceeds by an ambipolar diffusion process until recovery is complete and the control grid has reached its full bias value. During the recovery period the charging of the network has caused the anode voltage to rise. This charging must proceed at a rate which is slow compared with the rate of recovery, otherwise the anode will swing positive before recovery is complete. But with the grid region deionized and the control grid operative, the charging of the network may proceed as rapidly as desired. The completion of the network charging marks the termination of the pulse cycle and the ignitron is ready to be fired again.

In all our work to date we have had to use ignitrons which lacked any provision for directly measuring the pressure, the ion density or the electron temperature inside the tube. The only quantities which we can directly monitor are the voltages which appear at the external terminals and the currents which flow in the external circuits. However, these quantities are sufficient to provide a great deal of insight into the operation of the ignitron as a switch.

The most enlightening measurement we can make is a photographic record of the control grid voltage vs time. A typical oscillograph trace of V_g is shown in Fig. 5.

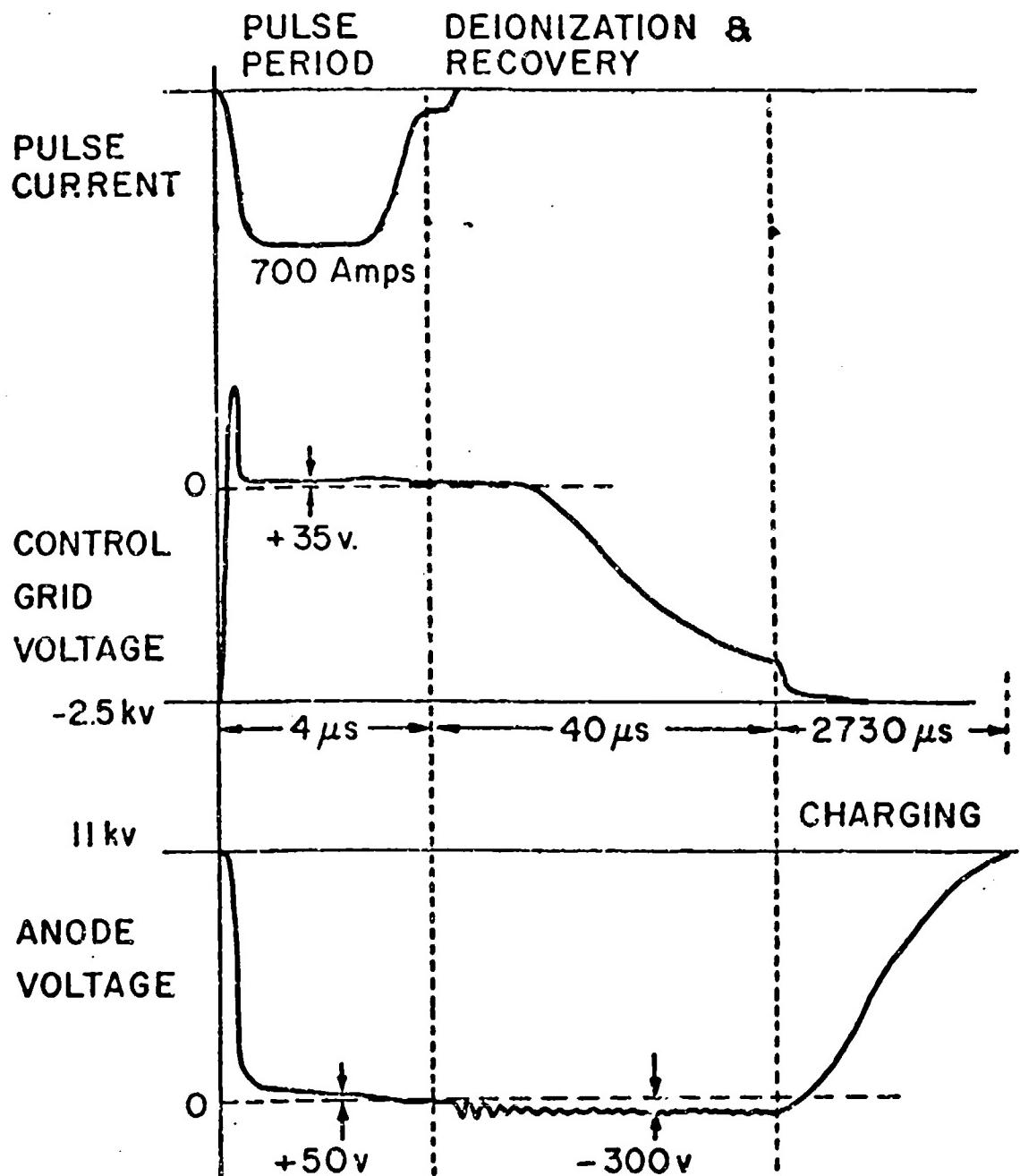


FIG. 4--PICTORIAL PRESENTATION OF THE RESPONSE
OF VARIOUS TUBE PARAMETERS
DURING THE PULSE CYCLE

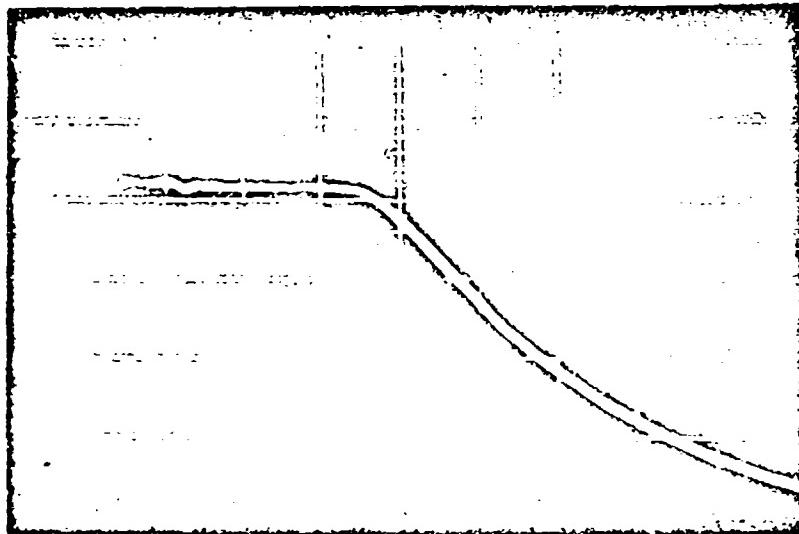


Fig. 5--The control grid voltage vs time. (5 μ sec/cm, 500 volts/cm)

The period between the end of the pulse and the knee of the curve is referred to as the deionization time. Its true significance will be made clearer later in the paper. By experiment we find that the deionization time: (1) increases with increasing grid resistance, (2) decreases with increasing bias voltage, (3) increases with increasing pulse repetition frequency, (4) increases with increasing cooling water temperature and (5) increases with increasing pulse current. Plotting the deionization time vs these various parameters gives useful information about the internal condition of the tube.

The deionization time for the control grid of the Z5233 is shown in Fig. 6 plotted against pulse current through the tube. For a given cooling water temperature the deionization time is seen to increase with increasing pulse current. This is a reflection of the fact that to carry the increased pulse current the ion density must be greater and the control grid requires a longer time to extract this increased number of ions from the grid region.

Fig. 7 presents the deionization time plotted against various cooling water temperatures for fixed pulse current for the GL-5223 and the Z5233. When the cooling water temperature is raised, the mercury vapor pressure in the tube rises; in fact, it about doubles with each 1°C temperature rise. The increased pressure decreases the mean free path of the particles in the gas which in turn decreases the drift velocity of the electrons. To carry the same current requires an increased number of ions and these added ions cause the deionization time to increase.

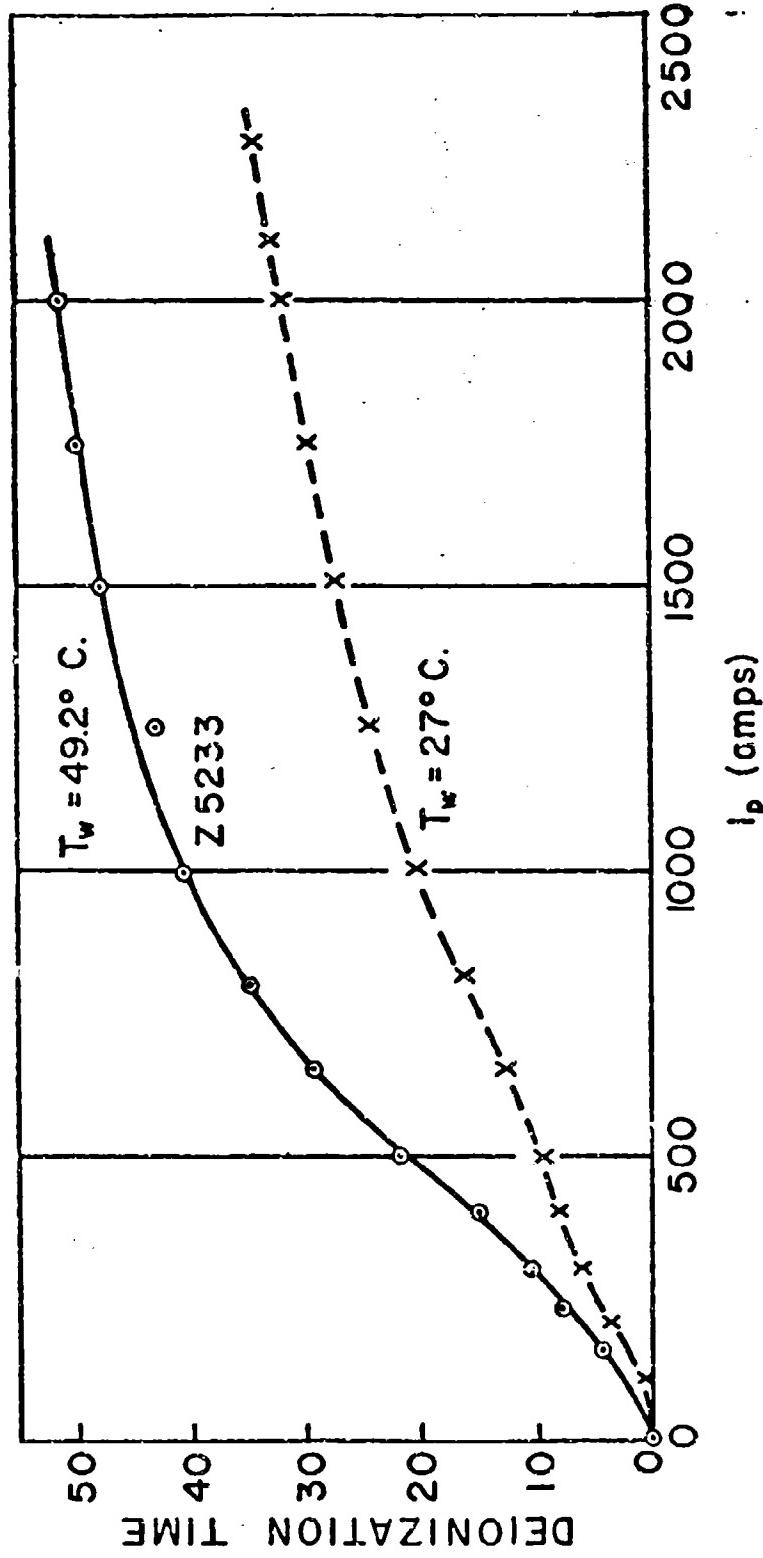


FIG. 6--DEIONIZATION TIME OF CONTROL GRID REGION OF A Z5233 FOR VARIOUS PULSE CURRENTS AT TWO COOLING WATER TEMPERATURES.

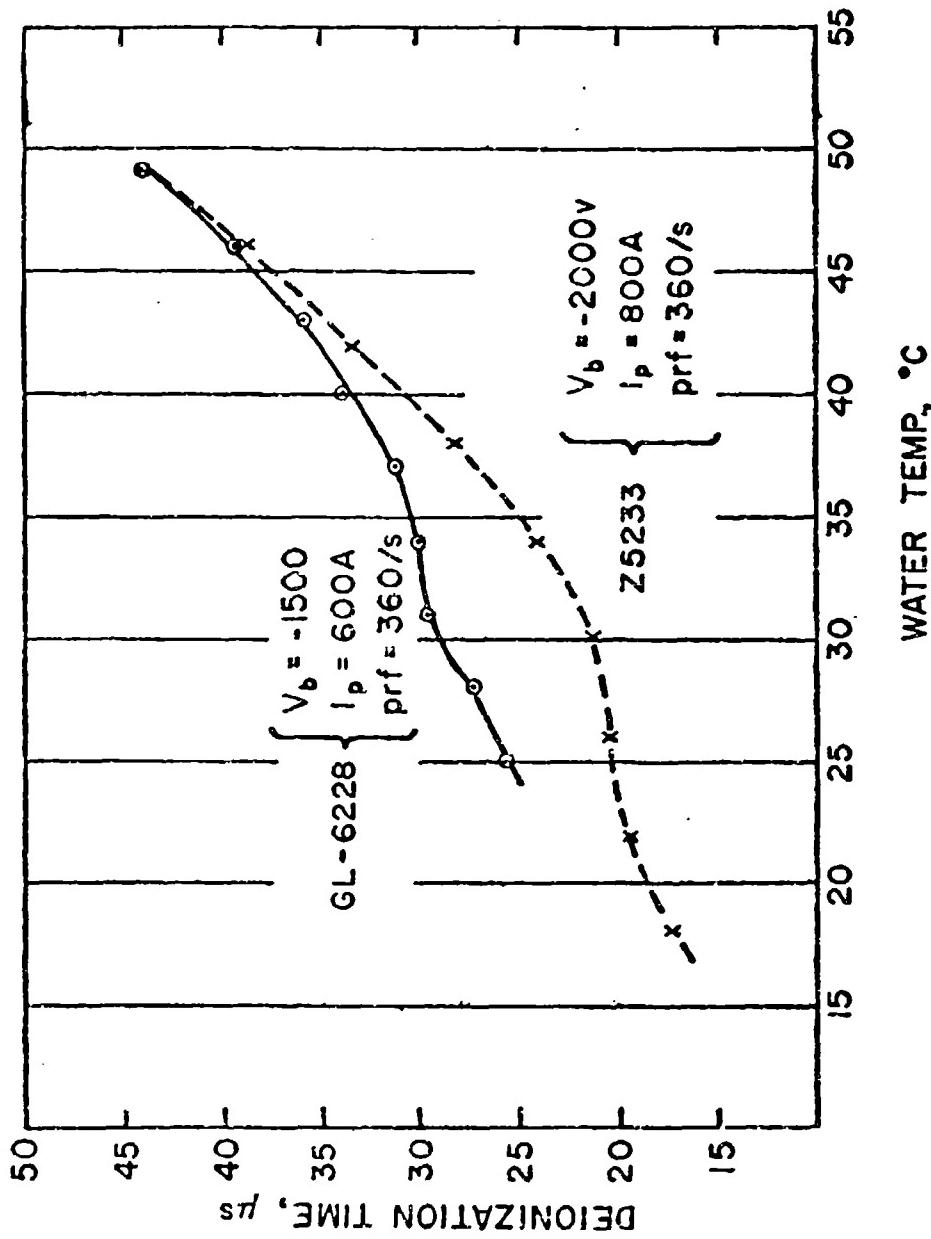


FIG. 7--DEPENDENCE ON COOLING WATER TEMPERATURE
OF THE DEIONIZATION TIME OF THE CONTROL
GRID REGION OF THE GL-6228 AND THE Z5233.

It is of interest to compare the deionization time vs pulse current for two different ignitrons. This is done in Fig. 8 for the GL-6228 and the Z5233. (Care must be taken to make the comparison at the same grid bias.) The deionization time for the GL-6228 is seen to be a few per cent greater in general than that for the Z5233. This probably reflects the slightly smaller tube diameter and grid hole size of the GL-6228.

DEIONIZATION MECHANISM

An interpretation of the physical process operating during the deionization period can be given with the aid of Fig. 9. Immediately following the end of the pulse, time t_p , a Debye sheath⁴ forms over the grid surface. This sheath forms at virtually every plasma-surface interface in order to equalize the electron and ion current flowing from the plasma to the surface. The thickness of the sheath is a function of the ion density of the plasma in the grid region. Because of the effective circuit shown schematically in Fig. 9, the ions are attracted to the control grid while the electrons move toward the grounded gradient and shield grids. At some later time t_d , the ion density in the grid region has decreased and the sheath has expanded accordingly. (Keep in mind that a sheath exists around each grid surface although only one sheath is shown here to prevent an overly complicated figure.) When the sheath reaches half way across the inter-grid space, that is, when the sheaths from adjacent grids meet, the deionization period ends. This point in time is marked on the grid voltage curve by t_d , the deionization time.

This process can be formulated mathematically as follows. The total number of ions in the grid region is given by

$$N = (A d X + A_1 d_1 X_1) n_0$$

where A is the cross sectional area of the ignitron barrel, d is the spacing between the grids, X is the degree of ionization in the region between the grids, A_1 , d_1 , and X_1 are the analogous quantities in the grid holes and n_0 is the gas density. Because the current is continuous through the tube, the following approximation is valid: $A X \approx A_1 X_1$. Also for the ignitrons of interest, $d \approx d_1$. Thus

$$N = 2 A d n \quad (6)$$

where n is now the ion density.

The thickness of the Debye sheath is given by

$$h^2 = kT_e / 4\pi n e^2$$

or, solving for n ,

$$n = b h^{-2} \quad (7)$$

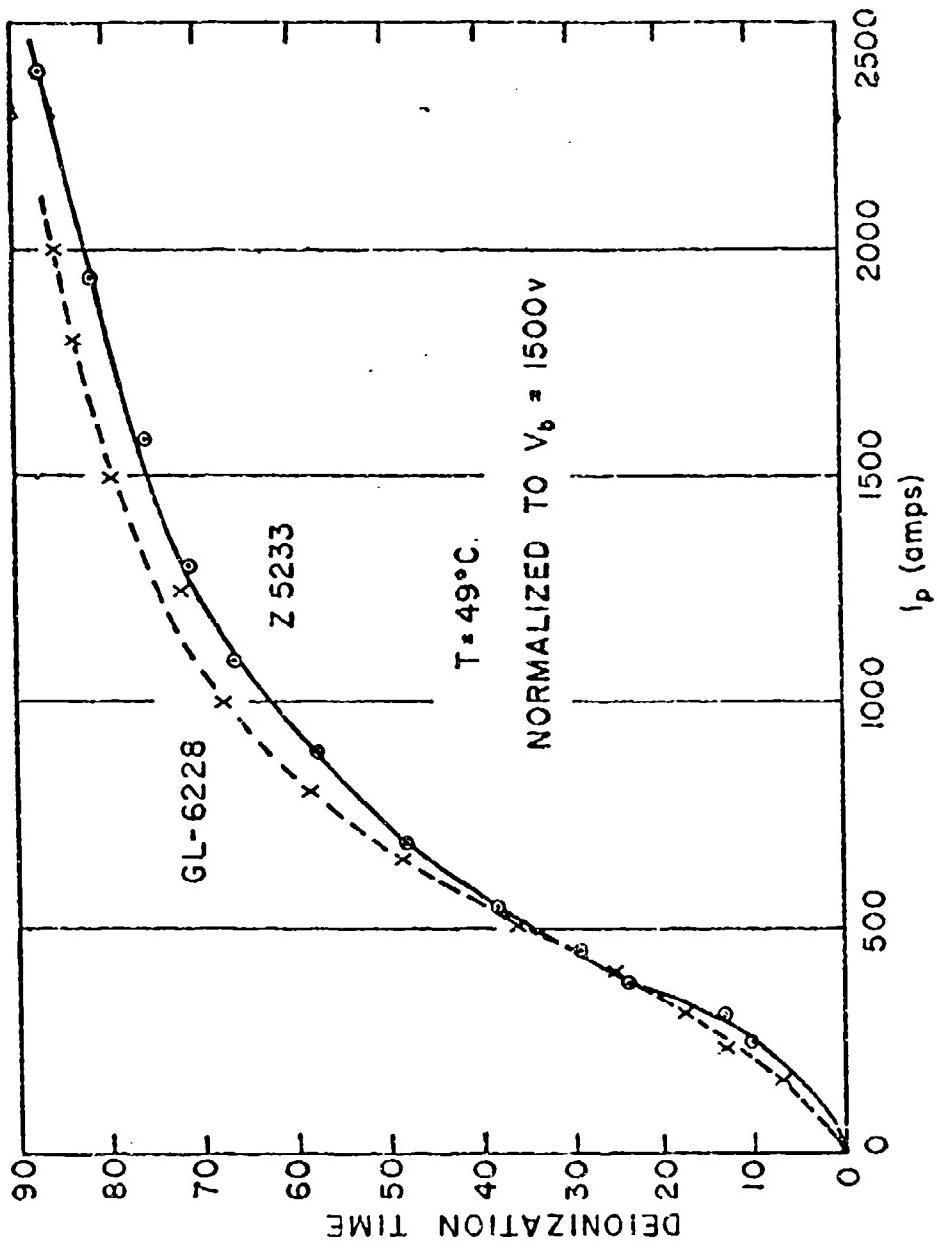


FIG. 8 -- COMPARISON OF DEIONIZATION TIMES OF THE
 CONTROL GRID REGION OF THE Z5233 AND THE
 GL-6228 FOR VARIOUS PULSE CURRENTS.

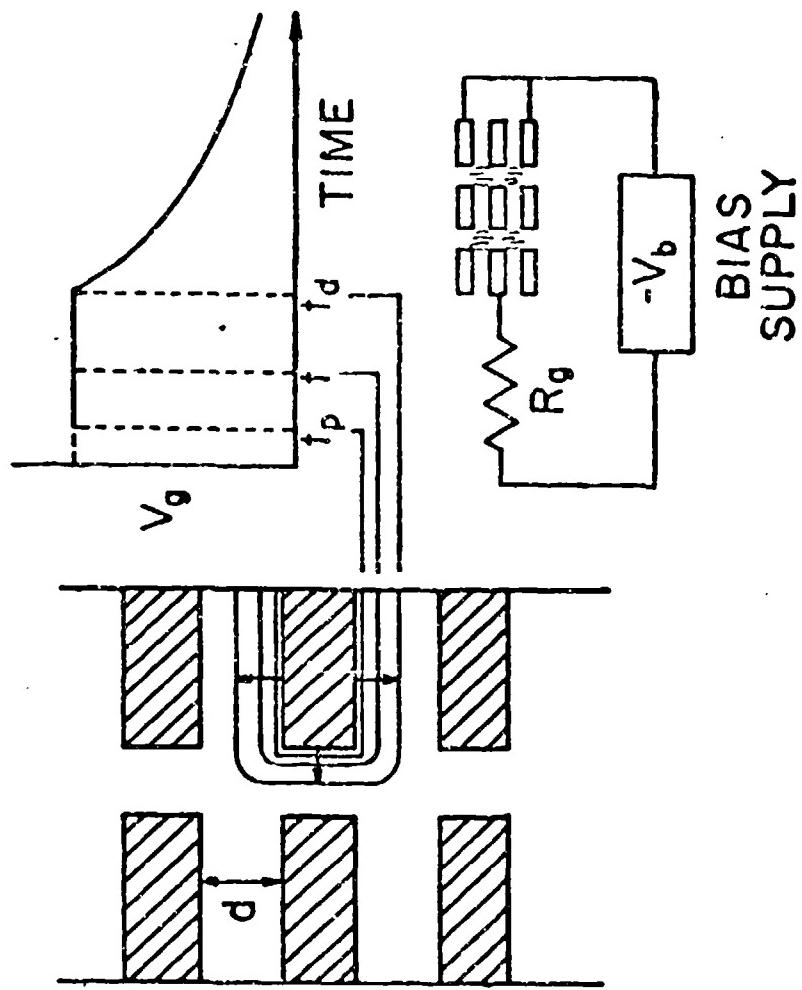


FIG. 9--PICTORIAL REPRESENTATION OF THE DEIONIZATION MECHANISM IN THE GRID REGION.

where

$$b = kT_e / 4\pi e^2 .$$

Substituting in (6) we have

$$N = 2 A d b h^{-2}$$

The time rate of change of the number of ions is given by

$$dN/dt = 2 A d b (-2h^{-3}) dh/dt$$

and experimentally we find this quantity to be a constant given by

$$-a = -V_b / eR_g$$

where V_b is the bias voltage, R_g is the grid resistance and e is the electronic charge. Equating this to dN/dt we have

$$-a = 2 A d b (-2h^{-3}) dh/dt .$$

Integrating this equation yields

$$(t_d - t_p) = -2 A d b (d^{-2}/4 - h_0^{-2})$$

where the following initial conditions have been used: $h = h_0$ at t_p and $h = d/2$ at t_d . Because $h_0 \ll d$, $h_0^{-2} \gg d^{-2}$ and we have

$$(t_d - t_p) = \frac{2 A d n}{V_b / eR_g} \quad (8)$$

where $b h_0^{-2}$ is the initial ion density from Eq. (7).

We see that the deionization time depends on the volume of the grid region, the ion density in the region, and the value of the grid bias and grid resistor. Comparison with experimental results has shown Eq. (8) to be qualitatively correct in its dependence on these quantities. Based on our best estimates of the ion density, as taken from the works of Langmuir⁵, Killian⁶, and Klarfeld⁷, Eq. (8) is also quantitatively correct.

We have another experimental observation with which we can compare Eq. (8). As shown in Fig. 10, the deionization time decreases with increasing grid bias. However, it decreases in such a way that the area under the curve is constant. Now the area under the curve, divided by eR_g , is nothing more than the time integral of the grid current. Rewriting Eq. (8) we have

$$2 A d n = N = \frac{1}{eR_g} (t_d - t_p) = \text{constant}$$

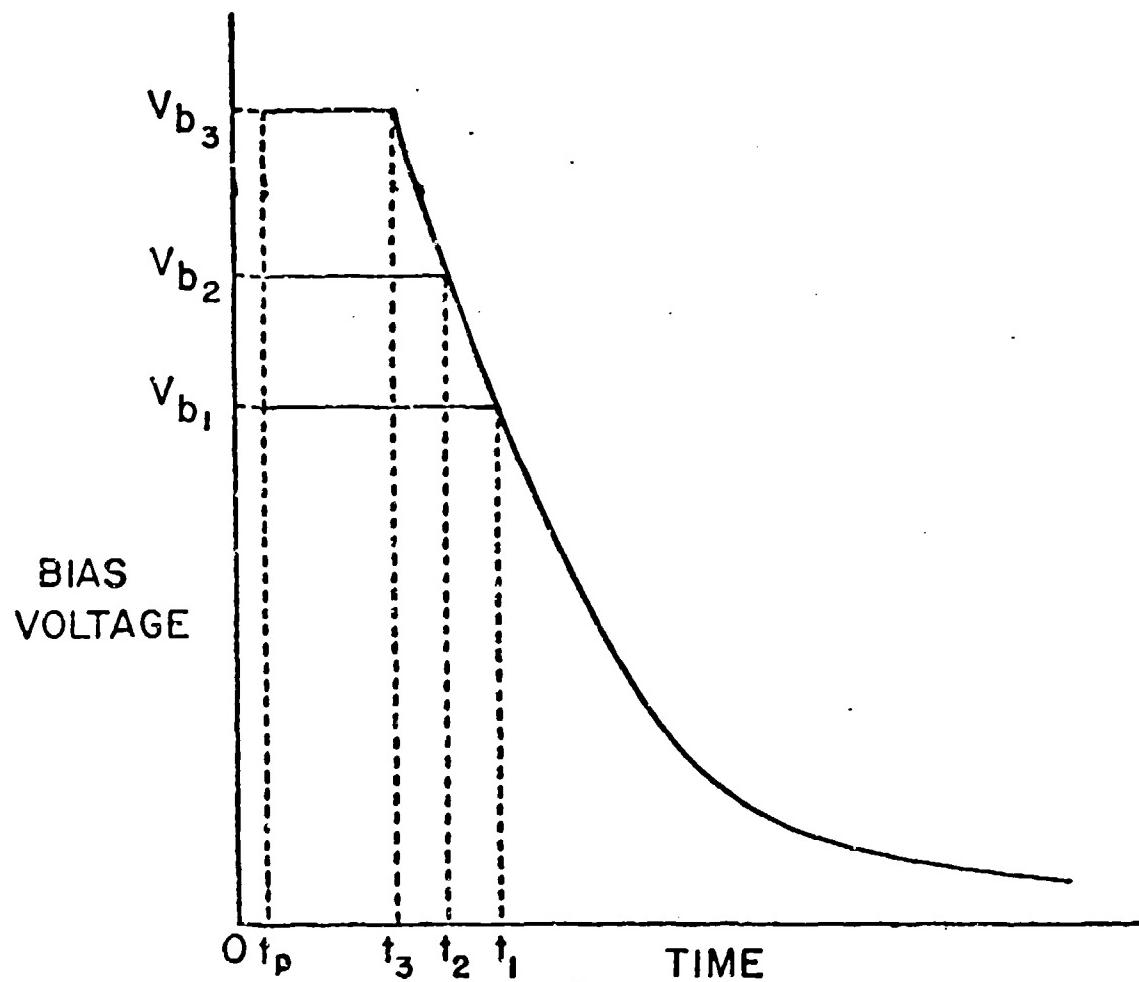


FIG. 10--PICTORIAL REPRESENTATION OF THE EXPERIMENTAL OBSERVATION THAT THE AREA UNDER THE DEIONIZATION PORTION OF THE CONTROL GRID VOLTAGE TRACE REMAINS CONSTANT INDEPENDENT OF BIAS VOLTAGE.

Thus Eq. (8) says that the total number of ions in the grid region is constant for a given pulse current and this is exactly what is shown by Fig. 10.

Following the deionization period, the shape of the grid voltage trace changes abruptly indicating a marked change in the recovery process. In an effort to gain insight into this period we plotted the logarithm of the grid current vs time and obtained, for example, the graph in Fig. 11. There are two distinct slopes indicating two decay constants, one of 15.7 μ sec, the other of 35.6 μ sec. The appearance of an exponential decay of current strongly suggests an ambipolar diffusion process, or a diffusion process of some kind. Considering the magnitude of the electric fields involved, one would expect to include a term in the diffusion equation to account for the field. There is a strong temptation to associate the two decay times with the decay of electrons of two different temperatures, but we have no direct experimental data to substantiate such an association. Moreover, in the solution of the diffusion equation, there are a series of eigenvalues, each representing a different decay constant. What we see in Fig. 11 may be the first two such eigenvalues.

CONCLUSIONS

Based on an extensive series of tests and accumulated practical experience at Stanford University, we believe that the following multi-grid ignitrons can be used successfully as high-power switch tubes in modulators: CL-6228, Z9233 and Z9234. The type 5630 ignitron should be added to the list as a result of its successful performance at another installation. An average power of 150 kw and a peak power of 260 mw represent the highest performance rates we have attained to date, but these were limited by the power capability of our equipment, not the ignitrons. The tube lifetime of an ignitron promises to be extremely long if properly treated.

If it were desirable to increase the maximum rep rate at which an ignitron can perform, Eq. (8) makes explicit the controlling variables. Given a specific ignitron, the grid bias should be made as large as possible, the grid resistor should be as small as possible, and the cooling water temperature (hence the ion density) should be kept as low as possible; all these adjustments being consistent with stable operation of the tube. If one were given the problem of designing an ignitron for higher rep rates, Eq. (8) tells one that the spacing between the grids should be as small as possible, the thickness of the grids as small as possible, and the diameter of the grid holes and overall tube diameter should be as small as possible consistent with maintaining control and handling the desired power. Designing the optimum tube for a given class of service would be a sophisticated problem and must await a more detailed knowledge of the manner in which all the tube parameters interact. One approach would be to use the work of Tonks and Langmuir¹ to relate the dependent variables in the plasma discharge (degree of ionization, axial electric field, ion density, electron temperature, positive ion current density and ion generation rate) to the independent variables of the tube (i.e. radius, gas pressure, bias current and well

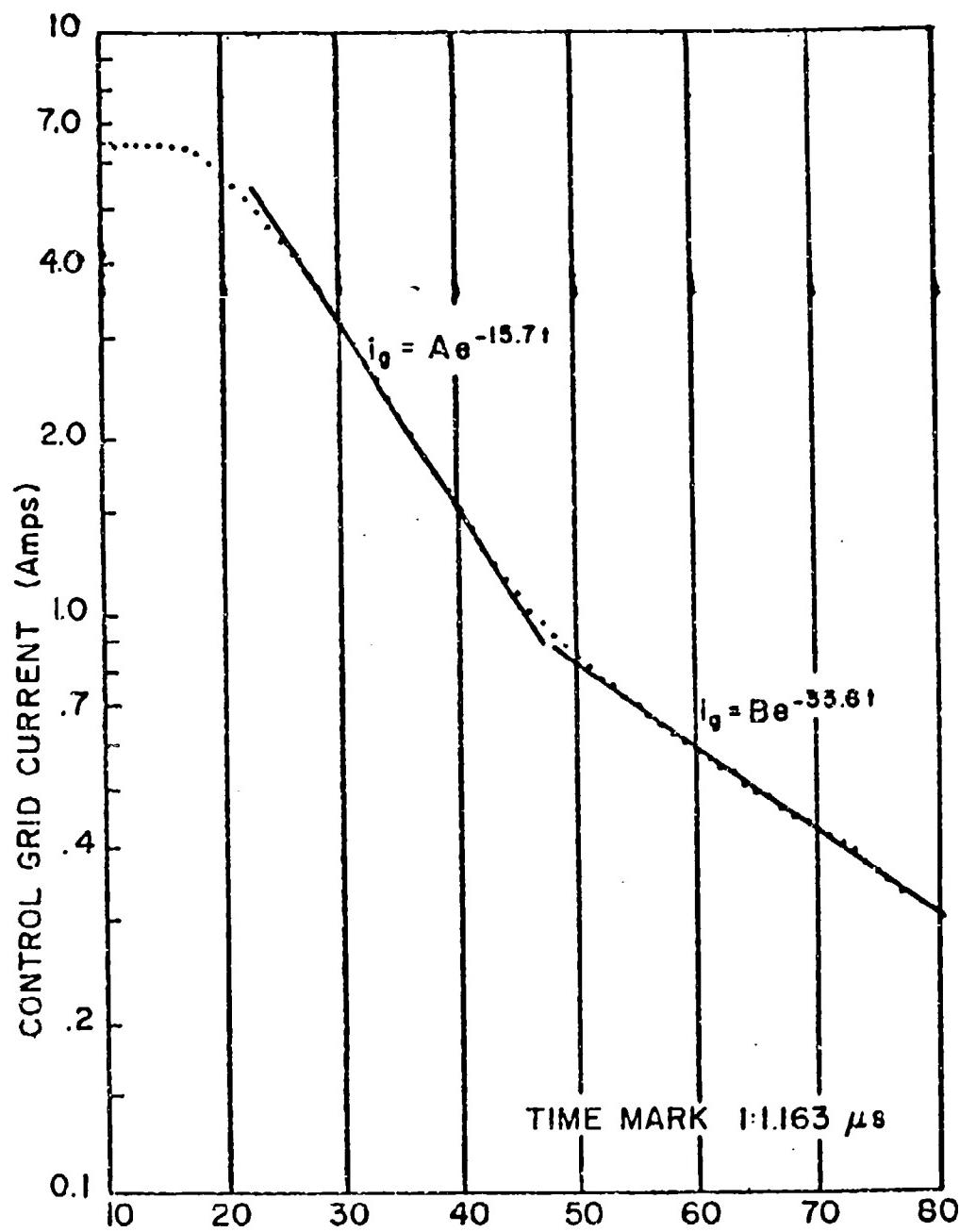


FIG. 11--LOGARITHM OF GRID CURRENT VS
TIME SHOWING THE EXPONENTIAL
DECAY OF GRID CURRENT DURING
THE RECOVERY PERIOD.

temperature). We hope to undertake such a theoretical study in the future along with our continued program of testing and study of the operation of the ignitron in pulse service.

REFERENCES

1. In its first phase of operation, the two-mile accelerator would produce a maximum electron energy of 20 Bev with an average beam current of 30 μ amps at that energy. Radiofrequency power would be supplied by 240 klystron amplifiers, each delivering up to 24 megawatts of peak power at the design frequency of 2856 Mc/sec. Each klystron would have its own modulator. By increasing the complement of klystrons to 900, it would be possible to increase the beam energy to 40 Bev and the average beam current to 60 μ amps. For a general description of the proposed Stanford machine, see R. B. Neal and W.K.H. Panofsky, "Progress Report on Proposed Stanford Two-Mile Linear Electron Accelerator," Proceedings of CERN Conference on High Energy Accelerators, CERN, Geneva, 1959.
2. T. F. Turner and H. S. Butler, The Microwave Journal, Vol. 5, No. 1, Jan. 1962, pp. 62-63.
3. D. B. Cummings, UCRL Report No. 5687, Electronic Engineering Department, Radiation Laboratory, University of California, Livermore, California (June 3, 1960).
4. L. Spitzer, Physics of Fully Ionized Gases, (Interscience Publishers, Inc., N. Y., 1956), pp. 16-18.
5. I. Langmuir and H. Mott-Smith, General Electric Review, 27, (1924), pp. 762-771.
6. T. J. Killian, Phys. Rev., 35, (1930), pp. 1238-52.
7. B. Klarfeld, Tech. Phys. of the USSR, 5, (1938), pp. 913-931.
8. L. Tonks and I. Langmuir, Phys. Rev., 34, (1929), pp. 876-922.

RESEARCH STUDY OF HARD TUBE MODULATOR LIMITATIONS

by

C. V. Weden

The Machlett Laboratories, Inc.

Introduction

The increasing use of vacuum tubes as switches of high pulse power led to a program, initiated in June 1959, to investigate the basic limiting factors in the design of tubes for these "hard tube" pulse generators. The scope of the study was restricted somewhat by the following major objectives: (a) high voltage hold-off in the region of 200 kV; (b) high current density, 10 amp/cm² or greater; (c) long pulse duration, 200 μ s or greater; and (d) pulse switching power of at least 35 megawatts. The goal of operation at a current density of 10 amp/cm², for example, dictated the use of an oxide type cathode. This type of emitter, in turn, influenced the choice of electrode geometry to be used in the model tubes built. The shielded-grid triode geometry, distinguished by a ground-potential "shield" between the control grid and the anode, has been shown to be highly desirable, and perhaps even necessary, for high-voltage pulse tubes using oxide coated cathodes.

First Year

The first year of the program was spent largely in improving processing techniques to reduce the residual gas pressure, and in improving stability by reducing cathode evaporation and interface resistance.

The first layout of an experimental structure to hold-off 200 kV was made using an active shield-grid to anode spacing of 6 cm. The state of the art on voltage breakdown vs. spacing between plane parallel electrodes was the 3/4-power relationship due to Kilpatrick⁽¹⁾. This relationship is plotted as Curve A in Fig. 1, which also includes the trend of observed data from several tubes of each cathode type up to about 100 kV. The breadth of curves B and C is a consequence of the field gradients on individual grid wires: tubes with higher amplification factor, and therefore higher screening fraction, have

(1) W. D. Kilpatrick, "Criterion for Vacuum Sparking Designed to Include both r-f and d-c," Rev. Sci. Instr., 28, 824-826 (1957).

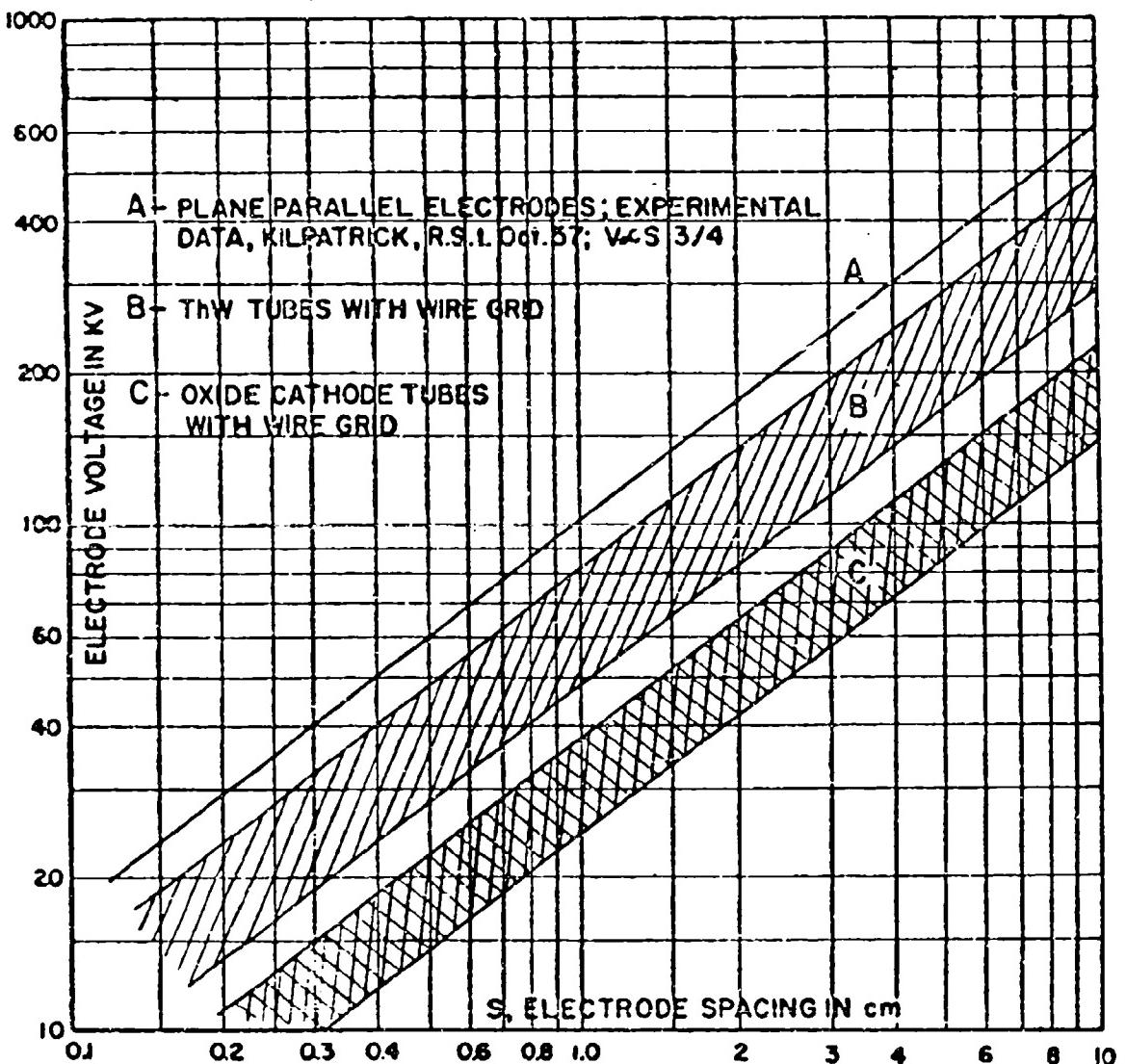


Fig. 1. Voltage breakdown vs. electrode spacing for plane, parallel electrodes (A), and trend of data from gridded tubes (B) with thoriated-tungsten cathodes and (C) with oxide coated cathodes.

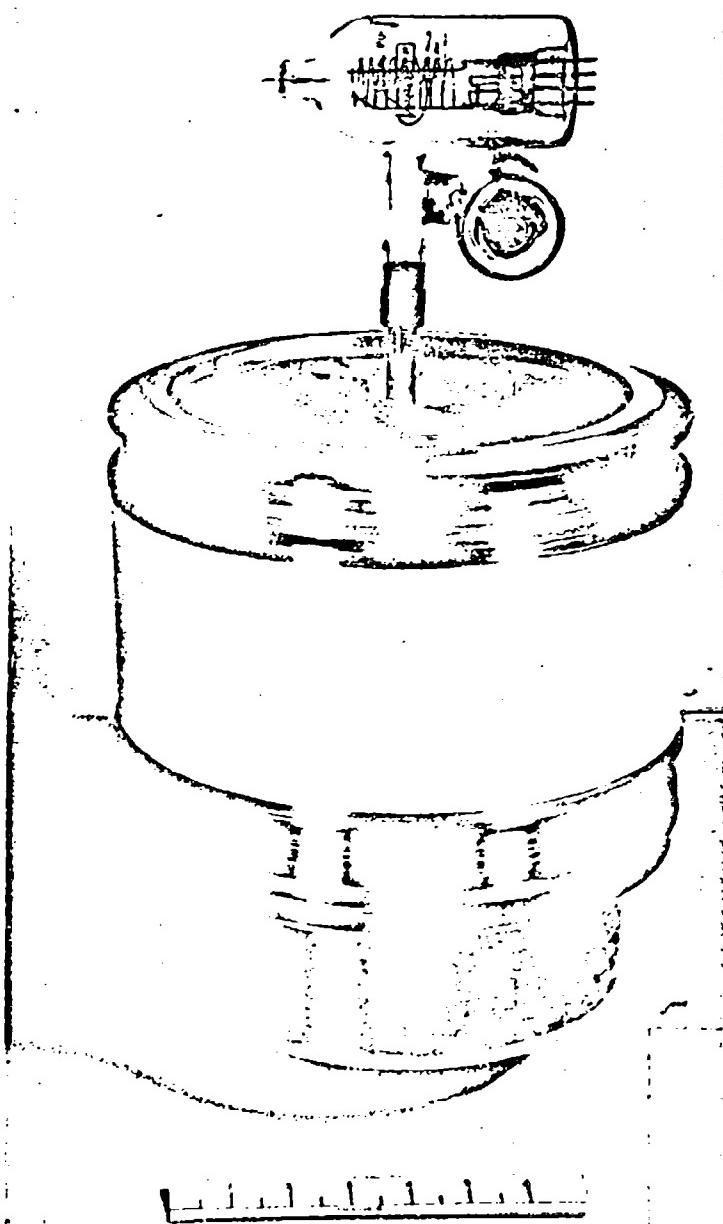


Fig. 2. High-voltage prototype tube Design L.

lower field gradients on the grid, and, for tubes with metallic cathode, approach curve A. One object was to test the validity of extrapolating curve C to 200 kV. Another object was to see if better processing of the oxide cathode, or some variation thereof, would shift curve B to the range of curve C. According to curve C, this layout could be expected to operate at about 150 kV.

The envelope design was aided by field plotting on resistive paper, although a compromise had to be made with a ceramic cylinder which could be procured in a reasonable time. Fig. 2 is a photograph of the resulting structure. Fig. 3 is a line drawing showing details of the envelope; the ceramic is 10" O.D. x 5" long x 1/4" wall. This "Design I" was "high-pot" tested to 160 kV and operational tested into a resistive load to 100 kV (equipment limitation). Subsequent high-votting resulted in failure at 160-165 kV due to puncture of the ceramic about an inch from the anode seal. Later internal examination confirmed that the limitation was the envelope insulator and not the active region of the tube.

The shielded-grid triode, with a ground potential shield adjacent to the anode, effectively protects the cathode and control grid from damage by transient arcs. At the beginning of this program, the beamng structures of this type geometry in use were suitable for cathode current densities up to 3.5 amp/cm^2 . Beyond this loading the plate to grid current division deteriorated rapidly. Concomitant to achieving 10 amp/cm^2 , therefore, was an implied objective to develop an electrode geometry to utilize this high current density. Gradual improvements resulted in a structure which fulfills this requirement. A sample tube of 30-cm^2 cathode area made with this electrode geometry was found to be capable of a pulse cathode current of 300 amperes. The plate/grid current ratio with equal grid and plate voltages (about 3250 volts) is nearly 30/1. It is significant that a current density of 10 amp/cm^2 has been achieved at this high a plate to grid current division without the use of a magnetic field.

The situation may be recapitulated by referring to Fig. 4. Curves A were taken from the ML-6904, a one-megawatt pulse tube which has been in production for five or six years. Curves B represent an attempt to attain a cathode current density of 10 amp/cm^2 . This goal was accomplished but grid current interception was unacceptable, as indicated by the divergence of the cathode and plate current curves. The end result is the desirable characteristics shown in Curves C. A schematic profile of a single beam unit for each case is given in the accompanying sketches. In each design the emitter is a concave strip, and the cathode-potential shield is the electrode between control grid and anode.

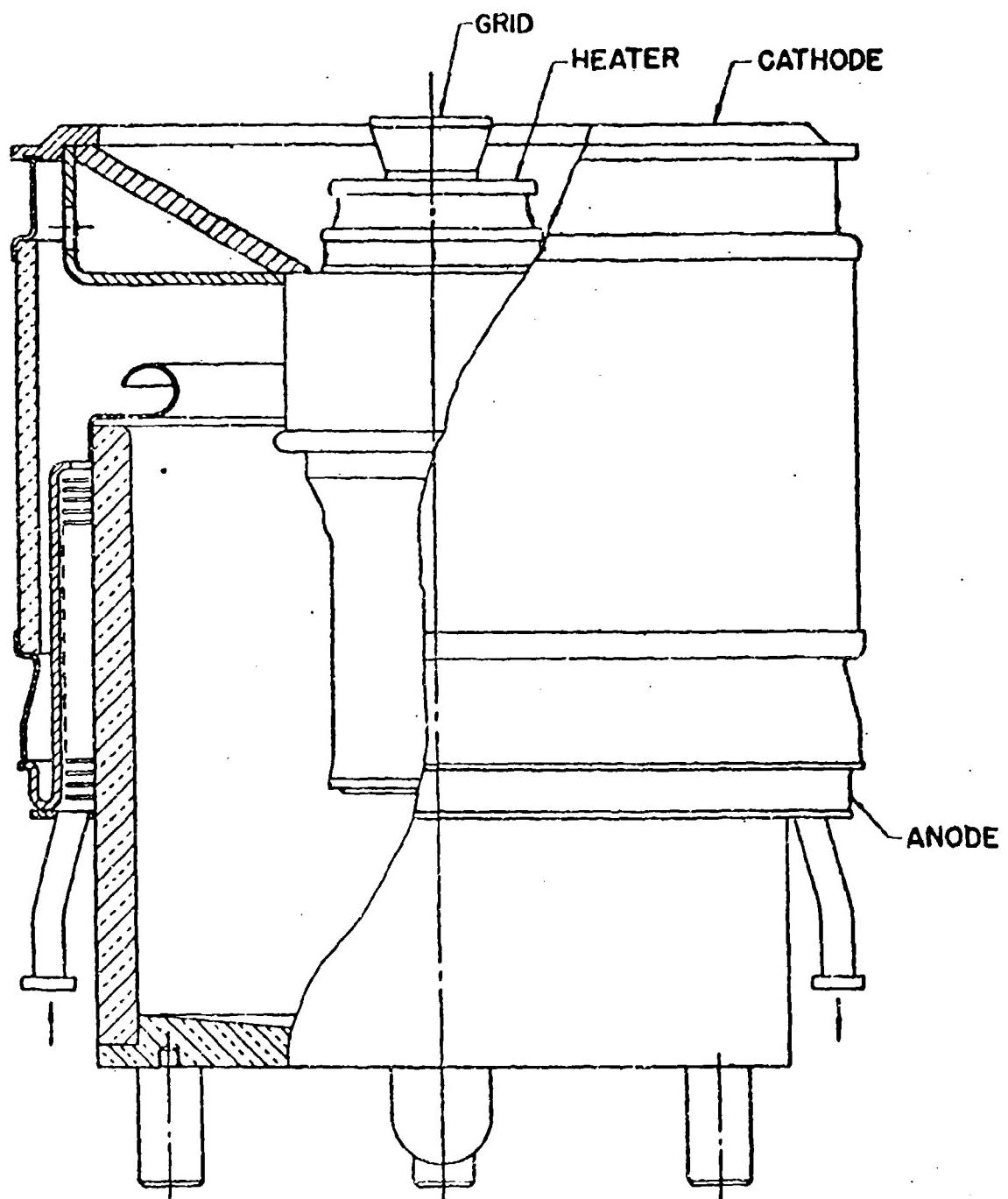


Fig. 3. Line drawing of Design I showing details of envelope.

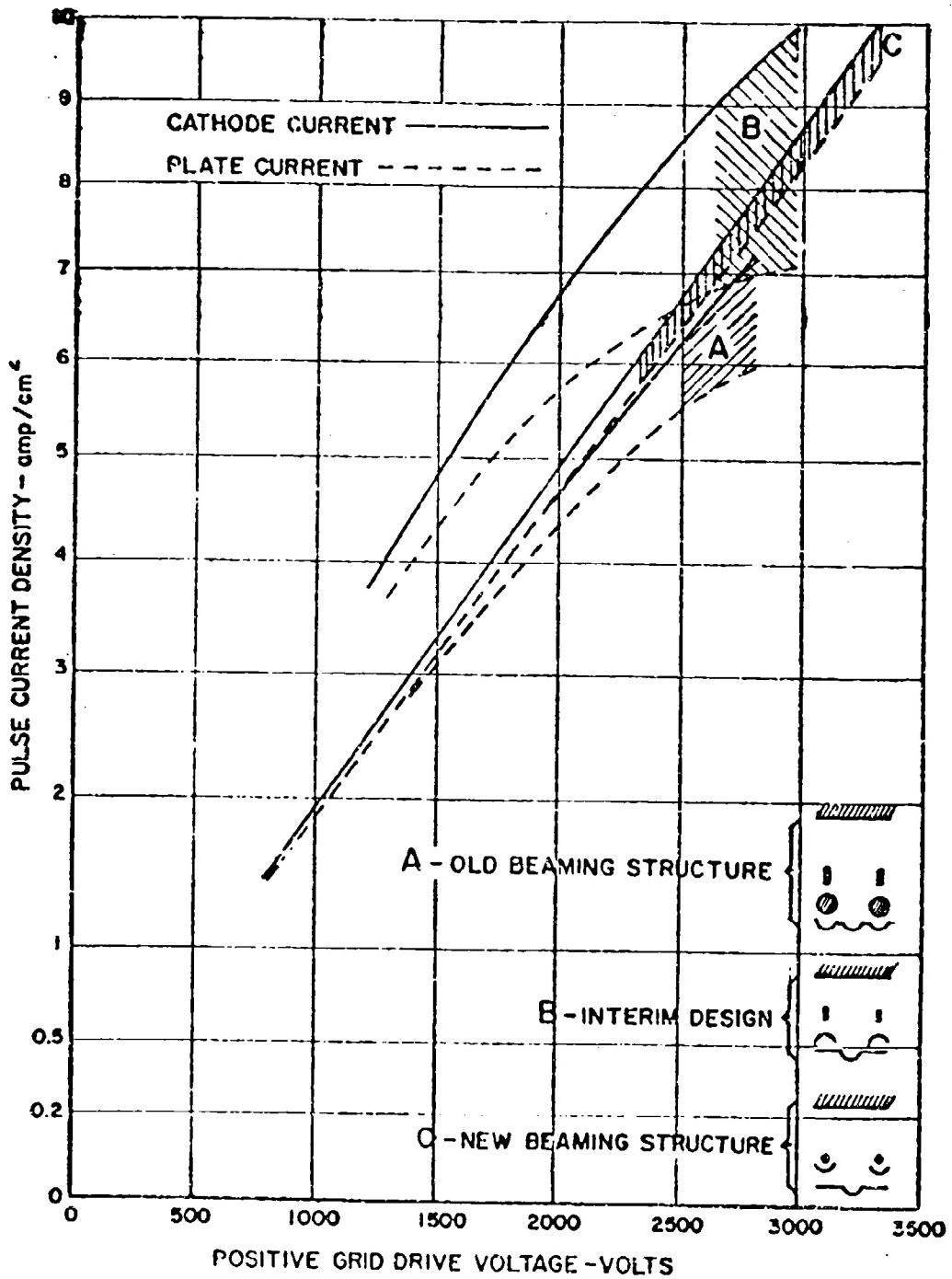


Fig. 4. Current density vs. positive grid drive voltage for three electrode geometries. Sketches show cross-section of single beam unit where concave strip is emitter and cathode-potential shield is electrode adjacent to anode.

Long pulse duration tests showed that with proper aging, a cathode current of 4-5 amp/cm² can be drawn for 200-microsecond pulses with negligible droop. In the range of 200-300 μ sec, observed droop is in the order of 2-3%. "Proper aging" consists of relatively long operation at high current density on short pulses.

An important part of the study was the use of an r-f mass spectrometer to make qualitative and quantitative analyses of the gases in typical tube structures. The device, as used in this experimental arrangement, is known as a total and partial pressure (TPP) gage.(2) The results of these experiments, in general, have since been corroborated by other researchers. In brief, it was observed that the major gas constituent in this type of tube is hydrogen, which accounts for more than 90 percent of the total pressure. The balance is made up of water vapor, carbon monoxide, and methane, with traces of other gases. Hydrogen and carbon monoxide are found to have strong temperature dependence, and methane shows a significant increase with the application of high voltage. Certain gases are detected under some operating conditions and not under others. The total pressure, furthermore, may remain almost constant as the operating conditions are changed, while pronounced and compensating changes take place in the constituent gases. Hydrogen in a large amount appears to have no detrimental effect on the cathode, however, this gas does impair high voltage stability.

Second Year

During the second year the initial work was carried to further refinement along with an investigation of a number of ancillary aspects of modulator tube design, such as anode heat transfer, effect of rms current density, peak charging current capability, x-radiation, and several other items. A discussion of these phases of the study is beyond the scope of this paper.

In addition, the overall objective was approached (1) by improved processing through the pumping of tubes in an external vacuum environment, and (2) by re-design of the envelope insulator and shielding.

A double vacuum pump station was built to pump tubes in a rough-vacuum environment in order to inhibit the diffusion of hydrogen and possibly other gases into the tube during the exhaust process. A vacuum of 20 microns was maintained in the

(2) P. F. Varadi, H. Langer, M. Saltzman, "Gas Composition During Pumping and in Sealed-Off Power Tubes", A.S.T.M. Special Tech. Pub. No. 300, pp. 193-203 (1961).

bell surrounding the tube, with the high-vacuum system capable of pumping down to 5×10^{-8} mm Hg. Interim evaluation did not produce any startling results, however vacuum-environment processing is considered a step in the right direction and worthy of further effort.

Prototype tube Design II was again a compromise. Although the ceramic cylinder was 1 inch longer, it was no larger in diameter, and did not offer much hope for improvement. The field on the end of the anode was reduced slightly by removing the shield. This model was tested to 200 kV for a short time, whereupon ceramic puncture occurred substantially as in Design I. In testing both of these models, sparking over the ceramic was observed prior to puncture, and the ceramic showed surface cracks close to the negative seal, suggesting that more effective shielding of this region was necessary.

With Design III the receipt of larger insulator and anode material permitted a more thorough redesign. Field gradients across the ceramic were reduced by using a cylinder 12" O.D. x 8" long x 3/8" wall, and the shield-grid to anode spacing was increased from 6 cm to 7.3 cm. The ceramic was also moved towards the negative terminal, to achieve better shielding of this seal.

From the tests on Design II and the improvements incorporated in Design III, it was considered feasible to switch power in excess of 35 megawatts at a d-c plate voltage at least up to 200 kV, using an oxide cathode with a 30 cm² emitting area. This represents a cathode current density of nearly 8 amp/cm². By making a straightforward increase in cathode length (and area) of 20-50 percent, the design would be capable of switching 45-55 Mw.

Towards the latter part of this phase the basic limitation to high-voltage operation gradually became apparent: bombardment of the envelope insulator by field-emitted electrons, probably from passive elements such as electrode supports and shields.

Third Year

The third year permitted time for evaluation of prototype tube Design III, and for a redesign of the structure based on these findings, striving principally to reduce the field gradient on apparent sources of field emission. Secondly, an investigation was begun on techniques to reduce the insulator resistivity in order to leak off wall charges which tend to accumulate. Additional areas of study in this phase of the project are (1) to develop an active getter of hydrogen, and (2) to investigate internal flash arc phenomena and methods of protecting the switch tube and its load. Further discussion is limited to testing and redesign of the high-voltage structures.

Design III was high-pot tested successfully to 250 kV, and then operational tested to 180 kV, again limited by the test equipment. Moderate instability was observed as the voltage was raised from 100- to 180 kV, however, the leakage current was low (less than 1 mA at 175 kV), and gas pressure and x-radiation appeared to be satisfactory.

In Design IV a 10"-long ceramic permitted the anode cylinder to be extended, providing more complete shielding of the insulator from the active region of the tube. It further permitted the cathode shield to be located further away from the anode, reducing the field gradient on this shield by nearly a factor of two.

Figure 5 shows section drawings of all four designs. In Design I, 80 percent of the field was concentrated over a length of 2.4 inches (6.0 cm), and the gradient at 165 kV where puncture occurred is 68 kV/inch (27 kV/cm). In Design II, 80 percent of the field covers 3.3 inches (8.4 cm), and the gradient at the maximum voltage attained (200 kV) is 60 kV/inch (24 kV/cm). In Design III the overall field gradient over the ceramic was reduced to about 40 kV/inch (16 kV/cm) at 200 kV. It will be appreciated from inspection of the drawing that Design IV further reduces the gradient over the ceramic and on the negative (cathode) shield.

Figure 6 is a photograph of the 200-kV, 40-kilowatt-average modulator test facility which Machlett Laboratories designed and built within the past year. This test set has been used for testing Design III, and will be used for Design IV. Fig. 7 is a photograph of Design IV, which we expect to fulfill all of the initial objectives of the contract.

While some additional refinement of this design is in order to reduce the frequency of kick-outs, it is significant that 200 kV hold-off voltage has been attained in a tube with an oxide cathode.

Acknowledgements

The research described in this paper has been pursued under sponsorship of BuShips on Contracts N0bsr-77593 and N0bsr-85440.

The author wishes to acknowledge the contributions of Dr. H. D. Doolittle for overall direction of the program, to Helmut Langer, Development Engineer, and to the supporting staff of engineers and technicians.

FIG. 5

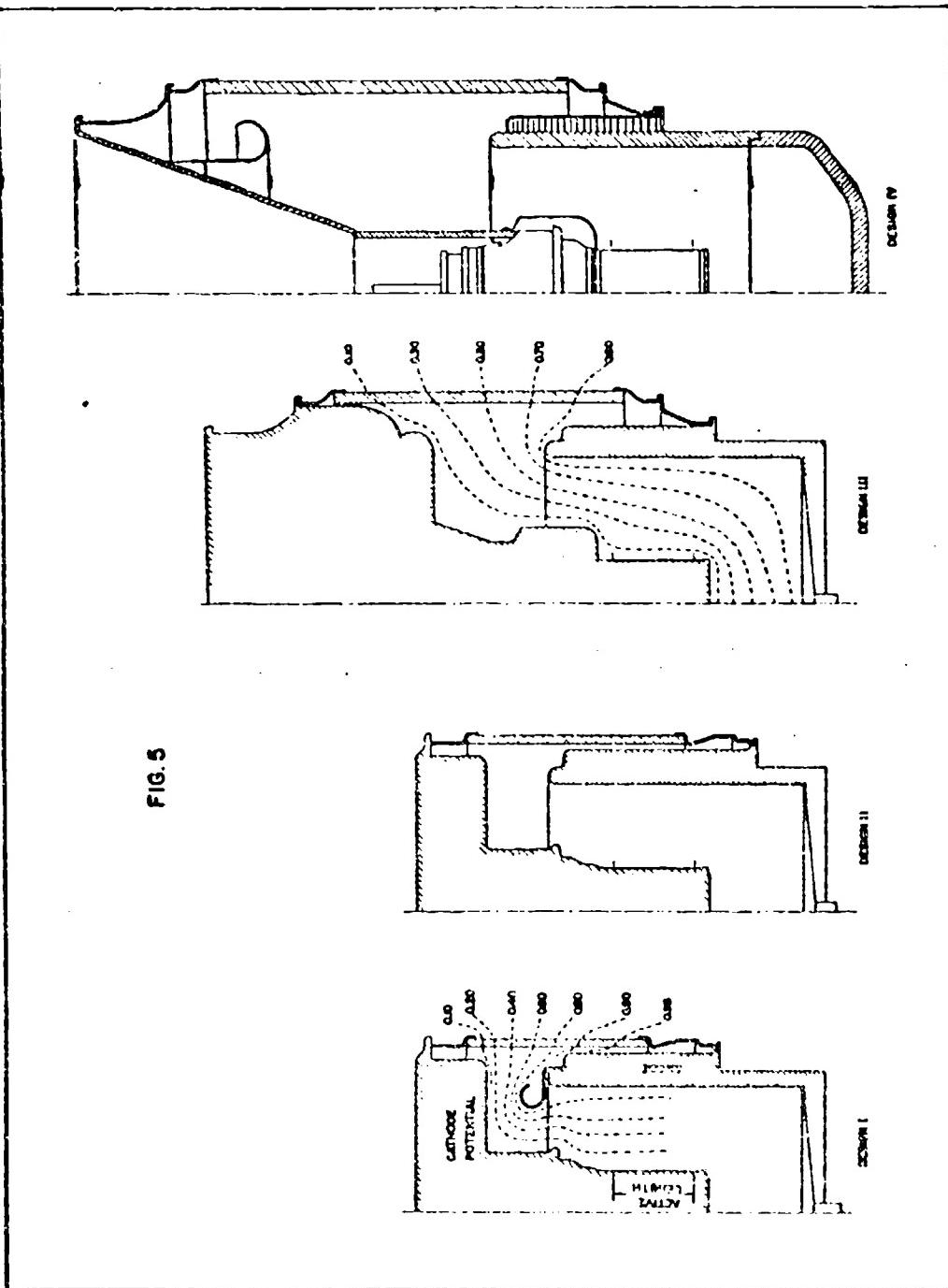


FIG. 5. Section drawings of all four designs of high-voltage prototype tube showing space-charge-free operation of equipotential lines on Design I and Design III.

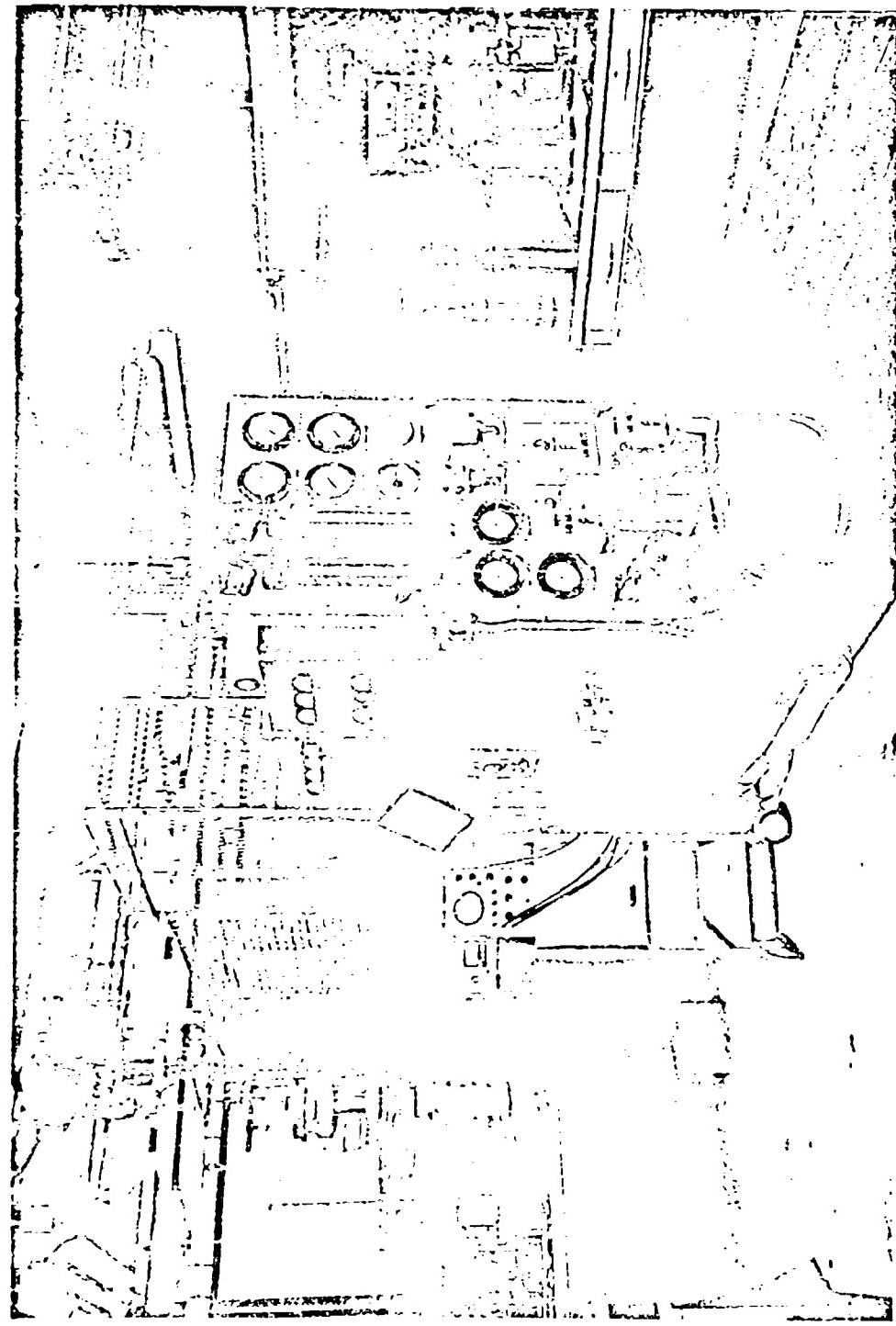


Fig. 6. 200-kilovolt, 40-kilowatt average pulse modulator test facility designed and built at Machlett.

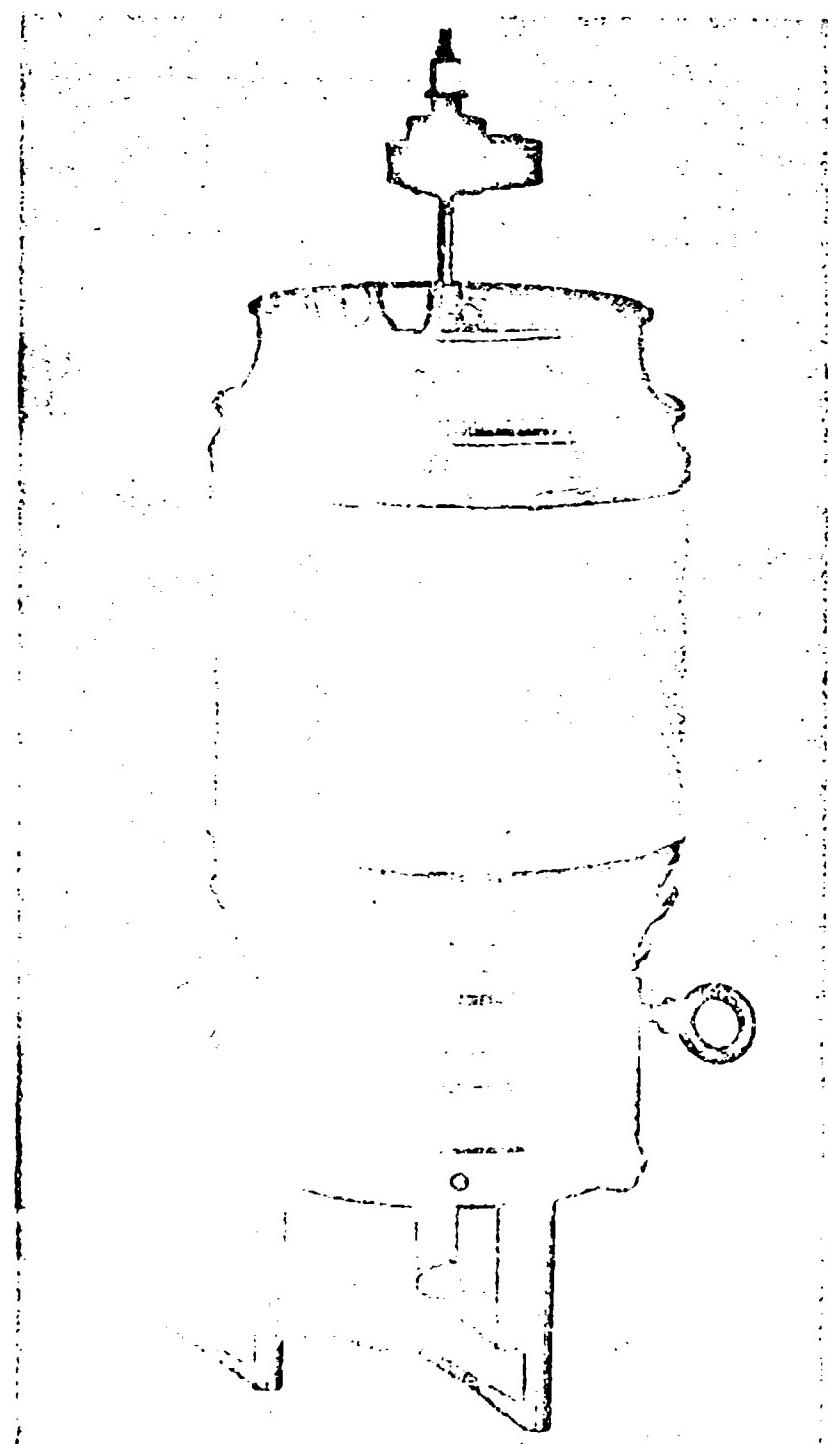


Fig. 7. High-voltage prototype tube Design IV.

ABSTRACT.

DESIGN AND APPLICATION OF THE "INJECTION"

Lowell J. Fox

Litton Electron Tube Corporation
San Carlos, California

The "Injection" is an oxide-cathode high-current, high-voltage modulator tube recently developed by the Litton Electron Tube Corporation. The basic format of this tube is the magnetron injection, a slot forms the cathode and control electrode, and eliminates the requirement for intercepting grid structures.

The design criteria that gives the "Injection" its unusual constant current characteristics and make the use of oxide-coated cathodes feasible at extremely high voltages will be discussed in the paper, in addition to some typical applications for which the "Injection" is particularly suited.

The magnetron injection gun geometry completely shields the cathode from the high voltage portion of the tube in such a manner that it is virtually impossible for an internal arc to terminate on the emitting surface. By employing a magnetic field, the control electrode is made practically non-intercepting, therefore requiring a relatively low power drive signal. This geometry also eliminates the requirement for fine grid wires and control electrodes that are susceptible to damage by internal arcs and high dissipation requirements.

The L-3408 was the first "Injection" developed for use in a floating deck modulator delivering a 150-kilovolt pulse at high repetition rates. Other tubes that are currently under development will be described.

In addition to the floating deck modulator application, other uses for the "Injection" based on its high control electrode dissipation capability and constant current characteristics will be discussed, along with photographs of typical circuits, data, and tube geometry.

SOME ADVANCES IN THE TECHNOLOGY
OF
MODULATING ANODE PULSERS
FOR
HIGH POWER KLYSTRONS

by

C. Pappas

Radio Corporation of America
Defense Electronic Products
Missile and Surface Radar Division
Moorestown, New Jersey

1. SUMMARY

With the advent of the modulating-anode pulser it has become possible to drive high voltage, high power klystrons operating at long pulse widths and low pulse repetition frequencies in a rather straight forward manner. However, the application of this same technique to high power klystrons operating at narrow pulse widths and high pulse repetition frequencies dictates the necessity for improvements and advances in the state of the art for mod-anode pulsers. For example, transmitters operating thus, which demand average power levels in the multi-kilowatt region require that the amount of power wasted during the pulse rise and fall time be minimized in the interest of economy and consistent with good design practice. In addition, the operation at high PRF's and narrow pulse widths imposes additional requirements for protection of pulser components from arcing within the tube. Finally, the design philosophy for the pulser for the TRADEX L-Band Transmitter utilizes a new type of Beam Switch Tube developed especially for TRADEX, as well as a unique mechanical configuration and packaging. Block diagrams, schematics, photographs and theory of operation are presented to illustrate this particular application of the modulating-anode pulser.

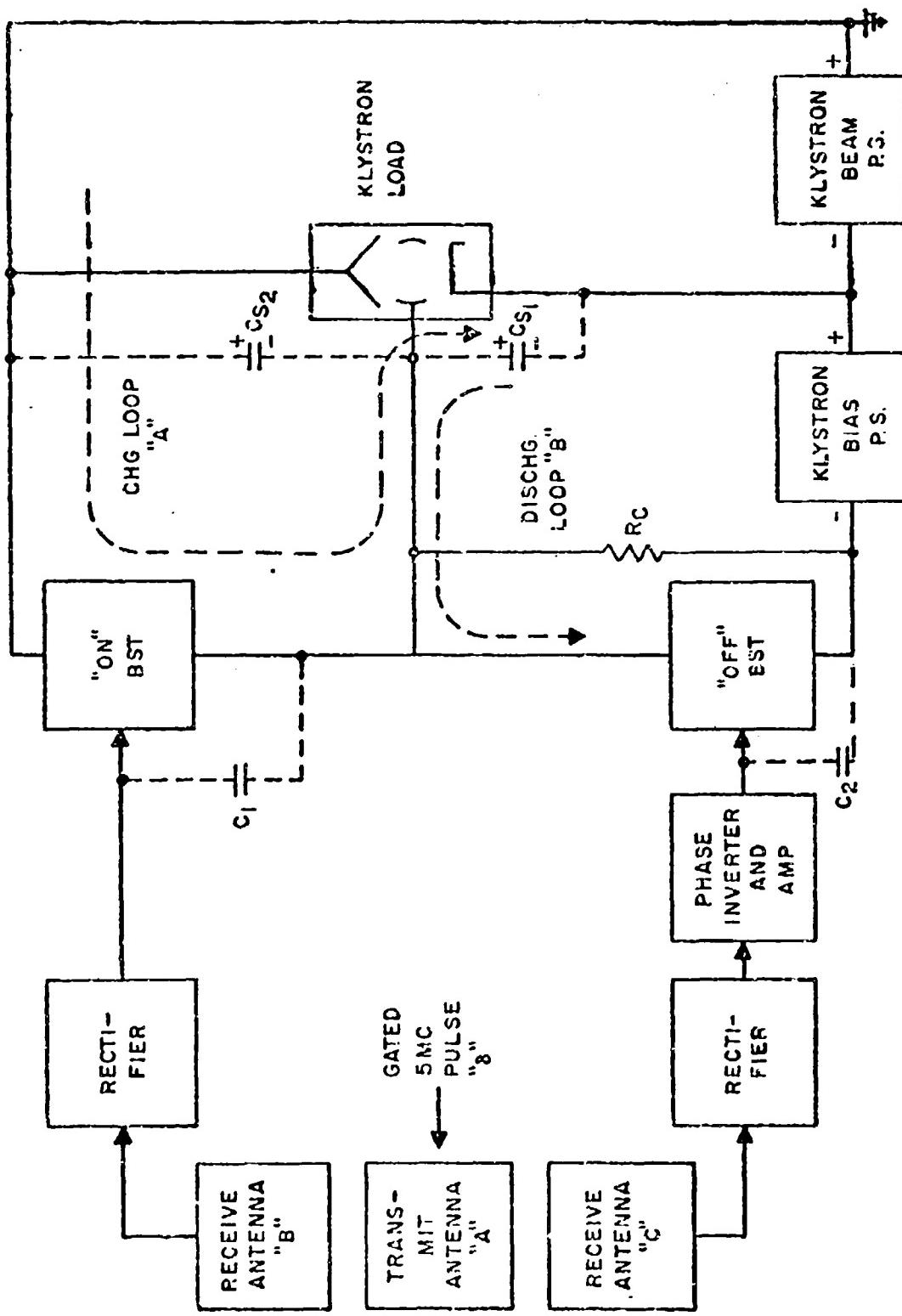
2. INTRODUCTION

Modulating-anode pulsers or floating deck pulsers for modulating the control element of high power klystrons are not new to the art. Literature shows that this type pulser has been used with a good deal of success especially with pulse rise and fall times measured in the order of 10 to 50 microseconds and with RF power output levels less than 100 KW average. Extending the operating range of this type of a pulser in both power level and improved pulse characteristics has posed some interesting and challenging problems. These include the development of a new beam switch tube type L-3408 by Litton Industries², the attainment of rise and fall times in the order of 5 to 10 microseconds (10 to 90%) and a means of accommodating the necessity for permitting a klystron to arc especially during a seasoning process. Combined with these features is the development of a unique packaging configuration for the pulser and the klystron load which it drives. A review of the modulating-anode pulser followed by a discussion of these new features is presented in this report.

3. MODULATING-ANODE PULSER BLOCK DIAGRAM AND THEORY

A simplified block diagram of a rather conventional mod-anode pulser is given in Figure 1. Basically it consists of an "ON" BST which has the dual function during the start of the pulse of charging the stray capacity C_{S1} of the mod-anode of the klystron via charge loop "A" and also of discharging C_{S2} . The "OFF" BST discharges the stray capacity C_{S1} via loop "B" and it also charges C_{S2} at the end of the pulse. The beam power supply is represented by E_{BB} and the bias for the klystron is E_C . Receiving "Antennas" "B" and "C" which supply a 5 MC signal for generating the mod-anode waveshape are coupled to a transmitter antenna "A". A pulse of 5 MC RF equal to the video pulse width desired on the mod-anode of the klystron is delivered to Antenna "A". It is coupled to the high voltage isolated antennas "B" and "C". In the "ON" channel, this RF signal is rectified and rectified pulse voltage is applied to the mod-anode element of the "ON" BST. As soon as the stray capacity of this BST begins to charge the BST will deliver a charging current up to 20 amperes via loop "A" to the stray capacity and it will also discharge C_{S2} . As this load stray capacity C_S is charged to a full beam voltage the tube and voltage drop across BST "A" gradually decreases also. This tube drop eventually becomes so low as to equal the mod-anode drive voltage on BST "A", at which time the impedance of the rectifier circuit and the loading effect of the mod-anode of BST "A" reduce the charging current through loop "A" to a small value sufficient to maintain a mod-anode beam interception of 0, 1% to 1.0%. Simultaneously while the "ON" BST is being turned on, the rectified pulse voltage developed in the "OFF" circuit is passed through a phase inverter and is used to turn off the "OFF" BST for the duration of the pulse width. At the end of the pulse, the pulsed 5 MC signal is turned off. The "OFF" BST is turned on and begins to discharge the stray capacity of the M-A of the klystron and pulser components and also charge C_{S2} . The waveforms for this type of operation are given in Figure 2. Typical operating conditions and a photograph of the L-3408 BST are shown in Figure 3. Characteristic curves and the outline drawing for the L-3408 BST are given in Figure 4.

FIGURE 1 - SIMPLIFIED BLOCK DIAGRAM OF MODULATING ANODE PULSER - SK-41662-3-CP



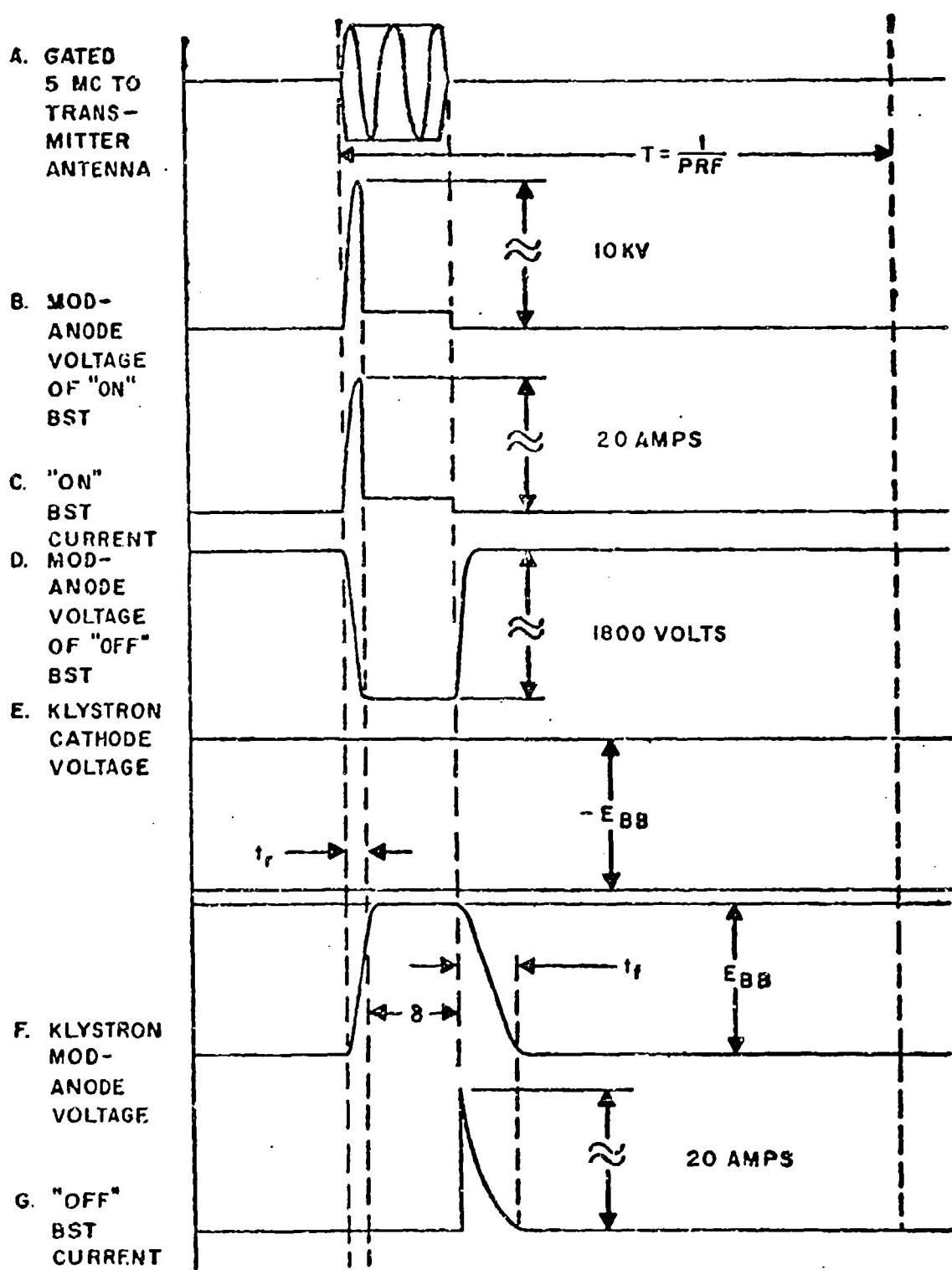


FIGURE 2 - IDEALIZED WAVEFORMS FOR MOD-ANODE PULSER - SK-41662-4-CP

SWITCH TUBE

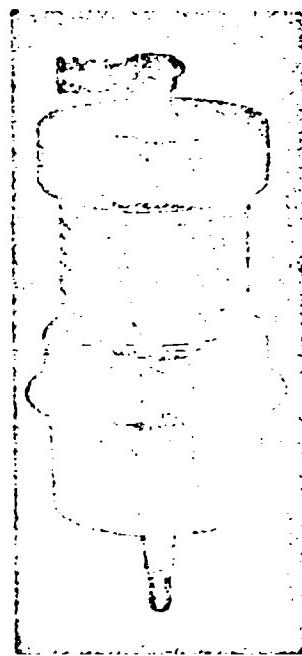
L-3408

The L-3408 Switch Tube is intended for use in high-voltage, high-switch rate, floating deck modulator applications. Features include unusually high hold-off voltage; low voltage drop at the operating current; high plate dissipation capability; pentode-like constant current characteristics; and rugged metal-ceramic construction.

Additional features: A cathode configuration permitting high peak current density with relatively conservative cathode loading; a high μ control element, which is virtually non-intercepting to the electron beam; a cathode configuration shielded from the high voltage of the collector; and ease of extension to high hold-off voltage or switching current, or both.

TYPICAL OPERATING CONDITIONS

Collector Voltage (hold-off)	150 Kv
Collector Current	20 Amps
Collector Dissipation	10 KW
Pulse Length		
t_c = 1 Amp	10 m.sec
t_c = 20 Amps	10 μ sec
Duty Cycle		
I_c = 1 Amp	0.1
I_c = 20 Amps	0.006
Mod. Anode Voltage at		
I_c = 1 Amp (max.)	2.5 Kv
I_c = 20 Amps (max.)	10 Kv
Mod. Anode Current (max.)*	100 mA
Mod. Anode Perveance (approximate) at		
I_c = 20 Amps	20×10^{-10}
Mod. Anode Bias (max.)	1000 v
Capacity (Mod. Anode to all electrodes)	$35 \mu\text{f}$
Heater Voltage	12 v
Heater Current	6 ± 5 Amps
* At $I_c = 20$ Amps and $E_o > 15$ KV		



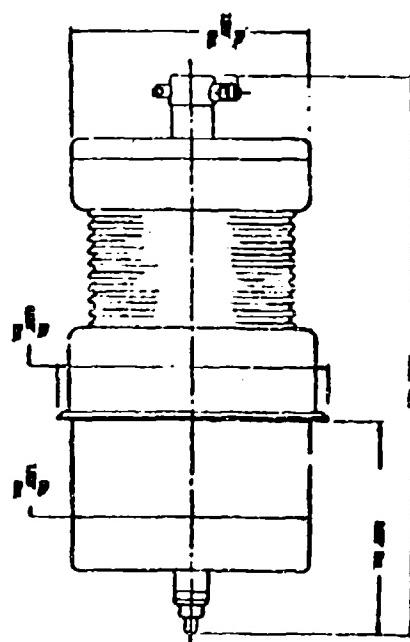
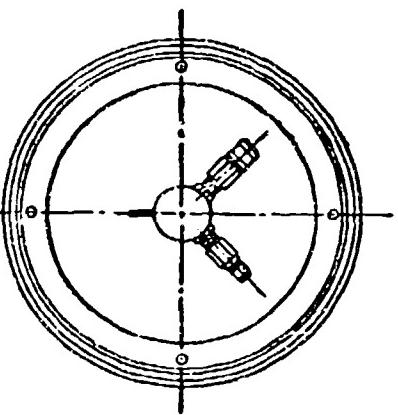
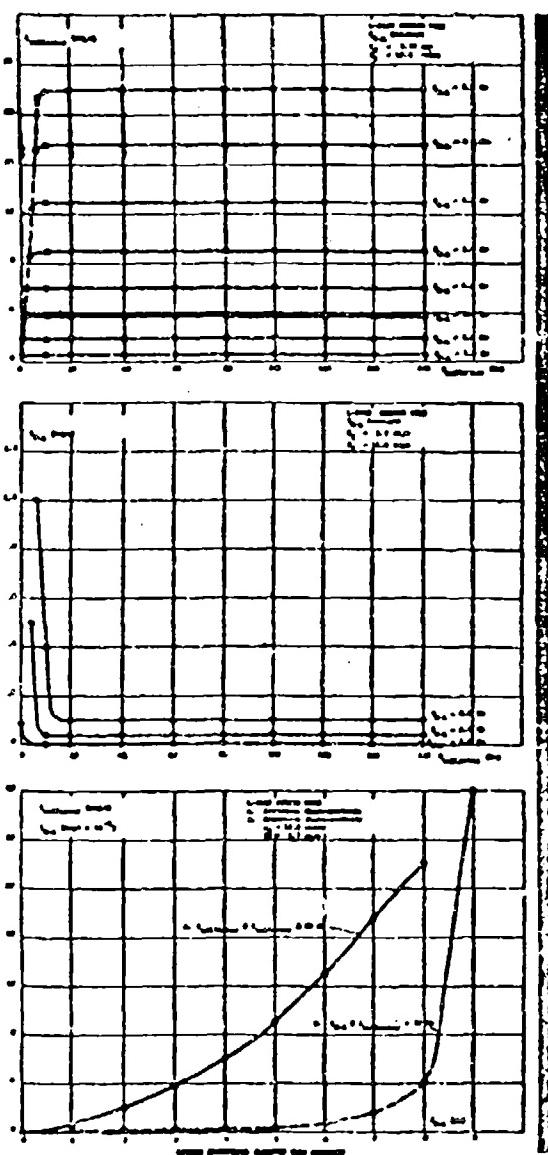
MAXIMUM RATINGS

Collector Voltage (hold-off)	200 Kv
Collector Current	30 Amps
Collector Dissipation	12 KW

MECHANICAL DESCRIPTION (approx)

Length	20 inches
Diameter, including magnets	8 inches
Weight, including magnets	45 pounds

FIGURE 3 - L-3408 BEAM SWITCH TUBE AND TYPICAL OPERATING CONDITIONS
REPRODUCED COURTESY OF LITTON INDUSTRIES,
ELECTRON TUBE DIVISION, SAN CARLOS, CALIF.



L-3408 SWITCH TUBE

FIGURE 4 - L-3408 BEAM SWITCH TUBE OUTLINE
DRAWING AND CHARACTERISTIC CURVES
REPRODUCED COURTESY OF LITTON INDUSTRIES
ELECTRON TUBE DIVISION, SAN CARLOS, CALIF.

4. PULSER WITH FEEDBACK CIRCUIT

One of the ways of decreasing the fall time of the voltage pulse applied to the mod-anode of the klystron is to use feedback. A pulse transformer placed in the cathode of the "OFF" BST with a step up ratio N of about 5:1 can be used to drive the mod-anode of the "OFF" BST. A circuit using this scheme is given in Figure 5. Figure 6 is an oscilloscope photograph of a typical mod-anode waveform using feedback to reduce the fall time. Here the 10 to 90% fall time is 5 microseconds at 100 KV mod-anode swing on a stray capacity of about 500 micro-microfarads. For purposes of comparison a typical fall time value without feedback would be 50 to 75 microseconds.

Another circuit modification can be made to avoid undesired effects of arcing between the anode and mod-anode of the klystron. One commonly used method is to insert a high value resistor in series with the mod-anode of the klystron as illustrated in Figure 7. When the mod-anode arcs in this circuit, the mod-anode is biased back by the current and the tube is cut off. This circuit works well where slow rise and fall times, and where dissipation in this biasing resistor can be tolerated. Where fast rise and fall times are a necessity, one may use a much smaller resistor; or what is better is to use a clamping circuit. This clamping circuit functions to clamp the mod-anode of the "OFF" BST back to its cathode. The clamping circuit is driven by the pulse transformer feedback circuit mentioned earlier. It employs 7665/KU-72 hydrogen thyratrons as the clammer tube. A typical circuit using a clammer tube is given in Figure 8. Sufficient resistance, R_2 , is inserted in series with the anode of the 7665/KU-72 to limit the current in the thyratron to a safe value when it goes into constant conduction. If desired, the thyratron can be left in a continuous conduction state for a short time after which a high voltage relay is used to open the anode circuit, and thus deionize the thyratron. Waveforms showing the tail of the pulse with and without the clammer tube firing are shown in Figure 9.

5. POWER DISSIPATION IN BST COLLECTOR

The dissipation in the collector of the "ON" BST may be determined a number of ways. These include graphical analysis, calorimetric measurement of the heat loss in the BST collector coolant lines, and a consideration of the stored energy in the mod-anode pulser stray capacity. The charging of this mod-anode stray capacity by means of a BST is a circuit problem in resistance charging. Therefore, the equations relating to this application will be developed first and then the various methods will be discussed. The simplified circuit for resistance charging is given in Figure 10.

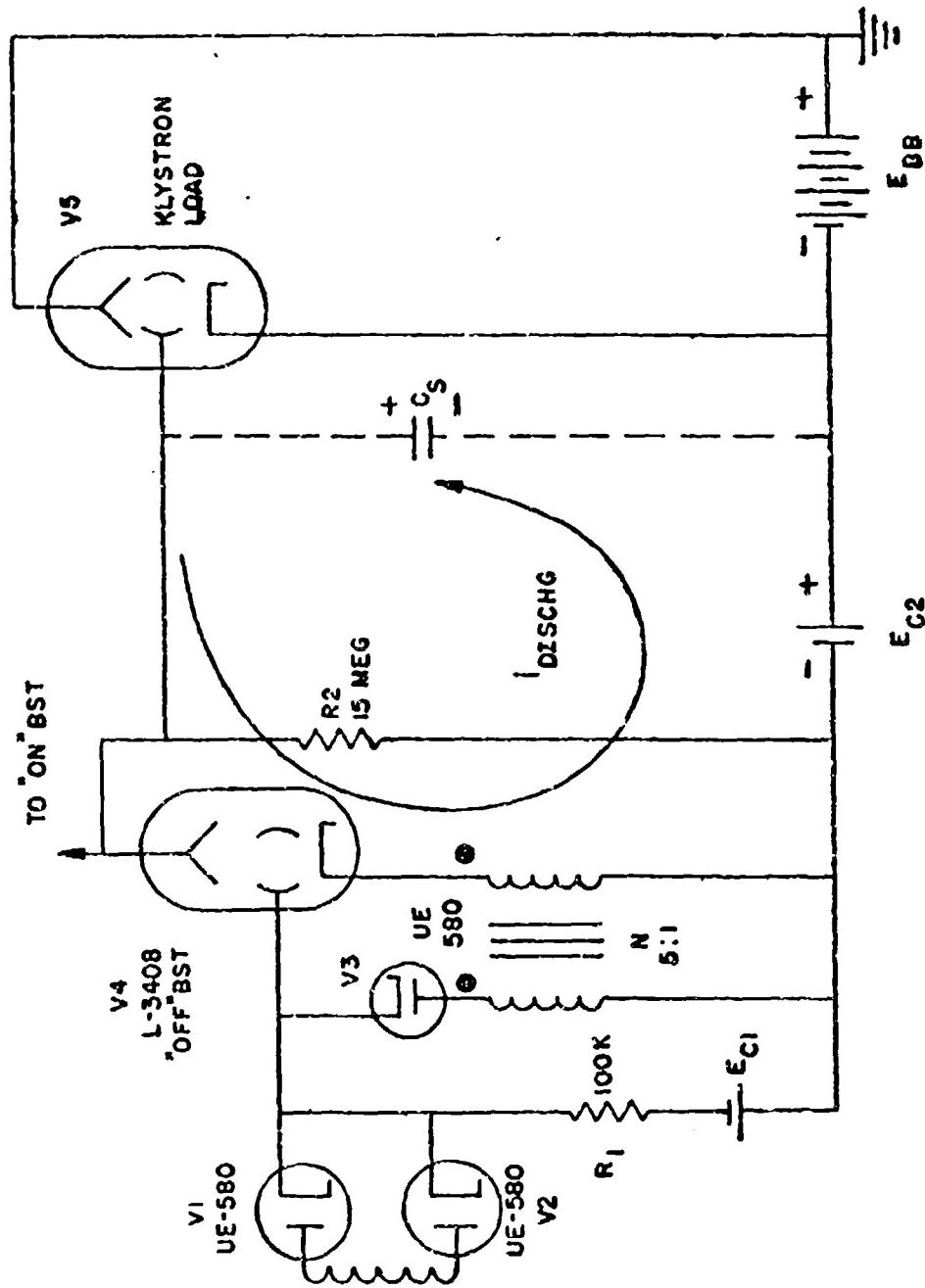
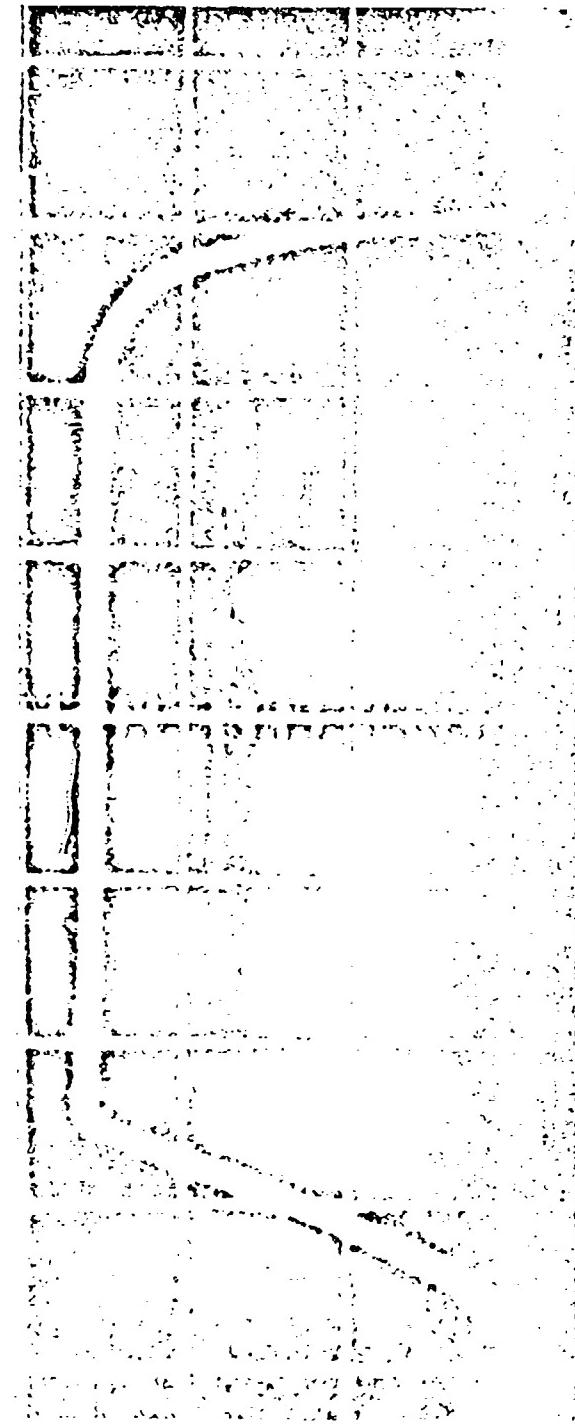


FIGURE 5 - "OFF" BST CIRCUIT SHOWING FEEDBACK CIRCUIT TO DECREASE FALL TIME
(PHASE INVERTER CIRCUIT OMITTED FOR SIMPLICITY) - SK-61062-1-CP



L3401 S/N 21 BEAM VOLTAGE APPROX. 100KV
AMP SENS = 20 V/CM SS = 10μ SEC/CM
REF: LOG #3 - PAGE 41 - SK-41862-1-CP

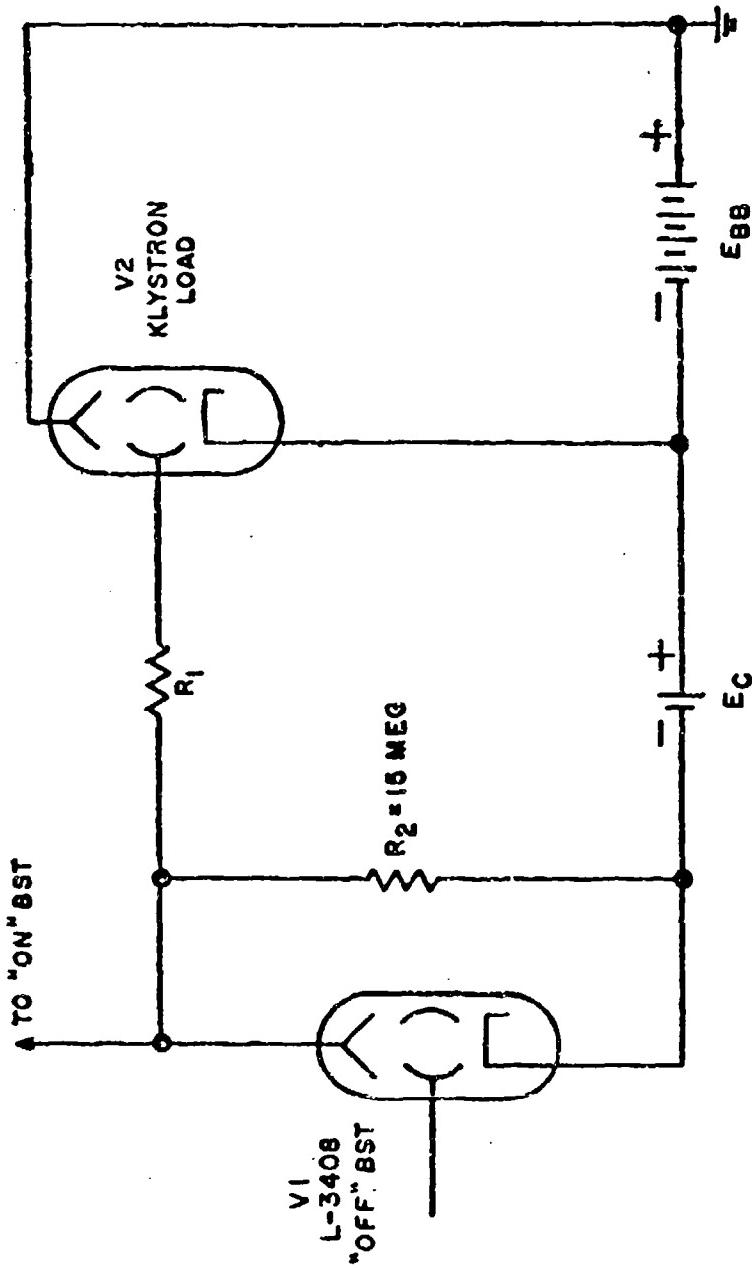
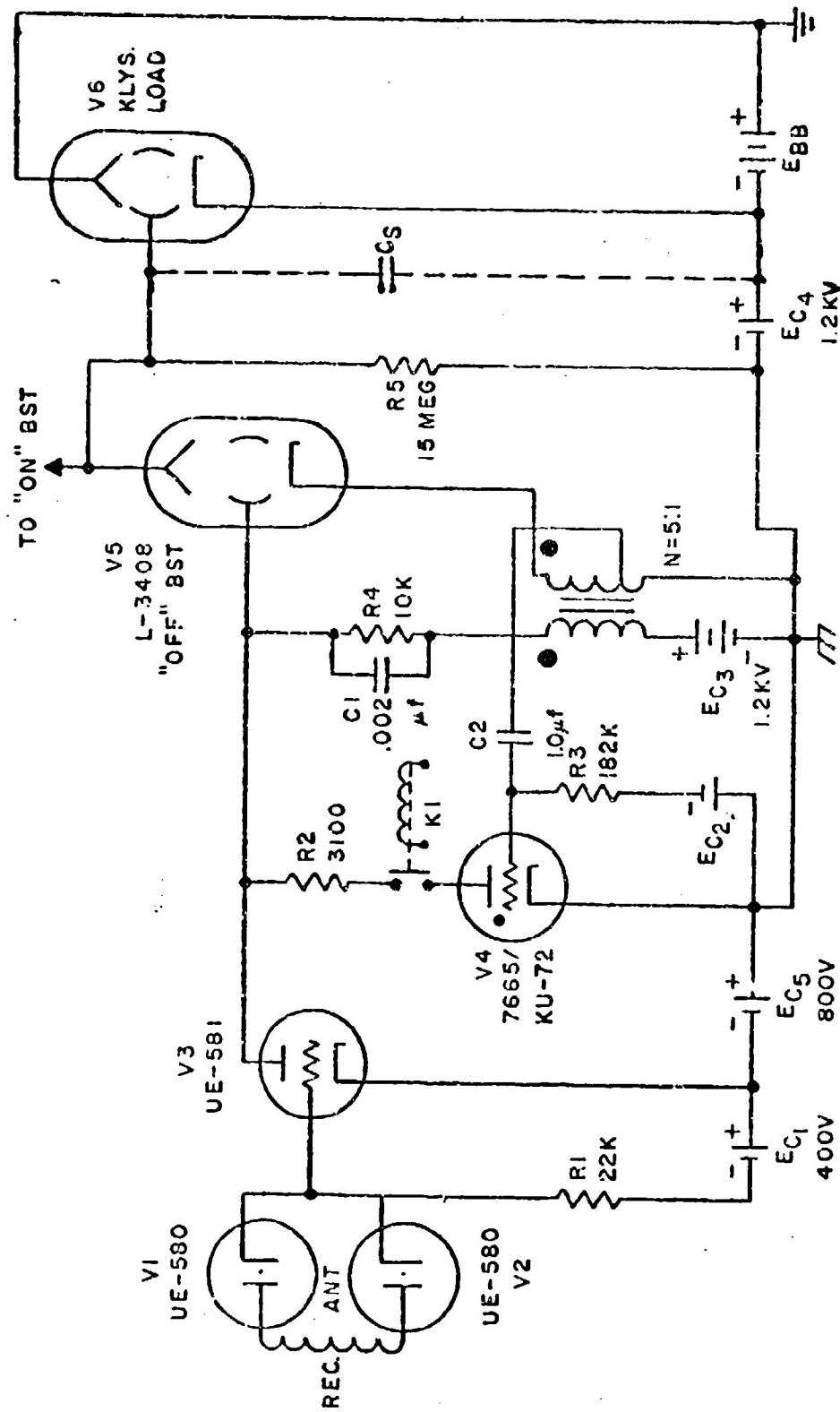


FIGURE 7 - "OFF" BST PULSER CIRCUIT WITH MOD-ANODE SERIES LIMITING RESISTOR, R₁ • SK-41162-4-CP

FIGURE 8 - "OFF" BST CIRCUIT EMPLOYING A CLAMPER TUBE - SK-51062-2-CP



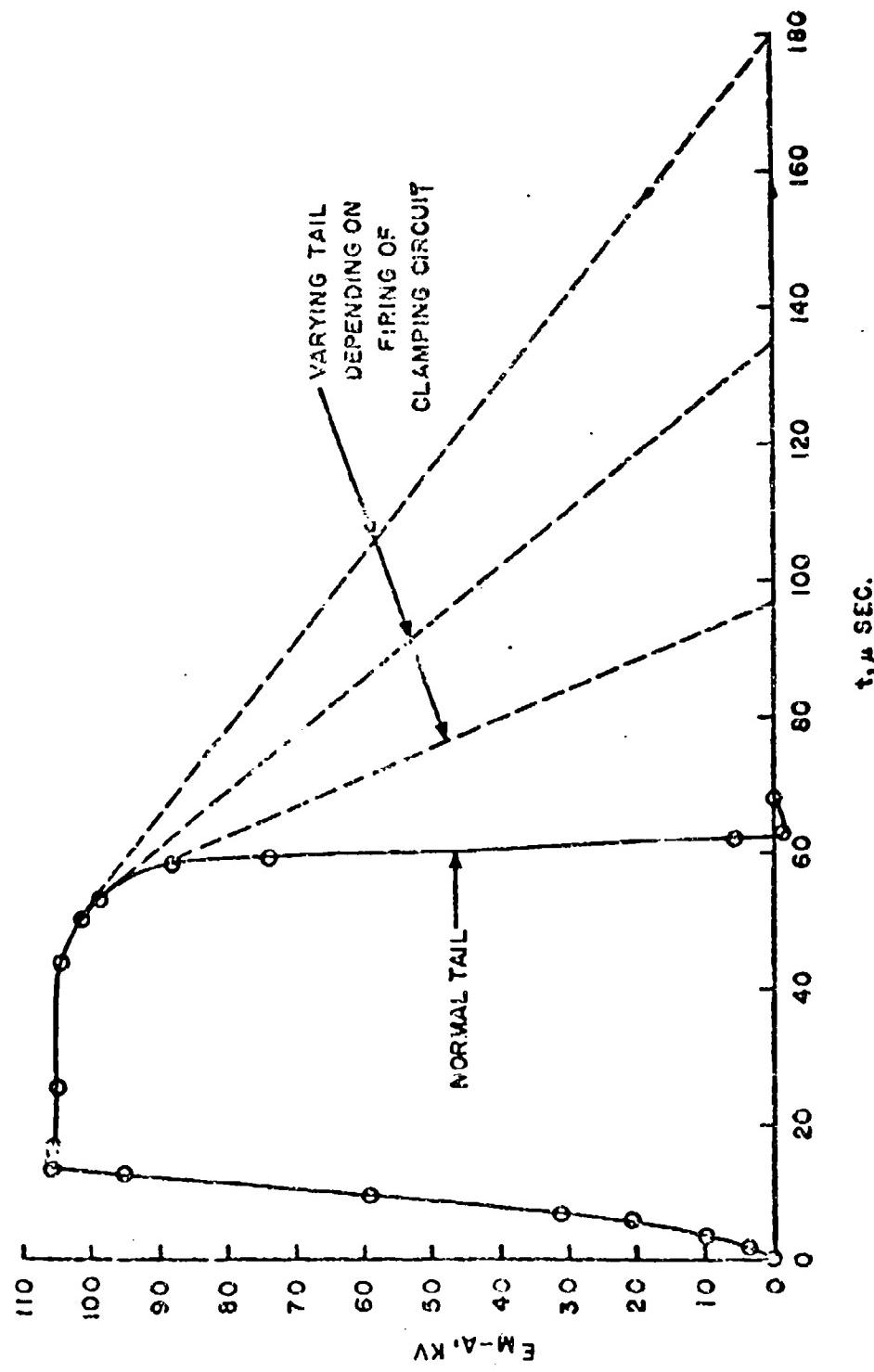


FIGURE 9 - TYPICAL KLYSTRON MOD-ANODE VOLTAGE WAVEFORM ILLUSTRATING EFFECT OF CLAMPING CIRCUIT ON TAIL OF PULSE - SK-42762-2-CP

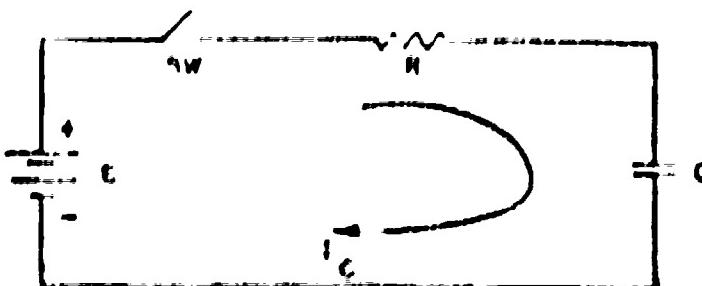


FIGURE 10 - EQUIVALENT CIRCUIT FOR RESISTANCE CHARGING

The current is given by

$$(1) \quad I = E - \frac{R}{L} Q^{-\frac{1}{LC}}$$

and the capacitor voltage is given by

$$(2) \quad C_o = E \left(1 - Q^{-\frac{1}{LC}} \right)$$

The dissipation in the resistor R is given by

$$(3) \quad P_R = \frac{1}{2} \int_0^t I^2 R dt$$

$$(4) \quad = \frac{1}{2} \int_0^t \left(E - \frac{R}{L} Q^{-\frac{1}{LC}} \right)^2 R dt$$

$$= \frac{E^2}{R} \int_0^t Q^{-\frac{2}{LC}} dt$$

$$= \frac{E^2}{R} \int_0^t Q^{-\frac{2}{LC}} dt$$

$$= \left(\frac{E^2}{R} \right) - \frac{E^2}{R} \int_0^t Q^{-\frac{2}{LC}} \left(-\frac{2}{LC} \right) dt$$

$$(5) \quad P_R = \frac{-E^2 C}{2T} \left[\Theta - \frac{2t}{RC} \right]_0^t$$

$$(6) \quad = \frac{-E^2 C}{2T} \left(\Theta - \frac{2t}{RC} - 1 \right)$$

$$(7) \quad = \frac{CE^2}{2T} \left(1 - e^{-\frac{2t}{RC}} \right)$$

Letting

$$(8) \quad t = T = \frac{1}{PRF}$$

and

$$(9) \quad \alpha = \frac{T}{RC}$$

and substituting in (7)

$$(10) \quad P_R = \frac{CE^2}{2T} \left(1 - e^{-2\alpha} \right), \text{ Watts}$$

The stored energy in C is given by

$$(11) \quad \text{Energy} = 1/2 C \Theta_0^2 \\ = 1/2 C E^2 \left(1 - e^{-\frac{t}{RC}} \right)^2$$

which is a maximum for

$$(12) \quad RC \ll T$$

and

$$\text{Energy} = 1/2 C E^2, \text{ Watt-seconds}$$

$$\text{or} \quad W_a = 1/2 \frac{CE^2}{T}, \text{ Watts}$$

$$\text{Returning to (11), (13)} \\ \text{Energy} = 1/2 C E^2 \left(1 - e^{-\frac{T}{RC}} \right)^2$$

and

$$(14) \quad W_c = 1/2 \frac{CE^2}{T} \left(1 - e^{-\alpha}\right)^2$$

Taking the ratio of W_c to P_R and defining

$$(15) \quad \eta_c = \frac{W_c}{P_R}$$

then

$$(16) \quad \eta_c = \frac{\frac{CE^2}{2T} \left(1 - e^{-\alpha}\right)^2}{\frac{CE^2}{2T} \left(1 - e^{-2\alpha}\right)} = \frac{\left(1 - e^{-\alpha}\right)^2}{1 - e^{-2\alpha}}$$

$$(17) \quad = \frac{\left(1 - e^{-\alpha}\right)^2}{\left(1 - e^{-\alpha}\right)\left(1 + e^{-\alpha}\right)}$$

$$(18) \quad = \frac{1 - e^{-\alpha}}{1 + e^{-\alpha}}$$

(19) Now for

$$T \ll RC$$

or

$$\eta_c = 1$$

$$(20) \quad P_R = W_c$$

also from (15)

$$(21) \quad \frac{W_c}{P_R} = \eta_c$$

or

$$(22) \quad W_c = \eta_c P_R$$

and

$$(23) \quad P_R = \frac{1}{\eta_c} \quad W_c$$

The functions η_c and $1/\eta_c$ are plotted in Figure 11. It is to be noted that when T/RC equals 1, then P_R is approximately $2.2 W_c$. Conversely, in order to minimize BST collector dissipation these

$$(9) \quad \alpha' = \frac{T}{RC}$$

should be at least

$$(24) \quad \alpha' \geq 4$$

and preferably

$$(25) \quad \alpha' \gg 1$$

Rewriting (9) and assuming a minimum value for α' of 4 one obtains

$$(26) \quad R \geq \frac{T}{4C}$$

For fixed values of T and C equation (26), among other considerations serves to specify the minimum size of the BST.

Now to compute BST collector dissipation and assuming negligible beam interception by the klystron

$$(27) \quad P_R = 1/2 CE^2 (\text{PRF}), \quad RC \ll T$$

Typical parameters are

$$C = 500 \mu\mu f$$

$$E = 120 \text{ kv}$$

$$\text{PRF} = 2000 \text{ PPS}$$

$$\text{BST Collector } R \approx 3000 \Omega$$

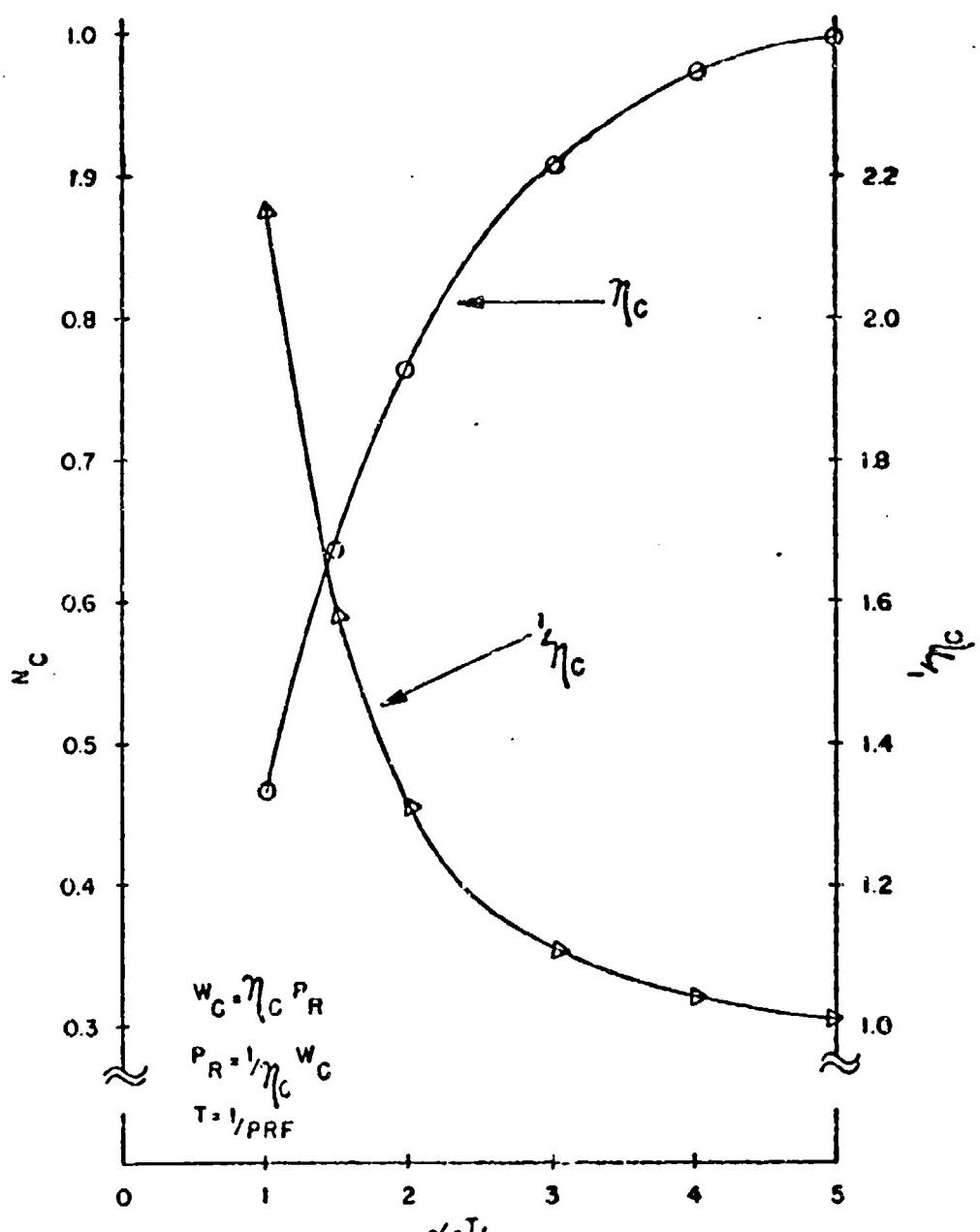


FIGURE 11-N N_c & $\frac{1}{N_c}$ VS α REF: SK-41462-1-CP

from which

$$\begin{aligned}\alpha &= \frac{T}{RC} \\ &= \frac{500 \cdot 10^{-6}}{3000 (500 \cdot 10^{-12})} \\ &= 333\end{aligned}$$

$$\therefore \alpha \gg 1$$

and therefore,

$$\begin{aligned}P_R &= 1/2 (500 \cdot 10^{-12}) (1.2 \cdot 10^5)^2 (20 \cdot 10^2) \\ &= \frac{500 (1.2)^2 (20)}{2} \\ &= 7200 \text{ Watts} \\ &= 7.2 \text{ KW}\end{aligned}$$

The BST collector dissipation may also be computed by means of heat loss transferred to the coolant lines from the collector of the BST. The loss for this measurement is

$$(28) \quad P_R = K_1 Q \Delta T, \text{ KW}$$

where

$$K_1 = 0.264, \text{ For Water}$$

$$Q = \text{GPM}$$

$$\Delta T = {}^\circ \text{C}$$

$$P_R = \text{KW}$$

Typical values for this method are

$$Q = 10 \text{ GPM of } 10-\text{C OIL}$$

$$\Delta T = 2.5 {}^\circ \text{C}$$

$$K_2 = 0.1017 \text{ For } 10-\text{C OIL}$$

from which

$$\begin{aligned}P_R &= L_2 Q \Delta T \\ &= 0.1017 (10) (2.5) \\ &= 2.53, \text{ KW}\end{aligned}$$

As mentioned previously, the BST collector dissipation may also be computed from the characteristic curves for the BST. However, one must know the voltage on the mod-anode of the BST as a function of time and this is not always easy to come by. If, however, one assumes a given function then this method reveals important information relative to parameters associated with the BST, i.e. peak power, average power, effective collector resistance, and effective pulse widths.

6. CAPACITY LOAD FOR "ON" BST

The capacitive load represented by " C_s " in Figure 1 is a major factor in the design of the pulser. As shown in the previous section it, among other factors such as rise and fall times, figures heavily in determining the size of the BST. The value of the capacity may be determined by several methods. These include the direct measurement by a capacity bridge, by calorimetric measurement of heat loss in the "ON" BST and by means of waveforms associated with the "ON" BST and the mod-anode of the klystron. These will be discussed now with the calorimetric method first.

By equating the calorimetric measurement to energy in the stray C_s there results

$$(29) \quad P_c = P_R$$

$$(30) \quad = \frac{1}{2} C_s E^2 (\text{PRF})$$

$$(31) \quad C_s = \frac{2 P_c}{E^2 (\text{PRF})} \cdot \text{Farad}$$

where $P_c = K Q \Delta T$ Watts as defined by (28)

E = peak mod-anode voltage on the klystron, volts

As an example of the use of this formula, typical parameters are

$$E = 120 \text{ KV}$$

$$\text{PRF} = 2000$$

$$P_c = 7.2 \text{ KW}$$

Assuming negligible convection and conduction heat losses of the coolant lines, then one obtains

$$\begin{aligned} C_s &= \frac{2 (7.2 \cdot 10^3)}{(1.2 \cdot 10^5) (2 \cdot 10^3)} \\ &= 5 \cdot 10^{-10}, \text{ Farad} \\ &= 500 \mu\text{f} \end{aligned}$$

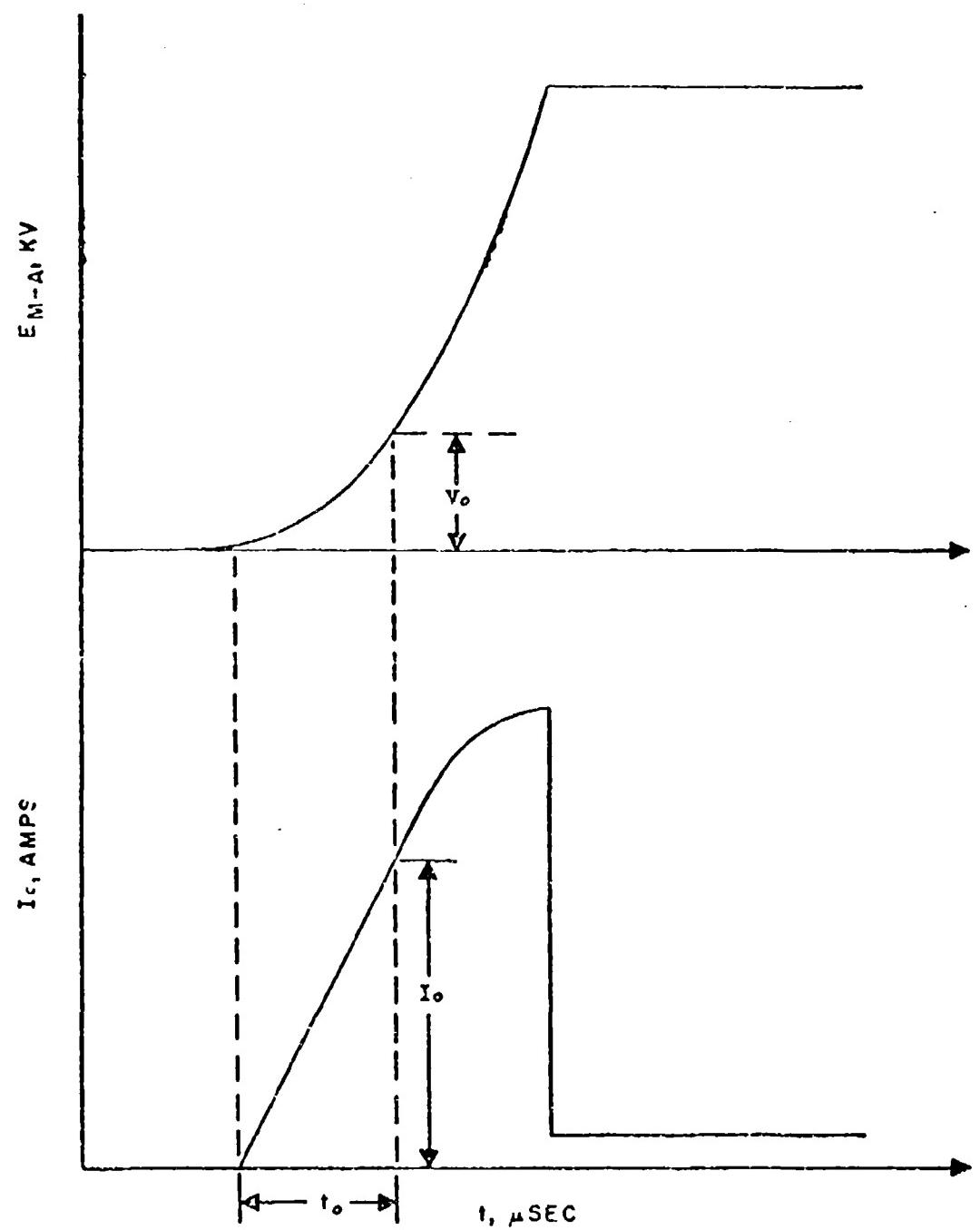


FIGURE 12 - DST COLLECTOR CURRENT AND KLYSTRON
MOD-ANODE VOLTAGE VS TIME - SK-41462-2-CP

Now returning to (38) removing the limits one obtains:

$$(42) \quad v_c = -\frac{I_0}{C_s t_0} - \frac{t^2}{2} + A$$

$$(43) \quad v_c = 0 @ t = 0$$

$$\therefore A = 0$$

$$(44) \quad v_c = -\frac{I_0}{C_s t_0} - \frac{t^2}{2}$$

Differentiating

$$(45) \quad \frac{dv_c}{dt} = -\frac{I_0}{C_s t_0} - t$$

$$(46) \quad = K_3 t$$

and

$$(47) \quad C_s = \frac{I_0}{t_0} - \frac{t}{\frac{dv_c}{dt}}$$

where t is restricted to the linear portion of i_c
if

$$(48) \quad t = t_0$$

then

$$(49) \quad C_s = \frac{I_0}{\frac{dv_c}{dt}}$$

and one obtains the well known formula

$$(50) \quad I_0 = C_s \left[\frac{dv_c}{dt} \right]_{t=t_0}$$

Again repeating I_0 and $\frac{dv_c}{dt}$ are both evaluated at $t = t_0$ and are restricted to the linear portion of i_c . Equation (50) therefore serves as a means of determining I_0 if one knows C_s and is able to determine $\frac{dv_c}{dt}$.

7. DESCRIPTION OF PULSER

Figures 13 and 14 are photographs of the mod-anode pulser unit. It contains four major assemblies. They are the "ON" BST assembly, the "OFF" BST assembly, the klystron bias supply of -1.2 KVDC and a 400 cps, 150 KV isolation transformer. The antenna drive motors for the tuning of the receiving antennas, and the shaft for the activation of the HV relay for the clumper tube can also be seen. The pulser is mounted in a tank filled with 10-C insulating oil. For purposes of orientation this pulser is shown mounted in the pulser tank (opened) in Figure 15.

8. ACKNOWLEDGEMENTS

Credit for the design of the modulating anode pulser is due to J. S. Walunas, Electrical Design Engineer and, in particular, to A. A. Gorski, the Design Project Engineer. The mechanical design was performed by E. F. Cahoon. Credit is also due to a very large supporting team of RCA personnel who were involved both directly and indirectly and who contributed so much to make this program a success. The mod-anode clamping circuit described in this report and the packaging configuration were developed jointly by A. A. Gorski and the author.

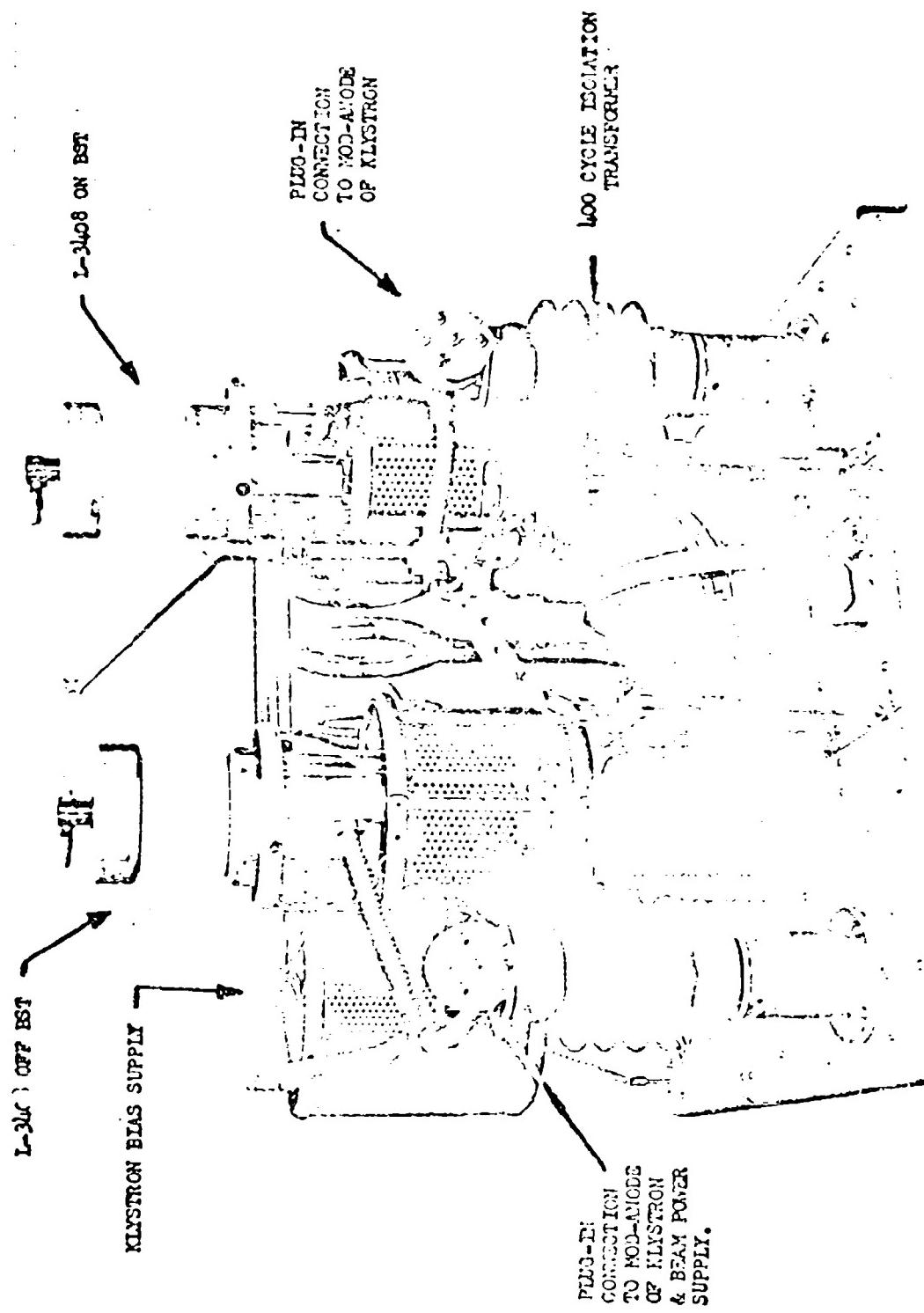


FIGURE 13 - REAR VIEW OF MODULATING ANODE PULSER - RCA ASSEMBLY 8332338-501

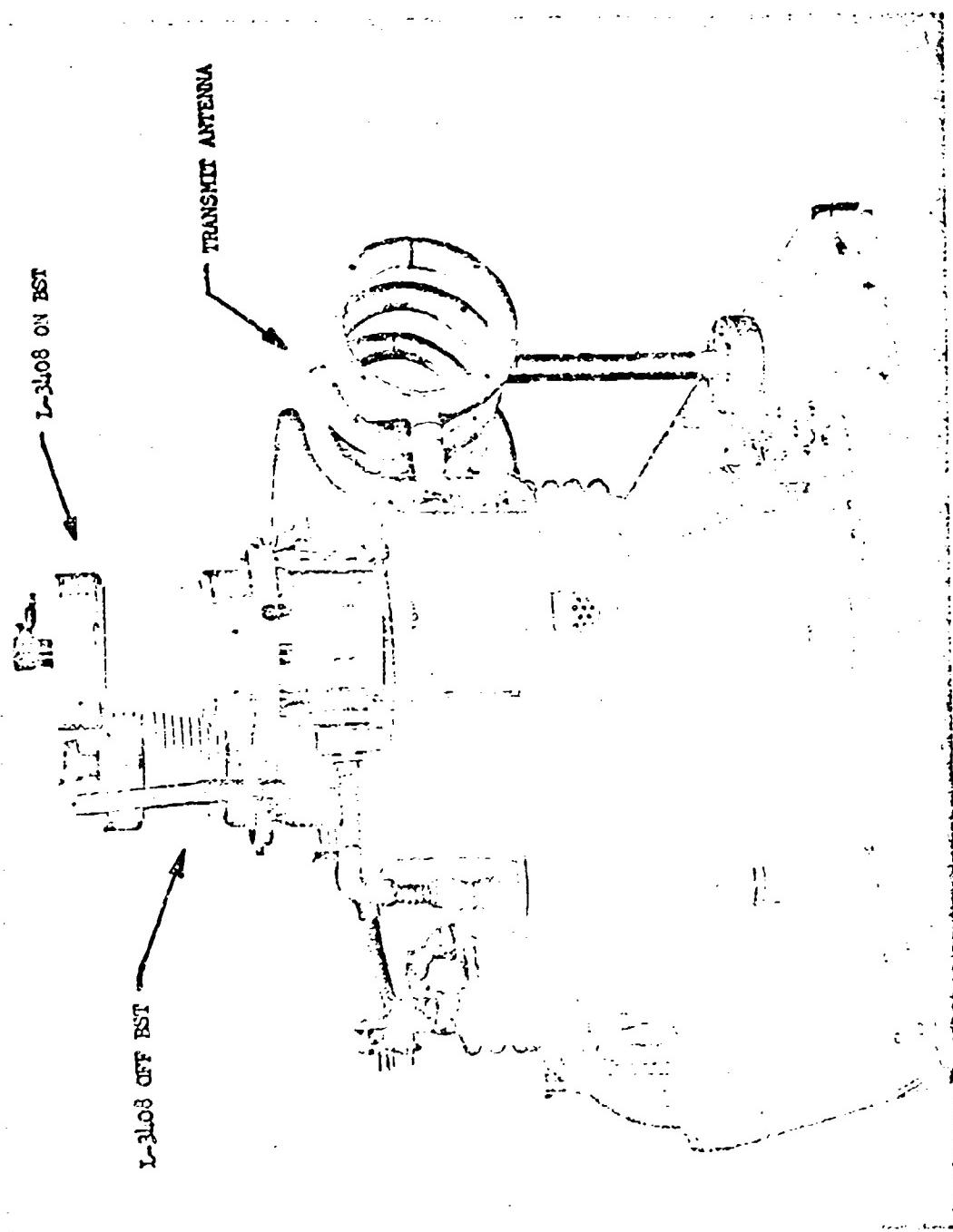
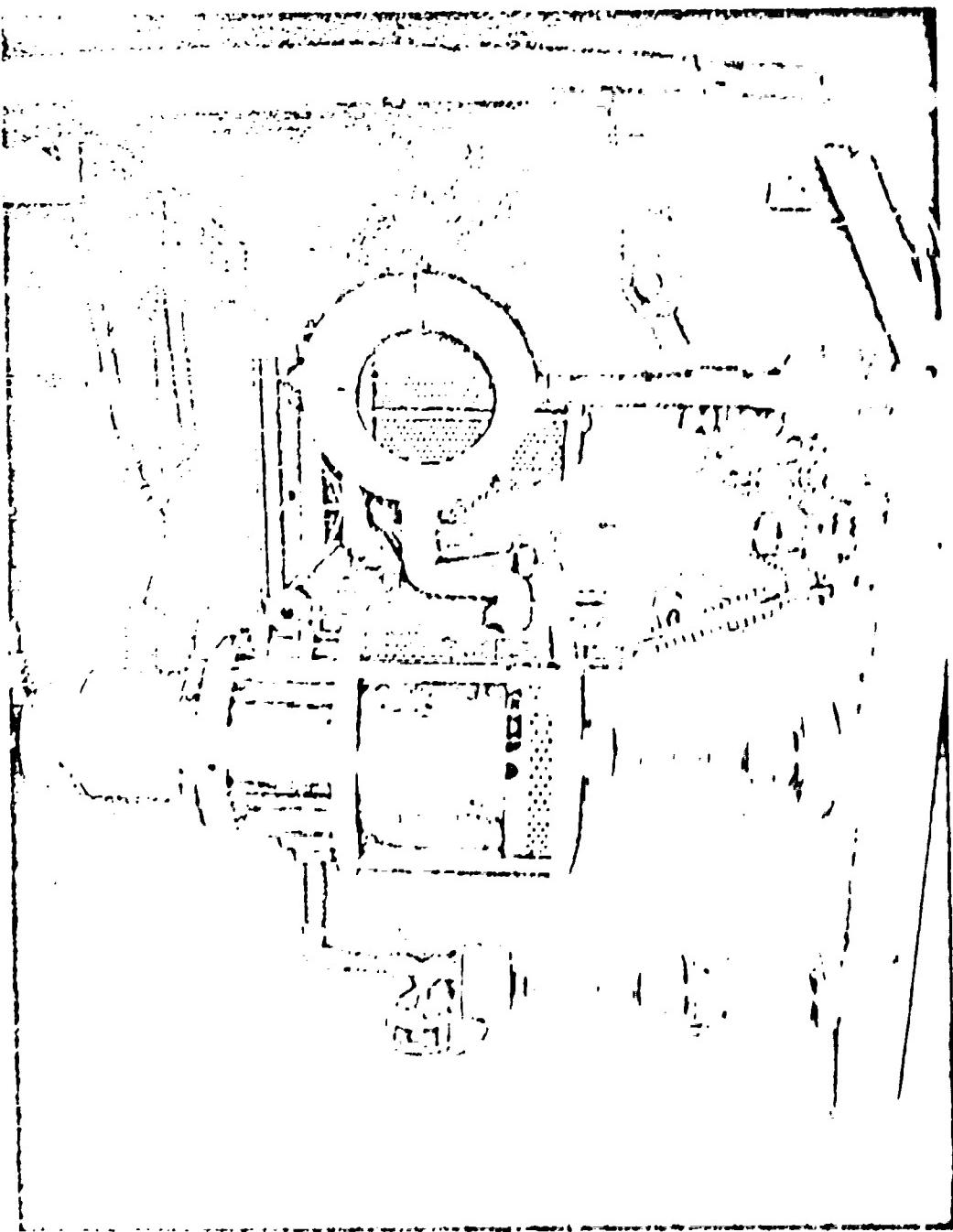


FIGURE 14 - SIDE VIEW OF MODULATING ANODE PULSER - RCA ASSEMBLY 6332338-601

100-35554-1 - 100-35554-2 - 100-35554-3
ACCES TAKEN BY STAFF - ANYONE GOING TO CAMP CREEK
SHOULD GO THROUGH THE GATE - 100-35554-4



REFERENCES

1. The equipment described in this report was developed by RCA under the Department of the Army Contract DA-36-034-ORD-2063(D), under the technical guidance of Army Ordnance Missile Center and sponsored by the Advanced Research Projects Agency.
2. The E-3408 Beam Switch Tube was developed for the equipment discussed in this report by Elettron Industries for D.E.P., M&HIC Division, Radio Corporation of America under P.O.G&R 996034 0001 70-Q72 under contract DA-36-034-ORD-2063(D).

FIELD EMISSION SWITCH TUBE STUDY[†]

by

E. E. Martin[#] and F. M. Charbonnier[#]

Linfield Research Institute, McMinnville, Oregon

ABSTRACT

The objective of this work is to determine the feasibility of using field emission cathodes in high vacuum switch tubes for radar pulser applications. Advantages derived from the use of compact multiple-needle cold field emission cathodes are elimination of heater power and warm up time, and ability to generate high current density beams ($>100 \text{ a/cm}^2$) with a well-defined boundary, which in turn allows low grid capacity, low grid current, and high voltage gain advantageous at large output voltages. Encouraging results have been obtained, and further work is planned.

A modular design was adopted; past work has been directed toward development of a satisfactory module, with emphasis on achieving effective operation of cathodes with up to 600 needles, and efficient beam collection and secondary suppression at plate voltages well below the peak grid voltage (to reduce tube power dissipation). Designs and techniques used to achieve these objectives are discussed. Peak currents of 26 amperes, voltage gains of 50, and switched powers of 1 megawatt have been demonstrated at low duty factor with 320-needle modules. Beam collection efficiencies in excess of 95% have been achieved with the plate at one-half of the peak grid voltage.

Future plans call for further refinement of the module design, construction of multiple module tubes with a minimum peak current capability of 100 amperes, and operation at increased duty factor.

[†]Paper presented at the Modulator Symposium, Fort Monmouth, 22-24 May 1962. This work was supported by Rome Air Development Center, Griffiss Air Force Base, N. Y., under Contract No. AF30(602)-2157, Project No. 5573, Task No. 55253. It is now being pursued at Field Emission Corporation under the same sponsor and Contract No. AF30(602)-2674.

[#]Now also at Field Emission Corporation.

I INTRODUCTION

This paper is based on work done under the sponsorship of Air Force Systems Command, Rome Air Development Center, Griffiss Air Force Base, N. Y. The objective of this effort is to perform a theoretical and experimental investigation to determine the feasibility of using field emission cathodes in high vacuum switch tubes for radar pulser applications.

Interest in field cathodes stems primarily from their demonstrated capability to yield extremely high emission densities. Multiple needle field cathodes are used in the present application and the significant parameters are the total current, the current density and the perveance of the beam near the plate, in addition to the current density at the field cathode emitting surface (which commonly exceeds 10^7 amp/cm²). Filamentary field cathodes of the T-F type are presently used in commercial high voltage flash x-ray tubes to produce electron beams with total peak currents above 1000 amperes and with current densities above 1000 amp/cm² at the anode, and the present work leads one to expect that comparable beam peak currents and current densities may be achieved at lower beam voltages (e.g., 10 to 20 kv) by the use of compact multiple-needle arrays of field cathodes.

High vacuum switch tubes using thermionic cathodes may be grouped into two categories: conventional close-spaced triodes or tetrodes, and focused beam "magnetron injection gun" triodes. The former are capable of high beam perveances and high switching power in relatively small structures. However, it appears in general difficult to avoid drawing large currents at the control grid, and the capacity between the grid and the other electrodes is large, thus requiring elaborate grid cooling and a large amount of power to drive the grid; also, the cathode is imperfectly shielded from the plate, which makes it difficult to handle very large output voltage pulses. Switch tubes of the "magnetron injection gun" type utilize well-defined hollow beams which allow considerable spacing between the modulating electrode and the plate, yield pentode-like characteristics, and thereby overcome some limitations of close-spaced triode switch tubes; however, the need to confine the beam over a fairly large transit distance tends to limit the beam perveance and results in relatively large size and weight.

Field emission switch tubes appear capable of combining to a fair extent the respective advantages of both types of switch tubes just described. Multiple tip field emission cathodes are capable of producing a very high density electron beam with a well defined edge. Thus, it is possible to extract the beam through a small aperture in the control grid without drawing a large grid current. The grid may be made small since it does not dissipate much power, and the grid capacity may be reduced; also, the cathode is well shielded from the plate and large output voltages can be

handled satisfactorily since the tube has a high voltage gain; high beam perveances may be achieved in relatively small structures because of the high beam current density. Finally, field emission switch tubes have the additional advantage of using a cold cathode, which eliminates warm-up time and the need for generating and dissipating heater power.

II GENERAL CONSIDERATIONS

A. The Field Emission Process

Field emission is the emission of electrons, usually from a metal into vacuum, by tunneling through the surface potential barrier which is lowered and thinned, as shown in Figure 1, by application of an intense electric field. The resulting emission is explained by quantum mechanics and described by the Fowler-Nordheim equation, which may be put in the form:

$$J = AF^2 e^{-\frac{B \phi^{3/2}}{F}} \quad (1)$$

where J is the emitted current density in a/cm^2 , F is the applied electric field in v/cm , and ϕ is the "thermionic" work function in ev. In the case of tungsten, which is at present the emitter material most often used in practice, the average work function is 4.5 ev and the corresponding values of A and B in Eq. (1) are respectively 3.5×10^{-5} and 6.12×10^8 , in the units shown above. The Fowler-Nordheim equation for field emission is formally similar to the Richardson equation for thermionic emission, the field in the former case playing the role of the temperature in the latter case; in both cases the emission is strongly dependent upon work function.

Thermionic emission (over the top of the potential barrier) and cold field emission (tunneling through the barrier) represent the two extremes of a continuous range of emission processes. Schottky emission and T-F emission are intermediate processes in which both temperature and field are combined to produce emission. T-F emission is defined as the emission from a heated conductor, in the presence of an applied electric field large enough so that a majority of the electrons are emitted through rather than above the barrier. Figure 2 shows the theoretical relationship between J , T and F for $\phi = 4.5$ ev (e.g., tungsten); cold field emission is included as a special case, $T = 0$. To the left of points B, tunneling accounts for less than 50% of the total emission, which is thermionic in nature: J is very sensitive to T and relatively insensitive to F . To the right of points B, emission occurs primarily by tunneling and it has the characteristic of field emission: J is very high, increases rapidly with F and becomes relatively insensitive to T . Typical conditions at the tip of a pulsed cold tungsten field emitter are: $F \geq 6 \times 10^7 v/cm$ and $J \geq 10^7 a/cm^2$.

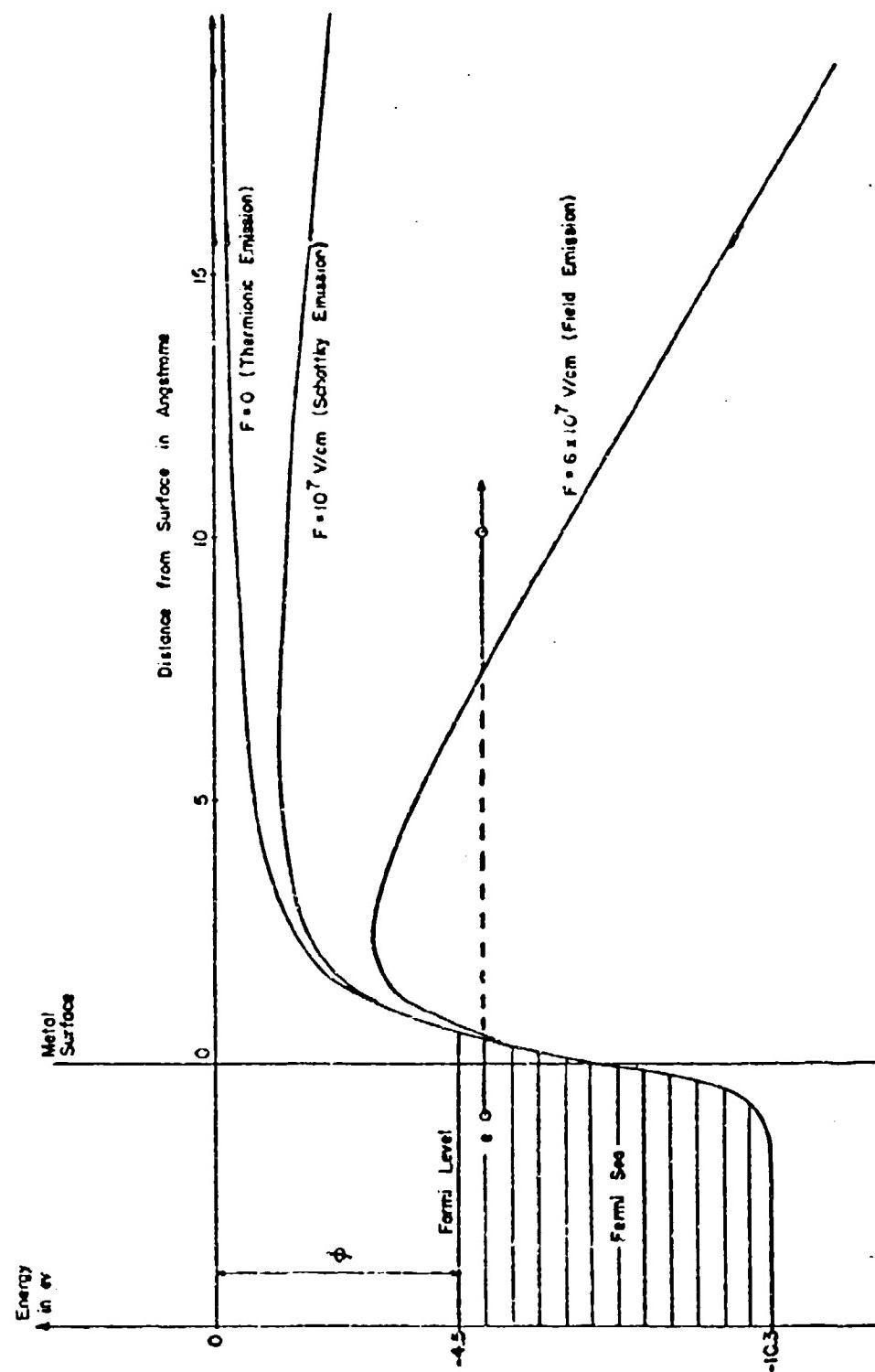


Figure 1. Potential barrier at the surface of a tungsten cathode, for various values of the applied electric field F .

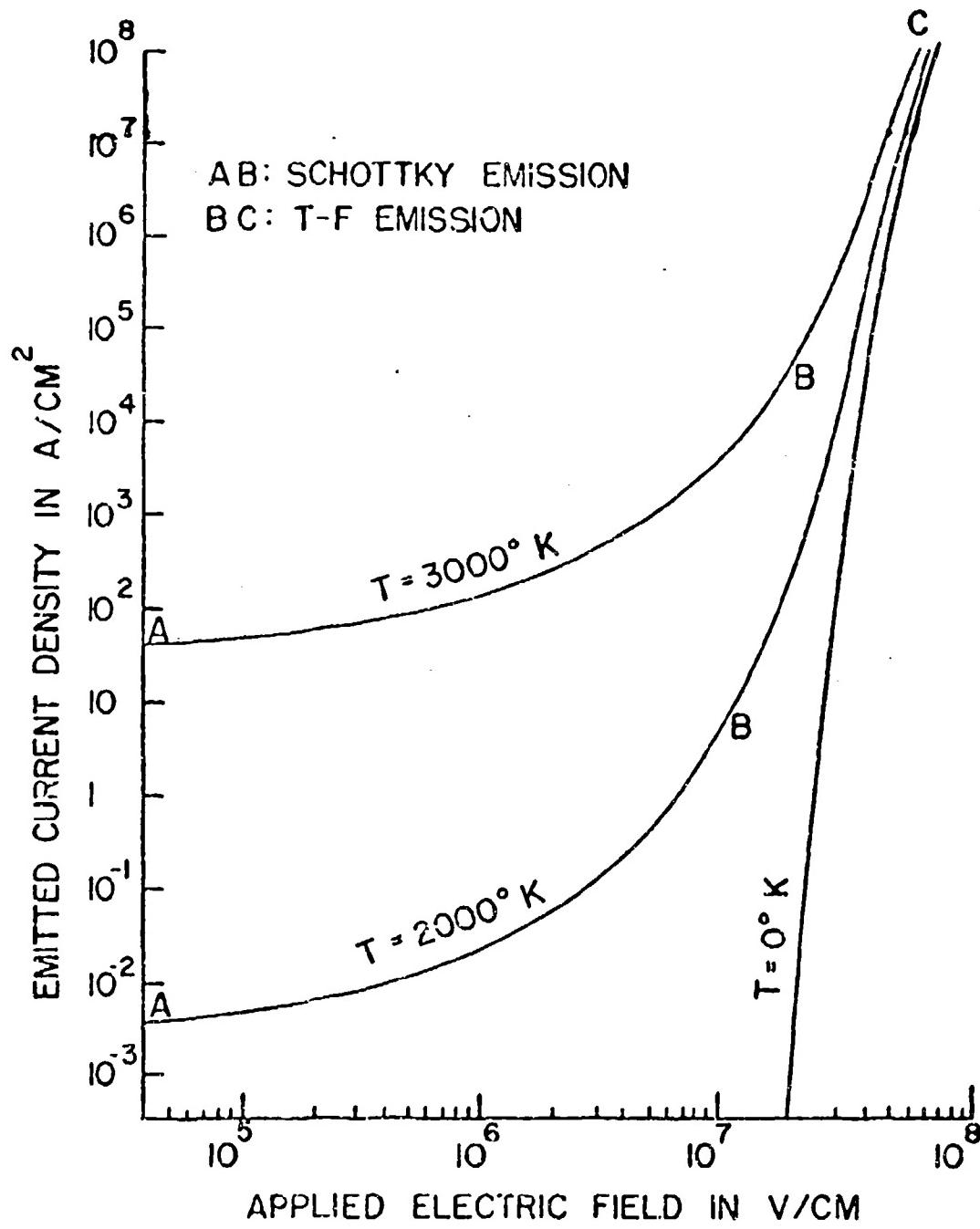


Figure 2. Emitted current density vs applied field, for $\Phi = 4.5$ ev (tungsten).

In practice, this high field requirement at the cathode is reconciled with moderate grid voltages and convenient spacings by using very sharp needle-shaped cathodes, such as is shown highly magnified in Figure 3. Such emitters are commonly electrolytically shaped from wire of a suitable material such as tungsten and, following smoothing and blunting of the tip by thermal migration, assume the geometry shown, which consists of an approximately hemispherical tip of radius r (typically a few tenths of a micron) smoothly fitted to a conical shank. Due to the decrease of electric field in the shank region, the emission from such a needle is confined to an area of the order of πr^2 centered at the emitter apex where field is maximum. The emitted electrons are accelerated in the intense field adjacent to the tip and form a beam which, although divergent, has a well defined edge. This permits production and modulation of the emission field by means of a control grid positioned wholly outside of the electron beam. The field at the emitter apex is approximately related to the control grid voltage V by the expression:

$$F = \beta V = \frac{V}{r \log_{10} \frac{4r}{R}} \quad (2)$$

where R is the grid-to-tip spacing.

B. Electrical Characteristics of Field Cathodes

A study of the electrical performance of pulsed field emission cathode at high emission density level reveals two significant phenomena. The first is the occurrence of space charge effects near the tip,¹ which become appreciable above 10^4 a/cm² and cause the field at the tip to rise less rapidly than the applied voltage. The second is tip heating which increases with emission density; at high current level, such heating can result in gradual geometric changes by surface migration or even, if a critical current I_M is exceeded, in evaporation of emitter material and initiation of a vacuum arc.^{2,3,4} I_M depends on cathode material and geometry and on pulse length. For tungsten cathodes and pulse lengths of interest in the present application, good agreement is found with the approximate theoretical expression:⁴

$$I_M = 3.6 \times 10^4 a r \quad (3)$$

in which I_M is in amperes, r is the tip radius in cm and a is the half angle of the conical cathode shank in radians.

¹ J. P. Barbour, et al., Phys. Rev. 92, 45 (1953).

² W. P. Dyke, et al., Phys. Rev. 91, 1043 (1953).

³ W. W. Dolan, et al., Phys. Rev. 91, 1054 (1953).

⁴ WADD Technical Report 59-20.

Experimental tests indicate that operation at approximately one-half the maximum current I_M normally yields long cathode life. Figure 4 shows the corresponding dependence on tip radius r of the peak beam current I_0 , assuming a typical cone angle $\alpha = 0.175$ radian (10°), a pulse length of 10 microseconds and an ideal (i.e., perfectly uniform) array. Also shown are the required grid voltage V_0 , the beam permeance $k = I/V_0^{3/2}$, and the "cut-off" voltage V_c required at the control grid to reduce the emitted current to $10^{-6} I_0$, assuming a typical cathode-to-grid spacing of $0.010"$ and ignoring the shielding effect to be discussed later.

Multiple-needle cathodes, such as that shown in Figure 5, have been developed for applications which require high values of beam permeance. The limitations of the single-needle cathode in this respect are quite apparent in Figure 4; large currents can be drawn only from large needles which require large grid voltages, and the beam permeance is almost independent of tip radius and of the order of 10^{-7} amp/v $^{3/2}$. For this reason, multiple-needle cathodes are used when a large beam permeance is required; a relatively low beam voltage is maintained by the use of sharp needles, and the desired beam current is achieved by using a sufficient number of needles.

The performance of actual multiple-needle cathodes deviates from that of "ideal arrays," i.e., arrays made up of perfectly uniform needles each of which contributes to the total emission current and permeance according to the performance predicted in Figure 4, because of inter-emitter "electrostatic shielding" and because of tip non-uniformity. For example, a 160 needle cathode was found, in an actual experimental case, to give performance equivalent to a 50 needle "ideal array."

The magnitude of these effects has been studied both theoretically and experimentally. For example, in a typical case where the emitter-to-grid distance R is equal to twice the inter-emitter spacing d of a double-row linear array, tests show that 25% more grid voltage is required to produce a given emission current density than would be needed for an isolated emitter having identical geometry.⁵ Figure 6 summarizes the results of such tests; in view of Eq. (2), the relative β values are inversely proportional to the grid voltages required.

The effects of geometric non-uniformity of the needles of an array are very pronounced at low emission densities, but become less so at high densities. As an example, an array, having a symmetrical distribution of emitter radii such that the largest emitters have radii 1.5 times those of the smallest, will in general deliver only 10% of the current emitted by a uniform array when operated with emission densities of the order of 100 a/cm^2 , but will deliver 50% as much current as the uniform array at an emission density of 10^7 a/cm^2 .

⁵ Quarterly Report No. 4 (15 March - 15 June 1961), Contract Nr. DA-36-039 SC-85368.

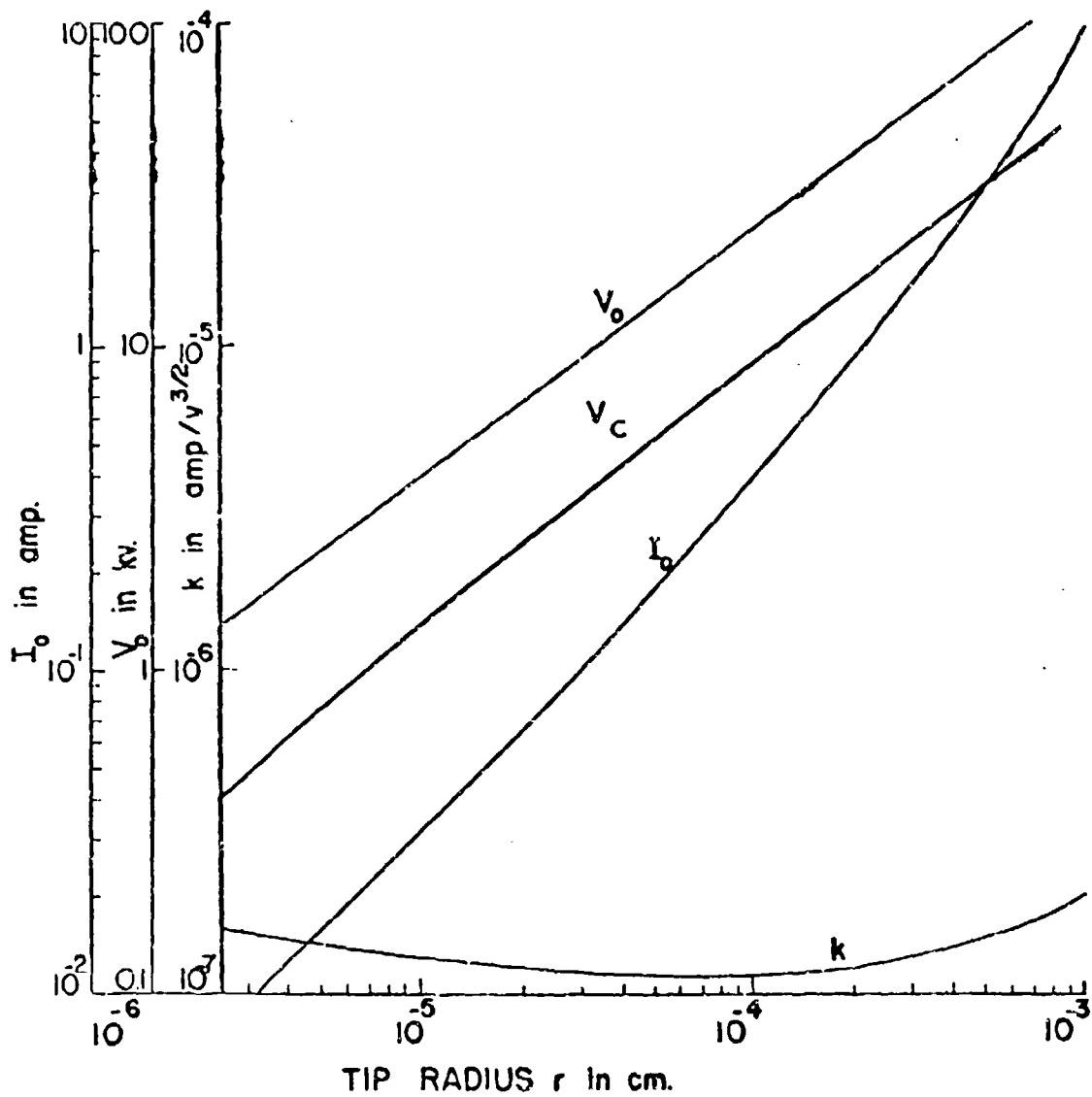


Figure 4. Electrical characteristics of a single-needle tungsten field cathode.

I_o = "safe" peak current ($0.5 I_M$)

V_o = peak grid voltage

k = $I_o/V_o^{3/2}$

V_c = "cut-off" voltage (corresponding to $I = 10^{-6} I_o$)

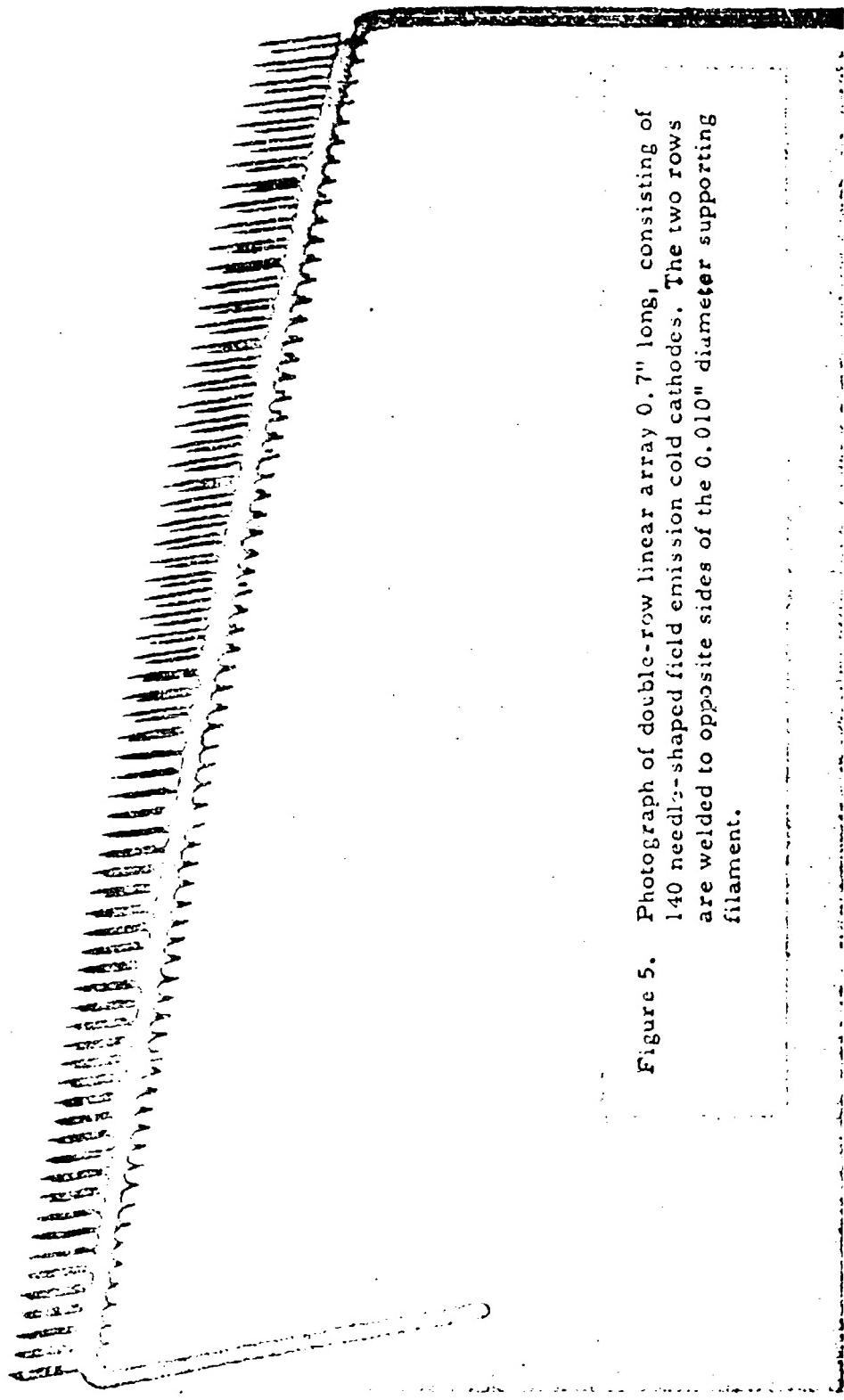


Figure 5. Photograph of double-row linear array 0.7" long, consisting of 140 needle-shaped field emission cold cathodes. The two rows are welded to opposite sides of the 0.010" diameter supporting filament.

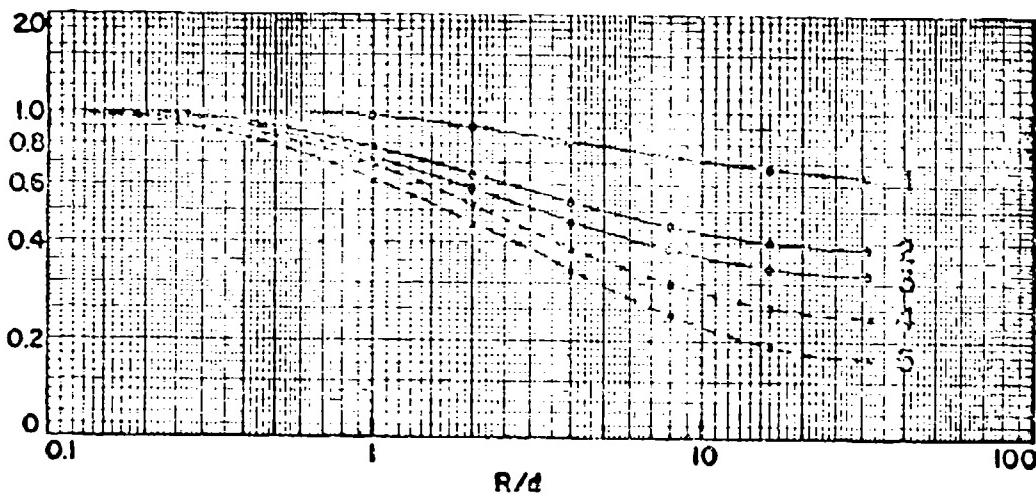


Figure 6. Relative β (solid lines) and relative perveance (dashed lines) of various cathodes, referred to an unshielded needle, as functions of the ratio of cathode-anode spacing to inter-emitter spacing, R/d . Curves 1, 2, 3 relative β for: a needle on an array filament, a single-row and a double-row array, respectively; Curves 4, 5 relative perveance per needle on a single-row and a double-row array, respectively.

C. Field Emission Switch Tube - Modular Design

With the preceding considerations as design parameters, testing of the feasibility of the use of field emission cathodes in high power switch tubes was undertaken. Ultimate objectives indicated in the contract included a peak current level of 2000 amperes, and achievement of a beam perveance of 10^{-3} amp/v^{3/2} at a current of 1000 amperes. The current and perveance requirements in either case imply the use of a very large total number of needles. Assuming the use of present double row linear arrays of tungsten needles a total perveance of 10^{-3} amp/v^{3/2} at the control grid aperture (where the beam voltage is highest and the beam perveance is lowest) corresponds to approximately 18,000 needles, and to a total array length of 45 inches if a typical spacing between needles of 0.005" is used. Mechanical and electrical considerations advise against the construction of a single array of this length, and it is proposed in the final switch tube to follow common practice and use a modular type of design, in which the switch tube consists of several identical sub-units or modules contained within the same vacuum envelope. A number of modules of the order of 50 appears reasonable at this time; however, a final choice of the number of modules has not been made. The immediate objective of the initial phase of this work was the design, construction and testing of an individual module consistent with the ultimate switch tube objectives, i.e., capable of switching a beam current of approximately 25 amperes, corresponding to a beam perveance of 25×10^{-6} amp/v^{3/2}.

A module design was sought which would incorporate the following:

- (a) a cathode with a sufficient number of needles for the required beam current and perveance
- (b) a control grid which would intercept a negligible portion of the primary beam despite a strongly positive potential and despite a relatively small cathode to grid spacing
- (c) a means for preventing return to the control grid of secondary electrons originating at the plate, even when using a plate potential substantially lower than the peak grid voltage in order to reduce tube voltage drop and internal power dissipation
- (d) a tube design compatible with a plate voltage in excess of 100 kv when in the off condition
- (e) a cathode environment compatible with stable cold cathode performance ($p < 10^{-10}$ Torr); if this should prove impossible due to the high average power dissipation level, satisfactory field cathode performance can be achieved by intermittent or continuous heating of the cathode⁶

⁶W. F. Dye, F. M. Charbonnier et al., J. Appl. Phys., 31, 790, May 1960.

- (f) a low grid capacitance
- (g) provision for dissipation of heat generated at the plate and control grid.

III DEVELOPMENT OF EXPERIMENTAL FIELD EMISSION SWITCH TUBE MODULES

A. General Description

Five types of experimental field emission switch tubes have been constructed and tested at this time, designated as FEST (field emission switch tube) 1, 2, 3, etc., in chronological order of construction. These tubes are of generally similar design and use the same materials; they differ primarily by the size and configuration of the cathode, by details in the geometry of the other electrodes and by details in the assembly techniques.

The cathode is made of tungsten, and other electrodes are made of molybdenum. The tube electrodes are enclosed in an external vacuum envelope made of alumino-silicate, Corning type 1720, glass. Therm bombardment filaments for outgassing the electrodes during evacuation of the tube and a titanium on tungsten getter filament are also provided.

Corning 1720 alumino-silicate glass was chosen because it offers several advantages as an envelope material for high power and ultra high vacuum devices: the 670° C strain point permits use of higher bake-out temperatures and more rigorous degassing procedures than would otherwise be possible, and its resistance to diffusion of atmospheric helium inhibits the accumulation over a period of time of substantial amounts of this gas within the tube. This is advantageous because roughening of the cathode surface by helium ion bombardment gradually leads to electrical instability of cold field emitters operated in envelopes of more conventional materials, e.g., Corning 7740 "Pyrex" glass.⁷

The multiple-needle cathodes presently used consist of a number of individual points fabricated from small tungsten wires spot-welded at regular intervals along both sides of a tungsten supporting filament, then etched electrolytically to form sharp needles.

B. Geometrical Tube Design

In a field emission switch tube the high field required at the needle tips, for emission densities of the order of 10^{12} a/cm², results in a relatively high control grid peak voltage (usually, though not necessarily, of the order of

⁷E. E. Martin, J. K. Trolan and W. P. Dyke, J. Appl. Phys., 31, 782, (1960).

15 kv).⁴ A lower plate voltage is desired (when the tube is conducting) in order to reduce internal power dissipation, and a satisfactory design requires a suppression technique which: 1) successfully prevents secondary electrons generated at the plate from striking the higher voltage control grid, 2) is compatible with a high beam pittance when the tube is conducting and with a high plate voltage when the tube is switched off and 3) results in negligible direct interception of beam.

1. Electrostatic Suppression - EEST-1 to 4

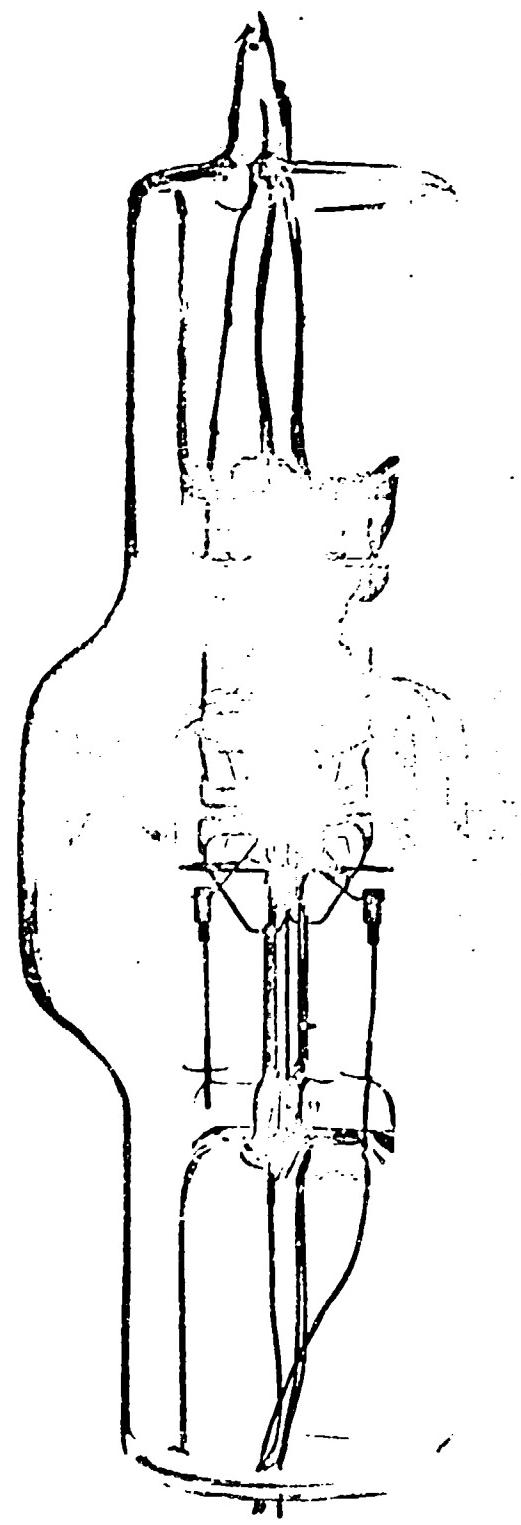
Switch tubes EEST-1 to 4 were electrostatically suppressed tetrodes of similar design incorporating cathodes with progressively larger numbers of tips. Because of this similarity only type EEST-4, shown in Figure 7, will be discussed. The cathode consists of two rows of needles welded on opposite sides of a 0.010" supporting filament centered in a 0.030" wide grid aperture; each row consists of 160 needles spaced 0.005" apart. Particular attention was given to the suppressor grid design. The mode of suppression which was used is apparent in Figure 8 which shows the distribution of potential and the path of a typical primary electron in a type 4 tube in the case where the plate voltage was 50% of the control grid voltage. Note that in this condition a potential minimum at 40% of control grid voltage exists between the plate and that electrode, since the great majority of secondary electrons have very low initial energies effective suppression would be expected even if the minimum in the auto-potential curve is relatively shallow. The potential curves which are shown ignore the beam space charge, which would further depress the potential minimum V_m and provide still more effective suppression of secondaries. In the absence of beam charge, the existence of a potential minimum and the corresponding suppression of plate secondaries occurs as long as the plate voltage exceeds approximately 40% of the control grid voltage. With the beam present, suppression would be achieved at still lower voltages, and the design provides effective suppression of secondary electrons for all values of plate voltage of practical interest. It will be noted that this design has the advantage of providing suppression of secondaries without placing a grid in the path of the beam.

In Figure 9 are shown the relative collection efficiency, i.e., the ratio of plate to cathode currents, obtained in a type 4 tube for different plate voltages, expressed as fractions of the control grid voltage, at several values of beam current.

2. Magnetic Suppression - EEST-5

The electrostatic suppression technique described above, while fairly satisfactory, requires a grounded suppressor grid which places limitations

⁴Note however that, with a field cathode, the cut-off voltage is positive and approximately equal to one third of the peak voltage, so that the required grid pulse amplitude is only about two-thirds of the peak grid voltage.



402

Figure 7. Type 4 field emission switch tube.

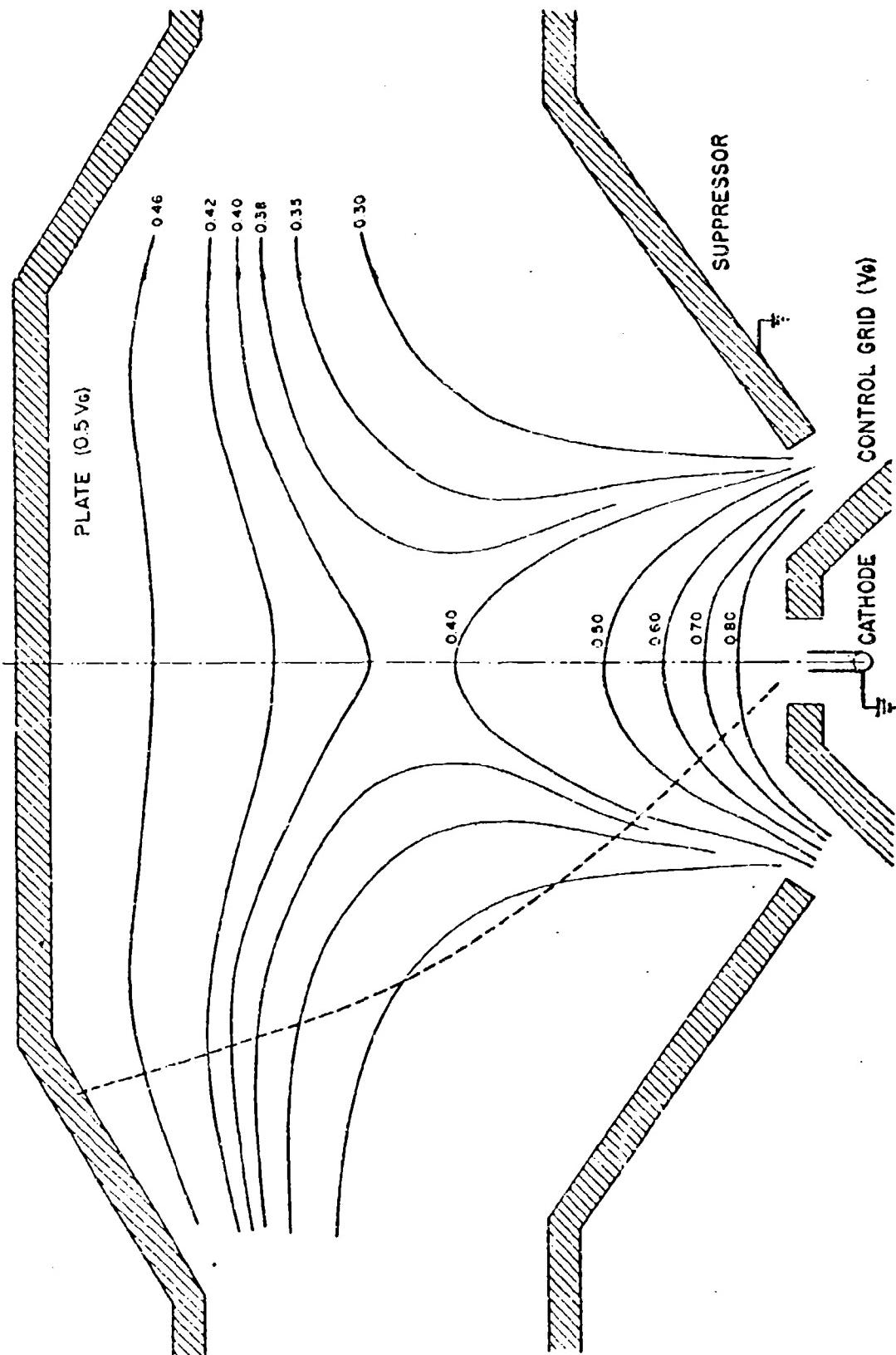


Figure 8. Plot of equipotentials in FEST-4 at $V_p = 0.5 V_G$.

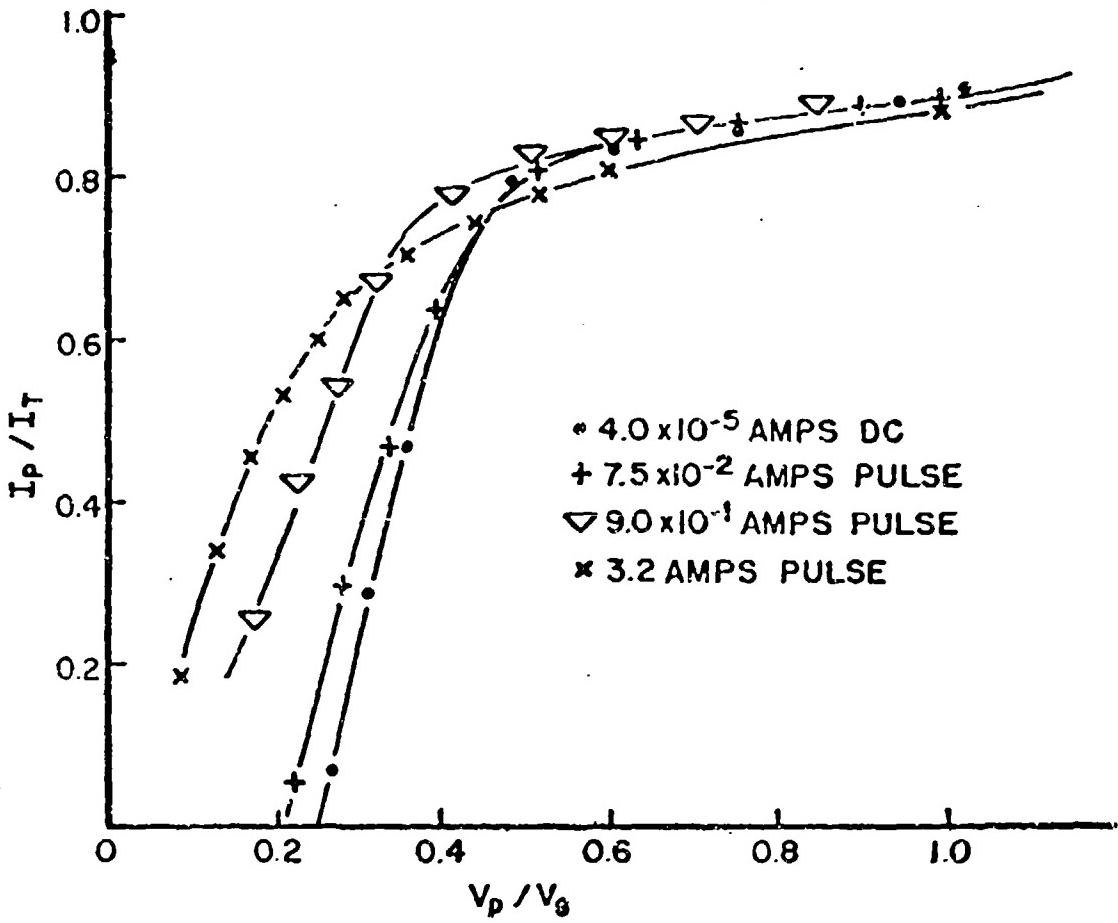


Figure 9. Collection efficiency at the plate in a type 4 tube.

on beam perveance and voltage stand off.

Because the field emitted electrons are accelerated to a large fraction of the grid voltage within a few microns from the tip, a moderate transverse magnetic field will perturb only slightly the primary electron paths, but will strongly deflect low energy secondary electrons and return them to the collector surface near their point of origin, as illustrated in Figure 10. A field emission triode, with a compact multiple-needle cathode and a spherical plate centered at the cathode, was built to test the practicality of this magnetic suppression technique. In Figure 11 are shown collection curves obtained by operating the triode in a 130 oersted magnetic field perpendicular to the tube axis. At all current levels investigated the collection efficiency exceeded that achieved in the electrostatically suppressed tubes FEST 1 to 4, and it was possible to maintain efficient collection down to $V_p \approx 1/3 V_g$.

Type FEST-5 switch tubes, as illustrated in Figure 12, differ significantly from earlier tubes in that they are magnetically suppressed field emission triodes with a 600 needle, $1/4 \times 1/4$ inch square cathode, consisting of 6 parallel double row-arrays interspersed with control grid wires. The plate is a 1 cm radius Mo hemisphere.

C. Evacuation and Processing

1. Evacuation

Attainment of ultra high vacuum conditions was sought in order to promote long term stability of the unheated cathode by reducing the rate of contamination of the cold surface. Baking of the entire tube at 560°C was alternated with outgassing of the electrodes at 1200 to 1400°C . Just before seal off the pressure was approximately 10^{-11} Torr, and a still lower value was probably achieved following gettering of the sealed-off tube.

2. Post Evacuation Cathode Tailoring

Present field cathodes are made of pure tungsten and require no activation. The purpose of cathode tailoring is to provide the desired uniformity of tip radii essential to effective operation of multiple tip cathodes.

In the past, thermally induced surface migration under the action of surface tension forces has been used with fair success to achieve the desired uniformity of emitter tip radii.⁶ In this process heating of the tungsten cathode to a sufficient temperature (e.g., 1800°C) enables surface atoms to migrate from regions of high curvature to regions of lesser curvature, at a rate which increases rapidly with local curvature. Thus when the cathode is first heated the sharp projections present on the surface of the

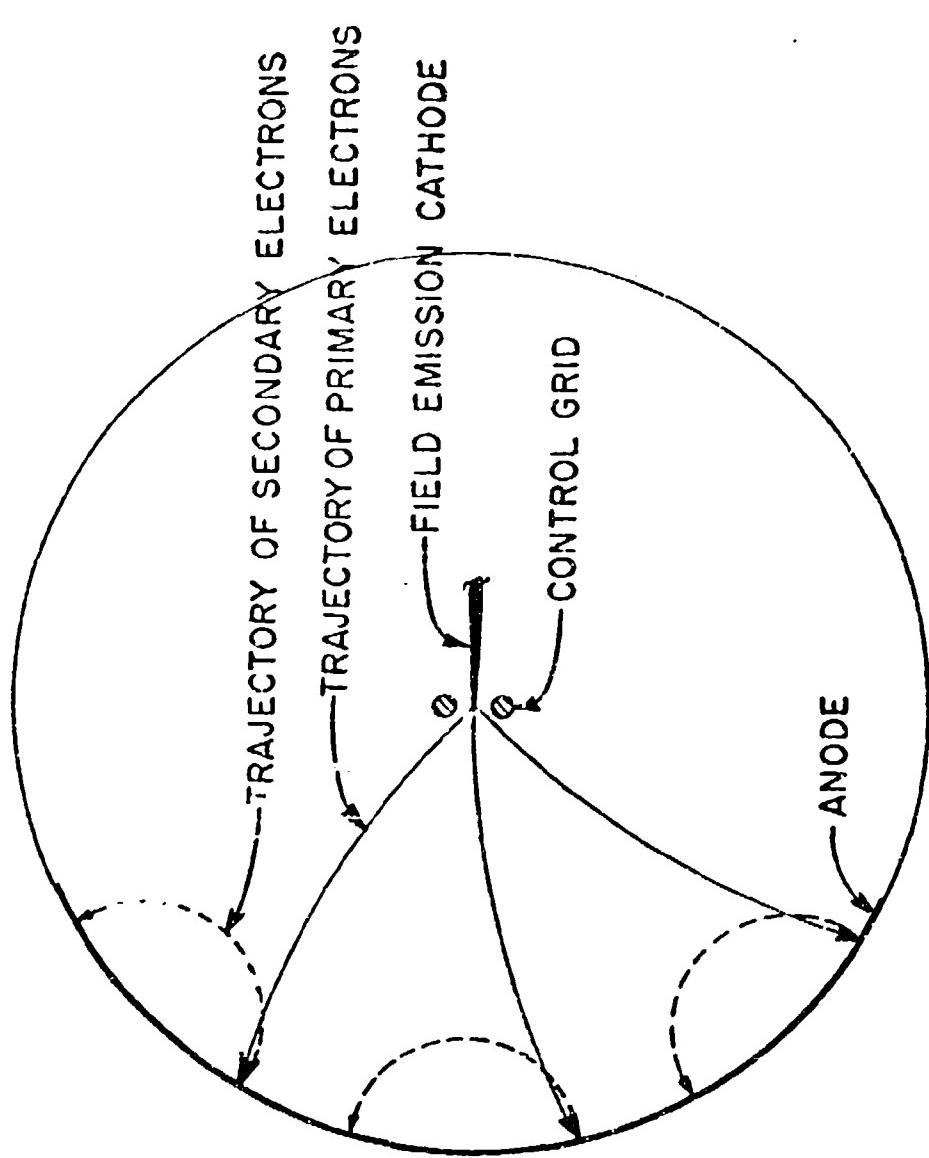


Figure 10. Sketch of primary and secondary electron paths in a magnetic field.

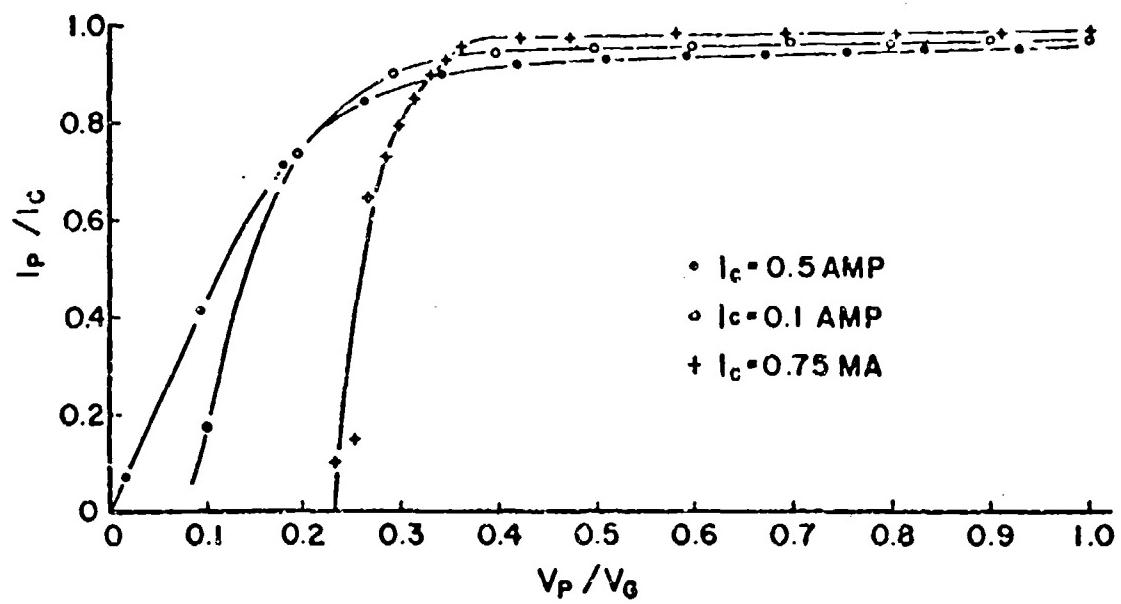


Figure 11. Collection curves obtained from experimental tubes suppressed by 130 oersted magnetic field.

emitters are rapidly smoothed out and the emitter tip assumes a roughly hemispherical form. Further heating of the cathode then leads to a gradual dulling of the emitter tips at a time rate inversely proportional to the cube of the tip radius. Thus there is preferential migration of the sharper tips and, assuming uniform temperature along the array, the variation in tip radii among the various needles decreases with time; by adjusting the heating temperature and heating time, it is possible to achieve fairly uniform and preselected values of tip radii and therefore of operating control grid voltages. However, in order to be fully effective this method requires uniform temperature and cone angle for all the needles, a condition which is difficult to achieve for cathodes containing a very large number of needles.

Thus an alternate procedure has been sought which would uniformize the field at various emitter tips. The use of the field evaporation process, in which application of a high electrostatic stress causes surface atoms to evaporate at a rate which is highly field dependent, seems to provide such a procedure. In the case of a cold tungsten cathode, the required field is extremely high and the procedure would be impractical because of the very high voltages which would then be required. However, by a combination of heating, thermal migration and field evaporation techniques it appears possible to reduce the required voltage and to achieve relatively uniform emission from the various emitters of a multiple-needle cathode, despite possible variations in emitter cone angle and in tip temperature during the process. The technique also has the advantage of yielding uniform emission even with sharp tips, as required for low voltage emission. Furthermore, one can, by choice of the applied voltage during treatment, pre-determine the operating grid voltage for the processed cathode.

3. Conditioning to Improve Voltage Stand-off

Field emission originating at microscopic surface protuberances on negative electrodes is a common mechanism leading to low impedance voltage breakdown in vacuum. The conditioning procedure used was aimed at improving voltage stand-off characteristics by controlled removal by a vacuum arc of those small protuberances which may be present on low voltage electrodes. Based in part on detailed studies of vacuum arc initiation at this laboratory,^{2,3,4} it was recognized that such a procedure, to be effective, requires ability to pass a substantial current to initiate the arc, but to limit very carefully the energy expended in the arc lest splatter products create new roughness on the electrode. For this purpose a 10 foot section of RG coaxial cable was charged to successively higher voltages up to 120 kv, and discharged several times a second, through a resistive load about three times the characteristic impedance of the cable, by means of a pressurized spark gap. The resultant pulses, which reached a peak voltage about 80% of the dc charging voltage and were less than 0.01 microsecond in length, were applied between the plate and grid structures of the tube

being processed. The four type 4 switch tubes which have been conditioned in this manner to date have subsequently all been capable of withstanding application of 75 kv dc at the plate, and have exhibited a field emission leakage current from the grid structures of only a few microamperes at the 75 kv dc gap voltage. Test of this technique at still higher processing voltages is planned in the near future.

IV ELECTRICAL PERFORMANCE OF EXPERIMENTAL MODULES

A. Electrostatically Suppressed Tetrodes (FEST 1 to 4)

Substantial progress has been made toward development of tetrode switch tube modules with compact multiple-needle cathodes to produce high beam current densities, and therefore high peak current and power capability in a very small structure. The general objectives of this work have been to increase beam perveance by increasing the number of needles and improving cathode tailoring, and to reduce internal power dissipation by achieving efficient collection of the beam at a plate voltage well below the peak grid voltage. Approximately 30 tubes of types FEST 1 to 4 were built, and half of these tested electrically. The main tests performed were the following:

1) field emission cathode characteristics. This is performed by measuring the dependence on peak control grid voltage V_g of the peak field emitted current I_e . Typical results are shown in Figure 13, which show the strongly positive voltage cut-off typical of field cathodes. A "Fowler-Nordheim" plot of the data, in the form $\log I_e$ vs $1/V$, yields the straight lines of Figure 14; this linearity which in view of Eq. (1) constitutes evidence that the observed current was due to stable field emission, maintained up to the highest current level investigated (26 amperes) which corresponds to a beam perveance of $9 \mu\text{A}/V^{3/2}$ (referred to the peak grid voltage, which is the highest electrode voltage in the conducting tube).

2) collection efficiency as a function of plate voltage. Typical results for the electrostatically suppressed tetrodes were shown in Figure 9. Satisfactory collection efficiency is maintained down to $V_p \approx 0.5 V_g$.

3) voltage gain. As noted earlier, the well defined edge of the field emitted beam permits use of a narrow grid aperture, so that the cathode is fairly well shielded from the plate. This leads to a relatively high voltage gain μ , defined as the ratio of the changes ΔV_p in plate voltage and ΔV_g in control grid voltage which produce the same change in cathode emission. Tubes types FEST 3 and 4 exhibited voltage gains in the range 40 to 60; thus a 50 kv variation in plate voltage, upon switching, is compensated by only 1 kv additional change in grid voltage.

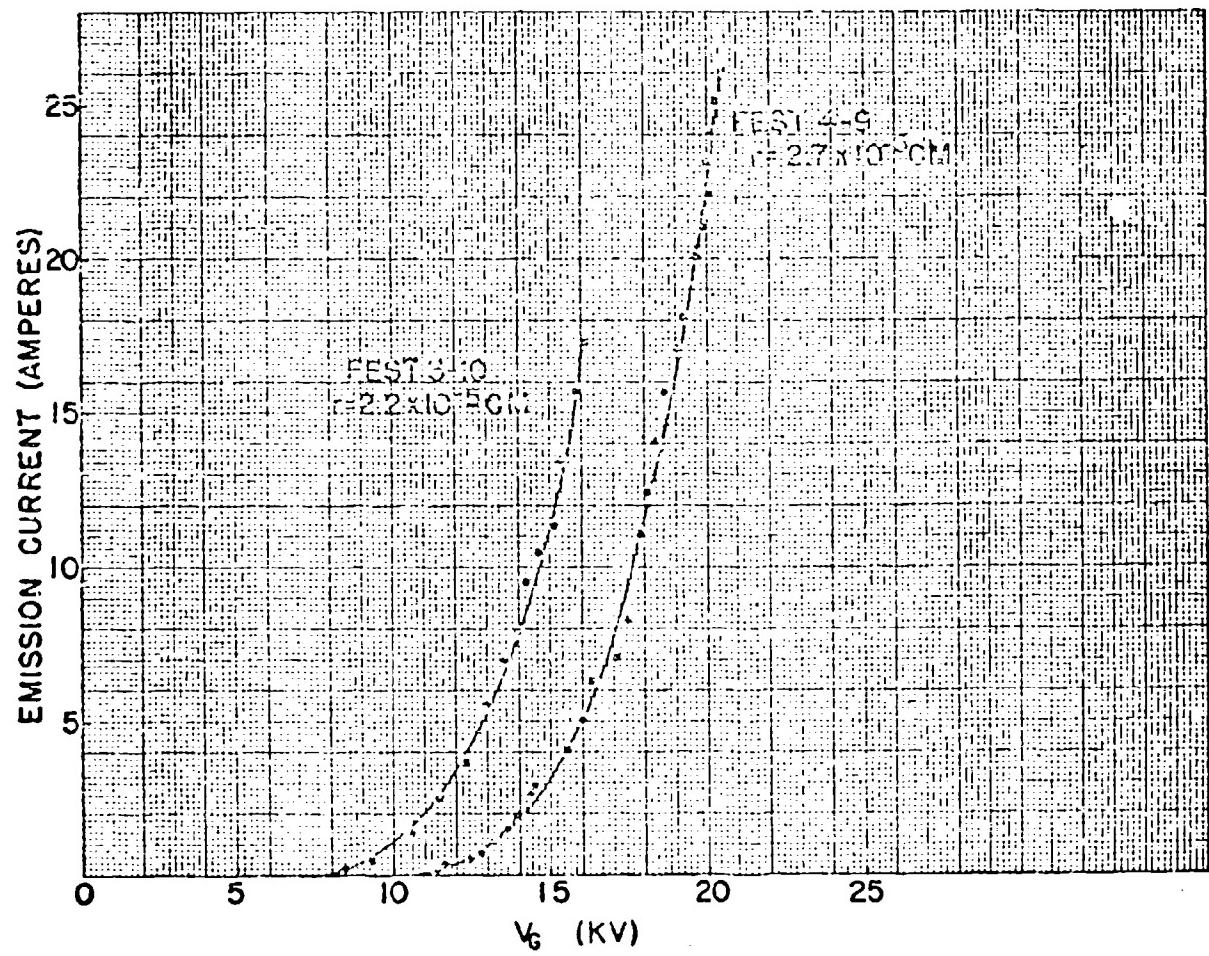


Figure 13. Emitted current vs control grid voltage for representative tubes FEST 3-10 and FEST 4-12.

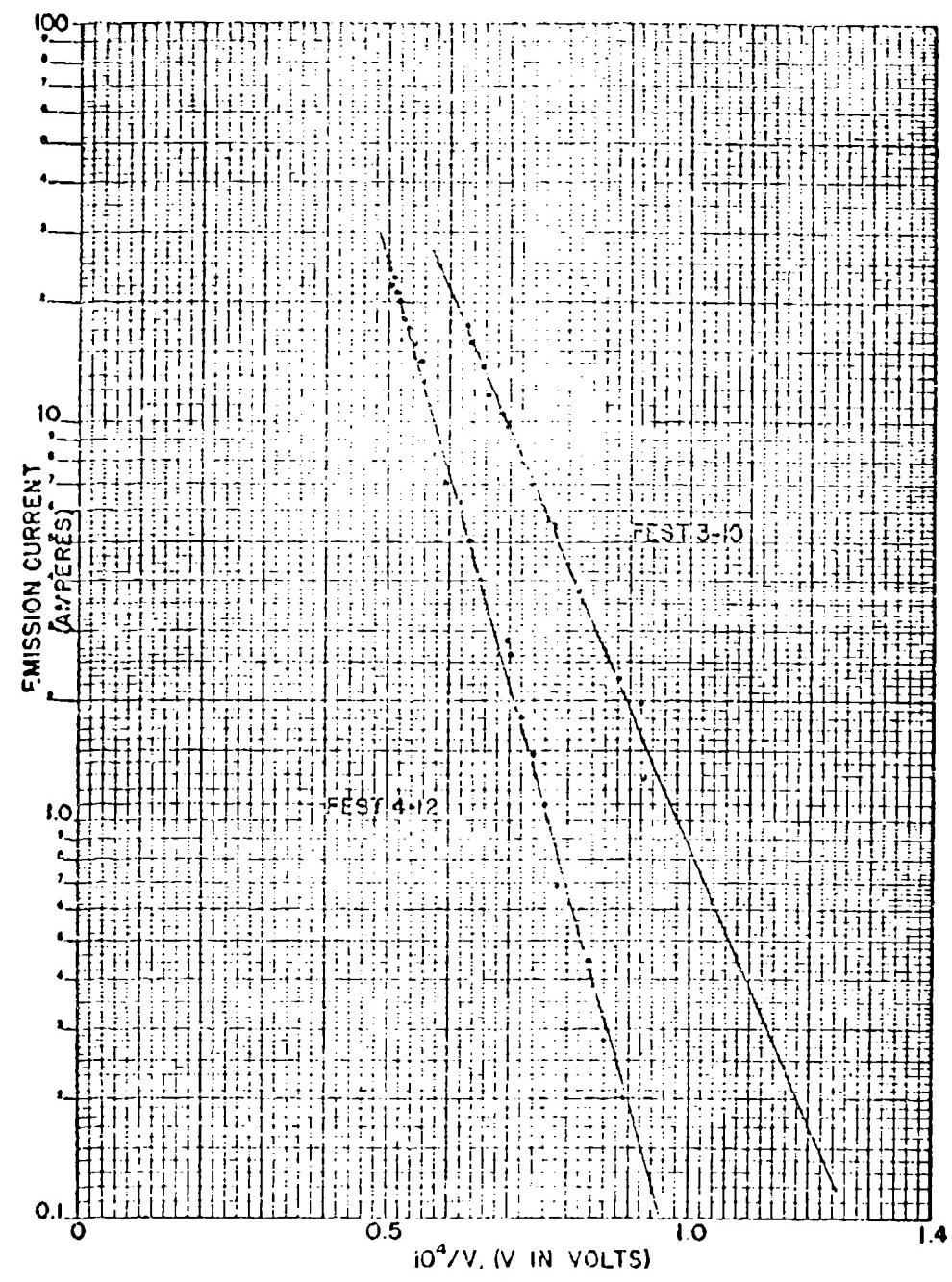


Figure 14. Fowler-Nordheim curves for representative tubes FEST 3-10 and FEST 4-12.

4) output power. One type FEST-4 switch tube was tested with the plate connected to a high voltage NJE dc supply through an appropriate resistive simulated load. Under these conditions, output pulses of approximately 1 megawatt (15 amperes and 65 kv) were obtained. The pulse waveform was identical to that which could be calculated from the known circuit capacities and time constants, corresponding to a rise time of 0.4 microseconds to 90% of full pulse voltage.

Table II based on the foregoing tests, illustrates the present state of the art for FEST-4 experimental field emission tetrode switch tubes.

TABLE II - FEST-4 - State of the Art Characteristics

Beam off conditions:

Plate voltage	4 75 kv
Control grid bias	4 5 kv
Residual cathode current (for the above voltage)	1 pa
Leakage current from grounded suppressor grid to plate	2 pa
Switching characteristics:	
Grid switching pulse	4 15 kv
Plate current	15 amp. peak
Output voltage pulse (with 4,300 ohm plate load used for the test)	65 kv

B. Magnetically Suppressed Triodes (FEST-5)

Work on these tubes started recently. Only two tubes were evacuated, and one electrically tested. The limited results obtained so far appear encouraging: ultra-high vacuum conditions were readily achieved; a substantial current (20 amperes) was reached, indicating the feasibility of effective processing of cathodes consisting of several multiple needle arrays in parallel; finally, the magnetic suppression scheme tested earlier at moderate current (0.5 amp), was found to remain effective at much high beam current and current density levels.

CONCLUSIONS

The initial phase of this work has established the feasibility of using high current density, multiple-needle, field emission cold cathodes in high voltage beam switching devices. A satisfactory sharing of the emission between the needles of extensive, densely packed multiple needle cathodes has been achieved, and effective operation of still larger cathodes of this type appears technically feasible. The good definition of the beam edge permits modulation and control of the beam by non-intercepting structures, alleviating grid power dissipation problems, and also leads to a high voltage gain which is a definite advantage when a large output voltage pulse is desired. Effective suppression of secondaries at the plate of both tetrode (electrostatically suppressed) and triode (magnetically suppressed) field emission switch tubes was demonstrated at plate voltages well below the peak grid voltage, leading to increased beam perveance and reduced power dissipation at the plate of the conducting tube. Both the small size of the control grid and the strongly positive cut-off voltage, which follow from the use of a high density field cathode, are favorable from the standpoint of reducing grid drive power requirements.

Work during the coming year will be directed toward testing at higher duty factor and peak current, with minimum objectives of 100 amperes peak at 0.002 duty factor set by available pulses and test equipment. Thus, particular attention will be given to technical problems associated with the construction, processing and operation of multiple module assemblies, to cooling techniques, and to materials selection and outgassing procedures which maintain the best possible environment at average power dissipation levels well above 1 kw. The degree of success of the latter will determine whether periodic reconditioning of the field cathode surface by a brief heating, which was not found necessary in the switch tubes tested so far but has been used successfully in other experimental field emission devices operating in a poorer environment, is needed to avoid marked long term variations of the cathode emission characteristic.

HARD TUBE MODULATOR TECHNIQUES IAT PERMIT UTILIZATION
OF MINIMUM SIZE CAPACITOR BANKS

by

Vadim N. Martinovitch

Lockheed Electronics Co. - Military Systems Division
Plainfield, N. J.

In hard-tube modulators, large banks of energy-storage capacitors are usually required to maintain the flatness at the top of the output pulses that are applied to RF amplifiers. This measure is taken to minimize the amount of RF phase shift in the output RF signals. One of problems studied at the Lockheed Electronics Company was the development of a means of minimizing the size of the required capacitor bank. Mention of this work was made in a recent paper.¹ Two methods of achieving the design objective were developed and are presented in this paper.

Conventionally, the required capacitance can be computed if the load impedance, maximum pulse duration, and allowable voltage droop are known. The method of computation is shown in Figure 1. Thus, for a tube having an impedance of 2000 ohms and operating with an allowable voltage droop of 5 percent during a 2-millisecond pulse, the capacity is computed to be:

$$C = \frac{19.2 \times 2 \times 10^{-3}}{2 \times 10^3} = 19.2 \text{ mfd}$$

In the application of super power klystrons, beam voltages of 90 - 120 KV are commonly used. The size requirements and cost of a capacitor bank rated at 20 mfd at 120 KV becomes prohibitively high. An example of a 300-mfd, 35-KV capacitor bank is shown in Figure 2. It was presented at the last symposium by Mr. T. Yingst,² and is shown again to give an idea of the size of representative energy-storage capacitor banks. Re-arranging this capacitor bank into 4 series sections of 75 mfd at 35 KV would provide an 18.75-mfd bank at 140 KV.

¹"Generation of Output Pulses Having a Continuously Variable Pulse Width in a Line-Type Modulator," V. N. Martinovitch, Lockheed Electronics Co., Military Systems Division. Presented at the Sixth Symposium on Hydrogen Thyratrons and Modulators, May 1960, USASKDL, Fort Monmouth, N. J.

²R. C. A. Power Tube Division, Lancaster, Pa.

The Lunar Radar Program of September, 1960, indicated a requirement for a 51-mfd at 125-KV capacitor bank if conventional techniques were employed. An advanced technique was therefore proposed for the Lunar Radar Program. Graphically, the conventional hard-tube modulator output pulse represents the differential between the energy-storage capacitor voltage and the constant-voltage tube drop through the series switch tube. This fact is shown in Figure 3a.

If it were possible to decrease the plate resistance of the switching tube with time, the output pulse voltage would have a smaller droop characteristic, as shown in Figure 3b. In order to maintain the droop of the final output pulse shown in Figure 3a while using half the original capacitor bank, the configuration of Figure 3c was employed to compensate for this droop by varying the plate resistance drop of the switching tube.

Machlett type DP-11R shielded-grid pulsed triodes were selected as switching tubes. They are in current production and are identified as Tube Type ML-8040. A more recent tube, the DP-15, is also suitable for this application. In the Lunar Radar S-band transmitter, which required 51 mfd at 125 KV, the modulator output voltage, having a 5 percent droop applied to the klystron cathodes at the end of 1 millisecond, would be 104.5 KV, as shown in Figure 4a. For a constant switch-tube drop of 15 KV, the output voltage across the capacitor bank would be $104.5 + 15 \text{ KV} = 119.5 \text{ KV}$, with the capacitor voltage decreasing by 5.5 KV.

If one-half of the capacitors were removed, the output voltage droop of the capacitor bank would double to 11 KV. However, in order to maintain the same 5 percent allowable droop at the output of the modulator—that is—110 KV to 104.5 KV, the tube voltage drop of the switching tube must vary from 15 KV to 9.5 KV, as shown in Figure 4b.

In order to obtain a variation in tube drop from 15 KV to 9.5 KV, the grid driver voltage must vary from 1150 volts to 1300 volts, as seen from points A and B, respectively, on Figure 5. For the operation of the tube at -1200 volts bias, a driver voltage swing of from 2350 to 2500 volts would be required, equal to a tilt on the top of the driver pulse of 6.18 percent. This tilt can be obtained in the lower power stages of the conventional drivers and amplified by the main output driver at no great expense.

The limitations of this technique are grid and plate dissipation as well as the possible requirement for a higher voltage power supply.

Figure 4c shows an application of the same technique in the proposed UHF transmitter for the Lunar Radar, wherein the capacitor bank size was decreased from 44 to 22 mfd at 120 KV.

The technique was applied in the proposed design for the M.I.T. "5-MW Versatile S-band Transmitter", which is shown in Figure 6. In this application, the capacitor bank was decreased in size by a factor of five.

The generation of trapezoidal-shaped pulses having a rising voltage characteristic was required recently to drive a hard-tube modulator. Size and weight requirements precluded the use of the conventional cascade of boot-strap, hard-tube amplifiers usually used as drivers.

COMPUTATION FOR CAPACITANCE REQUIRED IN KARD TUBE MODULATOR

WHERE
 $C = \frac{I}{E} \cdot t$
 E = ANODE CATHODE VOLTAGE
 I = ANODE CURRENT
 C = REQUIRED CAPACITANCE
 t = MAXIMUM PULSE DURATION

ZOR A 15 VOLTAGE DIODE
 $E_{DC} = 15 \text{ KV}$

$$+ 1.5 V_{DC} + 1.5 \times 15 = 15 + 2.25 = 17.25$$

$E_{DC} = 17.25 \text{ KV}$

$$C = \frac{I}{E} \cdot t$$

EMPLOYEE COMPUTATION

$$C = \frac{I}{E} \cdot t$$

$$C = \frac{17.25 \times 10^{-12}}{17.25 \times 10^{-12}} \cdot 10 \mu\text{s} = 1 \mu\text{F}$$

FIGURE 1

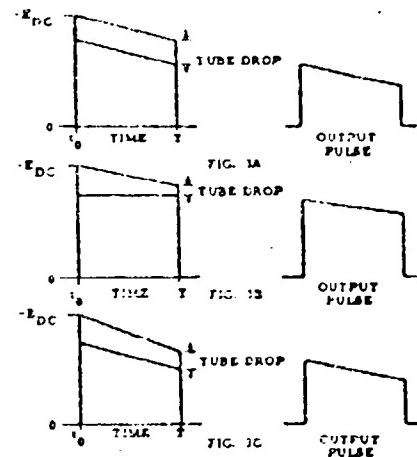


FIGURE 3

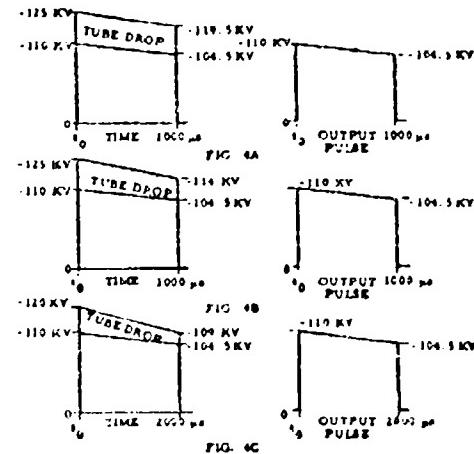


FIGURE 4



FIGURE 2

300 MFD AT 35 KV ENERGY STORAGE CAPACITOR BANK.

Courtesy of RCA

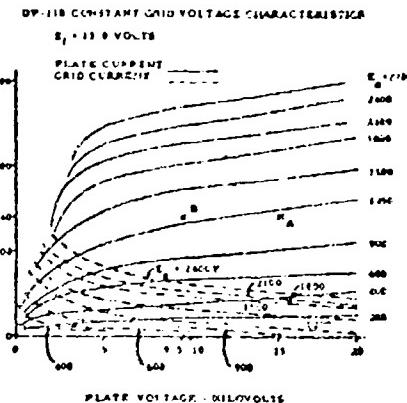


FIGURE 5

The circuit shown in Figure 7, incorporates a line-type modulator. The load consists of the grid-to-cathode impedance of a main hard-tube switch, V2. It is shunted by a series circuit, consisting of a diode, D, a variable resistance, R2, a capacitance C, and a fixed resistor R1, which is much greater than the grid-to-cathode impedance of V2.

When the thyratron, VI, fires, the network discharges through the load. As the positive leading edge of the pulse reaches a value A (see the output waveform) exceeding the voltage at point B, the capacitor, C, charges through the diode. The resulting waveform, when applied to the load, will have a positive ramp voltage.

The point of initiating the rising characteristic is controlled by adjusting the setting of potentiometer R3. The angle of tilt is controlled by varying the value of R2. R1 must be large enough to prevent the current passing through it from charging the output capacitance of the bias supply.

We, in the Advanced Techniques Department of the Lockheed Electronics Company, envisaged a non-dissipative means of providing pulse droop compensation. This plan resulted in the following approach, developed and tested in our high-voltage laboratory.

Figure 8 shows a pulse-forming network, which is substituted for a conventional energy-storage capacitor bank. Its impedance is approximately one-tenth the load impedance of the klystron. The equivalent circuit is similar to that of a line-type modulator working into a positively mismatched load. Hence, the beam voltage, at the time of modulating anode-voltage switching, is equal to ten-elevenths of the network voltage.

An isolating choke was installed in the circuit to isolate the network from the rectifiers. This technique was used successfully in one application wherein RCA ceramic, pulsed tetrodes were used. At that time, a slight increase in anode-pulse rise time was observed. The rise time can be optimized by adjusting the inductor closest to the load.

Assume a maximum pulse duration of 100 microseconds, a tube impedance of 1000 ohms, and a plate voltage of 20 KV. Then, for an allowable droop of 5 percent, the conventional energy-storage bank is computed to be:

$$C = \frac{I_t}{V} = \frac{20 \times 100 \times 10^{-6}}{1000} = 20 \text{ mfd.}$$

If a delay line having an impedance of 100 ohms were used, its total capacitance would be:

$$C = \frac{t}{Z^2} = \frac{100 \times 10^{-6}}{2 \times 100} = 0.5 \text{ mfd.}$$

The pulse voltage applied between cathode to anode of the tube load would be 20 KV, and the power supply voltage is:

$$\frac{1100}{1000} \times 20,000 = 22 \text{ KV.}$$

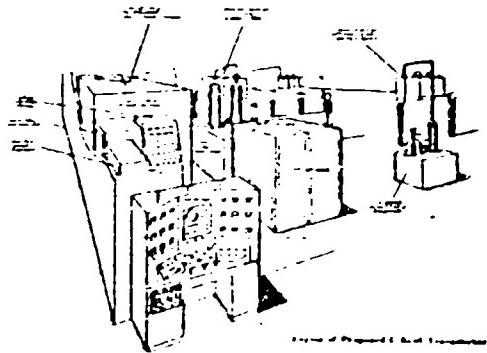


FIGURE 6

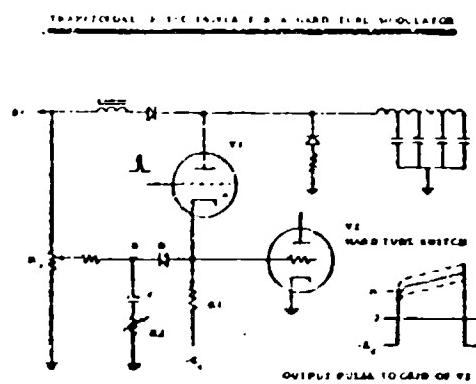


FIGURE 7

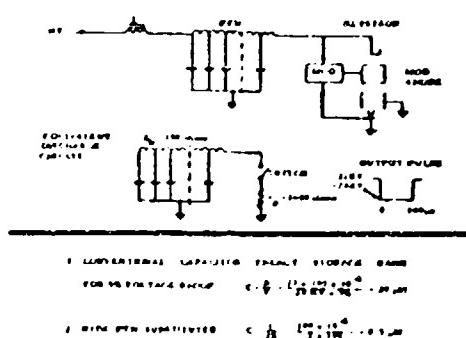


FIGURE 8

Thus, for a 2-KV increase in power-supply voltage and hold-off voltage capability of the tube load, the required capacitance of 20 mfd at 20 KV has been decreased to 0.5 mfd at 22 KV. Dividing this capacitance by 25 indicates the need for twenty 0.02-mfd pulse capacitors. These particular capacitors are inexpensive and relatively small in size and weight by comparison to those of the original requirement for a 20-mfd at 20-KV capacitor bank. Any ripple on top of the pulse can be optimized by adjusting the taps on the network inductor.

**"MODULATOR CONSIDERATIONS FOR MODULATING ANODE BEAM
TUBES IN BURST MODE RADARS"**

by

E. F. Weinburg and W. A. Vail

Raytheon Company - Missile & Space Division

There has been created a need for a new generation of high power radars because of the increased necessity for tools to make detailed studies in the area of space physics. These studies require radars with long range, as well as high range resolution, for making accurate position and attitude measurements. In addition, high data rates are necessary to get detailed velocity information. Gross system considerations indicate that some variation of a high power pulse radar is to be used for this task.

In general for long range, it is necessary to use long pulses as a tradeoff for extremely high peak power, while for high resolution it is necessary to have short pulse lengths. Thus, the two requirements would seem to have a basic incompatibility. One method of resolving this that is being explored currently is to break a long pulse up into a burst of sub-pulses. A radar employing this mode of operation imposes some unusual and stringent requirements on the modulator stages. It is the objective of this paper to examine some of the problems created by these requirements.

In order to discuss this "Burst Mode" type of operation, the following definitions are made:

Pulse Burst or Burst: Term used to refer to a complete complex of sub-pulses which are analogous in this system to a single pulse in a conventional radar.

Sub-Pulse: Part of a burst, the individual discrete pulses of energy that make up the major portion of a burst. There may be more than one type of sub-pulse in a single burst or there may be varying numbers of sub-pulses in successive bursts.

Burst Repetition Rate: Number of bursts per second, analogous to PRF.

Burst Interval: Time between corresponding points of successive bursts.

Sub-Pulse Spacing: Time between end of one sub-pulse and start of next succeeding sub-pulse - may be uniform or non-uniform.

A typical burst waveform is illustrated in Figure 1.

The objective of breaking a single pulse into a series of sub-pulses is to gain increased range resolution, while maintaining the long-range capability of the long pulse. The series of short pulses comprising the burst may be processed in the receiver after detection by a series of very short range gates and combined in a post detection integrator to give a form of pulse compression. Further refinements may be made by using a series of filters to obtain velocity information from the doppler frequency shift. The above by no means explains all the system possibilities, however, the system chosen will determine the detailed burst specifications and it is assumed that these are defined.

The choice of the RF amplifier to be used as the output tube of the transmitter is also primarily governed by the system specifications. These will determine the peak and average power objectives. As always, however, in radars where optimum range is an objective, the power level will most likely be determined by availability of a tube in the band of interest. As the burst waveform of the RF envelope would be determined from the system considerations, as previously discussed, the bandwidth required of the tube is thus defined. The selection of the tube and the finalizing of the system specification is almost always a compromise evolving from what the system attempts to do and what an available tube can do. In a burst mode radar the burst repetition rate is not only determined by the ratio of peak to average power capability of the RF tube, but must take into consideration other factors. A currently available high power tube capable of meeting the objective requirements and already designed into at least one burst mode radar, is the modulating anode type klystron.

A list of specifications for an available typical tube are as follows:

Gain	30-36 db
Efficiency	30%
Phase pushing figure, beam	10°/%
Phase pushing figure, mod. anode	2°/%
Amplitude pushing figure, beam	5/2%/%
Amplitude pushing figure, mod. anode	3/2%/%

Typical operating parameters of this tube are as follows:

Mod. anode voltage	30-40 kv
Mod. anode current	2 amps
Input capacitance	50-100 UUF

In a burst mode radar the phase and amplitude variation of the RF output pulse, during a sub-pulse, during a burst, and from burst to burst should be held to a minimum or at least to within the limits to obtain desired performance. From system consideration, exact limits on both the phase and amplitude variations may be established. In the design of an entire transmitter, these variations must be divided up among the various parts of the system. An assignment of the allowable phase and amplitude variations which may be caused by the final modulator must be made. This is done on the basis of examining each stage of the transmitter and allotting to each what seems to be an equitable share. This usually is a compromise.

In order to design a modulator to drive the modulating anode of the final klystron, it is necessary to translate the above-mentioned phase and amplitude variations into a variation in voltage of the pulse from the modulator. These variations may be such things as pulse droop or perturbations on the top of the pulse. To transfer the phase and amplitude variations into voltage variation, it is necessary to know the phase pushing figure of the klystron modulating anode as well as the amplitude pushing figure.

To compute the allowable voltage droop from the phase consideration, disregarding the beam voltage droop, one needs only the phase pushing figure α in degrees per volt and the allowable phase deviation $\Delta \phi$.

$$\text{The allowable droop } \Delta V \text{ is given by } \Delta V = \frac{\Delta \phi}{\alpha} \quad (1)$$

In a modulating anode klystron the beam current I_b is a three-halves power function of the modulating anode voltage E_{ma} .

$$I_b = k_m (E_{ma})^{3/2} \quad (2)$$

where k_m is the effective gun perveance, the beam power P_b is given by

$$P_b = E_b I_b = E_b k_m (E_{ma})^{3/2} \quad (3)$$

To compute allowable voltage variation from the amplitude variation criteria, we need the rate of change of beam power with modulating anode voltage. This assumes a constant tube efficiency for small changes in beam current so that a change in RF output power is directly proportional to a change in beam power.

$$\left. \frac{d P_b}{d E_{ma}} \right|_{E_b} = 3/2 E_b k_m (E_{ma})^{1/2} \quad (4)$$

$$= 3/2 P_b / E_{ma} \quad (5)$$

$$\frac{d P_b}{P_b} = 3/2 \frac{d E_{ma}}{E_{ma}} \quad (6)$$

$$\frac{\Delta P_b}{P_b} = 3/2 \frac{\Delta E_{ma}}{E_{ma}} \quad (7)$$

If the allowable amplitude variation $\Delta P_b\%$ is given in percent, it is readily seen that the allowable voltage variation ΔE_{ina} in percent is given by

$$\Delta E_{ma}\% = 2/3 \Delta P_b\% \quad (8)$$

With these expressions the allowable voltage droop on top of the modulator pulse may be calculated. These expressions may be used to compute the allowable voltage droop across either a sub-pulse, an entire burst, or a series of bursts.

It should be noted that whichever criteria (phase or amplitude) allows the least droop, will be the one which determines the modulator design.

In a typical burst mode radar, the allowable voltage droop across a burst is on the order of one percent.

The burst mode waveform defined by system considerations would be in terms of the RF envelope. A typical rise time and fall time of an RF pulse desired in this type radar would, given the parameters of the typical tube, be beyond the state-of-the-art if it were to be accomplished by switching the klystron. If this were possible, we would have an ideal utilization of the tube. There are now techniques, however, such as cascade varactor switches which will switch the RF this fast at a low power level in the chain. This technique allows the klystron to be turned on and come to full beam power before the RF drive is turned on and also allows the RF drive and the klystron to be switched off in sequence. (Figure 2) As the beam power of the klystron is limited, the ratio of beam power during RF on-time and total effective beam power becomes extremely significant and is defined as the waveform utilization factor. The effective beam on-time due to the rise time of the video pulse is defined as the time duration of a square pulse which would cause an equivalent beam power dissipation in the klystron as that which is actually produced by the rise time portion of the video. A similar definition can be made for the fall time. This must take into account the fact that the klystron beam current follows a three-halves power law for the modulator anode voltage. The total effective beam-on time τ_e is the sum of the effective rise time, the effective fall time, and the RF beam-on time τ_p .

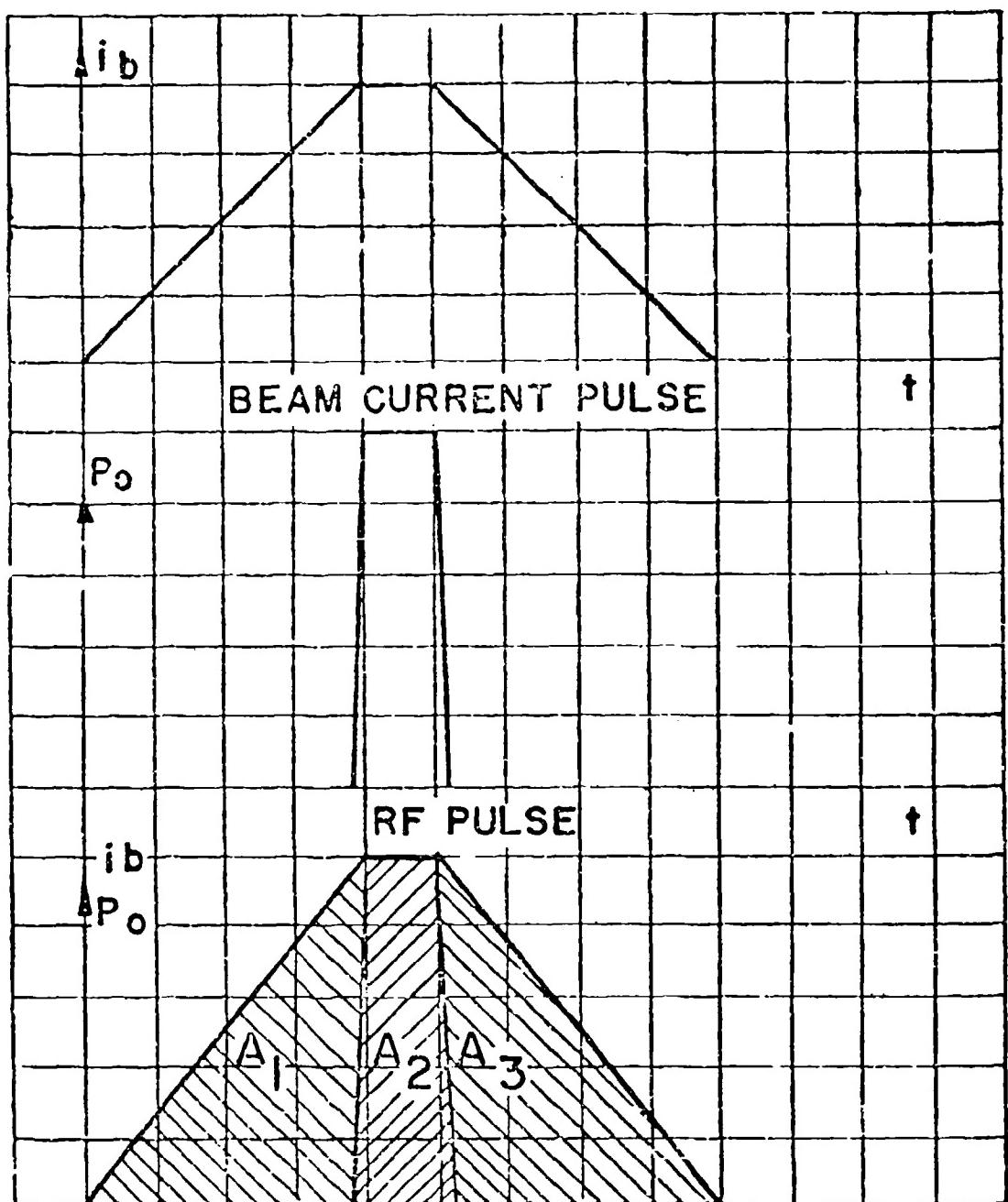
In Appendix I, τ_e is derived assuming the rise and fall times are full exponentials, five time constants long. The result is

$$\tau_e = .7 \tau_r + \tau_p + .13 \tau_f$$

The analysis in Appendix I is simplified by the fact that in this type tube the beam voltage remains relatively constant, the beam current is determined by the modulating anode voltage, and the modulating anode presents a relatively high impedance to the modulator during the pulse.

The waveform utilization factor is largely dependent on the ability of the modulator to switch the klystron with video pulses of short rise and fall times. It should be noted that realizable rise and fall times of practical modulators for this type tube may have an effective beam-on

FIG 2



WAVEFORM UTILIZATION FACTOR = $\frac{A_2}{A_1 + A_2 + A_3}$

WAVEFORM COMPARISONS

time which is equal to or less than the beam on-time of sub-pulse components in which it is being produced. The problem is further compounded by the fact that the total number of sub-pulses per second can be large.

It is informative to see the effect upon waveform utilization factor of various rise and fall times for a short duration sub-pulse (RF on time). The effective beam-on times are evaluated and the waveform utilization factor computed for various ratios of rise and fall times to RF beam-on times. The results are made emphatic when waveform utilization factor is plotted against this ratio in Figure 1. When it is realized the waveform utilization factor essentially indicates the proportion of the total beam power which is actually useful in producing RF during each sub-pulse, the advantage of fast video rise and fall times is obvious.

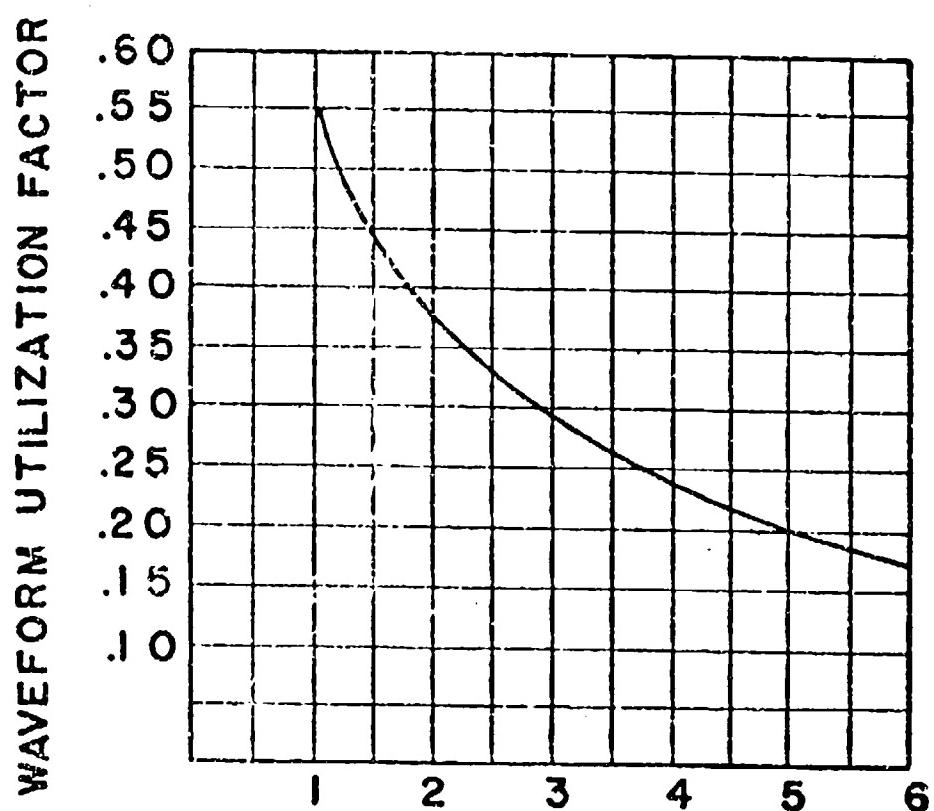
So far nothing has been said about the tubes inherent efficiency in converting beam power into RF energy. In the typical tube the efficiency is specified as 30 percent. In this tube, if all the beam power could be used to produce RF power, the typical tube could theoretically work at .009 RF duty factor. However, if a significant portion of the beam power is used during the time the tube is being turned on and off, as indicated by the waveform utilization factor, the RF duty capability will be reduced by this factor. This would effectively reduce the efficiency of the klystron stage also by the same factor. It also means that because of the limit on tube average beam power, this evaluation must be made to determine the actual RF duty that the tube can work at in any given situation.

If a radar used the above tube, with a ratio of 4 to 1 and a modulator with a waveform utilization factor of .25, the RF duty would be reduced to .00225. This would also have the effect of reducing the effective stage efficiency by a factor of 4.

As the RF sub-pulse components of the burst become longer relative to the video rise and fall time, the waveform utilization factor becomes less significant. Table I shows variations of this with different RF beam-on times for a .4 microsecond rise and fall time pulse. This is plotted in Figure 4.

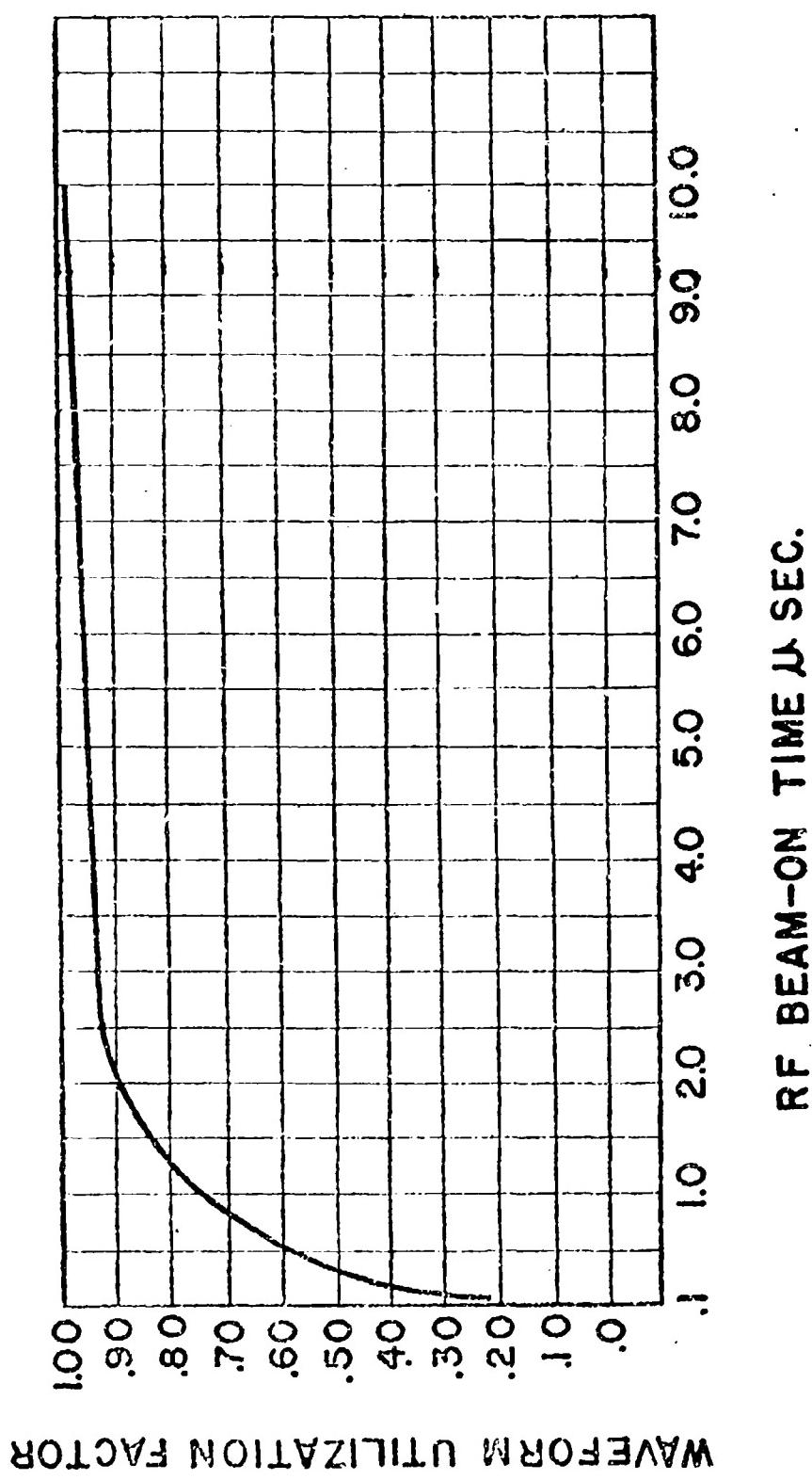
At most burst mode radars will have a mixture of sub-pulses where the number of short RF pulses will predominate and the number of long RF pulses will be limited, the short pulses will dominate the modulator design considerations. The design will have to take into account the waveform utilization factor for each pulse length. The design objective modulator rise and fall time, which can be achieved practically, must be determined. The effective rise and fall times for each component in the burst can be calculated and the waveform utilization factor for the whole burst can be derived by adding the total effective beam-on time components and taking the necessary ratio. The maximum possible burst repetition rate can now be determined by examining the tube specifications and parameters. Again, it has been assumed above that system considerations have determined the burst make-up. It is also obvious that other design input data may be the starting point and that many compromises may have to be made to achieve a final design.

FIG. 3



RATIO OF RISE AND FALL TO RF BEAM-ON TIME

FIG. 4



Video Rise Time	Video Fall Time	Effective Beam On-Time			Effective Beam-On Time	Waveform Utilization Factor
		Rise Time	Fall Time	RF On-Time		
μ s	μ s	μ s	μ s	μ s	μ s	
.4	.4	.28	.052	.1	.432	.232
.4	.4	.28	.052	.3	.632	.474
.4	.4	.28	.052	.5	.832	.601
.4	.4	.28	.052	1.0	1.332	.757
.4	.4	.28	.052	2.0	2.332	.900
.4	.4	.28	.052	5.0	5.332	.936
.4	.4	.28	.052	10.0	10.332	.967

TABLE I

Once the system and beam tube considerations have been evaluated and the necessary video waveform on the modulating anode has been defined, a review of the characteristics of the various modulator types must be made to determine their suitability in the application.

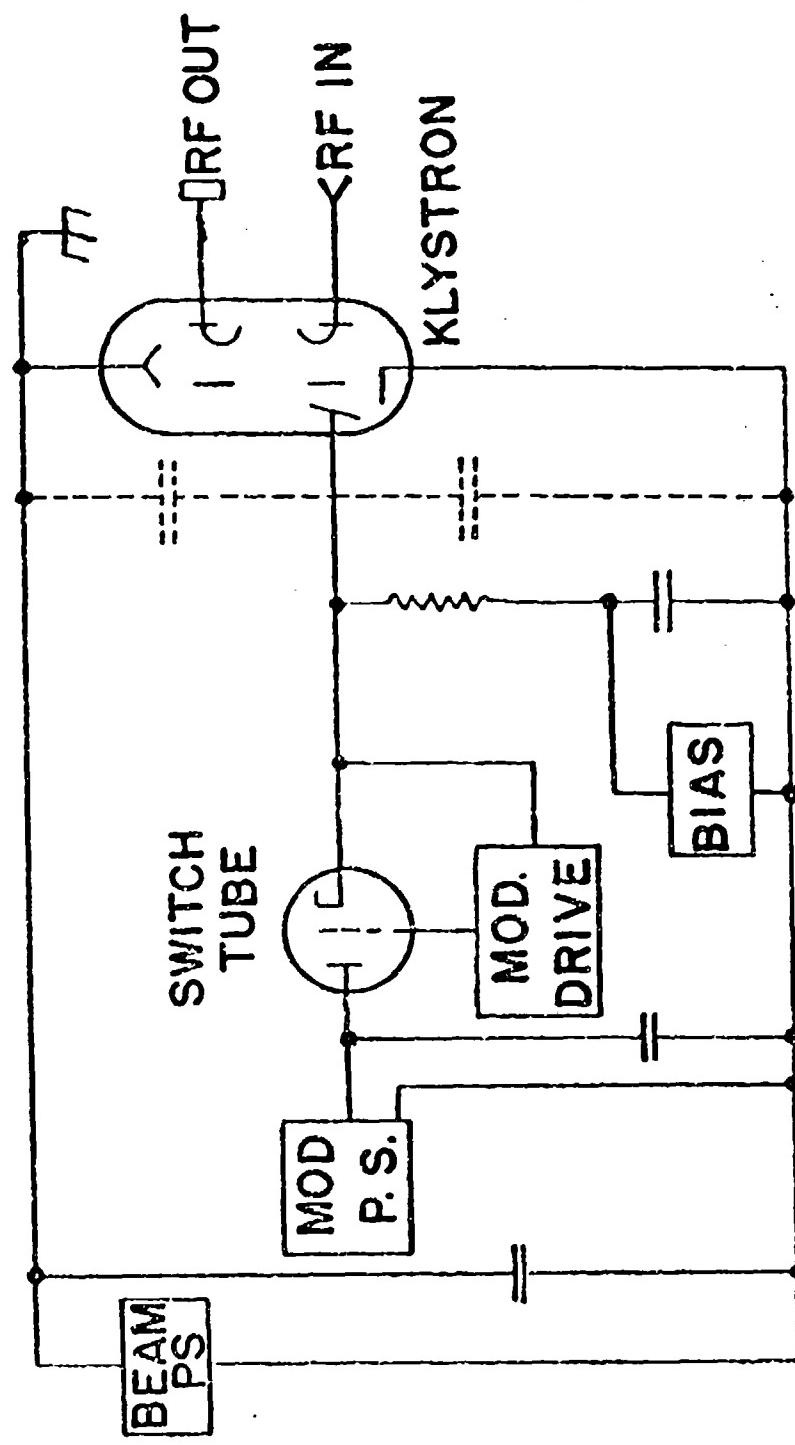
The line-type modulator employing a gas tube as a switch has the necessary rise and fall time capabilities and can be made to produce the short pulses. However, at the present time, the recovery time of available gas tubes is in the order of 50 to 100 microseconds. As the burst mode type of operation may require a recovery time as low as 5 microseconds, gas tubes are ruled out unless it is possible to employ multiple gas tube switches and sequence their firing. The usual practice of using low-voltage, high-current gas tubes with a pulse transformer also seems to have disadvantages inherent in the use of the transformer, that is, degradation of pulse rise and fall times and of pulse shape. This last is not insurmountable but the gas tube recovery time problem is most difficult to overcome and would seem to prohibit their use without extreme complications. A line-type modulator using hard tubes as switches offers some possibilities, however, the pulse forming network is a device limited to a single pulselength, and unless the additional circuit complexity of high-speed switching of pulse forming networks is to be tolerated, these are ruled out for bursts with sub-pulses of different time durations. A further possible problem of line modulators is that of perturbations on the top of the pulse which might exceed the video voltage limitations imposed by the phase and amplitude pushing figures of the klystron modulating anode.

The above discussion is not an attempt to review all the advantages and disadvantages of line modulators but only an attempt to point out those features that appear to determine the impracticality of their use in burst mode radars.

The use of a hard tube switch as a modulator has the advantage of flexibility in terms of pulse lengths, rise times, time between sub-pulses, and accommodation of sub-pulses of various lengths within a burst. The problem, of course, is to find a switch tube capable of switching the high voltage required (in this case 40 kv) and able to pass the peak current necessary to charge the input capacitance of the klystron and the circuit capacitance to achieve the desired rise times. Other limiting factors are the plate dissipation and (quite important) the grid dissipation of the tube. In investigating the switch tubes now available, it was found that at the duty factors at which the practical modulator could be operated as explained before, if these tubes were driven into the non-linear region of their constant grid voltage curves (high peak plate currents or bottoming) that their maximum grid dissipation would be exceeded. This interestingly enough is true for most of the switch tubes examined for a hard tube modulator stage regardless of the power levels. To achieve fast rise and fall times with hard tube modulators, it is necessary to go to essentially low impedance circuits. These circuits are by nature inefficient. Large amounts of power are used by a modulator supplying a modulating anode which in terms of power requires only a small drive. These last are disadvantages certainly, but they are not impossible restraints on the use of hard switch tubes. A possible circuit configuration is shown in Figure 5.

TYPICAL KLYSTON AND MODULATOR

FIG. 5



It may be concluded that a burst mode radar modulator will be required to generate a multiplicity of waveforms and that in order to make maximum use of tube capability and power, the video pulse shapes must include very fast rise and fall times. Further, the brief investigation we have made would indicate that satisfaction of these requirements can best be achieved at present through the use of hard tube switches in very low impedance circuitry to drive the modulating anode of a high power klystron.

APPENDIX I

Derivation of effective pulselwidth for beam current or beam power
(beam voltage constant).

i_b	instantaneous beam current
I_b	final peak value of beam current
e_{ma}	instantaneous value of mod. anode voltage
E_{ma}	final peak mod. anode voltage
k_m	effective perveance - equation (1)
τ_e	effective pulselwidth
τ_o	mod. anode circuit time constant = RC
τ_r	rise time = $5 \tau_o$
τ_f	fall time = $5 \tau_o$

$$e_{ma} = E_{ma} (1 - e^{-t/\tau_o}) \text{ DURING RISE}$$

$$= E_{ma} e^{-t/\tau_o} \text{ DURING FALL}$$

$$i_b = k_m e_{ma} = k_m E_{ma}^{3/2} (1 - e^{-t/\tau_o})^{3/2}$$

$$\tau_e = \frac{\int_0^{\tau_r} i_b dt}{I} + \frac{\tau_p I}{I} + \frac{\int_0^{\tau_f} i_b dt}{I}$$

$$= k_m E_{ma}^{3/2} \int_0^{\tau_r} (1 - e^{-t/\tau_o})^{3/2} dt + \tau_p + \int_0^{\tau_f} e^{-t/\tau_o} dt$$

$$= \tau_p + \int_0^{5\tau_o} (1 - e^{-t/\tau_o})^{3/2} dt + \int_0^{\tau_f} e^{-t/\tau_o} dt$$

EXPAND SECOND TERM BY: $(1 - X)^a \approx 1 - aX$

$$\tau_e = \tau_p + \int_0^{5\tau_o} (1 - \frac{3}{2} e^{-t/\tau_o}) dt + \int_0^{5\tau_o} e^{-t/\tau_o} dt$$

$$= \tau_p + (t + \frac{3}{2} \tau_o) e^{-t/\tau_o} \Big|_0^{5\tau_o} - 2 \tau_o e^{-\frac{3t}{2\tau_o}} \Big|_0^{5\tau_o}$$

APPENDIX I - Cont'd

$$\begin{aligned}\tau_e &= \tau_p + 5 \tau_o (1 + .3 e^{-5} - .3) - 5 \tau_o \frac{2}{15} (e^{-15/2} - 1) \\&= \tau_p + 5 \tau_o (1 + .0018 - .3) + 5 \tau_o \left(\frac{2}{15} - \frac{.014}{15} \right) \\&= \tau_p + 5 \tau_o (1.7018) + 5 \tau_o (.1322) \\&= \tau_p + 8.34 \tau_o \\&\approx \tau_p + .7 \tau_x + .13 \tau_f\end{aligned}$$

THE HIGH SPEED PROTECTION OF MICROWAVE TUBES AND SYSTEMS

by

Albert J. Morris and Joseph P. Swanson

RADIATION at Stanford

INTRODUCTION

The increase in power levels and energy densities in both pulse and cw systems has forced the microwave system designer to resort to high speed protection techniques formerly required only in systems utilizing relatively close spaced triodes and tetrodes.^{1,2,3} Unfortunately, the problem is frequently complicated by the very high voltages at which some microwave tubes operate. The use of thyratrons and ignitrons as "fault diverters" or "crow-bars" has had to be supplemented by spark gaps for systems operating typically in the 30 kv-400 kv range.⁴⁻⁹ High speed protection is defined as diverting the energy so that it is dissipated in the crowbar loop rather than in the load in times of the order of a few microseconds. For the purpose of this paper the load is defined as the microwave tube to be protected.

In order to better define the nature of the problem and why high speed protection is necessary, refer to Figure 1. This figure shows results of an experiment in which energies ranging from 5 Joules to 1000 Joules were discharged into a piece of aluminum foil 2 mils thick. In the experiment a known amount of capacity was charged to a known voltage through a very large resistance. The capacitor had placed across it a spark gap, one side of which was the foil under test. The voltage was then raised until the spark gap fired over, dumping the energy of the capacitor into the foil and also into the gap. No attempt has been made to measure how much of the energy stored in the capacitor was dissipated in the gap itself. The primary purpose of this figure is to demonstrate the order of magnitude of damage at atmospheric pressures done by various energy levels of interest in microwave systems. There is no reason to believe that equivalent damage inside a vacuum should not be expected. In fact, there is much experimental evidence to indicate that this type of damage has, in fact, happened in microwave tubes and that steps must be taken to avoid it.

In the course of protecting a load at microsecond rates, one imposes very significant transients on the system which is connected to the load. For this reason it is essential that a crowbar system design must be an "integrated" design, and that careful attention be paid to protecting not only the load but the equipment as well.^{10,11} These two major areas of protection are treated in this paper.

Destruction of the load can occur due to faults in the load, due to faults in the r-f transmission system connected to the load¹², or due to faults in equipment associated with the load. Prevention of destruction from all of these causes is treated in detail. All typical systems, both pulse and cw, are considered and the special problems and characteristics of each are discussed. In particular, the question of "when do we crowbar" receives considerable attention. Basic design criteria for crowbar systems, including a derivation of crowbar effectiveness as a function of crowbar and system parameters are presented. Finally, a standard test method which has been used successfully in the field is delineated.

WHEN DO WE CROWBAR?

The question of "when do we crowbar" is a dilemma for every system designer. The criteria discussed here will cover by far most cases and should provide a rational basis for decision. Final decision as to which of the potential problems outlined should be protected against will depend largely on the customer, the designer, the funds available, the specific system application, recommendations of the tube manufacturers, etc.

a. Transmission Line Faults:

In power amplifier systems an arc in the output r-f transmission line or excess reflected power can destroy the load. The mechanism can be dielectric breakdown of the output window due to excess electric field, burning at the window due to an arc propagating back to the tube, or mechanical destruction of the window due to the shock wave created by the initiation of arc breakdown. In all of these cases destruction can be prevented by turning off the r-f drive to the load in under a few microseconds. Techniques for doing this are well developed. Waveguide arcs are detected typically by photosensitive solid state diodes placed in the transmission system as close to the output window as possible. They should be positioned so that they can "see" an arc over the widest possible angle and yet they must be positioned out of the main power transmission path so that they do not in themselves initiate an arc. High reflected power is sensed by reflected power directional couplers placed as close as possible to the tube. The crystal output of these is used to drive a fast r-f shut-off circuit. Redundant couplers are often used to ensure operational reliability. The cost of redundancy may be cheap compared to the cost of a new load tube. The time scale for transmission line fault protection is important to pin down. High reflected power will result in an excess field at the load window at the speed of light in the transmission line. In this case, breakdown across the surface of the window will occur in a time equal to the formative time delay of the gas in the transmission line and this will be a function of the gas, the pressure and the electric field present. Fractions of a microsecond to microseconds may be involved. The damage done will be proportional to the energy available.

The window itself may be overstressed even if no surface breakdown occurs. In this case, if the window cracks, we've had it. When an arc occurs the pressure wave moves at the speed of sound in the line. Since this is slow compared to microseconds the pressure in the wave is proportional to the energy in the arc. Once the pressure wave is launched there is no way to stop it, we can only limit its pressure by minimizing the energy fed into the arc. The arc itself stops the instant we shut off r-f drive. Its propagation time is highly variable, certainly slower than the speed of light but sometimes faster and sometimes slower than the speed of sound.

If the load tube is an oscillator and there is a transmission line fault, then there is no way to turn the r-f off fast and crowbarring may be necessary.

The energy levels of concern in r-f transmission line problems are always much less than the system stored energy in pulsed systems. Even so, these r-f energy levels can be quite high. For example, the energy per pulse in the Cornell-Arecibo Radar Transmitter can be 25,000 joules. In the super-power tube program similar energies are involved. It is likely in pulsed systems that energies/pulse exceeding 50 joules can give trouble with energy density being a key criterion. A 50 joule arc in X-band waveguide can be much more harmful than the equivalent energy arc in WR2100 guide.

CW systems can continue to feed a transmission line arc until something burns up since system power supply overload circuitry can't tell when an arc occurs. If a transmission line arc occurs in a cw system it must be stopped quickly--the actual time again being dependent on the energy density involved. In low energy density systems 10-100 milliseconds shutdown time may be fast enough. This is typically achieved by the output of a crystal or photo-cell driving a microammeter meter relay tied into the main interlock chain or r-f drive chain.

Since most modern systems use power amplifiers instead of oscillators in the high power stages we have essentially eliminated r-f faults as typical inputs to our crowbar logic sensing circuits.

b. Load Faults:

This leads us to consider faults which occur in the load. Our load can be the equivalent of a diode such as either a klystron or TWT without a grid or modulating anode or a device such as a magnetron or an amplitron. Or, it can be a klystron or TWT or crossed-field device with one or more grids or a modulating anode. Independent of what the nature of the load is, if a power arc occurs between cathode and ground crowbarring is essential if the energy available to be dumped into the arc is high enough. The question of what is "high enough" is not an easy one to answer. It would be nice if the tube manufacturers could tell us but they can't. Perhaps referring back to the damage data previously discussed can help give guidance. As an opinion, allowing energies in excess of 50 joules to go into an arc in a

microwave tube is unduly risky. What the lower limit should be can at present only be determined by the specific system situation involved.

If the load has a grid or focus electrode or some equivalent electrode close to cathode potential, the arc will always occur between ground and this electrode. If the electrode is not tied to the cathode by a low voltage spark gap or other device which prevents it from going to ground potential, then even though you crowbar, you may destroy the insulation between grid and cathode. Introduction of a grid never eliminates the need for crowbarring, it always increases the need (discussed later) and requires additional protection means.

What about modulating anodes? In tubes with unity mod-anode gain the mod-anode intercept current is of the order of 0.1%. Typically, then in cw systems, the mod-anode is tied to ground through a large resistor. For example, in a 20 kw tube running at 4 amps beam current we could put 100 K ohms from mod-anode to ground and only develop 400 volts of bias in normal operation. If the tube arcs, the arc will always go to the mod-anode. This large resistor not only limits the arc current but also brings the mod-anode to cathode potential which tends to cut the tube off. While there is then residual voltage between mod-anode and ground, we have inhibited the formation of a power arc to ground. If the mod-anode is biased at some potential intermediate between cathode and anode, then the intercept current goes up, the size of the series resistor must go down, and we have a higher probability of a power arc to ground. We can conclude that mod-anodes in cw tubes reduce the probability of power arcs but don't necessarily prevent them completely.

In pulse tubes with mod-anodes essentially the same arguments hold except that in addition to a series resistor we also typically have a switch tube in series with the modulating anode. One essential difference however is that pulse systems always have large energy storage banks associated with them. In such systems there are other reasons for crowbarring so that including the insurance of an excess pulse current crowbar trip mode as added protection makes good sense.

It is important to bear in mind in connection with power arcs that such arcs do not usually go to the collector but to the body of the tube. The body structure is almost always such that very high power densities are involved in arcing situations.

One need only look into a typical tube destroyed by arcing to see that almost always the arc occurs to the most fragile, rather than the most rugged, parts of the tube structure.

In tube processing systems it is desirable not to have to crowbar every time the tube arcs. To avoid this some form of hard tube switch capable of opening in microseconds to isolate the energy storage system from the load is necessary. For high voltage, high power systems it is usually impossible

to find such a switch.

c. System faults:

We are concerned here with things which can happen to the power supply/modulator system which in turn can cause failure in the load. In the cw case there is no modulator and the tube is always connected to the power supply. For this case the only event which can hurt the load is slap on of the power supply at full voltage with the power supply designed such that in combination with the load it is underdamped. This can result in overvoltage and load breakdown. Most systems don't come on at full voltage but run up relatively slowly and don't have this problem. However, some tubes such as TWT's cannot be brought through a low voltage region slowly as they may oscillate in unwanted modes and burn themselves up. For such cases slap on with critical damping should be assured.

For pulse tubes with and without control electrodes the situation is quite different. If for any reason we stop pulsing the power supply will regulate, and if we haven't taken steps to reduce the voltage we can overvoltage the tube when we start pulsing again. Also, if we have a turn-on at full voltage capability and the tube is not being pulsed our problem of resonant charging the power supply is greater than in the cw case because in the cw case the load is always connected.

Figure 2 shows in simplified form six basic modulator circuits. Figure 2a shows a line type modulator. For this case a switch tube arc cannot hurt the load, it simply prevents PTN recharging and shuts down the system. If the load arcs, it can't usually be hurt during a single pulse because the maximum energy available is lost in the PTN and that would mostly go into the inverse load. However, the energy that does go into the load now goes to the body of the tube in beam type tubes rather than to a rugged collector. For this reason even in line type modulators one must think carefully of the total energy available during a pulse and face up to the possibility of crowbarring during a pulse in long pulse systems. Typical protection against load arcs is by an integrating inverse overload circuit in which the circuit will shut off the system trigger and/or power supply after a pre-determined number of successive load arcs. However, suppose we lose the inverse diode. In this case the network voltage can significantly exceed normal voltage. To protect against this, spark gaps across the pulse transformer primary, and/or the PTN, and/or the crowbar will prevent damage to the load.

Figure 2b shows a basic hard tube modulator circuit. In this case, if the switch tube arcs, the peak current does not greatly exceed normal, but there is no way to shut off the pulse and we must crowbar to prevent recharging all of the stored energy into the load. If the load arcs during the pulse off of the pulse, arcs at full switch tube saturation current. I_{sat} is the switch tube rating. It surely arc if it is not triggered off very quickly. Since we need the crowbar for the switch tube to be turned off anyway it is used as a back-up for the switch tube shut-off circuitry. In this case, loss of switch tube

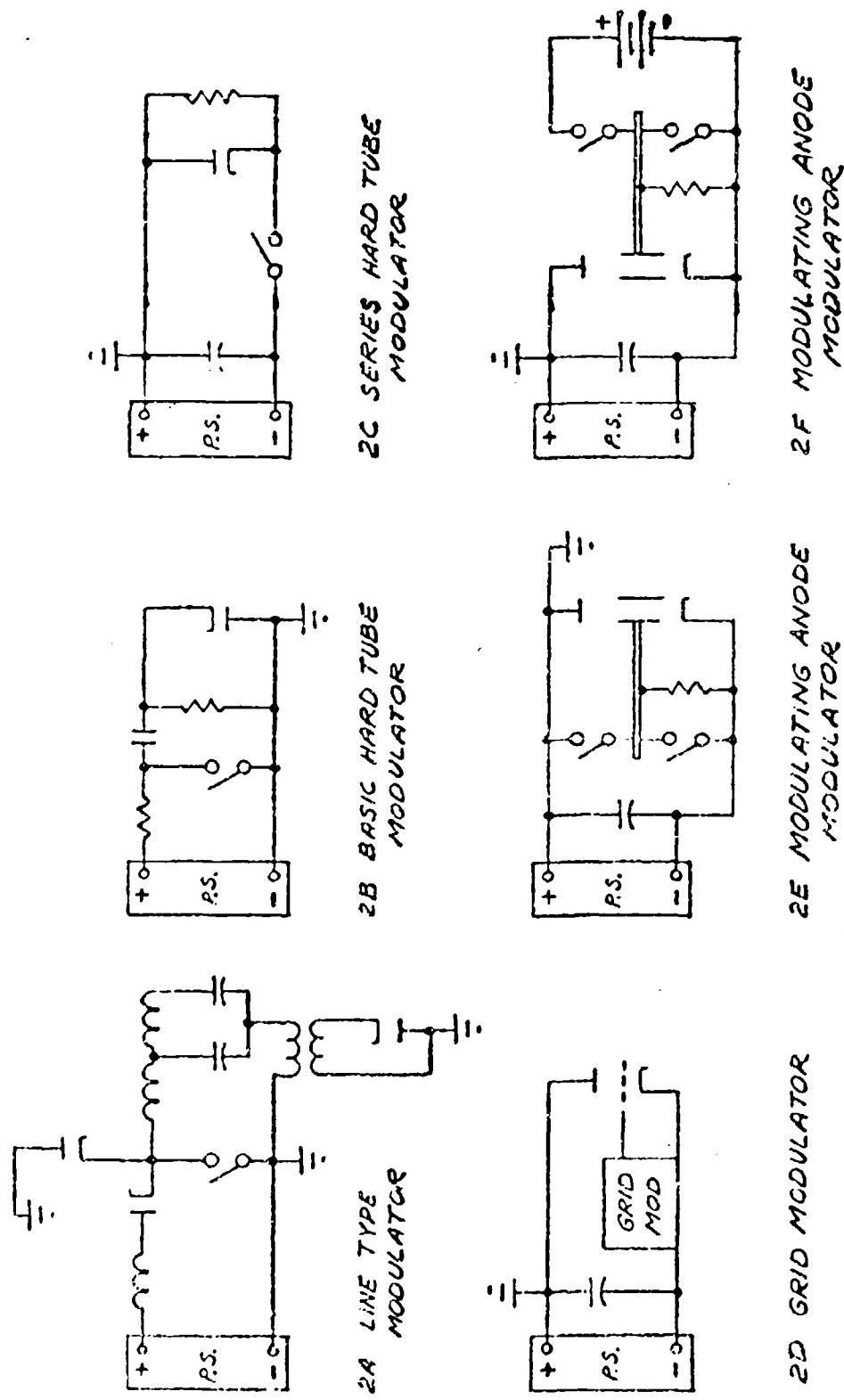


FIGURE 2
TYPICAL MODULATOR CIRCUITS

bias is equivalent to a switch tube arc in the protection required.

Figure 2c is a hard tube modulator configuration in which the switch tube and the load are in series across the power supply filter capacitor which also acts as the energy reservoir. Here, the problems are the same as for the basic hard tube modulator circuit except amplified by the fact that the storage capacitor now also acts as a filter capacitor and as such the stored energy needed for filtering is not isolated by the charging impedance shown in Figure 2b. Thus, our problems are aggravated by having more energy available for destructive purposes.

Figure 2d shows a circuit with a grid modulator. In this case, loss of bias will turn the load tube full on at 100% duty and will typically require crowbar action.

Figures 2e and 2f show tubes with a modulating anode and a pulser switching either to ground or to a bias supply. In these cases, a switch tube arc or loss of switch tube bias will turn the system on with no chance for turn off and may require crowbarring. Also, if the high voltage lead to the mod-anode shorts to ground (as has happened) crowbarring is necessary.

Finally, in pulse modulator systems relying on a stop pulse to turn the system off we must always face up to the possible loss of the stop pulse and be prepared to crowbar.

DESIGN CRITERIA FOR CROWBAR SYSTEMS

There are some fundamental design criteria for crowbar systems which can be treated as universal objectives. These are tabulated on Figure 3.

a. They should have infinite voltage range:

By infinite voltage range, we mean that the crowbar will fire at any voltage on the system from zero to full voltage with no electrical or mechanical adjustment of any kind being required. A minimum of 20% overvoltage hold-off capability of the crowbar device relative to the system open circuit voltage is a typical design goal. Nobody ever argues about infinite voltage range being desirable, but many have argued about whether it is necessary. The best argument of all is that since infinite voltage range can be achieved easily there is no excuse not to incorporate it and thereby take no chances of destroying the load tube.

b. They should be capable of multiple firing:

Multiple firing means triggering the crowbar device repetitively until the power supply primary contactor opens. Incorporating multiple firing with a few millisecond interpulse period eliminates the problem of power supply recharging after the crowbar device detonizes. Again, there may be arguments about how important this is in some systems. But again, since

- a. They should have infinite voltage range
- b. They should be capable of multiple firing
- c. They should be made as fail-safe as feasible
- d. They should be capable of being operated from multiple inputs
- e. They should be interlocked with the system power supply
- f. They should never be incorporated into systems without careful review of system design to insure that system components are specified and protected to take the brutal treatment imposed by crowbarring
- g. They should effectively divert the fault current in under a few microseconds
- h. The crowbar discharge loop should be as close to critically damped as feasible

Figure 3
DESIGN CRITERIA FOR CROWBAR SYSTEMS

multiple firing is simple and inexpensive to do, there is no reason not to incorporate this capability into most systems.

c. They should be made as fail-safe as feasible:

This requirement may seem obvious, but the need for operational reliability is nevertheless worth emphasizing. The crowbar clearly must work when needed and reasonable efforts to ensure this are required. Routine periodic testing of the crowbar to ensure operational reliability is often practiced. Test firing on system turn-on at low voltage is easy to do and represents cheap insurance.

d. They should be capable of being operated from multiple inputs:

All of the events tabulated on Figure 4 need not be used as trigger sources for the crowbar logic circuits. However, in designing any system all should be considered. In most cases, having an excess current input and an excess pulse length input will be satisfactory. It may seem foolish not to incorporate many inputs in all systems since the low level input circuitry is so cheap. Unfortunately, while this is true, the problem of integration of this circuitry into a large system to prevent false signals (noise) from firing low level circuits is not easy to solve and in the past has cost our company a great deal of time and money.

e. They should be interlocked with the system power supply:

Such interlocking ensures the quickest possible opening of the system primary which minimizes the power supply recharging problem and the energy to be dissipated in either the crowbar or the load.

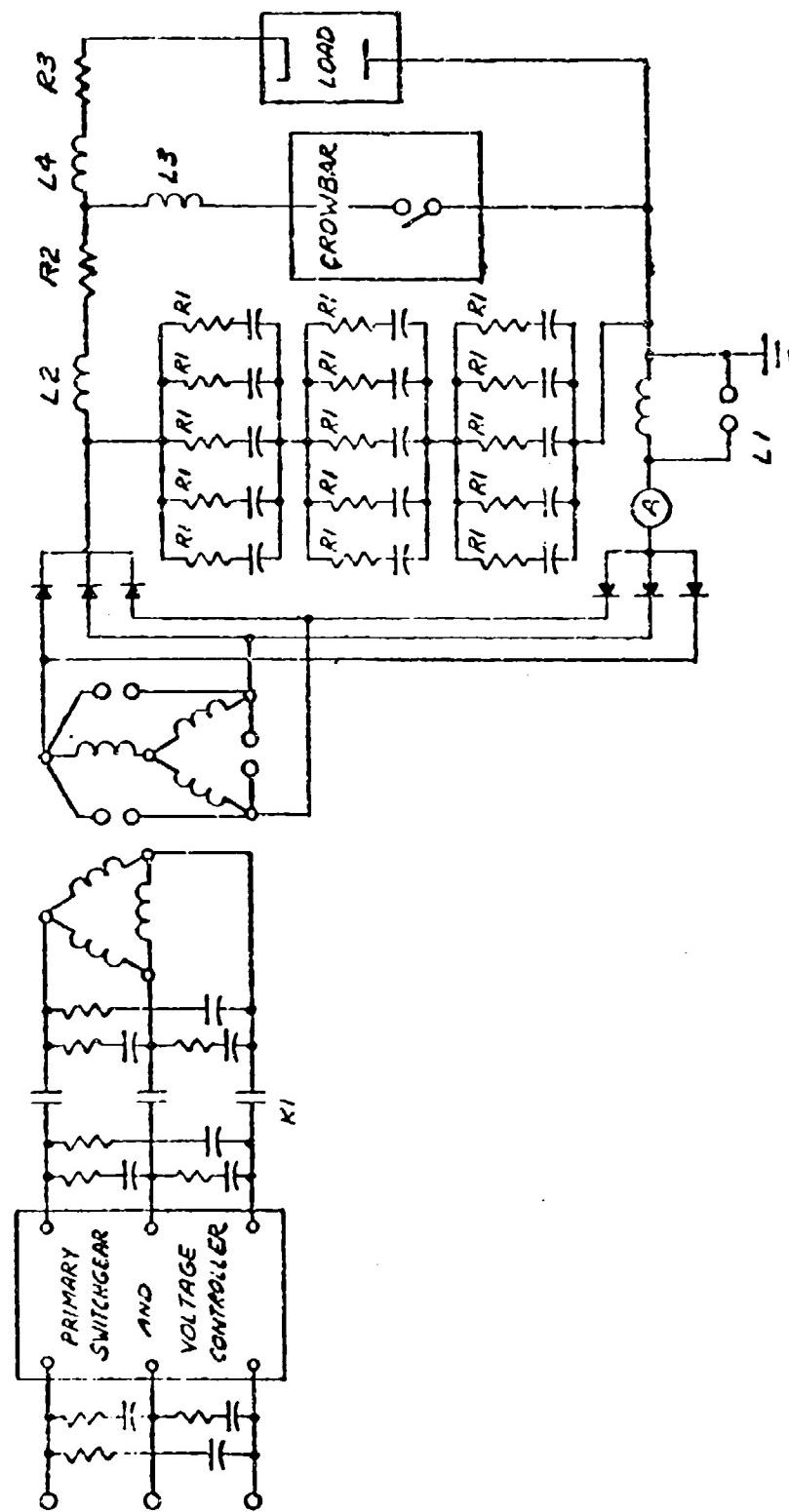
f. They should never be incorporated into systems without careful review of system design to ensure that system components are specified and protected to take the brutal treatment imposed by crowbarring:

To treat the system integration and protection problem in detail it is necessary to refer to Figure 5. This figure shows the essential parts of a typical high power, high voltage system in which the tube is connected directly to the power supply. One can immediately generalize and say that the series sum of $R_1 + R_2 + R_3$ should be as high as possible commensurate with how much power and voltage one can afford to throw away. In cw systems the problem is simplified by lower voltages and lower peak currents, so that very often, until energy densities get comparable to that in the Varian VA849 klystron, only R_3 is necessary and can be made so large that no crowbar is needed. The power rating of R_3 should be at least twice the normal maximum duty cycle rating. Its voltage rating must be such that it can take the full power supply surge voltage across it when the load arcs. Since R_3 is in the cathode lead it must be fully insulated off ground at full beam voltage.

<u>Event</u>	<u>How Detected</u>
1. Transmission line arc	Arc detector
2. Excess reflected power	Reflected power coupler and crystal
3. Excess r-f field in cavity or other component	Probe and crystal
4. Load tube arc	Excess current
5. Loss of bias in load or switch	Excess pulse length
6. Switch tube breakdown	Excess pulse length
7. Cable breakdown	Excess pulse length
8. Loss of stop pulse	Excess pulse length
9. Excess voltage	Compensated RC divider
10. Sputtering during interpulse period	Pulse during interpulse period
11. Capacitor breakdown in string of series capacitors	Compensated RC divider

Figure 4
TYPICAL INPUTS FOR CROWBAR LOGIC CIRCUITS

FIGURE 5
 TYPICAL HIGH POWER HIGH VOLTAGE SYSTEM WITH CROWBAR



If we do not have many capacitors in parallel then only R_1 or R_2 , but not both, are needed. Introducing R_1 reduces filtering but in large banks of series-parallel capacitors it may be easier to use R_1 only and eliminate R_2 . If one capacitor in a parallel string fails all of the energy in the parallel bank will dump into that capacitor. This cannot only cause the faulty capacitor to blow up, but it can also destroy the other capacitors. R_1 prevents this occurrence. Its resistance is made large enough where feasible so that if one capacitor faults the other capacitors in parallel have a critically damped discharge. The sum of $R_1 + R_2$ must not only be high enough to critically damp the capacitor bank discharge when crowbarring but their resistance must be high enough to limit the capacitor discharge current in individual cans to about 8000 amperes. R_2 must have the full system surge voltage rating and be designed using the same criteria as for R_3 . R_1 need only have a surge voltage rating equal to the rating of the capacitor that it is in series with. The wattage rating of R_1 for normal operation should be at least twice that required by maximum duty cycle. However, we are now faced with a choice of whether to consider R_1 as a fuse or make its thermal mass large enough to dissipate the full energy (less one can) of a parallel bank. This choice is dependent on specific system parameters. The L_2 , L_3 , L_4 shown on Figure 3 represent inductance values in the crowbar loop and the load loop which must be estimated so that one can determine the value of R needed for critical damping and for minimizing the energy available for discharge into the load loop.

By the introduction of R_1 and R_2 we have protected the capacitors from failure due to possible excess energy dumping, voltage reversal and excess pulse current. We must also protect them against failure of one of the capacitors in a series string which will short out one level and overvoltage all other levels. By doing this we now have protected the capacitor bank.

When we crowbar all of the power supply voltage appears across the filter choke L_1 . If it is not fully insulated for this surge it must be spark-gap or otherwise protected to prevent its destruction. When the gap across L_1 fires the full power supply voltage appears across the conducting diodes at the same time that they are conducting full short circuit current which can typically be at least 10 times normal current. To prevent rectifier destruction we must choose rectifiers which can take this kind of beating until the primary opens. Also, to minimize the problem, we must get the primary open as quickly as possible. In large systems we attempt to do this in 1-2 cycles of the line frequency. Thus, K_1 in Figure 5 must be a high-speed contactor or circuit breaker.

Among the critical components to protect when crowbarring are the meters in the system. The system ammeter must be located outside of the main crowbar loop. In many systems where we monitor body current the bottom end of the capacitor bank goes to ground through the body current meter. If we crowbar to ground this meter is subjected to a very fast rate of rise of current with the magnitude of the current usually at least 10,000 amperes. This imposes a requirement for a considerable amount of meter bypassing. It is

essential that the voltage across the meters be kept within the meter ratings by capacitor bypassing and voltage limiting devices. Placing the crowbar across the capacitors only and not from the high end of the bank to ground can help.

Another major problem area is the transient created in the system ground loop as a result of the very high rate of rise of current when the crowbar fires. Very low inductance grounds must be used and voltage limiting devices should be placed on all distribution transformers. It can be very distressing, indeed, to lose relays, meters, lights, cable bundles, etc., because of not incorporating transient voltage protection devices on our low voltage a-c lines.

The major problem in crowbarred systems is the voltage transient induced in the high power magnetic components. We've effectively shorted the power supply in microseconds. We've opened the primary in, say, 16 milliseconds. If we keep a dead short on the system we have no problem as the system energy dissipates in the crowbar and the series resistors. However, crowbars can and do deionize, at 50 kv and about 2000 joules deionization times of about 6 milliseconds have been observed. When this happens all magnetic components are carrying full short circuit current and then we open the primary fast. The transient voltages involved can be very high indeed. Extremely careful overvoltage protection on all magnetic components in the system primary as well as secondary is required. In Figure 5, we show a transient suppressing RC filter on the primary components. We have also used thyrites, lightning arrestors and spark gaps. We often use redundant protection. On the secondary for very high voltages we use spark gaps and lightning arrestors. At lower voltages thyrites and capacitors become feasible.

g. They should effectively divert the fault current in under a few microseconds:

By effectively divert we don't mean discharge the capacitor bank in a few microseconds. The capacitor bank voltage is not important as long as most of the energy goes in the crowbar loop and not the load loop. We want the crowbar to fire in under a few microseconds and as long as it looks like an effective short circuit it doesn't matter what the capacitor voltage is.

h. The crowbar discharge loop should be as close to critically damped as feasible.

Critical damping of the crowbar loop prevents voltage reversal on the capacitors. Allowing the capacitors to ring can overvoltage them and cause dielectric failure.

CROWBAR EFFECTIVENESS AS A FUNCTION OF CROWBAR AND SYSTEM PARAMETERS

It is possible to derive simple relationships which give a measure of crowbar effectiveness in protecting a faulted load as a function of crowbar and system parameters. To do this we compare the energy in the fault without a crowbar to the energy in the fault with a crowbar. Without a crowbar the energy dissipated in the load arc is:

$$1 - E_{A_0} = E_0 \frac{R_A}{R_2 + R_3} \quad \text{for } R_A \ll R_2 + R_3 \\ R_1 = 0$$

Where E_0 = system stored energy = $1/2 CV_0^2$

C = system capacity

R_A = effective arc resistance

V_0 = initial system voltage

For the purpose of this treatment, the assumption of $R_1 = 0$ does not limit the results as R_1 and R_2 are interchangeable and when both exist would merely add together. A further simplification will be made by assuming $L_2 = 0$ and $L_4 = 0$. In typical systems this approximation will have negligible effects on actual results.

In a system with a crowbar there is a delay between the formation of a load arc and the firing of the crowbar. During this time energy is dissipated in the arc in the amount:

$$2 - E_{A_1} \cong I_0^2 R_A t_1$$

Where E_{A_1} = energy dissipation in load arc in time t_1

t_1 = time delay between formation of load arc and crowbar firing

$$I_0 \cong \frac{V_0}{R_2 + R_3}$$

We can rewrite equation 2 as:

$$3 - E_{A_1} = \frac{E_0 R_A}{R_2 + R_3} \frac{2t_1}{C R_2 + R_3}$$

STANDARD TEST METHOD.

In the last analysis there is only one measure of effectiveness of a crowbar. Will it protect the load without at the same time destroying the equipment? The answer to this can only come by building the system and trying it out before connecting the load. To do this we use an experimental technique different than that described in the introduction. If we simply set a gap and let it break down as we raise system voltage, then we never know whether the power supply recharged significantly. The best test we know is to set the system voltage and then drop a shorting bar onto the test foil. If the extent of damage to our foil is negligible and we get protection without equipment failure in 100 out of 100 shots we breathe a sigh of relief and go on to our next problem.

REFERENCES

1. Parker, W. N., and Hoover, M. V., "High Speed Electronic Fault Protection for Power Tubes and their Circuitry," IRE Convention Record, 1955
2. Parker, W. N., and Hoover, M. V., "Gas Tubes Protect High Power Transmitters," Electronics, Jan. 1956
3. RCA Transmitting Tube Manual TT-4, pp. 74-77
4. Smith, Bob H., "The Fault Diverter - A Protective Device for High Power Tubes" UGRL Rpt. 3701 Rev. Aug. 1957
5. Goldfarb, Eli M., and Heard, Harry G., "Full Voltage Range Spark Gap Crowbar," Jour. of Applied Physics, vol. 32, Feb. 1961
6. "Crowbar Discharge Switch," Westinghouse Electric Corporation Distribution Apparatus Dept., Preliminary Application Data File 38-350, March, 1961
7. Nisbet, T. R., "Designing a Wide Range Spark Gap Switch," Electronic Design, Dec. 15, 1957
8. Wouk, Victor J., "Self-Triggering Spark Gap Crowbar," 1959 WESCON Convention Record
9. Wouk, Victor J., "Protective Spark Gap," Pat. #2,840,766, June 24, 1958
10. Mark, John T., "Improved Power Fault Protection," Electronic Design, March 5, 1958
11. Freier, L. J., "High Voltage Power Supply Protective Circuit," Electronic Equipment Engineering, Aug. 1960
12. Beust, Walter and Ford, Willard L., "Arcing in CW Transmitters," Microwave Journal, Oct. 1961, vol. 4, No. 10

PROTECTIVE CIRCUITRY CAPABLE OF
AUTOMATIC OPERATION OVER A WIDE DYNAMIC RANGE

by

H. F. Onusseit

Sylvania Electronic Systems, Waltham, Massachusetts

How does one sense a fault in a transmitter whose normal pulse current may be many times short-circuit current? We were faced with just such a problem. Our phased-array transmitter consisted of numbers of identical lower-powered transmitters whose RF outputs had to be adjustable to levels ranging from 4 KW to as much as 450 KW. The individual transmitters were all pulse modulated by means of line-type modulators. Consequently, the normal pulsed plate current at high level of RF output power was many times the short-circuit current at the lower levels of operation. Under these circumstances, it is obvious that the protective circuitry must be designed to sense a fault independently of the initial voltage across, or the inrush current into, the fault.

One must, therefore, rely on some other, less often employed, phenomenon to sense a fault. Among such phenomena available for service are: 1) visible light; 2) audible oscillations; 3) mechanical vibrations; 4) localized heating; 5) reduction in RF output; or 6) the initiation of high-frequency oscillations characteristic of arcs in air or in vacuum. The sensing means to be described used the last phenomenon and, in time, came to be affectionately known as the "corona sniffer."

Figure 1 shows the simplest sort of corona sensing circuit. Although rudimentary, such a circuit will actually work. However, this circuit will operate over only a relatively small range of voltages. Moreover, the triggering action is apt to be erratic and applicable only to a crowbar tube having very modest trigger requirements. The erratic behavior is due to the oscillatory nature of the trigger, the low energy level of this oscillation and the lack of discrimination against the pulse frequencies picked up during normal operation. The limitations of this circuit are, therefore, so restrictive as to warrant additional circuit sophistication.

The circuit of Figure 2, although representing only a modest improvement over Figure 1, has actually provided fault sensing over the range of 8 KV to 40 KV. In conjunction with a hydrogen thyratron crowbar, it successfully protected 1.9 mil wires simulating the delicate grid and screen wires of a super-power tetrode.

There is always a danger that a fault-sensing circuit will trigger spuriously because of the normal pulse voltages present. The circuit of Figure 2, however, can be designed to deliver a much higher triggering voltage without

FIGURE 1
ELECTRICAL CONCEPT OF AN ARC-STRIKING CIRCUIT

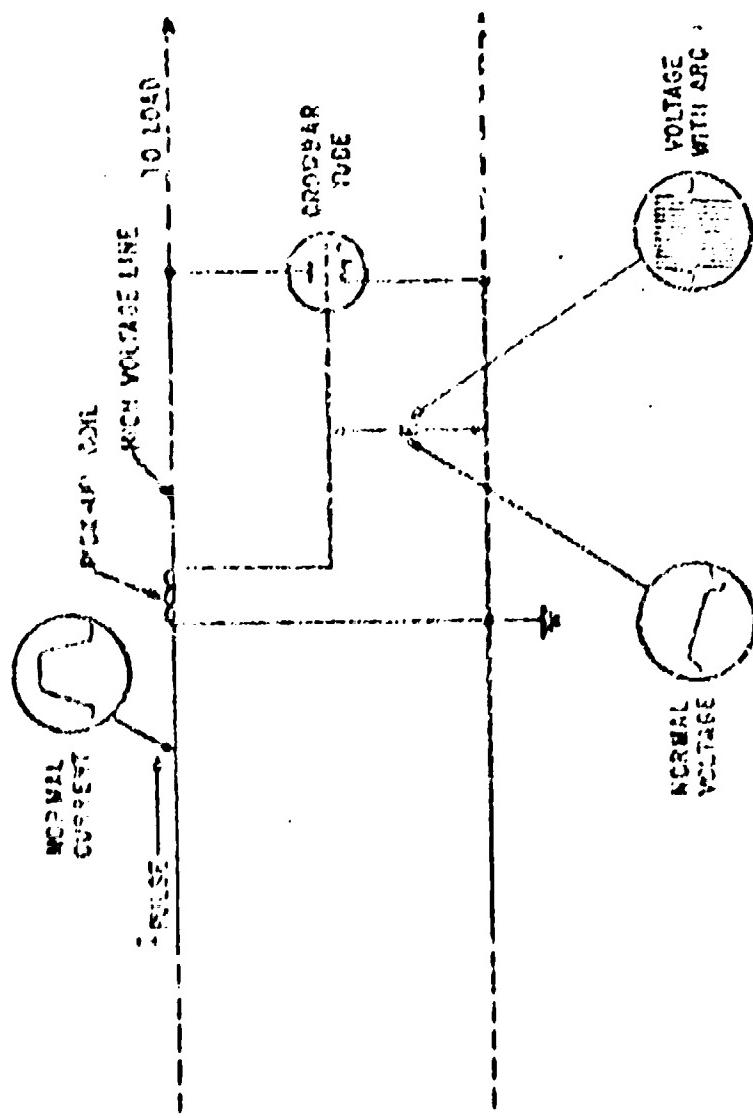
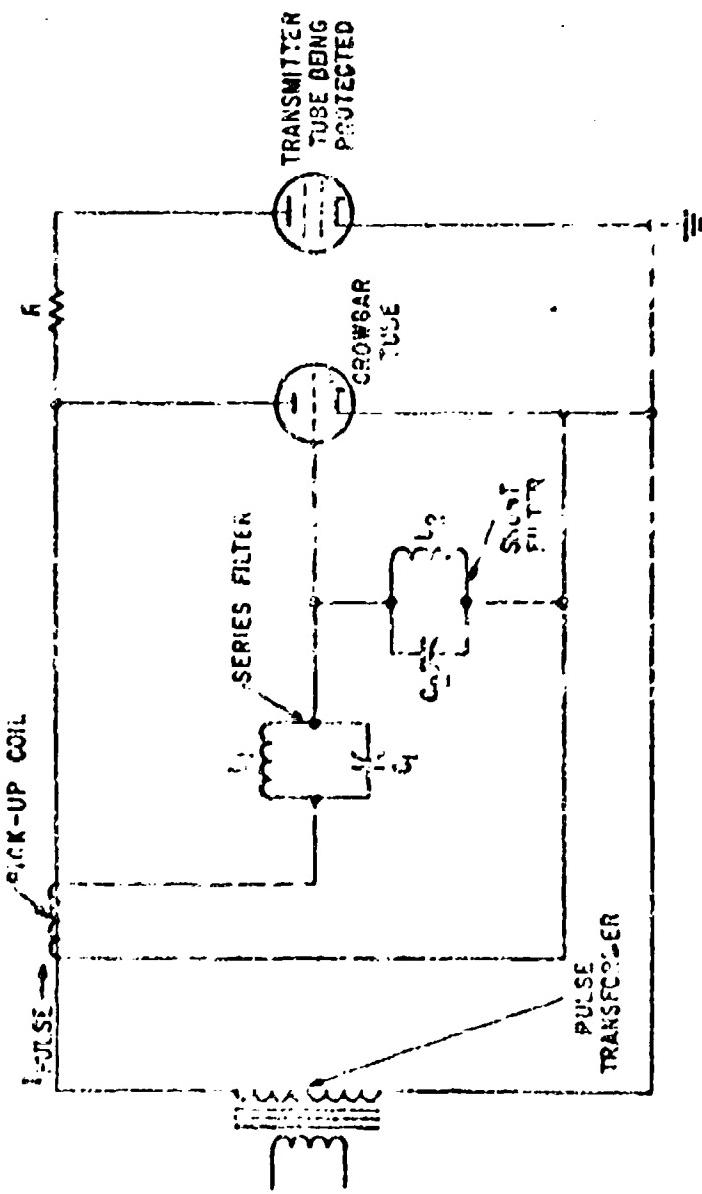


FIGURE 2
RIDIMENTARY BUT WORKABLE FAULT-SENSING
AND PROTECTIVE CIRCUIT



danger of spurious response from this source. The discrimination against the normal pick-up coil voltage is accomplished by means of the series and shunt filters. The series filter is tuned to present a very high impedance to the normal frequencies present and to present a low impedance to the high frequency oscillation initiated by an arc or by corona. The shunt filter is tuned for just the opposite condition. A further step can be taken to enhance the discrimination and to decrease even further the probability of spurious response. This step consists of inverting the voltage from the pick-up coil. With the proper coil polarity the voltage output due to the rise-time of the normal current pulse (normally the maximum output) will be negative when applied to the crowbar grid. This negative trigger will, therefore, have little tendency to fire the crowbar spuriously during normal operation.

The major fault of the circuit of Figure 2 is one previously mentioned in connection with the simple circuit of Figure 1. That is, the high frequency oscillations, because of their positive and negative reversals and their relatively low energy level are unable to provide consistently rapid and reliable triggering action. To overcome this major fault two improvements were incorporated, as shown in Figure 3.

The improvements are these:

1. A simple detector circuit has been added to derive unidirectional voltage from the high frequency alternating voltage existing across the shunt filter; and
2. A pulse amplifier has been added to provide an output pulse having sufficient energy to consistently trigger any crowbar device.

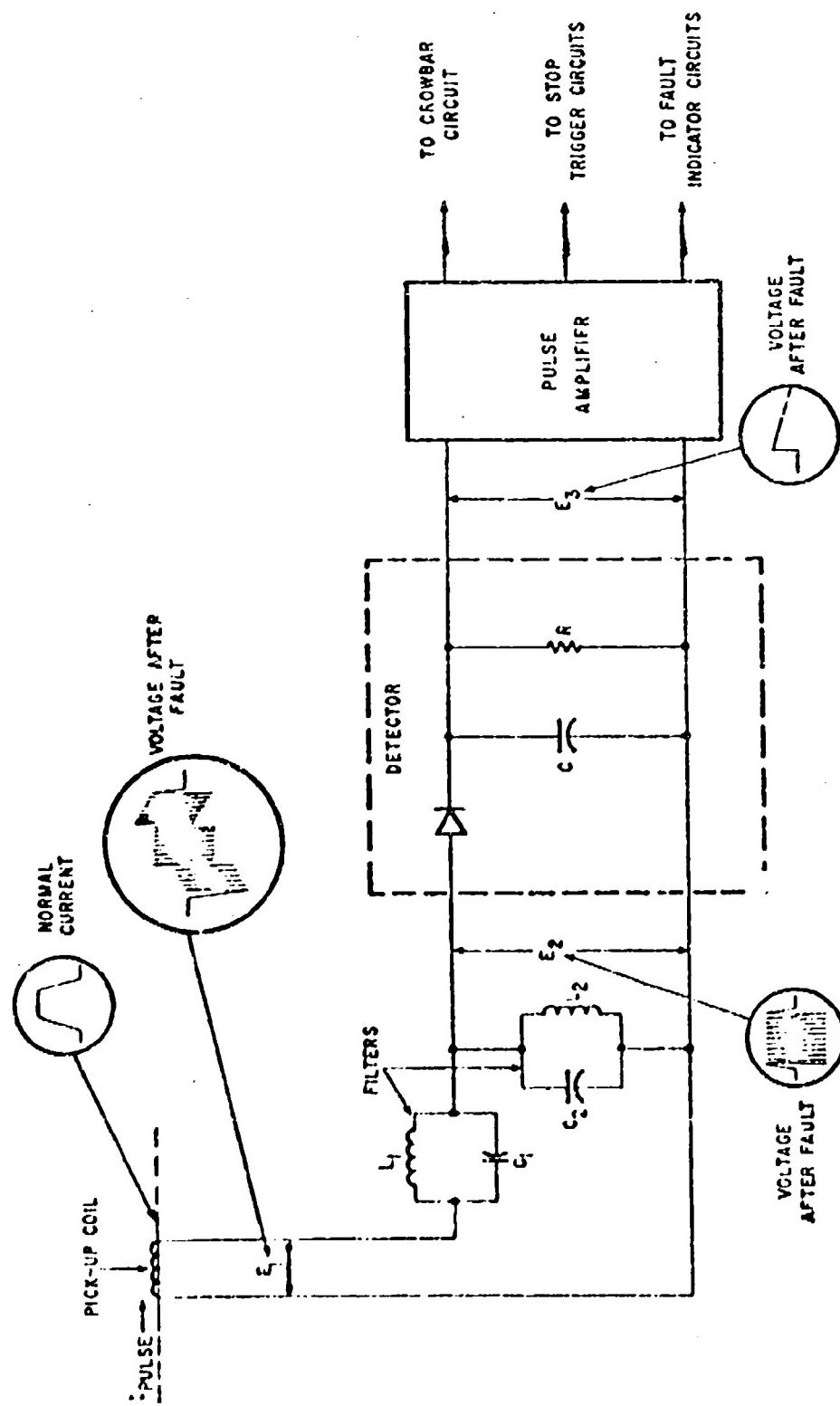
The detector circuit can be extremely simple. In our application it consisted merely of a high-frequency silicon diode, a small capacitor and an ordinary carbon resistor.

The pulse amplifier need not be sophisticated, either. For some applications, a cathode follower and a blocking oscillator will be sufficient. For other applications, the blocking oscillator may be followed up by a modulator driver having sufficient output to fire even the largest crowbar tubes.

Even the initial design of the circuit of Figure 3 was adequate for our application. Consequently, no further steps were required to improve the performance. The output trigger from the pulse amplifier occurred about a microsecond after the initiation of the arc or the onset of corona. This fast action of the sensing circuit enabled the crowbar system to provide mid-pulse interrupting service. The waveshapes labeled on Figure 3 as occurring after a fault, it should be noted, represent the voltages only if the fault is allowed to continue unhindered. Normally, the pulse amplifier will be triggered and the crowbar fired. The action of these circuits will ordinarily modify the waveshapes from those shown.

The fault-sensing circuit of Figure 3 was required to operate reliably with the high voltage line operating at a voltage level of from 5 KV to about 45 KV. The circuit was demonstrated to operate consistently within these limits. It was actually tested up to 75 KV without experiencing spurious

FIGURE 3
PRACTICAL WIDE-RANGE FAULT-SENSING CIRCUIT



triggering. With only slight changes in the component values, the same circuit was used to provide protection in a circuit operating as low as 1000 volts.

To summarize; a corona sensing circuit, although applicable to any type of modulator (or DC circuit), is particularly useful with line-type modulators which must operate over a wide range of output power. The sensing circuitry is simple, sensitive and extremely reliable. It has been demonstrated to provide automatic fault protection completely free of spurious response even when the output power varies over a range of 100 to 1.

FAULT SENSING AND PROTECTION FOR HIGH
POWER KLYSTRON TRANSMITTERS

by

C. Pappas

Radio Corporation of America
Defense Electronic Products
Missile and Surface Radar Division
Moorestown, New Jersey

1. SUMMARY

Modern day high power transmitters utilize large and expensive components in the Final RF Amplifier Stage. Typically speaking, the Final RF Amplifier Tube may cost \$15,000 to \$30,000 and the Klystron Beam Power Supply may be priced as high as \$200,000, or more. The protection of these high-cost items from destructive fires and overloads is, therefore, of paramount importance in terms of economy, component life and the successful completion of the prescribed mission for the transmitter. Some of the measures taken on the TRADEX L-Band Klystron Transmitter include the automatic monitoring, detection and correction of faults starting with the primary power line, thru the Klystron Beam Power Supply, the Final Klystron Amplifier and the associated waveguide system.

In addition to the automatic monitoring system, there have been incorporated special design features which include an electronic crowbar unit to dump the stored energy in the 130 KV Beam Power Supply Capacitor Bank, circuits to remove the primary AC power from the power supply when required, and circuits to momentarily interrupt the RF drive to the Klystron Amplifier when necessary. These features, among others, have been integrated on an overall transmitter basis with a logic readout which is located on the front of the Transmitter Control Console so as to provide the operator with a comprehensive status of the overall operation of the transmitter. The success of this philosophy of Fault Sensing and Protection is attested to by the fact that the major components performed as anticipated during the sub-system test of the TRADEX L-Band transmitter at RCA Moorestown, N. J. Block diagrams, schematics and photographs illustrating the application of a comprehensive Fault Sensing and Protection System to the TRADEX Transmitter are presented.

2. INTRODUCTION

Fault Sensing and Protection as developed at the M&SR Division of RCA is the outgrowth of experience accumulated on such high power transmitters as the AN/FPS-49 (BMEWS Engineering Model), the NIKE ZEUS Acquisition Radar Transmitter, installed at WSMR, White Sands, New Mexico, MADRE, and the TRADEX L-Band and UHF Transmitters. During the R/D phase of these transmitters at the M&SR Division at Moorestown, N. J., and during the latter phases of site checkout and field operation of these transmitters there was gradually evolved four basic requirements of fault sensing and protection for high power transmitters. These are:

- a. Protection - An adequate system must provide protection for large and expensive components in an R/D or operational environment which includes the arcing and seasoning of high power tubes, power supply overloads due to circuit and component malfunctions, and malfunctions in the RF transmission circuitry. Further, the protection system should operate to sense faults and to remove power and then permit the normal operation cycle to be resumed immediately; and it should restrict the component failures to small and easily replaceable items and to the component or area which caused the fault.
- b. Automatic Sensing and Logic Readout - Due to the fact that transmitters of the type discussed herein are in actuality large stations and may easily occupy 7,000 square feet and more, the fault sensing and protection system must be entirely automatic in its operation, and it must have a logic readout on the control console which eliminates ambiguity and which specifies the type and location of a malfunction. In addition, it must present sufficient information to a skilled operator such that in conjunction with other console status indicators it will enable him to make the decision whether to commence operation again or to initiate other action.
- c. Economy - Economy dictates that the cost of maintaining a large stock of very expensive components for replacement be minimized. In addition, the storage of large components such as transformers and inductors which may weigh 1 to 30 tons poses a major problem in itself. Likewise, the maintenance of expensive spares becomes a problem.
- d. Safety - Provisions must be included for the protection of personnel, the emergency removal of all primary power and, in some cases, a separate and backup scheme for removing all primary power from the transmitter area which is independent of the switchgear located immediately in the transmitter complex.

3. OVERALL SYSTEM

A simplified block diagram of the major areas covered in the overall fault sensing and protection system is shown in Figure 1. Referring to this figure it is seen that this includes the 3 phase/4160 volt switch gear and the associated beam

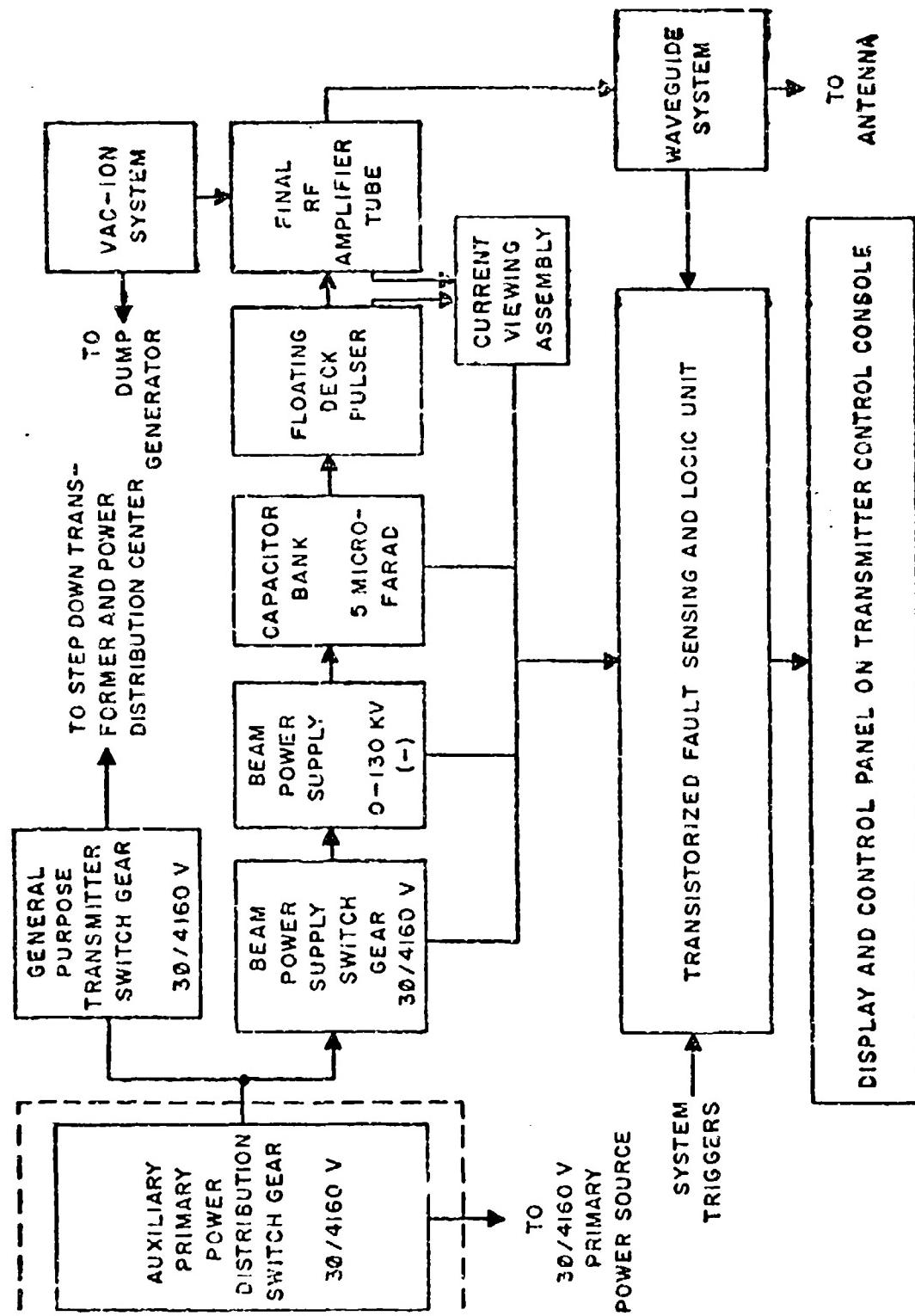


FIGURE 1 - SIMPLIFIED BLOCK DIAGRAM OF FAULT SENSING SYSTEM - SK-33062-1-WHE

power supply, the capacitor bank for the beam power supply, the beam deck pulser, the final RF amplifier stage and the waveguide system.

Figure 2 breaks this down further and includes the sensing elements and the protective devices as well. It is thus seen that eight sensing points are provided for monitoring the performance of the high power circuits. This includes overload relays for the 3 phase/4160 volt primary power, overvoltage sensing of the DC output of the beam power supply, inverse current arc-back detection in the F-7869 (D-1039) vacuum rectifiers for the power supply, crowbar current, beam switch tube arcing, klystron arcing, klystron vacuum, waveguide VSWR, and video duty cycle overload for the klystron. Each of these areas will now be discussed in detail.

4. KLYSTRON BEAM POWER SUPPLY OVERLOAD

A high speed remotely controlled GE Model AM-IIS circuit breaker is used to control the 4160 volt/3 phase power to the klystron beam power supply. It has an interrupting rating of 150 MVA and 30,000 amperes at full 4160 volts. It has a guaranteed 10,000 cycle trip life and a 2,000 hour performance rating without maintenance. Its interrupting speed is 1.96 cycles of 60 cps or 32.7 milliseconds measured from the application of the solenoid trip power. This time includes breaker operating time and arcing time, but not overload relay operating time. Overload relays type GE-1AC77 provide instantaneous and time delay tripping of the high speed circuit breaker when the 4160 volt line current reaches 600 amperes. A variable time delay as illustrated by Table I is provided also. This is based on a 100% full load line current of 208 amperes.

TABLE I

<u>% Load</u>	<u>Relay Time Delay (Seconds)</u>
150	0.5
200	0.22
300	0.15
500	0.05
800	0.035

5. BEAM POWER SUPPLY OVERVOLTAGE

The DC output voltage of the klystron beam power supply is monitored via a 150 megohm 1000/1 resistive divider. Its function is to guard against high voltage surges on the DC bus. The range of protection is adjustable from -126 KV to -155 KVDC. Tripping of the high speed circuit breaker is provided.

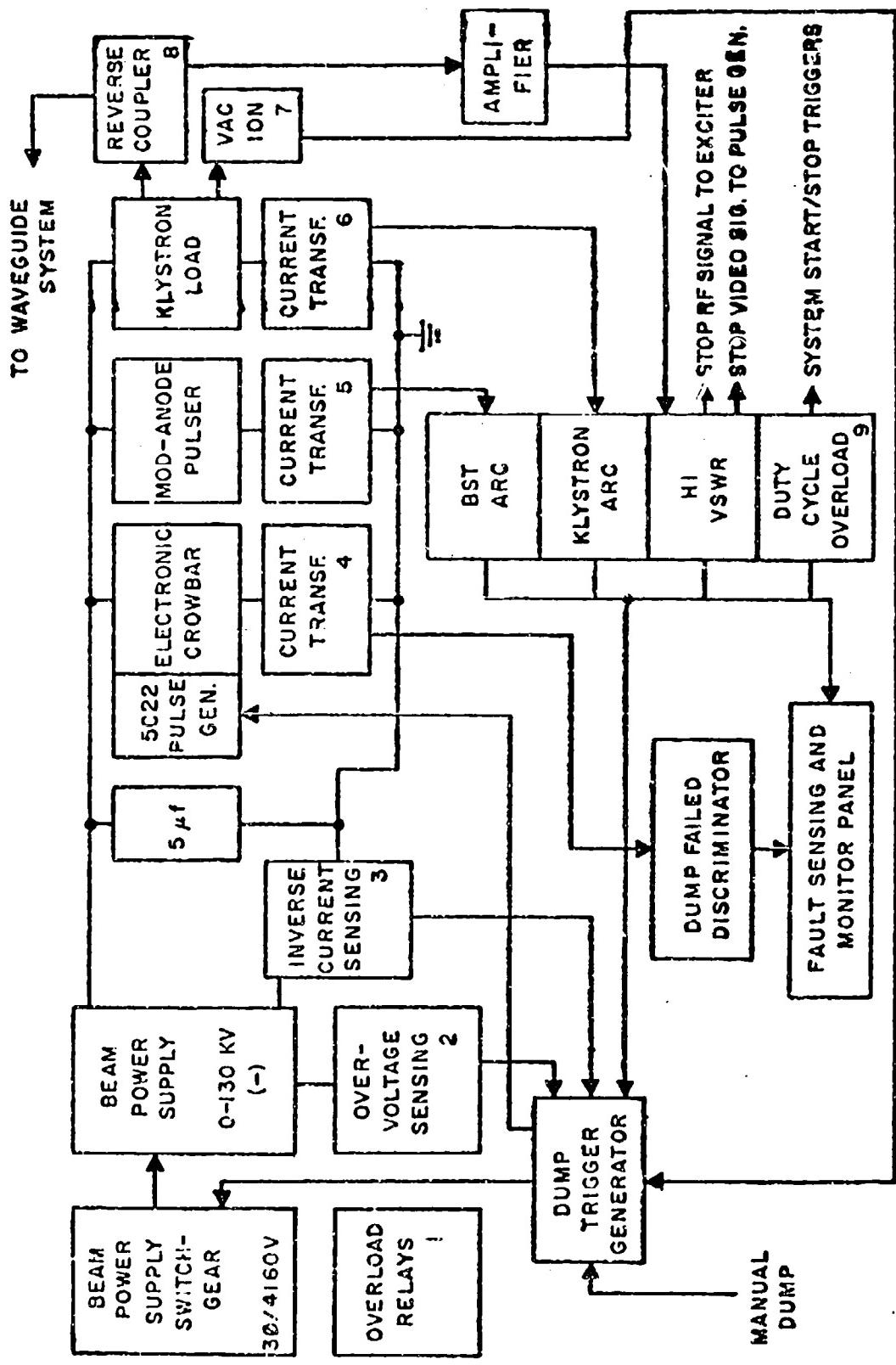


FIGURE 2 - BLOCK DIAGRAM OF FAULT SENSING AND PROTECTION INCLUDING
SENSING ELEMENTS AND PROTECTION DEVICES - SK-4962-2-CP

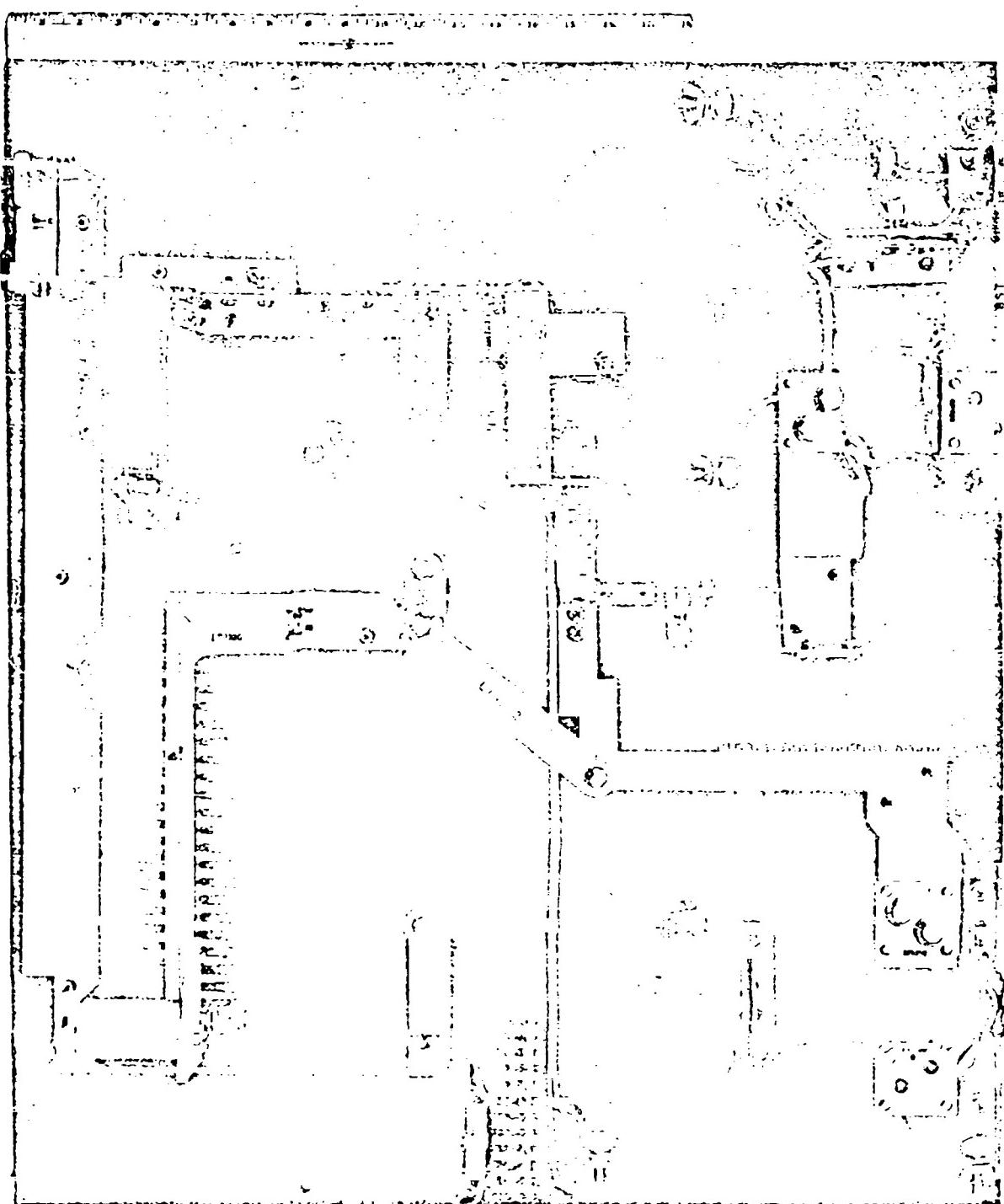


FIGURE 3 - KLYSTRON AMPLIFIER CURRENT VIEWING ASSEMBLY

generated when high reflected RF power occurs and a stop trigger is generated which triggers an SCR in the RF Exciter that, when triggered biases the second multiplier stage past cutoff. RF power in the RF Exciter that is re-applied gradually by means of a slow R-C time constant in this stage.

11. FAULT SENSING AND LOGIC UNIT

The aforementioned fault sensing and protection features are integrated in the Fault Sensing and Logic unit located in the front of the transmitter console. This area will be discussed next.

Figure 4 is a block diagram of the fault sensing and logic unit. It is to be noted that the entire logic function and automatic feature capability is provided by 13 plug-in modules. A typical module is shown in Figure 5.

Another feature not previously discussed is that manual operation of the crowbar unit is provided. In case of necessity, a manual dump may be executed by the operator; and it provides a means of checking the crowbar unit at the start of operation of the transmitter. Another important feature incorporated in the fault sensing and logic unit is the selection of the number of faults and its relation to the re-application of power after a fault. For instance, prior to operation, the operator has the option to choose manual or automatic re-operation after a fault. If manual operation is selected, then after a fault has occurred, the fault must be cleared manually by the operator before high voltage operation may be resumed. If automatic operation is chosen, then three faults can occur in succession in any 10 second interval after which an automatic lockout feature takes over and manual clearance of the fault is again required. If four faults occur within one minute, then automatic lockout takes over and manual re-operation is required.

Figure 6 is a front view of the panel containing the Fault Sensing and Logic Unit for the TRADEX L-Band Transmitter. It includes in addition to the lights, controls for the crowbar unit, counters, a neon lamp to indicate high VSWR, and it provides automatic readout of the type and number of faults which have occurred. The back side of the front panel is shown in Figure 7, and Figure 8 is a rear view of the unit showing the plug-in module nest. For purposes of orientation, there is shown a picture of the Transmitter Control Console in Figure 9.

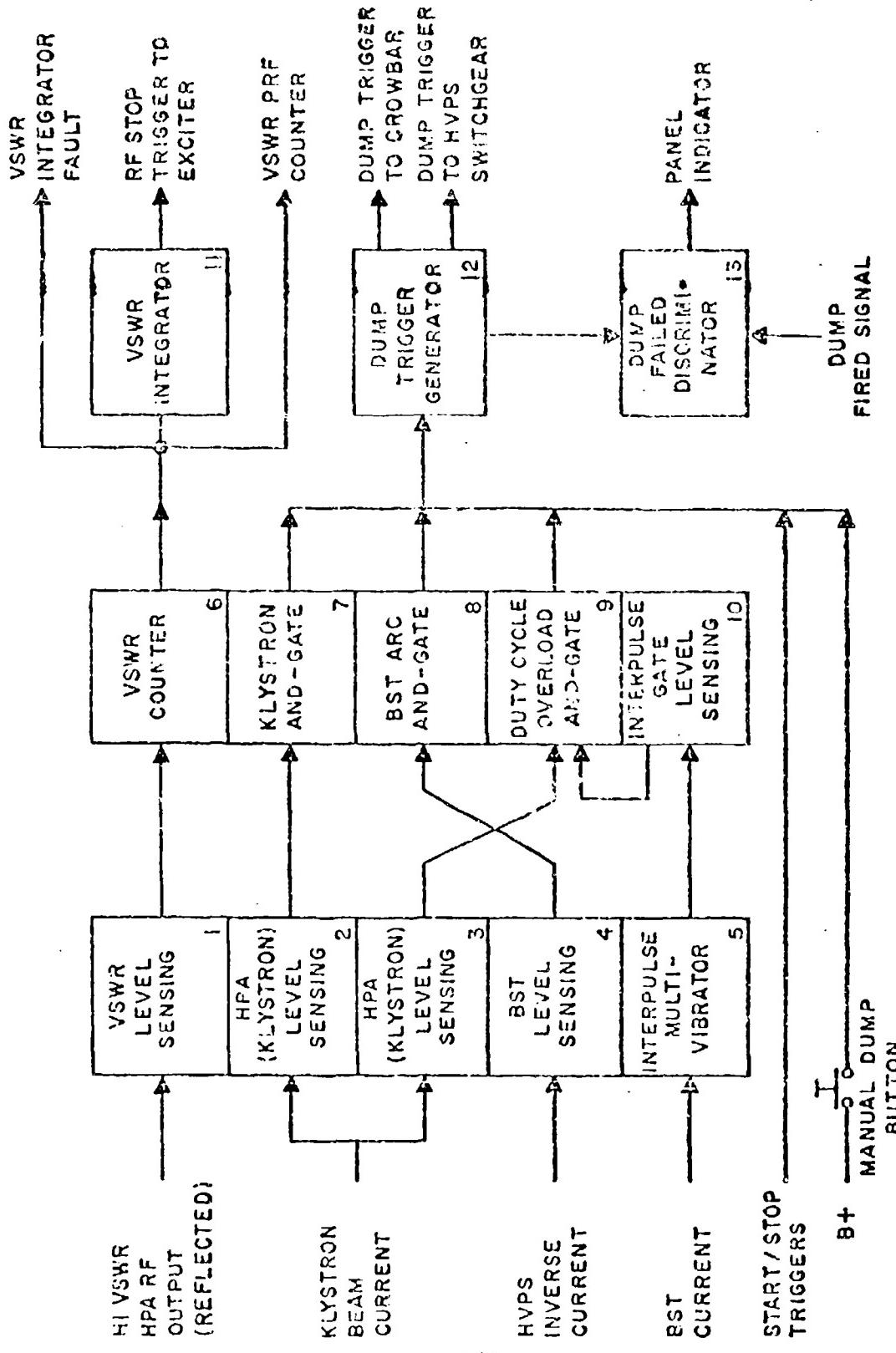


FIGURE 4 - FAULT SENSING LOGIC DIAGRAM - SK-4962-1-CP

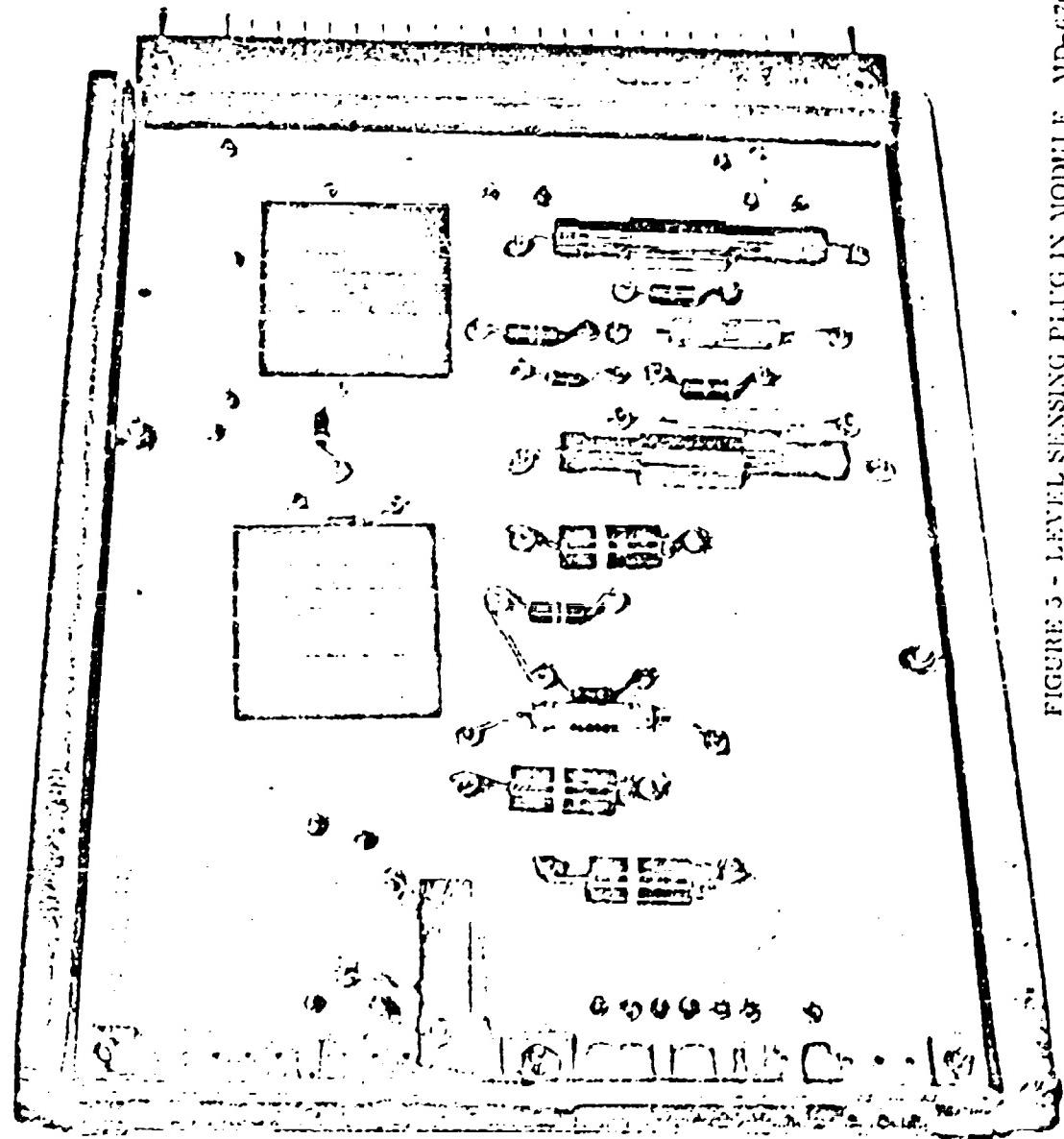


FIGURE 5 - LEVEL SENSING PLUG IN MODULE, MD-676
(RCA 8631153-503) FOR FAULT SENSING AND LOGIC UNIT

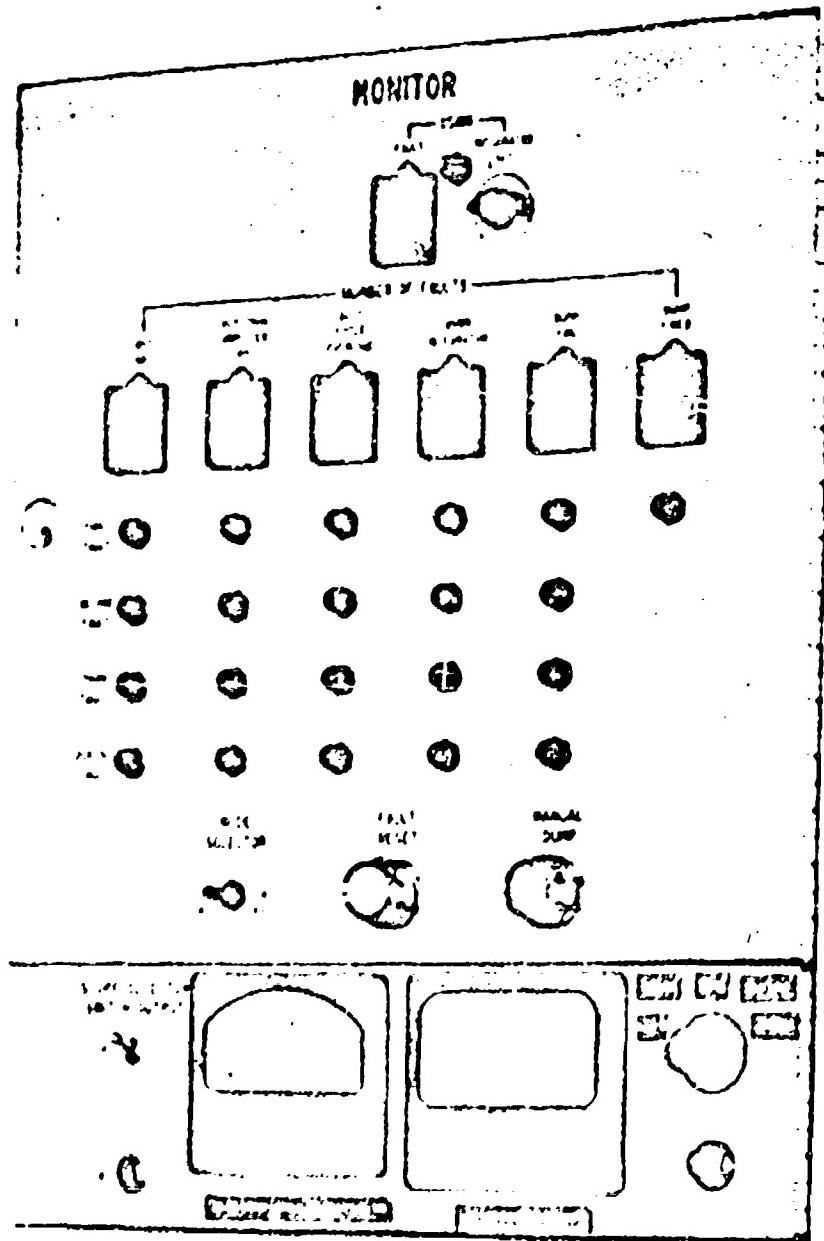


FIGURE 6 - FRONT PANEL VIEW OF FAULT SENSING AND LOGIC UNIT

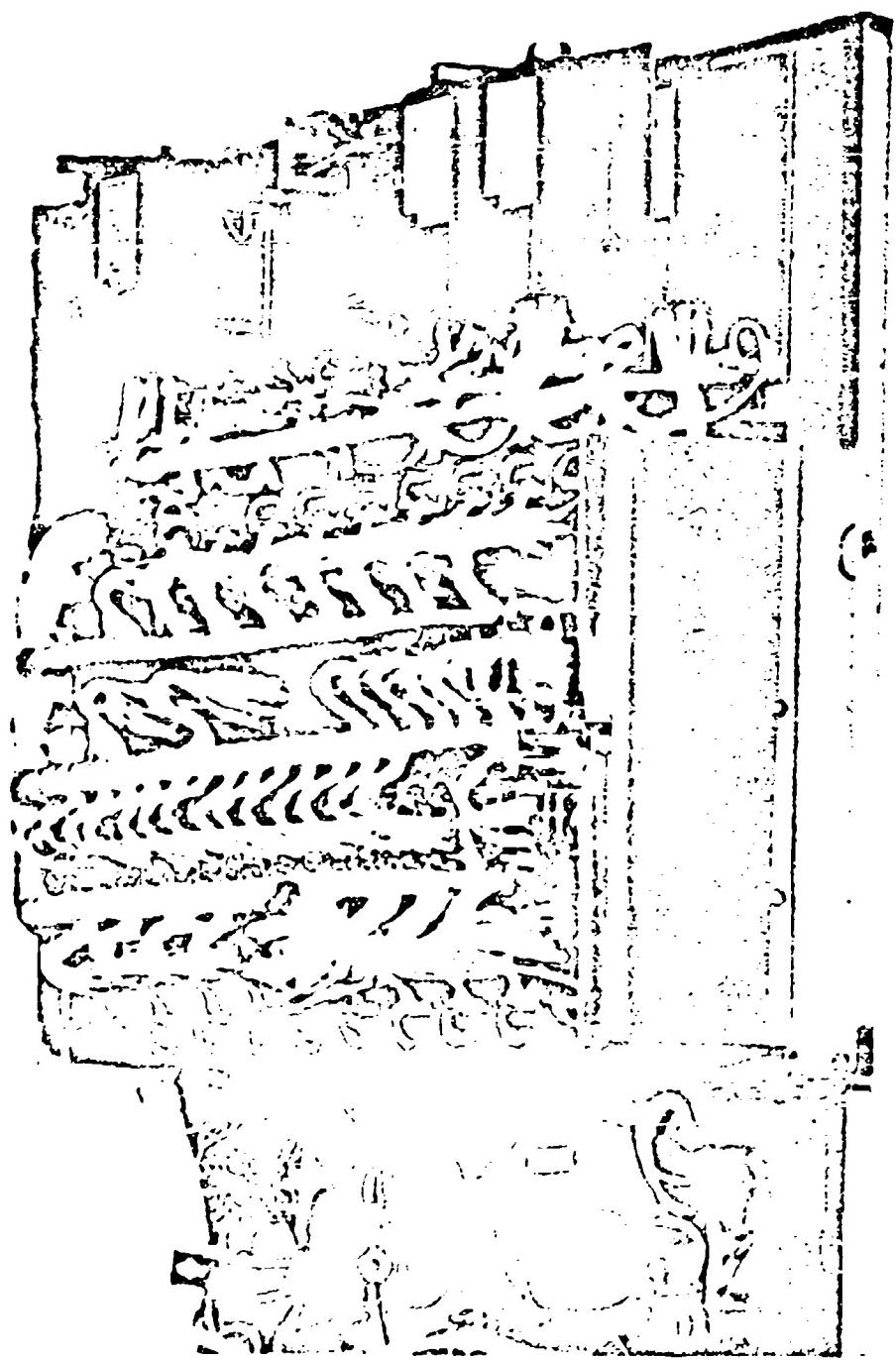


FIGURE 7 - REAR VIEW OF FAULT SENSING AND LOGIC UNIT PANEL

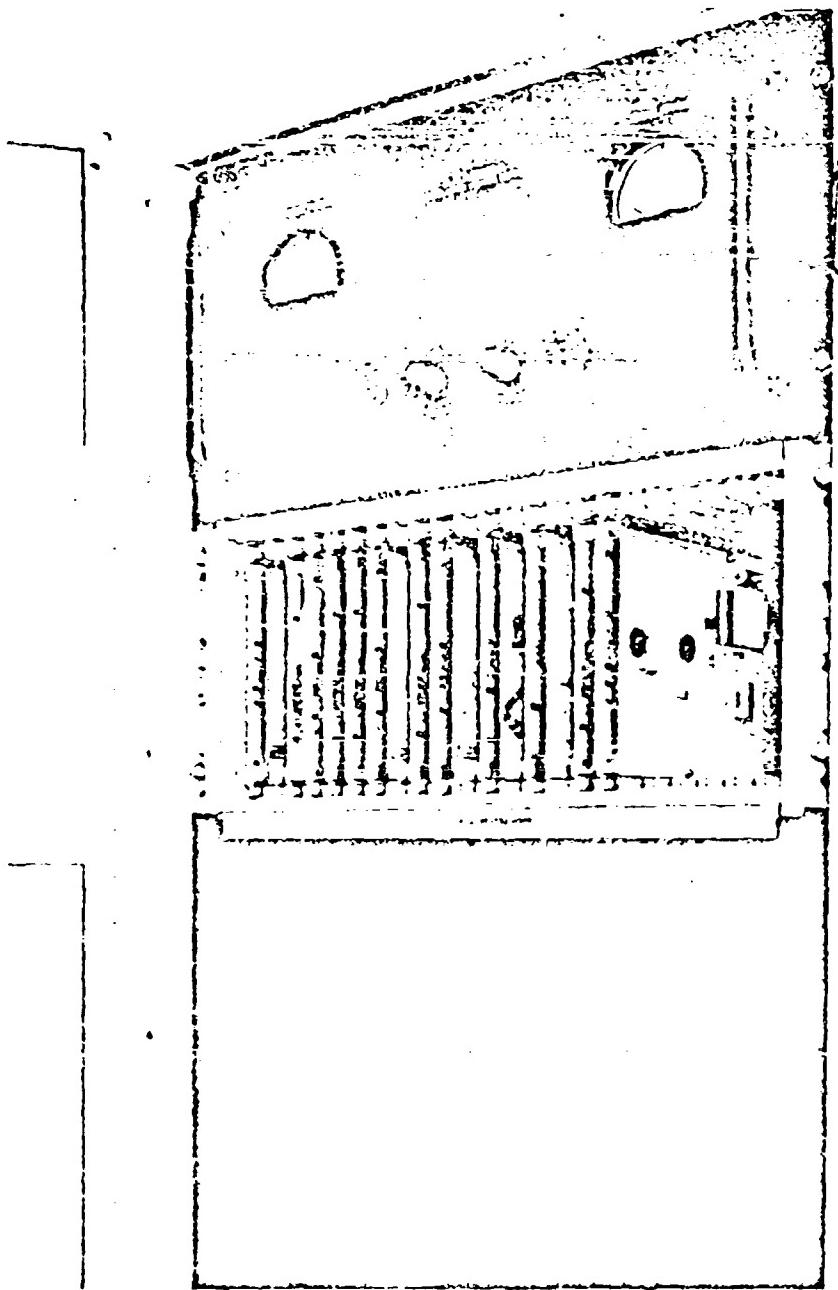


FIGURE 8 - REAR VIEW OF FAULT SENSING MODULE NEST

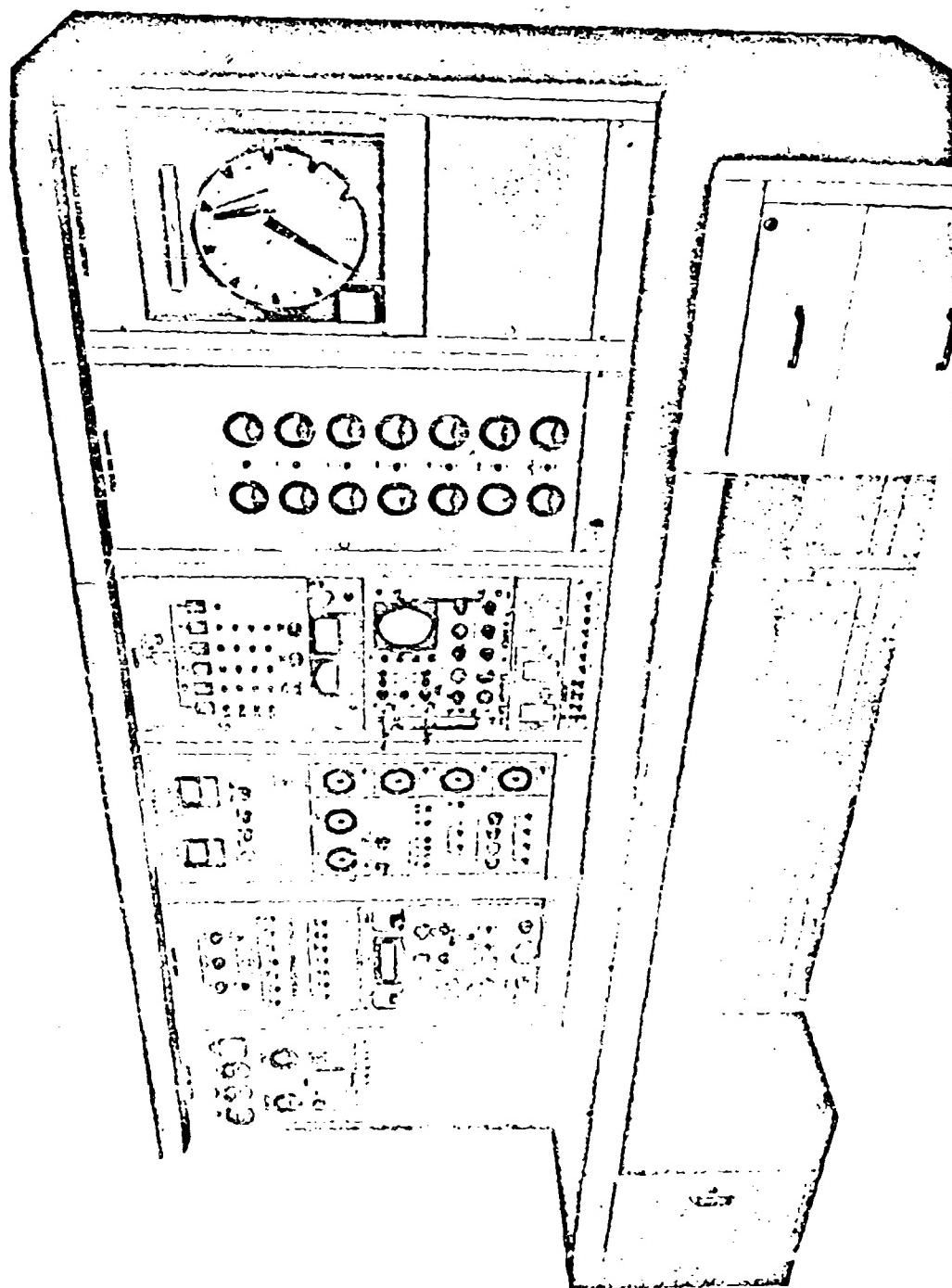


FIGURE 9 - TRANSMITTER CONTROL CONSOLE

12. CROWBAR UNIT

The crowbar unit discussed herein is patterned after a pulser switching device developed at Stanford University.¹ Electrically it is different in that it lacks a bias supply to extend the firing range to low voltage values and it incorporates modifications in the bottom two gaps. The voltage range of operation of the crowbar unit is approximately 60 KV to 140 KV. It is used to dump the energy in a 5 microfarad capacitor bank with a stored energy of 56,000 joules. A simplified block diagram of the crowbar unit is shown in Figure 10, and a schematic is given in Figure 11. Basically it consists of a series string of 5 air gaps with R-C dividing circuits mounted on a plexiglass frame. A load isolating resistor of 12 ohms is used to keep a shorting load from reducing the potential on the dump unit to zero prior to firing. A 6 ohm resistor is used to limit the discharge current of the 5 microfarad capacitor bank to less than 25,000 amperes. The 6 ohm resistor also establishes an overdamped discharge condition. Using the schematic in Figure 11, the sequence of operation is as follows. A trigger amplifier unit utilizing a 5C22 hydrogen thyratron is used to fire the gap (#1) closest to ground. This is accomplished by applying a damped oscillatory discharge to this gap. The first half cycle of this waveform is -100 KV in amplitude, and occurs in about 1 microsecond. An R-C discharge loop "A" is used to overvolt the next gap (#2) and likewise, another R-C discharge loop "B" overvolts the 3rd gap. Capacity divisor action fires the 4th gap and then the fifth gap fires. All the gaps are fired within one microsecond after application of the trigger by the 5C22 trigger amplifier and within seven microseconds after the detection of a fault. The gaps are composed of three inch diameter solid bronze balls. The limiting resistors are Globar type SP resistors. Based on experience with this unit, these resistors are operated at 30 KV peak and 3,000 amperes peak for crowbar discharge service. Experience and testing of this unit has shown that without this limitation, severe tracking and "fireball effects" on the outside surface of the resistor occur and an increase in resistance of about 3 to 1 occurs in the value of the resistor. This problem and one on the extinguishing of the gaps are the only significant problems which were encountered on this unit. Gap extinguishing was alleviated by making the gaps vertical firing and by increasing the storage capacity across the gaps. A typical set of waveforms of the crowbar unit firing is shown in Figure 12. Figure 12A shows the current in the 5 microfarad capacitor bank discharging through 12 ohms. Figure 12B shows the high voltage bus voltage during discharge. It is to be noted that at 4 milliseconds the gaps extinguish and then refire and then the voltage remains clamped at a low value until the high speed circuit breaker opens as evidenced by the small disturbance at 35 milliseconds. Also, the observed discharge time as shown by Figure 12C is 500 microseconds. In conclusion, it should be noted that crowbar service below 60 to 70 KV has not been found necessary to date and, hence, the range of 60 to 140 KV is considered satisfactory. Acoustically the unit makes a fair amount of noise when it fires, however, it is located in an enclosed capacitor room which is an uninhabitable area.

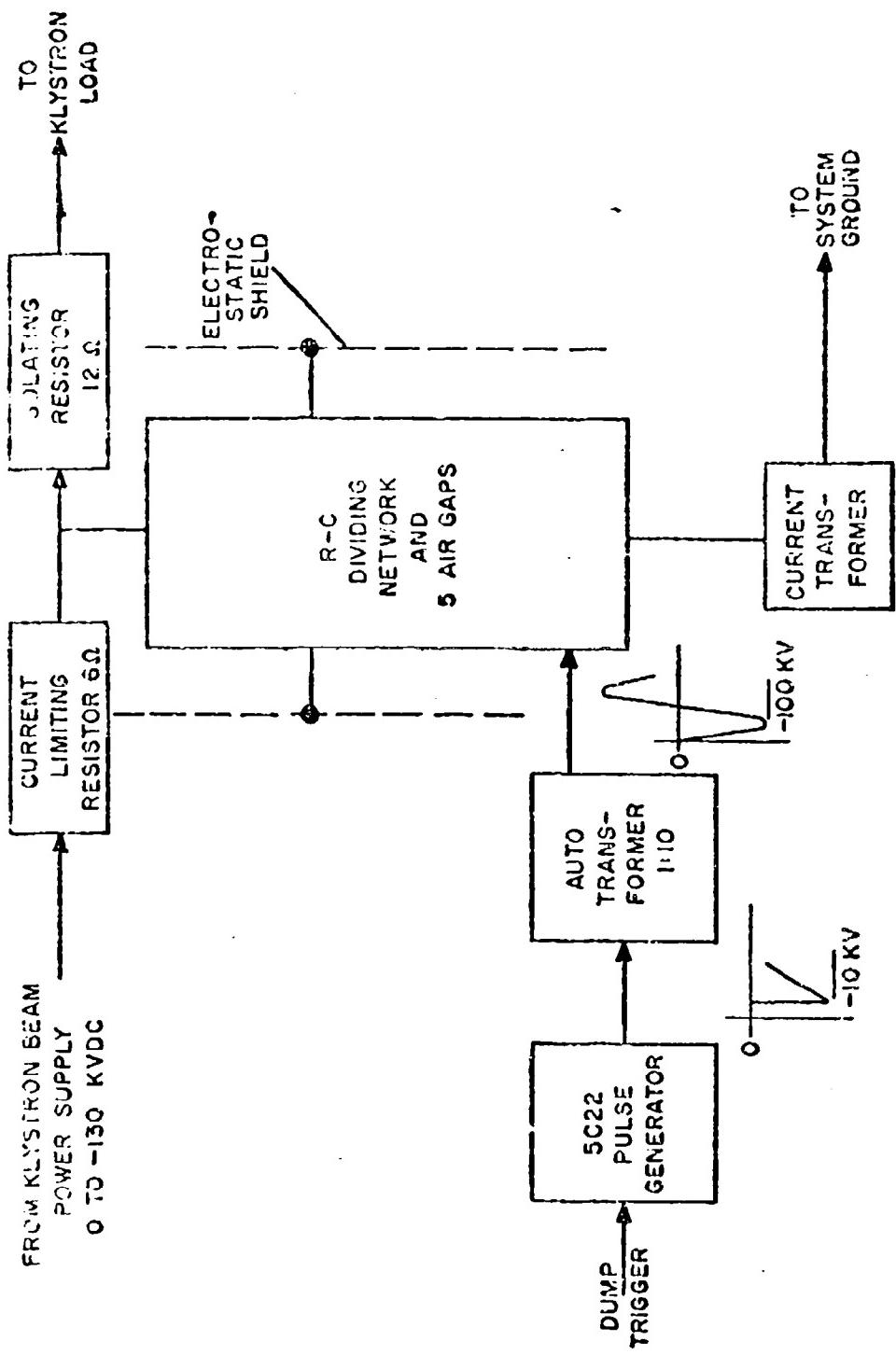


FIGURE 10 - SIMPLIFIED BLOCK DIAGRAM OF ELECTRONIC CROWBAR UNIT - SK-41162-2-CP

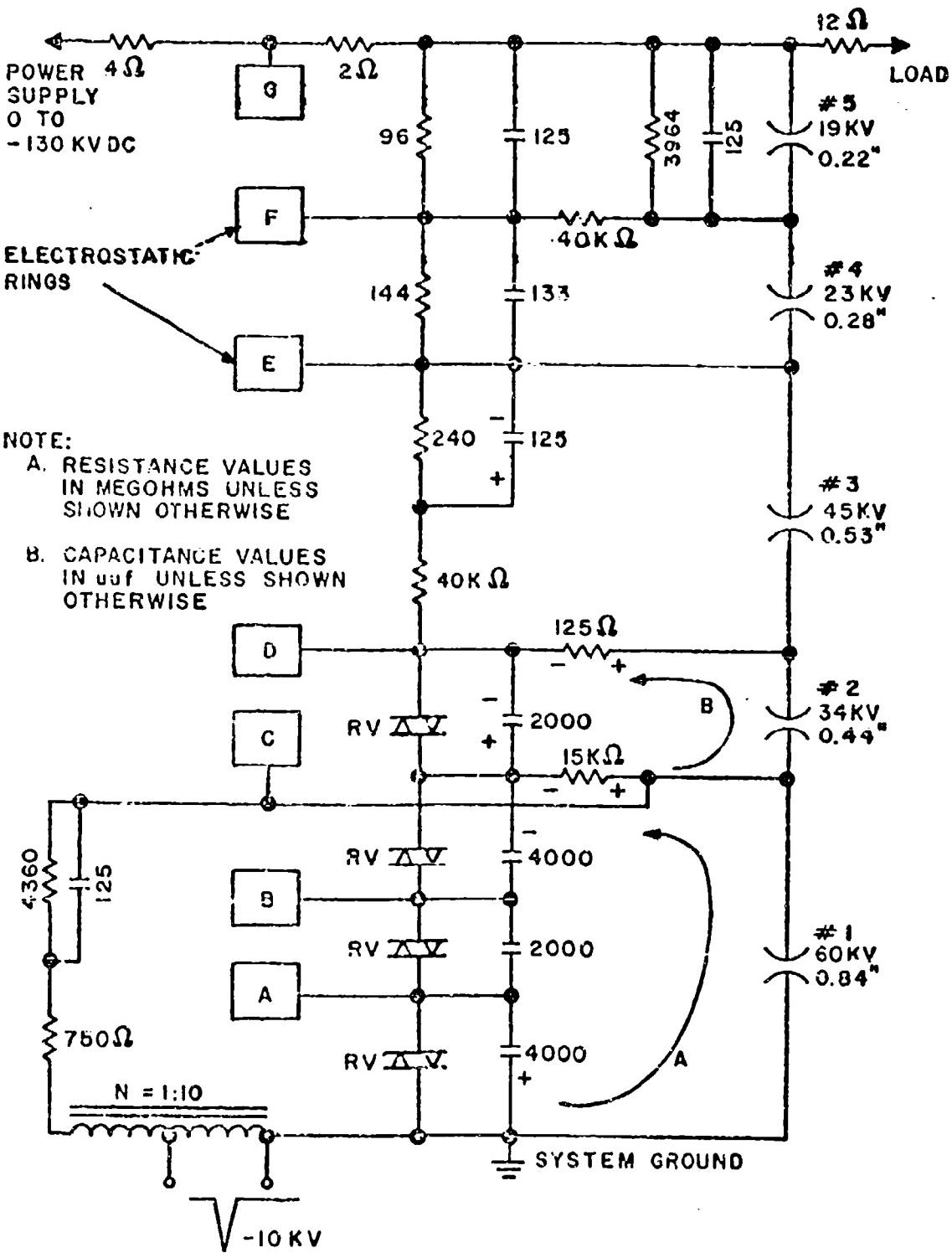


FIGURE 11 - SCHEMATIC OF ELECTRONIC CROWBAR - SK-41162-1-CP

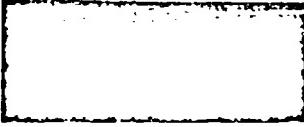
A. Current discharge waveform for 5 microfarad capacitor bank. Series limiting resistor is 18 ohms. Circuit is overdamped - $R/L > 1/\sqrt{LC}$. Loop inductance = 5 microhenry

E_{BB}	= -100 KV	<u>Analytical Solution</u>	<u>Measured</u>
		$t \text{ } (\mu\text{sec})$	$I \text{ (amps)}$
SS	= 100 $\mu\text{sec}/\text{cm}$	1.9 2.0	5380 5500
RC	= 90 μsec	2.5 3.0	5498 5490
L'DIV	= 1460 Amps/cm	4.0 200	5450 2050
			2040

Scope V/cm = 20

Current observed via transformer in ground lead of crowbar unit.

B. Voltage waveform on H. V. bus during firing of crowbar unit. Compensated R-C divider used.


 E_{BB} = -70 KV
 SS = 5 milliseconds/cm
 Scope V/cm = 2
 R-C divider ratio = 1100/1

Note gap extinguishing and resirring at 4 milliseconds. High speed circuit breaker also shown operating at about 35 milliseconds.


C. Voltage waveform on H. V. bus for 5 microfarad bank during crowbar firing. Series limiting resistor is 18 ohms.

E_{BB} = 70 KV
 RC = 90 μsec
 SS = 50 $\mu\text{sec}/\text{cm}$

FIGURE 12 - CROWBAR UNIT WAVEFORMS DURING DISCHARGE OF 5 MICROFARAD CAPACITOR BANK

SK-4262-1-CP
 REF: B #12776, pg. 23-26, WHC
 TTDM-L-189

Figures I3 and I4 are photographs of the crowbar unit. Physically it consists of a basic mounting structure consisting of a 1/2 inch thick plexiglass sheet. To this sheet are mounted the 5 ball gaps, various R-C dividing circuits, the series limiting resistors, electrostatic rings, a 10/1 auto-transformer and the associated trigger amplifier unit.

13. ACKNOWLEDGEMENTS

Credit for the design of the Fault Sensing and Logic System and the Electronic Crowbar Unit discussed in this report is due to W. H. Chester, the Electrical Design Engineer, and A. A. Gorski, the Design Project Engineer. The mechanical design of the Electronic Crowbar Unit was performed by J. M. Uzick, Mechanical Design Engineer. Credit is also due to the supporting team of RCA personnel who contributed heavily to the R/D of the equipment² described herein.

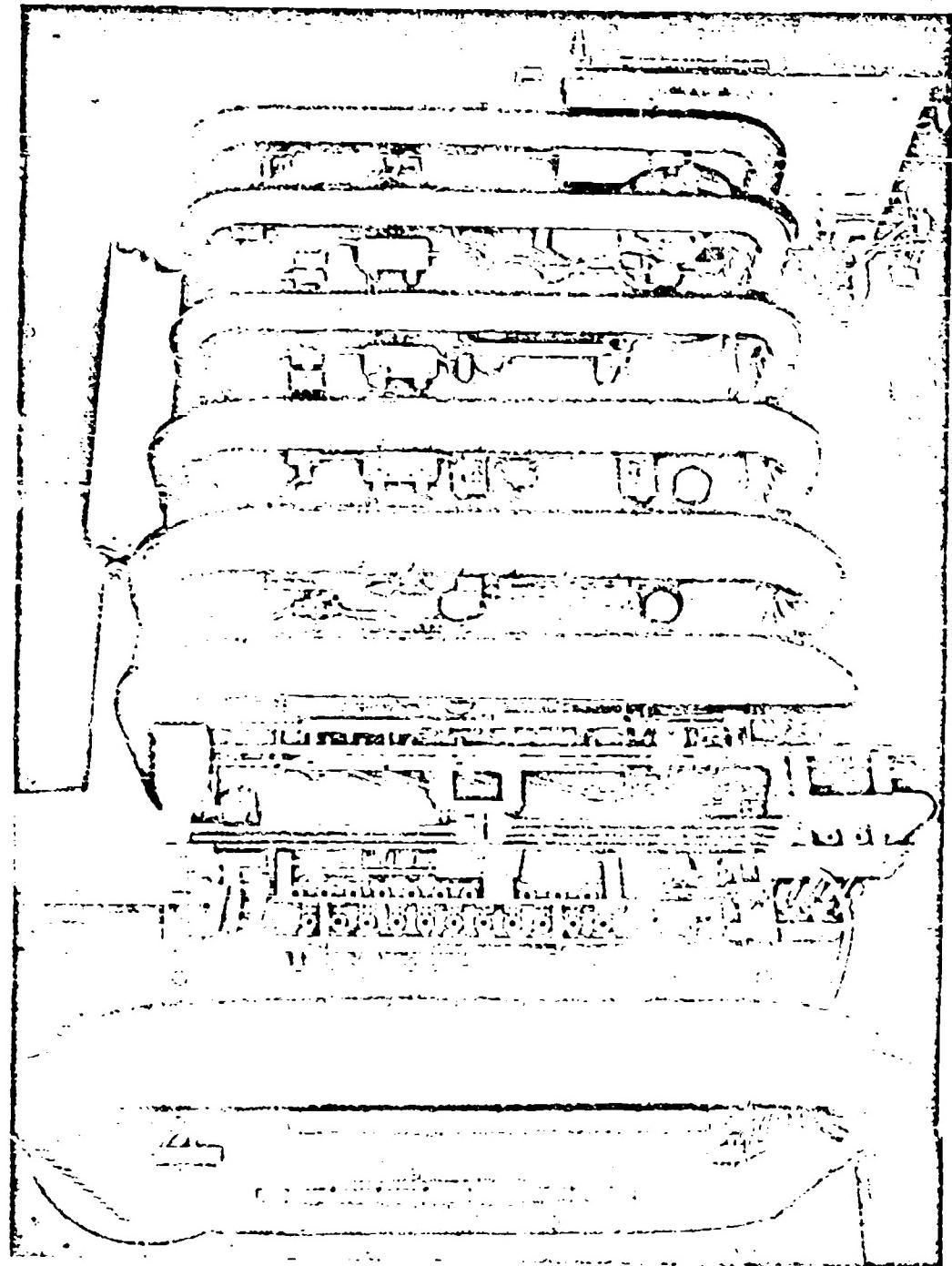


FIGURE 13 - PHOTOGRAPH OF BACK SIDE OF 140 KV CROWBAR UNIT

REFERENCES

1. M. Chodorow, E. L. Ginzton, W. W. Hansen, et al, "Stanford High Energy Linear Electron Accelerator (MARK III), Report No. 258, W. W. Hansen Laboratories of Physics, Stanford University, pp 172 - 174 February, 1955.
2. The R/D of the equipment described in this report was performed by RCA under the Department of the Army Contract DA-36-034-ORD-3063RD, under the technical guidance of AOMC and sponsored by the Advanced Research Projects Agency.

A VERSATILE ELECTRONIC CROWBAR SYSTEM

by

Sol Schneider, M. H. Zinn, and Anthony J. Buffa

U. S. Army Signal Research and Development Laboratory
Fort Monmouth, New Jersey

INTRODUCTION:

The utilization of high-power transmitters during recent years has spurred a need for the development of devices capable of protecting rf generators, high-vacuum modulator tubes, and high-voltage components in the event of an arc in any of these components. This need is particularly evident in equipment operating at high voltage with large values of stored energy in capacitor banks, since the high voltage increases the probability of arcing and the high energy increases the probability of catastrophic destruction of the components. At voltages under 80 kilovolts, use has been made of ignitrons, hydrogen thyratrons, triggered spark-gaps (of the sealed gas-filled variety), and open-air gaps of various configurations. Above 80 kilovolts, the only available devices have been of the open-air type. In this category various configurations have been used with varying degrees of success.

In order for a protective device or electronic crowbar to successfully protect the circuit in which it is used, it must have the following characteristics:

- a. Rapid firing after application of trigger pulse.
- b. Low voltage drop after firing.
- c. Low energy-triggering capability.
- d. Large range of operating voltage (i.e. V_{max}/V_{min} as large as possible).
- e. Repetitive firing.
- f. Self-triggering in the event of a fault.

The need for a. and b. above is evident; the crowbar must be caused to achieve a condition approaching that of a short circuit across the arcing component as rapidly as is possible so as to divert the energy from the arc before any damage has occurred. The crowbar obviously must be capable of passing the short-circuit current value without being damaged itself. The low triggering requirement is dictated by the usual desire for circuit simplicity and small size, but is also necessary to minimize any pulse signal that may appear in the main circuit during triggering of the crowbar. Requirement d. stems from the possible need for circuit operation over a wide voltage range for which protection is desired. This is particularly needed in high-power electron tube processing equipment where arcing is possible at the lower values of plate-supply voltage until seasoning of the

electron tube permits stable operation at the higher voltages. There is also a need for a low-plate-voltage triggering capability to provide for a repetitive firing of the crowbar during the period between initial firing of the crowbar and the opening of the circuit-breakers, in order to prevent reinitiation of the arc in an electron tube that may have evolved gas during the initial stages of the original arc. It should also be self-triggering in the event of a fault to provide protection against the main capacitor discharge even if the logic-driver fails.

In addition to the characteristics listed and discussed above, the crowbar must reliably hold off the desired high voltage without self-triggering induced either by atmospheric effects or the normal pulses appearing in the main circuit. Finally, a desirable feature would be a low value of acoustic energy generated by the firing of the crowbar.

When this Laboratory was faced with a need for a crowbar device, the crowbar art was surveyed in the light of the above requirements, and the devices presently being used in various equipments were found to fall short of the optimum. It occurred to us that the sequentially-fired spark gap, which had been studied by the University of California¹ and Carnegie Institute of Technology² as a pulse modulator device and a clipping device, could meet these requirements and could also be investigated and constructed in the shortest possible time.

A scale model of a prototype, sequentially-fired spark-gap crowbar was designed, constructed, and tested at this Laboratory. The test results indicated that it was possible to achieve all of the desired features, including the ability to fire the crowbar at zero plate voltage, i.e., the value of V_{max}/V_{min} achieved was infinite.

As a result of the success of these initial tests, a decision was made to design and construct at this Laboratory a full-scale crowbar for use in processing equipment for superpower klystrons. It is the purpose of this report to detail the general principles of operation of the sequentially-fired gap and the particular design features of the gap that was provided for this application.

DEFINITION AND PRINCIPLE OF OPERATION:

The electronic crowbar is a multiple fixed-gap system that is sequentially fired by a signal applied at approximately the mid-point of the gap system. A schematic diagram is shown in Fig. 1.

The electrodes of the gap system are in-line-staggered metal rods, each of which is connected to a dividing resistor (R) and a capacitor (C_g) to ground. Each end of the rod serves as an electrode of the adjacent gap. The two large resistors are all of equal value and provide uniform voltage division between gaps. This permits equal gap spacings to be used. The operating voltage is determined by the breakdown voltage of the atmospheric, the minimum operating voltage, and the desired degree of safety. The size of the coupling resistor is determined by a compromise between the amount of leakage current that can be tolerated and the time constant of the gap system dictated by the rate of application of voltage. The capacitor (C_g) from each electrode to ground is selected to be an order of magnitude greater than the total electrode capacitance (C_1) of the gaps. The coupling capacitor

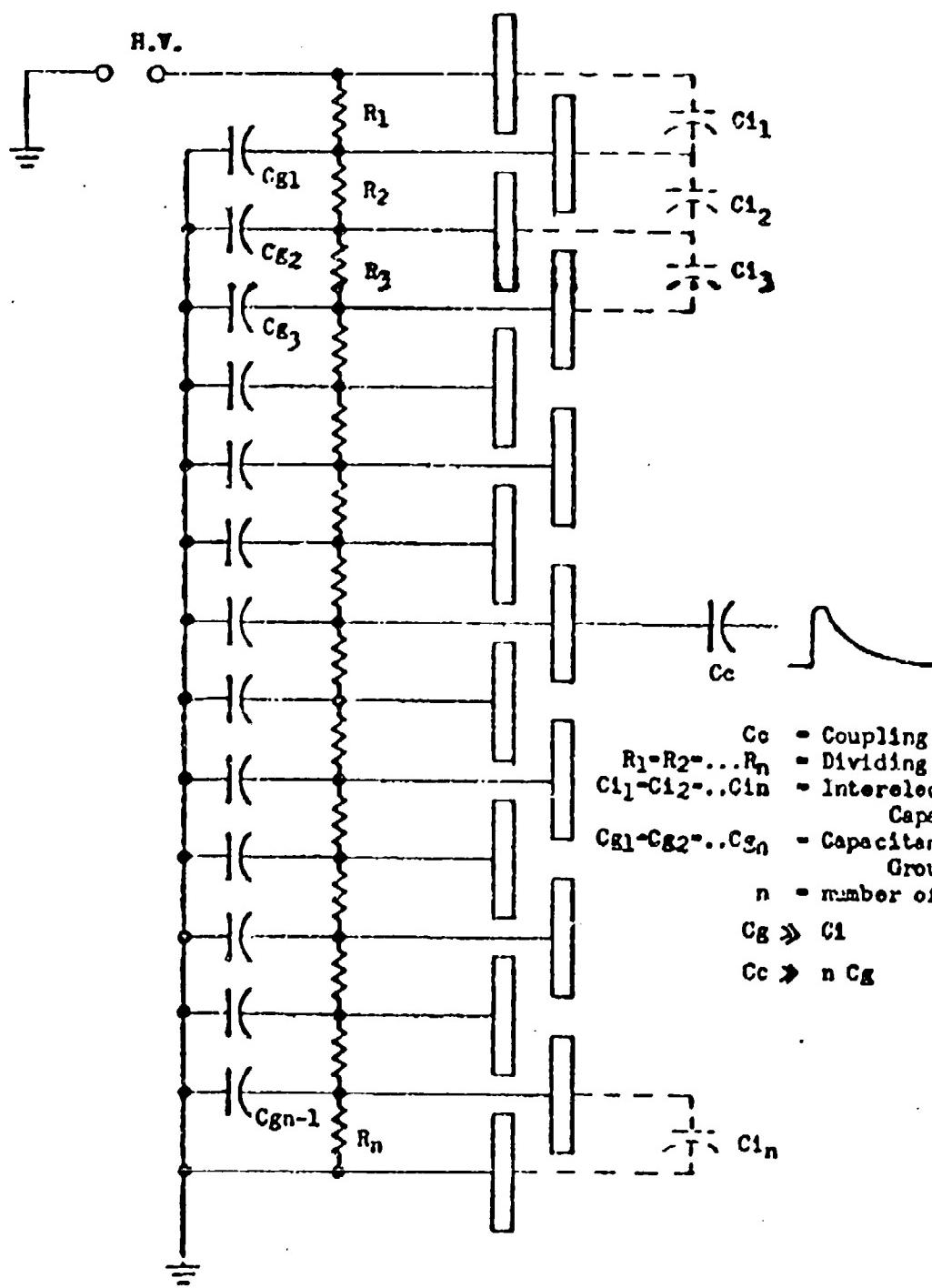


FIG. 1 Schematic Diagram of Electronic Crowbar

(C_c) is a minimum of five times the total capacitance ($n C_g$) of the system to ground.

The triggering mechanism of the series-gap system consists of over-volting each gap in turn with the discharges propagating in both directions from the center. The in-line structure permits irradiation of the next gap, thus stabilizing the breakdown voltage and minimizing statistical variations. The result is extremely-rapid breakdown of the gap system. The simplified circuit of Fig. 2 illustrates the triggering mechanism in the absence of any voltage in the main system. The trigger signal (e_t) is applied through the coupling capacitor (C_c) to the rod serving as one side of the gaps G_n and G_{n+1} . Assuming the trigger pulse has a very-fast rise time, the trigger voltage will divide across C_c , C_i (the gap capacitance), and C_g (the capacitance to ground) inversely proportional to the size of each capacitor. Since C_g is chosen to be approximately 10 times larger than C_i , and C_c is approximately 100 times larger than C_g , all the voltage will effectively appear across C_i and C_g with the voltage across C_i or the gaps G_n and G_{n+1} equal to $\frac{C_c}{C_c + C_g}$, which is approximately 0.9 e_t for this system.

If the trigger voltage is many times larger than the breakdown voltage of gaps G_n and G_{n+1} , both gaps will fire rapidly. The ultraviolet radiation produced in these two gaps will irradiate the neighboring gaps, thus stabilizing their behavior. With gaps G_n and G_{n+1} broken down, the trigger voltage will now be applied across gaps G_{n-1} and G_{n+2} and the same triggering process will be repeated. The process then continues in both directions until all the gaps in the system have fired.

The trigger source must have a low impedance in order to charge the capacitors (C_g) rapidly. The coupling capacitor is made as large as possible since as each set of gaps fire, $2C_g$ additional capacitance is added to the trigger load. The effect of this is a reduction in the trigger voltage available for the end gaps since the total capacitance of the system has to be considered with respect to the size of the coupling capacitor. For example, in a twenty-gap system, where $C_g \approx 10C_i$ and $C_c \approx 100C_g$, the trigger voltage for the first set of gaps is approximately 0.9 e_t and for the last set of gaps 0.77 e_t . It is also necessary that the trigger source be capable of delivering the full voltage (e_t) during the entire triggering process.

The energy required for the trigger can be simply computed. If the trigger potential required to ensure an infinite range and rapid firing of a gap system is known, the required energy can be computed as follows:

$$\text{Energy} = 1/2 n C_g e_t^2 \text{ joules} \quad (1)$$

For a system of twenty gaps, where $C_g = 30 \mu\text{fd}$ and $e_t = 50 \text{ kv}$, the energy required is 0.725 joule. If a step-up transformer is used to trigger the gaps, the trigger source can be a simple capacitor discharge. In this case the size of the capacitor can be computed as follows:

$$C_d = n C_g R^2 \quad (2)$$

where

C_d = discharge capacitor

R = turns ratio of transformer

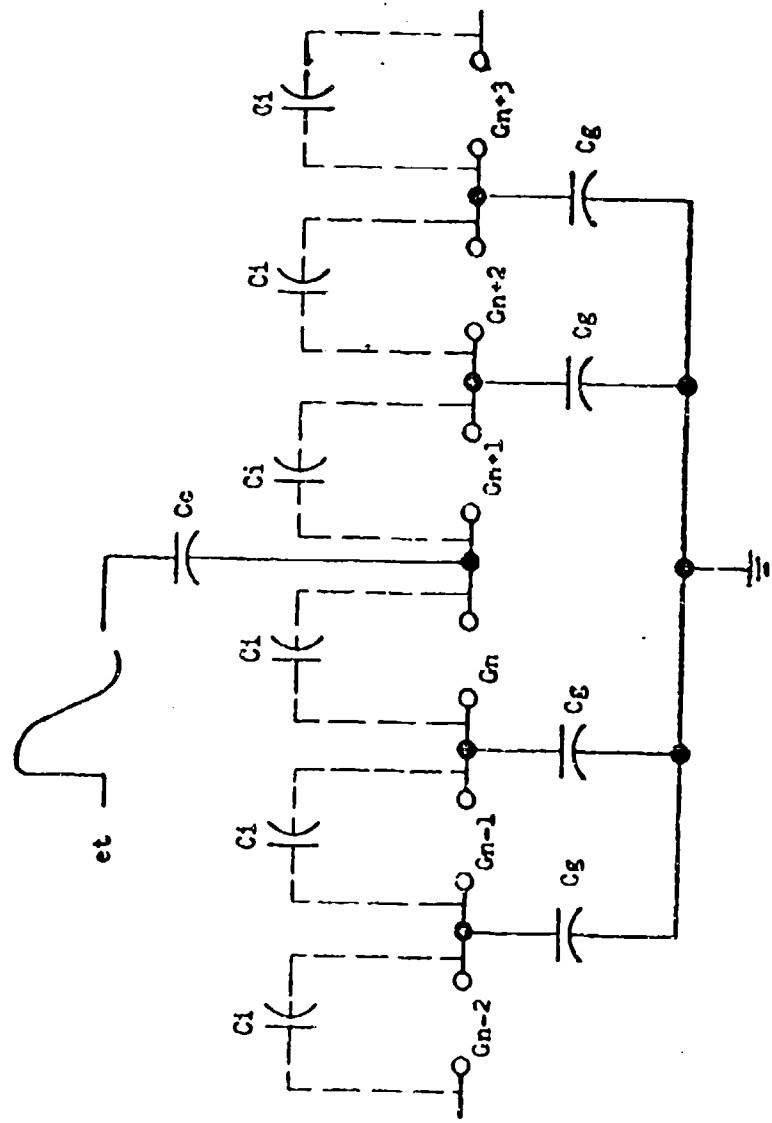


FIG. 2 Triggering Sequence

In the particular case mentioned above, if the turns ratio of the transformer is 5, the discharge capacitor (C_d) has to be a minimum of .015 μ fd. It should of course be slightly larger to compensate for circuit and transformer losses. The voltage applied to C_d in this case would be 10 kv.

Since the gap system is designed to fire with zero d-c potential on the gap, it provides an infinite-range switch limited only by the total breakdown voltage of all the gaps in series. The trigger signal itself is a narrow, high-voltage pulse requiring an energy of approximately one joule, and, therefore, a simple repetitive trigger source can be constructed. The repetitive trigger provides additional protection for a crowbar application since it continuously discharges the capacitor bank until the circuit breakers have had the opportunity to respond.

DESIGN PROCEDURE:

The system, independent of the trigger, consists of three basic components: the gaps; the capacitors to ground; and the dividing resistors. Since all of the gaps are the same, the capacitors to ground equal, and the dividing resistors of equal value, numerous configurations may be used. Therefore, dependent on the operating voltage and its regulation, availability of high-voltage components, energy to be switched, life requirements, safety factor, available space, and type of trigger, a system can be designed for any application.

1. The Klystron Test Equipment:

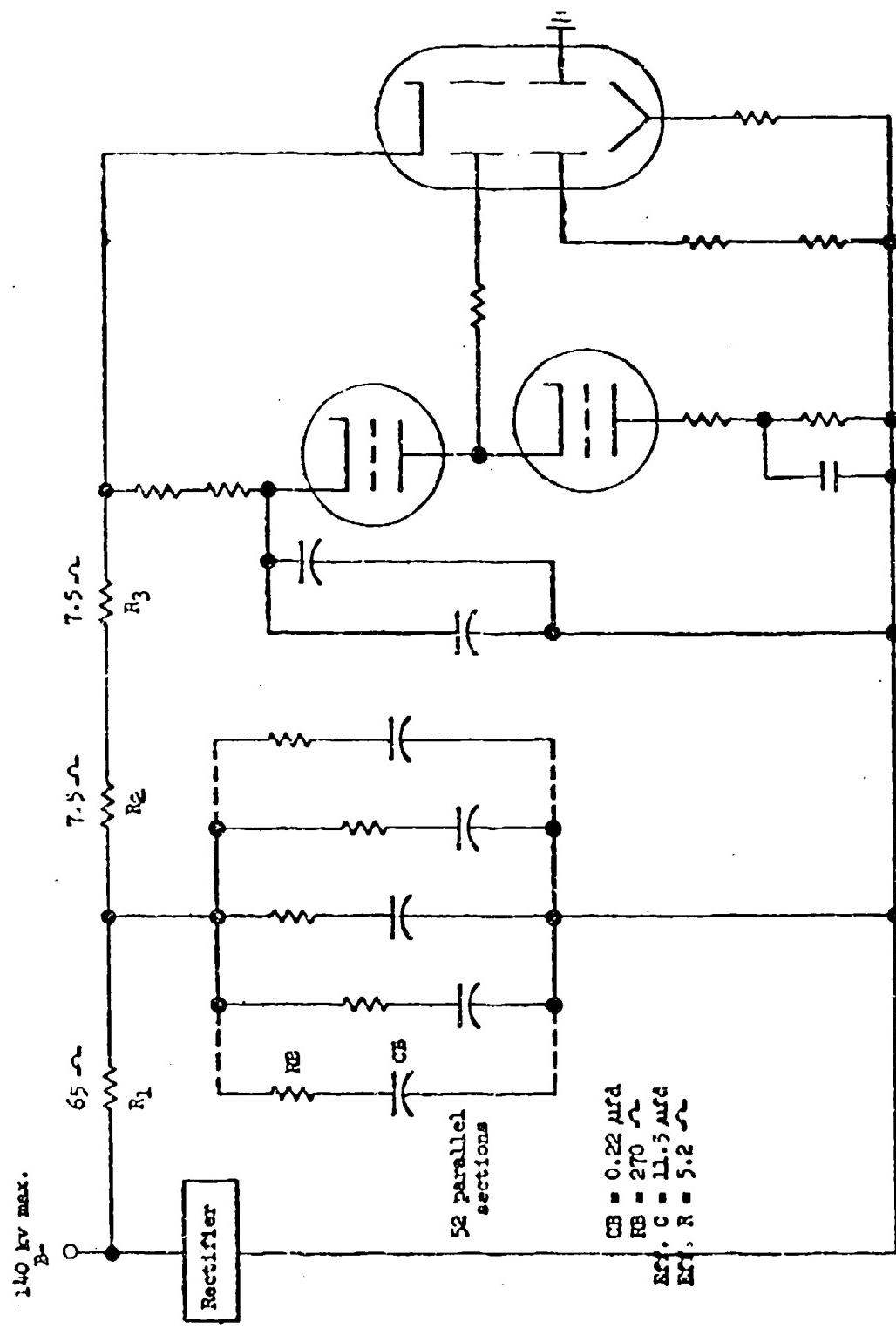
The basic diagram of the high-voltage portion of the klystron test equipment is shown in Fig. 3. The total capacitance of the energy storage bank is 11.5 μ fd. An effective series resistance of 20 ohms (5 ohms in the bank and 15 ohms external to the bank) is used to prevent exceeding the peak current capability of the capacitors, which is 140 amperes per capacitor, in the event of an arc in the klystron. If such a fault occurs, more than 100,000 joules will pass through the test equipment from the capacitor bank alone. Additional energy that may exceed this initial burst of energy will pass through the system until the circuit breakers have opened.

The installation of a crowbar in this equipment required a determination of the best location for the crowbar, both physically and electrically; the effect on the equipment and its components; the installation of a fault-sensing circuit; and, finally, the design and construction of a crowbar equipment to meet the physical and electrical boundary conditions imposed by the test equipment.

2. Physical Location of Crowbar:

The physical layout of the equipment was studied to determine if a crowbar of the type developed at USAGRL could be installed in a location readily accessible to the capacitor bank. Originally it was decided to place the crowbar in an adjoining room where the heat exchanger is located. The space available for the crowbar was $5\frac{1}{4}$ " L x 36" W x 166" H. This established the maximum size of the crowbar equipment. The basic unit could be designed to occupy a 36" x 36" area, with the additional floor space used for the coupling capacitor, the trigger transformer, and any other necessary gear. Unfortunately, when the klystrons were operated at higher power, condensation

FIG. 3 SCHEMATIC OF TEST EQUIPMENT



appeared in the heat exchanger room, and the moisture level became too high to permit installation of a high-voltage unit in the room. As a result, the crowbar was installed in another location on the other side of the capacitor room. Since the humidity problem was not known until the crowbar was completed, the original physical restrictions were adhered to in designing the crowbar.

3. Electrical Location of Crowbar and Resultant Equipment Modification:

From the standpoint of providing optimum protection to the high-voltage portion of the circuit, it would be desirable to place the crowbar directly across the capacitor bank, as shown in Fig. 4. In the event of a fault sensed to the right of the crowbar, this location provides a short-circuit placement across an arc in series with 15 ohms and should, therefore, reduce the energy available to the arc by orders of magnitude and lead to its being extinguished. With the circuit values present, however, this would result in only an effective resistance of 5 ohms in series with the capacitor bank. The peak-current rating of the capacitor would, therefore, be exceeded during crowbar firing with this placement. On the other hand, placing the crowbar beyond the 20-ohm series resistance would put it directly across the points where arcing is liable to occur. The firing of the crowbar would then produce an arc directly across an arc, and the two arcs would compete for the flow of current with no sure protection for the circuit component. It was therefore necessary to modify the existing circuit in order to permit the installation of the crowbar. Based on voltage ratings of available resistors, it was decided to modify the equipment and place the crowbar as shown in Fig. 5. This modification provided a total series resistance of 27.5 ohms; a resistance between the bank and the crowbar of 20 ohms; and a resistance in series with the klystron 7.5 ohms greater than that in series with the crowbar. With this arrangement, when an arc occurs in the klystron, the firing of the crowbar will place a shunt of approximately 0.1 ohm across the klystron and its 7.5-ohm series resistance. Assuming zero arc drop in the klystron, the klystron current cannot exceed 93 amperes compared to 7000 amperes possible without protection. In these changes, not only was the rms dissipation taken into consideration but also the instantaneous maximum voltage that could appear. Components were selected that are designed to withstand the rigors of the anticipated voltage and current surges.

4. Crowbar Design:

As discussed previously, the physical layout of the crowbar was dictated by the space originally available for location of the crowbar. Electrically, the crowbar was designed to hold off 140 kilovolts with no spurious triggering under main circuit quiescent or normal pulse operation. The normal pulse operation of the main circuit results in the application of an approximate voltage wave form as shown in Fig. 6, which appears across the top gap of the crowbar. The wave form is based on the assumption that at maximum plate voltage the klystron will draw 100 amperes peak current for a period of 500 μ sec. The 2-kv drop is due to the voltage drop caused by the 100 amperes that appears across the 20-ohm resistor. Its exact shape is a function of the time of rise and fall of the current pulse. The 4.5-kv change is due to the regulation of the capacitor bank and can be computed as follows:

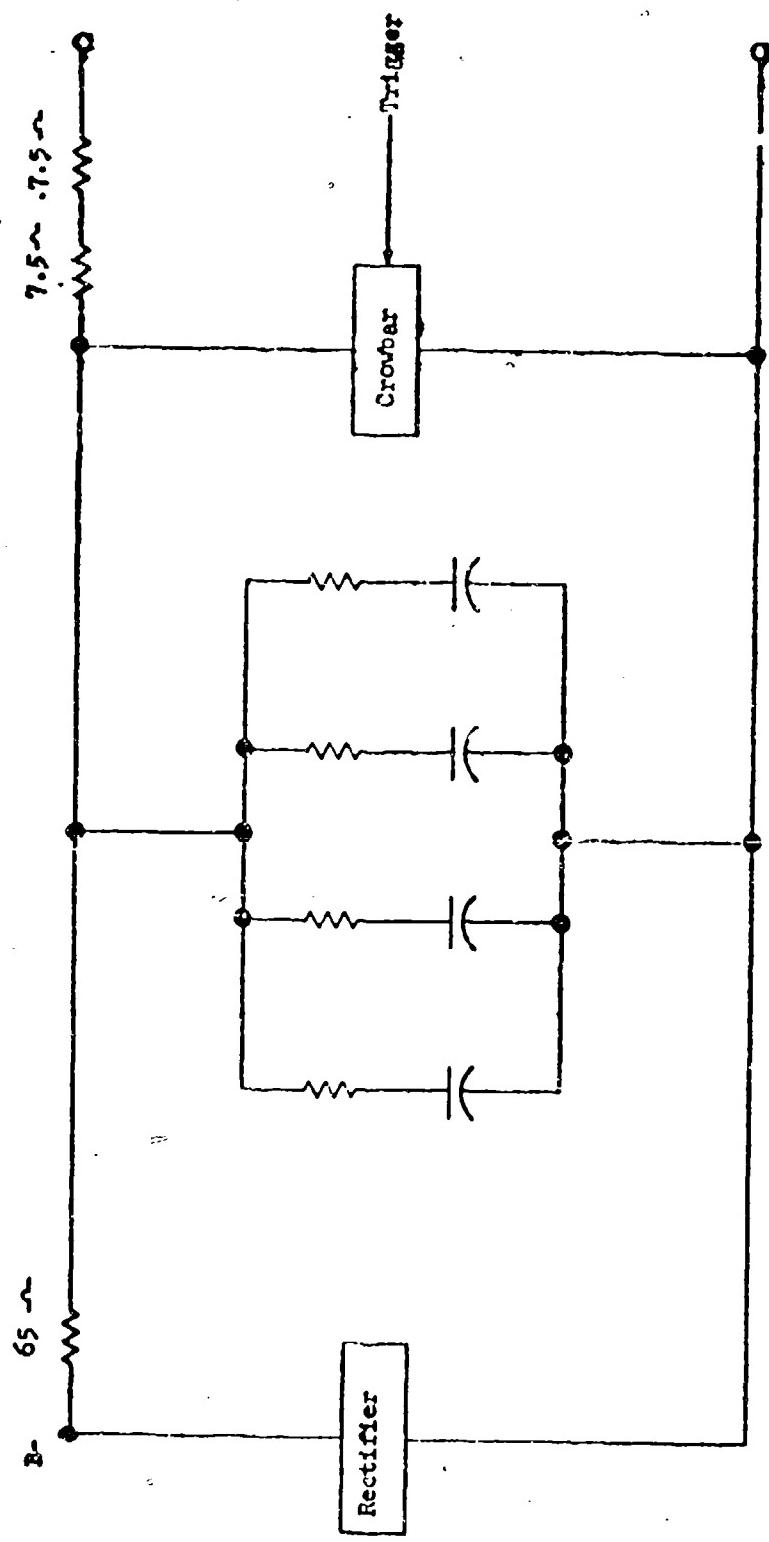
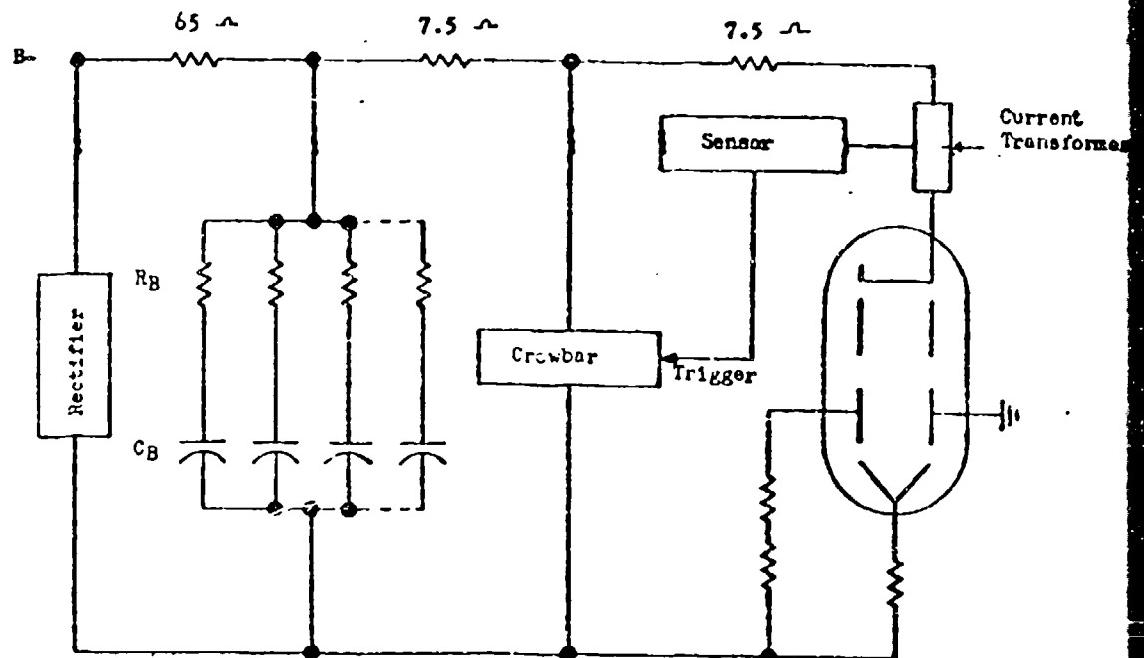


FIG. 4 Desirable Location of Crowbar



Each R_B changed to 627.5 ohms, thus providing an effective resistance of 12.5 ohms in the bank.

FIG. 5 Revised Circuit for Test Equipment

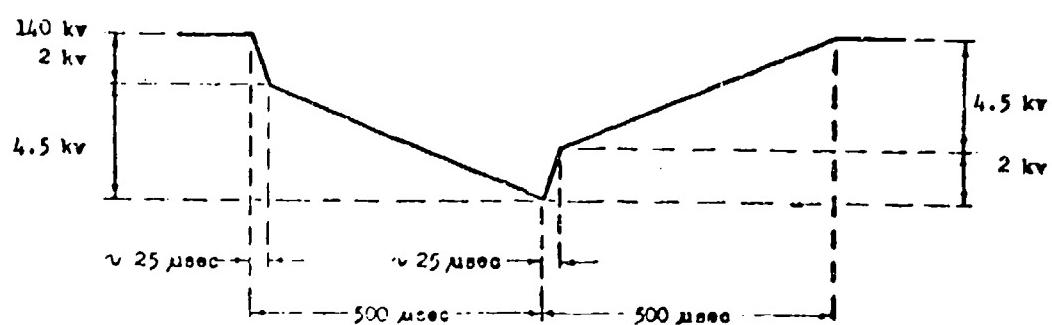


FIG. 6 Voltage Wave Form

$$\Delta V = \frac{i t_p}{C} \quad (3)$$

where i = peak current
 tp = pulse duration
 C = total capacitance

For this case

$$\Delta V = \frac{100 \text{ amperes} \times 500 \mu\text{sec}}{11.5 \mu\text{fd}} \approx 4500 \text{ kv}$$

The total voltage change that appears across the top gap is, therefore, 6.5 kv. The top gap should be capable of withstanding this voltage change without firing.

a. Gap Configuration:

Since the height was no restriction and 6.5 kv was the maximum change that would appear at the top gap, a 30-gap system was selected with individual gap settings of 10 kv. This provides a breakdown voltage for the system of 300 kv, which is a safety factor of 100%. At the same time it requires a lower breakdown voltage for the individual gaps than a system with a lesser number of gaps and the same safety factor. This advantage is somewhat offset by the larger intergap capacitance of the system.

On the basis of tests conducted on the feasibility model that was designed for 50-kv operation and was tested in our 3.0 gigawatt modulator³ (which provides a 30-usec pulse at a peak current of 120 kiloamperes), we had previously arrived at a conclusion for the best electrode geometry and materials. We had studied both ball and cylindrical electrodes and had determined that the cylindrical electrode was best. It provides a short length, large cross-sectional area conductor between gaps; a large potential discharge area within the gap; and an effective thermal conduction path. Our study also indicated that copper behaved best under the operating conditions and showed the least erosion. This is due, in great measure, to its high heat conductivity.

b. Physical Layout:

Having selected the number of gaps, the gap setting, the electrode configuration, and the electrode material, the design for the rest of the crowbar was now dictated by the operating voltage and the available floor area.

Prime consideration was given to evolving a physical design that would be corona free and would have sufficient structural strength to stand on its own base and be capable of shipment in one piece. The inner structure is a heavy Permalloy plywood trough that is bolted and epoxied together. It serves as the chassis on which the gaps, resistors, and capacitors are mounted. It is completely closed by a plexiglass window for sound-proofing and sealing the trough to enable use of nitrogen atmosphere. The plexiglass

permits viewing of the discharge. The outside structure is aluminum, and it provides a low-inductance ground return. It is completely smooth on the inside to reduce corona. The front panel has a plexiglass insert to permit viewing of the discharge. Examination of Figs. 7 thru 16 provides more detailed information of the structure.

c. Dividing Resistors and Mounts:

The dividing resistors are 5 megohms per section with a total resistance of 150 megohms. This limits the leakage current to less than one milliamper at full voltage and provides a low enough time constant to permit rapid application of the plate-supply voltage. The resistors and their mounts are shown in Figs. 10 and 12. Each section consists of two 10-megohm resistors in parallel. The mounts were designed to minimize corona. For lower voltages, they were made of square stock with rounded corners, and for higher voltages, they were constructed completely from round stock. The mounts are connected to the gaps by a lead from the mount to the capacitor fittings on the side. The uppermost resistor mount is of slightly different construction; it is of round stock but is mounted horizontally rather than vertically and it bends around the trough to make direct connection to the bolts holding the top electrode. It can be seen as the upper righthand connection in Fig. 9.

d. Ground Capacitors:

The capacitors used to connect each gap to ground represent one of the most severe problems of the crowbar design, since the top capacitor must be capable of holding the full plate voltage continuously. Although the voltage requirement for these capacitors is reduced in accordance with the equation:

$$VC_n = E_{bb} - 5(n-1) \text{ kilovolts} \quad (4)$$

where

$n = 1$ is the topmost gap

and

$n = 30$ is the lowest gap

it was decided to use the same capacitor design throughout to minimize the number of different parts and to simplify assembly procedures. Sections of RG-19/U cable were selected as the basis for the capacitors, since this cable was used in the basic equipment as a high-voltage cable required to hold off the 140-kilovolt plate voltage. The cables were constructed by utilizing a sleeve cut to a length suitable to provide $30 \mu\text{f/d}$ to replace the normal braided outer conductor of the cable. This sleeve serves as the high-voltage side of the capacitor. It is approximately 11 inches long. It is flared outwards at both ends and has corona rings. Silastic rubber is placed on these corona rings to increase their radii and to reduce corona. The silastic is also placed between the outer sleeve and the polyethylene of the cable. Its high dielectric constant forces all sharp voltage gradients to appear between the silastic and the polyethylene. The center electrode at each end of the cable is bolted to the outer case of the structure and serves as the ground connector. Figs. 9, 10, 11, and 12 present views of these capacitors. Examination of these figures shows that these capacitors effectively simulate graded corona rings down the length of the structure.

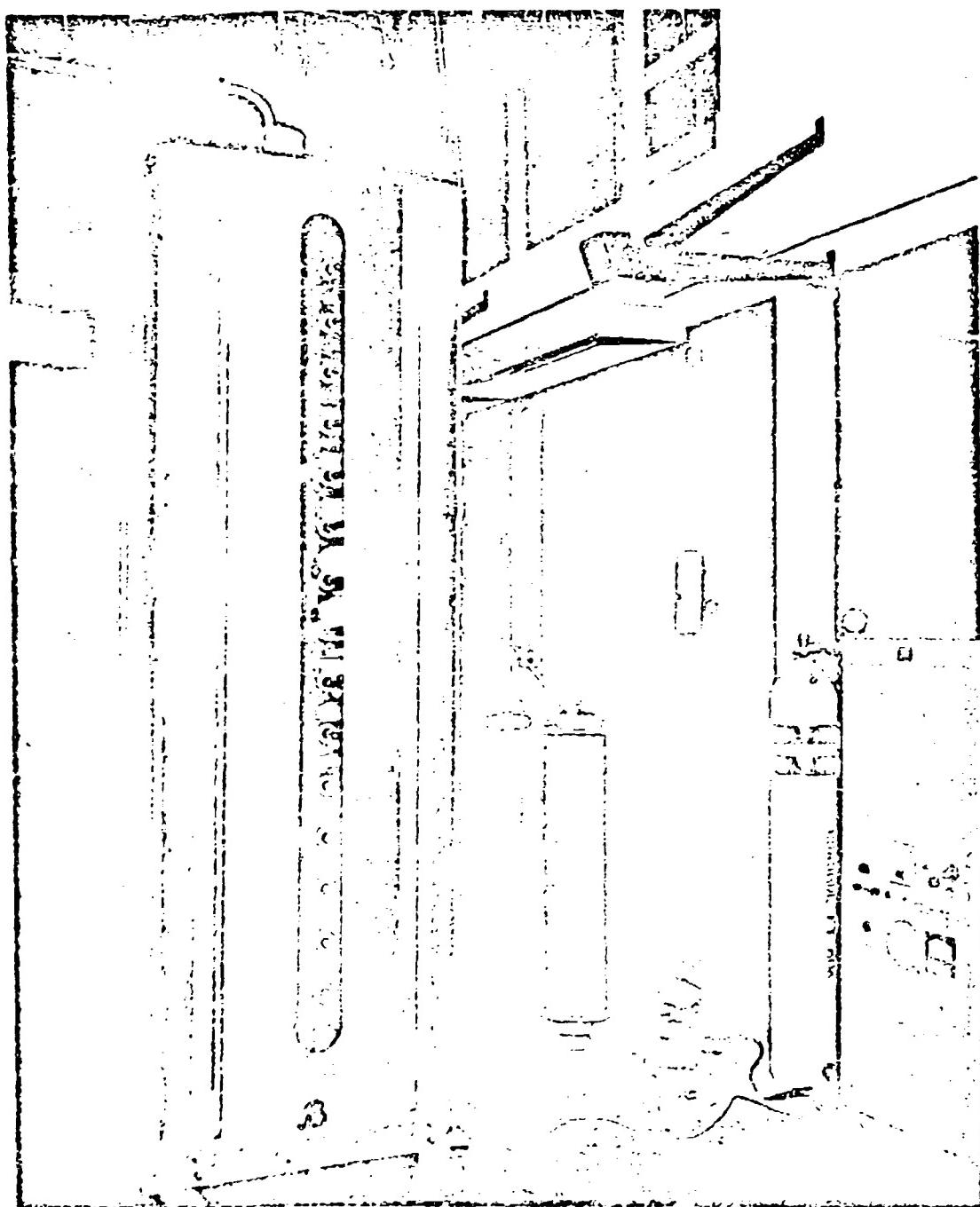


FIG. 8 FRONT VIEW OF COMPLETE EQUIPMENT, INCLUDING TRIGGER

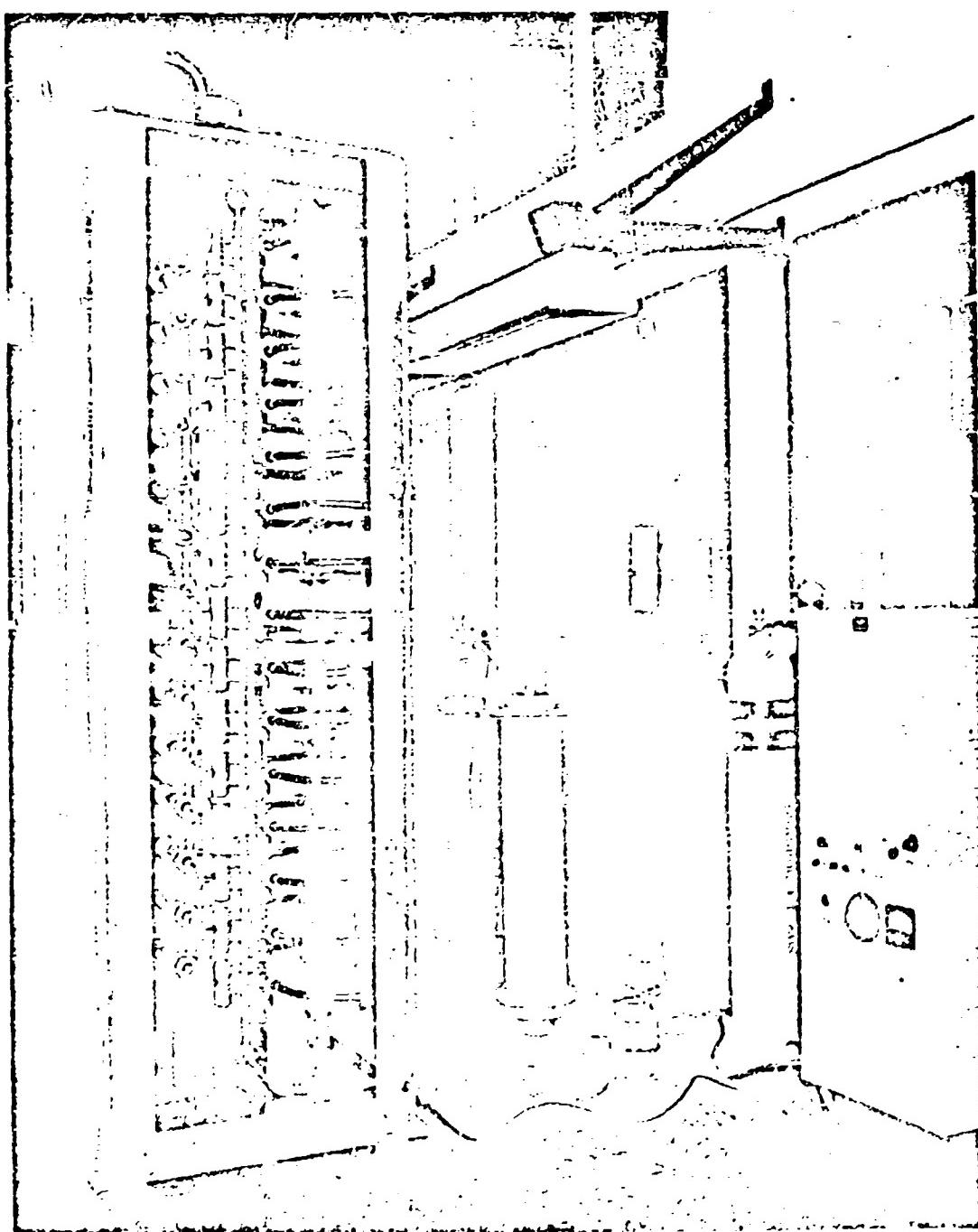


FIG. 9 FRONT VIEW OF CROWBAR, PANEL REMOVED, SHOWING INTERIOR

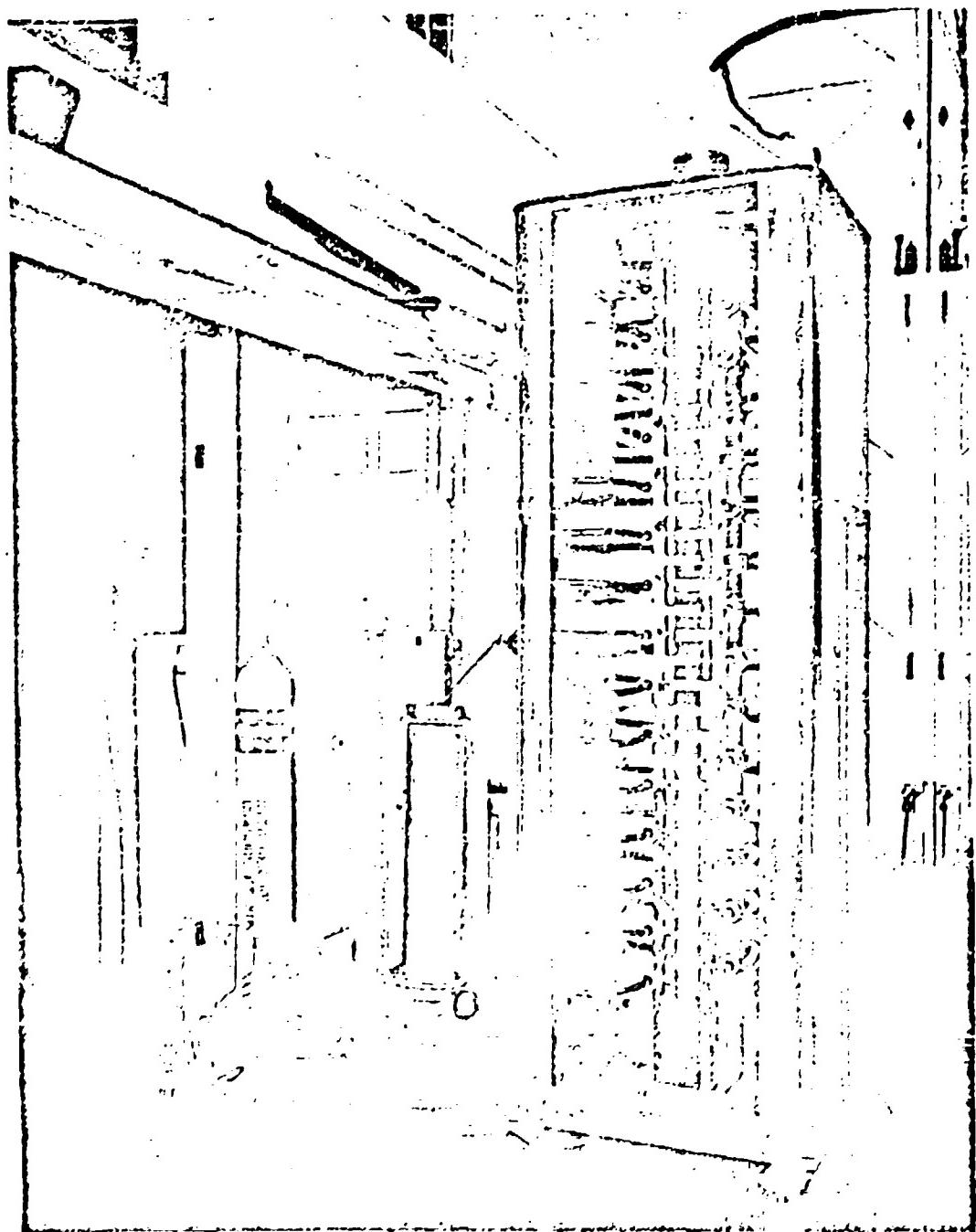


FIG. 10 REAR VIEW OF CROWBAR, PANEL REMOVED, SHOWING INTERIOR

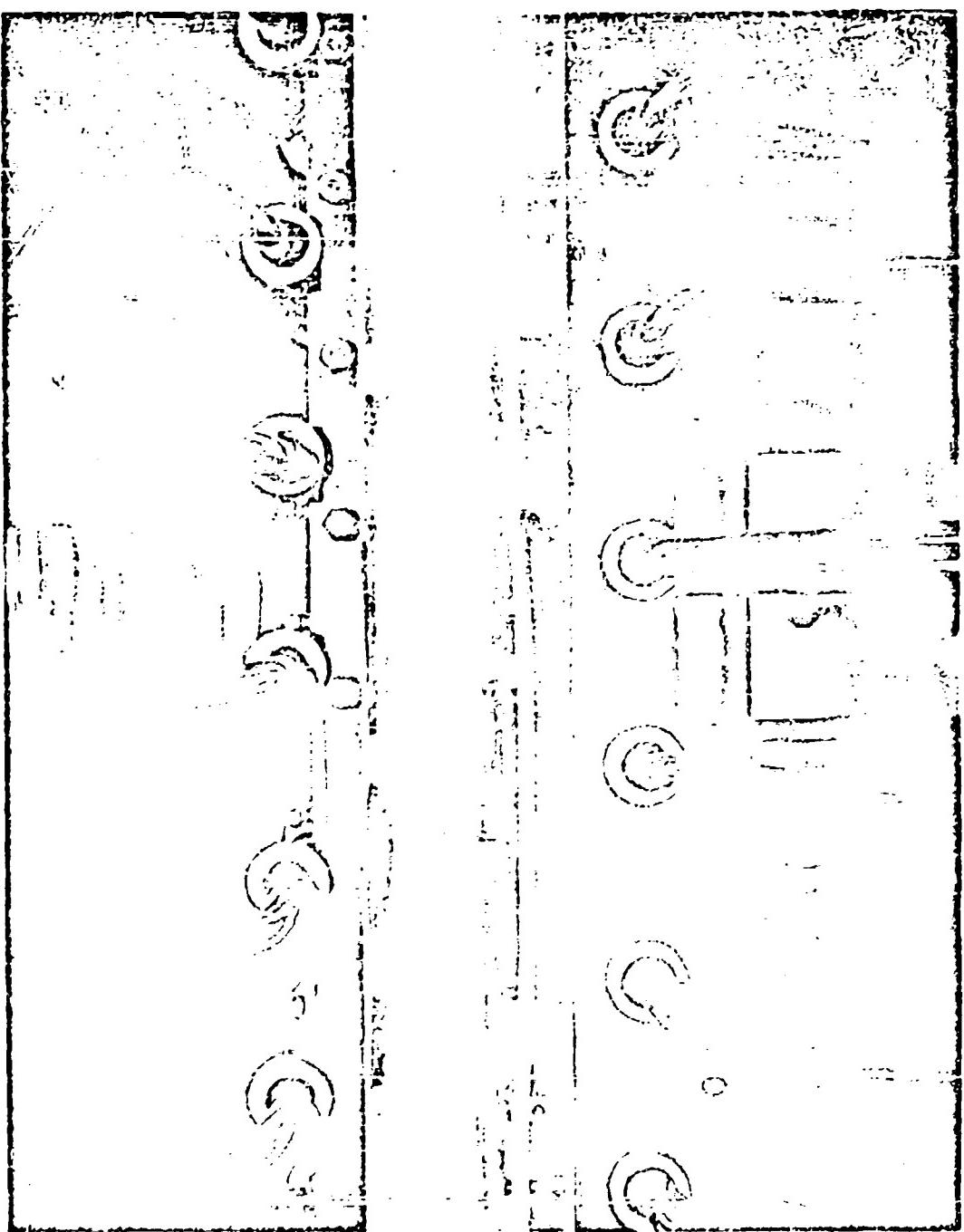


FIG. 11 CLOSE-UP VIEW, SHOWING DETAILS OF CONSTRUCTION AND DISCHARGE

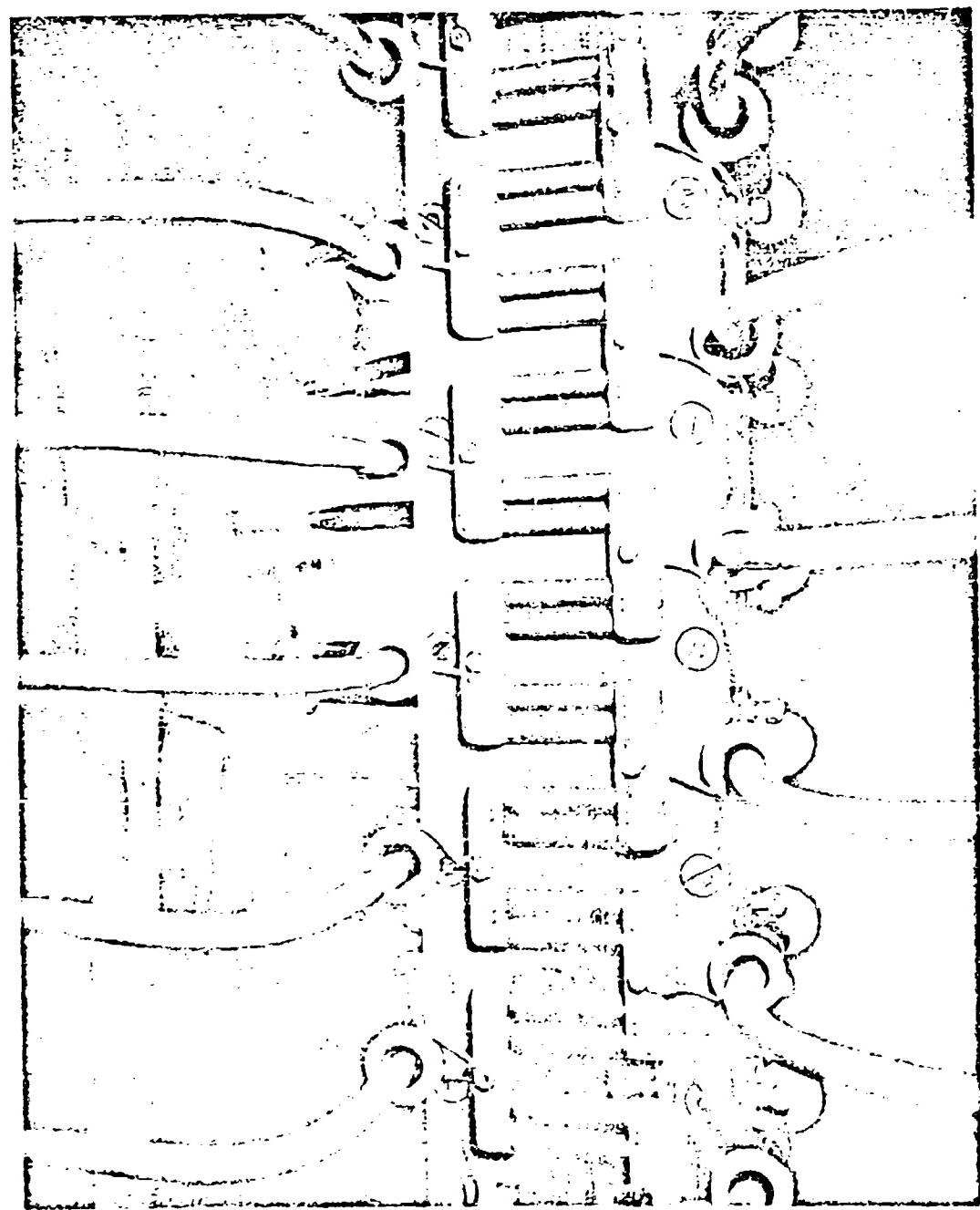


FIG. 12 REAR CLOSE-UP VIEW, SHOWING RESISTOR DIVIDERS AND CABLE CAPACITORS

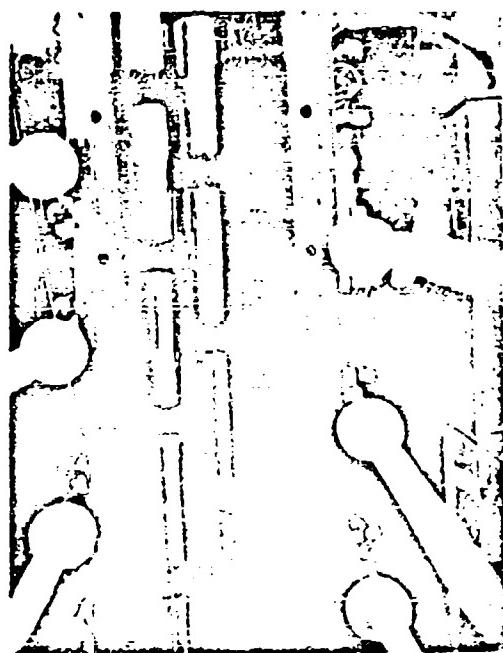


FIG. 13 Assembled Gap Electrodes

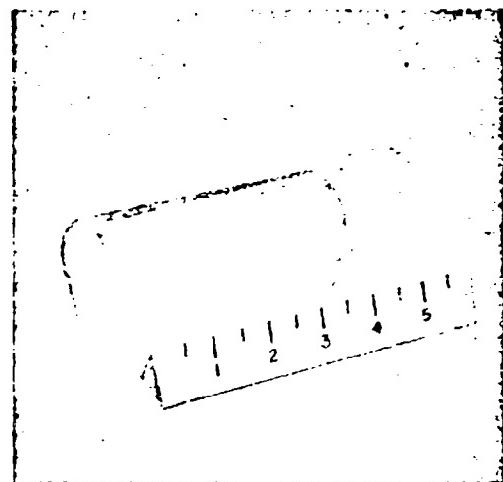


FIG. 14 Gap Electrode

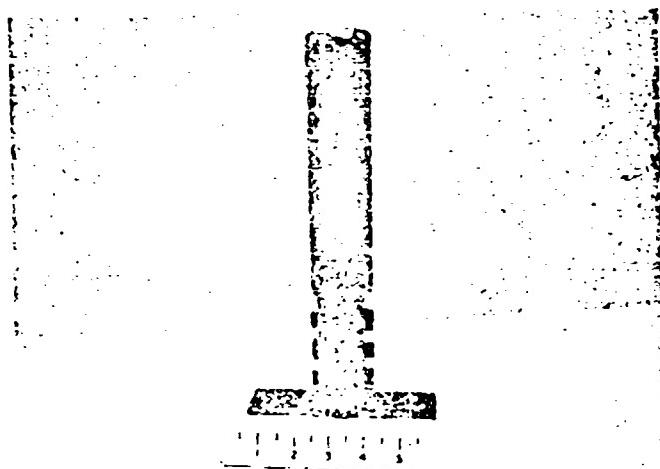


FIG. 15 Bottom Gap Electrode



FIG. 16 Top Gap Electrode

e. Coupling Capacitor:

The coupling capacitor was mounted externally and connected to the center electrode through a high-voltage bushing. Fig. 9 shows this connection.

f. High-Voltage Connection:

The high-voltage connection can be partially seen on the top of Figs. 9 thru 11. It is an aluminum cylinder placed on top of the rack. The connection from the capacitor bank to the top gap is made with this cylinder. The cylinder effectively shields the connectors and provides a corona-free bushing.

g. Trigger:

In accordance with the choice of a minimum of a 5-to-1 ratio of gap-applied voltage to gap-breakdown voltage, the trigger required is 50 kilovolts for a gap breakdown voltage of 10 kilovolts (1/8" gap setting). With a gap capacitance of $3 \mu\text{fd}$ (this high value is due to the large discharge area chosen) and an individual gap-to-ground capacitance of $32 \mu\text{fd}$ (including stray capacitance), only 80% of the supplied trigger voltage appears across the first set of gaps. A trigger supply voltage of 60 kilovolts is therefore required.

The discharge tube selected for the trigger is a 5949 hydrogen thyratron. To ensure that no misfires of the trigger discharge occur under standby conditions, a maximum d-c voltage to be applied to the thyratron of 16 kilovolts was selected. To ensure reliable firing with a d-c voltage as low as 10 kv, we therefore have to use a pulse transformer with a 6-to-1 ratio. The total capacitance of the gap system is approximately $1000 \mu\text{fd}$. This requires a discharge capacitor of $0.036 \mu\text{fd}$ in the thyratron circuit. The basic logic driver circuit used to fire the crowbar is shown schematically in Fig. 17. The fault signal is fed into the pulse amplitude selector, which has a variable bias; if it exceeds a pre-set level, it will trigger a biased blocking oscillator. The signal in turn is fed through the cathode follower output and fires the hydrogen thyratron. Measurements have shown that the crowbar fires in $0.55 \mu\text{sec}$ after receipt of a fault signal. A portion of the trigger signal is fed back to a univibrator, which applies a positive signal of a controllable length to the grid of the blocking oscillator, making it free running. The repetition rate is controllable and can be set for the needs of the system. As a general rule, a pulse separation of 1 millisecond appears desirable since the deionization time of the gaps appear to be in the order of 1-to-10 milliseconds dependent upon the energy flowing through the gaps and the degree of ionization.

TEST RESULTS:

After installation, a series of tests were conducted to determine the most effective manner of utilizing the crowbar. In this test the resistance in series with the klystron was varied and inductances were placed in various parts of the circuit. The results obtained led to the following conclusions for effective crowbar utilization:

- a. Add as much inductance in series with the rf tube on the capacitor side of the crowbar as can be tolerated in the circuit during normal

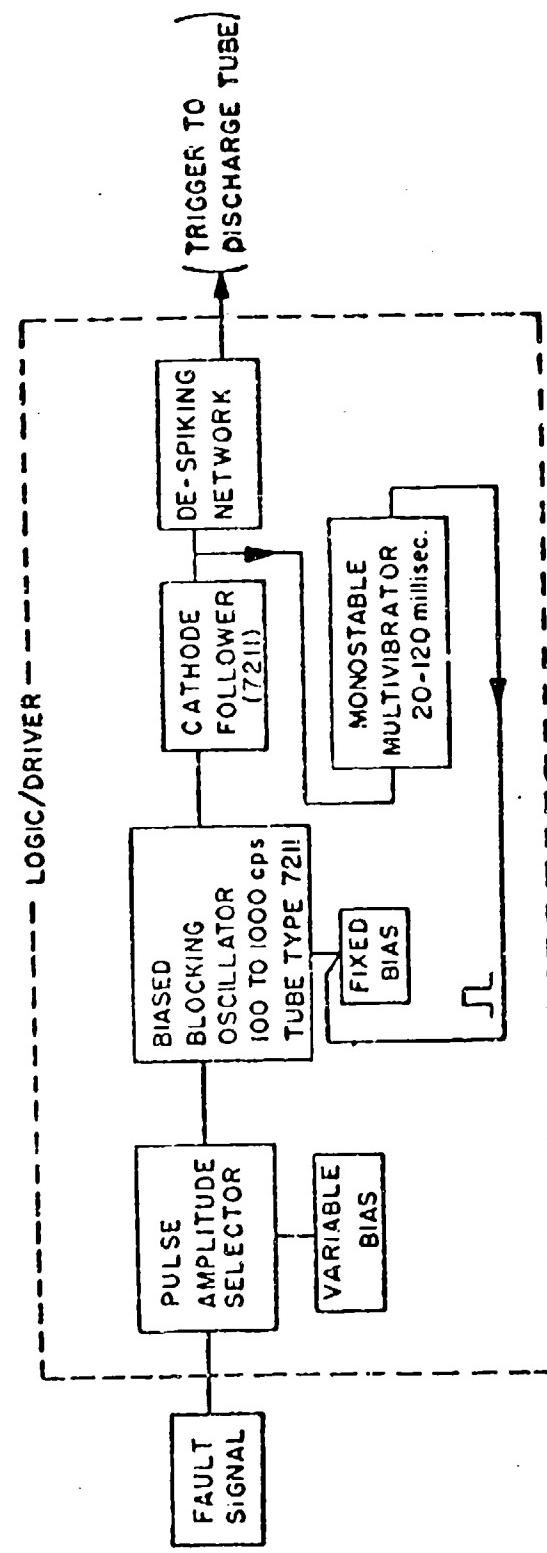


FIG. 17 SCHEMATIC OF LOGIC-DRIVER CIRCUIT

operation of the klystron. In most circuits the rise time of the output pulse is determined by other factors rather than this inductance. This limits the rate of rise of current during a fault, permitting the crowbar to fire before any sizable current is attained.

b. Eliminate inductance in series with the klystron on the klystron side of the crowbar. This assures a fast rate of fall of current in the klystron after the crowbar fires.

c. Place as much resistance as possible on the klystron side of the crowbar as can be tolerated during normal operation. If the klystron arc does not extinguish when the crowbar fires, the resistance determines the effective source impedance and the current that continues to flow in the klystron.

In Fig. 18(a) the fault current in an air gap is shown when no crowbar is used. The current reached a peak of 2600 amperes and decayed to zero in approximately 300 μ sec. Fig. 18(b) shows the result obtained with an air gap and the crowbar in the circuit. The peak current reached 300 amperes and decayed to zero. In this case the air gap was extinguished. In the cases where the air gap did not extinguish, current in the order of 50 amperes flowed for some hundreds of microseconds. This is quite reasonable, since the two arcs were competing with each other except that one had a 15-ohm series resistance.

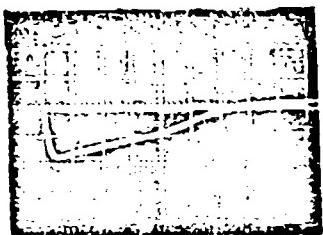
The data of most interest were that obtained with the klystron. Fig. 18(c) shows a typical klystron fault. In this case only 1.3 μ fd of the capacitance bank was used at 90 kilovolts. The current reached 2000 amperes or higher (the current transformer was saturated at 2000 amperes) and decayed to zero in approximately 50 microseconds.

Fig. 18(d) shows the effectiveness of the crowbar. In this fault the peak current never exceeded 100 amperes and decayed to zero in 2 μ sec. Pressure changes monitored with a Vac-Ion Gauge indicated negligible pressure changes in the tube. Fig. 18(e) is included, since it demonstrates the only observed fault where an arc did not immediately extinguish, and current can be seen flowing through the tube. In this case a pressure change of 1×10^{-7} mm Hg at 4×10^{-7} mm Hg was observed. This figure demonstrates the necessity of firing as rapidly as possible to avoid any gas evolution. It also demonstrates the need for multiple firing, since any increase in gas pressure is almost certain to lower the breakdown voltage of the tube and could cause reignition of the arc during the capacitor recharge period.

CONCLUSIONS:

In summary, a crowbar system design has been shown with the following features:

- a. Fast firing - 0.55 μ sec after initiation of fault.
- b. Low trigger energy - less than two joules.
- c. Repetitive firing - permits protection until main circuit breakers have opened.

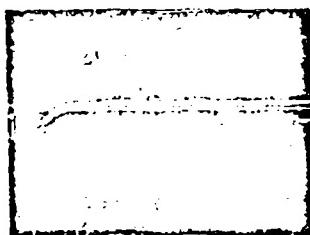


- a. Fault Current through Air Gap
Without Crowbar

Conditions: Full Capacitor Bank
at 140 KV

Current Scale = 2000 A/cm

Time Scale = 50 μ sec/cm

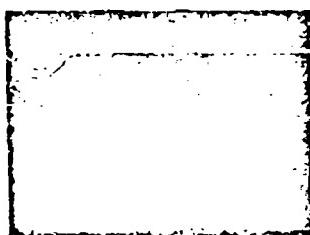


- b. Fault Current through Air Gap
With Crowbar

Conditions: Full Capacitor Bank
at 140 KV

Current Scale = 200 A/cm

Time Scale = 50 μ sec/cm

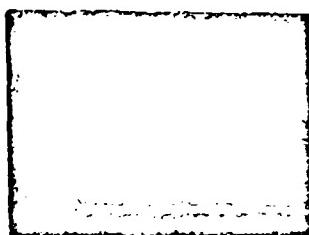


- c. Fault Current through Klystron
Without Crowbar

Conditions: Capacitor Bank 1.3 μ fd
at 90 KV

Current Scale = 2000 A/cm

Time Scale = 50 μ sec/cm

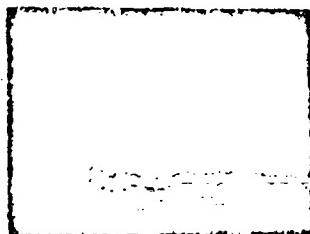


- d. Fault Current through Klystron
With Crowbar

Conditions: Full Capacitor Bank
at 140 KV

Current Scale = 200 A/cm

Time Scale = 2 μ sec/cm



Scale \rightarrow 1 cm

- e. Fault Current through Klystron
With Crowbar

Conditions: Full Capacitor Bank
at 140 KV

Current Scale = 200 A/cm

Time Scale = 2 μ sec/cm

FIG. 18

- d. Low acoustic energy - permits placement in working area without disturbing personnel.
- e. 100% overvoltage setting of gaps - reduces chance for spurious firing.
- f. Infinite voltage range - provides protection at any voltage level and permits checking at zero applied voltage on gaps by observing discharge.
- g. Self-triggering - if the logic-driver circuit fails at 90 kilovolts and over it will self-trigger in the event of a fault, never leaving the tube without protection at higher voltage. The reason for firing is that a fault superimposes a sufficiently large signal of a fast enough rise time to fire the crowbar. This type of operation is necessarily slower than normal triggering since the fault must develop to a level where the signal fires the crowbar.
- h. Low inductance - permits rapid decay of fault current in klystron.
- i. Flexible design - many different configurations may be used.

ACKNOWLEDGEMENTS:

The authors wish to express their appreciation to Mr. G. W. Taylor, Chief, Power Tubes Section, for his contributions in analyzing the test equipment and in making recommendations for its modifications, and to Mr. R. W. Brower, Technician, Model Shop, for his cooperation in constructing the crowbar.

REFERENCES:

1. Gardner, A. L., Sloan, D. H., Marshall, L. C., McBride, W. J., Jr., "High-Power, Pulse-Line Switching Devices," Final Report No. 5, Issue No. 10, Contract W-2E-099-ac-466, University of California.
2. Woodford, J. B., Roble, R. F., Bings, J; "12.5 Megawatt Spark Gap System," Final Report, Contract AF30(602)-915, Carnegie Institute of Technology.
3. Creedon, J. E., Schneider, S., Cannata, F., Buffa, A. J.; "Experiments in Switching High Peak Powers," Proceedings of the Sixth Symposium on Hydrogen Thyratrons and Modulators.

A HIGH-VOLTAGE MULTIGAP CROWBAR

by

G. Grotz

Surface Armament Division
Sperry Gyroscope Company
Division of Sperry Rand Corporation
Great Neck, L.I., New York

INTRODUCTION

Many high-power radar transmitters use mod anode klystrons in the final high-power stage. The klystrons are connected directly to a high-voltage dc power supply that usually has a large capacitor bank to minimize voltage droop during the transmitted pulse. As a consequence, a large amount of energy is stored in the capacitor bank, and if a fault occurs in the klystron, severe damage will result if all the capacitor bank energy is dissipated within the klystron.

To avoid damage to the klystron, a device is required that will remove the beam voltage in a short time, perhaps 10 to 20 microseconds, to keep the dissipated energy below a critical level. Ideally, a fast switch would suffice; however, no means presently exist to break a high-voltage dc circuit in this short period of time. The next alternative is to connect a short, or crowbar, across the klystron as rapidly as possible. Since a mechanical shorting switch is too slow, an electronic device is needed. Thyratrons or ignitrons function well as crowbars since they trigger rapidly and carry high currents. However, there are no commercial units operating in the 300-kv range, and series units appear impractical. Thus, one must turn to the common spark gap as the basic device.

Many configurations of spark gaps are suitable for klystron protection, e.g., the multigap, two-gap, or single-tracking-gap types of crowbar. This paper will discuss a particular multigap design and note the specific advantages it has over the others.

OPERATION

The circuit considered here is the multigap crowbar, shown in Fig. 1. The crowbar is connected across the klystron so that, after firing, the klystron voltage is reduced to the level of the crowbar arc drop. The capacitor-bank energy is therefore dissipated in R_1 . The value of R_1

usually is chosen for critical damping of the capacitor bank to avoid oscillations. Resistance R_2 insures arc extinction within the klystron after the crowbar fires. The crowbar conducts the capacitor-bank discharge current through R_1 until the current drops below the value needed to maintain the arc. If this value of current is greater than the dc power supply short-circuit current at that instant of time, then the arc may extinguish before the opening of the primary circuit breaker. In that event the capacitor bank will be recharged until the primary circuit breaker opens. Unfortunately, the recharged voltage on the bank may be sufficient to cause a second arc in the klystron since the klystron gas pressure still will be fairly high a fraction of a second after the first internal arc. To avoid recharging the capacitor bank, the crowbar is refired at 10-millisecond intervals until the primary breaker opens, so that the capacitor-bank voltage will not rise significantly.

The crowbar (bounded by the dashed lines in Fig. 1 and expanded in Fig. 2) consists of (1) series spark gaps that fire at 40 kv, (2) voltage-balancing resistors that apply 20 kv to each gap when the entire crowbar is connected to 300 kv, and (3) capacitors connected from each gap to ground. Zero voltage is assumed on the power supply capacitor bank. The crowbar is fired by increasing the charge on capacitor C_7 by a trigger pulse from pulse transformer T_1 and coupling capacitor C_{16} . Gaps G_7 and G_8 fire, and then capacitors C_6 and C_8 are charged through the previous gaps until gaps G_9 and G_{10} fire. This process continues until all gaps are fired and all capacitor charges fall to zero through the arc discharge to ground.

The pulse transformer T_1 is driven from a large pulse capacitor C_{17} that is switched by a 5C22 thyratron triggered at 10-millsec intervals for approximately one-half second. The open-circuit capability of the trigger is approximately 200 kv, or five times the breakdown potential of the gaps. The firing time is controlled by the impedance of the trigger source, the value of crowbar capacity to ground, and the voltage-time relationship for gap breakdown. The gaps are optically in line so that the ultraviolet radiation from the first gap will accelerate the firing of the subsequent gaps. In the event that high voltage is on the capacitor banks, then the firing is further accelerated by the potential of the capacitor bank aiding the applied trigger pulse.

DESCRIPTION

The multigap crowbar constructed for laboratory use (Fig. 3) is about 16 feet high and consists of brass electrodes, resistors, high-voltage dc cable, and automobile inner tubes, all mounted on a mahogany H frame. The coupling capacitor is connected to the center electrode and pulse transformer by RG 19U cable with the braid removed.

The electrodes (Fig. 4) are hollow brass cylinders, 12 inches long with a 3-1/2-inch diameter, placed over the center conductor and dielectric of two 300-kv cables with the braid removed. The cables have been placed in a

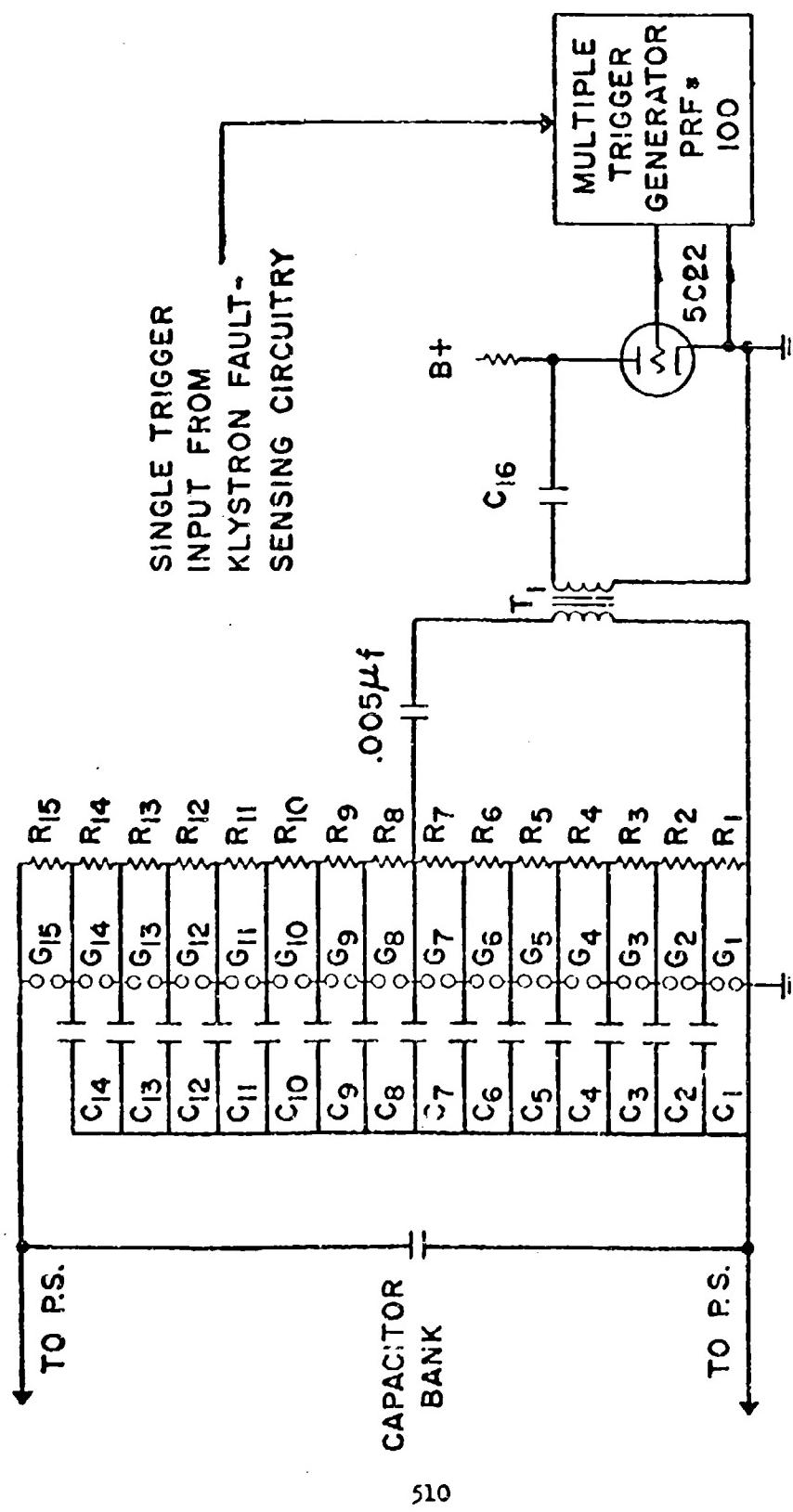


FIG. 2 MULTIGAP CROWBAR

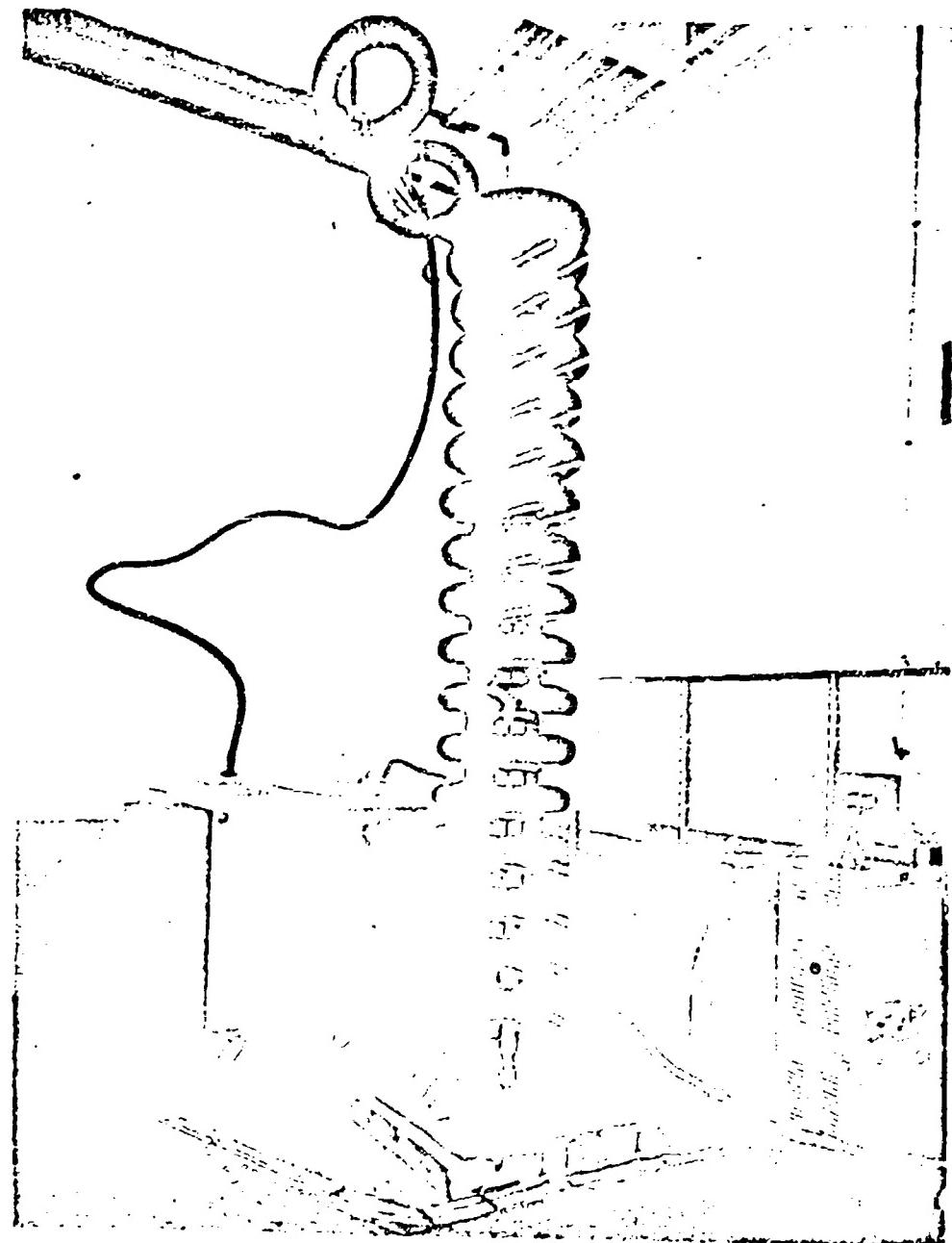


FIG. 3 MULTIGAP CROWBAR

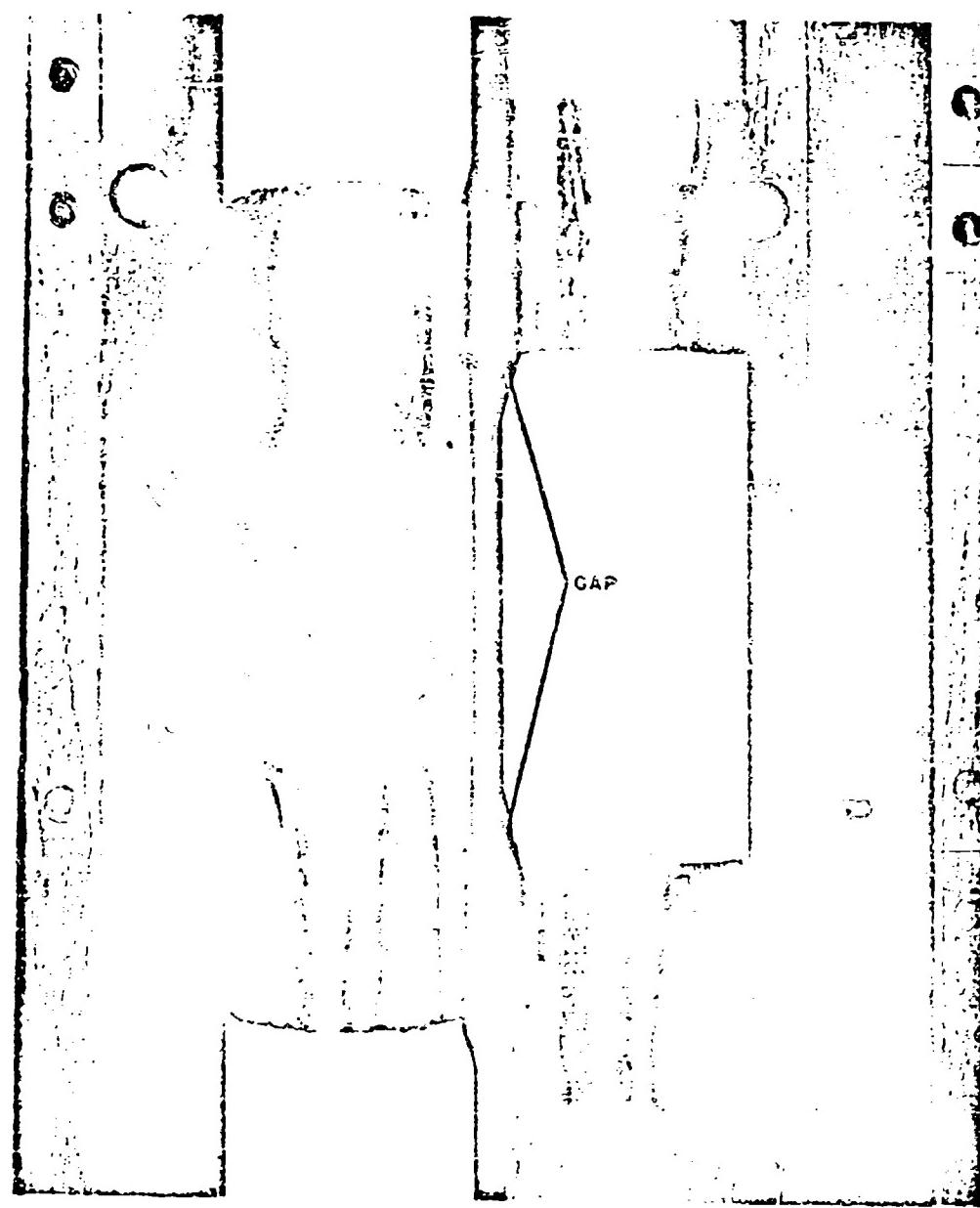


FIG. 4 SPARK GAP ASSEMBLY

vertical, parallel arrangement, with the electrodes staggered to form 15 gaps separated by approximately one-half inch. The capacitors are formed by the electrode-cable combination, since the center conductor of the cable is grounded.

To eliminate voids and consequent corona between the polyethylene surface of the cable and the electrode, the entire cable-electrode assembly was potted with vacuum-processed silastic rubber. In addition, a sphere was placed on the center conductor of each cable at the top of the assembly and enclosed in silastic. This technique prevented arcing from the top high-voltage electrode, along the surface of the cable, to the grounded center conductor of the cable at the top of the assembly.

Uniform dc potential distribution is assured by a series of 15 resistors across the 15 gaps (Fig. 5). The total number of gaps was determined by dividing the maximum operating dc voltage by the peak ripple and droop expected from the power supply capacitor bank. The right number of gaps eliminates the possibility of continuous arcing at the top gap during normal system operation. To provide reliable operation free from spontaneous arcs in a questionable atmosphere, each gap was spaced to break at twice the operating potential.

To avoid corona and consequent leakage currents that would upset the dc voltage distribution, an automotive inner tube was placed around each gap. The conductivity of an inner tube is approximately ten times greater than required to distribute the charge uniformly over the surface of the tube in the time required to build up the power supply voltage.

COMPARISON

One may ask how this unit compares in performance with related crowbars such as the tracking-gap or Marx-generator types. First, the two-gap crowbar described in Fig. 6a is considered. In the Marx-generator, a number of capacitors are charged in parallel and discharged in series through spark gaps to attain a potential across G_1 many times greater than the gap breakdown voltage. Gap G_1 fires and raises the potential across C_2 to its firing point. Gap G_2 fires and discharges C (the capacitor bank) through L and the critical damping resistance R_2 . Unfortunately, L is required to minimize the magnitude of the voltage spike delivered to the klystron during the interval of time between the firing of G_1 and G_2 .

Referring to the plot of klystron arc current (I_k) vs. time (Fig. 6b) it is seen that the current remains in the klystron during the time required to fire the crowbar G_2 (t_f) and slowly diminishes during an additional period of time, determined by the value of L , which is called circuit time (t_c). The crowbar arc will then extinguish, and the capacitor bank will recharge, applying voltage to the klystron V_k until the primary power is removed by the circuit breaker in time (t_{cb}). If the capacitor bank residual voltage is kept low, klystron arcs will not recur, and this usually requires an extremely fast primary circuit breaker. The two-gap crowbar can be



FIG. 5 RESISTOR ASSEMBLY

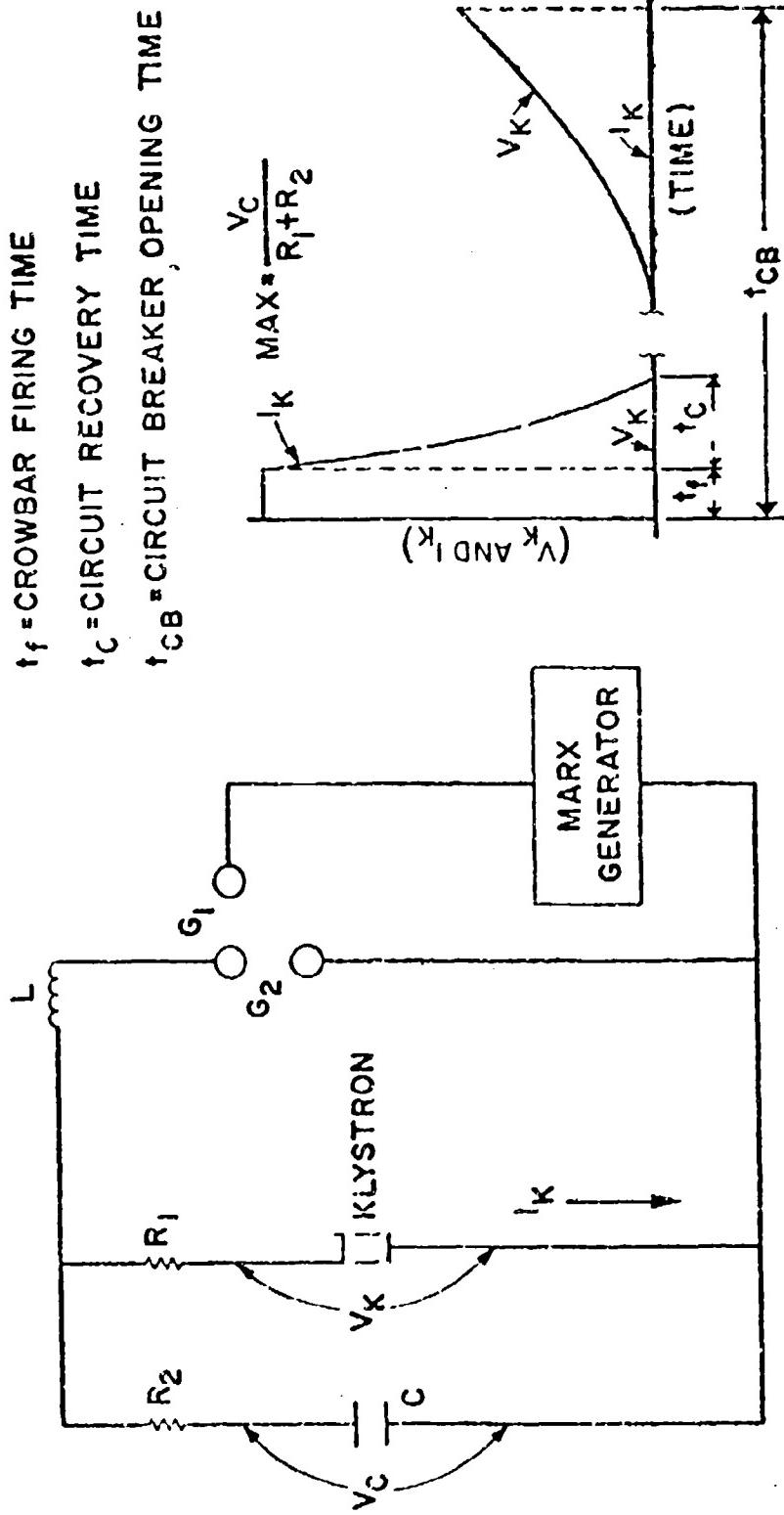


FIG. 6 TWO-GAP CROWBAR

repetitively fired to eliminate the capacitor-hank recharging problem, but the crowbar power supply will be fairly large in comparison to the other two types of crowbars.

Second, the single-tracking-gap crowbar (Fig. 7a) is considered. A single gap is formed by a fixed and movable electrode. The movable electrode is positioned by a servo motor so that the gap breakdown potential may exceed the operating potential by a predetermined amount and will track all operating potentials. The gap is fired by a low-voltage capacitor discharge through trigger electrodes contained in the main gap electrodes. However, in the event of a klystron arc, the voltage appearing across gap G_1 is reduced in accordance with the voltage division across R_1 and R_2 (Fig. 7b).

Resistor R_2 is chosen for critical damping, while R_1 is chosen so that the gap potential during a klystron arc will exceed a value of one half of the hold-off potential of the gap to provide reliable gap firing. The klystron current is reduced to zero immediately after crowbar firing, and the capacitor bank will discharge. The crowbar gap will de-ionize, and the capacitor bank will recharge until the primary voltage is removed. Unfortunately, the value of R_1 in this crowbar must be considerably larger than the value required in the other two types, which raises the total resistance in series with the klystron and results in slightly inferior performance of the over-all radar system. In addition, this type of crowbar cannot be repetitively pulsed, and thus the primary circuit breaker is more critical.

Third, the multigap crowbar is shown in Fig. 8a. In the event of an arc in the klystron, the arc current will attain a value of I_k (Fig. 8b) for a period of time (less than 2 microseconds) until the crowbar fires. After discharge of the capacitor bank C, the crowbar will de-ionize, and capacitor bank C will start to recharge. The crowbar then will be fired repetitively until after the primary breaker opens, to eliminate the residual capacitor-bank charge.

CONCLUSION

Performance capabilities of the various crowbars, are compared in table 1. It is apparent that the multigap crowbar will reduce the klystron arc current to zero in the shortest period of time and will prevent capacitor bank re-charging. To date, the multigap crowbar has been fired in excess of 4,000 times and has performed well.

ACKNOWLEDGMENTS

The author is indebted to Mr. S. Schneider and Mr. A. Buffa of the U. S. Army Signal Research and Development Laboratories, Fort Monmouth, New Jersey, who first proposed using a multigap crowbar for the protection

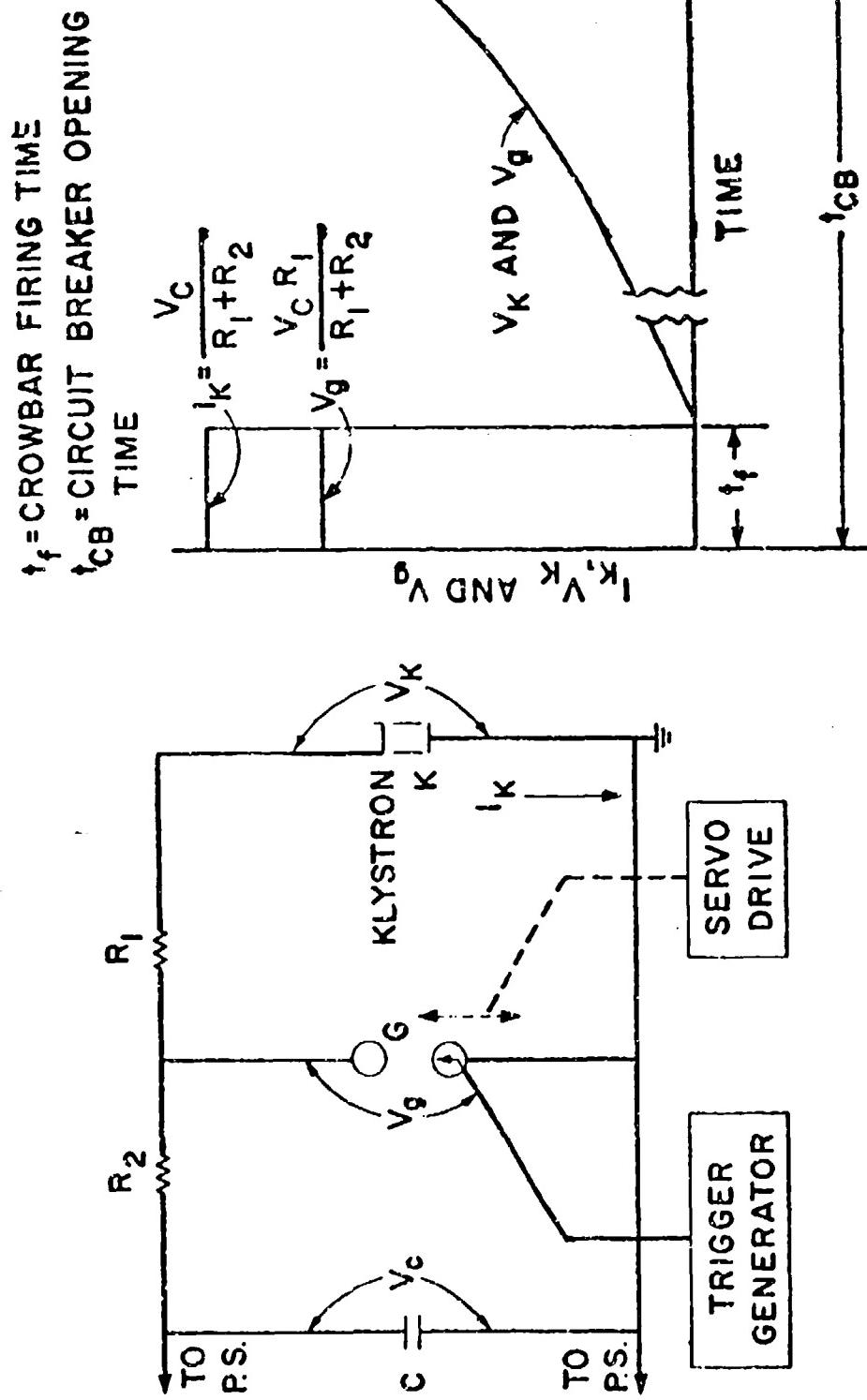


FIG. 7 SINGLE TRACKING GAP CROWBAR

t_f = CROWBAR FIRING TIME
 t_{CB} = CIRCUIT BREAKER OPENING TIME

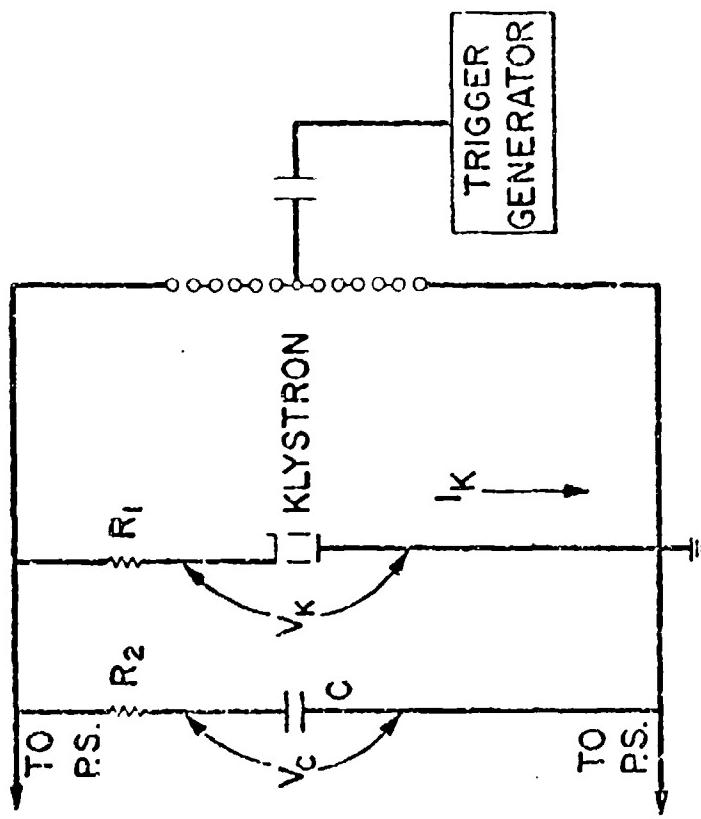
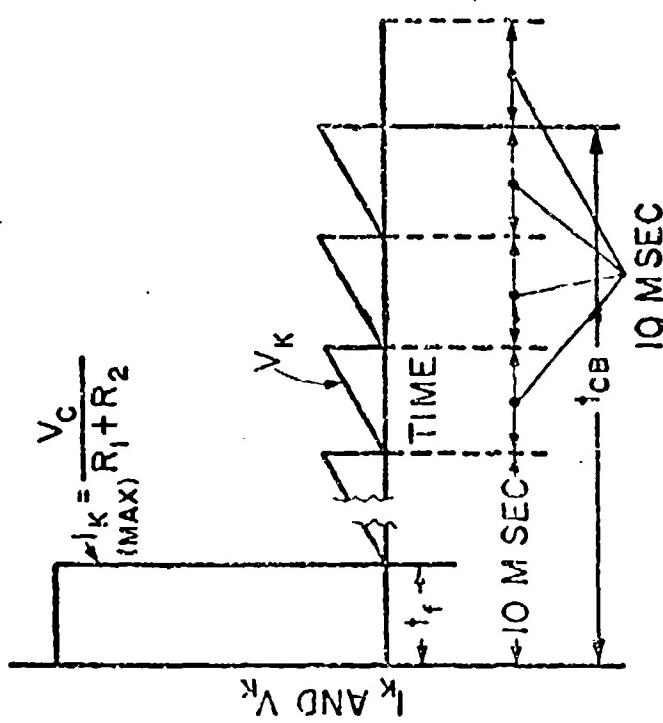


FIG. 8 MULTIGAP CROWBAR

TABLE I COMPARISON OF THREE TYPES OF CROWBARS

	SINGLE TRACKING GAP	TWO-GAP	MULTIGAP
FIRING TIME (INCLUDING TRIGGER GENERATOR)	LESS THAN 2 μ SEC	LESS THAN 2 μ SEC	LESS THAN 2 μ SEC
CIRCUIT TIME TO REDUCE KLYSTRON ARC CURRENT TO ZERO	LESS THAN 2	IN EXCESS OF 2	LESS THAN 2
ABILITY TO BE PULSED	NO	MODERATE	YES, AT ANY RATES LIMITED BY MARX GEN- ERATOR RE- CHARGING
KLYSTRON SERIES RESISTANCE	HIGH	LOW	LOW
MOVING PARTS	YES	NO	NO
PRICE	HIGH	MEDIUM	LOW

of a klystron, participated in preliminary discussions, and supplied the trigger generator for use with the crowbar.

Contributors to Program:

- A. Buffa USASRDL
- E. Cronauer Sperry Gyroscope Co.
- G. Grotz Sperry Gyroscope Co.
- A. Lesher Sperry Gyroscope Co.
- L. Reitman Sperry Gyroscope Co.
- S. Schneider USASRDL

THE USE OF TRIGGERED SPARK GAPS AS CROWBARS

by

Lawrence B. Woolaver

Edgerton, Germeshausen & Grier, Inc.

Introduction

The increased cost and working voltage of many present-day tube types has generated the need for an electronically controlled, fast acting switch to be used as a protective device or crowbar. To be successfully employed in this application, a switching device must possess at least the following four characteristics: high voltage holdoff capability, low impedance after firing, short delay time, and high peak current capability. Other features which greatly assist in the design of a successful crowbar circuit are such characteristics as easy triggering, wide working range, acceptable life, low standby power, size, and so forth. The triggered spark gap has now been developed to the point where it can compete very favorable with either thyratrons or ignitrons for the crowbar application.

Although not a new device, the characteristics of the triggered spark gap are probably less well understood than those of the thyratrons or ignitrons. In addition, a variety of operating circumstances exist for the spark gap, not all of which are recommended for the crowbar application. It is the purpose of this paper to review these characteristics and to illustrate how this device can best be employed in this application.

The work reported here refers principally to the type GP-12 spark gap which has been developed at EG&G and which is now commercially available as one member of a family of metal-ceramic spark gaps. This gap, illustrated in Figure 1, has been designed to have a working range of main electrode voltage approximately from 9 to 25 KV. It is a three-electrode device consisting of two main electrodes and a coaxially located trigger electrode. The main electrode which surrounds the trigger electrode has been termed the adjacent electrode, while the other main electrode is the opposite electrode.

Operating Modes

The three-electrode version of the triggered spark gap can be operated in four possible combinations of polarity. Following a suggestion of the Sandia Corporation made a number of years ago, EG&G has accepted the nomenclature for these operating modes as shown in Figure 2. The polarity signs as used in this nomenclature refer to the reference electrode, thus avoiding any possibility of ambiguity. The reference electrode need not be the grounded electrode. The characteristics of the spark gap depend heavily upon the mode of operation, as will be shown later.

Triggering Characteristics

The triggered spark gap transfers from a nonconducting state to a highly conducting state when an initiation trigger pulse is placed on the trigger electrode. If the peak voltage of this trigger pulse is too low or the voltage across the main electrodes is too low, the gap will fail to transfer from one condition to the other. A common method of illustrating this characteristic of a triggered spark gap is shown in Figure 3. These curves represent the data for the GP-12 in a slightly idealized form. This type of data is obtained by measuring the minimum peak trigger voltage required to reliably cause the spark gap to transfer versus the voltage applied to the main electrodes. The four principal characteristics illustrated by this graph are the static breakdown voltage, cutoff voltage, minimum trigger voltage, and operating range. The static breakdown voltage is the main electrode voltage at which the spark gap transfers spontaneously without an initiating triggering pulse. As the minimum electrode voltage is reduced, the peak trigger voltage required to reliably cause the gap to transfer increases rapidly and then reaches a relatively constant value which will successfully transfer the gap over a wide range of E-₁ voltages. The range of values of main electrode voltage over which the peak trigger voltage requirement remains essentially constant is the operating range. The value of peak trigger voltage required to fire the gap in the working range is frequently referred to as the minimum trigger voltage. As the main electrode voltage is reduced, a point is reached at which the peak trigger voltage requirement again increases rapidly and finally reaches a point where the gap fails to transfer regardless of the value of the peak trigger voltage. This value of main electrode voltage has been termed cutoff. It should be emphasized that although the operating characteristics of a triggered spark gap are plotted in this manner, the curve is, in

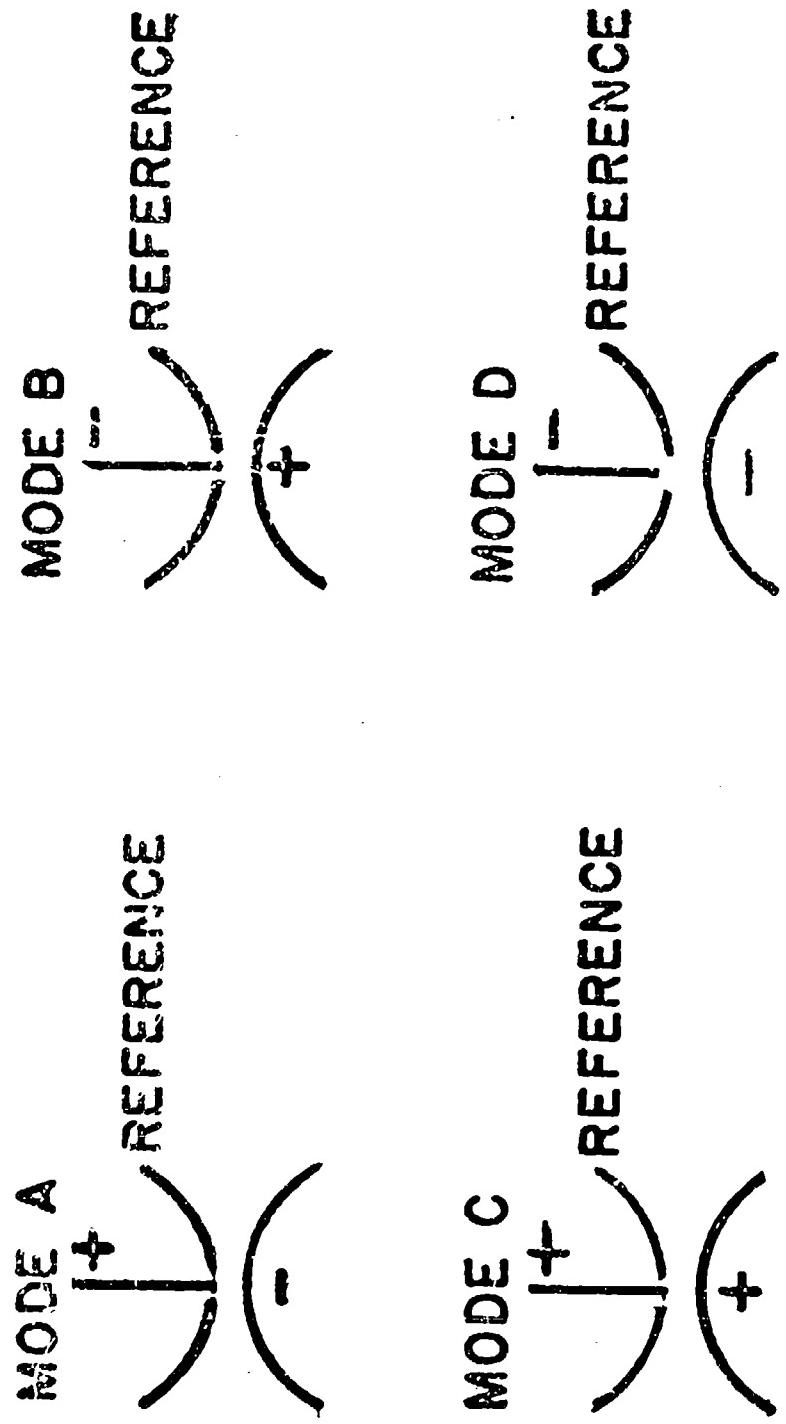
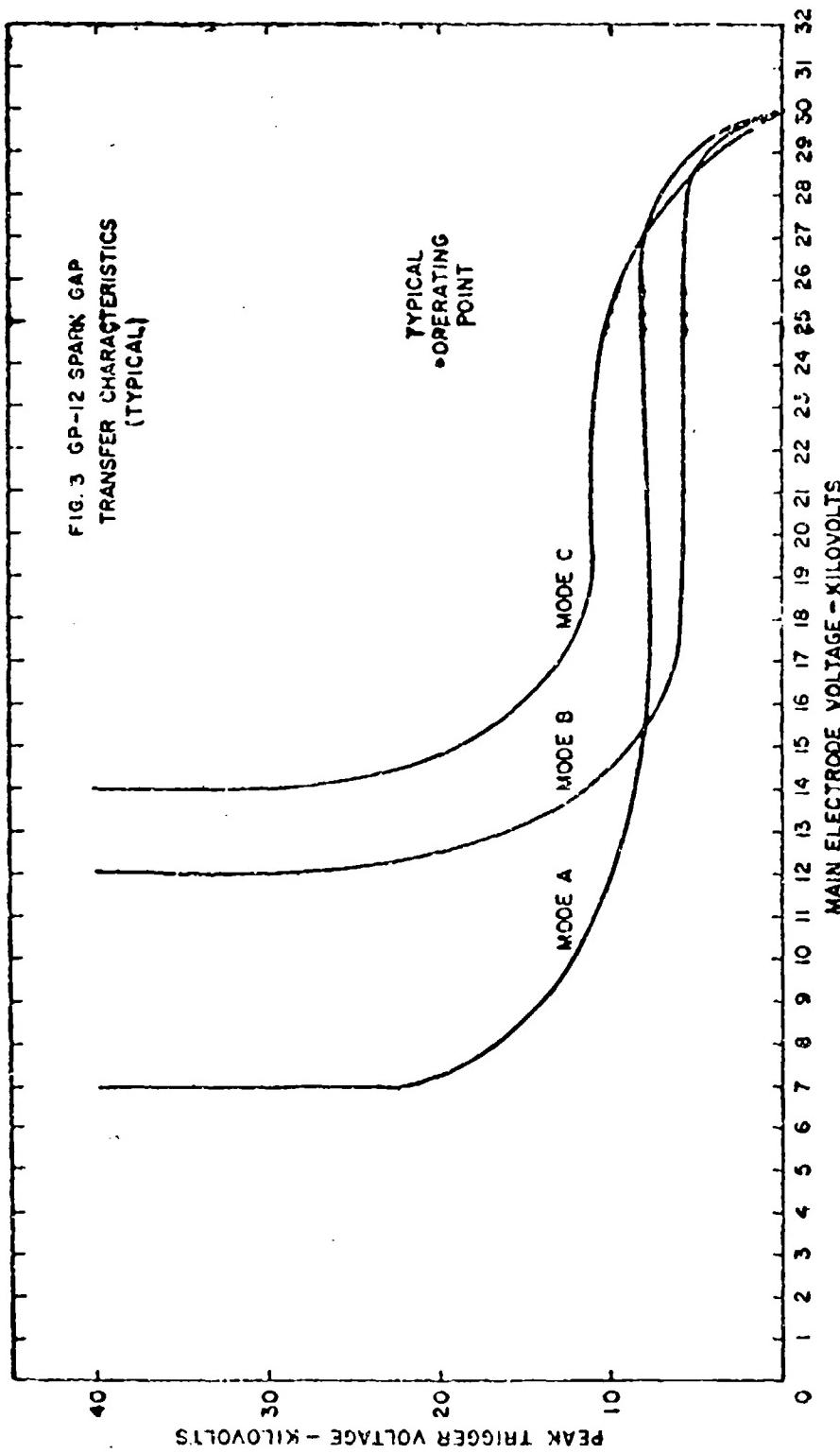


FIG. 2 SPARK GAPS
MODES OF OPERATION

FIG. 3 GP-12 SPARK GAP
TRANSFER CHARACTERISTICS
(TYPICAL)



fact, a boundary between two regions. The region above the operating characteristic curve represents combinations of values of peak trigger voltage and main electrode voltage which will produce reliable transfer of the spark gap. The region below and to the left of the curve are combinations which fail to cause transfer. Combinations of trigger voltage and minimum electrode voltage on or near the curve represent conditions which may prove to be unreliable. In normal practice, it is common to select an operating point well above the level of the minimum trigger voltage and sufficiently below the static breakdown voltage to avoid the possibility of a spontaneous transfer. Such a point has been marked on Figure 3.

The details of the transfer characteristics of a spark gap depends heavily upon the mode of operation as illustrated in Figure 3. The principal shifts are in the cutoff voltage which serves to shorten the working range and the minimum trigger voltage. Occasionally the static breakdown voltage shows a slight shift downward when the opposite electrode is positive. Any substantial downward shift indicates a poorly constructed gap.

Delay Time

The basic purpose of a switching device in a crowbar circuit requires a very rapid transition from the nonconducting to the conducting state after the application of an initiating trigger. The triggered spark gap is capable of making this transfer in as little as a few hundredths of a microsecond. This delay time can be measured by a technique illustrated in Figure 4. These photographs were obtained by displaying the trigger voltage on one plate of a direct coupled oscilloscope and the main discharge current on the other plate. In these photographs the beginning of the trigger pulse is not visible. It can be seen that just prior to trigger breakdown, the trigger circuit draws sufficient current to reduce the voltage. After a brief period in this condition, an arc forms and the trigger electrode becomes electrically connected to the voltage of the opposite electrode. After an additional delay period, current begins to flow in the main electrode circuit. This is an RC type discharge with some oscillations of local stray capacitance and inductance superimposed on the beginning of the pulse. The delay time has been measured from the period in time when the trigger circuit begins to draw current to the period where current begins to flow in the main electrode circuit. It can be seen that this period of time, the delay time, exhibits some variation which is the delay time jitter. The sine wave in



FIG. 4

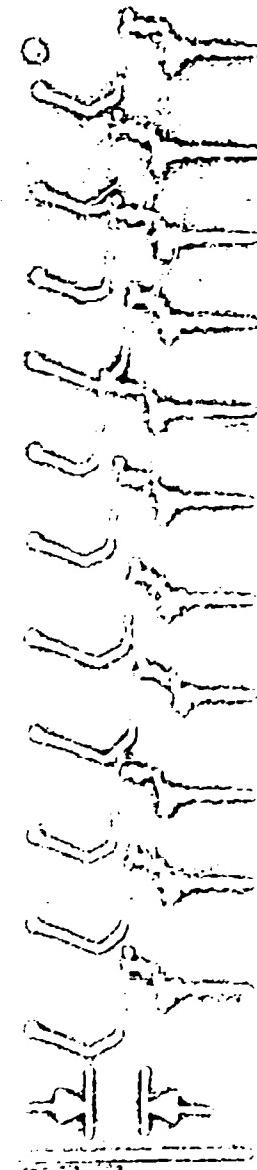
GP-12 DELAY TIME

MEASUREMENTS

MODE A

12 KV EE

12 KV PHOTOCOUP.



DELAY
TIME

DISCHARGE

Figure 4 is 10 megacycles.

The absolute value of delay time and the delay time jitter of a triggered spark gap is heavily dependent upon the mode of operation and the main electrode voltage as illustrated in Figure 5. It can be seen that once again Mode A is the most desirable operating condition for the crowbar application since the delay time remains low, down to voltages only slightly above cutoff. Mode B is nearly as good as Mode A. Mode C exhibits a transfer characteristic which is short when the applied main electrode voltage is near the static breakdown, but which rises sharply as the main electrode voltage is reduced towards cutoff. In those applications where a high degree of protection is not required during the initial turn-on period, this is not a serious drawback. In those cases where this type of protection is required, Mode A or B operation is strongly recommended since the delay time remains short.

The delay time of Mode D is so sensitive to main electrode voltage that it is not normally recommended for the crowbar application.

The delay time as measured above is not directly applicable to crowbar circuit design since the delay period does not begin at time zero. The total delay time will include the delay of the sensing circuit and trigger pulse generating circuit plus the time from the beginning of the trigger pulse to breakdown. These additional delays are not characteristic of the spark gap and have therefore been excluded from these data. In general, shorter total delay times can be obtained with faster rising trigger pulses with some slight adjustment for the fact that the voltage at which trigger breakdown occurs will increase slightly with increased trigger rise time. The rate of build up of current in the main discharge path is governed principally by the external circuit and is not characteristic of the spark gap. Therefore, this additional delay time has been excluded from the data presented above.

Life

The life of a spark gap in a crowbar application is difficult to predict since it depends upon many factors including peak current, pulse duration, electrode materials, and others. A GP-12 spark gap has been life tested at a peak current of 20,000 amperes with a pulse duration of a few microseconds for over 1000 operations without a significant change in its operating characteristics. It is believed that this may well

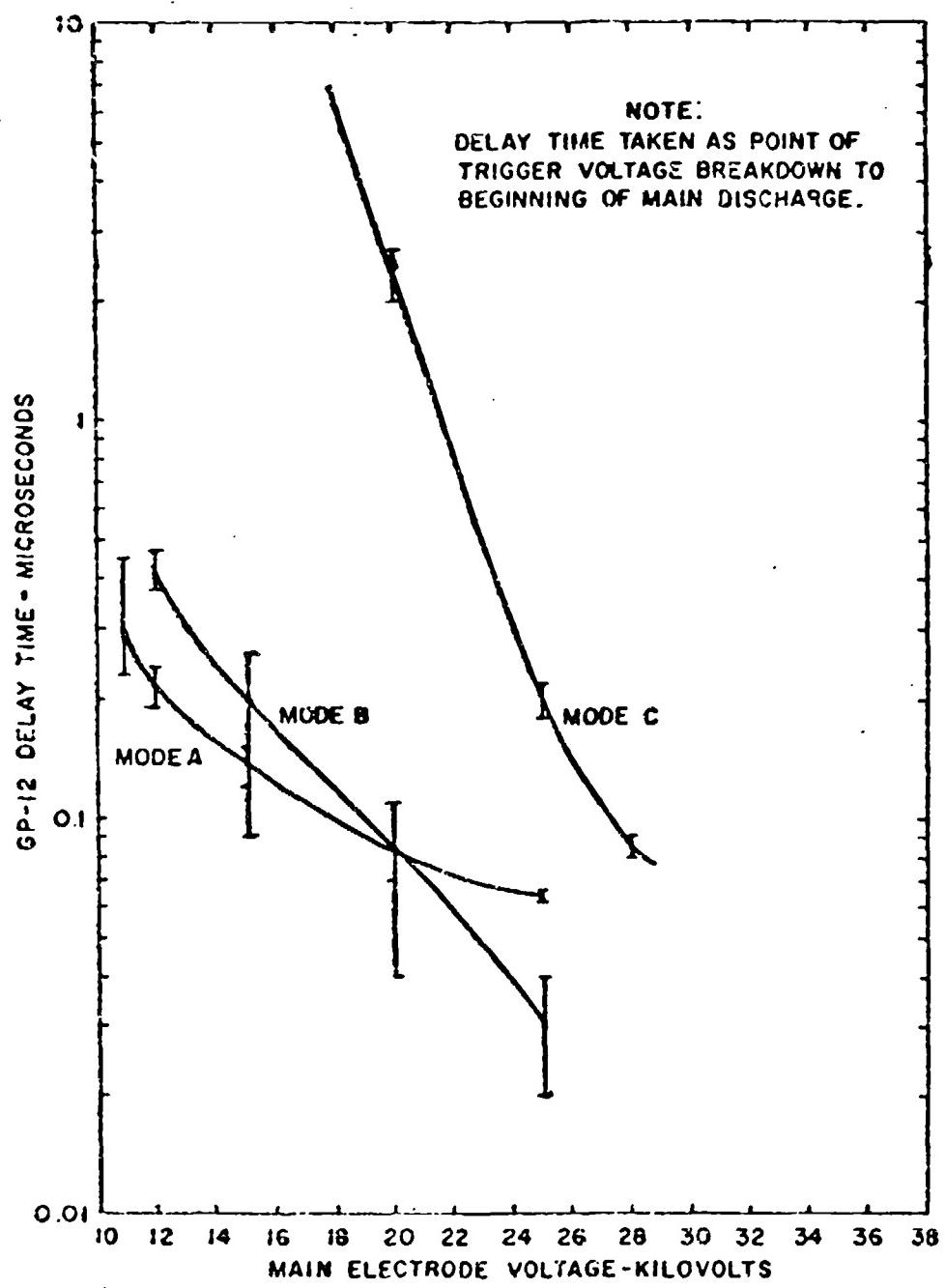


FIG. 5 GP-12 DELAY TIME CHARACTERISTICS

be a very conservative rating. Some experimental spark gaps have been made at EG&G which have been tested with a ringing pulse of several cycles duration at approximately 100 KC and a peak current of 100,000 amperes without a significant change in the characteristics or serious damage to the electrodes after 1000 operations. At lower peak currents, it can be expected that the life of a spark gap will be many thousands of operations.

Typical Crowbar Circuits

Of the four possible modes of operation, Mode A (positive trigger with negative opposite electrode) is most desirable for the crowbar application. A typical circuit for this application is shown in Figure 6. Since the main electrode opposite the trigger electrode in this mode is negative, it becomes necessary to employ a trigger transformer capable of isolating the trigger generator from the full main electrode voltage. For those crowbar applications where the cathode of the high power tube being protected is pulsed negatively, this requirement does not apply. The second recommended choice for crowbar applications is Mode B or C (see Figure 8). Since these modes employ a positive voltage on the electrode opposite the trigger electrode, it is most easily adapted to the common crowbar circuits. The price paid for operating this mode is somewhat reduced operating range for both modes and increased delay time with Mode C.

Summary

The triggered spark gap offers advantages over either the thyratrons or the ignitrons for many crowbar applications. The device is simple, rugged, easy to trigger and can be operated in any position or under severe environmental conditions. The stand-by power requirements can be reduced to essentially zero with cold cathode trigger generator tubes such as the krytron. The voltage holdoff capability is very high with 100 KV presently available. The peak power switching capacity is higher than the ignitron and very much higher than the thyratron. The efficiency as a switch is high since the arc drop is only a few hundred volts at very high peak currents. The life is more than adequate for the crowbar application even at very high operating conditions. It is felt the triggered spark gap has much to offer as a crowbar switch.

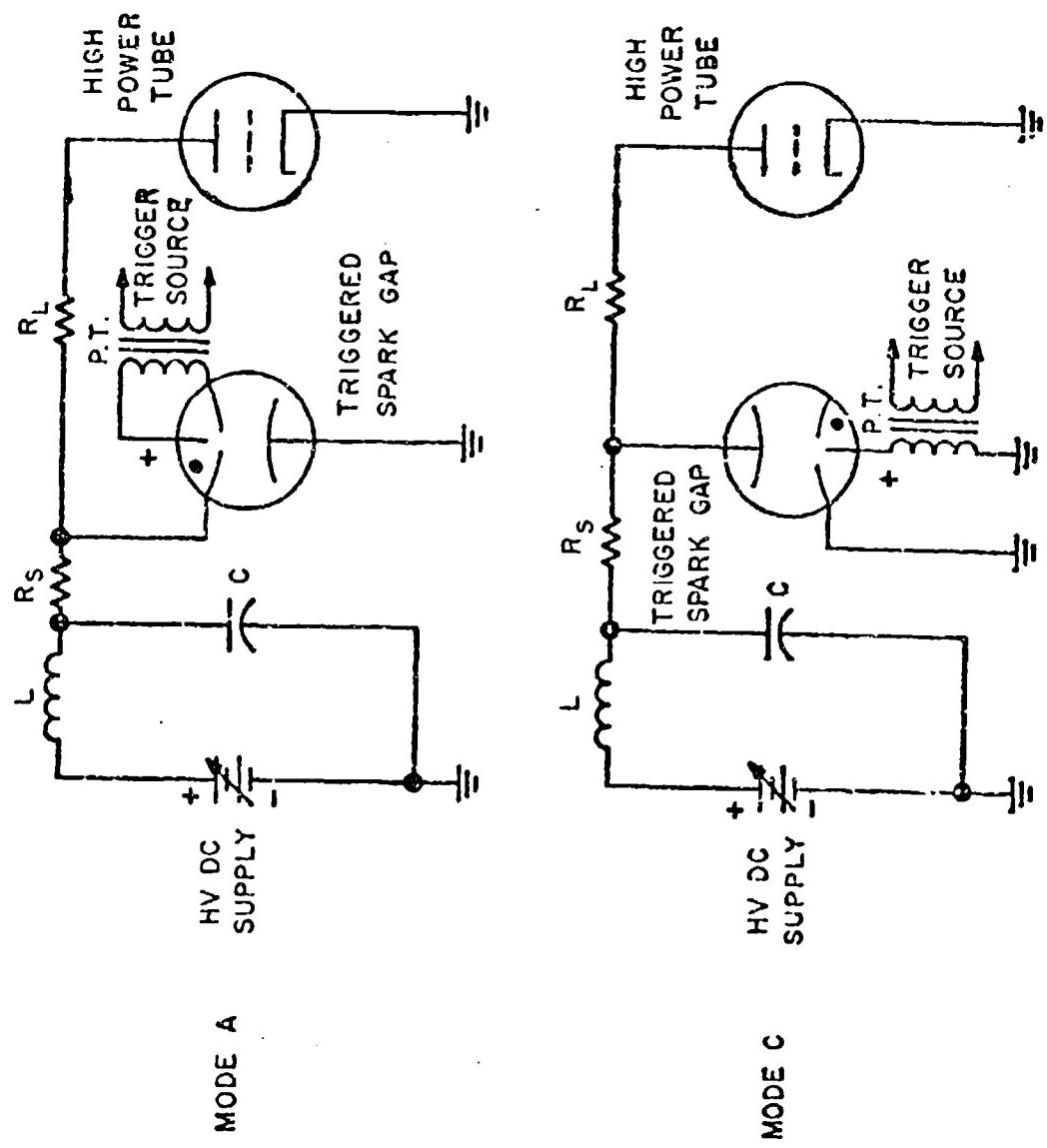


FIG. 6 TYPICAL CROWBAR CIRCUITS

A HIGH POWER GAS DISCHARGE SWITCH

by

B. G. Baker, B.Sc.(Eng.), A.C.G.I., A.M.I.E.E., and
K. G. Cook, B.Sc.(Eng.)

The General Electric Company Limited,
Central Research Laboratories, Hirst Research Centre,
Wembley, England.

SUMMARY

The paper describes a switch having a mercury pool cathode and a permanent gas filling. The switch has certain advantages over mercury pool devices of the ignitron and excitron type in reliability and accuracy of triggering, higher rate of increase of anode current, and improved anode voltage performance.

1. INTRODUCTION

The switch, which is essentially a mercury pool valve with a permanent gas filling, is not completely new. Patents dating back at least 25 years describe valves of this type, but there do not appear to have been any large scale commercial developments. Recent advances in design have made devices of this type more attractive; this will become apparent after a full description of the valve has been given. The advantages of the switch over conventional mercury pool valves and other switching devices will also be described.

A typical valve is shown in Figures 1 and 2. It comprises an anode A, which is partially enclosed by a metal screen G at grid potential, a baffle B and a mercury pool cathode C. The valve is enclosed in a glass envelope E and filled with hydrogen, deuterium or any of the rare gases. With hydrogen or deuterium filling a reservoir R may be included.

In operation the switch is triggered by applying a high voltage pulse to the grid, causing an arc spot to form on the mercury pool, thus initiating conduction between cathode and anode. The baffle prevents cathode vapour jets from reaching the control grid.

2. DESIGN PRINCIPLES

2.1. Cathode

The mercury pool is capable of high emission densities and is virtually

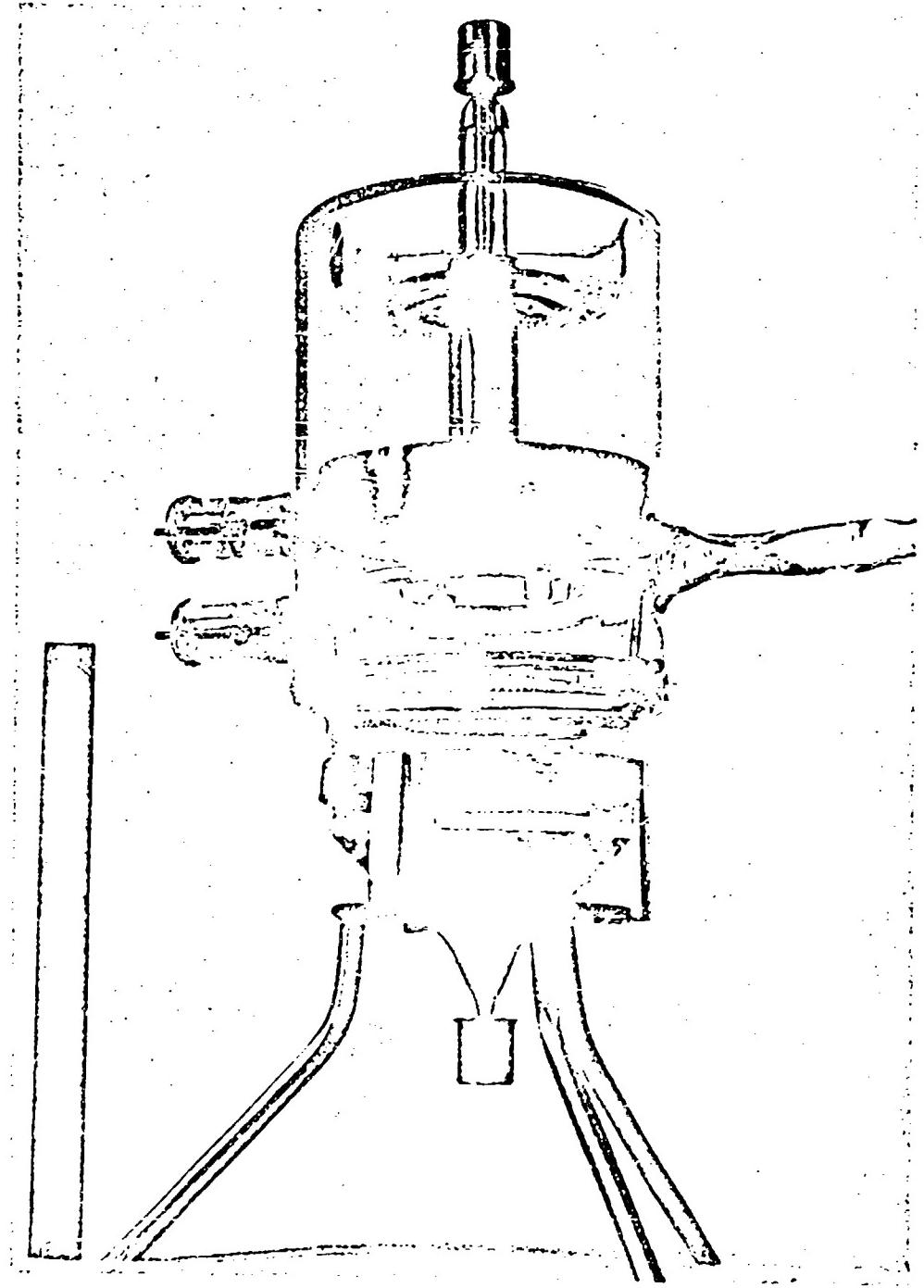
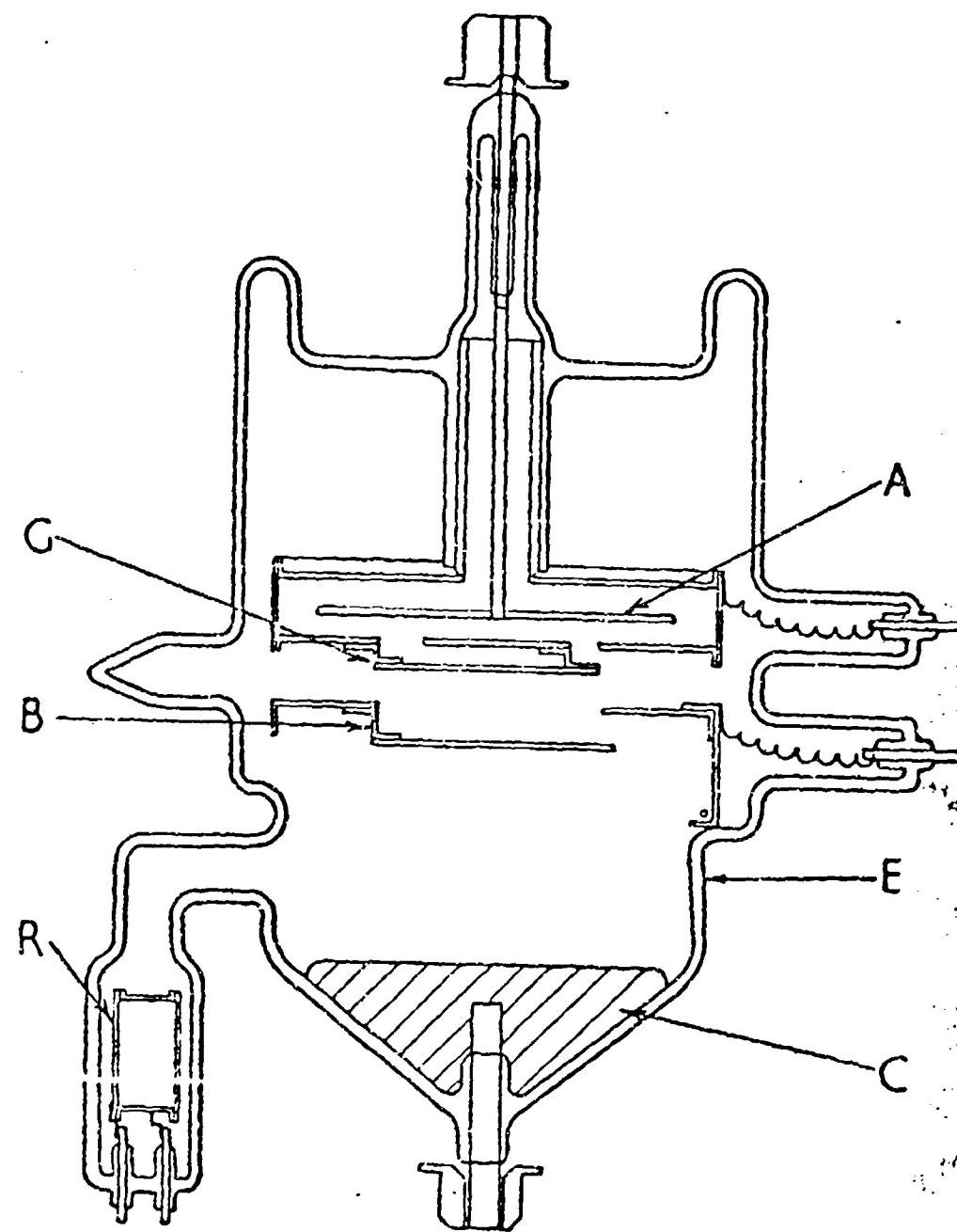


Fig. 1. Experimental Switch

FIG.2.
EXPERIMENTAL SWITCH



indestructible. It is desirable to contain the mercury pool in an insulating envelope: with a metal envelope there is a tendency for the cathode spot to transfer to the wall causing sputtering of the metal.

2.2. Baffle

At high peak currents jets of vapour are emitted from the surface of a mercury pool cathode. The baffle prevents these jets from reaching the grid structure, where condensed mercury would tend to reduce the voltage hold-off performance of the valve.

2.3. Grid

The grid has a two-fold purpose. Firstly, when a high voltage pulse is applied between grid and mercury pool, a cathode spot is formed on the mercury thus initiating the cathode-anode discharge. The permanent gas filling pressure and grid-cathode spacing are chosen so that the Paschen sparking potential of this gap is near the minimum. The application of a d.c. voltage to the grid-cathode gap produces a characteristic of the form shown in Figure 3. As the applied voltage rises the grid current increases steadily and the grid cathode region is filled with a diffuse glow. The voltage falls abruptly to about 50v when the current exceeds a critical value, and an arc spot forms on the surface of the mercury. If an anode voltage is applied under those conditions, a normal cathode-anode arc discharge develops.

At lower pressures a somewhat greater voltage must be applied before an arc forms. For breakdown to occur rapidly under pulse conditions an over-voltage must be applied. Table 1 shows the reduction in mean anode delay time as the grid trigger voltage is increased. The delay times are relatively independent of anode voltage, and accurately controlled initiation of the cathode-anode discharge can be achieved with anode voltages as little as 400v.

TABLE 1

<u>Grid Trigger Voltage</u> kv	<u>Mean Anode Delay</u> μsec
16	200
20	140
24	80
30	80

(Hydrogen pressure 0.26 torr.)

It is important that the mercury pool should be the only surface in the grid-cathode field which is at cathode potential. The pool must be

contained in an insulating envelope, and no metallic leads should protrude through the surface of the mercury, otherwise the cathode arc may form on the metal surface and fail to initiate a mercury cathode spot.

The second function of the grid is to enable the valve to hold off a high anode voltage during the period when the grid is not triggered. The device operates at pressures below the Paschen minimum and during the hold-off period the grid is virtually at cathode potential. If a high Paschen sparking voltage is to be achieved between anode and grid, at a sufficient gas pressure to support a high current discharge, the effective spacing between anode and grid must be a minimum, i.e. there must be no "long paths" between these electrodes. Therefore, the anode is virtually enclosed in a box at grid potential. The anode-grid spacing must not be so close that a "field emission" type breakdown occurs between those electrodes. Typically, for 40kv anode voltage, the gap should not be less than about 5 mm. With this spacing the following maximum filling pressures are attainable:- Deuterium 0.4 torr, Hydrogen 0.3 torr, Helium 0.7 torr, Argon 0.1 torr, Xenon 0.07 torr.

The design of the grid is a compromise between two conflicting requirements. Paschen breakdown requires that the grid apertures be sufficiently small to prevent long path breakdown between anode and cathode. The impedance offered to the discharge is, however, a minimum when the grid slots are very open. A good compromise is a long narrow slot and in practice a slot width of about 3 mm has been found suitable with deuterium and hydrogen. Some reduction in anode field penetration has been achieved by applying negative bias to the grid.

The recovery-time properties of the grid are unimportant in low duty cycle applications and for these a single layer grid has been found satisfactory. For valves which are to be used in high repetition rate circuits a more complicated double layer grid might be required.

2.4. Anode

The anode is a disc and is surrounded by the grid as described in Section 2.3. The material chosen for the anode will depend on the application. Where high peak currents and long pulse lengths are switched the transient heating of the face of the anode may raise the surface temperature to boiling point. In these cases it is desirable to use a material such as molybdenum.

The anode lead must pass through the grid box without introducing long path breakdown. To prevent breakdown a suitably designed moly seal, such as that shown in Figure 2, is used. In normal operation a lamp is shone

on the anode seal end, combined with a cooling air stream on the lower part of the valve, ensures that no mercury vapour condenses in the anode seal where it might lead to premature voltage breakdown.

3. RECENT DEVELOPMENTS

It is now possible to discuss why the switch has recently become a more attractive device. To achieve a high anode voltage, coupled with a sufficiently high gas pressure to obtain reliable triggering, it is desirable to use the more recently developed boxed-in anode structure. It would not, for example, be sufficient merely to fill an existing ignitron or excitron structure and hope that it could be triggered in the way described. In addition, in repetitive operation the rate of gas clean-up can become excessive; this can now be overcome by the use of titanium hydride or deuteride reservoirs controlled by barretter and thermistor.

4. COMPARISON WITH OTHER DEVICES

The switch possesses the following advantages compared with other devices:-

- (i) Hot cathode Thyatrons. The maximum current which can be drawn from a hot cathode reduces considerably at long pulse length. For high peak current operation at long pulse lengths a large cathode must therefore be used and the heater power becomes excessive. The use of a mercury pool cathode in the switch overcomes these difficulties.
- (ii) Ignitrons. Material sputtered from the electrodes of the ignitron can cause erratic operation if it settles on the surface of the ignitor and short circuits the triggering discharge. The grid-anode spacing in the switch described in the paper is large, and sputtered material is unlikely to short circuit the trigger voltage. At ambient temperatures below 0-10°C the mercury vapour pressure in the ignitron becomes too low to support a high rate of rise of current. The switch described will continue to operate even when the mercury pool is frozen.
- (iii) Triggered Spark Gaps. High pressure gaps will not trigger readily at anode voltages much less than 50% of the maximum static breakdown voltage. The new switch will operate satisfactorily at 1% of its maximum anode voltage.

5. PROBLEMS

Where the peak current and pulse length have been very high, difficulties have arisen due to erosion of the grid. Arc spots tend to form on the top surface of the grid, possibly due to the presence of unipolar arcs¹, and the discharge subsequently chooses to be collected on the lower side of the grid plate, and emitted on the upper, without passing through the grid slot. The difficulty is accentuated if the volt drop in the discharge through the grid slot exceeds the sum of the voltage drop through the material of the grid plus the drop in the arc spot formed on top of the grid.

Unipolar arcs form when the potential difference between grid and plasma exceeds approximately 10-20 volts. This potential difference is the sum of two voltages: a) the potential drop in the sheath produced around the grid by the high density plasma and b) the potential difference between the grid and the plasma due to the potential gradient through the plasma in the region of the grid.

The latter effect may be reduced by designing the grid so that it has a minimum depth in the direction of the plasma potential gradient, thereby minimising the potential difference between grid and plasma.

6. APPLICATIONS

Two possible applications of the switch are shown in Figure 4. In 4(a) the device is used to discharge a storage capacitor, thus preventing damage to an r.f. oscillator when the latter sparks. In this case the valve is initially holding off a high forward voltage. In 4(b) the switch is used to remove an overswing voltage from a capacitor in a thermonuclear switching application. Here the valve is initially holding off a high inverse voltage and is triggered when the anode voltage reaches a positive value. In circuits of this type peak currents up to 50kA have been passed for pulse lengths of about 1 msec.

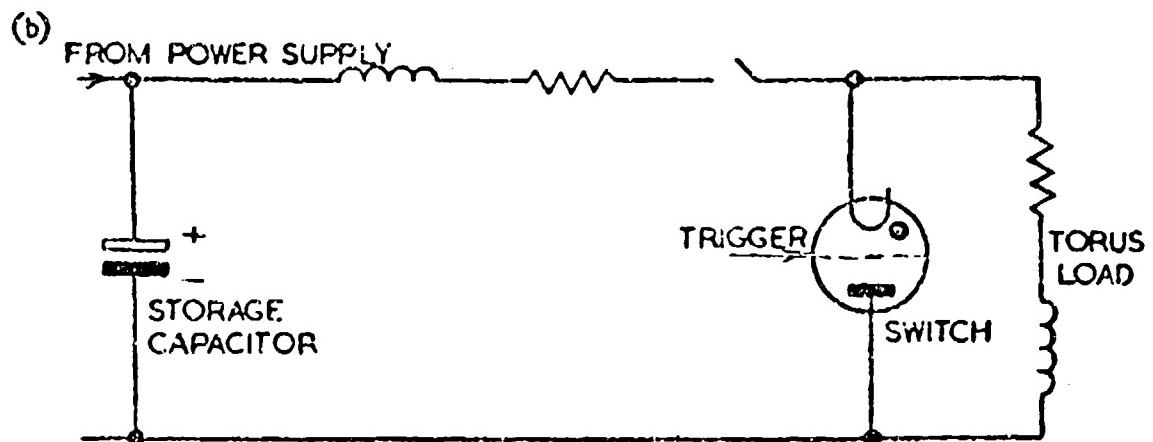
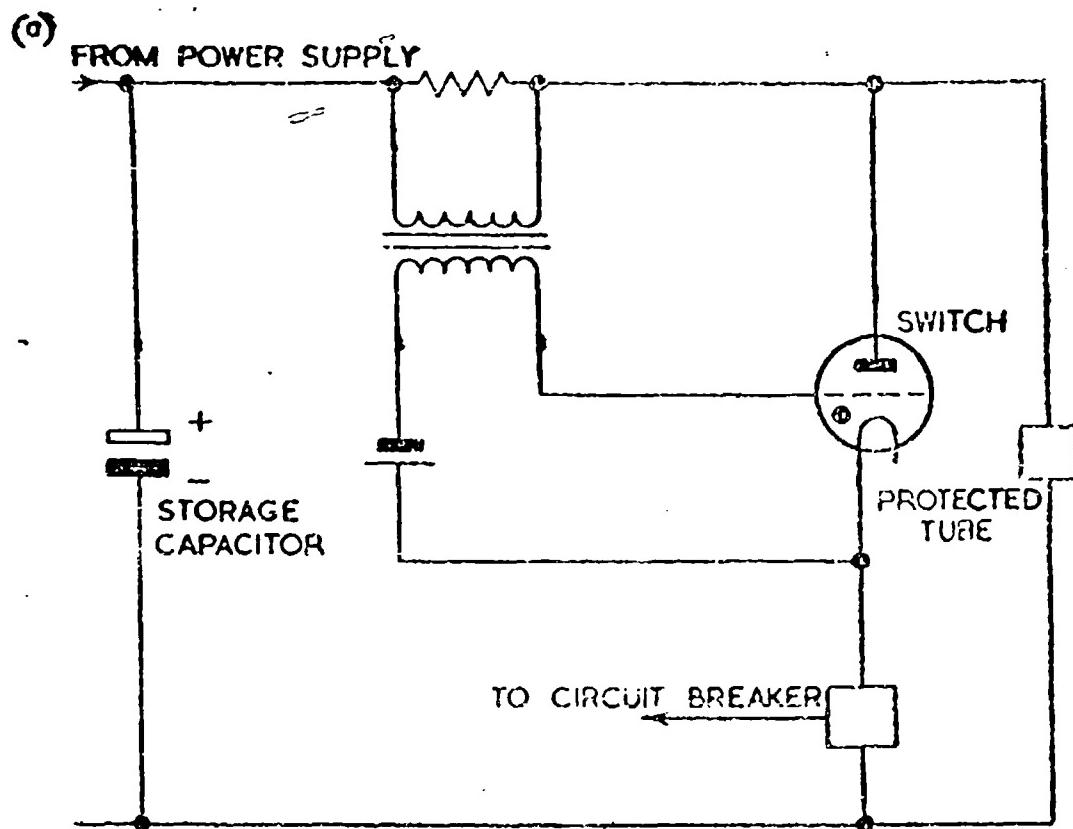
ACKNOWLEDGEMENT

This work has been supported by the United Kingdom Atomic Energy Research Establishment, Harwell, England, who have also given considerable assistance in testing experimental switches.

REFERENCE

1. A. E. Robson and P. C. Thonemann, Proc. Phys. Soc., Vol. 73, pp. 508-512, 1959.

FIG. 4. SWITCH APPLICATIONS



INFINITE VOLTAGE RANGE TRIGGERED ARC GAPS
FOR CROWBAR APPLICATION

By

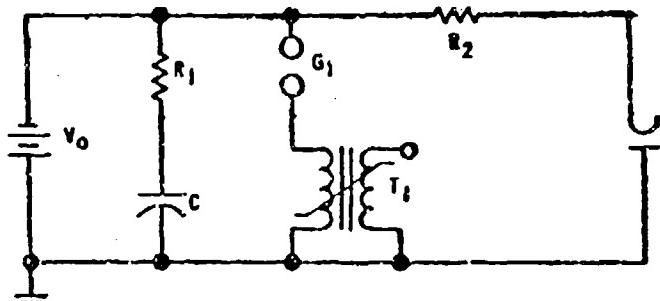
Joseph P. Swanson
RADIATION at Stanford

I. APPROACHES TO INFINITE RANGE CROWBARS

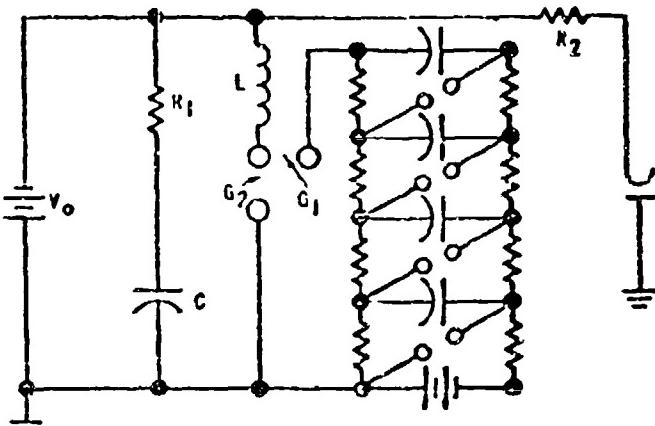
During the past several years three different approaches to the infinite voltage range triggered arc gap problem have been used at RADIATION at Stanford. These approaches include the two-ball arc gap discharged through a saturable transformer, an infinite voltage range three-ball arc gap triggered by a Marx generator, and most recently, an infinite voltage range needle-triggered arc gap.

These three approaches are shown schematically in Figure 1. Crowbar operation of the two-ball gap and saturable transformer shown in Figure 1-A is initiated by pulsing the primary of transformer T_1 and overvoltage arc gap G_1 . When G_1 breaks down, fault current passes through the secondary of T_1 , which rapidly saturates and produces a fault current diversion path. This approach has the advantage of extreme simplicity; but, it also has several disadvantages. First, the transformer has a constant ET product and thus the time required for the transformer to saturate is a function of the voltage it is crowbarring. Secondly, relatively large values of R_1 and R_2 are required because of the saturated inductance of this transformer so that rapid fault current diversion can be accomplished. Finally, the transformer must be constructed so that high fault currents can pass through its secondary and this becomes increasingly difficult at values of V_o larger than approximately 50 kv.

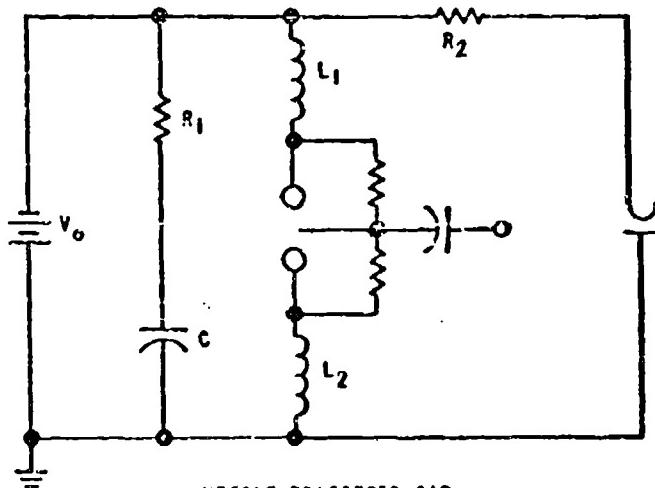
Another approach to infinite voltage range protection involves the use of a three-ball arc gap triggered by a Marx generator. This is shown schematically in Figure 1-B. Here, voltage V_o appears initially across both gaps G_1 and G_2 . When the Marx generator is triggered, it generates a positive voltage equal to approximately twice V_o . This voltage first breaks down gap G_1 , thus applying a positive potential of approximately $2 V_o$ across gap G_2 and causing its breakdown. This protective scheme works, but it has several disadvantages. First and most important, the Marx generator is not capable of being repetitively triggered for practical crowbar applications; secondly, field experience with this system has shown that at values of V_o on the order of 300 kv there is a capacitor reliability problem in the Marx generator.



TWO-BALL GAP AND SATURABLE TRANSFORMER
I-A



MARX GENERATOR TRIGGERED THRU BALL GAP
I-B



NEEDLE TRIGGERED GAP
I-C

FIG. I INFINITE VOLTAGE RANGE SWITCHES

Finally, in the light of what we now know about infinite voltage range triggered arc gaps, the Marx generator approach is too expensive a solution.

Figure 1-C shows schematically a crowbar system using an infinite voltage range needle-triggered gap. The operation of this type of gap will be discussed in the remaining portion of this paper.

II. THE OPERATION OF WIDE VOLTAGE RANGE NEEDLE-TRIGGERED ARC GAPS

If two spheres are considered to be isolated in space and have a voltage applied between them, equipotential planes similar to those shown in Figure 2 will be established. An equipotential plane having a voltage of $\frac{V_0}{2}$ is located

exactly halfway between the two spheres and has the shape of a flat plane perpendicular to the axis of the spheres. Now, if a straight conductor is aligned in this equipotential plane and if it is biased to the potential of this plane by some external means, this conductor will not distort the electrostatic field. Note also that this conductor (hereafter called the needle) will not corona since it is at the same potential as the space in its immediate vicinity would have been in the absence of the needle.

Figure 3 shows the method of inserting a biased trigger needle at the appropriate equipotential plane. Because this needle in no way influences the electrostatic field set up by the spheres, it does not lower the value of the breakdown voltage between these two spheres. It is, of course, assumed that other electrical elements such as R_1 and R_2 are sufficiently removed or so arranged that they negligibly affect the electric field between the spheres in the region where the field gradients are highest.

A triggered arc gap of the type shown in Figure 3 has a wide range of voltage operation and requires a very low energy trigger.

To fire the gap, the trigger pulse of opposite polarity from V_0 is coupled through C_1 to the needle. When the trigger electrode is pulsed to a potential other than that of the equipotential determined by the spheres, it forces a new electrostatic field configuration and the breakdown between the needle and upper ball is now determined by the needle point to sphere geometry and potential difference. Once the needle arcs to the upper ball, it is shorted to the potential of the upper ball and the breakdown potential of the needle to lower ball is again determined by a needle to sphere geometry. Because of the difference in geometries involved between the high voltage standoff situation, where breakdown is determined by sphere diameter and spacing, and the triggering situation, where breakdown voltages are determined by a needle-point to sphere geometry, it is possible to easily obtain an operating voltage range of 4 to 1.

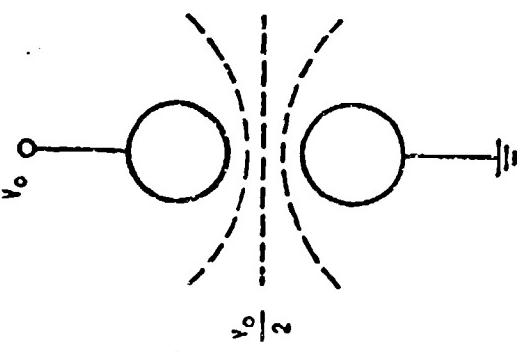


FIG. 2 EQUIPOTENTIAL PLANES DETERMINED BY TWO SPHERES

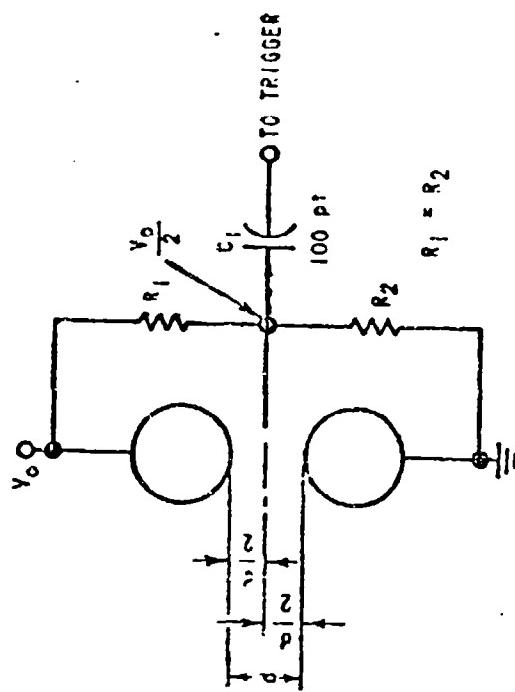


FIG. 3 METHOD OF BIASING NEEDLE TO THE $\frac{V_o}{2}$ EQUIPOTENTIAL PLANE

III. INFINITE VOLTAGE RANGE NEEDLE TRIGGERED ARC GAPS

Figure 4 shows the schematic diagram of a needle triggered gap similar to that described in the previous section, but which has been modified to trigger over a voltage range of 0 to -230 kv. As in the case of the gap shown in Figure 3, the needle is inserted halfway between the two sphere electrodes and biased to $\frac{V_o}{2}$. An inductance of 15 microhenries is added in series with each ball of the arc gap. The trigger pulse developed across the secondary of transformer T_1 is isolated from the trigger needle by an arc gap set to break over at about 110 kv.

The triggering sequence may be described as follows: Assuming that a negative supply is being protected, a positive trigger pulse is generated across the output winding of trigger transformer T_1 . As this trigger pulse rises it stores energy in capacitor C_2 . After about .75 microseconds, the voltage across C_2 reaches 110 kv and arc gap E_2 breaks down. A positive trigger pulse is then coupled to the needle through coupling capacitor C_1 . Assuming that the voltage across the main gap is zero when the arc gap is triggered, the needle has an equal probability of arcing to either the top or bottom ball. Because of the inductance in series with each ball, whichever ball the needle arcs to is pulled through a potential which is greater than $V_{o \text{ max}}$, and as mentioned in the first part of this paper, this is a high enough voltage to cause the needle to arc over to the other ball and thus completely light the gap.

As the minus potential on the top ball increases, the probability of arcing to the top ball first also increases, but the probability that the top ball will be pulled sufficiently positive to arc to the bottom ball decreases. However, note that the trigger signal applied to the top ball is oscillatory with a frequency determined by L_1 , C_1 and C_2 (neglecting distributed capacity). At the end of one-half cycle of trigger signal oscillation, both the top ball and the needle will be negative with respect to the bottom ball by a voltage equal to the applied d-c voltage plus some large fraction of the original input trigger signal amplitude. It can be shown that if the amplitude of the original trigger signal is great enough and its source impedance is low enough, reliable triggering to both balls can be obtained for any value of V_o . The purpose of capacitor C_2 and arc gap E_2 is to insure that the above requirements are met. Note that the triggering sequence described above is only needed during the first quarter of the arc gap's voltage range since for d-c voltages greater than $V_{o \text{ max}}$ firing of the needle to the lower ball is accomplished automatically once the needle has arced to the potential of the high voltage ball (as discussed in Section I).

Figure 5 shows the construction details of the 0-230 kv gap just described. For this gap we used two 11-inch steel balls separated by 4-1/4 inches and a steel trigger needle. Inductors L_1 and L_2 are seen at the top

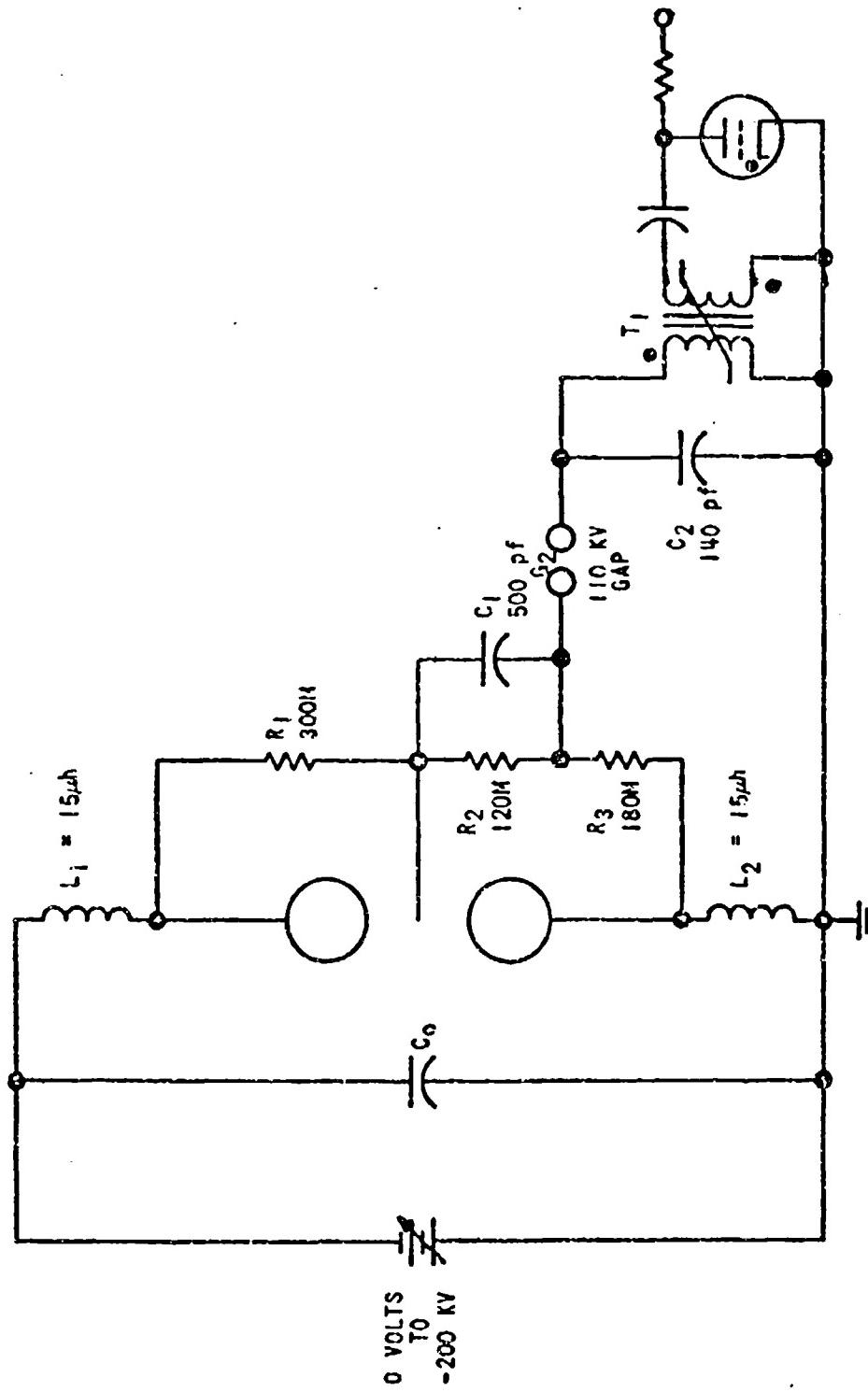


FIG. 4 SCHEMATIC DIAGRAM OF AN INFINITE VOLTAGE RANGE TRIGGERED NEEDLE GAP

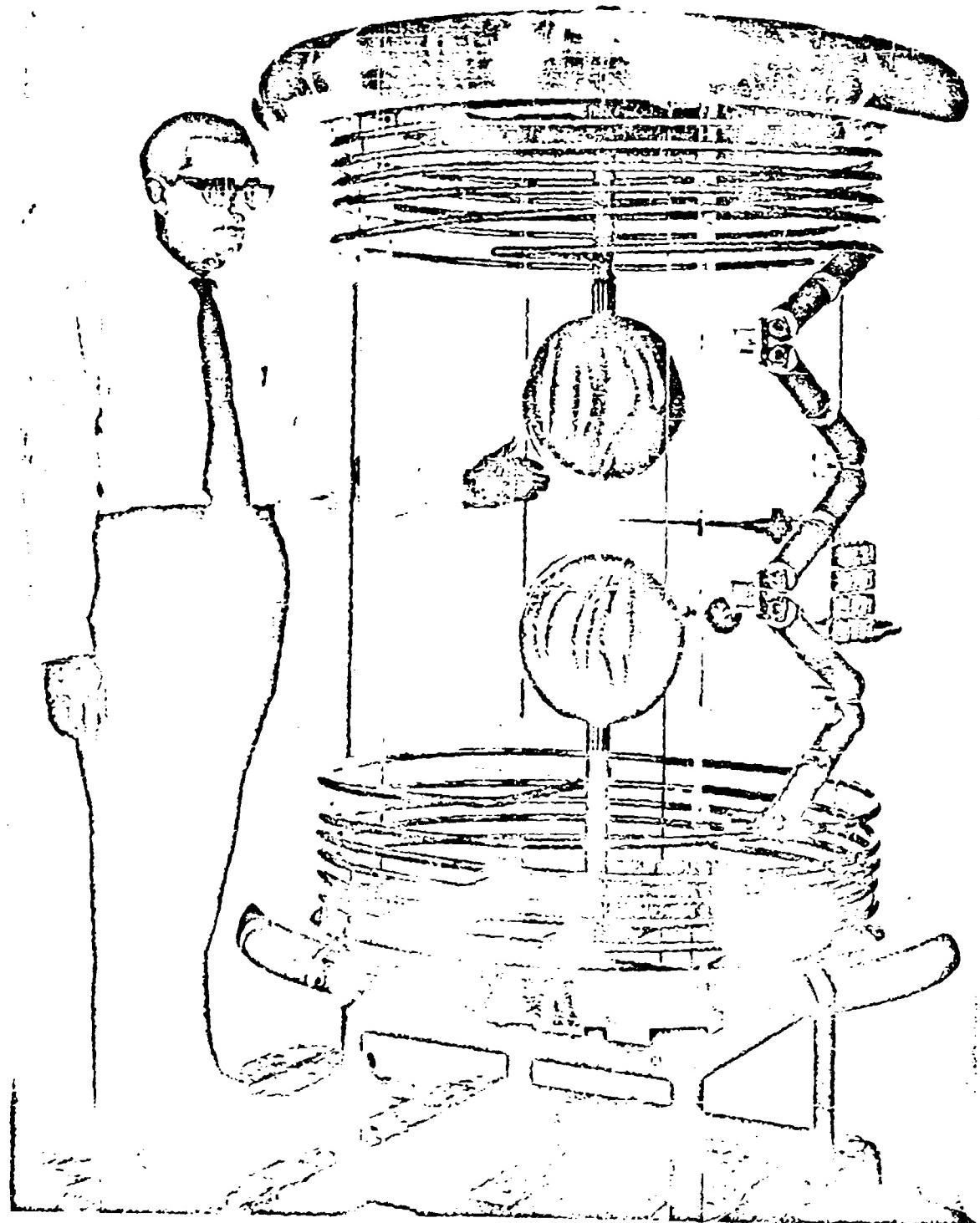


FIG. 5

and bottom of the gap. The inductance of L_1 and L_2 is not as large as might be imagined from looking at this photograph since the corona rings have the effect of coupling a shorted turn to each of these inductors. The trigger needle biasing resistors and coupling capacitor are shown on the right-hand side of the gap case, and one of the two 3-inch balls which make up the small 110 kv triggering gap may be seen on the rear panel of the lucite case.

Figure 6 shows construction details of a smaller gap built to trigger any voltage in a 0-60 kv range. This gap uses 2-inch steel balls spaced approximately 1-1/8 inches apart. In this design the trigger needle is physically positioned slightly closer to the upper ball than to the ground ball, and it is also biased to a potential slightly larger than V_{O_2} . This insures that the

$\frac{1}{2}$

needle will always arc to the top ball first, even with zero voltage across the gap thus permitting elimination of the inductor in series with the ground ball. Because of the ease of working with the lower voltages involved, it is possible to eliminate the coupling capacitor formerly shown in series with the trigger needle. The tall column immediately to the left of the arc gap contains needle biasing resistors, and the shorter column houses the capacitors which are connected across the secondary of the trigger transformer.

IV. SUMMARY OF TEST DATA

At the beginning of this program, the two most important questions to be answered were: First, could the 4.5:1 voltage range predicted by breakdown curves be achieved with a needle gap configuration of the type shown in Figure 3; and, secondly, what about erosion of the trigger needle in the presence of high energy discharges. Tests made on gaps using both 2-inch and 11-inch spheres showed a reliable operating voltage range of 4.1 to 1.

Our ability to test needle erosion phenomenon was limited by the equipment available for these tests. The first test performed consisted of discharging a 20-microfarad capacity bank charged to 150 kv into a needle gap using 11-inch spheres. This test was performed with a 17 ohm resistance in series with the needle gap. At the end of 20 shots there was some sign of needle discoloration due to heat but no observable erosion of the needle. During these tests the needle tip was positioned about 3/4 inch off the axis of the spheres and it could be observed that at high voltages the arc to both balls always formed off the tip of the needle, thus insuring that the needle did not enter into the discharge conduction path. However, it was noted that as the voltage across the gap approached the low end of its 4:1 firing range, there was a tendency for one arc to form off the tip of the needle and the other arc to form at some point behind the tip. When this happens, the needle at least initially enters into the discharge conduction path and is subject to erosion. To evaluate this, the 20 microfarad bank was charged to 50 kv and discharged through the gap 15 times. At the end of this test one could detect minute pock marks on the needle. To confirm the fact that the observed erosion was due to triggering the gap near its low-voltage limit, the gap using 11-inch spheres was replaced by a needle triggered gap using 2-inch steel balls set for a

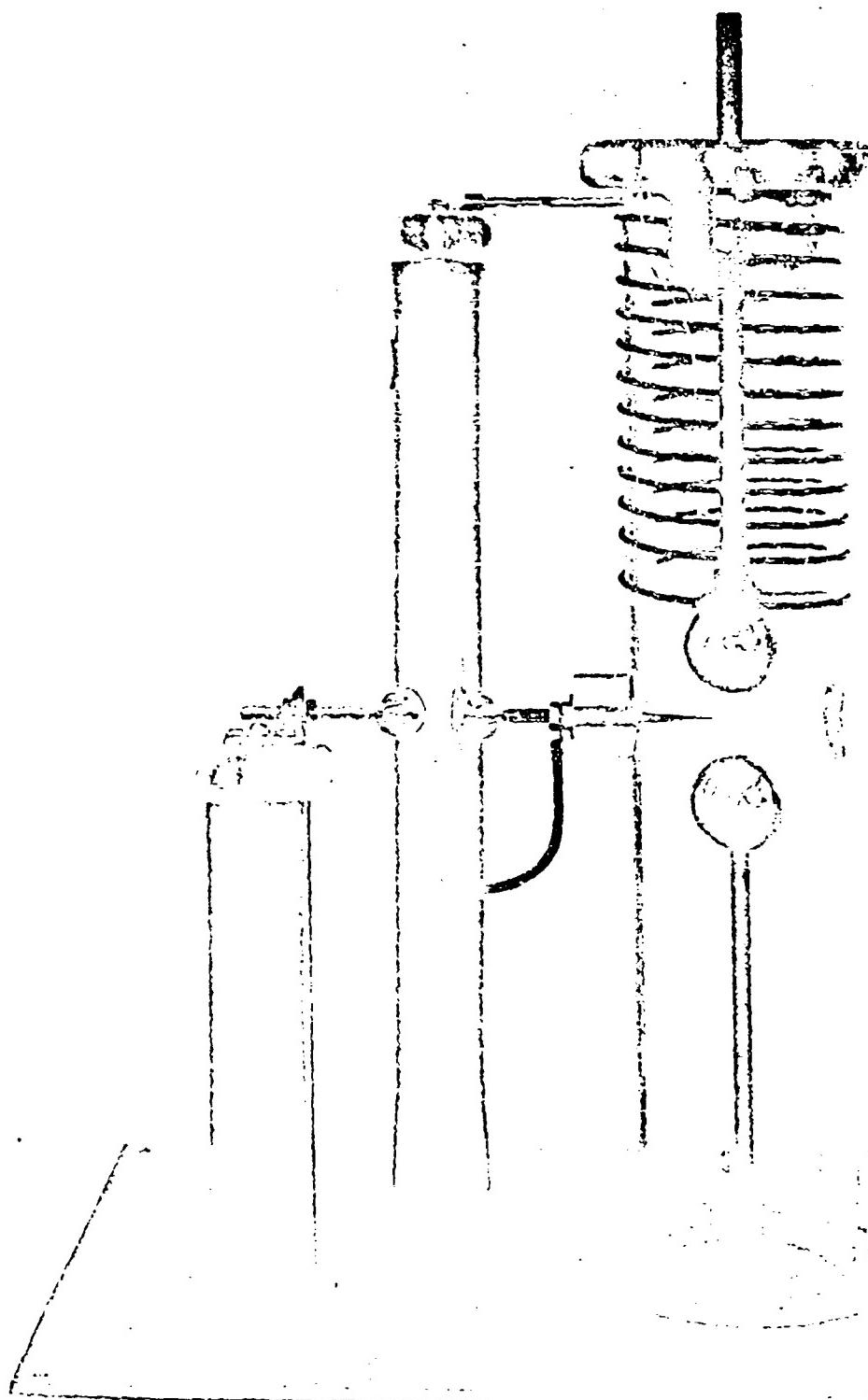


FIG. 6

Finally, tests were performed on the needle triggered gap shown in Figure 5 to determine its reliability of triggering at zero voltage and in the low voltage range. During these tests gap spacing was 4.25 inches. In the first test the high voltage and low voltage terminals of the arc gap were shorted together with an 8-foot length of RG 17/U cable. For this condition the gap triggered properly 100 out of 100 times.

Next, a .1 microfarad capacitor was charged to voltages varying between zero and 50 kv and discharged into the gap through a 35 ohm current-limiting resistor. During this test, trigger voltage was lowered 20% to explore the margin of triggering reliability. In spite of this 20% reduction of trigger voltage, during a total of 500 shots in the zero to 50 kv range, there were only two misfires.

Finally, the gap was connected to a power supply capable of varying its voltage from zero to 220 kv. There were no observed misfires at any voltage in this range.

V. THE OPERATION OF NEEDLE TRIGGERED GAPS ON POSITIVE AND NEGATIVE POWER SUPPLIES

Or work done with 1-1/2 inch spheres separated by 1 inch or less there seemed to be no significant difference in the ease with which one could trigger the gap for positive and negative power supplies. However, as the spacing between the sphere and trigger needle went out to 2-1/8 inches (4.25 inches between spheres) a significant difference developed in the case of triggering this gap for the zero and very low voltage case when a positive trigger pulse was applied, as against when a negative trigger was applied. Figure 7 shows the reason for this difference. Here, it is shown that for needle to plane spacings beyond 1/2 inch or so, it is significantly easier to trigger a needle to plane gap when the needle is positive with respect to the plane to which it must trigger. Since the trigger pulse for the needle triggered gap is of opposite polarity from that of the power supply being protected, it is easier to trigger the gap when protecting a negative power supply than to trigger the gap when protecting a positive power supply. From this same curve, it is seen that as one goes to higher and higher voltage gaps requiring spacings of 6-8 inches between spheres, the triggering problem becomes relatively easier as far as the protection of a negative power supply is concerned because of the curvature of the curve depicting breakdown voltage versus distance for needle to plane when the needle is positive with respect to the plane.

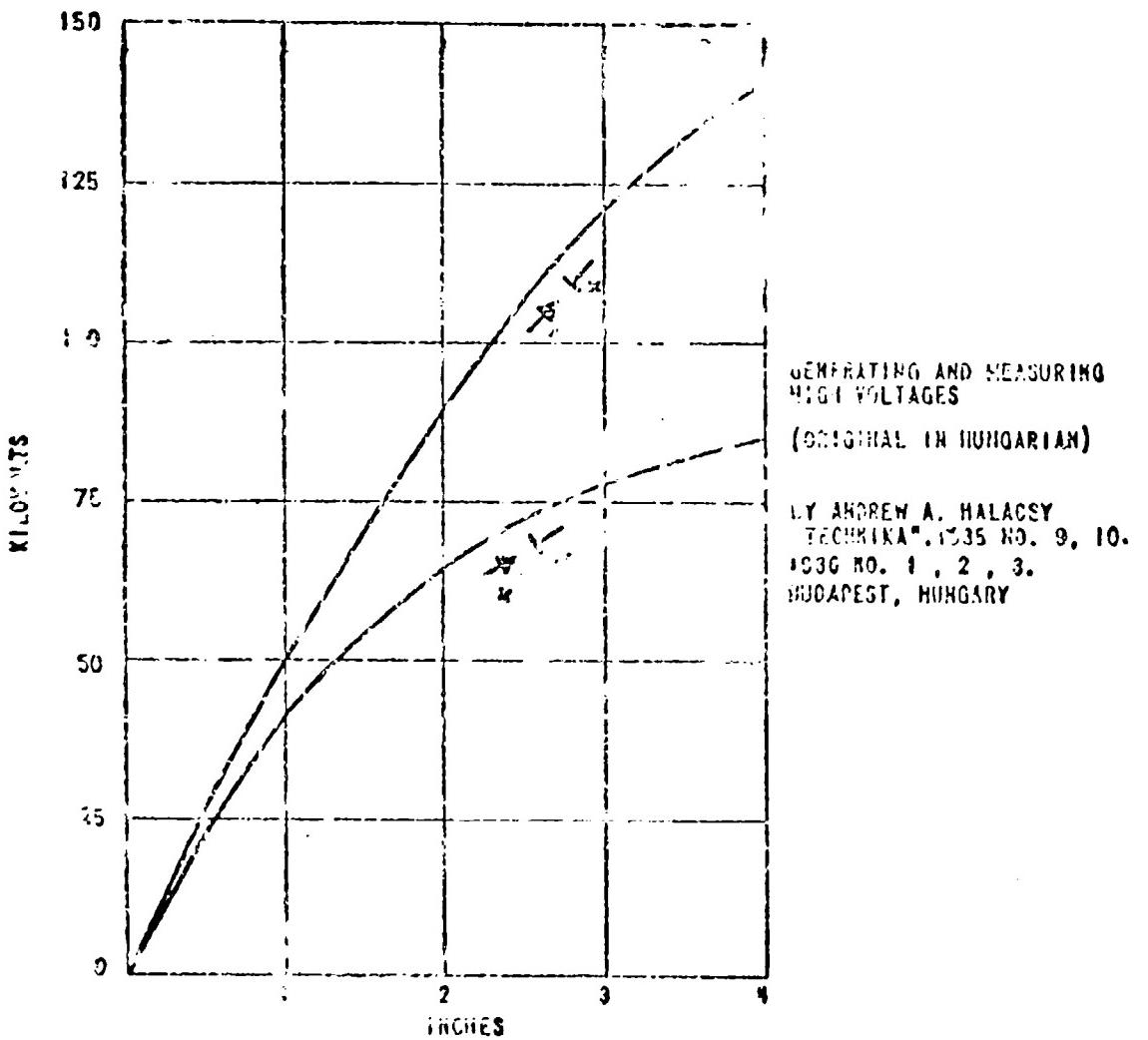


FIG. 7 NEEDLE BREAKDOWN VOLTAGE AS A
FUNCTION OF POLARITY AND DISTANCE

PRESSURIZED TRIGGERED HIGH VOLTAGE SPARK GAP
A POSSIBLE PROTECTIVE DEVICE

W. F. Westendorp

General Electric Research Laboratory

Introduction

The triggered spark gap developed in our laboratory in connection with fusion research may be of interest to the symposium as a short circuit device for the protection of high power klystrons in the case of internal failure. The present installation has a capacitor bank of 384,000 joules at 60 kilovolts (kv). It uses four simultaneously fired spark gaps to generate a magnetic field of 150,000 gauss with a total current of 3.1 million amperes in a single turn 4.5 in. in diameter, 13 1/2 in. long surrounding a 4 in. outside diameter alumina vacuum tube in which a high temperature deuterium plasma is produced. The resulting thermonuclear fusion reaction may be monitored by counting the neutrons that are produced.

The Installation

Fig. 1 shows a photograph of the system. There are four capacitor banks each with a spark gap connected to the one turn load which is centrally located in front. Each of the four banks is housed in two racks with six levels of eight capacitors of 5 microfarads each rated 20 kv or 1000 joules apiece. A wooden floor on which all the spark gaps and associated leads are placed is located 5 feet 6 in. above the concrete floor of the building. Three levels of the racks are below this wooden floor and three above it. This arrangement permits parallel connection by short wide leads of 4 groups of 3 levels in series to give 53.3 microfarads per bank with a maximum operating voltage of 60 kv. The leads are 3 feet wide, made of copper or Duralumin and the insulation is six layers of polyethylene each 0.030 in. thick operated with a maximum stress of 333 volts per mil. Six inch insulating margins prevent creepage discharges from lead to lead. Fig. 2 is a plan with the main elements sketched in.

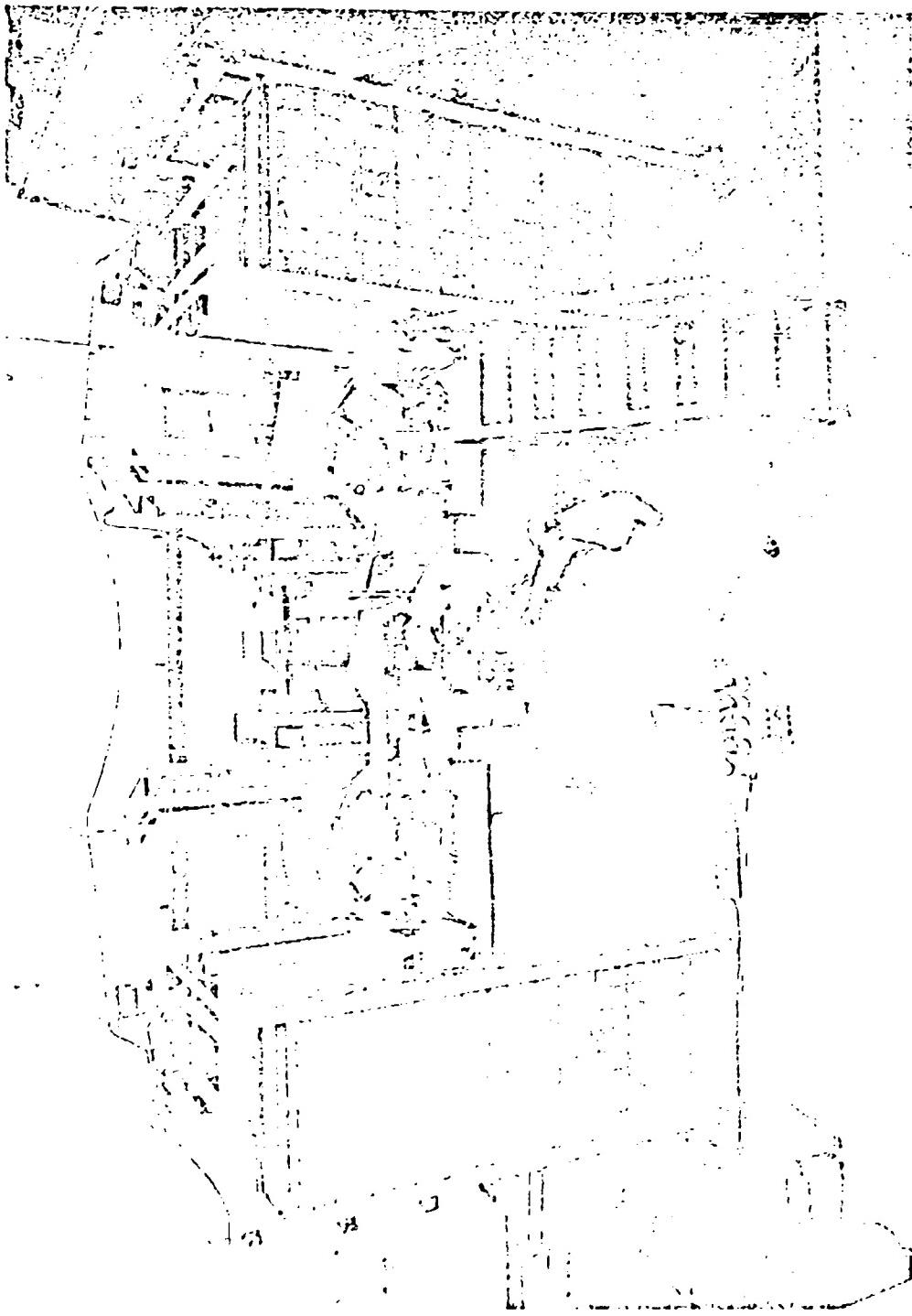
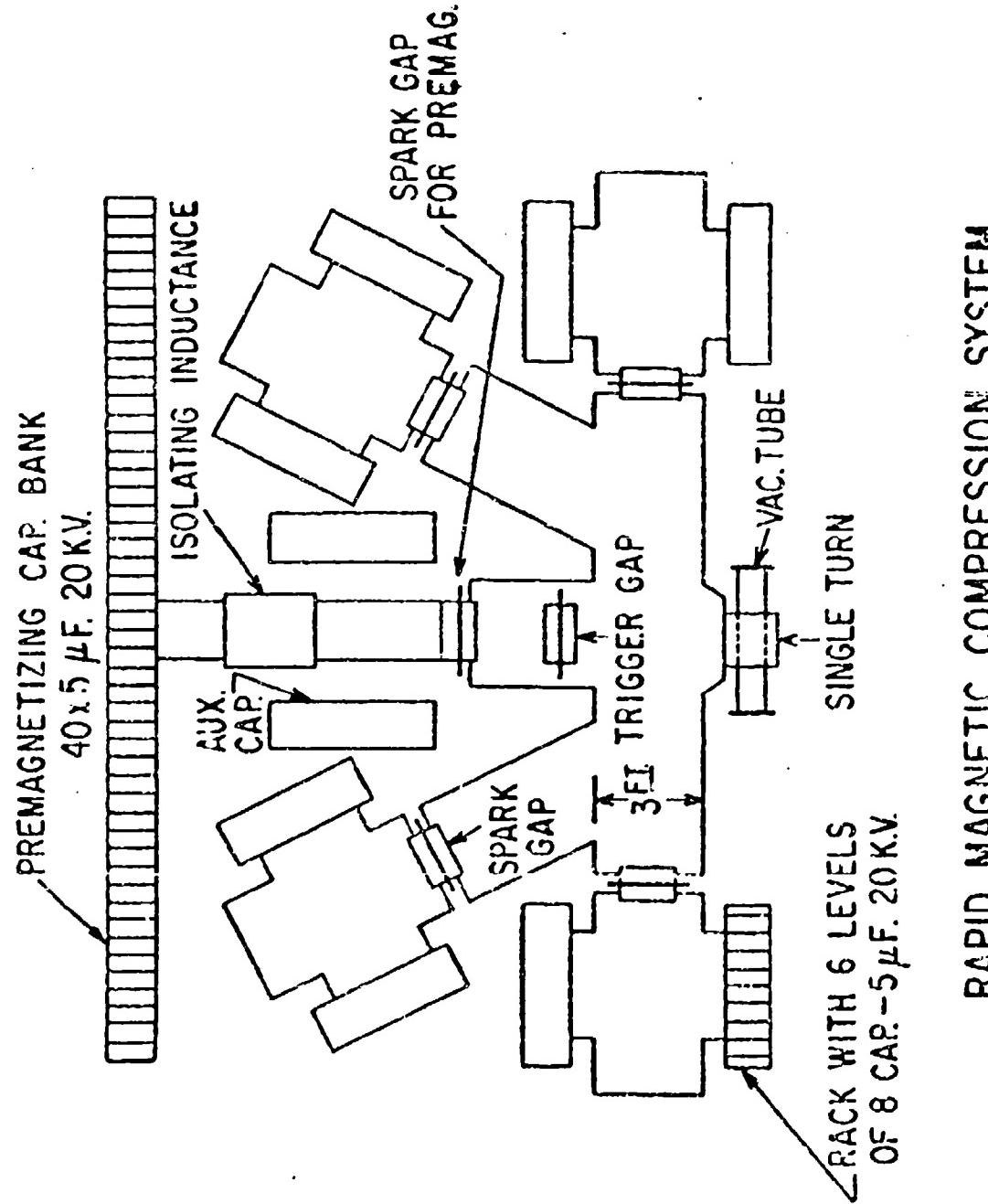


Fig. 1. General view of fast plasma compression installation.
Single turn with vacuum tube is in center foreground, capacitor
racks around periphery, spark gaps on elevated floor.



RAPID MAGNETIC COMPRESSION SYSTEM

Fig. 2. Floor plan showing location of principal parts.

The Circuit

Fig. 3 shows the circuit diagram; the ground symbols refer to one extensive return conductor system of copper sheets 3 feet wide laid directly on the wooden floor referred to above. For purposes of instrumentation there is an entirely independent copper ground plane measuring 20 feet by 28 feet under the installation on the concrete floor. The trigger electrodes of the spark gaps are maintained at half gap potential by two 20 megohm resistors. The capacitor connected to the trigger electrode joins on to a common trigger circuit shown at the top of Fig. 3. An auxiliary gap serves to apply simultaneous trigger pulses to all four main gaps. Care was taken to make the trigger leads also of low impedance and all four of equal length to insure simultaneity of firing. Fig. 4 is an oscillogram of the voltage of the bottom capacitors in each of the four banks taken by means of capacitor dividers and a two beam oscilloscope with two choppers. No difference in firing time can be detected in oscillograms of this kind. From the oscillograms we measure a natural frequency of 42 kilocycles per second and with the known total capacity of the bank of 213 microfarads we compute a total inductance of 0.068 microhenries. The current is computed to be 3.4 megamps peak in the four spark gaps, 3.1 megamps in the load inductance and 0.3 in the shunting pre-magnetizing circuit.

The pre-magnetizing circuit is also shown in Fig. 3. It may be used to establish a parallel or antiparallel field of the order of 10% of the main field before this is applied. The spark gap in this circuit is of the same design as the four others but the nitrogen pressure is 50 psig instead of 150 since the operating voltage is only 20 kv.

The Spark Gaps

The spark gaps¹ are the result of a long development necessitated by the requirements of low inductance (about 10 nanohenry), high voltage (60 kv), high current (0.85 megamp peak), reasonable life before overhaul (more than 100 discharges) and triggering with small jitter. Fig. 5 shows a simplified drawing of the cross section of the gap. A centrally located steel tie-rod with two 1 1/2 in. nuts serves to hold the parts sealed together against an operating pressure of 150 psig, and at the same time has the electrical function of a

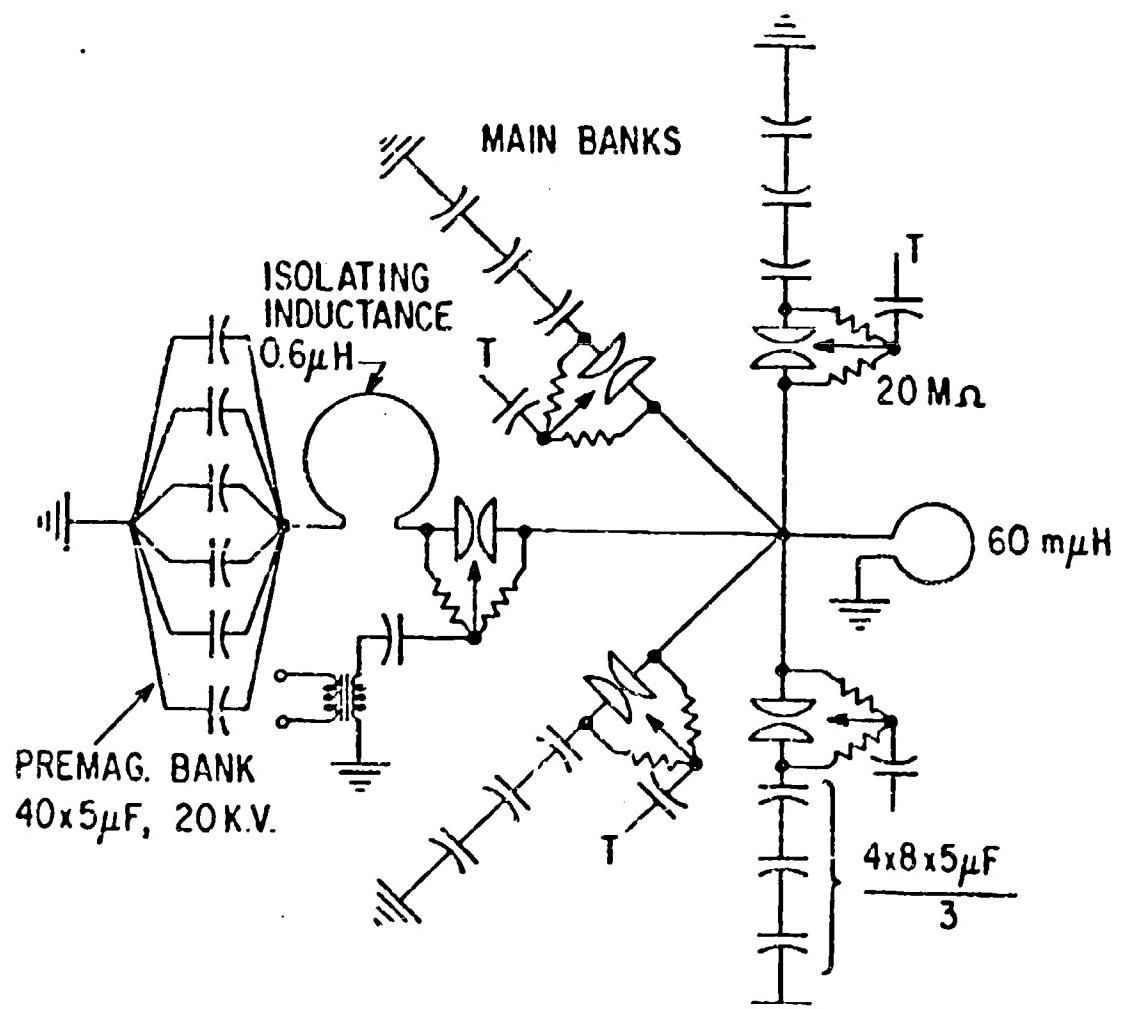
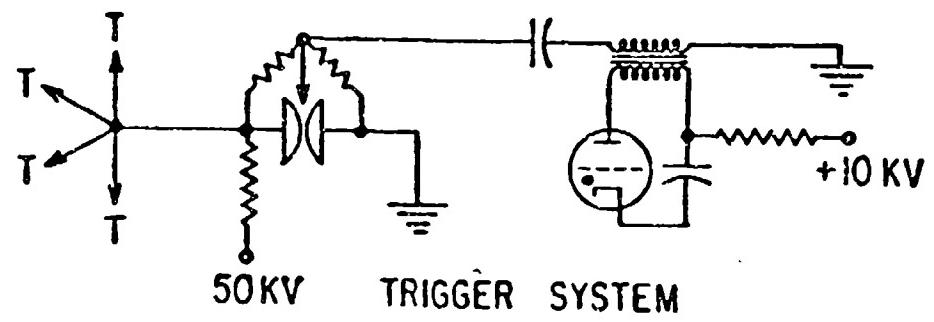


Fig. 3. Circuit diagram of fast compression systems.

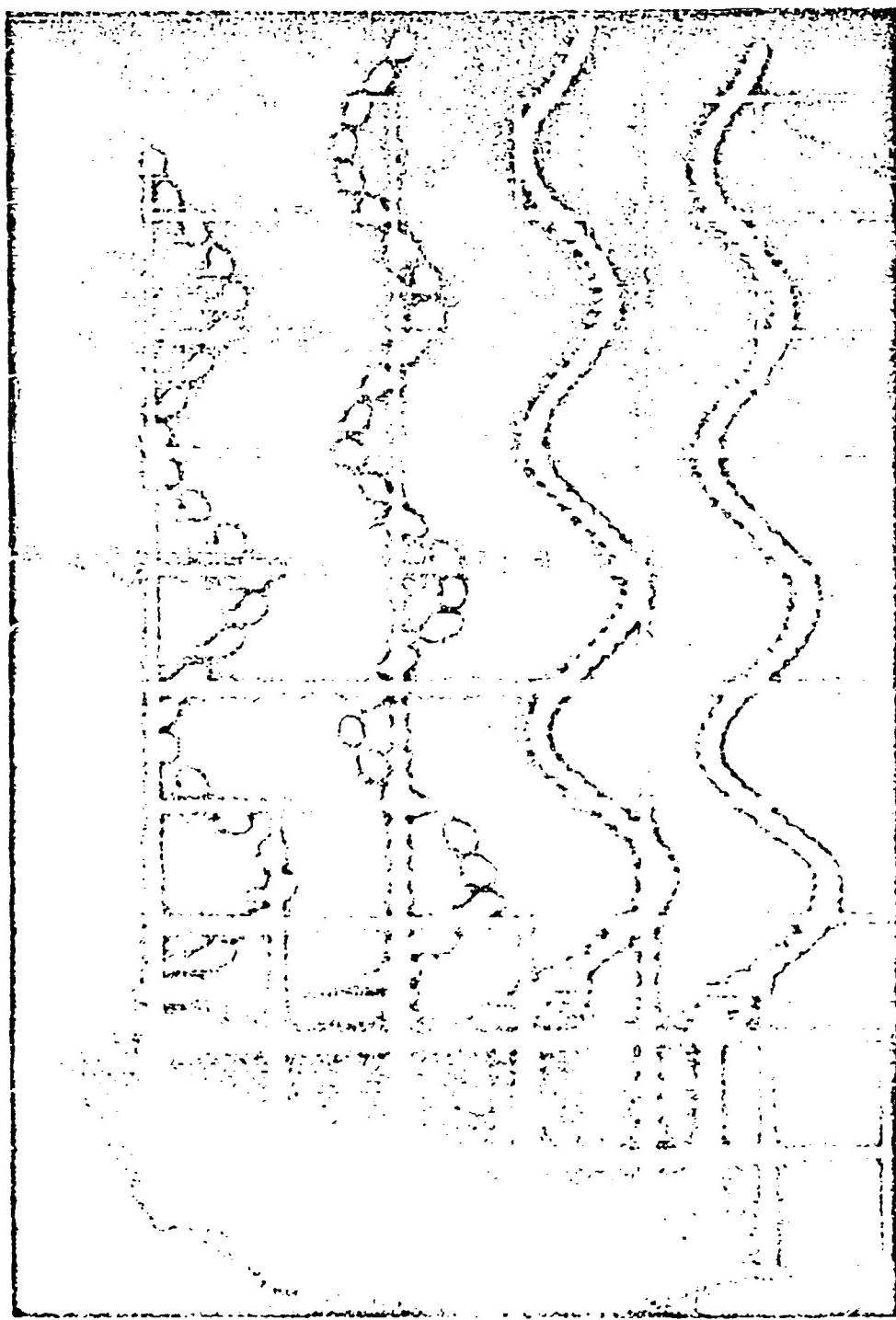
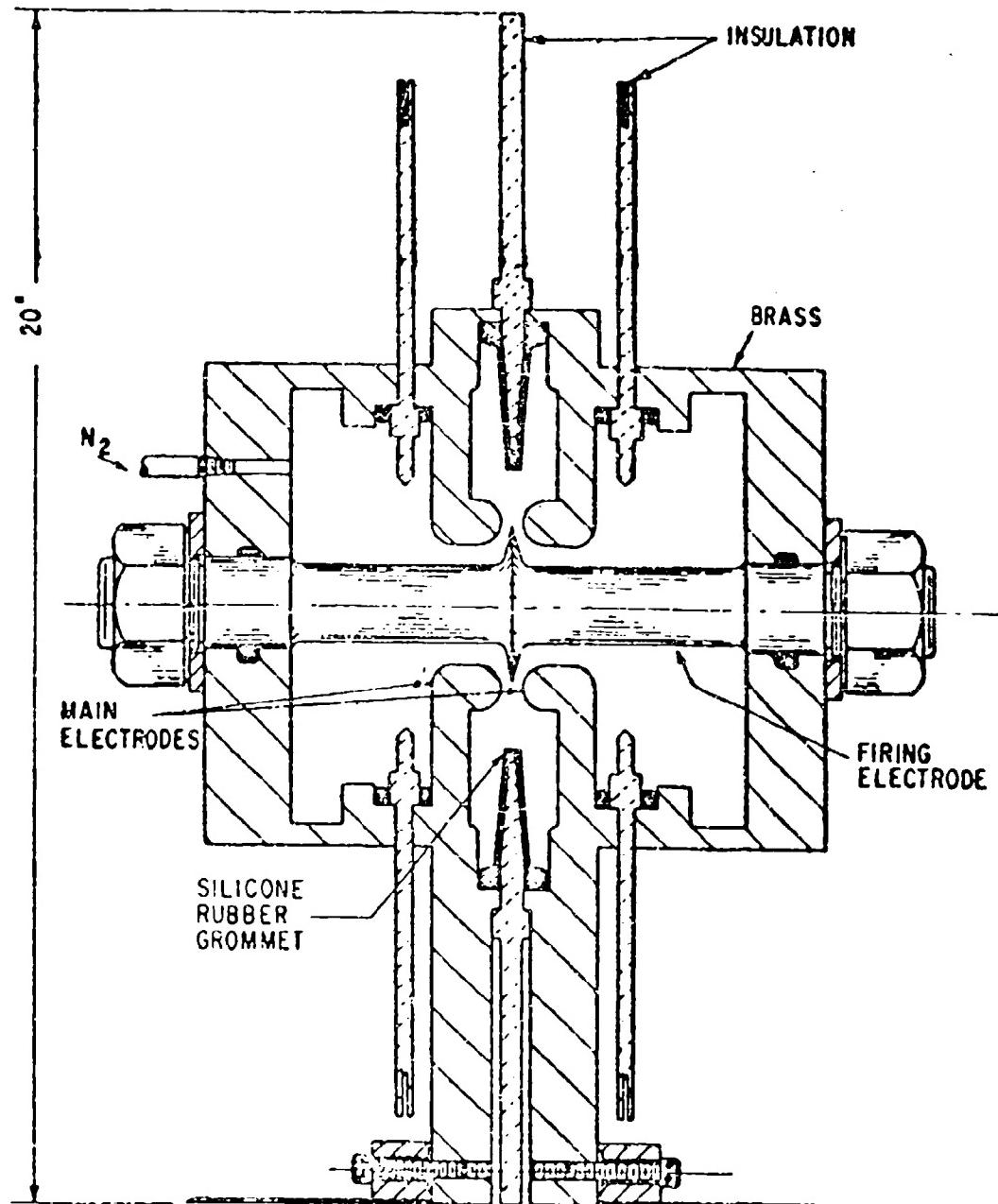


Fig. 4. Oscillosogram taken with two beam scope with two choppers showing four simultaneous traces of the capacitor voltages in the four banks. Total sweep time 100 microseconds.



PRESSURIZED TRIGGERED SPARKGAP

Fig. 5. Sketch of the cross section of the pressurized spark gap.

trigger electrode. To this end it carries in its center a flange with a sharp, 60 degree, circular edge, tipped with molybdenum. The large main electrodes machined out of brass slabs are located to either side of the fixing fin. The large hollow end bells that minimize the pressure rise caused by the arc and the three plane insulating sheets each three-eighths in. thick, show clearly in the figure. The action of the trigger fin is based on the fact that as long as it is kept at half gap potential by the two 20 megohm resistors, the electric field in this highly symmetric geometry shows no extreme stress regions, notwithstanding the sharp edge. However, if a high-voltage pulse is applied to the fin of the order of the gap potential, prompt breakdown takes place in the nitrogen near the fin and the main discharge starts. It was found that an 0.080 in. thick molybdenum insert at the sharp edge maintains a protruding edge, while arc erosion wears away some of the steel next to it. Most of the development was concerned with the insulating board in the median plane. Various glass cloth laminates with different organic bonding materials and different trade names did not stand up for more than 50 shots at full voltage and current to the hot, explosive blast of gas. They showed mechanical tearing and gouging and electrical creepage effects. The best results were obtained when the plastic bonded glass laminate central insulating board was provided with a one-eighth inch thick liner in the shape of a large grommet molded of silicone rubber. This grommet-shaped liner includes two thick edges which act as gaskets. Many other materials such as Mycalex, Mykroy, Micamat and Teflon were tried but none could compare with silicone rubber which so far has stood up for thousands of shots and shows no deterioration. Much less work was done on electrode materials; brass is used for the main electrodes for easy machinability and steel for the trigger electrode for extra strength since it serves as a tie-rod. The brass electrodes last about 2000 shots before remachining and the trigger electrodes have to be equipped with new molybdenum fins after about 200 discharges. A fine brass dust mixed with nitrides of copper and zinc is formed which is non-conducting. A provision is made for blowing off the nitrogen and the dust after every ten shots or so to prevent accumulations and consequent field distortions which lower the breakdown voltage. Normal operating pressure for 60 kv is 150 psig of nitrogen for the three-eighths inch gap. Outside the pressurized region the principal problem is to maintain a sufficient creepage margin over the boards that insulate the end bells from the main electrodes since the

trigger electrode is exposed to high voltage transients. Also proper overlapping of the polyethylene sheet insulation between the leads and the three insulating boards must be provided; this is not shown in Fig. 5.

Adaptation for Use as a Short Circuit Switch

The pressurized triggered spark gap described above may be fairly directly adapted for use as a protective switch across a klystron tube. For 150 kv it would probably be much simpler to use a series of three gaps of the existing design potential graded with a resistance divider rather than attempt to develop a single spark gap for the full voltage. Some consideration should be given to the energy stored in the rectifier filter which may cause an oscillatory discharge if no damping resistance is provided, with a detrimental effect on capacitor life.

Further Developments

In our laboratory the spark gap was still further developed by Goldman, Pollock and Reynolds mainly for the purpose of reducing the jitter between triggering and breakdown from a half microsecond to a few hundreds. This sort of accuracy of firing would presumably not be required for the klystron crow bar application. It was found that the delay between the application of trigger voltage and the breakdown of the gap could be reduced and made nearly constant by operating closer to the static breakdown voltage of the gap. To allow operation within 20% of the static breakdown voltage it is necessary to make this hold-off voltage level very much more stable than it is in the pressurized gap. By widening the gap and operating at atmospheric pressure without any enclosure residual dust in the gap blows away, the static breakdown voltage becomes very nearly constant and the operating level may be 60 kv when the breakdown level is 75 kv. This kind of operation results in an accuracy of firing or jitter time of 25 nanoseconds and increases gap life but has the disadvantage of doubled gap inductance and explosive noise generation. Fig. 6 shows the new atmospheric pressure gap as it is now being used in our laboratory. There are two half inch gaps in series between steel surfaces and the tie-bolt-trigger electrode is held suspended centrally in the main electrodes by four Mycalex insulating posts on each side. A very fast trigger

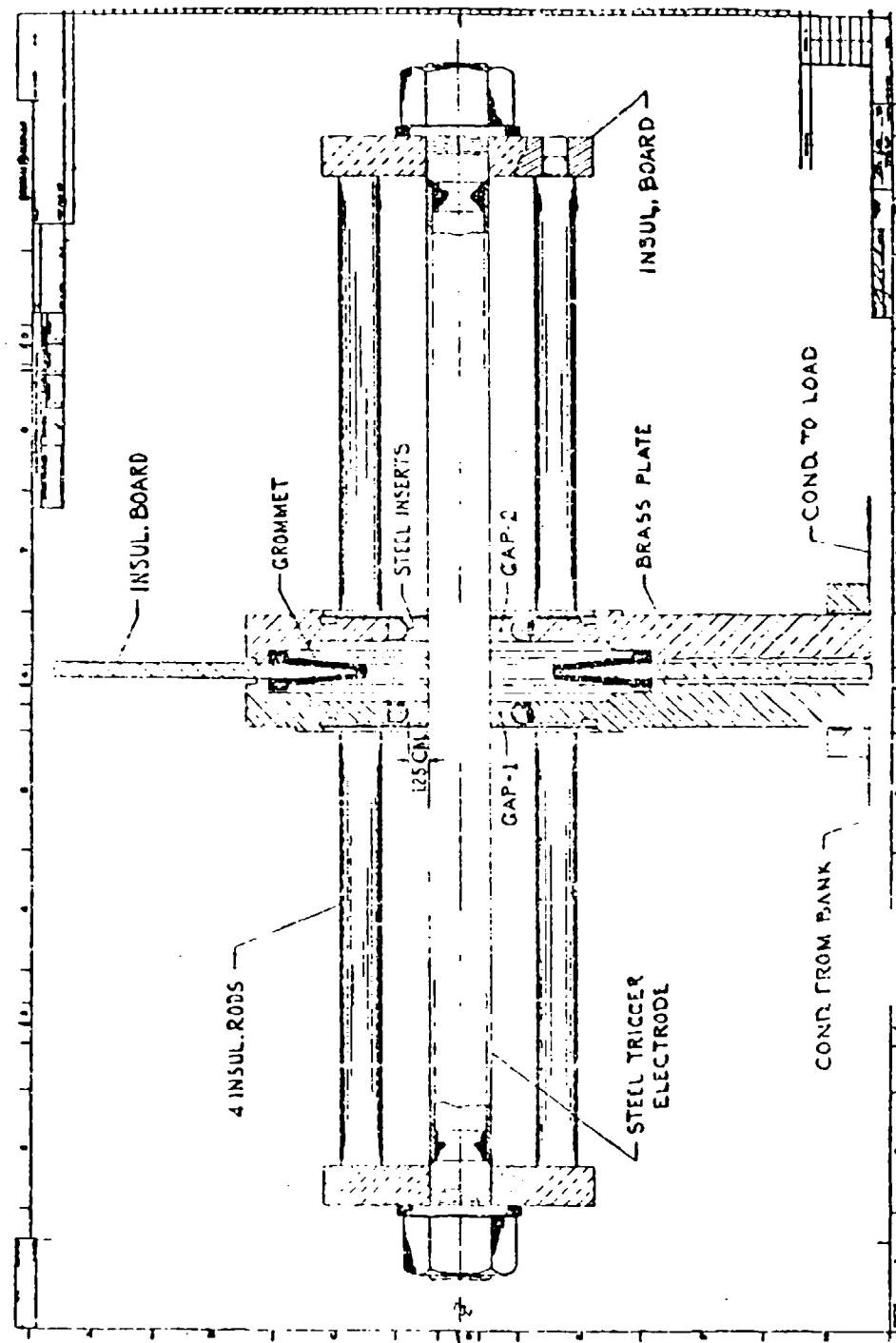


Fig. 6. Sketch of the cross section of the atmospheric air spark gap with 25 nanosecond action.

circuit is used which depends on the discharge of a transmission line thru an auxiliary gap.

References

1. Engineering Aspects of Magnetohydrodynamics, Columbia University Press, pp 542-548.
2. Switching a 384 Kilojoule Low Inductance Capacitor Bank. L. M. Goldman, H. C. Pollock and J. A. Reynolds, General Electric Research Laboratory report No. 62-RL-3047E, Class 1.

MILITARY ORGANIZATIONS (continued)

USARBL (continued)

H. A. Zahl
M. H. Zinn

U. S. Army Signal Supply Agency
225 S. 13th Street
Philadelphia 3, Pennsylvania
C. Mogavero
H. Shuenbloom
S. A. Sokolove

U. S. Naval Air Development Center
Johnsville, Pennsylvania
R. Cagliardi
G. Hazenfuss
J. Metz
P. Serenson

Rome Air Development Center
Griffiss Air Force Base
Rome, New York
H. L. Beard

UNIVERSITIES

Linfield Research Institute
McMinville, Oregon
F. M. Charbonnier

Massachusetts Institute of Technology
Lincoln Laboratory
P. O. Box 73
Lexington 73, Massachusetts
W. Both
A. Buckley
A. Funaro
E. O. Gronroos
P. B. McCorison
C. Price
J. R. Sandison
E. Silvermann
L. R. Swain, Jr.
A. Vierstra

University of California
Lawrence Radiation Laboratory
Box 208
Livermore, California
K. Aaland
B. M. Loth
W. I. Smith

Yale University
New Haven, Connecticut
J. Sheehan
G. W. Wheeler

Brookhaven Laboratory (ADC)
Upton, New York
E. Forsyth
H. Hahn

Stanford University
Microwave Laboratory
Stanford, California
H. S. Butler
C. H. Sphar
T. F. Turner

COMMERCIAL ORGANIZATIONS

ACF Electronics
11 Park Place
Paramus, New Jersey
V. Sacco

Airborne Instruments Laboratory
160 Old Country Road
Mineola, New York
W. Frey

Arinc Research Corporation
1700 K Street N.W.
Washington 6, D. C.
T. Jackson

Autonetics Division
N. American Aviation, Inc.
9150 E. Imperial Way
Downey, California
R. R. Trautwein

Avco Electronics & Ordnance Division
2630 Glendale-Milford Road
Cincinnati 41, Ohio
E. R. Young

Axel Electronics, Inc.
Jamaica, New York
E. F. Burns
M. Del Gross
M. Matnick

Bell Telephone Laboratories
Whippny Road
Whippny, New Jersey
H. J. Betzel
H. A. Reise

The Bendix Corporation - York Division
York, Pennsylvania
R. W. Sedgwick

Bendix Radio Division
Joppa Road
Towson 4, Maryland
R. Crowell
A. Bazarian
A. Hammel
R. H. Lee
D. J. Weber

Bomac Laboratories, Inc.
Salem Road
Beverly, Massachusetts
A. P. Waterman

Burmac Electronics Co., Inc.
142 So. Long Branch Road
Rockville Centre, New York
S. F. Delligatti

Cared Corporation
3381 Junipero Serra Boulevard
Palo Alto, California
D. Simmons

Chatham Electronics
Division of Tung-Sol Electric, Inc.
630-W. Mt. Pleasant Avenue
Livingston, New Jersey
S. Landstrom
J. R. Onifer
O. Schurek
C. S. Shackelford
W. W. Wetrous

Consolidated Engineering Company
Amherst, N. Hampshire
P. Martin

Continental Electronics Mfg. Co.
4212 S. Buckner Street
Dallas 27, Texas
J. H. Brown
R. E. Ramsey

Corson Electric Mfg. Corp.
540 30th Street
Union City, New Jersey
D. E. Corson
H. Oboryshko

Ethicon Corporation
U. S. Highway 22
Somerville, New Jersey
E. Roller

COMMERCIAL ORGANIZATIONS (continued)

Edgerton, Germeshausen & Grier, Inc. 160 Brookline Avenue Boston, Massachusetts	S. Goldberg J. J. Mulrey J. Murachver D. P. Riley A. D. Shea D. V. Turnquist Dr. L. B. Woolaver	General Electric Company 60 Jackson Street Holyoke, Massachusetts
Fitel-McCullough, Inc. 301 Industrial Way San Carlos, California	W. H. McAulay G. V. Miron W. Rate	D. M. Dimarest P. B. Headley R. D. Smith W. C. Stone J. W. Torrance R. S. Ringland
Electronic Enterprises, Inc. 65 7th Avenue Newark, New Jersey	R. H. Bloemeke D. Dubin	General Electric Company John Street Hudson Falls, New York
Emerson Electric Mfg. Co. 8011 Florissant Avenue St. Louis 36, Missouri	F. DeLurgio H. Robinson	D. H. Nichols S. R. Wilson
PXR, Div. of Amphenol-Borg Elec Corp. 25-26 50th Street Woodside 77, New York	D. J. Boston A. Feldman J. Hakimi F. Klarpanu R. J. Leff	General Electric Company Space Sciences Laboratory King of Prussia, Pennsylvania
General Dynamics Electronics San Diego, California	R. Kicar	C. J. Dudzinski R. C. Good, Jr.
General Electric Company Rectifier Components Department Auburn, New York	N. Mapham	General Electric Company 1 River Road Schenectady 5, New York
General Electric Company 200 Main Avenue Clifton, New Jersey	C. D. Ahlstrom H. L. Tate	W. H. Benning R. Bradford A. W. Coolidge J. E. Dillon A. Michaelson W. H. Nevins H. Price R. V. Pohl K. E. Wilson H. E. Zuvera
General Electric Research Laboratory Box 1038		General Electric Research Laboratory Box 1038
		Schenectady, New York
		C. J. Gallagher W. F. Westendorp
		General Electric Company Court Street Syracuse, New York
		E. R. Bosenfelder C. J. Eichenauer, Jr.
		General Electric Company 901 Broad Street Utica, New York
		P. Fenoglio

COMMERCIAL ORGANIZATIONS (continued)

General Electric Company
777 14th Street N.W.
Washington 5, D. C.
J. E. Kanan

Hughes Aircraft Company
P. O. Box 2097
Fullerton, California
J. V. Stover

ITT Components Division
Box 412
Clifton, New Jersey
P. Ehrhardt
K. Liddane
J. J. Tritchler

ITW Corporation
492 River Road
Nutley, New Jersey
R. T. Courtney
H. White

Kutite Laboratories, Inc.
730 S. 13th Street
Newark 3, New Jersey
J. Boeck
S. Cohen
A. E. Gordon
H. E. Krefft
J. J. Myers
M. K. Wilder

Litton Electron Tube Corporation
San Carlos, California
L. J. Fox
F. Oakes
S. W. Woolsey

Lockheed Electronics Company
U. S. Highway #22
Plainfield, New Jersey
P. Conier
V. N. Martinovitch

The Mechlett Laboratories, Inc.
1063 Hope Street
Springdale, Connecticut
C. Kirka
C. V. Weden

Magnetic Research Corporation
3160 W. El Segundo Boulevard
Hawthorne, California
T. Schweers

Manson Laboratories, Inc.
375 Fairfield Avenue
Stamford, Connecticut
N. Baske
H. Feldman
S. Jacobson
G. Lyuta
K. Yuan

Maxson Electronics, Corporation
460 W. 34th Street
New York City, New York
G. Gallios
J. Vergeichik

Microwave Assoc., Inc.
South Avenue
Burlington, Massachusetts
H. R. Durling, Jr.
R. W. McLaren

Moloney Electric Company
5390 Bircher Boulevard
St. Louis, Missouri
E. C. Hirschbuehler
C. J. Sievers

Norden Laboratories
Division of United Aircraft Corp.
121 W. Moreland Avenue
White Plains, New York
S. Brody

Radio Corporation of America
Front & Cooper Streets
Camden, New Jersey
L. Andrede
J. B. Fuller
G. F. Rosenzweig

Radio Corporation of America
100 So. 2nd Street
Harrison, New Jersey
D. Mawhinney

Radio Corporation of America
New Holland Pike
Lancaster, Pennsylvania
W. Harbaugh
T. E. Yingst

COMMERCIAL ORGANIZATIONS (continued)

Radio Corporation of America
Borton Landing Road
Moorestown, New Jersey
 T. Anderson
 T. Doma
 C. Pappas
 R. W. Scheyhing

Radio Corporation of America
Princeton, New Jersey
 B. Hazy
 E. M. Leyton

Radiation at Stanford
Palo Alto, California
 A. J. Morris
 J. P. Swanson

Raytheon Manufacturing Company
Box 312
Hartwell Road
Bedford, Massachusetts
 J. R. Caswell
 W. Vail
 E. F. Weinburg

Raytheon Manufacturing Company
P. O. Box 360
Newport, Rhode Island
 A. F. Pfeiffer

Raytheon Manufacturing Company
AEO, Box 211
Sudbury, Massachusetts
 R. C. Mong
 A. D. Porter

Raytheon Manufacturing Company
River Building 23
Waltham 54, Massachusetts
 G. W. Halder

Raytheon Manufacturing Company
Wayland Laboratory
Wayland, Massachusetts
 A. B. Fisher
 W. Hoover

Research-Cottrell Inc.
Bound Brook, New Jersey
 H. J. Hall
 R. E. Willison

S-0 Laboratories
8-0 Rahway Avenue
Union, New Jersey
 P. Fenster
 C. Gill
 D. Matthews
 G. Thornber

Sperry Gyroscope Company
Great Neck, New York
 M. Coyle
 G. Grotz
 W. Kestenbaum
 C. Lemmert
 F. Loeb
 I. A. Ross

Sperry Gyroscope Company
55 Denton Avenue
New Hyde Park, New York
 B. A. Michalak
 W. Orlowski
 J. Wolsiefer

Sperry Piedmont Company
Division of Sperry Rand
Charlottesville, Virginia
 P. R. Hamlin

Sperry Rand Corporation
Electronic Tubes Division
Gainesville, Florida
 D. Harper

Sprague Electric Company
Marshall Street
North Adams, Massachusetts
 C. W. Chase
 R. Lott
 J. A. White

Sylvania Electric Products
100 First Avenue
Waltham, Massachusetts
 G. C. Barker
 W. J. Boland
 H. F. Onusceit
 P. A. Robinson

Sylvania Electronic Systems
Electronic Defense Laboratory
P. O. Box 205
Mountain View, California
 F. V. Lewis

COMMERCIAL ORGANIZATIONS (continued)

Tung-Sol Electric Company, Inc.

200 Bloomfield Avenue
Bloomfield, New Jersey

H. Brady
C. E. Coon
R. Mann
R. P. Masek
F. Kauscher
D. Sanger
A. Skellett

Westinghouse Electric Corporation

P. O. Box 284
Elmira, New York

R. A. Freggens
L. H. Howe
R. M. Hieba
J. G. Sadler

Westinghouse Electric Corporation

Box 1297, Friendship Airport
Baltimore, Maryland

C. Festige
R. A. Gardenghi
B. V. Gerber
T. Hamburger
C. K. Hooper
M. L. Jones
H. Lehman
T. E. Olver
A. L. Quesimberry
F. J. Ritter
C. H. Wood

Baker, B. O.	11	Barber, R. S.
Banks, R.	12	Barlow, W. H.
Besenfelder, E. R.	13	Bartley, C.
Buffa, A. J.	14	Bassett, A. S.
Butler, H. S.	15	Battell, G. S.
Cannata, P.	16	Bazante, H. V.
Charbonnier, F. M.	17	Bearce, C.
Cook, K. G.	18	Bell, C.
Coolidge, A. W.	19	Bellinger, S.
Courtney, R. T.	20	Bengwick, R. W.
Creedon, J. E.	21	Beth, V. L.
Delligatti, S. F.	22	Smith, W. I.
Eichenauer, C. J.	23	Bever, J. V.
Fox, L. J.	24	Srain, L.
Froelich, R. J.	25	Branson, J.
Gardenghi, R. A.	26	Turner, T. P.
Goldberg, S.	27	Trotz, W. A.
Grotz, C.	28	Weden, C. V.
Hamburger, T.	29	Weinberg, E. F.
Huartson, A.	30	Westendorp, W. F.
Hill, R. A.	31	Sheldon, R. J.
Jarvis, R. E.	32	Wood, C. H.
Jordan, R.	33	Woolaver, L. L.
Loth, E. M.	34	Yinn, M. H.
Luna, A. R.	35	